The role of 3',4'-dihydroxyphenyl-γ-valerolactone, the gut microbiota metabolite of (−)-epicatechin, in reducing insulin resistance

Jenna Christine Helleur

Quadram Institute Bioscience

A thesis submitted to the University of East Anglia for the Degree of Doctor of Philosophy

December 2020

This work was supported by the UKRI Biotechnology and Biological Sciences Research Council Norwich Research Park Biosciences Doctoral Training Partnership [grant number BB/M011216/1, and project code KROON_F16HDTP].

Abstract

Background: Hydroxyphenyl-γ-valerolactones (HPVLs) are microbiota-derived metabolites of monomeric catechins and comprise about 33 % of total human catechin metabolites. HPVLs could therefore contribute to the previously reported beneficial effects of (−)-epicatechin (EC) on high-fat (HF) diet induced weight gain and insulin resistance (IR) in mice.

Aims: Assess the bioavailability and metabolism of 3',4'-dihydroxyphenyl-γ-valerolactone (34DHPVL) and determine its effects on IR, body weight gain, steatosis and hepatic gene expression changes when fed directly to mice on HF or low-fat (LF) diets.

Methods: Male C57BL/6J mice were fed LF (10 % kcal) or HF (60 % kcal) diets with or without 20 mg/kg body weight (BW) supplementation of EC or 34DHPVL for 15-weeks. A fasted glucose tolerance test was performed at week-13 to assess IR. Plasma and liver lipids were quantified, and the effects on global gene expression assessed via RNA-sequencing analysis of liver tissue.

Results: Gavaged 34DHPVL was highly bioavailable and present in plasma solely as sulfated and glucuronidated conjugates. 34DHPVL dietary supplementation reduced plasma glucose A.U.C (p = 0.12) albeit non-significantly (ns), paradoxically increased plasma insulin ($p < 0.01$) and liver lipids (ns) but had no effect on HF diet-induced BW gain. EC dietary supplementation improved insulin sensitivity (HOMA-IR, p = 0.07), and mitigated HF diet-induced BW and liver weight gain and hepatic lipid accumulation (all $p < 0.05$). Both EC and 34DHPVL protected against HF diet-induced increases in expression of genes involved in glucose production and increased expression of insulin signalling genes, but the effects of EC were much stronger.

Conclusion: These data suggest that 34DHPVL may contribute modestly to the beneficial effects of EC consumption on HF-diet induced IR, but it is clear that the effects of the parent EC are stronger. 34DHPVL is not responsible for the mitigation of HF diet-induced BW gain caused by EC, which suggests that this effect is caused by EC conjugates.

Contents

List of figures

List of tables

List of formulas

Abbreviations

345THPVL	3’,4’,5’-Trihydroxyphenyl-γ-valerolactone
34DHPVL	3’,4’-Dihydroxyphenyl-γ-valerolactone
35DHPVL	3’,5’-Dihydroxyphenyl-γ-valerolactone
3HPVL-4GlcA	3’-Hydroxyphenyl-γ-valerolactone-4’-glucuronide
3HPVL-4S	3’-Hydroxyphenyl-γ-valerolactone-4’-sulfate
4H3MVL	4’-Hydroxy-3’-methoxyphenyl-γ-valerolactone
4HPVL-3GlcA	4’-Hydroxyphenyl-γ-valerolactone-3’-glucuronide
4HPVL-3S	4’-Hydroxyphenyl-γ-valerolactone-3’-sulfate
A.U.C	Area under the concentration time-curve
ACC	Acetyl-CoA carboxylase
ACE	Angiotensin converting enzyme
ACLY	ATP-citrate synthase
ADME	Absorption, distribution, metabolism and excretion
Akt/PKB	Protein kinase B
ALDB	Aldolase B
ALT	Alanine transaminase
AST	Aspartate transaminase
Atg7	Autophagy-related protein 7
ATGL	Adipose triglyceride lipase
ATP	Adenosine triphosphate
$A\beta_O$	Amyloid-β oligomers
BAT	Brown adipose tissue
BBB	Blood-brain barrier
BH	Benjamini and Hochberg
BMP	Bone morphogenic protein
C/EBPα	CCAAT/enhancer binding protein α
CaMKK	Ca^{2+}/calmodulin-dependent protein kinase kinase
cAMP	Cyclic adenosine monophosphate
CAP	Cbl-associated protein
CAT	Catalase
CBG	Cytosolic-β-glucosidase
CCL	Chemokine ligand

CEACAM1	Carcinoembryonic antigen-related cell adhesion molecule 1
CGI-58	Comparative gene identification-58
CHO	Cholesterol
ChREBP	Carbohydrate response element binding protein'
C_{max}	Maximum concentration
COMT	Catechol-*O*-methyltransferases
CPE	Cocoa polyphenol extract
CPT	Carnitine palmitoyltransferase
CREB	cAMP Response Element Binding Protein
CVD	Cardiovascular disease
DAG	Diacylglycerols
DEG	Differentially expressed gene
DHBA	2,3-Dihydroxybenzoic acid
DHPAA	3,4-Dihydroxyphenylacetic acid
DMF	N,N-dimethylformamide
DMSO	Dimethyl sulfoxide
DNL	*De novo* lipogenesis
EC	(−)-Epicatechin
ECG	Epicatechin gallate
ECM	Extracellular matrix
EDTA	Ethylenediaminetetraacetic acid
EGC	Epigallocatechin
EGCG	Epigallocatechin gallate
EPIC	European Prospective Investigation into Cancer and Nutrition
ERK	Extracellular signal related kinase
FA	Formic acid
FASN	Fatty acid synthase
FDR	False discovery rate
FFA	Free fatty acid
fMRI	Functional magnetic resonance imaging
FOXO	Forkhead box O
G6Pase	Glucose-6-phosphatase

GEO	Gene Expression Omnibus
GI	Gastrointestinal
GIP	Glucose-dependent insulinotropic peptide
GLP	Glucagon like peptide
GLUT	Glucose transporter type
GPAT	Glycerol phosphate acyltransferase
GPCR	G Protein Coupled Receptor
GPx	Glutathione peroxidase
GR	Glutathione reductase
GSEA	Gene set enrichment analysis
GSH	Glutathione
GSK	Glycogen synthase kinase
GTE	Green tea extract
GTP	Green tea polyphenols
GTT	Glucose tolerance test
H&E	Hematoxylin and eosin
HBMEC	Human brain microvascular endothelial cells
HC	High carbohydrate
HDF	Human dermal fibroblasts
HDL	High-density lipoproteins
HF	High fat
HMGA1	High mobility group AT-Hook 1
HOMA-IR	Homeostatic model assessment of insulin resistance
HPAA	3-Hydroxyphenylpropionic acid
HPLC	High performance liquid chromatography
HPVA	Hydroxyphenylvaleric acid
HPVL	Hydroxyphenyl-γ-valerolactone
HSL	Human sensitive lipase
HT-29 and HCT-116	Human colon adenocarcinoma cells
HUVECs	Human umbilical vein endothelial cells
IEC-6	Rat intestinal epithelial cell
IGF	Insulin like growth factors
IKK	Inhibitor nuclear factor κB kinase
IL	Interleukin

iNOS	Inducible nitric oxide synthase
INT-407	Human intestinal epithelial cells
IR	Insulin receptor
IRS	Insulin receptor substrates
ITT	Insulin tolerance test
IκB	Inhibitor nuclear factor κB
JAK-STAT	Janus kinase (JAK)-signal transducer and activator of transcription
JNK	c-Jun N-terminal kinases
KEGG	Kyoto Encyclopedia of Genes and Genomes
KYSE150	Human oesophageal squamous cell carcinoma cells
LC	Low carbohydrate
LDL	Low-density lipoproteins
LF	Low-fat
LLE	Liquid-liquid extraction
LOD	Limit of detection
LPH	Lactase phloridzin hydrolase
LPS	Lipopolysaccharide
MAFLD	Metabolic associated fatty liver disease
MAPK	Mitogen-activated protein kinase
MCD	Malonyl-CoA decarboxylase
MCP	Monocyte chemotactic protein
MGL	Monoacylglycerol lipase
MMP	Matrix metalloproteinase
MRM	Multiple reaction monitoring
mTOR	Mammalian target of rapamycin
NADPH	Nicotinamide adenine dinucleotide phosphate
NASH	Non-alcoholic steatohepatitis
NES	Normalised enrichment score
NF-κB	Nuclear factor kappa-light-chain-enhancer of activated B cells
NO	Nitric oxide
NOD	Non-obese diabetic
NOX	NADPH Oxidase

NRF	Nuclear factor erythroid 2–related factor
PBS	Phosphate buffer saline
PDE3B	Phosphodiesterase 3B
PDK	Protein dependent kinasE
PEPCK	Phosphoenolpyruvate carboxy kinase
PGC1α	Proliferator-activated receptor gamma coactivator-1-alpha
PI3K	Phosphoinositide 3-kinase
PIP_2	Phosphatidylinositol 4,5-biphosphate
PIP_3	Phosphatidylinositol 3,4,5-trisphosphate
PKA	Protein kinase A
PKC	Protein kinase C
PLIN	Perilipin
PNPLA3	Patatin-like phospholipase domain-containing protein 3/adiponutrin
PP	Protein phosphatases
PPAR	Peroxisome proliferator-activated receptor
PPT	Protein precipitation
PTP1B	Protein Tyrosine Phosphatase 1B
PVL-34S	Phenyl-γ-valerolactone-3´,4´-di-sulphate
QUICKI	Quantitative insulin sensitivity check index
RFMs	Ring fission metabolites
RICTOR	Rictor-mTOR
rlog	*Regularised logarithm*
RNA-Seq	RNA-Sequencing
ROS	Reactive oxygen species
SBP	Systolic blood pressure
SCD	Stearoyl-CoA desaturase
SGLT1	Sodium-coupled glucose transporter
SH2	Src homology-2 domains
SHR	Spontaneously hypertensive rats
SIRT	Sirtuin
SOD	Superoxide dismutase
SPE	Solid-phase extraction

SREBP	Sterol regulatory element binding protein
SREMs	Structurally related epicatechin metabolites
STZ	Streptozocin
SULT	Sulfotransferases
$T_{1/2}$	Elimination half-life
t-BOOH	tert-butylhydroperoxide
TBS-T	TBS-Tween
TCA	Tricarboxylic citric acid
TCA	Trichloroacetic acid
TFAM	Mitochondrial transcription factor A
TGF-β	Transforming growth factor β
TLR	Toll-like receptors
T_{max}	Time for maximum concentration
TNF-α	Tumour necrosis factor-α
Trig	Triglycerides
TSC	Tuberous sclerosis complex
UCP	Uncoupling protein
UGT	Uridine-5'-diphosphate glucuronosyl-transferases
UPEC	Uropathogenic *E.coli*
UPLC-MS	Ultra-performance liquid chromatography-mass spectrometry
UTI	Urinary tract infection
VCAM	Vascular cell-adhesion molecule
vst	*Variance stabilising transformation*
WAT	White adipose tissue
ZDF	Zucker diabetic fatty
ZO-1	Zonula occluden
A-SMA	α-Smooth muscle actin

List of publications

Posters

Helleur J, Needs P.W, Vauzour D, Kroon P.A. How (−)-epicatechin and its gut metabolite influences type-2 diabetes. *The 9th International Conference on Polyphenols and Health*. November 2019.

Helleur J, Needs P.W, Vauzour D, Kroon P.A. Cocoa polyphenols & their role in mitigating type-2 diabetes. *NRP DTP Summer Conference*. June 2019.

Helleur J, Needs P.W, Kroon P.A. The role of colonic flora-derived hydroxyphenyl-γ-valerolactone's in the prevention of cardiovascular disease events. *IFR Student Science Showcase.* May 2017.

Oral presentations

Helleur J, Needs P.W, Troncoso-Rey P, Savva G.M, Vauzour D, Kroon P.A Cocoa polyphenols and their effects on hepatic gene transcription to mitigate high-fat diet induced insulin resistance. *Coffee Break Science*. November 2020.

Helleur J, Needs P.W, Troncoso-Rey P, Savva G.M, Vauzour D, Kroon P.A. The role of 3',4'-dihydroxyphenyl-γ-valerolactone, the gut microbiota metabolite of (−)-epicatechin, in reducing insulin resistance. *The 9th International Conference on Polyphenols and Health*. November 2019.

Helleur J, Needs P.W, Troncoso-Rey P, Savva G.M, Vauzour D, Kroon P.A. The role of 3',4'-dihydroxyphenyl-γ-valerolactone, the gut microbiota metabolite of (−)-epicatechin, in reducing insulin resistance. *NuGO Week 2019*. September 2019.

Helleur J. Stepping away from research and entering the entrepreneurial world. *Student QIB Seminar*. July 2019.

Helleur J, Needs P.W, Vauzour D, Kroon P.A. The health implications of a *cocoa* flavanol & its metabolite in the context of type-2 diabetes. *QIB Student Science Showcase*. June 2019.

Helleur J, Needs P.W, Vauzour D, Kroon P.A. The role of 3',4'-dihydroxyphenyl-γ-valerolactone, the gut microbiota metabolite of (−)-epicatechin, in reducing insulin resistance. *ISP Food and Health Meeting*. May 2019.

Helleur J, Needs P.W, Vauzour D, Kroon P.A. The role of gut microbiota metabolism of (−)-epicatechin in mitigating the onset of diet-induced type-2 diabetes. *Coffee Break Science*. January 2019.

Helleur J, Needs P.W, Vauzour D, Kroon P.A. The health benefits of dark chocolate, green tea, and broccoli. *Norwich Science Festival*. October 2018.

Helleur J, Needs P.W, Vauzour D, Kroon P.A. The role of colonic flora-derived hydroxyphenyl-γ-valerolactones in the health benefits of dietary flavanols. *Knowledge Exchange trip at the German Institute of Human Nutrition.* September 2017.

Helleur J, Needs P.W, Vauzour D, Kroon P.A. Hydroxyphenyl-γ-valerolactones and cardiac health. *IFR Student Science Showcase*. May 2017.

Other

Helleur J, Needs P.W, Troncoso-Rey P, Savva G, Vauzour D, Kroon P.A. Are hydroxyphenyl-γ-valerolactones responsible for mitigating the onset of type 2 diabetes? *Meeting with the Director of QIB*. June 2020.

Helleur J, Needs P.W, Troncoso-Rey P, Vauzour D, Kroon P.A. Are hydroxyphenyl-γ-valerolactones responsible for mitigating the onset of type 2 diabetes? *Meeting with the Director of QIB*. November 2019.

Helleur J. Awarded best poster award at *The 9th International Conference on Polyphenols and Health* for the poster titled: How (−)-epicatechin and its gut metabolite influences type-2 diabetes. November 2019.

Helleur J, Needs P.W, Vauzour D, Kroon P.A. The role of colonic flora-derived hydroxyphenyl-γ-valerolactones in the health benefits of dietary flavanols. *Meeting with the Director of QIB*. July 2018.

Acknowledgements

What an amazing last 4-years it has been! I have met some amazing individuals, travelled the world (quite literally), created a worldwide network and had some fantastic opportunities. I could also never have predicted finishing my PhD throughout a worldwide pandemic of Covid-19. But if I could turn back time and do it all again, would I? Yes, I would, and that's mostly because of the people I have met along the journey and the amazing opportunities I have had along the way.

Priscilla Day-Walsh, you are the most amazing person I have ever met. Not only have you helped me throughout my entire PhD, you have always lifted my mood and provided me with such a positive outlook in the world of research. You are so helpful, kind, knowledgeable, and the most hardworking person I have come across. I cannot thank you enough for being beside me throughout my PhD and I truly wish that one day you are granted the role of a research leader, not only do you deserve it, I know you would be amazing at it. So please keep following your dreams.

Perla Rey, you have been an incredible bioinformatics trainer. You have enabled me to process, extract and analyse terabyte sized datasets, that before were completely in-comprehendible to me. I have enjoyed working beside you on this project and you have provided me with new skills that I can now advance and utilise in the professional world of work. You are again an amazing person, and I will never understand how you can juggle working on 20 massive projects at once, but I admire that greatly about you.

Paul Needs, my PhD project would have been honestly impossible without you. You synthesised my phenyl-γ-valerolactones (that are not commercially available) and allowed me to work in such a new and fascinating area. So, thank you so much for giving me this opportunity, but more importantly thank you for being you. I enjoyed the conversations we had on a day-to-day basis and you most certainly humoured me on several occasions. Thank you for always being there and helping me out when the equipment misbehaved, and for steering me in the right direction for what seemed to feel like a never ending UPLC-MS method development process to quantify my compounds. You will be missed.

Karen Chambers, I believe the reason I was able to apply and be offered a PhD was because of your fantastic training and guidance throughout my MSc research project you supervised. I learnt so much from you and because of this I was prepared to enter a world of research and apply the fantastic skills that you had given me. You were honestly the best trainer I could have had, and although you could not be there for most of my PhD, I am very grateful for having worked with you and for you to have shared your knowledge with me.

To my colleagues and friends, Jasmine Percival, Gemma Beasy, Aleena Mushtaq, Sophie Prosolek, Emad Shehata, and Federico Bernuzzi. We have had an interesting time haven't we! We have shared all our PhD stories together and we have always helped each other out whenever we wanted and needed to. Could you ever have imagined that we would all become Dr's! Well, you are all extremely deserving, and I am so glad that I had the opportunity to meet you all and build a long-lasting friendship. And Emad, thank you for travelling the world with me on the EIT Global Food Venture programme, you were hilarious and great company.

I would also like to thank the side projects I have engaged in throughout my PhD, I would like to thank Andy Boyce for providing me with the most fantastic internship with BrisSynBio and entering me into the world of entrepreneurship, you were a great manager and a great trainer. I would also like to thank EIT food and all the trainers, and specifically Chryssa and Carmen who provided me with entrepreneurial skills that I can translate into every job that I now enter and for giving me the opportunity to build a global network and friendship circle. In addition, I would like to thank my iTeams group who have been so hardworking, and I believe we really have been the best team together.

Although this may be uncommon, I would like to thank my lovely 104 mice that I worked with (and on) throughout my PhD, without them my PhD would have been a very different story, and I definitely got attached to them by the end of the studies.

Finally, I would like to thank my supervisory team, but most importantly I would like to thank Paul Kroon. Paul, thank you for selecting me for this PhD and for believing that I could deliver this project. Your expertise and guidance has enabled me to complete this PhD and I really have enjoyed it, despite the never-ending challenges that I seemed to face. Also, thank you for being such an easy supervisor to talk to, you make your students feel comfortable and it's great to have a laugh with your boss!

Chapter One

AN INTRODUCTION TO POLYPHENOLS AND THEIR PROTECTIVE EFFECTS AGAINST INSULIN RESISTANCE

Chapter 1: An introduction to polyphenols and their protective effects against insulin resistance

1.1 Structure of the thesis

The results presented in this thesis covers three main objectives, the first being an exploratory analysis of how (−)-epicatechin and 3',4'-dihydroxyphenyl-γ-valerolactone differ in the bioavailability of their ring fission metabolites, second the effects of metabolites on the mitigation of insulin resistance and hepatic lipid accumulation in high-fat (HF) diet fed mice, and the third the mechanisms through which the metabolites may confer protective effects against HF diet induced insulin resistance using analysis of RNA-Sequencing data for gene and pathway changes in the liver tissue of the mice on dietary interventions. This general introduction will therefore provide information on polyphenols and more specifically flavan-3-ols and their health benefits, their bioavailability and metabolism, their effects on insulin resistance, and then set-out to investigate the current research gaps in this area through the overarching objectives of the research described in this thesis. Each results chapter focusses on different objectives and because the methods used in the experiments in each results chapter are distinct, the material and methods are included within each chapter.

1.2 Classification of dietary polyphenols

Polyphenols are naturally derived plant compounds that have been shown to possess bioactive properties. Rich polyphenol sources include fruits, vegetables, whole grains, nuts, seeds, flowers, tree barks, along with foods and beverages such as tea, chocolate, wine, and coffee (6, 7). The basic monomeric unit of polyphenols is the phenolic ring, but they are mostly characterised by at least two phenyl rings (7, 8). There are four main groups of polyphenols, one of the groups are flavonoids (flavonols, flavones, flavanols which include proanthocyanidins, flavanones, flavanonols, isoflavones, anthocyanidins – anthocyanins) and the other non-flavonoids are phenolic acids (hydroxybenzoic acids, hydroxycinnamic acids), stilbenes and lignans (Figure 1.1) (9). They are classified by the number of phenol rings present and from the nature of the substitutions and condensation of the rings (4, 10).

Flavonoids are the most common polyphenol throughout the plant kingdom, constituting more than half of the 8000 phenolic structures currently recognised (6). They possess two phenolic rings (ring A and ring B) linked by a heterocyclic ring (ring C), as seen in Figure 1.1. The flavonoid

structures are displayed in Figure 1.2 and describes the most common structures within each class (4). For catechins, they are isomers, where (+)-catechin has a cis configuration and (−)-epicatechin has a trans configuration, each having two stereoisomers. They can also exist in polymer forms as proanthocyanidins, for example procyanidin A1 is a dimer of epicatechin and catechin, whereas procyanidin B2 is a dimer of two epicatechin units, and there are oligomers of procyanidins which have three or more degrees of polymerisation (11). Anthocyanidins supply the dark blue/red/purple pigments of plants, fruits, vegetables and grains such as black rice (6).

For relevance and food ubiquity, the rest of this review will be focussing on flavonoids rather than polyphenols in general, and their metabolism and effects on health.

1.3 Flavonoid food sources

Manach *et al* (2004) reviewed the food sources of most flavonoid groups and their respective concentrations by weight (4) (Table 1.1). Most flavonoids are typically found as parent compounds in foods with most of them glycosylated. Typically, the flavonol quercetin is the most common polyphenol in diets (12), whilst flavanones are present at high concentrations only in citrus fruits (4). Flavones are present at much lower concentrations than flavonols, but they are not very common in foods, with the exception of parsley that contains high apigenin. Isoflavones are almost exclusively found in legumes and found as aglycone or malonylglucoside derivatives and are glycosylated during industrial food processing, unless they are fermented which can cause deglycosylation. Flavanols are found in a diverse range of food and drink products, but are richest in cocoa, green tea, and apples (4).

Table 1.1: The classes of flavonoids found in foods
This information has been extracted from Manach et al (2004) (4) and the food sources are not exhaustive.

Flavonoid class	Class types	Food sources
Anthocyanins	Cyanidin	Aubergine
	Pelargonidin	Blackberry
	Peonidin	Black currant
	Delphinidin	Blueberry
	Malvidin	Black grape
		Cherry
		Rhubarb
		Strawberry
		Red wine
		Plum
Flavonols	Quercetin	Yellow onion
	Kaempferol	Curly kale
	Myricetin	Leek
		Cherry tomato
		Broccoli
		Blueberry
		Blackcurrant
		Apricot
		Apple
		Beans
		Black grape
		Tomato
		Black tea infusion
		Green tea infusion
		Red wine

Table 1.1: The classes of flavonoids found in foods (continued)

Flavonoid class	Class types	Food sources
Flavones	Apigenin	Parsley
	Luteolin	Celery
		Capsicum pepper
Flavanones	Hesperetin	Orange juice
	Naringenin	Grapefruit juice
	Eriodictyol	Lemon juice
Isoflavones	Daidzein	Soy flour
	Genistein	Boiled soybeans
	Glycitein	Miso
		Tofu
		Tempeh
		Soy milk
Flavan-3-ols	Catechin	Chocolate
	Epicatechin	Beans
		Apricot
		Cherry
		Grape
		Peach
		Blackberry
		Apple
		Green tea
		Black tea
		Red wine
		Cider

Hydroxybenzoic acids

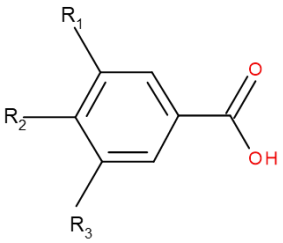

$R_1 = R_2 = OH$, $R_3 = H$: Protocatechuic acid
$R_1 = R_2 = R_3 = OH$: Gallic acid

Hydroxycinnamic acids

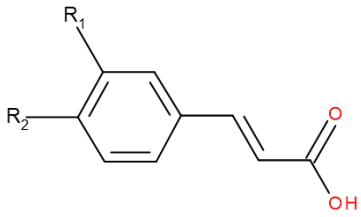

$R_1 = OH$: Coumaric acid
$R_1 = R_2 = OH$: Caffeic acid
$R_1 = OCH_3$, $R_2 = OH$: Ferulic acid

Chlorogenic acid

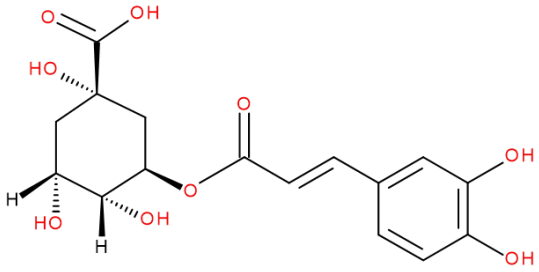

Stilbenes

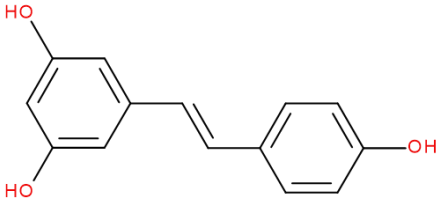

Resveratrol

Lignans

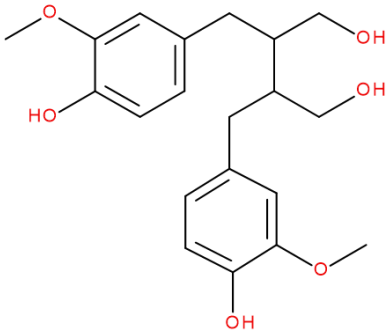

Secoisolariciresinol

Flavonoids

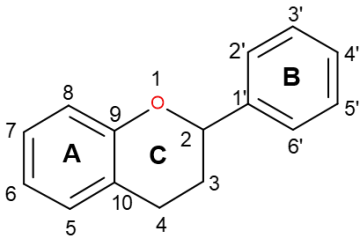

See Figure 1.2

Figure 1.1: Classifications of polyphenols and their structures

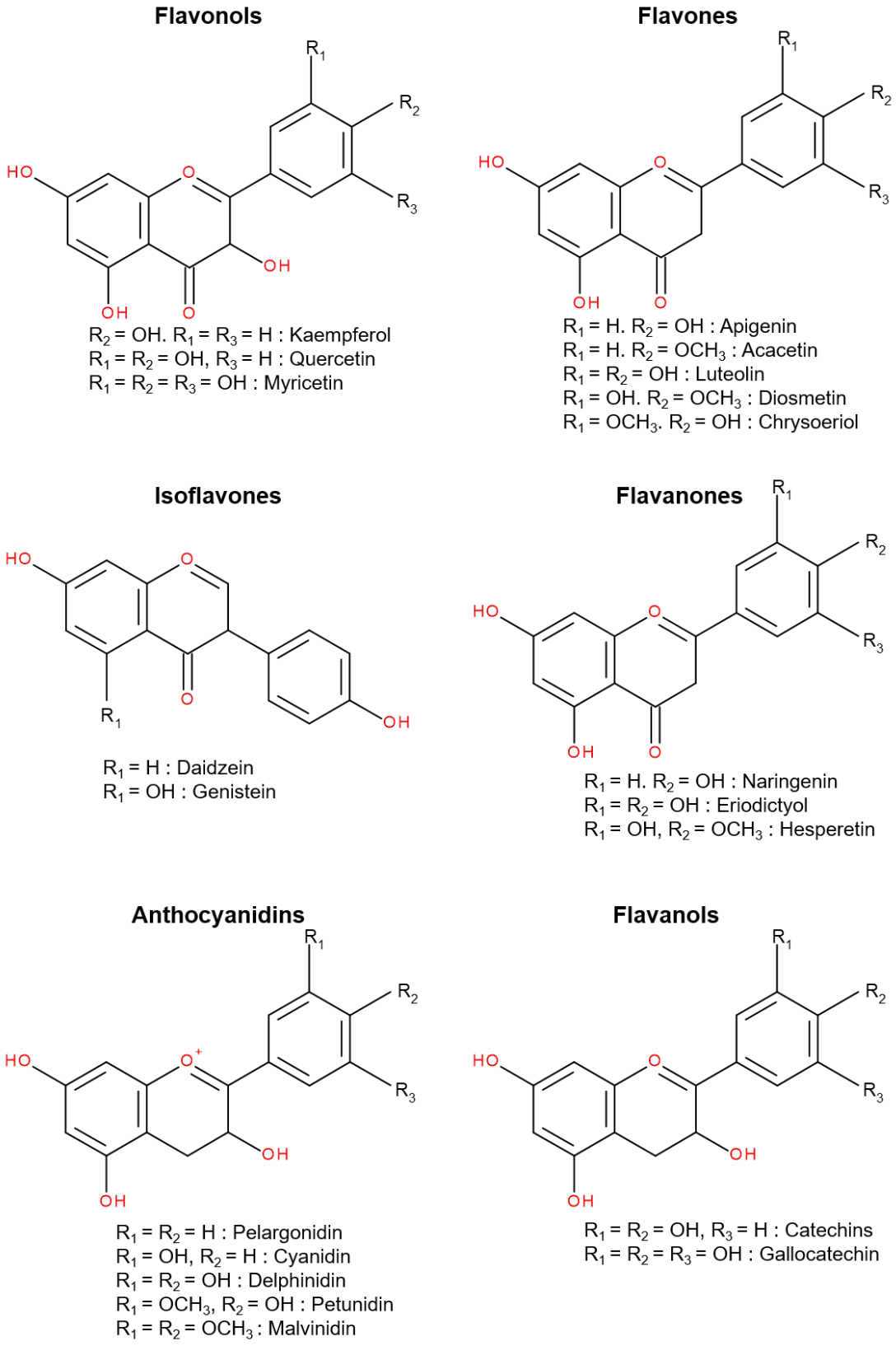

Figure 1.2: Structures of the classes of flavonoids

The most common flavonols are kaempferol, quercetin, and myricetin; flavones - apigenin and luteolin; isoflavones - daidzein and genistein; flavanones - naringenin, eriodyctiol and hesperidin; anthocyanidins - pelargonidin, cyanidin, delphinidin, petunidin and malvidin; and flavanols or flavan-3-ols - catechins ((+)-catechin and (−)-epicatechin) and gallocatechin (4).

1.3.1 Dietary flavan-3-ols – cocoa and green tea

Daily dietary flavanol intakes vary greatly on the types of foods and drinks consumed, but on average it is estimated to be around 60 mg/day from a total polyphenol consumption between 1-2 g/day (9, 13). Databases such as Phenol-Explorer (14-16) eBASIS (17) and USDA (18) exist to report the average polyphenol concentrations found in foods. But the levels still vary greatly depending on how old the foods are (there are reduced polyphenol concentrations in fruit the longer it is ripened), as well as how the foods are processed, cooked and stored (4).

Pure cocoa has the highest flavan-3-ol content on a per weight basis over other foods (19-21). The phenolic levels of cocoa products are as follows: 72-87 % in cocoa powder, 45-49 % in baking chocolate, 20-30 % in dark chocolate, 15-19 % in milk chocolate and 5-7 % in white chocolate (22), where phenolic compounds compose 12-18 % of the total weight of dried cocoa nibs (19). It has been estimated that 11 g of 70 % cocoa content in chocolate can contain 100 mg flavan-3-ols, whereas 52 mg of milk chocolate or 50-100 mL of cocoa drink containing 8 % (w/v) pure cocoa is required to achieve the same amount (23). Polyphenols constitute around 5-6 % of the content of fresh cocoa beans mostly as flavonoids, which can be further subdivided as 58 % proanthocyanidins, 37 % monomeric flavan-3-ols, and 4 % anthocyanins (24, 25). Of the flavan-3-ols (−)-epicatechin is the most abundant (~37 %) with much smaller quantities of (+)-catechin, (+)-gallocatechin and (−)-epigallocatechin (25, 26).

Meanwhile, tea, derived from the *Camellia sinensis* plant contain higher concentrations of flavan-3-ols compared to other polyphenol groups. Catechins derive around 3-8 % of the total flavonoid content in black tea, and 30-42 % in green tea for a typical 235 mL serving and 2 minute brew time (27, 28). The four major catechins present in tea include (−)-epigallocatechin gallate, (−)-epigallocatechin, (−)-epicatechin gallate, and (−)-epicatechin (29, 30), providing 142 mg, 65 mg, 28 mg and 17 mg of the compounds respectively (30). The differences between green and black tea arise from their processing, where green tea is processed in a way that doesn't lead to the enzymatic oxidation of catechins, whereas black tea is derived from the fermentation of green tea leaves which promote the oxidation of catechins which gives the brown colour and contributes to the complex flavour of black tea (29).

Because of the high flavan-3-ol content of cocoa and green tea, these food products have been highly researched in the context of their possible health benefits. This will be reviewed later in this chapter.

1.4 Absorption, metabolism and bioavailability of flavonoids

Dietary flavonoids have been reported to be associated with several health benefits, including the prevention of cardiovascular diseases, cancers, osteoporosis, neurodegenerative disease and diabetes mellitus (31, 32). More specifically, flavonoids are known to trap and scavenge reactive oxygen species (ROS), upregulate nitric oxide (NO) production, inhibit cell mitosis, promote apoptosis, and decrease inflammatory leukocyte attachment to cell membranes (33). However, due to the rapid absorption, metabolism and conjugation and limited bioavailability of polyphenols, it becomes hard to identify the active compounds that drive these positive health effects. As such, this section will discuss these points from the onset of consumption through to absorption, metabolism and the excretion of compounds from flavonoid diets.

1.4.1 Absorption

Approximately 5-10 % of total ingested polyphenols are absorbed from the stomach and small intestine (34). As a brief overview of compound absorption and metabolism, polyphenol structures in their native glycosylated form are unable to be absorbed, hence the requirement for hydrolysis by intestinal enzymes or colonic microflora (4). Other than catechins and procyanidins, most polyphenols are glycosylated in foods, which for anthocyanins enhances their absorptive capacity (35), as an example, quercetin glucosides are absorbed at a two to three times higher rate than their aglycone forms (36) because of the instability of the aglycone and the different mechanisms of absorption and metabolism of anthocyanins (37, 38). For most other glycosylated polyphenols, the removal of the glycoside is required before passive diffusion, and it has been demonstrated that the β-glucosidase in the human small intestine can do this for *O*-glycosides and *O*-galactosides (39). The intestinal border contains the enzyme lactase phloridzin hydrolase (LPH), a luminal β-glucosidase that can perform this action (40). If they are able to enter the enterocyte, cytosolic β-glucosidase (CBG) may act on polyphenol glucosides (39, 41). Aglycones and acylated compounds are absorbed by enterocytes in the small intestine through passive diffusion without hydrolytic or deconjugating mechanisms (42). Since flavanols are almost always present in foods as aglycones, they do not require deconjugation/hydrolysis prior to intestinal absorption (12).

However, anthocyanins that enter the small intestine can be transported into the enterocyte by a sodium-coupled glucose transporter (SGLT1) and then deglycosylated via β-glycosidases in the enterocyte, they can also enter following prior deglycosylation via LPH (43).

1.4.2 Metabolism

Following enterocyte absorption, phase II metabolic events for methylation, sulfation and glucuronidation occurs by catechol-*O*-methyltransferases (COMT), sulfotransferases (SULT), and uridine-5'-diphosphate glucuronosyl-transferases (UGT), respectively (12). These metabolites can then enter the circulatory system and pass to the liver via the hepatic portal vein; the liver can facilitate further phase-II metabolism of the compounds to give glucuronidated, methylated and sulfated derivatives (44). These can re-enter the bloodstream via hepatic veins and are later excreted in urine. Alternatively, compounds can undergo enterohepatic circulation, where they are excreted into bile and back into the small intestine and later may be re-absorbed (42). Methylation of polyphenols by COMT occurs in a wide range of tissues, whereas the liver is the main tissue for the site of glucuronidation, but it can be affected by environmental and genetic factors, consequently creating interindividual differences (12). Polyphenol sulfation by SULTs mainly occurs in the liver or colon and they are not largely affected by environmental factors (12).

The colon will receive polyphenols that have either not been absorbed by the stomach or small intestine or have undergone enterohepatic circulation. Here they become deglycosylated and catabolised into more simple compounds, commonly to phenylacetic, phenylvaleric, benzoic, and phenylpropionic acids and phenyl-γ-valerolactones (12). Gut microbes also have the capacity to cleave *O*-glucuronides and catalyse carbon-carbon cleavage of heterocyclic and aromatic rings in flavonoids, in addition to dehydroxylation and decarboxylation (45). However, the composition of the gut microbiota does vary due to disease, diet and environmental and genetic factors, which can influence the metabolism of polyphenols (46, 47).

Almost all polyphenols found in the plasma will have undergone conjugation to glucuronides or sulfates (35). The main exception to this is through the provision of pharmacological doses, which seems to saturate the conjugation process (8).

1.4.2.1 Flavanol metabolism

Flavanols are rapidly metabolised into phase I and phase II conjugates for glucuronidation, sulfation and methylation by the small intestine and liver in less than 1-hour (13). Whilst aglycones and conjugated flavanols that pass into the colon are further catabolised and re-absorbed into the blood or excreted by 6 hours and more. There are very few species of microbiota that have been currently recognised to metabolise polyphenols out of the 500-1000 different species present, e.g. *Escherichia coli, Bifidobacterium sp., Lactobacillus sp., Bacteroides sp., Eubacterium sp*., *Eggerthella sp.* (34).

Procyanidins are not well absorbed per se and are generally degraded into monomers and dimers prior to absorption (13), although the epicatechin dimer (procyanidin B2) has shown to be absorbed intact in small quantities. Almost all procyanidins are metabolised by the gut microbiota (48) and mostly form the metabolites 2-(3,4-dihydroxyphenyl)acetic acid and 5-(3,4-dihydroxyphenyl)-γ-valerolactone (49). Anthocyanins are poorly absorbed in the small intestine and are extensively catabolised by the gut microbiota (50). They undergo hydrolytic conversion to their aglycone anthocyanidins through the removal of their glycoside, but both the glycosides and aglycone variants are found in the urine of mammals (51, 52). Anthocyanidins can be further metabolised to more than 30 different metabolites and include degradants protocatechuic acid and phloroglucinaldehyde, and further metabolites (53) which can be initiated by the neutral or basic pH conditions of the small intestine and further transformed by the gut microbiota (50). For quercetin, it can be metabolised into protocatechuic acid and 2-(3,4-dihydroxy)-phenylacetic acid (54) and further into *O*-methyl metabolites in the colon (55).

Gut microbial metabolism of catechins involves an A-ring cleavage to form compounds such as 3-hydroxyphenylpropionic acid, 3,4-dihydroxyphenylacetic acid and 3-hydroxyphenyl-γ-valerolactone (49). The latter can be further metabolised into 3,4-dihydroxyphenyl-γ-valerolactone. A proposed mechanism for this is for a hydride attack on the methide carbon to yield a 3,4-dihydroxyphenyl metabolite and eventually give rise to 3,4-dihydroxyphenyl-γ-valerolactone (45). Alternatively, catechins can undergo C-ring opening by *Eggerthella lenta* rK3 to form 1-(3,4-dihydroxyphenyl)-3-(2,4,6-trihydroxyphenyl)propan-2-ols, which is then dehydroxylated to 1-(3-hydroxyphenyl)-3-(2,4,6-trihydroxyphenyl)propan-2-ols (56, 57). Both these compounds then undergo ring fission of the phloroglucinol ring to form 5-phenyl-γ-valerolactones (5-(3,4-dihydroxyphenyl)-γ-valerolactone), and 4-hydroxy-5-phenylvaleric acids (4-hydroxy-5-(3,4-dihydroxyphenyl)-valeric acid) (56), a biotransformation that has been shown to be performed by *Flavonifractor plautii* aK2 (57). The 4-hydroxy-5-phenylvaleric acids are then dehydroxylated to 4-oxo-5-phenylvaleric acid and further to 5-phenylvaleric acids (56). These can later be degraded to 3-phenylpropionic acids most likely through a β-oxidation process (58). Please see Figure 1.3 for the detailed metabolism of catechins described in a schematic.

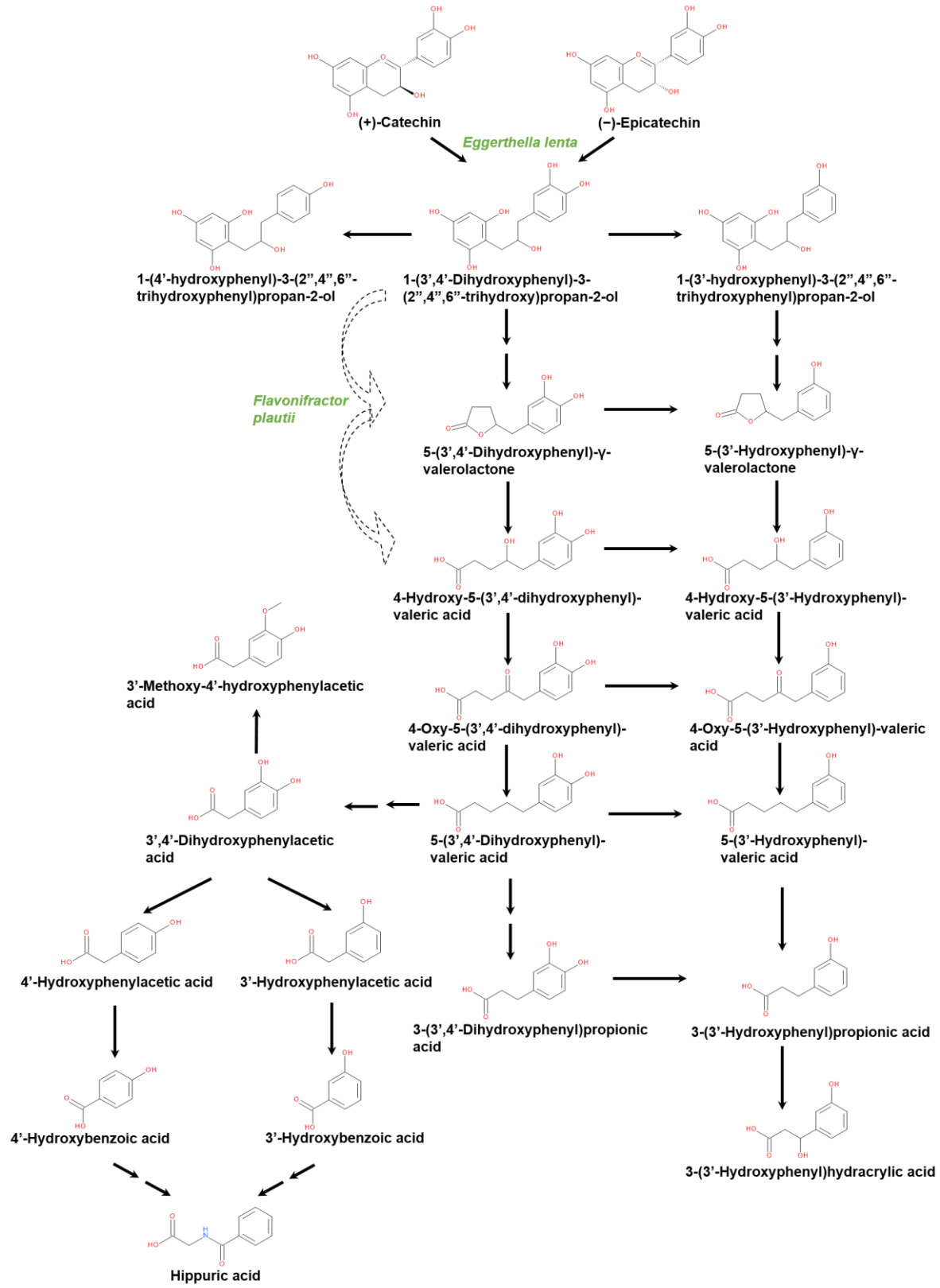

Figure 1.3: Proposed pathways involved in the colonic metabolism and urinary excretion of catechins
Unmetabolised catechins that pass from the upper gastrointestinal tract into the large intestine are subjected to colonic degradation. Kutschera et al (57) identified the role of the microbiota Eggerthella lenta to open the C-ring of catechins to form a metabolite that undergoes further metabolism by Flavonifractor plautii to cause

Figure 1.3 (continued): *ring fission of the phloroglucinol ring. Following the identification of metabolites in urine and faeces (1, 5) alongside faecal slurry incubations with the catechins (56, 59), the proposed colonic degradation pathways are illustrated. Double arrows indicate where unknown intermediate metabolites are formed but are not detected. Please note, not all the compounds displayed are detected following consumption. Please refer to Figures 1.6 and 1.7 for the metabolites detected in urine, faeces and plasma following (−)-epicatechin consumption in humans and rats.*

1.4.3 The general features of flavonoid bioavailability

Bioavailability is defined as the fraction of compound intake that reaches the circulation (13), and in this thesis the term refers to both the intact flavonoid and the fraction that is absorbed post gut microbiota transformation. The differences in flavonoid structures causes different metabolites to be produced and subsequently causes them to appear at different concentrations and times within the circulation and excretory products. Therefore, a summary of flavonoid bioavailability shall be provided, mostly using information reported in a review by Manach *et al* (2005) (9) and more recently by Williamson *et al* (2018) (60).

Flavanone aglycones are generally reported to be absorbed and metabolised quickly and typically peak in the circulation within 30 mins (61), however, flavanone and flavonol glycosides take approximately 5-hours for the hydrolysis of the sugar rhamnoglycoside which can only occur via catalysis from the gut microbiota (9), and consequently appear at maximum concentrations in the plasma between 4-9 hours, dependent on the flavonoid (62-64). Because of the delayed absorption of flavanone glycosides, they can circulate for up to 36-hours, with urinary excretion being almost complete by 24-hours (62), but only 1-30 % of the ingested intake is found to be recovered in urine (65-68).

For anthocyanins, there have been 35 metabolites reportedly recovered in the serum, urine and faecal samples of participants following consumption of an isotopically labelled anthocyanin, including anthocyanin degradation products, phase-I/II/III metabolites and very low concentrations of parent compounds (69). Plasma concentrations for parent compounds peaked around 1.8-hours whilst colonic metabolites peaked between 6-30 hours, and urinary excretion of anthocyanins and their metabolites appeared between 1-48 hours, and faecal samples were detected from 6-48 hours, with an overall low recovery of 12 % of the ingested compound (53).

The pharmacokinetic profile of isoflavones has been predominantly explored from the consumption of soy products, with plasma T_{max} of ~6-7 hours and urinary and faecal concentrations detected from 6-72 hours, with peak concentrations detected between 6-12 hours and 24-48 hours, respectively (70). Recovery ranges have been detected to be 1-2 % and 21 % of the ingested dose

in faeces, and in urine for 9, 21, 22 and 62 % (71, 72). The profile of isoflavone metabolites detected were mostly *O*-glucuronides and *O*-sulfates and very low levels of aglycones and glycosides (9).

For flavones, they have been reportedly detected up to 12-days in the plasma of rats due to their long-half-lives but peaked at ~24-hours (73). High recoveries have been detected from the ingested dose, 51 % in urine, 12 % in faeces and 1.2 % in plasma and mostly consisted of *O*-glucuronides and *O*-sulfates. In contrast, glycosylated flavones are very rarely absorbed but are quickly excreted (74).

The extensive metabolism and bioavailability of flavanol's epigallocatechin-3-gallate (EGCG) and (−)-epicatechin (EC) are discussed in detail in sections 1.4.3.1 and 1.4.3.2 respectively.

1.4.3.1 EGCG metabolism and bioavailability

The high absorptive capacity of flavan-3-ols and their metabolites have made them interesting for investigating their potential health benefits (1, 5). Epigallocatechin-3-gallate (EGCG) has been widely researched, mostly because of its high concentrations found in tea products, so it is important to understand its bioavailability in humans. However, its research has mostly been explored from the consumption of green tea extracts, with a few studies providing EGCG directly to mammals.

Oral administration of EGCG has shown to provide poor absorption, poor bioavailability, and low accumulation in the body due to their poor stability in the gastrointestinal tract. Studies have shown that under simulated gastrointestinal conditions, 49 % of free EGCG was retained after digestion at simulated gastric pH, while 20 % of free EGCG was retained after digestion at simulated intestinal pH (75). In a rat study, 42 % of the provided oral dose of radiolabelled EGCG was present in the stomach within 15-30 mins and had mostly disappeared by 8 hours, but by 4-hours most of it had moved into the small intestine and by 8-hours into the cecum and large intestine (~42-45 %) (76). Although the stability and absorption of free EGCG is shown to be low, it undergoes extensive metabolism in the colon and their absorption and excretion accounts for most of the circulatory compounds detected (76-78).

A few studies have reported a low (< 1 %) absorption of free EGCG into the blood via the small intestine (79-82), but its metabolites peaked within 1-2 hours post-consumption and are almost undetected by 24-hours (80, 82-85) and mostly consist of *O*-glucuronides which account for ~90 % of the EGCG detected in the urine of mice (80). However, in humans, glucuronidated and sulfated derivatives of EGCG were found in the plasma at very low concentrations (82), whilst only *O*-methyl metabolites were detected in mouse faeces (80).

To assess the metabolic distribution of EGCG and its metabolites, Kohri *et al* (2001) radiolabel tagged EGCG and provided it to rats via intragastric administration (76). Plasma and blood radioactivity had a small peak at 2-hours and a penultimate peak at 24-hours post dosage. Liver radioactivity followed the same trend (0.2 % and 0.5 % of the dose respectively), whilst tissues for the brain, eye, thymus, lung, heart spleen, kidney, and testis showed peaks at 24-hours. After the 72-hour assessment period, 32.1 % of the dose appeared in the urine and 35.2 % in the faeces, where most of the radioactivity was excreted between 8-24 hours. The main compounds detected in urine and faeces were for epigallocatechin (EGC), EGCG, 5-(3',5'-dihydroxyphenyl)-γ-valerolactone and 5-(5'-hydroxyphenyl)-γ-valerolactone 3'-*O*-*β*-glucuronide. For 5-(3',5'-dihydroxyphenyl)-γ-valerolactone, this was absorbed through the colon after metabolic degradation of EGCG and later metabolised by the liver and/or the microbiota to produce the glucuronide derivative. The detection of free EGCG in the urine is conflicted by other studies, where only EGCG metabolites were detected, and therefore this requires more investigation (86). Further EGCG phase-II metabolites are found to mostly arise in the bile after liver metabolism of EGCG to produce 3'-*O*-methyl-EGCG, 4'-*O*-methyl-EGCG, 3''-*O*-methyl-EGCG, 4''-*O*-methyl-EGCG, and 4',4''-di-*O*-methyl-EGCG, and their conjugates, although conjugates were unidentified due to β-glucuronidase/sulfatase treatment prior to analysis (87). Because of this, most phase-II metabolites of EGCG do not reach the circulation but are instead excreted via the bile.

In an earlier radiolabelled EGCG study performed in mice, they discovered that ~6.5 % and ~35 % of radioactivity was excreted in the urine and faeces respectively, where the largest concentrations were detected at 24-hours post-consumption (78). Radioactivity was detected in the systemic circulation within 1-hour, rising steadily till 6-hours and peaked at 24-hours, accounting for ~2 % of the total radioactive dose to be absorbed into blood.

Takagaki *et al* (2010) investigated the metabolism of EGCG *in-vitro* with rat enterobacteria and *in-vivo* in male Wistar rats to devise the image reconstructed in Figure 1.4 for EGCGs metabolism (77). They identified bacteria involved in hydrolysing EGCG and in its subsequent degradation steps. Initially, EGCG is hydrolysed to EGC and gallic acid, EGC then forms the basis for further metabolism. Following this is the opening of the C-ring through a retro-Michael reaction which reductively cleaves carbons 1 and 2 to liberate the hydroxyl group on the meta position to form the phloroglucinol ring in product 1-(3,4,5-trihydroxyphenyl)-3-(2,4,6-trihydroxyphenyl)propan-2-ol, which peaks at 24-hours post EGC formation. Later is the formation of 1-(3,5-dihydroxyphenyl)-3-(2,4,6-trihydroxyphenyl)propan-2-ol, which peaks at 48-hours post EGC formation, and is subjected to decomposition of the phloroglucinol ring to form 5-(3,5-dihydroxyphenyl)-4-hydroxyvaleric acid, the most dominant metabolite found in the cecum and faeces of the rats, peaking at 96-hours post

EGC formation. This pathway is shown to be route 1 in Figure 1.4, and accounts for more than 90 % of the microbial metabolites; encompassing this are two further less favoured degradation routes, routes 2 and 3 in Figure 1.4. As such, further metabolites for 5-(3,5-dihydroxyphenyl)-γ-valerolactone, 5-(3,5-dihydroxyphenyl)valeric acid, and 5-(3-hydroxyphenyl)valeric acid are formed.

To summarise, EGCG absorption and bioavailability is low, particularly when compared to (−)-epicatechin (EC) and EGC flavanols. However, when assessing the metabolic profile of EGCG and their absorption and distribution profile, these contribute more greatly to the circulatory and tissue distribution. Thus, it is reasonable to suggest that EGCG colonic metabolites could contribute more greatly to the overall health benefits that have been seen to be induced following EGCG interventions. The provision of pharmacological doses could also provide a greater protection against disease.

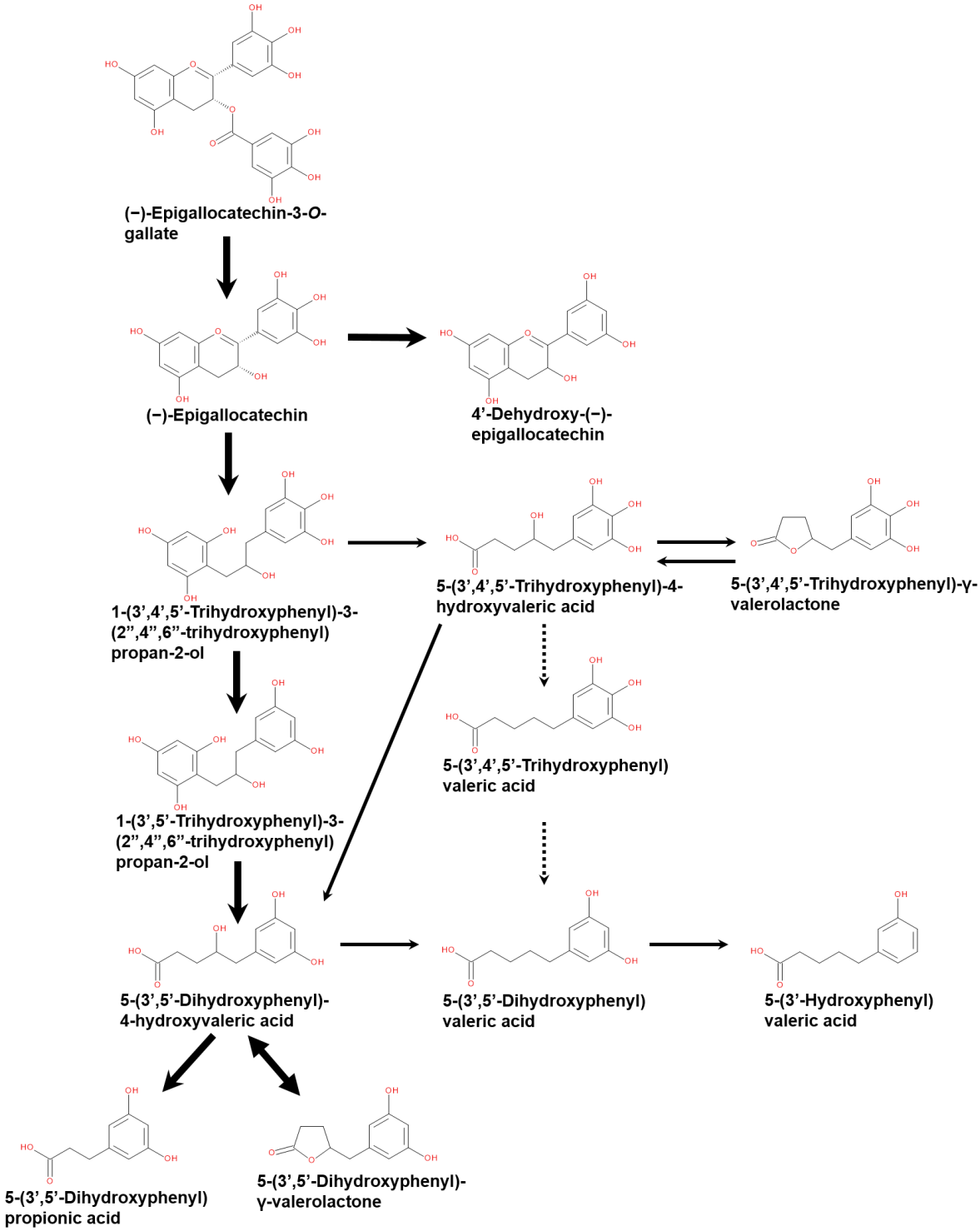

Figure 1.4: Proposed pathways involved in the colonic metabolism and urinary excretion of (−)-epigallocatechin gallate (EGCG)

This image has been reconstructed from Tagakai et al (2010) (3) and illustrates the colonic degradation of EGCG. Thick arrows demonstrate the main pathway of colonic degradation (route I). Thin solid arrows demonstrate a second route for colonic degradation (route II), and the thin dashed arrows represent the third route for colonic degradation (route III).

1.4.3.2 (−)-Epicatechin metabolism and bioavailability

As with EGCG, EC has been widely researched for its protection against disease. Because of this, it is necessary to understand the bioavailability and metabolism of EC in-order to comprehend what metabolites of EC are responsible for the protective effects. For instance, if a metabolite circulates for a longer period of time in the system than other metabolites, then it may have a greater capacity to exert biological effects due to its long exposure to cells and their receptors.

Bioavailability studies have been conducted to explore the metabolism of EC, and have been primarily investigated from the consumption of cocoa derived products (88). Once consumed, EC undergoes quick sulfation, methylation and glucuronidation (89-92), with rapid absorption by the upper GI tract into the circulatory system, resulting in detectable levels of these compounds within 1-4 hours (1, 93-95). These rapidly absorbed compounds are known as structurally related EC metabolites (SREMs), and are also quickly excreted with elimination half-lives of around 2-hours (1, 96). Later absorbed compounds are known as ring fission metabolites (RFMs), and are produced via catabolism by the gut microbiota (1). Approximately 70 % of SREMs formed in enterocytes efflux back into the intestinal lumen, along with unabsorbed EC, where they pass to the colon and are converted to RFMs (96). The main groups of RFMs from EC are hydroxyphenyl-γ-valerolactones (HPVL) and hydroxyphenyl-valeric acids (HPVA) (1, 5, 95), both of these compound types have much longer elimination half-life's of around 6-hours in humans, compared to SREMs (1, 96) following the ingestion of EC or cocoa.

Two major studies have investigated the metabolism of radioactively labelled (−)-epicatechin, one in humans (1) and one in rats (5). Ottaviani *et al* (2016), (1) explored in detail ECs absorption, distribution, metabolism and excretion by having participants to consume 60 mg of radiolabelled [2-^{14}C](−)-epicatechin in a drink. They monitored the radioactivity levels in blood, urine and faecal matter and profiled the compounds on HPLC-MS (high performance liquid chromatography - mass spectrometry). Circulatory radiolabelled products appeared as soon as 15-minutes after ingestion for SREMs, with peaks at 1 and 6-hours for both plasma and whole blood. The sum of SREMs in the circulation was twice the concentration of the sum of RFMs, but the amounts were 3.5-fold less than the sum of RFMs in urine. Subsequently SREMs declined rapidly, with full clearance from the circulatory system after 8-hours. The complete clearance of whole blood radioactivity took 36-hours and in plasma after 72-hours. Within 24-hours, 82 % of radioactivity was excreted in urine and 12 % in faeces. Almost half, ~42 % of total radioactivity was attributed to HPVLs, data for metabolites are depicted in Figure 1.7. Ottaviani also concluded that "70 % of the ingested ^{14}C-EC was absorbed into the circulatory system via the colon compared to the 20 % absorbed from the small intestine". This reinforces how important the colonic microflora is in the metabolism of EC

and the production of bioavailable flavanol derivatives. Figure 1.5 depicts the metabolism of EC over time in humans.

Borges *et al* (2016) (5) took a similar approach to Ottaviani, but investigated the metabolism of ^{14}C-epicatechin in rats, instead of humans, thus allowing for a detailed account of the species dependent differences (Figure 1.6). Due to the different measurement recordings of the radiolabelled samples, it is not feasible to compare the concentrations of the metabolites between studies, but it is possible to identify the metabolites produced at timed intervals. Table 1.2 summarises some of Borges *et al* (5) data.

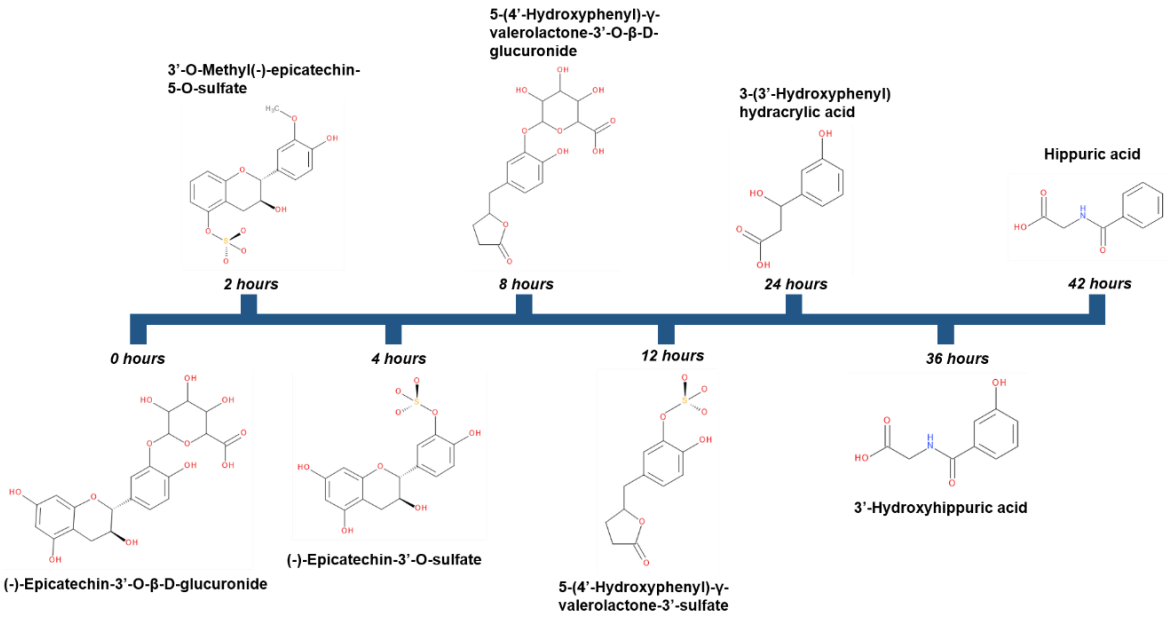

Figure 1.5: Metabolism of (-)-epicatechin in humans over 42-hours
Time represents the number of hours following the consumption of (-)-epicatechin. This figure has been re-drawn from Ottaviani et al (2016) (1).

As an overview of the results, no sulfated SREMs were detected in the plasma of rats (5), which was also confirmed briefly by Ottaviani *et al* (1). Furthermore, the SREMs in rats were also detected up to 9-hours post intervention (5), whereas no SREMs were detected past 4-hours in humans (1). An additional contrast between the studies included the detection of only two RFMs in the plasma of rats, compared to the detection of six in humans. Urinary excretion products were also different between the two species; but both studies confirmed the lack of detection of any EC SREMs after 24-hours, whilst RFMs appeared in human's urine within 4-hours, and in rat's urine after 6-hours.

Another disparity between both studies, was the presence of un-metabolised ^{14}C-epicatechin in the plasma and urine of rats, which was not reciprocated in humans.

Borges *et al* (5) continued to compare their data to that of Ottaviani *et al* (1) with some of the main differences relating to the types of metabolites found (5). The main variations in the two datasets were for the profiles of the methylated, sulfated and glucuronidated phase-II metabolites, where methylated metabolites were only detected in humans after sulfation and glucuronidation of ^{14}C-epicatechin.

Table 1.2: Radioactivity of ^{14}C-Epicatechin in rats
The information in this table has been extracted from Borges et al (2016) (5). They monitored the radioactivity of EC, following EC consumption at 1.3 µM in rats, throughout organs and excretory products over 72-hours.

Time	Location	Percentage of Radioactivity
1-hour	Stomach	52 %
	Duodenum	2 %
	Jejunum/Ileum	45 %
	Circulatory system	0.7 %
6-hours	Jejunum/Ileum	72 %
12-hours	Urine	52 %
6-72 hours	Urine	78 % of total intake
9-hours	Colon	13 %
9-hours	GIT	34 % remaining
0-72 hours	Faeces	19 %

Ottaviani *et al* (1) also performed radiolabelled EC tracing in C57BL/6 mice, but only reported the major differences for the circulatory metabolites found to those of humans and rats (1). They revealed that the metabolic profile from EC is larger in mice than in rats, with plasma detection of (−)-epicatechin-3'-sulfate, (−)-epicatechin-5-*O*-β-D-glucuronide, 3'-*O*-methyl(−)-epicatechin-5-*O*-β-D-glucuronide, (−)-epicatechin-7-*O*-β-D-glucuronide and 3'-*O*-methyl(−)-epicatechin-7-*O*-β-D-

glucuronide, in mice, versus the detection of 3'-*O*-methyl(−)-epicatechin-5-*O*-β-D-glucuronide and (−)-epicatechin-5-*O*-β-D-glucuronide in rat plasma.

1.4.3.2.1 Colonic metabolites of EC and a focus on hydroxyphenyl-γ-valerolactones (HPVL)

Section 1.4.2.1 discussed the microbial metabolism of flavan-3-ols that is specific to EC. In addition to the microbe specific roles involved in its metabolism, Chen *et al* (2020), investigated the time course for microbial conversion of EC and EC conjugates, via *in-vitro* fermentation of rat faecal samples (97). From this, they discovered that by 4-hours around 50 % of EC was converted to metabolites by C-ring opening, and by 8-hours, 95 % conversion had taken place. This was followed by A-ring opening of metabolites to result in complete conversion by 12-hours. The results were very much dependent on the mass of faecal matter used and the concentration of EC supplied. Throughout the experiment, HPVL production occurred immediately in the faecal slurry, with a sharp increase in their production after 4-hours and peaking at 12-hours. Accompanied, was a later peak at 18-hours for hydroxyphenyl-valeric acids (HPVA), that accounted for 90 % of all the metabolites. By the end of their study, at 24-hours, both groups of compounds still appeared at high concentrations (97).

In Ottaviani *et al's* (1) human study, RFMs appeared at peak concentrations in the circulatory system after 6-hours and expressed longer elimination half-lives than SREMs. HPVL was maximally detected in the serum of individuals after 8-hours of EC (1 mg/kg body weight) ingestion and up to 48-hours later in some participants (1). There was a total of 6 RFMs detected in human plasma, 11 RFMs in urine, and 3 RFMs but no SREMs in faeces (Figure 1.7). Up to 18.6 % of ingested EC was excreted in urine as HPVLs and conjugates. Unfortunately, measurements were only taken up to 48-hours for urine and plasma and for no longer than 24-hours for faeces, but it is known that levels can be detected up to 72-hours following ingestion (1, 5).

In rats, HPVLs appeared in the contents of cecum and colon after 6-hours following EC ingestion but peaked after 12-hours, the same also applied to its detection in urine (5). A total of 8 RFMs were detected in colon contents, 5 RFMs in faecal material and 11 RFMs in urine (Figure 1.6). There were no HPVLs detected in plasma between 0-9 hours (5), because they do not get absorbed into the circulation until 9-24 hours (1).

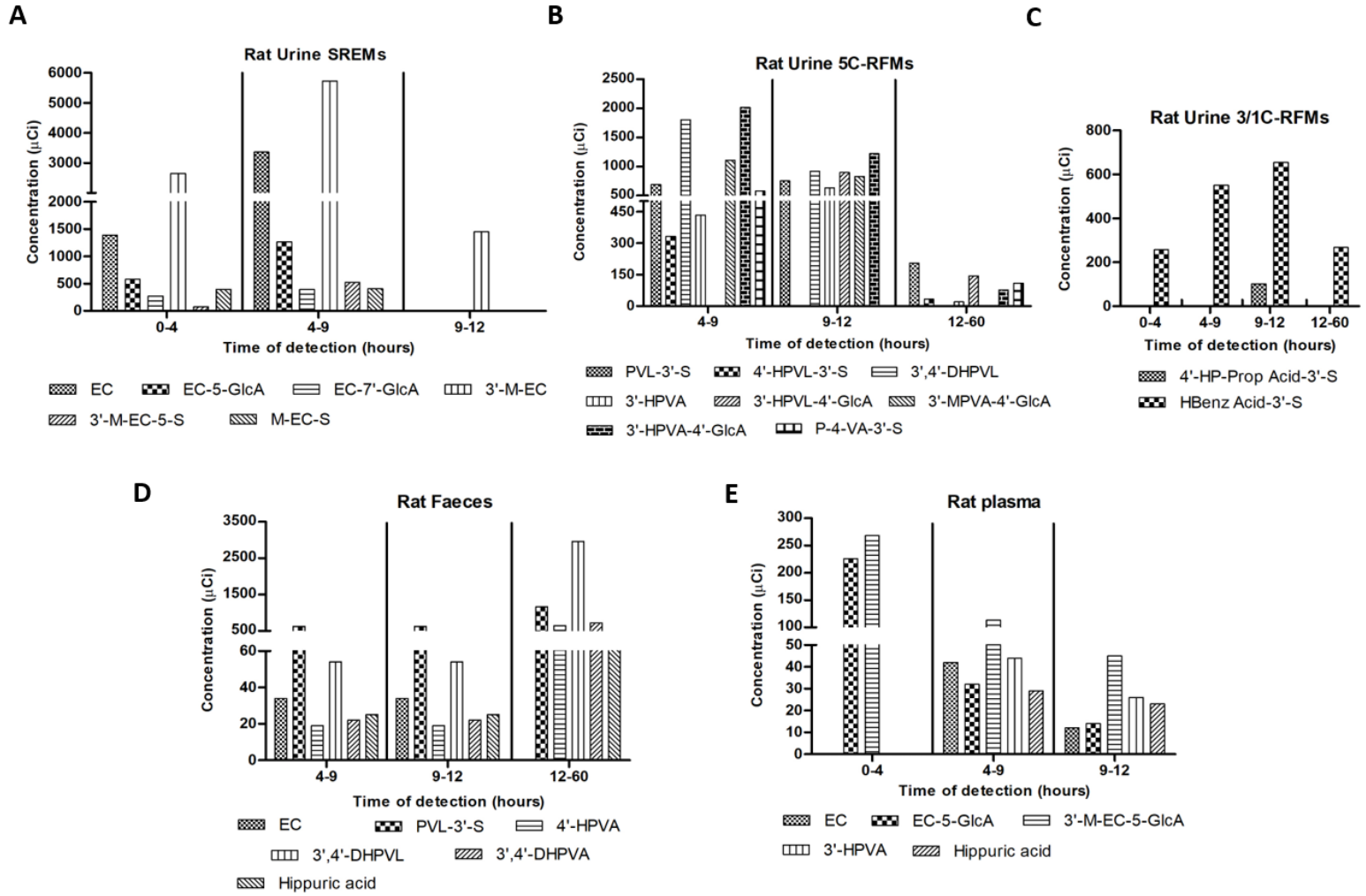

Figure 1.6: Pharmacokinetics of EC metabolism in rats

The graphs have been drawn from data reported by Borges et al (5). Rats were fed 20 µCi radiolabelled (−)-epicatechin (EC) and levels were monitored in plasma, urine and faeces over time. A-C) Urine EC metabolites detected for structurally related EC metabolites (SREMs), and ring fission metabolites (RFMs). D) Faecal metabolites, and E) plasma metabolites. GlcA: glucuronide; M: methyl; S: sulfate; D: di-; H: hydroxy; PVL: phenyl-γ-valerolactone; VA: hydroxyvaleric acid; P: phenyl; Prop acid: propionic acid; Benz acid: benzoic acid.

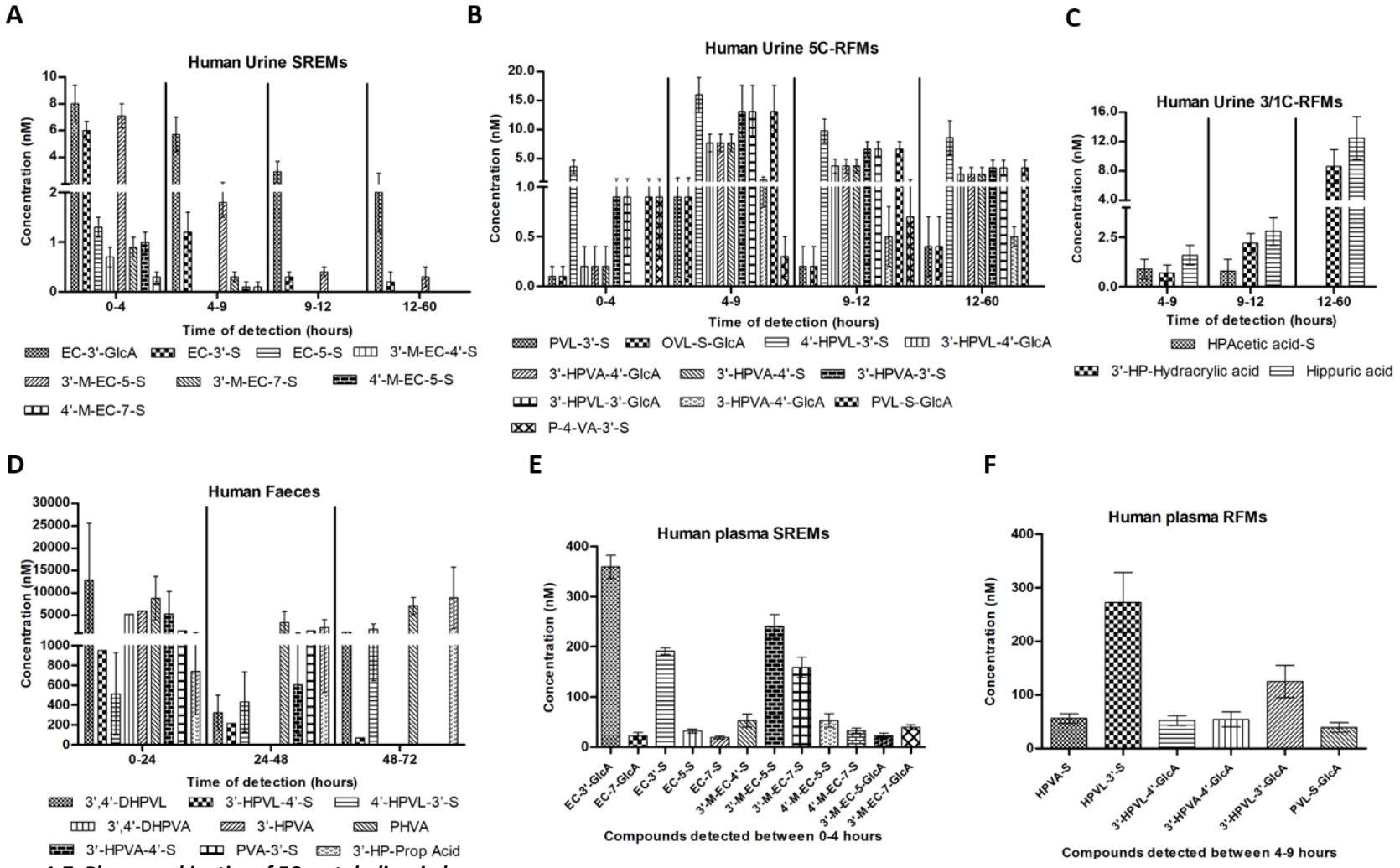

Figure 1.7: Pharmacokinetics of EC metabolism in humans

The graphs have been drawn from data reported by Ottaviani et al (1). Humans were fed 1 mg/kg body weight of radiolabelled (−)-epicatechin (EC) and levels were monitored in plasma, urine and faeces over time. A-C) Urine EC metabolites detected for structurally related EC metabolites (SREMs), and ring fission metabolites (RFMs). D) Faecal metabolites, and E-F) plasma metabolites for SREMs or RFMs. GlcA: glucuronide; M: methyl; S: sulfate; D: di-; H: hydroxy; PVL: phenyl-γ-valerolactone; VA: hydroxyvaleric acid; P: phenyl; Prop acid: propionic acid; Benz acid: benzoic acid.

There are more studies that detail the bioavailability of HPVLs following ingestion of specific food products in human, mice and rats (57, 81, 98, 99) which suggests their physiological levels from food consumption. Meng *et al* (2002) (99) studied human consumption of 20 mg/kg of body weight of green tea solids, which comprised of 2.78 mg EGCG (epigallocatechin gallate), 2.2 mg EGC (epigallocatechin), 0.64 mg EC (epicatechin) and 0.66 mg ECG (epicatechin gallate). 5-(3',4',5'-Trihydroxyphenyl)-γ-valerolactone (345THPVL) peaked in the urine of the volunteers between 3-9 hours at 14 μM, whilst 3',4'-dihydroxyphenyl-γ-valerolactone (34DHPVL) peaked between 3-6 hours at 4.7 μM. Very similar findings were reported by Lee *et al* (2002) for 34DHPVL detection in plasma following green tea solid consumption, but with a cumulative detection in urine of 5.0 ± 2 mg (81). In a separate study, ingestion of 150 mg of green tea solids in humans caused urine levels of 345THPVL to peak at 2.8 ± 1.5 μM and 34DHPVL to peak at 36.7 ± 34.4 μM, with a 1.2 mg cumulative excretion of 345THPVL (100). Faecal matter contained a total net wet weight of 11 μg/g of 345THPVL and 34DHPVL up to 9 hours following ingestion, and plasma contained up to 6 ng/mL of the compounds (100). In rats and mice, following the provision of 0.6 % green tea solids, 0.3 % EGCG or 0.1 % EGCG for 3 days in drinking water (composition as a percentage of that spoken from the solids above), mice excreted 8.3 μM of 345THPVL and 6.6 μM of 34DHPVL in urine (plasma was not recorded) (99). They also reported lower levels of EGCG in the liver and kidneys of rats compared to mice, and so mice demonstrated a greater bioavailability of EGCG and its metabolites than rats. In comparison, mice fed epicatechin gallate (10 mg) had detectable levels of 34DHPVL in plasma (562 ± 307 pmol/mL) and urine (201 ± 113 nmol/mL) between 24-48 hours (73).

The collation of evidence highlights that HPVLs are the main metabolites circulating in plasma and excreted after flavan-3-ol consumption, but their pharmacokinetics are highly dependent on the concentration consumed and the species used. There are larger differences in the metabolism of EC between rats (5) and humans (1) (Figures 1.6 and 1.7) than between mice and humans (101), where the latter have been shown to produce a greater more consistent metabolic profile following flavan-3-ol consumption. It is therefore very important to consider the model used when trying to relate to the health benefits in humans. Furthermore, dependent on the species, HPVLs have been shown to circulate in plasma over a 0-3-day period, which is vastly longer than other flavan-3-ols and their metabolites (102). Due to this, HPVLs may exert biological effects on organs, cells, signalling pathways and metabolic processes over a longer timescale than other compounds; however, very little is known about them and the effects (if any) they have on human physiological functions and disease. Nonetheless, because of the known health benefits of consuming the parent flavan-3-ol compounds, there is the suggestion that HPVLs could in part contribute to these effects, but this is an area for further exploration.

1.5 Current evidence of possible health beneficial effects of hydroxyphenyl-γ-valerolactones, gut microbiota-dependent metabolites of (−)-epicatechin

With the knowledge that HPVLs are the main group of colonic metabolites from EC, they require further investigation for their potential bioactive effects. The following is a summary of the existing published data relating to the biological activities of HPVLs.

HPVLs effects have been investigated using *in-vitro* models for anti-inflammatory activity in RAW264.7 macrophages where a 50 % reduction in nitric oxide was measured (NO) following treatment with 345THPVL (20 μM) (103) and with 34DHPVL (1.3 μg/mL); 34DHPVL also induced a dose dependent decrease in NO and iNOS expression at concentrations from 0.1-50 μg/mL (0.48-240 μM) (104). In addition, evidence was provided to suggest the facilitated diffusion of 34DHPVL into the macrophages via GLUT1 transporters (104). Moreover, HepG2 cells incubated with 34DHPVL dose dependently decreased tumour necrosis factor-α (TNF-α) induced NF-κB transcription (105). It is reported that NF-κB drives inflammatory marker expression and can directly influence iNOS activity and this could therefore be a mechanism for how 34DHPVL lowers iNOS and NO levels (106).

Both 34DHPVL and 4'-hydroxy-3'-methoxyphenyl-γ-valerolactone (4H3MPVL) have also been explored for their effects on lowering matrix metalloproteinase (MMP) levels (107). MMPs are involved in the pathogenesis of atherosclerosis where they degrade collagen and allow for smooth muscle cell migration into the vessel (108). Grimm *et al* investigated inflammatory lipopolysaccharide-stimulated MMP release in a model of primary human monocytes and reported that 0.5 μg/mL of 34DHPVL or 4H3MPVL inhibited MMP-9 secretion by 50 % (107). In addition, incubation of MMP-1 or MMP-2 proteins with either HPVL inhibited enzyme activity by 50 % at concentrations between 10-23 μg/mL, while 2-10 μg/mL was sufficient to inhibit MMP-9 activity (IC_{50}). Because MMP activity is dependent on zinc ions that reside within their active site, it was further shown that the addition of Zn^{2+} to the enzyme assay reversed the inhibitory activity of the HPVLs on MMP-2 and MMP-9 activity and thus may interact directly with the active site of MMPs.

A further study that demonstrated the potential of HPVLs to mitigate the development of atherosclerosis involved the incubation of human umbilical vein endothelial cells (HUVECs) with 34DHPVL (7.5-30 μM) following TNF-α incubation (109). In comparison to only TNF-α stimulated cells, the results showed a dose-dependent reduction in protein and mRNA expression of vascular cell-adhesion molecule (VCAM)-1 (109), an endothelial cell adhesion molecule that is expressed

following inflammatory stimulation to support cholesterol accumulation within the vascular intima (110). Reductions in monocyte chemotactic protein-1 (MCP-1) secretion, NF-κB mRNA levels and the TNF-α induced phosphorylation of IKK were also observed following 34DHPVL incubation (109).

In a spontaneous hypertensive rat model, 100-200 mg/kg body weight of 34DHPVL or 3',4',5'-trihydroxyphenyl-γ-valerolactone (345THPVL) was provided via gastric gavage and systolic blood pressure(SBP) was recorded (111). This study reported a decrease in SBP 4-hours post-gavage of 100 mg/kg or by 2-hours following 150 mg/kg body weight of 345THPVL administration, and by 4-hours following 200 mg/kg body weight of 34DHPVL administration, when compared to the saline control and to baseline. It was reported that these effects may have occurred from the inhibition of angiotensin converting enzyme (ACE), although there were marginal inhibitory effects seen from both these HPVLs (111) they were not able to influence endothelial elasticity in arteries collected from mice, alongside other HPVL metabolites (112).

More recently, the therapeutic potential of HPVLs was investigated using a brown adipose tissue (BAT) thermogenic *in-vitro* model (113), where BAT activity has been reported to be inversely correlated with adiposity and body mass index. For this, brown pre-adipocytes were differentiated in the presence of 10 μM of either 34DHPVL, 3´-hydroxyphenyl-γ-valerolactone-4'-sulfate (3HPVL-4S) or phenyl-γ-valerolactone-3´,4´-di-sulfate (PVL-34S) with or without hydrogen peroxide stress (113). However, the HPVLs used in this study were not able to induce gene transcriptional changes that were different from the control for adipocyte differentiation and neither were they able to modify norepinephrine stimulated lipolysis. Nonetheless, the antioxidant potential of the HPVLs was confirmed following their ability to counteract the increased reactive oxygen species (ROS) levels following hydrogen peroxide treatment (113).

Furthermore, 34DHPVL, 3HPVL-4S, PVL-34S, 4HPVL-3S were assessed for their ability to decrease the adherence of uropathogenic *E.coli* (UPEC) to bladder epithelial cells (114), a situation that occurs in the presence of a urinary tract infection (UTI). All the HPVL metabolites caused inhibition of UPEC adhesion by 20-30 % when treated with concentrations in the range 50-100 μM.

To assess HPVLs ability to mitigate cancer cell proliferation, incubations were performed with 34DHPVL, 345THPVL and their *O*-methoxy derivatives on several cancer cell lines (103). 345THPVL was the most active metabolite with IC_{50} values between 15-73 μM for human oesophageal squamous cell carcinoma cells (KYSE150), human colon adenocarcinoma cells (HT-29 and HCT-116), immortalized human intestinal epithelial cells (INT-407), and an immortalized rat intestinal epithelial cell line (IEC-6). However, the loss of a hydroxy group significantly reduced the bioactivity of the compound and stronger concentrations were required to achieve similar results. In contrast,

34DHPVL, 35DHPVL, and 345THPVL were unable to initiate an anti-proliferative effect on human cervical ovarian cancer (HeLa) cells (0.4-50 μg/mL over 72-hours), however their hydroxyphenyl-valeric acid (HPVA) metabolic derivatives were able to inhibit proliferative activity in HeLa cells (115). This highlighted the importance in the bioactive potential of the aliphatic side chain.

To determine if HPVLs were able to protect against skin ageing (wrinkling), human dermal fibroblasts (HDF) were incubated with 1 μM of racemic (*S*) and (*R*)-DHPVLs. The results showed that DHPVLs inhibited photoinduced MMP-1 protein expression where the (*S*) isomer was two times more potent than the (*R*) isomer. MMP-1 was the marker assessed because ROS levels are increased in the skin following UV radiation and subsequently this increases the transcription factor AP-1 and its transcribed protein MMP-1, and is thus a marker of photo-ageing (116).

The ability of HPVLs to cross the blood-brain barrier (BBB) was confirmed by Unno *et al* (2017) using a BBB model kit. The same authors also incubated human neuroblastoma SH-SY5Y cells with 35DHPVL, which was shown to cause cell proliferation at 0.5-1.0 μM incubations, whilst its *O*-sulfate and *O*-glucuronide derivatives had no effect. All three metabolites were able to increase the number of neurites, whilst only 35DHPVL and its *O*-sulfate increased neurite length (although it was unconfirmed whether this was for both isomers) (117). A further study by Angelino *et al* (2019) also confirmed the ability of 34DHPVL, 3HPVL-4S and 4HPVL-3S to cross the BBB by use of *in-silico*, *in-vitro* and *in-vivo* models (118). The *in-silico* model provided a predictive score for the HPVL and HPVAs to cross the BBB, whilst incubation of 5 μM of each of the metabolites for 2-hours on human brain microvascular endothelial cells (HBMEC) (trans-well inserts) showed that 4HPVL-3S crossed the barrier and was quantified in both the 'brain' and 'blood' sides of the chamber. To determine the ability of HPVLs to cross the BBB *in-vivo*, rats were intraperitoneally injected with 34DHPVL at 2 mg/kg body weight per day for seven days; alternatively, rats were provided with 100 mg/kg body weight of lyophilised red grapes for 10-weeks; an additional swine model was used where the animals were provided with a 20 g/day cocoa powder supplement for 27-days; in all scenarios the brain was harvested and frozen (118). This study revealed that the aglycone 34DHPVL was not detected in the brains of any of the animals, but there was the presence of the *O*-sulfate metabolites (although it was unconfirmed whether this was for both variants). Despite this, there was also the detection of HPVL-sulfates in the brains of the control and treated grape supplemented mice but only in the treated cocoa supplemented pigs.

Lastly, in a recent study, the effects of HPVLs were reported to reduce amyloid-β oligomers ($A\beta_O$) in a mouse model of Alzheimer's disease (119), these are aggregates that lead to neuroinflammation and cognitive impairment (120). To determine this, mice were injected with

$A\beta_O$s pre-incubated with or without 4HPVL and it was shown that the $A\beta_O$s induced memory impairment in the mice, but this was dose-dependently relieved with 4HPVL and object recognition was preserved at the highest concentration used (10 μM) (119). Alongside this result was a reduction in Iba1 immunoreactivity in the brain, which was assessed via immunostaining procedures; Iba1 are microglia markers that are active during immune defence. This research also supported the *in-vitro* work performed in the same study by Ruotola *et al* (2020) for the anti-cytotoxic effects of HPVLs on $A\beta_O$s (119).

The scarce but current evidence on HPVLs therefore implies that these metabolites have bioactive potential and can mediate mitigations in disease. However, the lack of evidence means that more research is required into this interesting group of metabolites.

1.6 Glucose homeostasis and insulin resistance

Body homeostasis of glucose and insulin is imperative to prevent the onset of insulin resistance and diabetes. The continual consumption of high fat and/or high carbohydrate diets is a driver for the progression of type-2 diabetes (121, 122) and in keeping with the observation that more than 90 % of those with type-2 diabetes are overweight or obese (123). It is known that the flavan-3-ols EGCG (124-126) and EC (127-130) can exert protective effects against the onset of type-2 diabetes even under the continual consumption of high calorie foods. This section will therefore cover the basic signalling processes involved in glucose and insulin signalling and how this can impact on insulin resistance when disturbed. It will go on to describe how EC has been shown to protect against insulin resistance using *in-vivo* and *in-vitro* models.

1.6.1 Normal glucose homeostasis

Glucose is a source of energy for the body but it is not synthesised by the brain (131). Therefore, the brain is the only organ that is insulin independent and maintains glucose uptake at the same rate in the absorptive and postabsorptive periods (132). In the hypoglycaemic state, glucagon is released by pancreatic α-cells, small intestine L-cells, and hypothalamic cells, all of which help to stimulate organs to release glucose, with an 85 % contribution by the liver (131, 132). An equal 50 % split of glucose is produced by processes of gluconeogenesis and glycogenolysis (132). Glycogen is a polymer of glucose subunits through α-1,4 glucosidic bond and an α-1,6 glucosidic bond that is stored in the liver and muscles (133). Only liver glycogen can contribute to blood glucose via glycogenolysis, the breakdown of glycogen into glucose, whilst muscle glycogen provides glucose only to the muscle fibres. Gluconeogenesis is the alternative pathway for the production of glucose, and it does so through the use of amino acids and citric acid cycle intermediates (Figure 1.8) (131, 133).

Glycogenolysis is controlled by hormones, namely epinephrine in the muscles and glucagon in the liver (133). Glucagon binds to its G Protein Coupled Receptors (GPCRs) to activate adenylyl cyclase via its α-subunit and subsequently cAMP. Likewise, protein kinase A (PKA) becomes activated to stimulate a series of enzymes involved in glycogenolysis (134). Energy release by ATP stimulates a series of phosphorylation reactions in the sequence of: phosphorylase kinase, phosphorylase, and finally glycogen synthase (133, 134). Glucose 1-phosphate is the final product from glycogenolysis, so the liver enzyme phosphoglucomutase converts it to glucose-6-phosphate, and finally glucose-6-phosphatase converts this into glucose. Glycogenolysis becomes inactivated when cAMP is

degraded to AMP and when protein phosphatases PP1, PP2a, PP2b, PP2c, dephosphorylate the phosphorylated enzymes (133). This process is summarised in Figure 1.8.

Gluconeogenesis is a reverse process of glycolysis using amino acids. When glucagon binds to GPCR and activates PKA, it stimulates CREB (cAMP Response Element Binding Protein) that initiates binding to CRE. CRE triggers transcription factors to synthesise PEPCK (phosphoenolpyruvate carboxy kinase), that converts oxaloacetate to phosphoenolpyruvate. Oxaloacetate is the intermediate formed from the conversion of pyruvate in the mitochondria, itself formed from amino acids but mostly alanine, and can also be produced as a keto acid of aspartate via aspartate aminotransferase and from citric acid cycle intermediates which can originate from fatty acids (135). Phosphoenolpyruvate undergoes a series of reactions to produce fructose-1,6-bisphosphate, this is further catalysed by fructose-1,6-biphosphatase to fructose-6-phosphate, and to glucose-6-phosphate by phosphoglucose isomerase (Figure 1.8). The final transformation to glucose is mentioned previously.

The reverse of the mentioned processes will occur in the presence of hyperglycaemia to allow for insulin release and ultimately lower blood glucose. In the pancreas, β cells possess GLUT2 receptors that facilitates the diffusion of glucose into the cytoplasm, and further enters into pathways for glycolysis and the TCA cycle (136, 137). An increase of cytoplasmic glucose causes depolarisation of the cell via efflux inhibition of K^+ through an ATP dependent mechanism, leading to a rise in cytoplasmic current (137). Voltage-gated Ca^{2+} channels open in response to the polarisation and influx into the cell, resulting in the exocytosis of insulin containing vesicles to raise circulatory insulin concentrations. Additionally, insulin release can be stimulated through the binding of GLP-1 (glucagon like peptide 1) and GIP (glucose-dependent insulinotropic peptide) to GPCRs, that are excreted by small intestinal endocrine cells. Their binding increases the sensitivity of β-cells for glucose by increasing cAMP and potentiating insulin release (136, 137) (Figure 1.9).

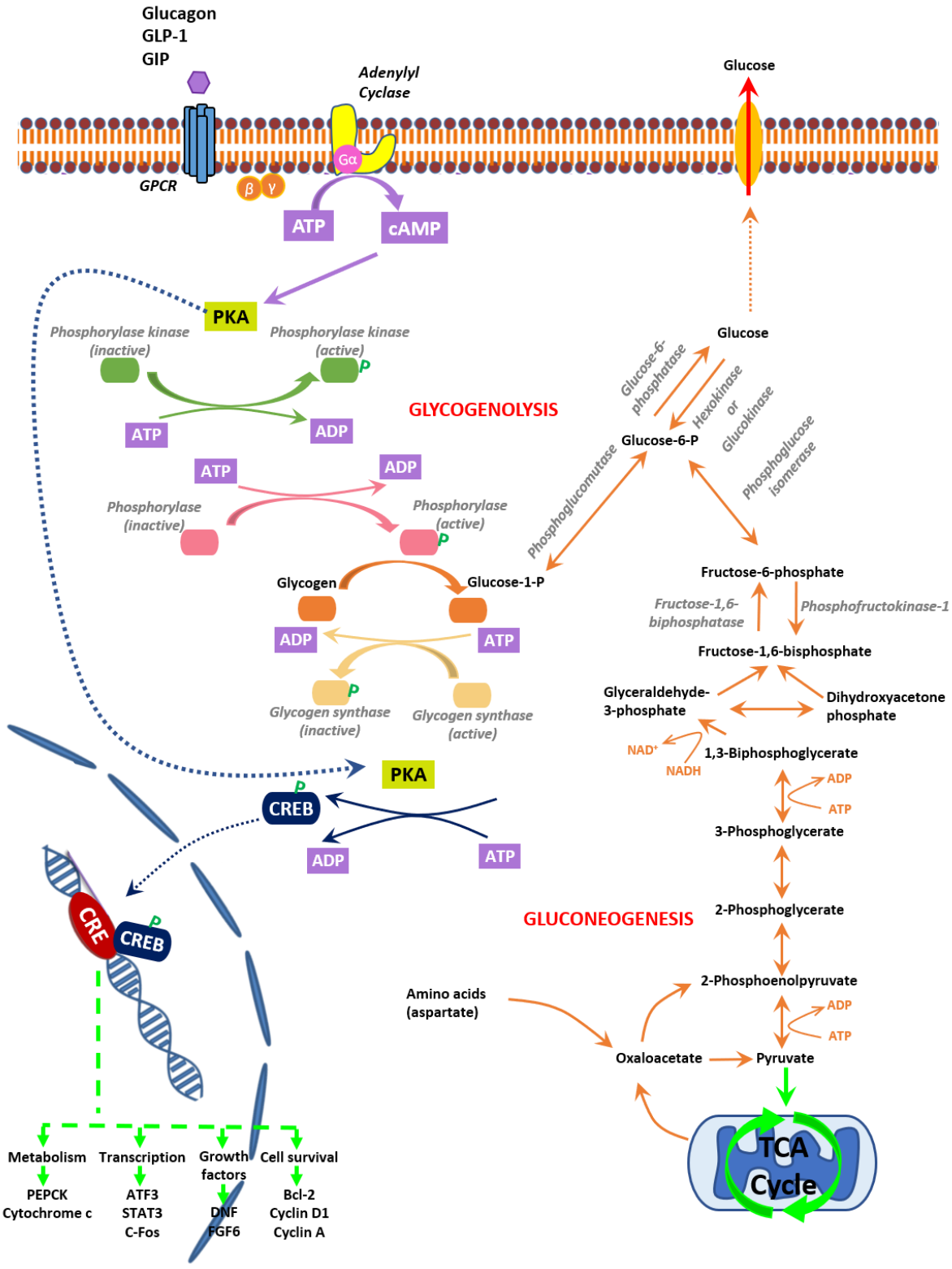

Figure 1.8: Mechanistic overview of glucagon initiating glycogenolysis and gluconeogenesis in liver cells
Glucagon binds to its G-protein coupled receptor where its α subunit activates adenylyl cyclase and increases the levels of cAMP. In return this activates PKA that triggers a series of events to activate enzymes involved in glycogenolysis that ends with the formation of glucose. Gluconeogenesis is a backwards process of glycolysis, forming glucose from pyruvate by a series of energy activated reactions and enzymes where highlighted.

1.6.2 Insulin signalling pathway

Insulin signalling promotes glycogenesis to lower blood glucose levels and restore homeostatic conditions. It is also stimulated by the ingestion of carbohydrates through GLP-1 and GIP (138), but half of insulin produced is metabolised by the liver (138).

The insulin receptor is an allosteric enzyme consisting of an α-subunit and a β-subunit located in hepatocytes, skeletal muscle cells and adipocytes (139). Upon the binding of insulin or insulin like growth factors (IGFs), the receptor dimerises to form an $\alpha_2\beta_2$ complex which causes autophosphorylation of tyrosine residues on the β-subunits at positions 1158, 1162, 1163 (140). This activation step recruits and further activates several substrates with SH2 (Src homology-2 domains) (141), in return activating signalling pathways such as the PI3K, Akt (also known as protein kinase B - PKB), mTOR (mammalian target of rapamycin), MAPK (mitogen-activated protein kinase), GSK-3 (glycogen synthase kinase-3), and cbl-associated protein (CAP) pathways (142) as detailed below.

The best understood signalling pathway is the PI3K/Akt pathway. PI3K possesses two SH2 domains, a catalytic subunit (p110) and a regulatory subunit (P85). P85 binds to the activated insulin receptor substrates (IRS), stimulating the PI3K enzyme to phosphorylate the second messenger molecule phosphatidylinositol 4,5-biphosphate (PIP_2) to phosphatidylinositol 3,4,5-trisphosphate (PIP_3). This further leads to the recruitment of protein dependent kinase-1 (PDK1) towards the plasma membrane and thus the phosphorylation of its downstream target Akt. When Akt is phosphorylated it becomes active, initiating downstream effector pathways involved in cell survival, inhibition of apoptosis and cell proliferation (Figure 1.10). Its activation is mediated by the phosphorylation on two residues, Thr308 and Ser473; two different pathways lead to the phosphorylation of each residue. Thr308 is phosphorylated by active PDK1 whereas Ser473 is phosphorylated by rictor-mTOR (RICTOR) – both phosphorylation sites are required to achieve maximal Akt activation. Phosphorylated Akt can then go on to de-phosphorylate GSK-3 and phosphorylate TSC-2 (tuberous sclerosis complex-2), SREBP-1c (sterol regulatory element binding protein-1c), and FOXO (forkhead box O), all of which are transcription factors. Deactivated GSK-3 can regulate glycogen synthesis by preventing the phosphorylation of a cluster of serine residues on the enzyme (143). TSC1/2 regulates mTOR and protein synthesis. FOXO regulates gluconeogenic genes.

Another important activated pathway from the insulin receptor is the Cbl-CAP complex that occurs in adipose tissue and muscles (144). This pathway is mainly involved in stimulating the translocation of GLUT4 (glucose transporter type 4) receptors to the membrane of the cell. Once insulin binds to the insulin receptor, it initiates the phosphorylation on the tyrosine residue of Cbl, activating it

(144). As a result, CAP binds to Cbl and the whole complex translocates to the plasma membrane where CrkII followed by C3G and TC10 binds to the complex. TC10 catalyses the conversion to GTP from GDP, resulting in a release of energy to signal to GLUT4 vesicles from inside the cell to translocate to the plasma membrane.

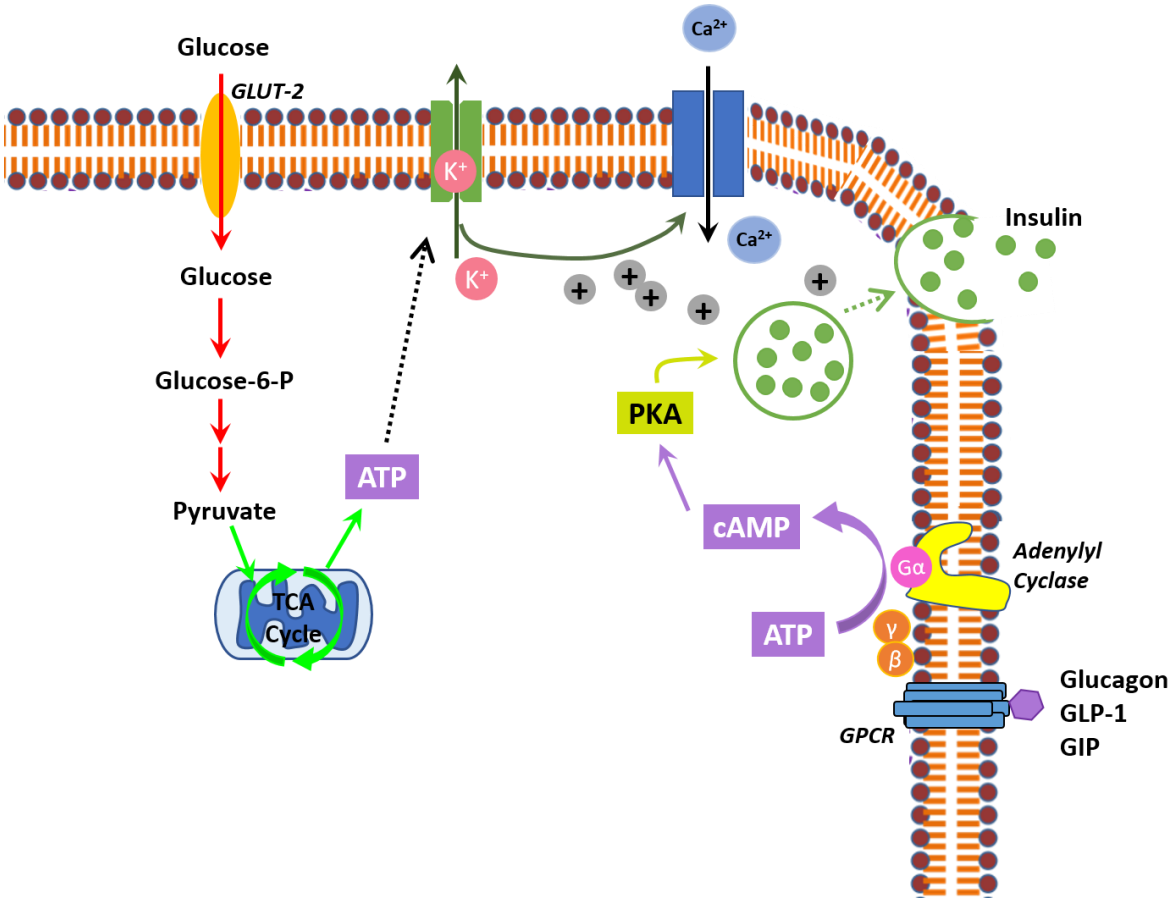

Figure 1.9: Mechanisms of insulin secretion
Glucagon and GLP-1 bind to G-protein coupled receptors that activates adenylyl cyclase and increases cAMP levels that stimulates PKA. PKA can in turn trigger the exocytosis of insulin containing granules. Additionally, cell depolarisation from the influx of glucose via GLUT-2 receptors in pancreatic β-cells triggers insulin release through ATP dependent closure of K^+ channel. This depolarisation initiates the opening of Ca^{2+} channels to increase cytoplasmic stores that again triggers the exocytosis of insulin containing granules.

In addition to insulin's role in transforming glucose into glycogen, it also regulates cell growth through the MAPK/ERK pathway, as illustrated in Figure 1.10. If insulin insensitivity occurs or the pathway is inhibited, cell growth can become arrested. Insulin signalling is also involved in lipid synthesis via activation of the SREBP-1c transcription factor and inhibition of enzyme lipases such as lipoprotein lipase, adipose triglyceride lipase, hepatic lipase and hormone sensitive lipase, thus inhibiting lipid degradation (145).

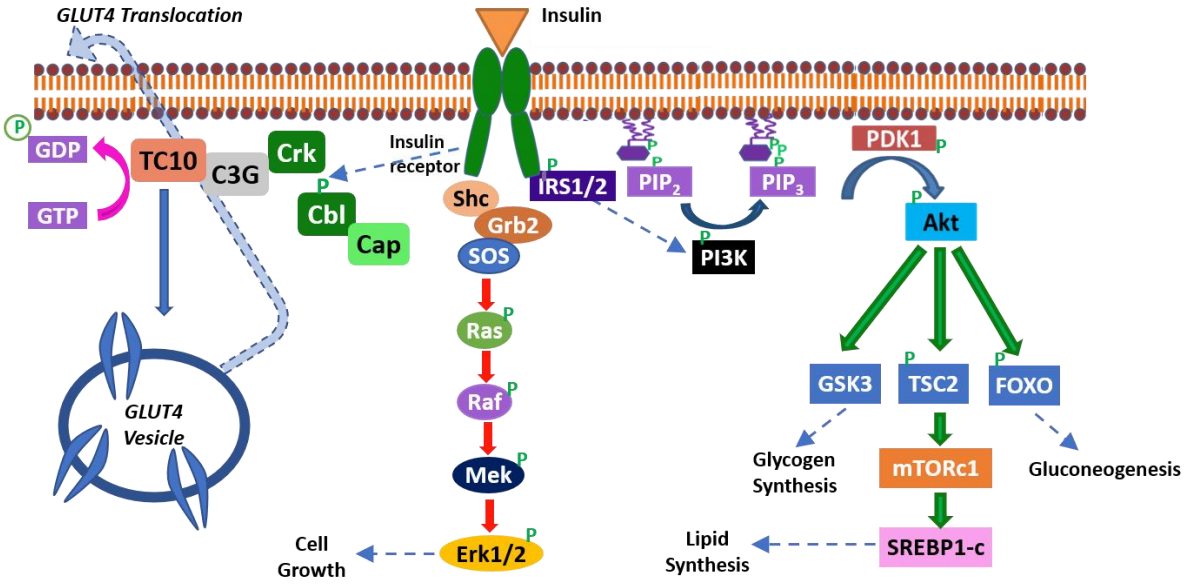

Figure 1.10: Insulin signalling in hepatic cells
Insulin binds to IR/IRS-1 receptors and can trigger a series of activation pathways. One pathway is through the phosphorylation of PI3K which phosphorylates PIP_2 to PIP_3. This activates PDK1 by phosphorylation which phosphorylates Akt. Akt can then go on to activate several pathways: GSK3 to trigger glycogen synthesis; TSC2 to trigger lipid synthesis through SREBP1C; and FOXO to initiate gluconeogenesis. Alternatively, insulin binding can recruit Shc to the receptor that binds to Grb2-SOS complex, to trigger the phosphorylation of Ras, Raf, Mek and Erk1/2, ultimately triggering cell growth through transcription factors. Another important pathway is the triggering of Cbl and Cap following insulin binding. Cbl is phosphorylated by the receptor and recruits Cap. The Cbl-Cap complex translocates to the plasma membrane and binds to CrkII-C3G-TC10 complex. TC10 causes a release of energy from GTP to GDP which stimulates the recruitment of GLUT4 vesicles to the plasma membrane and increases the uptake of glucose.

1.6.3 Pathogenesis of insulin resistance

Insulin resistance is defined to occur "when normal concentrations of insulin produces a less than normal biological response" (146), resulting in a decreased uptake of glucose in the periphery in addition to the increased production of glucose endogenously (132). Beta cell function is impaired in type-2 diabetes, although in early stages they release more insulin as a compensatory mechanism to lower glucose levels. Type-2 diabetes is inherently associated with metabolic associated fatty liver disease (MAFLD) (formerly known as non-alcoholic fatty liver disease, NAFLD (147)), such that over 90 % of obese patients with type-2 diabetes have MAFLD (148).

Insulin resistance mostly arises when there is an interference between insulin and its receptor, which is normally due to a reduction in receptor numbers (149). Intracellular signalling interferences following insulin binding to its receptor will induce decreased responsiveness, which is defined differently to resistance. Type-2 diabetic patients have been shown to have a 30 % lower

glycogen store in muscle tissues in addition to a 50 % reduction in glycogen synthesis; reduced glucose transportation has been shown to be the rate limiting step in this process (150).

An increase in the concentration of lipids, either from dietary consumption or from the accelerated lipolysis of adipose tissue, results in an increased delivery of fatty acids and overwhelms the capacity for cells to oxidise fats to diacylglycerols (DAGs) (151). The reduction in fatty acid oxidation induces the phosphorylation of protein kinase C-θ (PKC-θ), in turn phosphorylating IRS-1 on its serine/threonine amino acids, thereby inhibiting it. It's inhibition prevents the activation of the PI3K/Akt pathway (152, 153), which desensitises the receptors to stimulation from insulin, in return leading to continued glycogenolysis and gluconeogenesis (153-158), and induces muscle insulin resistance over time. Although this process is the same in liver tissue, the PKC responsible is PKC-ε. Another method shown to desensitise insulin receptors is through the transportation by F-actin of PKC-ε to the cellular nucleus (159). This downregulates the expression of the insulin transcription factor HMGA1 (high mobility group AT-Hook 1) through phosphorylation, and drastically impacts upon the detection and signal transduction of insulin.

Accumulation of free fatty acids (FFA's) in the liver can also stimulate inflammatory pathways, in particular toll-like receptors (TLRs), that increases the synthesis of *de novo* ceramide (153, 160). Ceramides can inhibit Akt phosphorylation and therefore contribute towards insulin resistance. In addition to increasing ceramides, PP2a is activated by FFA's and will phosphorylate and inactivate Akt. Its inactivation prevents the inhibition of transcription factor Forkhead Box-01 (FOXO1) that would otherwise activate gluconeogenesis enzymes (161). Despite these other pathways, hepatic diacylglycerol (DAG) accumulation is the best predictor for insulin resistance, as confirmed by liver biopsies in obese subjects (153, 155, 162).

1.7 Flavonoids and insulin resistance

Flavonoids have been reported to contribute to the prevention of cardiovascular diseases, cancers, osteoporosis, neurodegenerative disease, chronic inflammation and diabetes mellitus (6, 31, 32, 163). More specifically, flavonoids have been reported to trap and scavenge ROS, upregulate NO production, inhibit cell mitosis, promote apoptosis, and decrease inflammatory leukocyte attachment to cell membranes (33). The focus of the rest of this review will be on flavonoids and insulin resistance which was the purpose of the research project described here.

Flavonoids have been shown to mitigate type-2 diabetes via improved insulin sensitivity, improved glucose tolerance, enhancing the uptake of glucose in tissues through an increase in the number of glucose receptors, and inhibit and regulate enzymes involved in carbohydrate metabolism (60).

1.7.1 Associations of flavonoid consumption and protection from insulin resistance inferred from epidemiological studies

The associations of polyphenol intake and the risks of type-2 diabetes have been explored by several authors. In the European Prospective Investigation into Cancer and Nutrition (EPIC) InterAct study (EPIC-InterAct), where polyphenol intake was estimated in 12,403 type-2 diabetic patients, it was reported that there were significant inverse associations for flavanol and flavonol intake against type-2 diabetes (164). EPIC-InterAct is a case-cohort study nested within the EPIC study, comprising cohorts recruited in the 1990s from 8 European countries (Denmark, France, Germany, Italy, The Netherlands, Spain, Sweden, and the United Kingdom) across 26 participating study centres. In this study they analysed 26,088 participants which included 11,559 who had type-2 diabetes from the start of the trial, 729 who developed type-2 diabetes during and 15,258 who did not have type-2 diabetes. Dietary questionnaires were used to estimate polyphenol intake using the Phenol-Explorer database (15). For flavanol consumption, EGCG was found to be the highest contributor, followed by ECG, EGC, EC, catechin, catechin-3-gallate, and gallocatechin, comprising 45.6 %, 14.2 %, 13.8 %, 13.2 %, 9.2 %, 2.5 % and 1.5 % of the ingested flavanols respectively (164). Alongside this was the consumption of flavonols quercetin, kaempferol, myricetin and isorhamnetin, comprising 70.2 %, 18.5 %, 9.3 % and 2 % of the flavonol intake. A significant negative association for the prevalence of type-2 diabetes was found for all the listed compounds except for isorhamnetin and quercetin but included proanthocyanidins.

Del Bo *et al* (2019) reviewed the health effects of polyphenols from food related sources and highlighted 12 papers to have investigated these in the context of insulin resistance and/or type-2 diabetes in humans based in the United States, South America, Europe and Asia (165). The results of this found the following associations for a decreased risk of type-2 diabetes, 15 % with total flavonoid intake (US males and females) (166), 8 % with myricetin consumption (European populations) (167), 14 % with proanthocyanidin dimer consumption (European populations) (167), 7 % with EC consumption (European populations) (167), 6 % with (+)-catechin consumption (European populations) (167), 2 % with (+)-gallocatechin consumption (European populations) (167), 10 % with total flavonoid consumption (European populations) (164), 18 % with total flavanol consumption (European populations) (164), 27 % with flavan-3-ol monomers (European

populations) (164), 19 % with flavonol consumption (European populations) (164), and 32 % with total polyphenol intake (Polish males and females) (168). There was also a decreased risk for type-2 diabetes with flavanol intake (US males and females) (169) and flavone intake (Korean women) (170), but not for total flavonoid consumption (US males and females) (169). Additionally, there were reductions in the homeostatic model assessment of insulin resistance (HOMA-IR) with anthocyanin and flavone intake (UK women) (171). Moreover, there was a 3.18 % reduction in insulin and 3.10 % reduction in HOMA-IR with flavone intake, and a 3.11 % reduction and a 4.01 % reduction in HOMA-IR with isoflavone intake (US males and females) (172). Sex specific reductions were found for insulin and HOMA-IR by flavonol consumption in men and flavanone consumption in women (Korean women) (170), but no gender differences were detected for decreased fasting plasma glucose with high total polyphenol intake (168).

The current evidence therefore strongly supports an association for a decreased risk of type-2 diabetes and insulin resistance with increased flavonoid intake. The differences between studies for the percentage reduction in type-2 diabetes risk highlights how study design and length can affect the outcome, alongside with how differently ethnic populations respond to diets, but may also reflect how the composition of the gut microbiota affects individual's metabolism of the compounds that proceed to initiate protective effects (34).

1.7.2 Associations of targeted dosing of flavonoids and protection from insulin resistance inferred from intervention studies

To induce insulin resistance in mice, it is common to provide a HF diet for a period of time, as it imitates the western diet lifestyle. The effects seen in mice can be somewhat comparable to humans, although this model does not account for the many variables in a human's lifestyle that can influence the effects induced by the diet, for example, mice are maintained in a strict environment for humidity, temperature and air flow whilst humans are faced with different environmental factors, and mice are maintained on a strict regulated diet, whereas humans diets will consistently vary. Before summarising the protective nature of flavonoids on insulin resistance, it is important to understand the tests performed to collate data. The most commonly used tests are the insulin tolerance test (ITT) and the glucose tolerance test (GTT). The ITT involves a bolus insulin injection into the subject and blood samples are taken to determine glucose levels over time to establish how the subject responds to insulin. In insulin resistance/type-2 diabetes, the glucose level will remain high despite the insulin injection, this is due to the subject's resistance to insulin where they fail to respond in lowering plasma glucose efficiently, through mechanisms discussed

in previous sections. In the case of GTT, a bolus glucose dose is injected, and blood samples are taken to monitor the glucose and insulin levels. Type-2 diabetic patients have impaired recovery of their glucose levels - a rapid spike in their blood glucose concentration that is sustained for a long period of time despite the high recording of insulin in their blood. In contrast to this, a 'healthy' subject responds with a smaller rise in glucose concentration that returns to baseline more rapidly. The HOMA-IR is a model to assess insulin resistance and is calculated using the glucose and insulin levels following a GTT performed in the fasted state. To explore the mechanisms for how flavonoids protect against type-2 diabetes, this section will detail the glucose and insulin changes with treatments as well as the alterations in specific protein and gene markers linked to insulin resistance following the intervention of flavonoids in mice, rats and humans.

Feeding Goto-Kakizaki rats 1 % (w/w) hesperidin for 4-weeks prevented the elevation of blood glucose and insulin levels and increased PPARα and PPARγ, signalling markers known to stimulate the insulin signalling pathway (173). PPARγ was also shown to be raised following oral administration of hesperidin (50 mg/kg body weight) for 15-days in diabetic Wistar rats induced by Streptozotocin (STZ) injections (174). In C57BL-KsJ-db/db mice, hesperidin and naringin (0.2 g/kg diet) lowered blood glucose and gluconeogenesis enzymes glucose-6-phosphatase (G6Pase) and phosphoenolpyruvate carboxykinase (PEPCK), and raised plasma insulin and hepatic glycogen and glucokinase levels after 5-weeks (175, 176). In addition to this, in the same study, hepatic glucose transporter 2 (GLUT2) protein expression was reduced whilst adipogenic GLUT4 and hepatic PPARγ were upregulated in both hesperidin and naringin groups (176). In diabetic Wistar rats (STZ diabetes induced), hesperidin (10 g/kg diet) lowered blood glucose through a reduction in hepatic enzymes G6Pase and glucokinase after 4-weeks (177). Furthermore, in humans, hesperidin (500 mg/day) supplementation for three weeks improved insulin sensitivity as shown by a lower QUICKI (quantitative insulin sensitivity check index) and reduced fasting plasma glucose levels (178).

An intervention study in Djungarian hamsters administered orally with 10 mg/kg body weight of naringenin or quercetin prevented rises in plasma glucose levels when administered 15 mins prior to a fasted glucose challenge (179). Myricetin may also have anti-hyperglycaemic properties as has been reported in rat models following intravenous or intraperitoneal injections (180-182), accompanied with decreases in HOMA-IR (182), and increased hepatic glycogen associated with increases in glycogen synthase I activity, and is consistent with hepatic glycogen storage (180). Catechin (10 mg/kg body weight) had a similar effect in Sprague-Dawley rats after 60-days of feeding for the increase in hepatic glycogen and glycogen synthase activity, but with a decrease in glycogen phosphorylase levels (183). Quercetin (10 mg/kg body weight) reduced blood glucose in diabetic STZ treated Sprague-Dawley rats after 8-10 days of treatment, but it was unable to reduce

the glucose area under the concentration time-curve (A.U.C) following a glucose tolerance test (184).

The effects of the flavan-3-ol EC are described in detail in section 1.7.2.1. Meanwhile, a 3-week administration of EGCG (200 mg/kg/day) in spontaneously hypertensive rats (SHR) was reported to improve insulin sensitivity (185). When EGCG was administered for seven weeks in db/db mice at 0.25-1.0 % and in ZDF rats at 0.5 %, blood glucose levels decreased dose dependently alongside an increase in mRNA expression for glucokinase and a decrease for PEPCK in both the liver and adipose tissue (186). However, in humans, EGCG (400 mg) has not been reported to improve insulin resistance after 8-weeks, although there were effects seen to be positive such as a reduction in diastolic blood pressure (187). Green tea polyphenols (100 mg/kg body weight) that are high in EGCG lowered blood glucose levels in Wistar albino diabetic (alloxan treated) rats within 8-hours of oral administration (188), in db/db mice within 6-hours of administration (300 mg/kg body weight) (189), and in humans after 3-months of administration (379 mg) (190, 191), where the levels of insulin were also lowered alongside HOMA-IR (191). Despite this, there was a study that provided humans with 544 mg of green tea polyphenols for 2-months, but there was no improvement in blood glucose levels or insulin resistance (192). Green tea extract consumed at 500 mg for 16-weeks in humans with type-2 diabetes improved insulin resistance and increased GLP-1, a hormone that stimulates insulin release from the pancreas (193).

Cocoa polyphenols, that are rich in catechins and mostly EC, have been routinely shown to positively influence insulin sensitivity through the lowering of blood glucose in humans (194-198) and rodents (199-206), reducing insulin in humans (194-198) and rodents (199, 201-203), improving HOMA-IR in humans (194-198, 207, 208) and rodents (201, 209), and reducing hepatic PEPCK and G6Pase accompanied with increased hepatic glucokinase in rodents (199). For a detailed example, in Zucker diabetic fatty rats, a 10 % cocoa diet (fed for 9-weeks) prevented hyperglycaemia in addition to improved insulin sensitivity which was associated with reduced serine phosphorylation of IRS-1, inactivation of GSK-3 and improvement in antioxidant defences (19, 199). The cocoa diet also suppressed the activation of JNK and P38 pathways which are otherwise active in insulin resistance (199). Meanwhile, human intervention studies have demonstrated that dark chocolate without polyphenols did not relay any health benefits, whilst the presence of polyphenols caused a decrease in blood pressure, increased insulin sensitivity, and improved HOMA-IR and β-cell function (197, 207, 210-212). The same improvements were also seen in patients who were type-2 diabetic (195, 213). However, there have also been studies that show no effect on improving insulin sensitivity with cocoa intake, though these are largely thought to be due to the acute length of the intervention studies (214, 215).

For the isoflavones genistein and daidzein, their supplementation at a low dose of 0.02 % (w/w) for 9-weeks in non-obese diabetic (NOD) mice caused a reduction in the hepatic mRNA expression for PEPCK, G6Pase and fatty acid β-oxidation together with a reduction in blood glucose levels (216). Accompanying this was a rise in insulin levels, where daidzein was 20 % more effective in raising insulin than genistein. Similar findings were found by genistein and daidzein supplementation at 0.02 % in C57BL/KsJ-db/db mice after 6-weeks for the reduction in blood glucose and glucagon, whilst increasing the insulin/glucagon ratio and hepatic glucokinase, but reduced hepatic G6Pase and PEPCK, and lowered the expression of enzymes involved in fatty acid metabolism (217). Furthermore, STZ treated mice fed 10 mg/kg body weight of areca nut procyanidins for 4-weeks lowered blood glucose and hepatic PEPCK and G6Pase mRNA with increases in active AMPK (218). For the anthocyanin cyanidin-3-glucoside, when fed to db/db or high fat diet fed C57BL/6J mice at 0.2 % for 12-weeks, there was an improvement in insulin sensitivity through the lowering of blood glucose levels accompanied with lower insulin levels, reduced JNK1 (c-JUN) protein expression, along with increased phospho-Akt (Ser473) and phospho-FOXO1 (Thr24) levels in adipose tissue (these are signalling molecules involved in insulin signalling) (219). Grape seed procyanidins administered orally to STZ rats at 250 mg/kg body weight also had an immediate anti-hyperglycaemic effect, as determined following oral gavage of the compounds with or without insulin and recording blood glucose for 4-hours after(220).

Flavonoids protect pancreatic β-cells from glucose induced damage and therefore restore insulin secretion in response to glucose, i.e. they are more sensitive. β-cell restoration has been shown to occur by quercetin-3-rutinoside and quercetin in STZ rats and diabetic mice through restoring the cell proliferation capacity and therefore raising insulin levels (184, 221-223).

1.7.2.1 (−)-Epicatechin effects in-vivo on insulin resistance

High-fat (HF) diet fed mice are routinely used as a model of insulin resistance, alongside the genetically induced models. Research has shown that mice fed EC supplemented into a 60 % kcal HF diet, enables the reduction of plasma glucose in response to insulin, therefore highlighting ECs potential to mitigate insulin resistant effects (127, 130, 224).

Studies using EC in mice fed a HF diet have routinely shown that EC can improve the insulin response to a glucose injection where their blood glucose levels return to baseline comparably quicker than those on a HF only diet (130, 224-227). Mice on an EC supplemented HF diet have also been shown to express increased activity of insulin stimulated IR, IRS-1, Akt and ERK1/2 in adipose and liver, whilst a high fat only diet decreased this activation compared to control treatments. Further

observations of adipose and liver from EC fed mice showed that EC prevented activation of IKK (kinase activating NF-kB pathway), JNK and adipose PKC (228). Transcriptomic studies from EC fed mice showed the reduced genetic expression of PTP1B when compared to HF mice; this gene is involved in negating the insulin signalling response, whilst the HF diet alone significantly increased its expression compared to control fed mice. Further findings using mice that were fed a 60 % kcal HF diet with or without 200 mg/kg body weight EC (224), or 20 mg/kg body weight EC (229), highlighted that EC prevented obesity in mice, and also resulted in lower adipose tissue weight, in addition to the reduction in serum levels of CCL19 and the downregulation of inflammatory genes TNF-α and IL-6, amongst others (130, 224, 229). EC was also able to restore mitochondrial proteins within adipose tissue and skeletal muscle (226, 230) and increase mitochondrial levels.

Cremonini *et al* (2018) sought to understand how EC could mitigate steatosis and insulin resistance (130) based on the knowledge that increased intestinal permeability is associated with an increased risk for steatosis and insulin resistance (231, 232). They demonstrated that a 60 % kcal HF diet in mice increased intestinal permeability and made the gut 'leakier', evidenced by increased plasma TNF-α and inflammatory cytokine concentrations (130). The HF diet caused a reduction in tight junction proteins within ileal epithelial cells ZO-1, occludin, and claudin-1, where the supplementation of 20 mg/kg body weight of EC for 15-weeks prevented this. Additionally, EC prevented the increase in ERK1/2, AMPK, NF-kB (nuclear factor kappa-light-chain-enhancer of activated B cells) and p65 phosphorylation - pathways that are required to increase intestinal permeability. Oxidative stress is another factor that can increase intestinal permeability, and is reported to be significantly induced by HF diets via increases in NOX1 and NOX4 - changes that were mitigated by EC (130). Moreover, GLP-2 (glucagon like peptide-2) plasma levels were also raised by EC in the mice, this is a protein that can decrease intestinal permeability as well as exert a beneficial effect on glucose metabolism via the increase in the number of glucose transporters and the facilitation of glucose uptake (141, 142). This study therefore supports a further underlying role for how EC could mitigate insulin resistance and hepatic steatosis.

Very few human studies have been performed with pure EC to investigate the effects on insulin resistance (233, 234). Gutierrez-Salmean (2014) investigated the effects of 1 mg/kg body weight of EC on blood glucose levels prior to consumption of a commercial supplement containing fat, protein, and carbohydrates, totalling 246 kcal (234). Respiratory quotient was assessed in the subjects to measure the ratio of CO_2 consumed to O_2 produced whilst food was being metabolised, and it was apparent that EC significantly lowered the respiratory quotient by sustaining fat oxidation in both normal weight and obese subjects. In addition, EC significantly lowered blood glucose and triglyceride levels even after meal ingestion in both obese and normal weight subjects,

but bigger changes were observed in those who were obese. A double-blinded crossover study in humans was performed by Dower *et al* (2015) (233), with one arm of the study involving the daily intake of 100 mg/day EC for 4-weeks in a form of a supplement. After the 4-weeks there was a significant reduction in plasma insulin concentrations, ultimately leading to a lower HOMA-IR index (233). Although plasma lipids were lower, the change was not significant. After a 4-week washout period, the same participants were provided with quercetin-3-glucoside supplements, but caused no significant effects on insulin or HOMA-IR. These data support the notion that the effects of EC consumption on insulin resistance are somewhat specific, and this is not a flavonoid-wide effect (233).

In addition, there are several clinical studies published on *clinicaltrials.gov* involving epicatechin and its effects on diabetes, and as of the 2nd April 2021 using the search criteria with 'diabetes + epicatechin' returns 10 completed study results. Of these, they were then narrowed down to studies that used cocoa and/or EC in the interventions to narrow down the data where EC is the most likely cause for any positive effects observed. A total of 5 intervention studies will therefore be highlighted, however two of the studies have already been mentioned previously under section 1.7.2 with the references from Curtis *et al* (2012 and 2013) (195, 213). In pre-diabetic participants, the consumption of 30 mg/day of (+)-epicatechin (please note this is the least naturally occurring epicatechin not found in cocoa) for seven days had no effects on plasma glucose or insulin levels when compared to placebo treatments, however, there was a tendency for the reductions in plasma TNF-α and MCP-1 levels (borderline significant) which tended to rise seven days after having stopped the intervention (235-237). A study in type-2 diabetic participants who consumed either high polyphenol content (3.5 % total polyphenols or 1 mg/day EC content) of milk or 70 % dark chocolate exhibited a non-significant reduction in P-selectin and E-selectin levels compared to those who consumed milk chocolate with low polyphenol content (0.9 % total polyphenols or 0.05 mg/day EC content) which is reflective of EC's antioxidant potential and ability to improve endothelial dysfunction, however, there was no improvement in other diabetic markers (214, 238). On the other hand, type-1 diabetes is associated with impaired cognitive function, and as such, a study was performed in type-1 diabetic patients to monitor cognitive reaction times via a 'flanker' test and functional magnetic resonance imaging (fMRI) following the consumption of a high (900 mg cocoa flavanols: 185 mg (−)-epicatechin, 20 mg (+)-catechin, and 691 mg procyanidins) or low (15 mg cocoa flavanols) cocoa flavanol drink with a standardised breakfast (239, 240). The results of this demonstrated a marginal improvement in cognitive performance and an increased response in the supramarginal gyrus parietal lobe and inferior frontal gyrus in both healthy subjects and patients with type-1 diabetes.

In summary, obesity caused by a western diet can increase the risk of developing type-2 diabetes and other disorders. This involves insulin resistance occurring via a reduction of insulin receptors on cells, causing a reduced capacity to respond to glucose through insulin secretion. It is apparent that EC protects against the effects of a western diet in inducing insulin resistance through: an increase in antioxidant defences, maintenance of insulin receptor number on cells, increased activation of the insulin signalling pathway, increased insulin secretion, a decrease in inflammatory responses, and an improved HOMA-IR.

1.7.3 In vitro studies and cellular mechanisms

1.7.3.1 Flavonoids and their effects on insulin resistance in-vitro

Some flavanols have been shown to inhibit the enzymatic activity of α-amylase and α-glucosidase and thus reduce starch digestion. Hanhineva *et al* (2010) reviewed the effects of polyphenols on carbohydrate metabolism (241) and discussed the reported effects for all flavonoids and phenolic acids that have been shown to possess inhibitory activity. To summarise, the flavonoids that have been shown to inhibit α-amylase include: cyanidin 3-sambubioside (242), quercetin (243), myricetin (243, 244), luteolin (243, 245), and luteolin 7-glucoside (245), whilst the flavonoids that have been demonstrated to inhibit α-glucosidase include: cyanidin 3-galactoside (246), cyanidin 3-rutinoside (247, 248), cyanidin 3-sambubioside (242), acylated anthocyanins (249), (+)-catechin (250), (+)-catechin gallate (250), EGC (250-252), EGCG (243, 253), theaflavin gallate (253), quercetin (243, 250), quercetin 3-rhamnoside (254), myricetin (243), luteolin (243, 245), luteolin 7-glucoside (245), genistein (243, 255) and daidzein (243, 245). It is thought that the inhibition of starch digestion therefore contributes to the reduction in blood glucose levels in subjects on polyphenol interventions when compared to controls.

Several flavonoids have also been shown to inhibit glucose transportation in Caco-2 cells at 100 μM (256) and between 31-2570 μM concentrations (257) and enhance insulin-mediated glucose uptake from EGCG (20-40 μM) stimulation of GLUT-4 in L6 myotubes (258); and by kaempferol and quercetin in 3T3-L1 cells (5-50 μM) (259); genistein in 3T3-L1 cells (50 μM) (260); grape-seed procyanidins in L6 myotubes and 3T3-L1 adipocytes (140 μg/mL) (220) (100 μg/mL) (261); acyl-EC in L6 myotubes (100 nM) (262); and by hesperidin and other fruits (0.1 % v/v) (263, 264). EGCG (20-40 μM) can also stimulate the activation of AMPK and Akt, in return triggering the insulin signalling cascade (258, 261), and similar effects are reported for grape-seed procyanidins for Akt and MAPK activation (100 μg/mL) (261). Furthermore, glucose is also absorbed into enterocytes by active transport via the sodium-dependent glucose transporter (SGLT1) and by facilitated diffusion (265).

This process has been shown to be inhibited in porcine jejunum cells by quercetin glucosides (0.6 mM) (266), in rat jejunum cells by ECG (1 mM) (267), and in Caco2 cells by ECG (100 μM) (256, 268), EGC (100 μM) (256), EGCG (100 μM) (256), and in rabbit and rat jejunum cells by naringenin (500 μM) (269).

Myricetin incubated with rat adipocytes caused increased glucose uptake that was not due to increased GLUT4 translocation (270). This was also reciprocated in soleus muscle cell culture from STZ rats, where myricetin increased glucose uptake dose dependently and caused an increase in glycogen (181), and increased the active phosphorylated levels of IR, IRS-1 and Akt, in addition to enhanced GLUT4 levels (182). All of this supports a myricetin-induced restoration of insulin signalling and glucose uptake. In contrast to these positive findings, naringenin incubation on 3T3-L1 adipocytes was reported to exacerbate insulin resistance effects through the inhibition of insulin-stimulated glucose uptake via Akt phosphorylation inhibition (271). The same was discovered for genistein treatments in the same cell model, but this did not occur through the alteration of GLUT4 translocation, rather it affected their conformation and thus their activity to uptake glucose (272). A further study found inhibition of insulin-stimulated glucose uptake in isolated rat adipocytes by quercetin, myricetin and catechin-gallate but not by catechin through the direct interaction with GLUT4 (273).

Isolated rabbit muscle cells treated with quercetin (5-21 μM), luteolin (16-29 μM), ECG (13-50 μM), EGCG (8-34 μM), cyanidin (3-9 μM), delphinidin (3-11 μM) and peonidin (25-18 μM) in enzyme assays have been reported to inhibit phosphorylated active glycogen phosphorylase-a and unphosphorylated glycogen phosphorylase-b, but quercetin, cyanidin and delphinidin were the most potent (274). This is evidence that the general flavonoid structure is capable of inhibiting enzymes involved in the production of glucose. However, it should be mentioned that these parent compounds rarely interact with these enzymes physiologically because they are rapidly degraded, conjugated and metabolised before being absorbed into the systemic circulation. Moreover, in purified rat liver microsomes, the flavonoids kaempferol 3-*O*-α-(2″-galloyl)rhamnoside, quercetin 3-*O*-α-(2″-galloyl)rhamnoside, quercetin 3-*O*-α-rhamnoside, kaempferol 3-*O*-α-rhamnoside, quercetin 3-*O*-α-arabinoside, quercetin and kaempferol inhibited enzymatic activity of glucose-6-phosphatase (G6Pase), listed by their order of potency (275). Quercetin 3-*O*-α-(2″-galloyl)rhamnoside, purified from Bauhinia megalandra leaves, was further reported to competitively inhibit G6Pase dose dependently (276).

Treatment with 10 μM EGCG on rat pancreatic β-cells (RIN-m5F) stimulated IRS2, Akt and AMPK signalling under high glucose conditions and increased insulin secretion in the presence of 0.1 μM

and 10 μM EGCG (277). Additionally, there were increases in the expressions of GLUT2, glucokinase, β-cell differentiation, and PDX-1 (Pancreatic and Duodenal Homeobox 1), a transcription factor that regulates insulin transcription. Under a high glucose environment, the treatment of isolated rat islets with EC (0.8 mM) or quercetin (0.01 mM) induced insulin secretion but not in the presence of naringenin (278). However, these concentrations are not physiologically achieved from food consumption.

Insulin secretion levels have been monitored in INS-1E cells after polyphenol treatment. Genistein treatments (1-5 μM) caused glucose mediated insulin secretion, but this was not due to modulation of insulin synthesis, and so the pancreatic cells responded better to glucose (279). This was found to mostly occur through a Ca^{2+} signalling AMPK dependent mechanism. Similarly, anthocyanins, specifically cyanidin-3-glucoside and cyanidin-3-galactoside, also increased insulin secretion in the presence of glucose (280).

In HFIIE rat hepatoma cells, EGCG at 50 μM and 100 μM decreased PEPCK and G6Pase mRNA expression, along with many genes involved in lipid metabolism (186). Similar findings were reported for a study with HFIIE cells when treated with 12.5 μM and 25 μM EGCG, that caused a reduction in the mRNA levels of PEPCK and G6Pase mRNA, and a reduction in glucose production (281). These were accompanied by increases in IRS-1 phosphorylation levels, and active PI3K and MAPK. Furthermore, in primary mouse hepatocytes, 0.25-1.0 μM of EGCG significantly decreased glucose production, and the levels of PEPCK and G6Pase mRNA (282). Additionally, there were increases in the levels of active AMPK but without stimulation of insulin signalling proteins. Finally, when primary mouse hepatocytes were treated with areca nut procyanidins, the rate of gluconeogenesis was dose dependently inhibited via the reduction in mRNA levels of PEPCK and G6Pase (218).

1.7.3.2 (–)-Epicatechin effects in-vitro on insulin resistance

The liver is an organ that will encounter insulin resistance in response to a high fat diet prior to other organs such as the pancreas, kidney, skeletal muscle, adipose and cardiac tissue (283). There are a few reports that investigated effects of EC and its metabolites on liver cells. High glucose incubation is mostly selected as an *in-vitro* treatment on cells to induce insulin resistance effects. This is because hyperglycaemia is known to induce damage to cells by five major mechanisms concluded by Giacco and Brownlee (2010): increased flux of glucose and other sugars through the polyol pathway, increased intracellular formation of advanced glycation end-products (AGEs), increased expression of the receptor for advanced glycation end products and its activating ligands,

activation of protein kinase C (PKC) isoforms and overactivity of the hexosamine pathway (284). Evidence suggests that the overproduction of ROS by mitochondria activates all the above.

The incubation of cocoa polyphenol extract (CPE) (1 μg/mL) or EC (10 μM) with HepG2 cells (immortalised human liver carcinoma cells) stimulated the insulin signalling pathway through increases in the phosphorylation of tyrosine and total protein levels of IR, IRS-1 and IRS-2, in addition to the activation of PI3K and AMPK (285). The latter mitigated the phosphorylation of serine on IRS-1 and caused an induction of gluconeogenesis, when compared to cells in high glucose conditions (199, 286). Moreover, it initiated the recovery of hepatic GLUT-2 expression to uptake extracellular glucose and increase glycogen synthesis through glycogenesis (199, 286). The data in a report by Cordero-Herrera *et al* (2015) reinforced these findings above for the ability of EC and CPE to prevent the inhibition of insulin signalling caused by glucose (287).

Rat kidney NRK-52E cells incubated with EC (10 μM) or one of its metabolites, 3,4-dihydroxyphenylacetic acid (DHPAA) (10 μM), prior to or post to glucose challenge, prevented the induction of ROS and prevented the reduction in antioxidant defences for proteins SIRT1 (sirtuin 1), MAPK, and NOX-4 (NADPH Oxidase 4) (288). In brief, SIRT1 influences metabolism by regulating transcription factors in the liver, skeletal muscle, pancreas, adipose tissue and the brain (289). It can regulate lipolysis, adipogenesis, ROS production, and stimulate glucose uptake and GLUT4 translocation. Impairment of NOX-4 can induce a distinct pattern of insulin resistance/responsiveness that includes the abolishment of FOXO1 activation and glucose uptake from insulin (290). Further evidence supporting the protective role of EC and DHPAA against ROS production, includes the restoration of GSH (glutathione), SOD (superoxide dismutase), GPx (glutathione peroxidase) and CAT (catalase), that are otherwise decreased under high glucose conditions; all these enzymes are actively involved in antioxidant defences and the scavenging of ROS (288).

EC (10 μM) antioxidant effects were also demonstrated in HepG2 cells that had been previously exposed to a high glucose environment (287). Incubation with EC prevented glucose stimulated ROS production and prevented the depletion of GSH and GPx. Further observations included increases in NRF2 activity, a transcription factor that regulates antioxidant defences, alongside a reduction in active p38 and an increase in active ERK. Furthermore, cell incubation with an inhibitor of ERK, blocked the increase in NRF2 from EC or CPE (1 μg/mL), thus confirming that both these extracts act through the ERK pathway.

EC treatment (5-20 μM) in rat pancreatic cells (INS-1E) exposed to high oxidative stress caused by treatment with tert-butylhydroperoxide (t-BOOH), mitigated the induced oxidative effects (291).

Consistent with previously reported studies, EC prevented the depletion of GSH and GR (glutathione reductase) whilst recovering GPx and reducing the levels of phosphorylated JNK. Importantly, EC significantly increased insulin secretion from the cells in basal conditions and in the presence of glucose, which was otherwise depressed with t-BOOH treatment in the presence of glucose. To add to this, Fernandez-Millan (2014) studied the effects of phenolic metabolites from EC (3,4-dihydroxyphenylacetic acid (DHPAA) (5 μM), 2,3-dihydroxybenzoic acid (DHBA) (10 μM) and 3-hydroxyphenylpropionic acid (HPPA) (1 μM)) on glucose or t-BOOH stimulated INS-1E cells (292). DHPAA and DHBA were shown to increase insulin secretion from the cells only in the presence of glucose. However, in the presence of ERK and PKC inhibitors, DHPAA and DHBA failed to stimulate insulin release, indicating that these metabolites initiate effects via these pathways. Consistent with the other report, DHPAA and HPPA prevented oxidative stress from t-BOOH and restored insulin secretion from t-BOOH treated cells (292).

The concentrations of EC used to exert protective effects varies across reports in the published literature and appears to depend on the cell line used and the conditions of the culture itself, and most effects were observed at physiologically relevant concentrations. Yang *et al* (2018) incubated INS-1 cells in a high glucose environment, and only in the presence with EC (30 μM) was there a significant reduction in ROS levels. In contrast, a low concentration of EC (0.3 μM) had no effect, but unfortunately there were no intermediate concentrations used to determine the bioprotective concentration of EC (293). Furthermore, following the induction of β-cell damage from glucose, EC at 0.3 μM increased insulin secretion via the activation of CaMKII, but no effects were observed for EC at 30 μM. Kim *et al* (2003) repeated similar effects *in-vivo* in rats and *in-vitro* in primary rat cultured cell islets (294). Meanwhile, Hii *et al* (1984) repeated the effects of EC for the induction of insulin secretion at concentrations of 1 mM in primary cultured rat islets (295). These data demonstrate bioactive effects of EC at different concentrations, which therefore causes inconsistency with regards to what EC concentration should be used.

The co-culture of 3T3-L1 adipocytes with RAW264.7 macrophages in the presence of EC (50 μM, or 0.5-10 μM) and challenged by lipopolysaccharide (LPS) (1 ng/mL, or 0.5 μg/mL) or TNFα (1 ng/mL, or 20 ng/mL), mitigated the increase in CCL19 (inflammatory cytokine) and TNF-α, alongside other inflammatory cytokines (224, 225) (concentrations are sourced from the references, respectively). This was evidenced to occur through the inactivation of the NF-kB signalling cascade, which would otherwise act to increase inflammatory precursors. Such effects were not seen in isolated adipocytes; thus, EC mitigated the inflammatory effects on adipocyte cells from macrophages. This finding was also supported in a HF diet fed mice study where EC mitigated the recruitment of macrophages in adipose tissue (229).

1.7.4 Summary

In conclusion, the evidence obtained from epidemiological, interventional and *in-vitro* studies for the protective role that flavonoids and polyphenol-rich foods play towards insulin resistance and type-2 diabetes is equivocal. Nonetheless, due to discrepancies in the literature and the differences found between humans and rodents from flavonoid effects, the mitigation of insulin resistance by flavonoids cannot be exclusively stated. Because of this, more tightly controlled interventions need to take place, specifically in humans to fully identify the role of polyphenols in insulin resistance.

1.8 Conclusion and future perspectives

High fat and high carbohydrate diets are known to cause metabolic syndrome and the induction of insulin resistance. Polyphenols have been investigated for their effects in controlling glycaemia and improving insulin resistance, but the exact mechanisms for their actions are not fully understood and require further investigation. There is a distinct shortage of human studies and animal studies for pure polyphenol compound interventions, and interventions using food sources does not allow for the identification of the active components in the diet that bring about the positive changes observed. As such, there is the requirement for intervention studies to be performed in humans and in rodents using isolated flavonoids to examine tissues and dissect the mechanisms involved. Because of the greater similarity in the metabolic profile of compounds from flavonoid/food ingestion in mice than other animals such as rats and rabbits, this model is recommended for investigative studies.

Moreover, flavonoids are metabolised rapidly following consumption, where there are a subset of phase II/III and microbial metabolites that are most likely to reach the circulation and encounter endogenous organs. Therefore, it would be valuable to investigate specific metabolites in rodents and humans in intervention studies, and with more *in-vitro* studies specifically treating cells with these metabolites and measuring effects on metabolism and associated biomarkers.

Although polyphenols are reported to confer many health benefits, this review has focussed primarily on insulin resistance and type-2 diabetes because that was the aim of the research in this thesis. EC has been investigated in rodents for their protective effects towards insulin resistance and it is known that hydroxyphenyl-γ-valerolactones (HPVLs) contribute around one third of the circulatory metabolites produced. Because of this, and the lack of understanding surrounding the active metabolites from EC metabolism, it is of interest to determine if HPVLs contribute to the

beneficial effects of EC consumption to protect against insulin resistance. Thus, the rest of this thesis will focus on understanding the bioavailability of HPVLs following their ingestion in C57BL/6J mice, followed by an intervention study of this compound performed in a HF diet induced diabetic C57BL/6J mouse model to explore potential effects on the processes included in insulin resistance.

1.9 Thesis objectives

The overall aims of this thesis were two-fold:

(1) Assess the bioavailability of hydroxyphenyl-γ-valerolactones following oral consumption
(2) Understand whether 3',4'-dihydroxyphenyl-γ-valerolactone (34DHPVL), a metabolite of (−)-epicatechin, protects against the development of insulin resistance in a diabetic mouse model.

For the reasons outlined in section 1.8, the next sections of this thesis are divided into 6 chapters which address the following objectives:

1. Chapter 2 – Investigate the bioavailability of hydroxyphenyl-γ-valerolactones in C57BL/6J mice
    a. Develop a fit-for-purpose analytical method for the quantification of HPVLs and their phase-II conjugates from mouse plasma and urine.
    b. Design and execute a mouse single acute dose pharmacokinetic study investigating the absorption, metabolism and excretion of 34DHPVL with (−)-epicatechin (EC) as a control.
    c. Quantify the concentrations of 34DHPVL and its phase-II metabolites in mouse plasma and urine samples.
    d. Determine the pharmacokinetic parameters of HPVLs: maximum concentration (C_{max}), time for maximum concentration (T_{max}), and elimination half-life ($T_{1/2}$).
2. Chapter 3 - Directly compare the effects of (−)-epicatechin and its microbial metabolite 34DHPVL on insulin resistance in a high-fat diet mouse model of diabetes
    a. Design a powered study using previous literature as a reference to guarantee insulin resistance and EC protection effects.
    b. Prepare mouse pellets for the inclusion of EC and 34DHPVL at carefully selected concentrations.
    c. Perform a glucose tolerance test in mice and measure plasma glucose and insulin levels to calculate an insulin-sensitivity index.
    d. Statistically evaluate the data at a 95 % confidence interval to extract conclusions.
3. Chapter 4 - Evaluate the physiological actions of EC and 34DHPVL in the mice and other markers
    a. Quantify plasma lipids and liver damage markers.
    b. Histologically examine liver tissue for lipid deposition, fibrosis and inflammation.
    c. Extract and quantify liver lipids.

   d. Perform enzyme assays on alpha amylase with 34DHPVL to assess inhibitory action on starch digestion.

4. Chapter 5 – Assess the mechanisms involved from dietary supplementation with EC versus 34DHPVL on gene expression in mouse liver tissue using transcriptomics
   a. Randomly select liver samples to extract RNA and quality check for RNA-Sequencing preparation.
   b. Perform RNA-Sequencing through a third-party.
   c. Use bioinformatics to process the RNA-Sequencing data to compare the effects of the dietary interventions for 7-pairwsie comparisons on gene expressions and pathway enrichments.
5. The final chapter 6 will bring the whole thesis together by way of discussion and explore the future directions and impact the findings of this work may have in terms of future interventions and dietary advice.

Chapter Two

A PHARMACOKINETIC STUDY OF THE ORAL BIOAVAILABILITY AND PHASE-II METABOLISM OF 5-(3’,4’-DIHYDROXYPHENYL) -γ-VALEROLACTONE IN MICE

Chapter 2: A pharmacokinetic study of the oral bioavailability and phase-II metabolism of 5-(3',4'-dihydroxyphenyl)-γ-valerolactone in mice

2.1 Abstract

Background: There is a substantial body of preclinical and clinical scientific evidence describing the beneficial effects caused by the consumption of (−)-epicatechin (EC) rich foods and beverages such as dark chocolate, cocoa, and apples. The absorption, distribution, metabolism, and excretion (ADME) of EC have been extensively reported, including after oral consumption of ^{14}C-labelled EC. These studies have shown that a proportion of the EC is absorbed intact and undergoes phase-II metabolism so that it is found exclusively as EC *O*-methylated, -sulfated and -glucuronidated conjugates in plasma and urine. Meanwhile, a greater proportion is transformed into hydroxyphenyl-γ-valerolactones (HPVL) by the gut microbiota; these are also accumulated in plasma and urine as phase-II conjugates and may be responsible for the beneficial effects of EC consumption. It is not possible to determine the pharmacokinetic properties of HPVLs from EC because HPVLs are generated over an extended period of time, and the exact dose of EC that reaches the colon is unknown due to prior absorption of EC from upper gastrointestinal tract.

Aim: To directly investigate the absorption, metabolism, and excretion of the most common HPVL, 3',4'-dihydroxyphenyl-γ-valerolactone (34DHPVL).

Methods: Eighteen 12-week old C57BL/6J mice were oral gavaged with 80 mg/kg body weight of 34DHPVL and sacrificed after 1, 2, 3, 6 or 24-hours when blood and urine were collected. An additional group of four mice were oral gavaged with 80 mg/kg body weight of EC and sacrificed at 24-hours. Plasma and urine samples were processed prior to analysis using UPLC-MS^2 in MRM mode for analysis of metabolites with quantification achieved using authentic standards.

Results: The following metabolites were identified and quantified in mouse plasma/urine: 34DHPVL; 3'-*O*-glucuronide, 4'-*O*-glucuronide, 3'-*O*-sulfate and 4'-*O*-sulfate of 34DHPVL; 3'-*O*-methylated 4HPVL. No HPVL metabolites were detected in samples that had not been gavaged with 34DHPVL. The highest concentration of total HPVL metabolites in plasma was observed at 1-hour with concentrations declining to 24-hours. Although HPVL-glucuronides accounted for 62 % of total plasma HPVLs at 1-hour, the balance between glucuronides and sulfates shifted dramatically with time such that HPVL-sulfates had the highest area under the pharmacokinetic curve (A.U.$C_{0\text{-}24h}$) values and accounted for 74 % of the total HPVL metabolites excreted in urine. HPVL-sulfates

exhibited the longest plasma elimination half-lives, with the aglycone ≥ glucuronides. Together, these observations are consistent with a rapid early glucuronidation of 34DHPVL as a result of small intestinal phase-II conjugation, which is followed by a longer hepatic-driven process of de-glucuronidation and subsequent sulfation occurring continuously post-absorption. A minor second plasma peak of 34DHPVL metabolites at 3-6 hours suggested that enterohepatic recirculation was occurring. Total urinary excretion of HPVL metabolites accounted for an estimated 45 % of the oral 34DHPVL dose. The mean plasma concentrations of 34DHPVL metabolites were similar in 24-hour samples from mice gavaged with 34DHPVL or with EC.

Conclusion: These data show that 34DHPVL is absorbed rapidly from the small intestine and undergoes phase-II conjugation, with small intestinal *O*-glucuronidation dominating early on followed by sulfation that later dominates, presumably as a result of hepatic metabolism. Evidence of enterohepatic recirculation shows that phase-II conjugated 34DHPVLs can be conjugated in the lower gut and the aglycone absorbed.

2.2 Introduction

EC is widely distributed in the diet, with especially high levels being found in cocoa and green tea (14-16). These foods have been primarily investigated for their health protective effects in humans, with strong evidence supporting their protection towards cardiovascular disease, cancer, insulin resistance and cognition (296). Very few studies have assessed individual flavanols and their protective effects, but the collation of *in-vitro* and *in-vivo* studies provides a collection of evidence supporting specific flavanols and in particular EC for their strong bioactive potential (163, 297, 298). Nonetheless, there is a distinct lack of evidence in understanding the mechanistic actions of EC and polyphenols more general. Irrespective of this, the absorption, distribution, metabolism and excretion (ADME) of EC is becoming better understood and it will help in interpreting the modes of action of EC and/or its metabolites (299).

Chapter 1 has reviewed extensively the ADME of EC following its ingestion in humans (1), mice and rats (5). Almost immediately, EC becomes phase-II conjugated by enterocytes of the small intestine to produce structurally related EC metabolites (SREMs), -*O*-sulfated, -*O*-glucuronidated and -*O*-methylated. This is followed by the colonic metabolism of unmetabolised EC that has passed through the gastrointestinal (GI) tract, alongside the further metabolism of phase-II conjugates that re-enter the gut following enterohepatic circulation. These catabolites can be further conjugated by phase-II enzymes by intestinal enterocytes and/or the liver for -*O*-sulfates, -*O*-glucuronides, and -*O*-methylates. The large recovery of EC and their metabolites in urine for 78 % (5) and 82 % (1) in rats and humans respectively highlights how efficiently EC is absorbed. For the SREMs that efflux back into the intestinal lumen and also for those that appear following enterohepatic circulation, alongside unabsorbed EC, these pass into the colon, approximating 70 % of the ingested EC (96). The main colonic metabolites are those of HPVL and hydroxyphenylvaleric acids (HPVA), representing 42 % of the ingested EC that passes into urine, and ~74 % of the detected metabolites found in plasma (6.9 % of the ingested EC intake $_{0\text{-}24\,h}$) (1, 96). Although the main catabolites of EC are HPVLs, it is not possible to identify their pharmacokinetic parameters due to the unknown concentrations of EC and phase-II metabolites that reach the colon. Due to the long half-life of HPVLs (5.7 ± 0.7 hours) (1) and the high exposure of tissues to these compounds, it is plausible that they are mostly responsible for the positive effects brought around by EC. Because of this, the pharmacokinetic profile of HPVLs requires investigation to understand the retention and elimination of these compounds by the body.

This chapter reports on a study performed in C57BL/6J female mice for the plasma and urinary distribution of HPVLs following oral gavage of 34DHPVL over a 24-hour period. Identification and

quantification of HPVLs was performed using methods optimised for their detection by use of UPLC-MS^2.

2.3 Aims and approach

There are no published reports describing the pharmacokinetics of any orally ingested HPVL; the only available data currently available are for orally ingested catechins, especially EC, part of which is transformed to HPVLs in the lower gut over a period of many hours. The overall aim of the research presented in this chapter was to determine the pharmacokinetics of 34DHPVL following administration of a single dose to mice. The following approach was taken to achieve this:

(1) Female C57BL/6J mice were orally gavaged with 80 mg/kg body weight of 34DHPVL or EC, and urine, plasma, and faecal samples collected after 1, 2, 3, 6 and 24 hours after.

(2) A fit-for-purpose analytical method for the quantification of HPVLs and their phase-II conjugates from mouse plasma and urine was developed.

(3) The concentrations of 34DHPVL and its phase-II metabolites in mouse plasma and urine samples were quantified after extraction using UPLC-MS^2.

(4) The pharmacokinetic parameters for C_{max}, T_{max}, area under the curve and elimination half-life ($T_{1/2}$) were calculated.

The resulting data was used to address the following questions:

(1) How bioavailable is 34DHPVL and what is the profile of its phase-II metabolites when provided as an oral dose in female mice?

(2) How does the bioavailability and metabolism of orally ingested 34DHPVL differ from that for HPVLs generated in the lower gut by the action of the gut microbiota on catechins?

2.4 Methods

2.4.1 Materials

Seven hydroxyphenyl-γ-valerolactones: 5-(3',4'-dihydroxyphenyl)-γ-valerolactone, 5-(3',4',5'-trihydroxyphenyl)-γ-valerolactone, 5-(4'-hydroxy-3-methoxyphenyl)-γ-valerolactone, 5-(4'-hydroxyphenyl)-γ-valerolactone 3-*O*-glucuronide, 5-(3'-hyroxyphenyl)-γ-valerolactone 4-*O*-glucuronide, 5-(3'-hydroxyphenyl)-γ-valerolactone-4'-*O*-sulfate sodium salt, 5-(4'-hydroxyphenyl)-γ-valerolactone-3'-*O*-sulfate sodium salt, were synthesised by in house chemist Dr Paul Needs using methods as described in sections 2.4.2 and 3.4.1. Taxifolin, dimethyl sulfoxide (DMSO), trichloroacetic acid (TCA), protocatechuic acid, syringic acid, N,N-dimethylformamide (DMF), hippuric acid, Whatman® Mini-UniPrep® syringeless filters (0.45 µM pore, cat: WHAUN203NPUORG), mouse serum, and animal feeding needles (sterile, disposable, PTFE, size 18G, L × diam. 1.2 in. × 2 mm ball (cat: CAD9933-100EA), were purchased from Sigma Aldrich (UK). Methanol (MeOH), acetonitrile and UPLC glass vials with a 300 µL insert (cat: 10003264), were purchased from Fisher Scientific (UK). (−)-Epicatechin was purchased from Toronto Research Chemicals (Canada). Regular wall butterfly needles 25G¾" were purchased from Terumo (UK). Microvette 200 µl EDTA blood collection tubes were purchased from Sarstedt (Germany, cat: 20.1288.100).

2.4.2 Synthesis of hydroxyphenyl-γ-valerolactones

5-(3',4'-Dihydroxyphenyl)-γ-valerolactone (34DHPVL) was synthesised according to the procedure in chapter 3, section 3.4.1.

5-(4'-Hydroxy-3'-methoxyphenyl)-γ-valerolactone (4H3MPVL) and 5-(3',4',5'-trihydroxyphenyl)-γ-valerolactone (345THPVL) were synthesised according to the procedure by Chang *et al* (2010) (300).

All remaining hydroxyphenyl-γ-valerolactones were synthesised by an in house synthetic organic chemist (Dr Paul Needs, Quadram Institute Bioscience, UK). The synthetic routes were designed by Dr Needs and full descriptions are reported in Hollands *et al* (2020) (2). 5-(4'-Hydroxyphenyl)-γ-valerolactone 3'-*O*-glucuronide (4HPVL-3GlcA) and 5-(3'-hydroxyphenyl)-γ-valerolactone 4'-*O*-glucuronide (3HPVL-4GlcA) were synthesised as shown in Figure 2.1. A mixture of 5-(4'-hydroxyphenyl)-γ-valerolactone-3'-*O*-sulfate, ammonium salt (4HPVL-3S), 5-(3'-hydroxyphenyl)-γ-valerolactone-4'-*O*-sulfate, ammonium salt (3HPVL-4S) was prepared as per Figure 2.2.

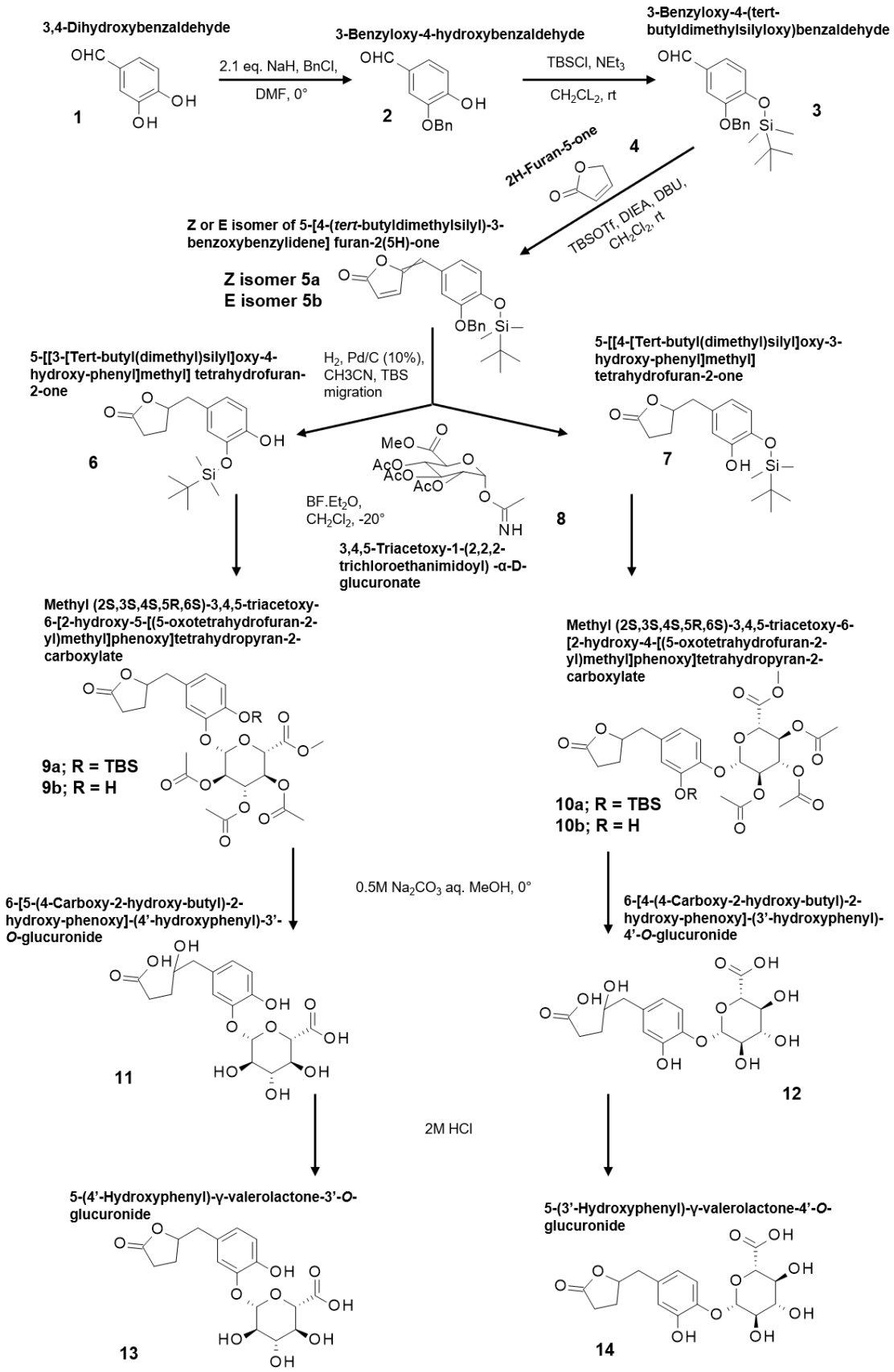

Figure 2.1: Synthetic steps to produce 3HPVL-4GlcA and 4HPVL-3GlcA

This Figure has been reproduced with permission by Hollands et al (2020) (2). Complete synthesis was performed by synthetic chemist Dr Paul Needs at the Quadram Institute Bioscience, UK, via the following steps.

Figure 2.1 (continued): *3-benzyloxy-4-hydroxybenzaldehyde 2 was silylated to give 3-benzyloxy-4-(tert-butyldimethylsilyloxy)benzaldehyde 3. Reaction of 3 with 4 by the general procedure of Chang et al (22) gave 5-[4-(tert-butyldimethylsilyl)-3-benzoxybenzylidene]furan-2(5H)-one as a mixture of its Z and E isomers 5a and 5b. Hydrogenation of 5a and 5b led to debenzylation and reduction, but also induced tert-butyldimethylsilyl group migration between the 3- and 4-hydroxyl groups, to give a mixture of the 3-silylated and 4-silylated products 6 and 7. Glucuronidation of the mixture of 6 and 7 with 8 gave the expected products 9a and 10a. During chromatography, smaller amounts of the desilylated 9b and 10b were formed. De-esterification and desilylation of 9a and 10a and 9b and 10b were achieved by hydrolysis with methanolic sodium carbonate, and undesired lactone ring-opening was reversed by treatment of 11 and 12 with hydrochloric acid. Finally, pure 13 and 14 were obtained by reverse phase preparative chromatography.*

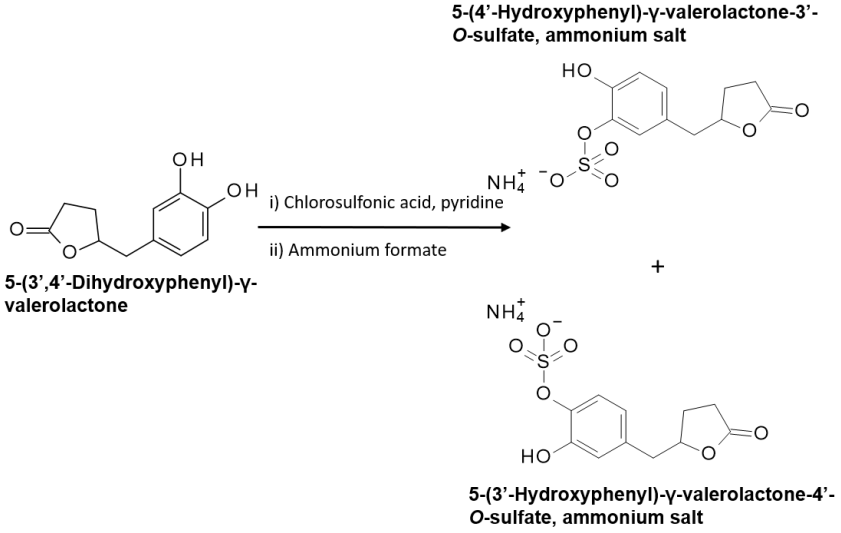

Figure 2.2: Synthetic steps to produce 4HPVL-3S and 3HPVL-4S
This Figure has been reproduced with permission by Hollands et al (2020) (2). Complete synthesis was performed by synthetic chemist Dr Paul Needs at the Quadram Institute Bioscience, UK, via the following steps. A mixture of 5-(3'-hydroxyphenyl)-γ-valerolactone-3'-O-sulfate, ammonium salt, and 5-(4'-dihydroxyphenyl)-γ-valerolactone-4'-O-sulfate, ammonium salt, was prepared by direct sulfation of 5-(3',4'-dihydroxyphenyl)-γ-valerolactone with chlorosulfonic acid.

2.4.3 Preparation of 34DHPVL and EC solution for use in the mouse study

A dose of 400 mg/70 kg body weight of compound was selected on the basis that this is an average flavonoid dose from tea, cocoa, and fruit consumption for humans in a day (301-305). Although EC consumption is estimated to be around 25 mg/day in Europe (306), this study was designed to attribute the total flavonoid dose consumed to EC, and to detect analytes in mice plasma and urine at concentrations above the limit of detection (LOD). This equates to 5.71 mg/kg body weight and was converted to the mouse equivalent dose using Formula 2.1, according to Nair *et al* (2016) (307). A 70.29 mg/kg body weight of compound was therefore required for a mouse, which when based

on the average weight of a 25 g mouse equates to 1.76 mg/25 g mouse. For convenience this value was rounded up to 2 mg/25 g mouse, which is equal to 8 mg/mL in solution. 34DHPVL and EC were given to the mice at equivalent doses to allow comparisons of plasma end-point concentrations.

$$\text{a) } MED\left(\frac{mg}{kg}\right) = Human\ dose\left(\frac{mg}{kg}\right) \times 12.3_{\text{ human to mouse ratio}}$$

$$\text{b) } 5.71\frac{mg}{kg} \times 12.3_{\text{ human to mouse ratio}} = 70.29\frac{mg}{kg}\ \text{mouse equivalent dose}$$

Formula 2.1: Conversion of human equivalent doses to mice equivalent doses
(a) Generic Formula where MED indicates mouse equivalent dose; (b) Actual calculation used to estimate the mouse equivalent dose for this study (307).

34DHPVL and EC were not fully soluble at the target concentration of 8 mg/mL, and so the lowest concentration of DMSO for solubilisation was determined. This was 1.34 % DMSO for 34DHPVL and 1.8 % DMSO for EC. Both 34DHPVL and EC were therefore dissolved in DMSO and made up to final volumes/concentrations with sterile ddH_2O on the same day as use and kept at 4 °C and were warmed to room temperature for 1-hour prior to use.

2.4.4 Study design

All experiments described here were performed in compliance with the European Union regulations concerning the protection of experimental animals and with the UK Home Office Animals (Scientific Procedures) Act of 1986 under personal license I39D37621 and project license 70/8710.

A total of 24 female C57BL/6J mice at 12 weeks old were purchased from the University of East Anglia's in-house breeding facility (Norwich, UK) and separated into six groups of four animals: 34DHPVL gavaged and sacrificed at 1, 2, 3, 6, and 24 hours, and a final EC gavaged group sacrificed after 24-hours. Female mice were selected because they are generally smaller than male mice and would thus require less weight-administered of the in-house synthesised 34DHPVL (308). All mice were maintained on the chow diet (RM3-P, SDS Special diet services, UK) provided by the housing facility before experimental procedures commenced. Baseline blood samples were obtained from all mice one week before the pharmacokinetic study commenced, to allow time for the removed blood to be replenished. Mice were warmed in a heating chamber at 39 °C for 10 mins prior to bloodletting. Afterwards, a tail bleeding procedure was performed, where a 25G¾" regular wall butterfly needle was inserted into the lateral vein of the tail and blood was collected into 200 µL

EDTA tubes. Baseline urine samples were obtained from the mice as and when they urinated during weighing or regular checks; a total of 8 baseline urine samples were obtained (in clean weighing chambers). All blood collections were centrifuged at 2000 g for 15 mins at 4 °C to collect the serum and stored at -80 °C until use.

To perform oral gavage, a tight scruff of the mouse neck and body was performed to allow for a wide-open mouth and no movement. The mouse was then held vertically upright where an 18-gauge feeding needle attached to a 1 mL syringe was inserted down through the mouth and into the stomach where 80 mg/kg body weight of 34DHPVL or 80 mg/kg body weight EC was released (prepared as per section 2.4.3). 34DHPVL was provided to five groups of 4 mice and EC was provided to one group of 4 mice. Each of the five 34DHPVL groups were sacrificed at either 1, 2, 3, 6 or 24-hours after gavage. The EC gavaged group were sacrificed at 24-hours post gavage.

Housing conditions consisted of 4 mice per cage which were kept in ventilation at 22 ± 2 °C with 55 ± 5 % humidity and 12-hour light-dark cycles. Mice cages were checked daily, and bedding, food and water changed weekly by housing facility staff. Pellets were kept in the cage hoppers and replenished weekly. All measurements and pellet changing was performed in ventilated cabinets.

2.4.5 Terminal anaesthesia and biological fluid harvest

Mice were sacrificed by cardiac puncture and PBS perfusion at times according to section 2.4.4. Initially, mice were anaesthetised using 4 % isoflurane (Abbott laboratories, US) in a mixture of nitrous oxide (70 %) and oxygen (30 %) and maintained throughout the whole procedure until death was confirmed. To determine the depth of the anaesthesia, patellar reflex measures were performed. Ethanol at 70 % was sprayed lightly onto the chest of the mouse and a lateral incision was made through the integument and abdominal wall. The diaphragm was cut through to allow access to the heart, and the sternum was clamped and placed over the head using a haemostat. Injection using a 1 mL syringe and 25G ¾" BD Precision Glide syringe needle was made into the left ventricle of the heart and blood was drawn into the syringe. Once blood was extracted, the right atrium was snipped, and PBS supplemented with EDTA was perfused into the left ventricle of the heart until organs turned pale and PBS circulated out clear (~50 mL). To collect urine, an open Eppendorf was placed at the base of the urethral orifice throughout the cardiac puncture procedure, this ensured urine dripped into the tube upon loss of muscle control. The number of mouse urine samples obtained for 1-hour post gavage was two, 2-hour timepoint was one, 3-hour timepoint was three, 6-hour timepoint was three, and 24-hour timepoint was four for 34DHPVL gavaged mice, and four for EC gavaged mice.

All blood collections were centrifuged at 2,000 g for 15 mins at 4 °C to collect the plasma and stored at -80 °C until use.

Two mice died before they were scheduled for termination, one because it was severely underweight and the second because of complete ingestion of the oral gavage tubing, and as a result only 3 sets of mouse biological fluids were collected for the 2 and 6-hours 34DHPVL gavaged mice.

2.4.6 Development of a quantitative analytical method for 3',4'-dihydroxyphenyl-γ-valerolactone and its metabolites in mouse plasma

Hydroxyphenyl-γ-valerolactones have proven difficult to extract from plasma and erythrocytes. Mülek and Högger have published several papers and a thesis that details the challenges and suggest suitable approaches for extraction and analysis of HPVLs from both plasma and erythrocyte samples (309-313). It has been reported that 34DHPVL strongly binds to serum proteins with the estimate of the bound fraction being 98.3 ± 4.4 % (309) and an erythrocyte/plasma partition ratio of 32.8 ± 64.6 (310).

Mülek's thesis (312) and subsequent published paper (311) highlights the method development steps for the extraction of HPVLs from plasma and erythrocytes. A method development protocol was devised for the detection of these compounds in the plasma of mice with aim for a reliable method to obtain good yields and consistent recoveries of the compounds. Due to the complexity to achieve this, Table 2.1 describes the 16 methods that were trialled. One of two final methods selected produced some unexplained disparities in the results of the run; this is detailed in section 2.5.1 later in this chapter.

Table 2.1 outlines the main methods attempted, the problems that surfaced and whether the method(s) were pursued further. To summarise, initial attempts provided low recoveries of 4H3MPVL, and following suitable checks, Dr Shikha Saha (analytical chemist, Quadram Institute, UK) optimised the UPLC-MS^2 parameters for compound detection. Consequently, good recoveries and low concentrations were detected.

For other compounds, there were regular issues for providing consistent results. Method 6 in Table 2.1, proved to provide strong recovery values for all compounds, but these were inconsistent between replicate standards. Because of this, new methods were trialled for protein precipitation (PPT), liquid-liquid extraction (LLE), solid-phase extraction (SPE) and combinations of these, PPT:LLE, LLE:PPT, and PPT:SPE. Method 14, an SPE method, provided greater consistency between

replicates, but not for *O*-sulfates. Adjustment of the elution pH above the *O*-sulfates pK_a value greatly improved this. An acidic elute step was used in conjunction to wash the aglycone and *O*-glucuronides off the SPE cartridge, method 16.

The two methods, 6 and 16, were selected for two final processes of the mouse plasma samples. The two methods would allow for the full detection of all HPVLs in the mouse plasma, where all compounds except for 34DHPVL and 345THPVL would have consistent reliable recoveries.

The detection of EC and conjugates were identified in plasma using a routine method from within our laboratory (2). The same applies for the detection of hydroxyphenyl-γ-valerolactones and EC conjugates in urine (2).

Table 2.1: Method development steps for the processing of mouse plasma for UPLC-MS² detection of hydroxyphenyl-γ-valerolactones

The main methods attempted are listed alongside a brief overview of the results and whether it was pursued further or not. References are listed for those where the method has been obtained and edited from. FA: formic acid; PPT: protein precipitation; SPE: solid phase extraction; LLE: liquid-liquid extraction.

Method number	Method	Preparation type	Mobile phase	Results	Conclusion	References
1	10 µL of formic acid + 10 µL of N,N'-DMF, vortex, stand 20 mins, vortex centrifuge at 13,300 rpm.	PPT	A - 0.1 % FA in H_2O B - 0.1 % FA in MeCN	Only able to detect 4HPVL-3GLcA and 3HPVL-4GlcA	Lack of detection of HPVLs	In house method
2	12 µL of 50 % H_3PO_4 +120 µL of KH_2PO_4, vortex, centrifuge 15 mins at 13,300 rpm. ProElut™ PLS SPE cartridges (Dikma Technologies) - preconditioning: 3 mLs MeOH, 3 mLs H_2O; plasma loaded; wash: 3 mLs H_2O, 3 mLs 60:40 0.1 % FA:methanol; elute: 0.1 % formic acid aqueous solution: methanol, 10:90 (v/v).	SPE	A - 0.1 % FA in H_2O B - 0.1 % FA in MeCN	1st run: No detection of 4H3MPVL in the first run. 2nd run: Poor recovery of all compounds.	Further tests proved 4H3MPVL was not adhering to the column and had not degraded. There were also no signs of the solvent causing compound degradation. Further investigation showed poor ionisation of 4H3MPVL, to account for this the collision energy was altered to allow for increasing sensitivity in detection of the compound. The wash step was found to elute target analytes prior to sample collection (in 3x elution collections).	(314)
3	2 parts MeCN to 1-part plasma with 1 % FA, vortex, centrifuge 15 mins 13,300 rpm.	PPT	A - 0.1 % FA in H_2O B - 0.1 % FA in MeCN	Poor recovery of all target analytes. Lots of background noise.		In house method

Table 2.1: Method development steps for the processing of mouse plasma for UPLC-MS2 detection of hydroxyphenyl-γ-valerolactones (continued)

Method number	Method	Preparation type	Mobile phase	Results	Conclusion	References
4	3:1 ratio of 2 % FA in MeCN to plasma, vortex, sonicate 10 mins, centrifuge 3 mins 13,300 rpm. Extract supernatant. To the same matrix: add in 3:1 ratio of MeCN with 0.1 mM NH_4OH to plasma matrix, vortex, sonicate 10 mins, centrifuge 3 mins at 13,300 rpm (do this a total of 3 times). Collect all supernatants into one tube, evaporate to dryness and reconstitute in MeOH:H_2O:FA (10:89:1). Vortex, centrifuge 13,300 rpm 3 mins.	PPT	A - 0.1 % FA in H_2O B - 0.1 % FA in MeCN	No detection of 345THPVL at low concentrations.		In house modified version from (315)
5	Dilute plasma 1:2 in H_2O. ProElut™ PLS SPE cartridges (Dikma Technologies) - preconditioning: 3 mLs MeOH, 3 mLs H_2O; load diluted plasma; wash - 4 mLs H_2O in 0.1 % FA; elution: - 500 µL 4:4:2 MeOH:MeCN:FA, perform 3 times. Run elutes separately in the UPLC-MS.	SPE	A - 0.1 % FA in H_2O B - 0.1 % FA in MeCN	40-60 % recovery of all compounds.	Target analytes lost during the wash phase; target analytes not fully eluted during first standard elution step, at least two additional elution steps required.	In house modified version from (314)
6	50 µL plasma with 30 µL 35 % TCA, 10 µL MeCN. Ice 5 mins, centrifuge 15 mins at 13,300 rpm	PPT	A - 0.1 % FA in H_2O B - 0.1 % FA in MeCN	Good recoveries of all target analytes, however, there were highly variable and inconsistent recovery values, even for duplicate standards.	Good working method with minor problems for inconsistent recoveries.	In house

Table 2.1: Method development steps for the processing of mouse plasma for UPLC-MS2 detection of hydroxyphenyl-γ-valerolactones (continued)

Method number	Method	Preparation type	Mobile phase	Results	Conclusion	References
7	3:1 ratio of 2 % FA in MeCN to plasma, vortex, sonicate 10 mins, centrifuge 3 mins at 13,300 rpm. Extract supernatant. To the same matrix repeat 3 times. Evaporate supernatant to dryness and reconstitute in 4:4:2 MeOH:MeCN:FA, vortex, centrifuge at 13,300 rpm 3 mins.	PPT	A – 0.1 % FA in H_2O B – 0.1 % FA in MeCN	Poor recovery of all target analytes. No detection of 345THPVL.		
8	Dilute plasma 1:2 in H_2O. ProELUT™ PLS SPE - preconditioning: 3 mLs MeOH, 3 mLs H_2O; load diluted plasma; wash – 4 mLs H_2O in 0.1 % FA; elution: - 4:4:2 MeOH:MeCN:FA, perform 3 times. Dry down elutes and resuspend in volume of elution buffer. (The drying stage and pooling of elutions makes this different to method 5).	SPE	A – 0.1 % FA in H_2O B – 0.1 % FA in MeCN	No detection of 34DHPVL and 345THPVL. Lower recovery of all target analytes in comparison to method 5.	The drying step caused significant loss of target analytes as the lack of a drying step (in method 5) resulted in higher recovery of the target analytes.	In house method
9	25 µL of 4 % H_3PO_4 and 450 µL EA (ethyl acetate)/MTBE (tert-butyl methyl ether) (1:1, V/V) to plasma. Collect the supernatant, repeat the process again on the matrix and pool the supernatants together. Vortex 1 min, centrifuge at 3,300 g for 15 mins 4 °C. Evaporate to dryness, reconstitute in 100 µL MeOH. Vortex 15 mins 2500 g, centrifuge at 18,000 g 15 mins 4 °C.	LLE	A – 5 mM NH_4HCO_2 with 0.065 % (v/v) formic acid (Ph = 3.2). B - 0.1 % formic acid in MeOH	Better recoveries of 34DHPVL and 345THPVL, but poorer recoveries for 4HPVL-3GlcA, 3HPVL-4GlcA and 4H3MPVL when compared to method 6.		(312)
10	30 µL 35 % TCA, 10 µL MeCN. Ice 5 mins, centrifuge 15 mins at 13,300 rpm. Extract supernatant, and on the same matrix add 25 µL of 4 % H_3PO_4 and 450 µL EA/MTBE (1:1, V/V). Collect the supernatant and repeat the liquid liquid extraction on the same matrix. Pool the supernatants together and vortex 1 min, centrifuge at 3,300 g 15 mins 4 °C. Evaporate to dryness, reconstitute in 100 µL MeOH. Vortex 15	LLE & PPT	A – 5 mM NH_4HCO_2 with 0.065 % (v/v) formic acid (Ph = 3.2). B - 0.1 % formic acid in MeOH	Poor recovery of all target analytes, low concentrations barely detected.		In house modified version from (312)

Table 2.1: Method development steps for the processing of mouse plasma for UPLC-MS2 detection of hydroxyphenyl-γ-valerolactones (continued)

Method number	Method	Preparation type	Mobile phase	Results	Conclusion	References
	mins at 2500 g, centrifuge at 18,000 g for 15 mins at 4°C.					
11	25 µL of 4 % H_3PO_4 and 450 µL EA /MTBE (1:1, V/V). Collect the supernatant and then repeat the process again on the matrix and pool the supernatants together. Then on the same matrix add 30 µL 35 % TCA, 10 µL MeCN. Ice 5 mins, centrifuge for 15 mins at 13,300 rpm. Pool the supernatant with the other aliquots and vortex 1 min, centrifuge at 3,300 g for 15 mins at 4°C. Evaporate to dryness, reconstitute in 100 µL MeOH. Vortex for 15 mins at 2500 g, centrifuge at 18,000 g for 15 mins at 4°C.	LLE & PPT	A – 5 mM NH_4HCO_2 with 0.065 % (v/v) formic acid (Ph = 3.2). B - 0.1 % formic acid in MeOH The same samples were also run with different mobile phase A – 0.1 % FA in H_2O. B – 0.1 % FA in MeCN.	Poor inconsistent recoveries. 345THPVL and HPVL-GlcA signal intensities were slightly lower in comparison to method 6. The change of mobile phase produced better results which improved the detection of 345THPVL and the glucuronides. But, this did not improve the inconsistencies.	Overall, poor inconsistent recovery of all target analytes.	In house modified version from (312)
12	Using a 96 well µ-SPE OASIS PRIME HLB plate. Pre-condition: 250 µL MeOH, and 250 µL 0.2 % acetic acid. Load sample. Wash: 200 mL H_2O and further with 200 mL of 0.2 % acetic acid. Samples eluted with 60 µL MeOH.	SPE	A – 0.1 % FA in H_2O B – 0.1 % FA in MeCN	Poor detection and recovery for all target analytes.	Although this method has been published and used by several authors. It has provided poor recovery values for all the target analytes.	(316-318)

Table 2.1: Method development steps for the processing of mouse plasma for UPLC-MS2 detection of hydroxyphenyl-γ-valerolactones (continued)

Method number	Method	Preparation type	Mobile phase	Results	Conclusion	References
13	STRATA-X cartridges of 33 µm pore size and a 30 mg capacity with a 3 mL maximum used. Precondition: 3 mL 0.25 % FA in MeOH, 3 mL of 0.1 % FA. Cartridge loaded with 500 µL of 0.1 % FA, do not drain. Load 1:1 diluted plasma with 4 % H_3PO_4. Load 500 µL of 0.1 % FA. Drain. Wash: 3 mLs of H_2O, 3 mLs of 2 % MeOH. Dry cartridge for 20 mins. Elute: soak for 10 mins with 2 mLs 0.25 % FA in MeOH, collect elute, elute with a further 2 mLs 0.25 % FA in MeOH. Centrifugal evaporated to 200 µL.	SPE	A – 0.1 % FA in H_2O B – 0.1 % FA in MeCN	Poor and inconsistent recoveries for all target analytes.		In house modified version of (319)
14	STRATA-X cartridges of 33 µm pore size and a 500 mg capacity with a 6 mL maximum used. Precondition: 6 mL 0.25 % FA in MeOH, 6 mL of 0.1 % FA. Load: 500 µL of 0.1 % FA, not drained. Load 1:1 diluted plasma diluted with 4 % H_3PO_4. 500 µL of 0.1 % FA loaded. Drain. Wash: 6 mLs of H_2O, 6 mLs of 2 % MeOH. Dry cartridge for 20 mins. Elute: soak for 10 mins with 5 mLs 0.25 % FA in MeOH, collect elute, elute with a further 2 mLs 0.25 % FA in MeOH. Centrifugal evaporate to 200 mL.	SPE	A – 0.1 % FA in H_2O B – 0.1 % FA in MeCN	Consistent recoveries around 50-60 % for all standards except for 34DHPVL, with a recovery of 10-15 %. 345THPVL was almost undetectable with this method. Really low detection limits for the sulfate compounds.	Method further optimised to allow for the detection of sulfate analytes (method 16).	In house modified version of (319)
15	STRATA-X SPE Microelution in a 96 well plate. Precondition wells: 250 µL 0.25 % FA in MeOH, 250 µL of 0.1 % FA. Load wells: 100 µL of 0.1 % FA, do not drain. Load 1:1 diluted plasma diluted with 4 % H_3PO_4. Load 100 µL of 0.1 % FA. Drain. Wash: 200 µL of H_2O, 200 µL of 2 % MeOH. Dry cartridge for 10 mins. Elute: soak for 5 mins with 100 mL 0.25 % FA in MeOH, collect elute.	SPE	A – 0.1 % FA in H_2O B – 0.1 % FA in MeCN	Poor and inconsistent recoveries for all target analytes.		In house modified version of (319)

Table 2.1: Method development steps for the processing of mouse plasma for UPLC-MS2 detection of hydroxyphenyl-γ-valerolactones (continued)

Method number	Method	Preparation type	Mobile phase	Results	Conclusion	References
16	STRATA-X cartridges of 33 µm pore size and a 500 mg capacity with a 6 mL maximum volume were used. Precondition: 6 mL 0.25 % FA in MeOH, 6 mL of 0.1 % FA. Load: 500 µL of 0.1 % FA, do not drain. Plasma diluted 1:1 with 4 % H_3PO_4 loaded. 500 µL of 0.1 % FA loaded. Drain. Wash: 6 mLs of H_2O, 6 mLs of 2 % MeOH. Dry cartridge for 20 mins. Elute: soak for 10 mins with 5 mLs 0.25 % FA in MeOH, collect elute, elute with a further 2 mLs 0.25 % FA in MeOH. Soak a further 5 mL of MeOH with 2 % NH_4OH (pH 10.50), soak for 10 mins. Elute through. Elute again with 1 mL (MeOH with 2 % NH_4OH (pH 10.50). Centrifugal evaporate to 200 µL.	SPE	A: 10 mM Ammonium Acetate in water, Ph 5 B: 10 mM Ammonium Acetate in acetonitrile, Ph 5 The same samples were also run with different mobile phase A – 0.1 % FA in H_2O. B - 0.1 % FA in MeCN.	Good consistent recoveries for all target analytes around 50-60 %, except for 34DHPVL, with a recovery around 15 %. 345THPVL was almost undetectable with this method. Almost 100 % recovery of the sulfates using this method.	Good consistent recoveries with and reliable method. This method would be used on the mouse plasma samples in conjunction with method 6. By using two methods, it allows for the detection of 34DHPVL and 345THPVL in the samples whilst providing consistent recoveries for the remaining analytes.	In house modified version of (319)

2.4.7 UPLC-MS analysis for plasma

2.4.7.1 Stock preparation of seven hydroxyphenyl-γ-valerolactones

Seven hydroxyphenyl-γ-valerolactones: 5-(3',4'-dihydroxyphenyl)-γ-valerolactone (34DHPVL), 5-(3',4',5'-trihydroxyphenyl)-γ-valerolactone (345THPVL), 5-(4'-hydroxy-3-methoxyphenyl)-γ-valerolactone (4H3MPVL), 5-(4'-hydroxyphenyl)-γ-valerolactone-3'-*O*-glucuronide (4HPVL-3GlcA), 5-(3'-hyroxyphenyl)-γ-valerolactone-4'-*O*-glucuronide (3HPVL-4GlcA), 5-(3'-hydroxyphenyl)-γ-valerolactone-4'-*O*-sulfate sodium salt (3HPVL-4S), 5-(4'-hydroxyphenyl)-γ-valerolactone-3'-*O*-sulfate sodium salt (4HPVL-3S), were resuspended in 100 % DMSO to make final stocks of 1 mg/mL, stored at -20 °C until use. Aliquots of all the seven HPVLs were pooled together to make a stock that contained each metabolite at 143 µg/mL. A standard curve was prepared from the 143 µg/mL stock for concentrations ranging from 195 ng/mL to 50 µg/mL in final solvent concentration of 65 % methanol with 35 % DMSO (v/v).

2.4.7.2 Serum standard curve preparation with hydroxyphenyl-γ-valerolactones

Triplicate serum standard curves were prepared using 50 µL volumes of mouse serum (Sigma, UK) spiked with 2.895 µL of pre-prepared pooled phenyl-γ-valerolactone stocks in 65 % methanol with 35 % DMSO (v/v) (195 ng/mL to 50 µg/mL) (from section 2.4.7.1), ranging from final plasma concentrations of 2500 ng/mL to 0 ng/mL, using a total of ten concentrations. A 5 µL aliquot of 1 mg/mL of the internal standard syringic acid, prepared in 100 % methanol, was spiked into the serum standard curve. For post-spiked plasma samples, 50 µL of plasma was processed according to section 2.4.7.3, and the final samples were spiked with the HPVLs and internal standard stocks in the same volumes and concentrations as the pre-spiked samples, in triplicate.

All processed pre-spiked and post-spiked standards were spiked with 5 µL of 1 mg/mL protocatechuic acid in 100 % methanol, to act as a volume standard for the run, giving a final volume of 60 µL (50 + 5 + 5 µL).

2.4.7.3 Hydroxyphenyl-γ-valerolactone detection in mouse plasma: plasma crash technique

Plasma samples in 50 µL volumes from the C57BL/6J mice study, detailed in section 2.4.4/2.4.5, were spiked with 5 µL of 1 mg/mL syringic acid in 100 % methanol. Plasma was processed prior to UPLC-MS^2 analysis as follows: 65 µL of 100 % acetonitrile was added to plasma and vortexed, followed by 30 µL of ice cold 35 % trichloroacetic acid (in water, v/v) and further vortexing. Samples

were placed on ice for 15 mins and then centrifuged at 13,300 rpm for 15 mins at 4 °C. The supernatant was collected into 300 µL glass vial inserts and 5 µL of the volume standard (1 mg/mL protocatechuic acid in 100 % methanol), was added. All samples and standards were injected at 2 µL with a flow rate of 0.4 mL/min into an Agilent 1200 series LC 6490 Triple Quad LC-MS mass spectrometer (Agilent Technologies, CA, US), using a Waters Acquity UPLC HSST3 Column (100 x 2.1 x 1.7 µm), and with mobile phase A (0.1 % formic acid in H_2O), and B (0.1 % formic acid in acetonitrile). The gradient was run according to Table 2.2. The retention times, parent and daughter ions, collision energies, polarity and cell accelerator voltage for each of the compounds investigated are shown in Table 2.4.

Response areas from samples were acquired using Agilent Masshunter Quantitative Analysis software as supplied by the instrument manufacturer. Standard curves were plotted (Appendix Figure 1) for the post-processed spiked standards and these used to calculate the response factors for each of the compounds (Table 2.4). Recoveries of the standards from the pre-spiked to post-spiked samples were calculated following concentration determination according to Formula 2.2. Recovery ranges for each compound are also displayed in Table 2.4, alongside limits of detection (LOD) values.

$$R = \frac{A_x}{A_{IS}} \div \frac{C_x}{C_{IS}}$$

Formula 2.2: Calculation of the response factors following UPLC-MS²
Peak area values following quantification of UPLC-MS results were subjected to this formula to obtain response factors and concentration values for each compound in biological samples. R: response factor for post-spiked standards; A_x: response area of the compound of interest; A_{IS}: response area for the internal standard; C_x: concentration of the compound of interest (ng/mL); C_{IS}: concentration of the internal standard (ng/mL).

Table 2.2: Gradient applied throughout the UPLC-MS² run in the Agilent 12000 series LC 6490 Triple Quad
This gradient was used for the methods outlined in sections 2.4.7.3, 2.4.7.4 and 2.4.8.2 for plasma and urine processed samples.

Time (mins)	% Mobile A	% Mobile B
0.00	100	0
0.50	100	0
20.00	82	18
30.00	5	95
30.10	100	0
35.00	100	0

2.4.7.4 Phenyl-γ-valerolactone detection in mouse plasma: cartridge filtration technique

Standards were prepared as per section 2.4.7.2 for the pre-spiked and the post-spiked standards (n = 6 replicates).

Mouse plasma samples (50 µL) volumes were spiked with 5 µL of 1 mg/mL syringic acid in 100 % methanol and processed as follows: STRATA-X cartridges (500 mg capacity, 6 mL maximum volume load, 33 µm pore size) were hydrated by loading 6 mL of 0.25 % formic acid in MeOH and drained under vacuum, then equilibrated with 6 mL of 0.1 % formic acid with draining, loaded with 500 µl of 0.1 % formic acid (without draining), sample loaded (100 µL) and a further 500 µL of 0.1 % formic acid loaded; the cartridge was drained to dryness around 1 drop/second and then washed with 6 mL of ddH_2O and 6 mL of 2 % MeOH (both under vacuum) before being completely dried (30 mins under vacuum); the cartridge was eluted at 1 drop per second: 5 mL of 0.25 % formic acid in MeOH, after soaking for 10 mins 1 mL of 0.25 % formic acid in MeOH; a 5 mL of 2 % NH_4OH in MeOH (pH 10.5), after soaking for 10 mins 1 mL of 2 % NH_4OH in MeOH (pH 10.5). The final 12 mL of eluted sample was dried to approximately 200 µL using a Genevac EZ-2 Elite centrifugal evaporator (Biopharma, UK). If the sample volume was significantly below the 200 µL then it was made up to approximately 200 µL with 0.25 % formic acid in MeOH. Samples were then centrifuged for 10 mins at 17,000 g to pellet any remaining debris and the supernatant placed into vials where 5 µL of 1 mg/mL protocatechuic acid was added as a volume standard.

Samples were run on the UPLC-MS^2 exactly as described in section 2.4.7.3. The recovery values are displayed in Table 2.4.

2.4.7.5 Serum standard curve preparation with (−)-epicatechin conjugates and hydroxyphenyl-γ-valerolactones

Stock standards of five hydroxyphenyl-γ-valerolactones: 34DHPVL, 3HPVL-4S, 4HPVL-3GlcA, 3HPVL-4GlcA, 4H3MPVL, and (−)- epicatechin were resuspended in 100 % DMSO to make final stocks of 1 mg/mL, stored at -20 °C until use. Aliquots of all the six compounds were pooled together to make a stock of 167 µg/mL. A standard curve was prepared from the 167 µg/mL stock for concentrations ranging from 50 ng/mL to 40 µg/mL in final solvent concentration of 76 % methanol with 24 % DMSO (n = 3). These were prepared using 50 µL of mouse serum (Sigma, UK) spiked with 2.5 µL of pre-prepared pooled stock in 76 % methanol and 24 % DMSO ranging from final plasma concentrations of 1730 ng/mL to 0 ng/mL, using a total of nine concentrations. A 5 µL aliquot of 3 µg/mL internal standard taxifolin (prepared in 100 % methanol), was added to the serum standard curve. Final pre-processed plasma was therefore 57.5 µL and processed according to section

2.4.7.6. For post-spiked plasma samples, 50 µL of plasma was processed according to section 2.4.7.6, and the final samples were spiked with the 76 % methanol and 24 % DMSO stocks of compounds as well as internal standard, in the same volumes and concentrations as the pre-spiked samples (n = 3).

2.4.7.6 (−)-Epicatechin and conjugates detection in plasma

Only EC gavaged mice plasma samples were monitored using this method alongside the pre-prepared standards (section 2.4.7.5). Plasma mouse samples were spiked with 5 µL of 3 µg/mL taxifolin in 100 % methanol. Plasma was processed prior to UPLC-MS analysis by performing the following: 65 µL of 100 % acetonitrile was added to plasma and vortexed, followed by 30 µL of ice cold 35 % trichloroacetic acid (in water, v/v), and vortexed; samples were placed on ice for 15 mins and centrifuged at 13.3 rpm for 15 mins at 4 °C; the supernatant was collected into 300 µL glass vial inserts.

All samples and standards were injected at 2 µL with a flow rate of 0.4 mL/min and separated with a Waters Acquity UPLC HSST3 Column (100 x 2.1 x 1.7 µm) on a Waters Acquity i-Class UPLC with Waters Xevo TQ-S micro triple quadrupole MS (Waters Ltd, Wilmslow, UK). The mobile phase A consisted of 0.1 % formic acid in H_2O, and the mobile phase B consisted of acetonitrile with 0.1 % formic acid. The column was kept at a 35 °C temperature and samples kept at 10 °C during the run. The gradient was run according to Table 2.3. The retention times, MRM and collision energies for each of the compounds investigated are shown in Tables 2.5. Please note, no recovery values, LOD, or response factors from the standard curves are provided because no compounds were detected, with the exception of spiked standards, in the 24-hour post gavage plasma samples of EC-gavaged mice.

Response areas from the samples were analysed using Waters MassLynx MS software as supplied by the instrument manufacturer. There was no standard for epicatechin sulfate or epicatechin glucuronide, so it was searched for based on its MRM transitions and by reference to (−)-epicatechin which was used to confirm the retention time.

Table 2.3: Gradient applied throughout the UPLC-MS^2 run in the Waters Acquity i-Class UPLC
This gradient was applied to the method outlined in section 2.4.7.6.

Time (mins)	% Mobile A	% Mobile B
0	97	3
2	97	3
6	80	20
10	50	50
12	5	95
13	5	95
13.10	97	3
15.00	97	3

Table 2.4: UPLC-MS² input and output data for compound detection in plasma and urine

In addition to the ion-pairs and the retention times, the recovery values and response factors for each compound for the methods used have been listed. Response factors are calculated from the standard curves obtained from matrix-matched standards that were SPE extracted and analysed in the same way as real samples, and the recovery ranges are calculated from the standard curves obtained for blank matrix samples spiked pre-processing compared to those spiked post-processing. The protein-precipitation (PPT) method is detailed in section 2.4.7.3, solid-phase extraction (SPE) method in section 2.4.7.4, and urine method in section 2.4.8. Rows highlighted in bold were the MRM transitions used for the final compound quantification in the samples.

Compound	Parent Ion	Daughter Ion	Dwell	Collision Energy	Cell Accelerator Voltage	Polarity	Retention Time (mins)	Response Factor for plasma standard curve	Response Factor for urine standard curve	Recovery range (%) – plasma PPT method	Recovery range (%) – plasma SPE method	Recovery range (%) – urine method	Limit of detection (ng/mL)
4HPVL-3GlcA	**383.09**	**207.1**	**80**	**26**	**4**	**Negative**	**12.65**	**38.899**	**0.527**	**73-108**	**47-61**	**67-94**	**5**
4HPVL-3GlcA	383.09	162.9	80	42	4	Negative	12.65	20.526	0.210	60 -105	48-70	70-92	15
4HPVL-3GlcA	383.09	113	80	25	5	Negative	12.65	10.054	0.084	48-129	43-77	68-93	12
3HPVL-4GlcA	**383.09**	**207.1**	**80**	**26**	**4**	**Negative**	**11.85**	**30.993**	**0.450**	**64-106**	**47-73**	**71-90**	**5**
3HPVL-4GlcA	383.09	162.9	80	42	4	Negative	11.85	17.547	0.181	65-107	46-68	71-93	5
3HPVL-4GlcA	383.09	113	80	25	5	Negative	11.85	9.427	0.079	65-138	43-64	66-92	7
4HPVL-3S	**287**	**207**	**80**	**26**	**5**	**Negative**	**12.43**	**242.61**	**4.911**	**66-99**	**45-97**	**66-89**	**2**
4HPVL-3S	287	163	80	26	5	Negative	12.43	458.65	2.471	63-94	45-97	70-96	3
3HPVL-4S	**287**	**207**	**80**	**26**	**5**	**Negative**	**12.11**	**153.15**	**1.543**	**53-106**	**22-30**	**62-90**	**10**
3HPVL-4S	287	163	80	26	5	Negative	12.11	83.98	0.774	55-108	22-30	63-86	6
4H3MPVL	**223.1**	**103**	**80**	**38**	**4**	**Positive**	**18.80**	**159.53**	**1.569**	**73-114**	**47-75**	**72-91**	**4**
4H3MPVL	223.1	76.9	80	62	4	Positive	18.80	87.752	1.005	69-109	47-67	74-91	15
345THPVL	223.06	179	80	18	5	Negative	9.00	5.912	2.38	0-39	0	51-102	900
345THPVL	**223.06**	**138**	**80**	**26**	**5**	**Negative**	**9.00**	**1.16**	**0.488**	**0-42**	**0-6**	**59-100**	**200**

Table 2.4: UPLC-MS^2 input and output data for compound detection in plasma and urine (continued)

Compound	Parent Ion	Daughter Ion	Dwell	Collision Energy	Cell Accelerator Voltage	Polarity	Retention Time (mins)	Response Factor for plasma standard curve	Response Factor for urine standard curve	Recovery range (%) – plasma PPT method	Recovery range (%) – plasma SPE method	Recovery range (%) – urine method	Limit of detection (ng/mL)
34DHPVL	207.06	162.8	80	18	5	Negative	13.39	104.21	2.733	53-199	0-12	87-101	12
34DHPVL	**207.06**	**122**	**80**	**26**	**5**	**Negative**	**13.39**	**33.912**	**0.955**	**43-109**	**5-11**	**87-101**	**3**
Syringic Acid	**196.7**	**181.8**	**80**	**26**	**5**	**Negative**	**12.45**	**NA**	**NA**	**NA**	**NA**	**NA**	**NA**
Syringic Acid	196.7	123.1	80	26	5	Negative	12.45	NA	NA	NA	NA	NA	NA
Protocatechuic Acid	**152.9**	**108.9**	**80**	**26**	**5**	**Negative**	**5.87**	**NA**	**NA**	**NA**	**NA**	**NA**	**NA**

Table 2.5: Additional compound detection from the urine of mice by UPLC-MS²
This table includes the additional compounds searched for from the urine of mice, that are not listed in Table 2.4.

Compound	Parent Ion	Daughter Ion	Dwell	Cell Accelerator Voltage	Collision Energy (V)	Polarity	Retention Time (mins)	Response Factor for urine standard curve	Recovery range (%) in urine	Limit of detection (ng/mL)
Epicatechin glucuronide	465.1	289.1	80	5	18	Negative	Undetectable	NA	NA	NA
Epicatechin sulfate	369.03	289.03	80	5	15	Negative	14.76	NA	NA	NA
Epicatechin	289	245	80	5	11	Negative	14.07	0.389	73-92	15
Hippuric acid	179.84	104.9	80	5	15	Positive	9.90	0.821	80-97	0.25

Table 2.6: UPLC-MS^2 parameters used in the analysis of (−)-epicatechin and its phase-II conjugates in mouse plasma samples
The method is detailed in section 2.4.7.6.

Compound	Parent Ion	Daughter Ion	Dwell	Collision Energy (V)	Cone (V)	Polarity	Retention Time (mins)
Epicatechin	290.88	122.98	0.006	20	20	Positive	6.25
Taxifolin	304.90	149.00	0.006	24	26	Positive	7.57
34DHPVL	206.78	121.92	0.006	20	40	Negative	6.65
3HPVL-4S	286.78	108.86	0.006	36	20	Negative	6.23
4HPVL-3S	286.78	108.86	0.006	36	20	Negative	6.40
Epicatechin sulfate	369.03	289.03	0.006	15	25	Negative	6.48
3HPVL-4GlcA	382.78	207.02	0.006	20	20	Negative	5.79
4HPVL-3GlcA	382.78	207.02	0.006	20	20	Negative	6.06
Epicatechin glucuronide	465.10	289.10	0.006	18	25	Negative	5.41

2.4.8 UPLC-MS analysis of urine

2.4.8.1 Stock preparation of compounds

Five hydroxyphenyl-γ-valerolactones: 34DHPVL, 345THPVL, 4H3MPVL, 4HPVL-3GlcA, 3HPVL-4GlcA, as well as epicatechin and hippuric acid were resuspended in 100 % DMSO to make final stocks of 1 mg/mL, the remaining two hydroxyphenyl-γ-valerolactones, 3HPVL-4S, and 4HPVL-3S were resuspended in 100 % MeOH at 1 mg/mL, and stored at -20 °C until use. Aliquots of all the seven hydroxyphenyl-γ-valerolactones, (−)-epicatechin and hippuric acid were pooled together to make a stock of 100 µg/mL at 77.7 % DMSO with 22.2 % MeOH (v/v) concentration. A standard curve was prepared from the 100 µg/mL stock for concentrations ranging from 195 ng/mL to 50 µg/mL in final solvent concentration of 38.8 % DMSO with 61.1 % MeOH.

2.4.8.2 Methanol standard curve preparation for quantification of urine compounds

Standard curves were prepared (n = 3) using 190 µL of 100 % MeOH spiked with 10 µL of pre-prepared pooled compounds (section 2.4.8.1), ranging from final standard concentrations of 2500 ng/mL to 0 ng/mL, using a total of ten concentrations. A 10 µL aliquot of 1 mg/mL internal standard taxifolin (prepared in 100 % methanol) was spiked into the MeOH standard curve. Final pre-processed standards were therefore of 200 µL volume. Standards were then processed according

to the method outlined in section 2.4.8.3. For post-spiked MeOH samples, 190 µL of MeOH was processed according to section 2.4.8.3, and the final samples were spiked with the compound stocks and internal standard stocks in the same volumes and concentrations as the pre-spiked samples (n = 3).

All processed pre-spiked and processed post-spiked standards were spiked with 5 µL of 1 mg/mL protocatechuic acid (in 100 % methanol), to act as a volume standard for the run.

2.4.8.3 Hydroxyphenyl-γ-valerolactone and (−)-epicatechin conjugate analysis of mouse urine

The target volume of mouse urine for analysis was 190 µL, but for collected samples of less than this volume, the maximum available volume was used, and the method was scaled down accordingly. Mouse urine samples (190 µL) were spiked with 10 µL of 1 mg/mL taxifolin (in 100 % methanol). Urine was processed prior to UPLC-MS^2 analysis as follows: 200 µL of 5 % TCA was added and vortexed followed by 100 µL of DMF; the samples were vortexed and left at room temperature for 20 mins and vortexed again before being centrifuged (10 mins at 13,300 rpm) and spiked with 5 µL of 1 mg/mL protocatechuic acid; these were then filtered through Whatman® 0.45 µM filter vials, which held a maximum capacity of 400 µL.

Samples were then run on the UPLC-MS^2 according to the exact specifications outlined in section 2.4.7.3. There were further additional ion pairs screened for the compounds listed in Table 2.6.

The maximum concentration run for the standard curve was lower than the maximum concentration detected in the samples (typically the 1-hour samples). Because of this, an additional standard curve was run up to 121 µg/mL for a total of eight concentrations (5-fold dilutions). Overall, the standard curves were linear up to 10 µg/mL and then the gradient decreased, and the line of best fit followed a $y = x^2 + x + c$ pattern. Therefore, for the compounds that were detected in the samples at concentrations much higher than 2500 ng/mL, then the response factor from the more concentrated standard curve was used. The response factors from both standard curves were almost identical for the aglycones, *O*-methylated and *O*-glucuronidated metabolites, but the *O*-sulfates were different. The response factors for the 3HPVL-4S and 4HPVL-3S were 4.56 and 4.01, respectively, and these values were used to calculate the sample concentrations beyond 10 µg/mL.

2.4.9 Calculation of elimination half-lives

Once concentrations were calculated for plasma and urine HPVL metabolites, a concentration over time curve was drawn for each metabolite and for the total metabolites detected (Figure's 2.3 and 2.4). From this, the area under the pharmacokinetic curve (A.U.C) was calculated using the standard integration trapezium rule formula (manually calculated in Microsoft Excel). The peak concentration (C_{max}) and time for peak concentration (T_{max}) were taken from the peak analytical points. Elimination half-lives ($T_{1/2}$) for each compound were calculated according to Byers *et al* (2009) (320). Briefly, the elimination rate constant (k) was calculated according to Formula 2.3 a/c, taking the average of the k constants over the entire study length, the $T_{1/2}$ was then calculated according to Formula 2.3 d.

$$a)\ C_{t+1} = C_t \times e^{-kt}$$

$$b)\ k = \frac{\ln \frac{C_t}{C_{t+1}}}{-t}$$

$$c)\ k_{\bar{x}} = \sum_{k_0}^{k_N} \frac{k_N + k_{N-1} + K_{N-2} + \cdots k_0}{N}$$

$$d)\ T_{\frac{1}{2}} = \frac{ln(2)}{k}$$

Formula 2.3: Elimination half-life formula
Steps a-d were performed to calculate the elimination half-lives for all HPVL metabolites from both urine and plasma pharmacokinetic curves, b) is the rearrangement of the formula in a). C_t = Concentration (C) at time (t) after dose; C_{t+1} = concentration at time (t+1) after t; k = elimination rate constant; $T_{1/2}$ = elimination half-life; N = number of HPVL concentrations recorded; $\bar{x}$ = mean.

2.5 Results

2.5.1 Method selection for plasma processing

Following processing, mouse plasma samples were separated on a Waters reverse phase C18 Column and passed through a UPLC-MS^2 to quantify the concentrations of seven HPVLs. Two processing steps were tested on the plasma samples; one was a PPT method (section 2.4.7.3), and the other was an SPE method (section 2.4.7.4). The PPT method allowed the determination of all seven HPVL concentrations in all the plasma samples, but with lower precision due to inconsistent recoveries of standards, whereas the SPE method allowed the determination of only five of the HPVLs (4HPVL-3GlcA, 3HPVL-4GlcA, 4HPVL-3S, 3HPVL-4S and 4H3MPVL) but with better precision, which reflected the more consistent recoveries of standards.

The PPT method gave recovery ranges ("Recovery range (%) – plasma PPT method" in Table 2.4) that varied from 0-114 % across the different compounds. The SPE process gave much more consistent recoveries, except for 34DHPVL and 345THPVL, which may be as a consequence of their high limit of detections (LOD). However, the data obtained for mouse samples processed with the SPE method were considered unreliable; this is because the peak areas for the target metabolites in mice samples were considerably lower than the peak area obtained for the same compounds that had been processed using the PPT method, even though the peak areas for the internal standards was similar. Moreover, the greater number of replicate standards quantified from the SPE extraction method resulted in the UPLC-MS^2 to run considerably longer than when it was run for the PPT extracted samples. Consequently, this caused trailing retention times and a reduced level of responsiveness. Furthermore, the addition of the drying step following SPE extraction caused further loss of the metabolites. And so, the unreliability of the SPE procedure was not pursued for the final quantification of the HPVL metabolites.

2.5.2 HPVL metabolites peak in the plasma 1-hour following ingestion

HPVLs and EC conjugates were quantified in plasma samples processed using the PPT methods described in, section 2.4.7.3 and section 2.4.7.6. EC conjugates were assessed in only the 24-hour post EC gavaged mouse samples, and HPVLs were quantified in all plasma samples. Figure 2.3 displays the resulting concentrations of each HPVL up to 24-hour's post oral gavage of 80 mg/kg body weight of 34DHPVL or EC, and Table 2.7 summarises the data. In total, the combined C_{max} of HPVL metabolites in plasma was 7.18 µM (1-hour) which estimates to be a tiny 0.11 % of the ingested 34DHPVL dose. This was calculated from the average mass of 1.84 mg of 34DHPVL

provided to the mice (8.85 µmol), and the average blood total volume in the mice was 1.34 mL (58.5 mL/kg body weight of blood (321)), consequently, the 7.18 µM of HPVL metabolites is equal to 9.62 nmol (0.11 % of the ingested dose). The area under the pharmacokinetic plasma curve (A.U.C) for the total HPVL metabolites detected was 14.31 µM (Figure 2.3 H).

There was no detection of (−)-epicatechin, epicatechin-glucuronide or epicatechin-sulfate in any of the 24-hour post EC gavaged mouse samples. This was as expected, as there are several published reports highlighting the quick metabolism and excretion of these SREMs. The only detectable concentrations in the EC gavaged mice were for 3HPVL-4S and 4HPVL-3S (Figure 2.3 G), however, the concentrations were very low (6 and 2 nM respectively).

4HPVL-3S, 3HPVL-4S, 34DHPVL, and 4H3MPVL were detectable in the plasma of 34DHPVL-gavaged mice at 24-hours, but 3HPVL-4GlcA and 4HPVL-3GlcA could not be detected and 345THPVL was only detected in the plasma of one mouse at 24 hours post-gavage. The glucuronides were the most concentrated compounds found in mice plasma in the early timepoints, peaking 1-hour post gavage at 3.97 ± 1.41 µM and 0.70 ± 0.30 µM, for 3HPVL-4GlcA and 4HPVL-3GlcA respectively. It is possible that the concentrations could have been higher in the plasma prior to or soon after the 1-hour timepoint, however since there were blood samples collected between 0-1 or 1-2 hours, it was not possible to evaluate this. HPVL-*O*-glucuronide concentrations were drastically lower at the 2-hour timepoint, with estimated concentrations of 0.64 ± 0.21 µM and 0.10 ± 0.03 µM, and negligible concentrations after 6 hours. They also expressed quick elimination half-lives between 0.33-0.35 hours and so this demonstrates the rapid clearance of the glucuronides from the circulation.

HPVL-sulfates were also found at relatively high concentrations in plasma, with highest concentrations observed in 1-hour samples (2.26 ± 0.78 µM and 0.18 ± 0.04 µM for 4HPVL-3S and 3HPVL-4S, respectively). Concentrations then dropped gradually from 1 to 6-hours and were still detectable in plasma after 24-hours (4.8 nM and 1.8 nM for 4HPVL-3S and 3HPVL-4S, respectively). Sulfate HPVLs appeared over a long timeframe and at high concentrations throughout; this could be because they are metabolised or synthesised more slowly than HPVL-glucuronides or because there are differences in the excretion rate. This is partly demonstrated by the longer circulation time of the *O*-sulfates, with elimination half-lives of 0.94-1.18 hours, almost 3-4 times longer than the glucuronides.

34DHPVL and 4H3MPVL aglycones were detected at much lower concentrations in plasma samples than glucuronides and sulfates, which is consistent with efficient phase-II conjugation and rapid conversion of aglycones to phase-II conjugates by small intestinal enterocytes and the liver. Both aglycones were found at the highest concentration in 1-hour post gavaged samples (0.22 ± 0.04 µM

and 0.10 ± 0.02 µM for 34DHPVL and 4H3MPVL, respectively). 34DHPVL was more slowly cleared in the mice than 4H3MPVL, with a $T_{1/2}$ of 0.66-hours and a mean concentration at 24-hours of 2 nM for 4H3MPVL.

345THPVL was included in the list of targeted metabolites because it could plausibly arise from hydroxylation of 34DHPVL. An ion current response was observed for the 345THVL ion pair; however, this peak was below the estimated limit of detection for 345THPVL. No peak was observed in 25 % of mouse samples, and inter-mouse variance was very high, so if the observed peak was due to 345THPVL, then the observed concentrations were approximately 10-fold lower than for the 34DHPVL aglycone (low nM). Overall, the evidence suggests that this is not an important metabolic route and possibly not a metabolic route at all.

Table 2.7: 34DHPVL metabolites detected in mouse plasma
This table summarises the results for the detection of hydroxyphenyl-γ-valerolactones in the plasma of mice from the pharmacokinetic study. C_{max}: the maximum concentration detected at a time; T_{max}: time at which the maximum concentration was observed; A.U.C: area under the plasma concentration over time curve (estimated from the graphs produced in Figure 2.3); $T_{1/2}$: estimated elimination half-life.

Epicatechin metabolites	C_{max} (µM)	T_{max} (hours)	A.U.C (µM/hour)	$T_{1/2}$ (hours)
34DHPVL	0.22	1	0.91	1.05
4HPVL-3GlcA	0.70	1	0.96	0.33
3HPVL-4GlcA	3.97	1	5.75	0.35
4HPVL-3S	2.26	1	6.36	0.94
3HPVL-4S	0.18	1	0.60	1.18
345THPVL (putative)	0.03	1	0.17	1.57
4H3MPVL	0.10	1	0.24	0.66

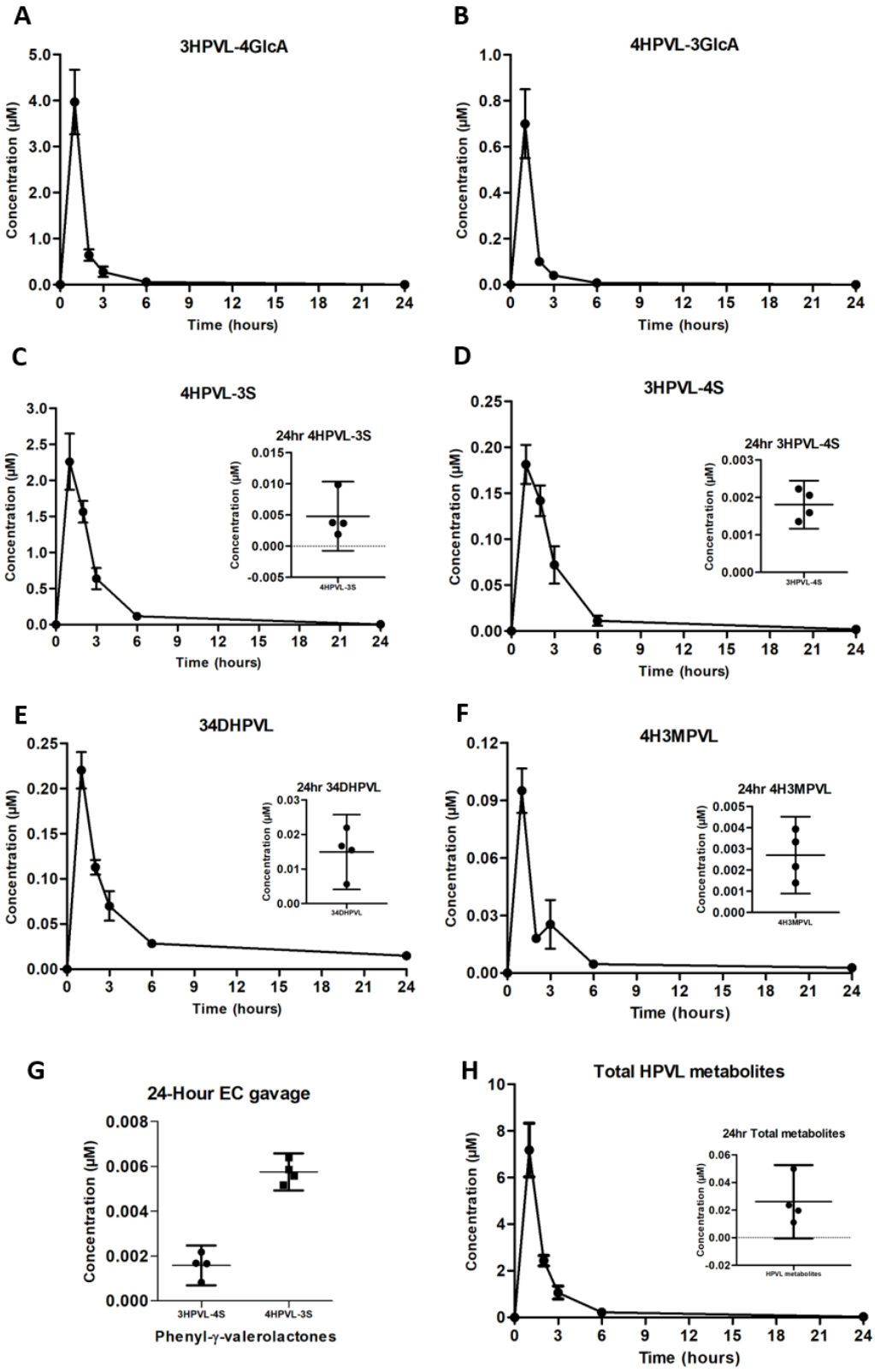

Figure 2.3: Hydroxyphenyl-γ-valerolactone concentrations in 0-24 hour plasma samples of mice fed 34DHPVL

Mice were oral gavaged with 80 mg/kg body weight of 34DHPVL, and plasma concentrations for compounds (A) 3HPVL-4GlcA; (B) 4HPVL-3GlcA; (C) 4HPVL-3S; (D) 3HPVL-4S; (E) 34DHPVL; (F) 4H3MPVL, were quantified over time. (G) 24-hour detection of 3HPVL-4S and 4HPVL-3S following oral gavage of 80 mg/kg body weight of EC. Error bars represent the standard error of the mean (SEM) for the line graphs and 95 % confidence interval for the dot plot graphs.

2.5.3 4HPVL-3S is the most concentrated urinary excreted metabolite following 34DHPVL ingestion

Mouse urine samples processed and analysed according to the method detailed in section 2.4.8.3 were used to estimate the concentrations of metabolites in urine samples collected over time following 34DHPVL gavage at 80 mg/kg body weight. It was not possible to collect urine samples at each timepoint for each mouse, and so the data presented here are for a limited number of animals at each timepoint and the number involved has been indicated. The data for urinary concentrations for each metabolite over time are shown in Figure 2.4 with a summary in Table 2.8. Data for only the 24-hour timepoint samples collected following EC administration are also shown.

After dosing with 34DHPVL, HPVL-sulfates were excreted highest at 1-hour (561 µM and 132 µM, n = 2 for 4HPVL-3S and 3HPVL-4S, respectively) post-gavage, (Figure 2.4 C/D). These compounds were excreted gradually over the 24-hour time period, with concentrations still high at 24-hours (4.27 ± 1.55 µM and 1.26 ± 0.95 µM, n = 4, mean and SD values) and $T_{1/2}$ values of 3.01 and 1.18 hours, after a 24-hour gavage for 4HPVL-3S and 3HPVL-4S, respectively. These observations are consistent with a process in which 34DHPVL is rapidly conjugated to sulfated forms following ingestion, circulate in the plasma, and are then excreted, with excretion via the kidneys (urine) appearing to be the major route.

The concentrations of HPVL-glucuronides peaked in urine samples collected 1-hour after gavage, reaching 94 ± 29 µM and 66 ± 63 µM for 3HPVL-4GlcA and 4HPVL-3GlcA, respectively (Figure 2.4 A/B). Concentrations then dropped rapidly in samples after the 1-hour timepoint and were only 0.17 ± 0.06 µM and 0.11 ± 0.03 µM at 24-hours, with $T_{1/2}$ estimates of 1.22 and 0.56 hours, for 3HPVL-4GlcA and 4HPVL-3GlcA, respectively. The glucuronide conjugates have much shorter elimination half-lives than the sulfate conjugates.

The aglycones 34DHPVL and 4H3MPVL appeared to be rapidly cleared from the plasma by the kidneys, evidenced by the highest concentrations in urine being in the earliest 1-hour timepoint (84 ± 92 µM and 116 ± 146 µM, respectively). These aglycones possessed the shortest elimination half-lives of all of the quantified metabolites at 0.53 and 0.36 hours, with only nanomolar concentrations being detected in urine 24-hours after gavage.

Since urine was collected periodically and there was no urine collected between 6-24 hours, it is not possible to accurately determine the recovery of HPVL metabolites from the concentration ingested. However, an estimate was calculated based on the area under the urine pharmacokinetic curve (A.U.C) for the total HPVL metabolites over time (Figure 2.4 I) and from the amount of

34DHPVL ingested. There was an average mass of 1.84 mg of 34DHPVL provided to all the mice, which equates to an amount of 8.85 µmol. The A.U.C for total HPVL urinary metabolites was 5012 µM/hour, and so, when making the assumption of an average urinary excretion of 0.8 mL by the mice over 24-hours (322) then the amount of HPVL metabolites excreted in urine is 4.01 µmol; accounting for an estimated recovery of 45 % of the ingested dose.

There was a correlation between the detected concentrations in mouse urine and plasma for 345THPVL. However, in keeping with the literature (1, 5), the concentrations of the 34DHPVL metabolites in urine should be far greater than the observed concentrations in plasma, this is typical for the rapid excretion of xenobiotics by the kidneys into urine. Because of this and the high LOD for 345THPVL, it is likely that the peak detected for 345THPVL could be an artefact of the analysis.

For the majority of the pharmacokinetic time courses for the urinary excretion of the different 34DHPVL conjugates, there was a smaller second peak, typically between 3 and 6-hours. This is the hallmark for enterohepatic recirculation where a fraction of the peripheral blood metabolites are excreted via the liver into bile, which is later emptied into the small intestine, allowing for later reabsorption by the intestine and further intestinal/hepatic metabolism.

In 24-hour samples from EC-gavaged mice, there were detectable concentrations of 3HPVL-4GlcA, 4HPVL-3GlcA, 4HPVL-3S, 3HPVL-4S, 34DHPVL and 4H3MPVL. This is different from what was observed for 24-hour plasma samples for which only 4HPVL-3S and 3HPVL-4S were detected (Figure 2.4 G/H). This reflects the substantially lower concentrations of metabolites present in plasma when compared to urine, where the majority were below the LOD after 24-hours. The order of concentrations of the individual HPVL metabolites from EC-fed mice was similar to that observed for 34DHPVL-fed mice (sulfates > glucuronides > aglycones), showing that once HPVLs are formed by microbiota in the colon following EC ingestion, their metabolism for phase-II conjugation is similar to that for 34DHPVL when fed directly and absorbed by the small intestine.

The 24-hour urinary concentrations for the HPVL conjugates were similar for EC-gavaged and 34DHPVL-gavaged mice (Figure 2.4 G/H), as were the 24-hour plasma concentrations for 4HPVL-3S and 3HPVL-4S (section 2.5.2, Figure 2.3 G). Finally, no EC-sulfates, EC-glucuronide or EC aglycone were detected in 24-hour urine samples of EC-gavaged mice. This is likely due to the rapid clearance of these compounds in mice, such that the concentrations in 24-hour samples were low and below the LOD.

Table 2.8: 34DHPVL metabolites detected in mouse urine

This table summarises the results for the detection of hydroxyphenyl-γ-valerolactones in the urine of mice from the pharmacokinetic study oral gavaged with 80 mg/kg of 34DHPVL. C_{max}: the maximum concentration detected at a time; T_{max}: time at which the maximum concentration was observed; A.U.C: area under the urinary concentration over time curve (estimated from the graphs produced in Figure 2.4); $T_{1/2}$: estimated elimination half-life.

Epicatechin metabolites	C_{max} (µM)	T_{max} (hours)	A.U.C (µM/hour)	$T_{1/2}$ (h)
34DHPVL	84.1	1	141.8	0.53
4HPVL-3GlcA	65.6	1	134.6	0.56
3HPVL-4GlcA	93.8	1	492.0	1.22
4HPVL-3S	561.0	1	3466	3.01
3HPVL-4S	131.7	1	595.5	1.18
345THPVL (putative)	0.03	1	0.04	0.73
4H3MPVL	116.3	1	208.6	0.36

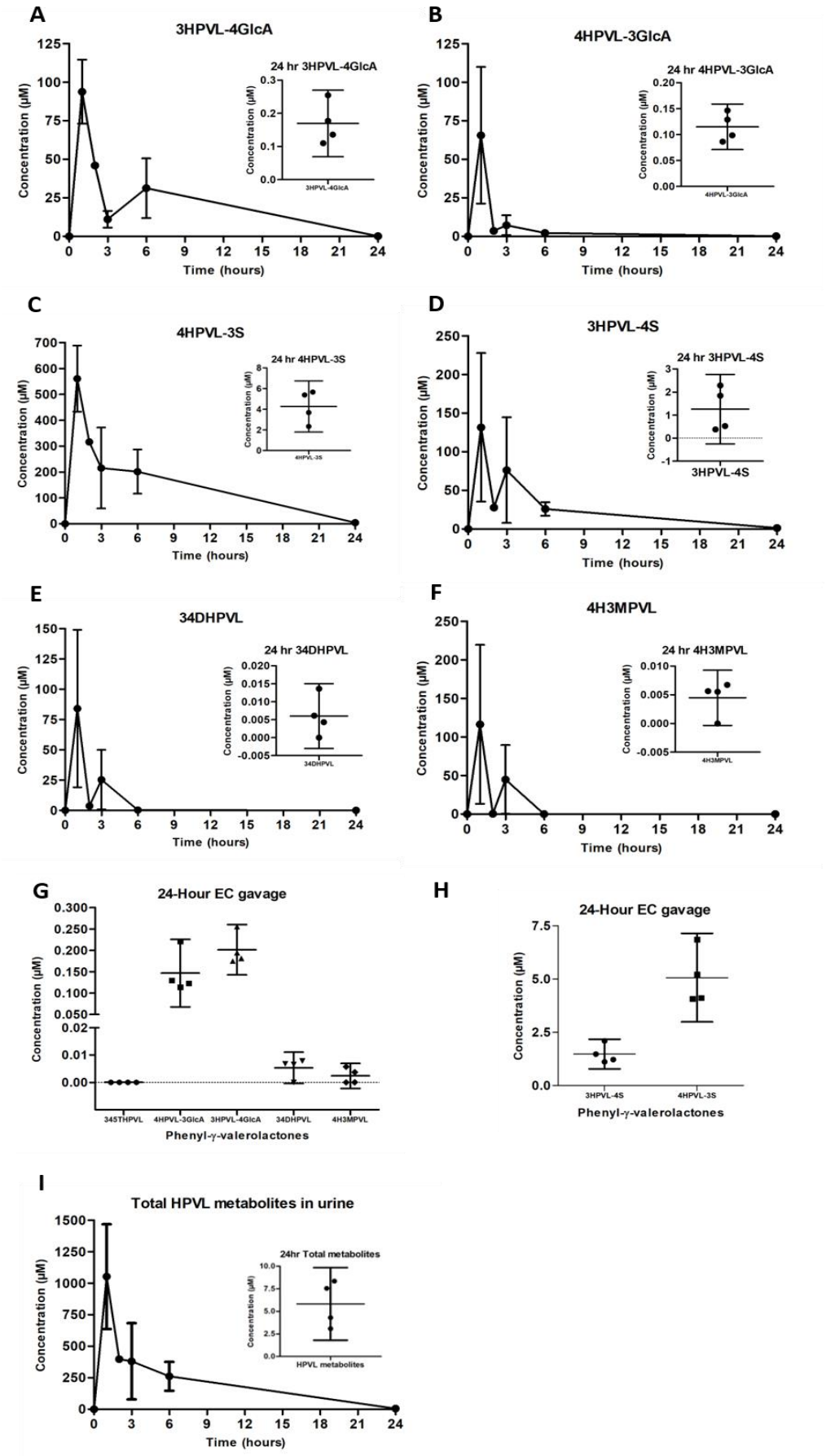

Figure 2.4: Hydroxyphenyl-γ-valerolactone concentrations in 0-24 hour urine samples of mice fed 34DHPVL

Figure 2.4 (continued): *Mice were orally gavaged with 80 mg/kg body weight of 34DHPVL, and urinary excretion concentrations for compounds (A) 3HPVL-4GlcA; (B) 4HPVL-3GlcA; (C) 4HPVL-3S; (D) 3HPVL-4S; (E) 34DHPVL; (F) 4H3MPVL, were quantified over time. Mice oral gavaged with 80 mg/kg EC had detectable concentrations in 24-hour urine samples for (G) 4HPVL-3GlcA, 3HPVL-4GlcA, 34DHPVL and 4H3MPVL; and, (H) 3HPVL-4S and 4HPVL-3S. Total hydroxyphenyl-γ-valerolactone metabolites following 34DHPVL gavage over time are shown in (I). Error bars represent the standard error of the mean (SEM) for the line graphs and 95 % confidence interval for the dot plot graphs.*

2.6 Discussion

The purpose of the pharmacokinetic study was to compare the absorption and excretion profile of HPVLs when provided as an oral dose compared to providing its parent compound as an oral dose. In doing so, this study has revealed that:

(1) There is rapid conjugation and absorption of HPVLs, that provide peak plasma concentrations after 1-hour.

(2) This is followed by rapid urinary excretion of the compounds which again is highest in 1-hour post-gavaged samples.

(3) HPVL metabolites are still excreted after 24-hours, although at substantially lower concentrations.

(4) HPVL-*O*-sulfates have longer elimination half-lives than HPVL-*O*-glucuronides and aglycones.

This study was novel in directly feeding a HPVL to rodents and this is therefore the first report for the pharmacokinetic behaviour in such instance. Consequently, there is no possibility of comparing the results reported here with other studies for the pharmacokinetics of HPVLs. However, the appearance of HPVLs following oral consumption of the flavanol EC and flavanol-rich foods and extracts has been reported, and these provide the backdrop to understand the novelty of this new data and the insights it has uniquely provided.

2.6.1 There is rapid absorption and excretion of 34DHPVL and its metabolites

Maximal plasma and urinary concentrations of all 34DHPVL metabolites occurred within 1-hour of 34DHPVL oral gavage, showing that these compounds are rapidly absorbed, distributed, and quickly excreted in the urine in mice in the current study. Although timepoints prior to the 1-hour and very soon after this were not taken, it is likely that the maxima detection at 1-hour is true of the HPVL metabolites pharmacokinetic profile; this is indeed true for the pharmacokinetic profile of EC conjugates following EC-gavage (1, 5). When EC is directly fed to humans, there is the requirement for microbial catabolism of EC and EC-conjugates to HPVLs and further phase-II conjugation by the enterocytes/hepatocytes, consequently the T_{max} times for HPVLs in the circulation are much later at ~6-hours (1). In contrast, this study has shown that 34DHPVL-gavage in mice causes the rapid absorption and production of HPVL metabolites (4HPVL-3GlcA, 3HPVL-4GlcA, 4HPVL-3S, 3HPVL-4S and 4H3MPVL) by phase-II conjugation from enzymes within small intestinal enterocytes and the liver, subsequently they appear maximally in plasma at around 5-hours earlier than when EC is

gavaged. In keeping with this observation, 34DHPVL metabolites are rapidly processed by the kidneys and excreted in urine when dosed orally (approximate T_{max} of 1-hour), compared to the delayed detection of HPVL metabolites in urine following EC-gavage (T_{max} 4-8 hours) (1).

2.6.2 O-glucuronide and O-sulfate HPVL distribution in mice

A very interesting observation was that the *O*-glucuronides were initially the main conjugated form of 34DHPVL and accounted for 62 ± 1.98 % of all the circulatory compounds screened at 1-hour; this was followed by the *O*-sulfates (34 ± 1.73 %) and then the aglycones (5 ± 0.97 %). This is different to that reported for humans fed (^{14}C)-EC where 4HPVL-3S accounted for 60 % (mol %) of the total concentration of HPVLs in peripheral blood samples taken 6-hours post-consumption (1, 96). In addition, 3HPVL-4S was detected in the plasma of mice fed 34DHPVL in the current study, whereas this compound was not detected in plasma samples from previously reported studies where flavanols were consumed and the HPVLs were generated by the gut microbiota (1, 5). Although the glucuronides accounted for the majority of total conjugated metabolites at their C_{max} in mice, the sulfates had the highest exposure over time evidenced by the highest A.U.C values and the longest elimination half-lives (Tables 2.7 and 2.8). This is also reflected in a previously reported human study, where 4HPVL-3S was reported to account for the largest plasma and urinary A.U.C and had the longest elimination half-life (1). In contrast, in EC-gavaged rats, 3HPVL-4GlcA dominated the total urinary excretion over 4HPVL-3S (5). It is noteworthy that the elimination half-lives of all the 34DHPVL conjugates were reported to be significantly longer in humans in comparison to values estimated for the mice in this study. This is consistent with humans having slower metabolic activity compared to mice (323, 324). This might be relevant when considering the length of treatments to be used when planning *in-vitro* experiments to determine their biological activities, for example cultured mammalian cell models. Regardless, this study has shown that the mouse model is a closer fit with what is observed in humans. This might reflect the relative genetic closeness of mice to humans in comparison to other animals such as rats and rabbits. Although, it must be taken into account that there are often large differences between mice and humans in terms of metabolic activity (323, 324).

2.6.3 The detection of 34DHPVL at 24-hours post-gavage

At 24-hours post 34DHPVL-gavage in mice, there were still detectable plasma concentrations of 34DHPVL, and these were detected to be the most concentrated HPVL screened at this time-point

(~15 nM) with a high $T_{1/2}$ of 1.05-hours. This occurred despite enterohepatic recirculation where further conjugation is highly likely, as evidenced by the second peak of 34DHPVL and conjugates in urine at 3-hours. So, despite the evidence for the rapid absorption and phase-II conjugation of 34DHPVL, when provided orally at concentrations of 2 mg/25 g mouse, not all of it is converted to conjugates after 24-hours and there is a long elimination clearance of the metabolite. This observation cannot be explained by this study, but the persistence of 34DHPVL in 24-hour plasma samples of the mice appears to be a rodent phenomenon, because it has previously been reported that the 34DHPVL aglycone was not detectable in human plasma after EC-consumption, but it was detectable in the plasma of rats administrated with EGCG; first appearing at 6-hours from consumption and peaking later (98).

Similarly to humans (1), the biggest A.U.C was for the HPVL-sulfates in this mouse study followed by the glucuronides, whilst in rats 3HPVL-4GlcA dominates over 4HPVL-3S (5). This reiterates how the mouse model is a better choice when trying to make biological judgements in humans, versus other animal models, such as rats, rabbits and amongst others, due to their greater similarity in genetics (325), although still vastly different in terms of metabolic activity.

Within this mouse study there was an estimated recovery of 45.3 ± 34 % of the ingested 34DHPVL. This value is low compared to other studies mostly because of the short 24-hour period where measurements were taken. In humans and rats, there is excretion of metabolites, particularly ring-fission metabolites (RFMs), between 48-72-hours (1, 5). There is still the detection of HPVLs after 24-hours in both plasma and urine in this study, informing that there will be further excretion of the compounds beyond this. Additionally, only two biological matrix markers have been assessed in this study, to find a greater recovery of the compounds following ingestion there would need to be an assessment of faeces, red blood cells, and synovial fluid (309), where 34DHPVL has been shown to bind to these latter two matrices. Finally, there are also further metabolites of HPVL's that have not been screened for in this study, these are namely, hydroxyphenyl valeric acids, hydroxyphenyl propionic acids and hydroxyphenyl benzoic acids (1, 5); thus screening for these additional compounds would increase the recovery of the ingested dose.

2.7 Conclusion

The mouse pharmacokinetic study performed in this chapter has shown that:

(1) 34DHPVL is very rapidly absorbed (within 1-hour).

(2) 34DHPVL is very rapidly metabolised to phase-II conjugates.

(3) There is rapid urinary excretion of 34DHPVL and its metabolites (peak in 1-hour). The data also shows that *O*-glucuronides are the dominant early metabolic form, consistent with conjugation in the small intestine whereas the dominant later forms are *O*-sulfates, which is consistent with liver *O*-sulfation, and indeed 34DHPVL-*O*-glucuronides appear to be transformed into *O*-sulfates in the liver post first pass metabolism.

(4) Finally, evidence that 34DHPVL undergoes enterohepatic circulation has been reported.

There are several limitations from the study design that do not allow for a complete picture with regards to the pharmacokinetics for 34DHPVL and its metabolites. If this study were to be repeated:

(1) More mice would have been used to decrease the error surrounding the observed concentrations at each timepoint, in addition to the use of both male and female mice to observe differences in HPVL pharmacokinetics between the sexes.

(2) Samples would have been taken at several additional earlier timepoints following oral gavage to allow a more accurate estimation of the T_{max} and C_{max} in particular (e.g. 15, 30, 45, 60 and 90 mins).

(3) Metabolic organs would have been harvested to allow determination of the concentrations in them at each timepoint.

(4) Measurements of the concentrations of 34DHPVL metabolites would have been performed in other biological samples such as faeces, red blood cells, and the gut (duodenum, jejunum, ileum, cecum and colon), to provide a more complete picture of HPVL absorption, distribution, metabolism and excretion parameters.

Chapter Three

A DIETARY INTERVENTION STUDY TO EXPLORE THE EFFECTS OF 3',4'-DIHYDROXYPHENYL-γ-VALEROLACTONE AND (−)-EPICATECHIN ON INSULIN RESISTANCE IN HIGH FAT DIET FED MICE

Chapter 3: A dietary intervention study to explore the effects of 3',4'-dihydroxyphenyl-γ-valerolactone and (−)-epicatechin on insulin resistance in high fat diet fed mice

3.1 Abstract

Background: There are numerous reports showing that (−)-epicatechin (EC) consumption has beneficial effects on health and in particular biomarkers of type-2 diabetes. Such evidence includes the protection against hepatic steatosis and insulin resistance in high fat diet fed mouse models supplemented with EC. However, since a substantial proportion of ingested EC is converted to hydroxyphenyl-γ-valerolactones (HPVL) by the gut microbiota, and these HPVLs are efficiently absorbed and account for about one third of EC metabolites that reach the peripheral circulation, it is not clear if the effects of consuming EC are caused by EC and its phase-II metabolites per se, or by HPVLs, or a combination of both.

Aim: The purpose of this study was, for the first time, to directly compare the effects of EC and its microbial metabolite 34DHPVL on insulin resistance in a high-fat diet fed mouse model to produce metabolic changes causing insulin resistance.

Methods: A total of eighty C57BL/6J mice were fed six different diets containing 20 mg/kg body weight of EC or 34DHPVL or no supplement into either a low fat 10 % kcal (LF) or high fat 60 % kcal (HF) base diet for 15-weeks. Plasma insulin and glucose levels were recorded after 13-weeks of dietary intervention via a fasted glucose tolerance test (GTT).

Results: The HF diet significantly increased body weight in mice by 56 ± 8.5 % ($p < 0.0001$) and impaired insulin sensitivity when compared to the LF diet (79 ± 5.1 % higher glucose A.U.C, $p < 0.05$). The supplementation of EC into the HF diet (HF+EC) caused a significant reduction in blood glucose concentrations by 26 ± 3.8 % at 2-hours after intraperitoneal glucose injection during the GTT ($p = 0.007$) and significantly reduced body weight gain in the mice by 12 ± 5.8 % ($p = 0.03$). Although EC supplementation lowered fasting plasma insulin in HF diet fed mice and consequently almost halved the HOMA-IR, the glucose A.U.C was not significantly different to HF fed mice (77.4 mg/dL versus 82.5 mg/dL, $p = 0.32$) and the absolute HOMA-IR still indicated the mice were insulin resistant. Interestingly, there was no difference in epididymal fat mass between EC supplemented and non-supplemented mice on HF diets. In contrast, 34DHPVL supplemented into HF diet fed mice did not prevent body weight gain and increased the fasting insulin concentrations in comparison to the non-supplemented HF diet fed mice ($p = 0.008$) and increased their HOMA-IR by 1.8-fold ($p =$

0.08). Remarkably, 34DHPVL supplementation did reduce the glucose A.U.C but not significantly (p = 0.12). Additionally, 34DHPVL supplementation increased the dietary intake in mice with borderline significance to the non-supplemented HF diet fed mice (p = 0.07).

Conclusion: EC significantly lowered plasma glucose and protected against HF diet induced weight gain compared to non-supplemented HF diet fed mice. On the other hand, 34DHPVL was not able to protect against body weight gain, and instead raised plasma insulin concentrations compared to non-supplemented HF diet fed mice, which is suggestive of impaired hepatic insulin clearance. Regardless, the reduced blood glucose A.U.C in 34DHPVL supplemented HF diet fed mice showed a response to the raised insulin which was indicative of an improved insulin sensitivity compared to non-supplemented mice. Because this is the first study of its kind to feed HPVLs over a long intervention period to mice, there is a requirement for further research in-order to understand the mechanisms underlying HPVL's actions, nonetheless, this study has proved to be hypothesis generating and has provided novel insights into this particular group of EC metabolites.

3.2 Introduction

Overweight and obesity is a worldwide health concern and it is predicted to affect 18 % of men and 21 % of women at a global level by 2025 (326) and 8 % of the UK by 2035 (327). Obesity increases the prevalence for cardiovascular disease, cancer risk, mobility problems, osteoarthritis, mental illnesses, and type-2 diabetes (328-333). Lifestyle factors can influence the development of these conditions and diet is a major influencing factor that can drive or mitigate against the development of type-2 diabetes. Type-2 diabetes is a reversible condition and dietary polyphenols, in particular flavanols, have been shown to provide protection against insulin resistance (334-337). In chapter 1, the pathogenesis of insulin resistance and the current evidence surrounding the actions of the flavanol EC and its actions *in-vitro* and *in-vivo* on insulin resistance were discussed in some detail, and only a brief re-visit will be provided here. The review of the literature on HPVLs was discussed extensively in chapter 1, but because there are no reported effects of HPVLs on insulin resistance, it can only be assumed that they will contribute to the protective effects seen by EC against insulin resistance.

3.2.1 The actions of (–)-epicatechin in the protection against insulin resistance

EC constitutes around 37 % of flavanols in cocoa products (25, 26) and ~7 % in green tea (29, 30). Estimated consumption of flavonoids is around 400 mg/day, of which an estimated 25 mg/day is attributed to EC, with growing evidence for flavonoids role, and more particularly ECs role, in preventing the onset of insulin resistance (301-305). In high fat diet fed mouse models, the consumption of EC at doses of 1-200 mg/kg body weight has been shown to significantly mitigate body weight gain and insulin resistance that are induced by consumption of the high fat diets (127, 129, 130, 224, 227). Blood glucose and insulin have been primarily recorded through performing GTT's in the fasted state, and later allows for the calculation of the HOMA-IR and the area under the concentration over time curves, providing clear metrics to quantify the level of insulin resistance. Rat models have also been used and the reported results mirror the effects of EC for improving insulin sensitivity (226, 338).

In a human intervention study, EC consumption of 100 mg/day for 4-weeks by overweight and normal weight subjects caused a reduction in their HOMA-IR and concomitantly an improvement in their insulin sensitivity when compared to placebo treated controls (233). Meanwhile, one-time consumption of EC caused an improvement in patients oral metabolic tolerance, which indicated

towards sustained fat oxidation by EC post prandially, but the effects were seen to be greater in overweight versus normal weight subjects (234).

Investigative studies have been performed to identify the mechanistic actions of EC. These have been accomplished through the analysis of protein/mRNA expression in the liver and adipose tissues from rodent models and from *in-vitro* cell culture models in HepG2 (liver), 3T3-L1 (adipose) and INS-1E (β islet) cells. EC has been shown to negate the redox potential in cells, largely through preventing the activation of c-Jun N-terminal kinase 1/2 (JNK) or of the inhibitor nuclear factor κB (IκB) kinase (IKK) (129, 338) which are increased during inflammation, subsequently preventing redox induced phosphorylation of IRS-1 and so preventing inhibition of the insulin signalling pathway (339, 340). Further, EC has been shown to interact with protein kinase C which also exhibits redox sensitivity and further phosphorylates IRS-1, but EC has been demonstrated to prevent this (338).

Inflammation is also a big driver for the development of insulin resistance, largely through the activation of nuclear factor kappa-light-chain-enhancer of activated B-cells (NF-κB). EC has been demonstrated to inhibit NF-κB activation in metabolic tissues, and consequently caused a reduction in the inflammatory markers TNF-α and monocyte chemo-attractant protein-1 (MCP-1) (229, 338). Other mechanisms by which EC may impact upon insulin resistance is through the modulation of intestinal permeability via the prevention of high fat diet-induced paracellular transport and endotoxemia which could in part contribute to the improvement of insulin sensitivity (130); and by EC directly targeting the stimulation of glucose regulating proteins via an increase in the levels and activation of insulin signalling AMPK, IR and IRS-1 (129, 285, 341) and decreasing the levels of the gluconeogenic enzyme PEPCK (341). Finally, EC treatment with INS-1E cells enhanced insulin secretion through a CaMKII dependent mechanism (293).

Overall, the existing published evidence supports the beneficial effects of EC on insulin resistance is strong and that is the basis of the research described in this chapter which seeks, for the first time, to investigate the potential role of gut microbiota-derived metabolites of EC in mitigating against the insulin insensitive effects of high fat diets.

3.3 Aims and approach

HPVLs are the most concentrated group of colonic metabolites generated by EC metabolism that enter the circulatory system. Because of our lack of understanding surrounding what the bioactive metabolites from EC are with regards to disease protection, and specifically for mitigating the onset of type-2 diabetes, it is necessary to investigate this using a targeted approach. The overall objective approached was to directly compare the effects of EC with its main microbial metabolite, 34DHPVL, on insulin resistance in a high-fat diet fed mouse model of type-2 diabetes. The key aspects of the study design were to:

(1) Induce insulin resistance in mice by feeding a 60 % kcal HF diet from fat and comparing against a control 10 % kcal LF diet from fat over a course of 15-weeks.

(2) Measure differences in body weight and insulin resistance caused by supplementation of the diet with 20 mg/kg body weight of EC in mice.

(3) Determine the effects of supplementation of the diets with 20 mg/kg body weight of 34DHPVL on body weight and insulin resistance and compare the effects with EC.

The resulting data was used to address the following questions: 1) does EC dietary supplementation significantly mitigate against HF diet induced insulin resistance and body weight gain? 2) Does direct dietary supplementation with the microbial metabolite 34DHPVL significantly improve insulin resistance and body weight gain induced by the HF diet? 3) Does dietary supplementation with EC or 34DHPVL improve the glycaemic index when supplied in the LF (high carbohydrate) diet and compared to the LF treatment group? The following linked hypotheses were addressed by this research:

(1) Both EC and 34DHPVL significantly mitigates HF diet induced body weight gain in mice.

(2) Both EC and 34DHPVL significantly mitigates HF diet induced insulin resistance in mice.

3.4 Methods

3.4.1 Synthesis of 3',4'-dihydroxyphenyl-γ-valerolactone

34DHPVL was synthesised by an in house synthetic organic chemist (Dr Paul Needs, Quadram Institute Bioscience, UK) using a modified version of that published by Chang *et al* (300) (Figure 3.1). Full details can be found in Hollands *et al* (2020) (2).

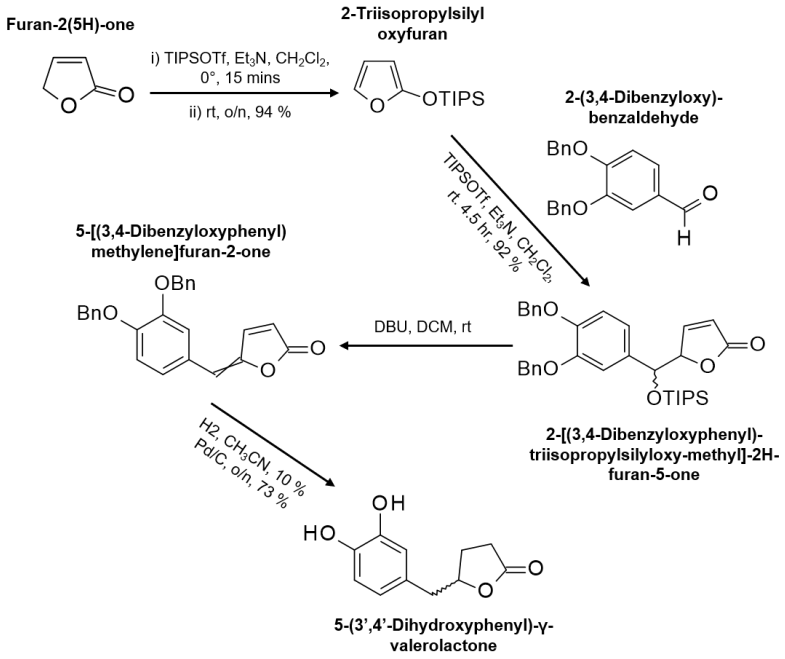

Figure 3.1: Synthetic steps to produce 5-(3',4'-dihydroxyphenyl)-γ-valerolactone
Initially, 2-triisopropylsilyloxyfuran was prepared, with high yields from purification and distillation. The intermediate 2-[(3,4-dibenzyloxyphenyl)-triisopropylsilyloxy-methyl]-2H-furan-5-one was isolated as a diastereomeric mixture and purified before conversion to 5-(3',4'-dihydroxyphenyl)-γ-valerolactone via 5-[(3,4-dibenzyloxyphenyl)methylene]furan-2-one. The above image has been edited from that published by Hollands et al (2020) (2) with permission. All synthetic steps were performed by Dr Paul Needs, Quadram Institute Bioscience, UK.

3.4.2 Preparation of mouse pellets

(−)-Epicatechin was purchased from Toronto Chemicals (Ontario, Canada) and 34DHPVL was synthesised in house as previously described (see section 3.4.1). The diets were prepared with help from Research Diet Inc (New Jersey, USA) according to the formulations described in Table 3.1. Formulations were such that low-fat diets contained 10 % kcal energy from fat (fat: lard and soybean oil) (Research Diets D12450 J) and high-fat diets contained 60 % kcal energy from fat, an increase in the saturated fat from lard (Research Diets D12492). The amount of compound required was calculated based on the estimated average daily food consumption of 3.5 g per mouse and to

contain 20 mg/kg body weight of either EC or 34DHPVL. In total this accounted to 200 mg compound/kg diet when using Formula 3.1. Please see Table 3.1 for the complete ingredient list for each of the six different diets. Pellets were slow dried during formulation to reduce the risk of compound breakdown and were then sealed in airtight bags and irradiated for sterility at 10-20 kGy.

Table 3.1: Dietary constituents of mouse pellets
This table has been taken directly from the pellet manufacturer Research Diets (US).

Product	**LF**		**HF**		**LF + 200 mg/kg diet 34DHPVL**		**HF + 200 mg/kg diet 34DHPVL**		**LF + 200 mg/kg diet EC**		**HF + 200 mg/kg diet EC**	
	D12450 J		**D12492**		**Formula 1**		**Formula 2**		**Formula 3**		**Formula 4**	
%	**g**	**kcal**	**g**	**kcal**	**g**	**kcal**	**g**	**kcal**	**g**	**kcal**	**g**	**kcal**
Protein	19	**20**	26	**20**	19	**20**	26	**20**	19	**20**	26	**20**
Carbohydrate	67	**70**	26	**20**	67	**70**	26	**20**	67	**70**	26	**20**
Fat	4	10	35	60	4	10	35	60	4	10	35	60
Total		**100**		**100**		**100**		**100**		**100**		**100**
kcal/gm	3.8		5.2		3.8		5.2		3.8		5.2	
Ingredient	**g**	**kcal**	**g**	**kcal**	**g**	**kcal**	**g**	**kcal**	**g**	**kcal**	**g**	**kcal**
Casein	200	800	200	800	200	800	200	800	200	800	200	800
L-Cystine	3	12	3	12	3	12	3	12	3	12	3	12
Corn Starch	506.2	2025	0	0	506.2	2025	0	0	506.2	2025	0	0
Maltodextrin 10	125	500	125	00	125	500	125	500	125	500	125	500
Sucrose	68.8	275	68.8	275	68.8	275	68.8	275	68.8	275	68.8	275
Cellulose	50	0	50	0	50	0	50	0	50	0	50	0
Soybean Oil	25	225	25	225	25	225	25	225	25	225	25	225
Lard	20	180	245	2205	20	180	245	2205	20	180	245	2205
Mineral Mix S10026	10	0	10	0	10	0	10	0	10	0	10	0

Table 3.1: Dietary constituents of mouse pellets (continued)

Product	LF		HF		LF + 200 mg/kg diet 34DHPVL		HF + 200 mg/kg diet 34DHPVL		LF + 200 mg/kg diet EC		HF + 200 mg/kg diet EC	
	D12450 J		D12492		Formula 1		Formula 2		Formula 3		Formula 4	
%	g	kcal	g	kcal	g	kcal	g	kcal	g	kcal	g	kcal
DiCalcium Phosphate	13	0	13	0	13	0	13	0	13	0	13	0
Calcium Carbonate	5.5	0	5.5	0	5.5	0	5.5	0	5.5	0	5.5	0
Potassium Citrate, 1 H2O	16.5	0	16.5	0	16.5	0	16.5	0	16.5	0	16.5	0
Vitamin Mix V10001	10	40	10	40	10	40	10	40	10	40	10	40
Choline Bitartrate	2	0	2	0	2	0	2	0	2	0	2	0
34DHPVL	0	0	0	0	0.212	0	0.155	0	0	0	0	0
EC	0	0	0	0	0	0	0	0	0.212	0	0.155	0
FD&C Yellow Dye #5	0.04	0	0	0	0	0	0.05	0	0	0	0.025	0
FD&C Red Dye #40	0	0	0	0	0.05	0	0	0	0.025	0	0.025	0
FD&C Blue Dye #1	0.01	0	0.05	0	0	0	0	0	0.025	0	0	0
Total	**1055.05**	**4057**	**773.85**	**4057**	**1055.26**	**4057**	**774.005**	**4057**	**1055.26**	**4057**	**774.005**	**4057**
34DHPVL (mg/kg)	0	0	0	0	200.898	0	200.257	0	0	0	0	0
EC (mg/kg)	0	0	0	0	0	0	0	0	200.898	0	200.257	0

$$DD = \frac{SD \times BW}{FI}$$

Formula 3.1: Formula to calculate the required pellet concentrations of EC or 34DHPVL
DD: Diet dose; SD: Single daily dose; BW: Body weight; FI: Daily food intake. For this study, values had the following input: SD = 20 mg compound/kg body weight; BW = 35 g; FI= 3.5 g diet/day. Resulting in DD = 200 mg compound/kg diet.

3.4.3 Power calculation

Cremonini *et al* (127) have reported a mouse dietary intervention study feeding C57BL/6J mice EC at 20 mg/kg body weight in combination with a low-fat (10 % kcal) or high-fat (60 % kcal) diet for 15-weeks (N = 10). They reported that EC supplemented into HF diet fed mice improved insulin sensitivity (measured by a glucose tolerance test) compared to non-supplemented controls, and this did so with a power of 50 %. This study was therefore used as a backbone to perform a power calculation to identify the numbers of mice required in the current study presented in this chapter.

Power calculations were performed using R Studio (version 3.6.1) with an effect size of 0.9829, a *p*-value of 0.05 and a power of 60 %. This computed a minimum mouse number of 12 mice per group. However, the batch differences in the mice arrivals meant there were uneven housing numbers of 2, 3 or 5 mice per cage with a total of 12-14 mice per group (specified in section 3.4.4).

3.4.4 Study design

All experiments described here were performed in compliance with the European Union regulations concerning the protection of experimental animals and with the UK Home Office Animals (Scientific Procedures) Act of 1986 under personal license I39D37621 and project license 70/8710.

Eighty healthy C57BL/6J male mice, aged 6-weeks, were purchased from Charles River, UK, and batches delivered every two weeks for a total of seven batches. They were acclimatised on chow diet RM3 (SDS Special diet services, UK) as supplied by the housing facility for 2-weeks. At 8-weeks of age, all mice were placed on a low-fat diet (10 % kcal) (LF) for 2-weeks. At 10-weeks of age, all mice were placed onto their respective intervention diets for 15-weeks: LF (14 mice), LF supplemented with 20 mg/kg body weight EC (LF+EC) (13 mice), LF supplemented with 20 mg/kg body weight 34DHPVL (LF+34DHPVL) (13 mice), high-fat (60 % kcal) (HF) (14 mice), HF supplemented with 20 mg/kg body weight EC (HF+EC) (12 mice) or HF supplemented with 20 mg/kg body weight 34DHPVL (HF+34DHPVL) (14 mice), see Table 3.1 for formulations. Body weight and food intake were measured weekly throughout the study.

Housing conditions consisted of between 2, 3 or 5 mice per cage and were kept in ventilation at 22 ± 2 °C with 55 ± 5 % humidity and 12-hour light-dark cycles. Mice cages were checked daily, and bedding and water was changed weekly by housing facility staff. Pellets were kept in the cage hoppers and freshly supplied every 2-3 days with continuous monitoring of cage consumption by weighing the amount consumed and subtracting this from the amount provided. All procedures throughout the study were performed in ventilated cabinets.

3.4.5 Glucose tolerance test and plasma glucose and insulin recording

During the 13th week of the intervention, mice were fasted for 16-hours overnight. Tails were locally anaesthetised using a lidocaine spray (Intubeaze® spray; Chapelfield Veterinary Partnership, UK) before bloodletting. An approximate 3 mm of tail length was cut and removed and allowed for blood sampling. Prior to glucose injection (0 mins), blood was collected into Microvette 200 µL EDTA blood collection tubes (Sarstedt, Germany, cat: 20.1288.100) and blood glucose concentration was recorded using a glucometer (Alphatrak 2 Starter Kit, Animed Direct, UK, cat: 15089). A 20 % D-glucose (Sigma, UK, cat: G8270) solution was prepared with PBS, and filtered (0.22 µm) on the same day as use. The glucose tolerance test (GTT) was then performed by intraperitoneally injecting the mice with the prepared glucose at 2 g /kg body weight, calculated as per Formula 3.2:

$$\mu L \text{ of } 20\ \% \text{ solution to inject} = \ 10\ \times Body\ Weight\ (g)$$

Formula 3.2: Calculating the volume of 20 % glucose solution to inject into mice

Glucose was administered via a 27G ½" BD Precision Glide syringe needle (Sigma, UK, cat:Z192384). Blood was then drawn by stroking the tail in a downwards direction and blood glucose was recorded at 15, 30, 60 and 120-mins post-injection, and blood was collected. Collected blood samples were centrifuged at 2000 g for 15 mins at 4 °C to collect the serum and immediately stored at -80 °C until use.

For intraperitoneal injection, mice were held via a tight scruff and turned onto their backs with head angling towards the ground at around a 60° angle. Their hind limbs would splay out, leaving enough room to inject into the intraperitoneal sack. Prior to needle removal, a light twist was performed to allow the injection site to seal. The mouse was then returned to its home cage.

To record plasma insulin from the GTT, an Insulin ELISA (Crystal Chem, Netherlands, cat:90080) was performed as per the manufacturer's protocol. Insulin concentrations in ng/mL were converted to mIU/mL (milli insulin units per millilitre) by using Formula 3.3 (342). The homeostatic model of insulin resistance (HOMA-IR) was later calculated using Formula 3.4 according to Matthews *et al* (1985) (343) and the QUICKI index by Formula 3.5 according to Katz *et al* (2000) (344).

$$\frac{\frac{ng}{ml}\text{insulin}}{1000} = \frac{mg}{L}\text{insulin} \quad \rightarrow \quad \frac{\frac{mg}{L}\text{insulin}}{\frac{0.0347mg}{U}\text{insulin}} = \frac{U}{L}\text{insulin} \quad \rightarrow \quad \frac{\frac{U}{L}insulin}{1000} = \frac{U}{mL}\text{insulin}$$

$$\rightarrow \frac{U}{mL}insulin \times 10^6 = \frac{\mu U}{mL}insulin$$

Formula 3.3: Conversion of ng/mL to µU/mL for insulin

$$HOMA\text{-}IR = \frac{I_0\ \left(\frac{\mu U}{mL}\right) \times G_0\ (mM)}{22.5}$$

Formula 3.4: HOMA-IR formula
I_0: is fasting plasma insulin, G_0: is fasting plasma glucose (343).

$$QUICKI = \frac{1}{Log(I_0)\left(\frac{mIU}{mL}\right) + Log(G_0)(\frac{mg}{dL})}$$

Formula 3.5:QUICKI formula
I_0: is fasting plasma insulin, G_0: is fasting plasma glucose (344).

3.4.6 Terminal anaesthesia and tissue harvest

Mice were sacrificed by cardiac puncture and PBS perfusion at 15-weeks into the intervention. This was performed by the described procedures in chapter 2, section 2.4.5 without urine collection. All blood collections were centrifuged at 2,000 g for 15 mins at 4 °C to collect the serum and stored at -80 °C until use.

Tissues were harvested immediately after cardiac puncture as per Table 3.2, these included: liver, brain, prostate, duodenum, jejunum, ileum, colon, aorta, epididymal fat, inguinal fat, and brown adipose tissue.

Table 3.2: Tissues harvested from C57BL/6J mice and their storage conditions

Tissue	Storage
Liver	• RNA later and stored at -40 °C • Snap frozen in liquid nitrogen and stored at -80 °C • Formalin 24-48 hours, 50 % ethanol for up to 2-weeks, embedded in paraffin and stored at 4 °C • Formalin 24-48 hours, 15 % sucrose until sunken, 30 % sucrose until sunken, OCT embedded, stored at -80 °C
Aorta	• RNA later and stored at -40 °C • Formalin 24-48 hours, 70 % ethanol for up to 2-weeks, embedded in paraffin and stored at 4 °C • OCT embedded, stored at -80 °C
Inguinal Fat	• RNA later and stored at -40 °C • Formalin 24-48 hours, 70 % ethanol for up to 2-weeks, embedded in paraffin and stored at 4 °C • Snap frozen in liquid nitrogen and stored at -80 °C
Epididymal Fat	• RNA later and stored at -40 °C • Formalin 24 - 48 hours, 70 % ethanol for up to 2 weeks, embedded in paraffin and stored at 4 °C • Snap frozen in liquid nitrogen and stored at -80 °C
Prostate	• RNA later and stored at -40 °C
Brown Adipose Tissue	• RNA later and stored at -40 °C • Snap frozen in liquid nitrogen and stored at -80 °C
Brain	• Snap frozen in liquid nitrogen and stored at -80 °C
Duodenum	• RNA later and stored at -40 °C • Snap frozen in liquid nitrogen and stored at -80 °C • Formalin 24-48 hours, 50 % ethanol for up to 2-weeks, embedded in paraffin and stored at 4 °C • Formalin 24-48 hours, 15 % sucrose until sunken, 30 % sucrose until sunken, OCT embedded, stored at -80 °C
Jejunum	• RNA later and stored at -40 °C • Snap frozen in liquid nitrogen and stored at -80 °C • Formalin 24-48 hours, 50 % ethanol for up to 2-weeks, embedded in paraffin and stored at 4 °C • Formalin 24-48 hours, 15 % sucrose until sunken, 30 % sucrose until sunken, OCT embedded, stored at -80 °C

Table 3.2: Tissues harvested from C57BL/6J mice and their storage conditions (continued)

Tissue	Storage
Ileum	• RNA later and stored at -40 °C • Snap frozen in liquid nitrogen and stored at -80 °C • Formalin 24-48 hours, 50 % ethanol for up to 2-weeks, embedded in paraffin and stored at 4 °C • Formalin 24-48 hours, 15 % sucrose until sunken, 30 % sucrose until sunken, OCT embedded, stored at -80 °C
Colon	• RNA later and stored at -40 °C • Snap frozen in liquid nitrogen and stored at -80 °C

3.4.7 Statistical Calculations

All statistical calculations were performed in R Studio, version 3.6.1. Linear mixed models were used through packages "lme4" (345) and "nlme" (346) with cage effects introduced as a random variable. Once a linear model was designed, residual variances were checked using "plot(linearmodel)", and checked for group residual variances by adding the diet (treatment) as an aesthetic:

```
data$residuals, <- resid(linearmodel)
ggplot(data , aes(y=residuals, x=treatment)) + geom_point()
```

Normality of the residuals was determined using "qqnorm(resid(linearmodel))". Only once the linear model assumptions were met (normally distributed residuals, equal variance distribution across all groups) was then "lme4::lmer" applied. If residuals were normally distributed but distinct differences across group residuals occurred, then "nlme::lme" was used to allow for a grouping factor for unequal residual variance, "weights=varIdent(form=~1|HFvsLF)". If, however, none of the above were met and grouping for unequal variance did not improve the residual scatter, then the data was transformed as specified in Table 3.3 and applied to the same methods. Statistically significant *p*-values were obtained through default methods 'Sattherthwaite', however 'Kenward-Roger' was also examined to determine if values were distinctly different, this was not the case for any of the data.

Table 3.3: Transformations made on the data for statistical analysis and the linear model R package used

Mouse Measurement	Transformation	R package used
Carbohydrate consumption	Log_{10}	lmer
Fat consumption	Log_{10}	lmer
FER	Log_{10}	nlme
Body weight	N/A	nlme
Liver weight	N/A	nlme
Epididymal weight	N/A	nlme
Glucose data	N/A	nlme
Insulin data	N/A	nlme
HOMA-IR	$\sqrt{x}$	nlme
QUICKI	$\frac{1}{\sqrt{x}}$	nlme

3.5 Results

3.5.1 (–)-Epicatechin but not 3',4'-dihydroxyphenyl-γ-valerolactone supplementation inhibited high-fat diet induced body weight gain in mice

Body weight was continuously monitored throughout the 15-week dietary intervention study to determine whether the different diets influenced body weight gain. Table 3.4 displays the final weights for each dietary group and Figure 3.2 shows the overall change in body weights throughout the intervention period. Before the mice commenced the intervention, they weighed an average of 24.62 ± 1.32 g, this was regardless of the different batch arrivals of mice over several weeks. At the end of the 15-week intervention, all mice on diets of LF, LF+EC and LF+34DHPVL had consistent body weights within 1-2 g of each other, and thus the supplementation of EC or 34DHPVL into low calorie diets did not influence changes in body weight between groups.

For LF diet fed mice, at the end of the study they had gained 5.78 ± 1.43 g in weight from when they commenced the study, whereas HF diet fed mice gained 23.4 ± 3.59 g in weight (Figure 3.2 B). For the mice on HF diets supplemented with or without compound, they weighed significantly more than all LF dietary intervention fed mice ($p < 0.0001$), gaining an average of 0.176-0.223 g in body weight per day when compared to LF intervention fed mice (0.049-0.055 g body weight gain per day) at the end of the study. HF diet fed mice supplemented with EC weighed significantly less than HF diet fed mice (43.18 ± 6.59 g versus 47.92 ± 3.80 g, $p = 0.028$, respectively), showing that an effect of EC supplementation was bioprotective against high-fat diet induced body weight gain. In contrast, 34DHPVL supplemented into HF diet fed mice did not affect body weight gain when compared to non-supplemented controls (46.43 ± 1.94 g), and so, HPVLs did not contribute to the protective effects seen by EC consumption on body weight.

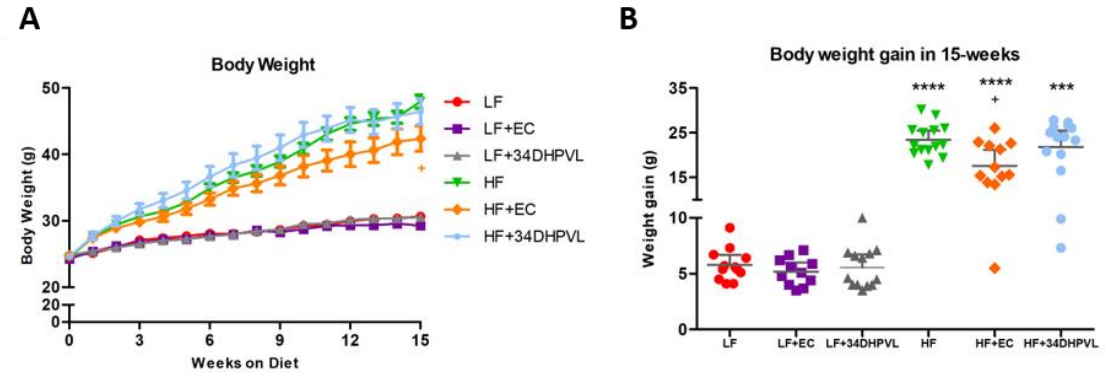

Figure 3.2: Mouse body weight data

*A) Body weights of each dietary intervention group over the 15-week intervention; B) Body weight gain in mice over 15-weeks of dietary intervention, each point represents an individual mouse. All errors bars represent standard error. Significance ***p < 0.001, ****p < 0.0001 compared to LF diet. $^{+}$ p < 0.05 compared to HF diet.*

Table 3.4: Mouse weights and dietary consumption data
*Unless otherwise specified, all weights presented are final values at the end of the 15-week intervention. Food intake and food efficiency ratio (FER) are calculated as average intakes over the entire 15-weeks. All errors represent standard deviation. Significance *p < 0.05, **p < 0.01, ***p < 0.001, ****p < 0.0001 compared to LF diet. $^{+}$p < 0.05, $^{++++}$ p < 0.0001 compared to their respective controls (HF with supplements are compared to HF, LF with supplements are compared to LF).*

	LF	LF+EC	LF+34DHPVL	HF	HF+EC	HF+34DHPVL
Initial body weight (g) (week 0)	24.8 ± 1.07	24.4 ± 1.37	24.7 ± 1.68	24.5 ± 1.04	24.7 ± 1.73	24.6 ± 1.54
Final body weight (g)	30.7 ± 1.20	29.5 ± 1.83	30.2 ± 2.48	47.9 ± 3.80 ****	42.4 ± 6.59 $^{****+}$	46.4 ± 7.21****
Weight gain (g/mouse/day)	0.06 ± 0.01	0.05 ± 0.01	0.05 ± 0.02	0.22 ± 0.03 ****	0.18 ± 0.05 $^{****+}$	0.21 ± 0.06****
Food intake (g/mouse/day)	3.10 ± 0.21	3.13 ± 0.07	2.86 ± 0.28^{++++}	2.67 ± 0.16 ****	2.60 ± 0.13****	2.73 ± 0.15****
Calorie consumption (kcal/mouse/day)	11.8 ± 0.47	11.8 ± 0.77	10.5 ± 0.76 $^{++++}$	13.9 ± 0.83 ****	13.7 ± 0.69 ****	14.4 ± 0.89 $^{+****}$
EC or 34DHPVL consumption (mg/mouse/day)	-	0.62 ± 0.04	0.55 ± 0.04	-	0.52 ± 0.03	0.55 ± 0.03
FER	1.75 ± 0.22	1.56 ± 0.22	1.87 ± 0.25	8.06 ± 1.06 ****	6.15 ± 1.36****	7.31 ± 2.44****
Liver weight (g)	1.26 ± 0.24	1.21 ± 0.20	1.17 ± 0.19	1.79 ± 0.39 **	1.57 ± 0.35	1.93 ± 0.64***
Liver weight to body weight ratio	0.04 ± 0.01	0.04 ± 0.01	0.04 ± 0.01	0.04 ± 0.01	0.03 ± 0.01	0.04 ± 0.01
Epididymal weight (g)	0.74 ± 0.30	0.54 ± 0.12	0.70 ± 0.31	2.60 ± 0.39 ****	2.39 ± 0.81****	2.18 ± 0.66****
Epididymal weight to body weight ratio	0.02 ± 0.01	0.02 ± 0.00	0.02 ± 0.01	0.06 ± 0.01 ****	0.06 ± 0.02***	0.05 ± 0.01**

3.5.2 High-fat consumption caused significant weight increases in the liver and epididymal adipose tissues compared to the low-fat treatment group

At the point of sacrifice, livers and epididymal fat mass from the mice were weighed. This helped to identify whether the different interventions caused weight changes in these internal organs and whether these organs were responsible for the differences seen in final body weights.

For HF diet fed mice, their livers weighed an average of 1.79 ± 0.39 g, and this was significantly heavier than LF diet fed mice (1.26 ± 0.24 g, p = 0.0022), however, liver weight gain was lower when

EC was supplied into the HF diet (1.57 ± 0.35 g), whereas liver weight gain was higher when 34DHPVL was supplied into the HF diet (1.93 ± 0.64 g), but the differences by either supplement were not significant (Figure 3.3 A, Table 3.4). For EC supplemented into HF diet fed mice and compared to LF non-supplemented mice, there was borderline significance between their liver weights (p = 0.0786). Therefore, EC supplementation does appear to have a modest effect in inhibiting liver weight gain by 12 % from fat.

Liver to body weight ratio was also calculated to understand whether liver weight gain in HF diet fed mice occurred irrespective of body weight gain. However, the consistent mean data values across all dietary interventions (Figure 3.3 B) suggests that liver weight gain occurred because of body weight gain, i.e. EC mitigated liver weight gain in HF diet fed mice when compared to HF controls because they had a reduction in body weight.

Surprisingly, EC supplementation into the HF diet caused no significant reduction in epididymal adipose weight, when compared to the non-supplemented diet (2.39 ± 0.81 g versus 2.60 ± 0.39 g, p = 0.29), (Figure 3.3 C). The same was true for 34DHPVL supplemented into HF diet fed mice, although the mean was lower compared to the HF diet fed mice, the high variance likely prevented a significant effect from being detected (2.18 ± 0.66 g, p = 0.16). Furthermore, for all HF intervention fed mice, their epididymal mass to body weight ratio was significantly higher than the LF fed mice (Figure 3.3 D). This suggests that all HF fed mice stored the extra calories they consumed as white adipose tissue.

Regression analyses were performed to determine whether a correlation existed between liver weight or epididymal weight to body weight (Figures 3.3 E/F) to identify whether body weight caused an increase in weight of these tissues. The results highlight a strong positive correlation for both liver weight (p < 0.0001, R^2 = 0.64) and epididymal weight (p = 0.0001, R^2 = 0.74) to body weight.

Finally, changes in the weights of the livers of LF diet fed mice supplemented with 34DHPVL or EC were not different to the values of non-supplemented controls.

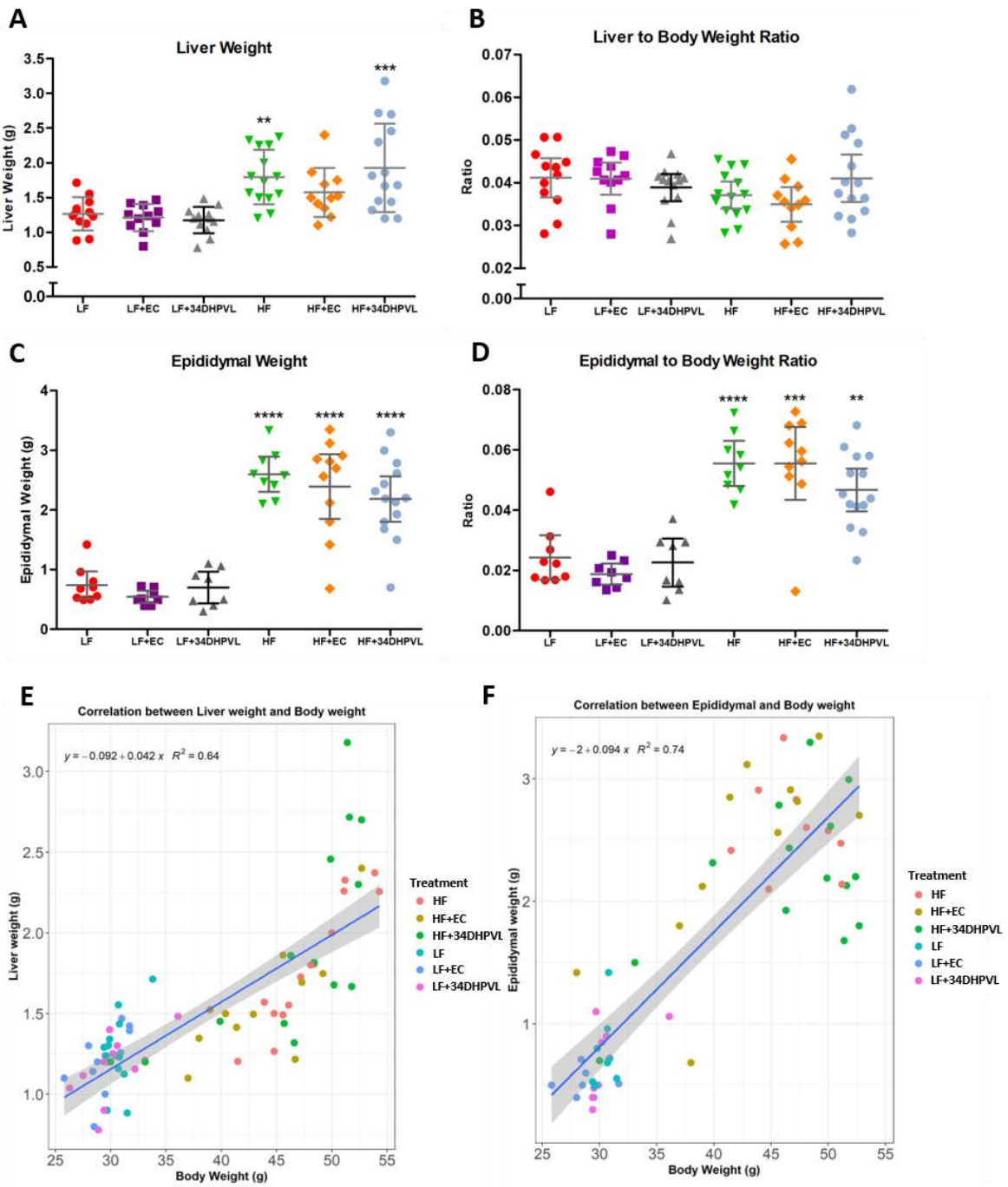

Figure 3.3: Epididymal adipose and liver tissue weights from mice

*All weights were recorded at the point of sacrifice. A) Final liver weights; B) Liver weight to body weight ratio; C) Epididymal adipose tissue weight; D) Epididymal adipose tissue weight to body weight ratio; E) Regression analysis for liver weight and body weight; F) Regression analysis for epididymal weight and body weight. Each point represents an individual mouse on that respective diet. Bars represent 95 % confidence intervals with means. Significance **p < 0.01, ***p < 0.001, ****p < 0.0001 compared to LF diet.*

3.5.3 Mice on low-fat diets consumed more food compared to those on high-fat diets

Cage food consumption was monitored throughout the duration of the intervention study. It was anticipated that this data would be useful in the interpretation of differences between diets in the weight gain observed, i.e. were differences in weight gain correlated with the rates of food consumption.

For LF diet fed mice, food consumption was higher by 0.24-0.54 g/mouse/day than mice on the HF fed diet (3.10 ± 0.21 g/mouse/day versus 2.67 ± 0.16 g/mouse/day, $p < 0.0001$, respectively) (Table 3.4), which suggests that satiety was reached earlier on from the HF diet. The same was true for mice on LF diets supplemented with EC but not for those supplemented with 34DHPVL where their food intake was reduced (2.86 ± 0.28, $p < 0.0001$) by an average of 0.26 g/mouse/day when compared to LF diet only fed mice. An assumption made to understand this could be that 34DHPVL influenced the palatability of the LF diet (possibly bitterness), or because it caused satiety to be reached earlier. In contrast, 34DHPVL supplemented into the HF diet caused mice to consume more food than those on the non-supplemented diet, but with borderline significance ($p = 0.065$). It is possible that the greater lard content of the HF diet compared to the LF diet overcame the potential palatability issue with 34DHPVL (similar to the situation with chocolate where the fat and sugar mask the bitterness of the cocoa polyphenols). However, because of the differences in dietary consumption across the groups, the mass of polyphenol consumption was different in all supplemented groups, refer to Table 3.4 for values.

Figure 3.4 A shows a graph of the nutritional intake following each dietary intervention. For all HF dietary interventions, the mice consumed significantly more protein ($p < 0.0001$), more calories ($p < 0.0001$), more fat ($p < 0.0001$) and less carbohydrates ($p < 0.0001$), compared to LF diet fed mice. 34DHPVL supplemented into the HF diet caused a significant increase in calorie and protein intake compared to non-supplemented mice, which is due to the greater food consumption observed for mice in this group. However, because mice on the diet of 34DHPVL supplied in combination with the LF diet consumed less food compared to the LF control, this was also accompanied by a significant reduction in their calorie ($p < 0.0001$), protein ($p = 0.0002$), carbohydrate ($p < 0.0001$) and fat ($p < 0.0001$) intake, nevertheless this caused the consumption in the amount of 34DHPVL to be equal in both the LF and HF supplemented diets (0.55 ± 0.04 mg).

The average daily consumption of EC and 34DHPVL in mice was between 0.52-0.62 mg/day, which when converting to a human equivalent dose using the reverse of Formula 2.1 in chapter 2, section 2.4.3 and the final body weights of the mice, equates to a human daily intake of 67.42-119.5 mg/day

(for 70 kg person body weight). Humans in Europe consume an average daily EC dose of 24 mg/day (306), but there is large interindividual and intercountry variation where doses are shown to exceed 100 mg/day as discussed by Vogiatzoglou *et al* (306). The amount consumed by mice in this study therefore reflects a physiological amount consumed in humans, especially those consuming a variety of food sources high in polyphenols.

To determine how efficient the mice were at converting their food intake into body weight, a feed efficiency ratio (FER) was calculated as per Formula 3.6:

$$FER = \frac{Weight\ gain\ (g)}{Food\ Intake\ (g)}$$

Formula 3.6: Feed efficiency ratio calculation

The results showed that all HF dietary intervention fed mice had a significantly higher FER when compared to LF fed mice (Figure 3.4 B, Table 3.4), and so smaller quantities of food intake resulted in greater mass gain. Furthermore, the addition of either EC or 34DHPVL into either HF or LF diets did not affect the FER.

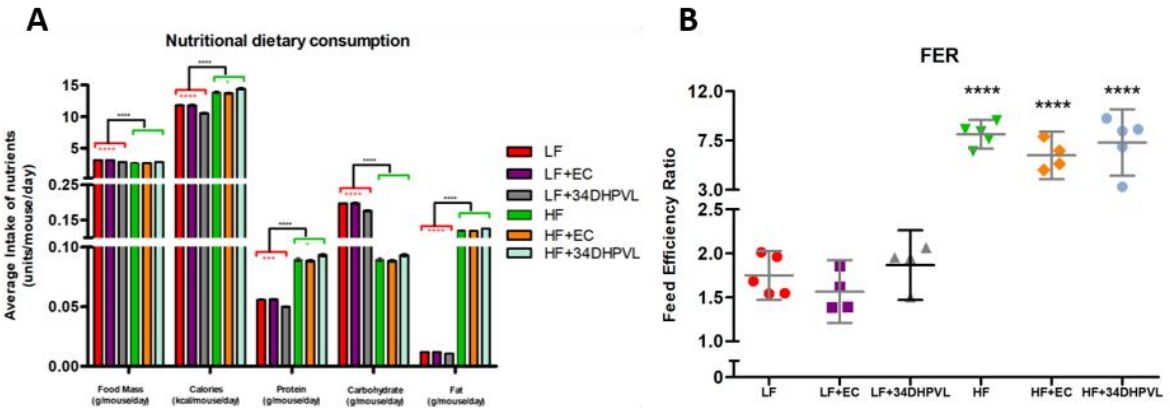

Figure 3.4: Mice dietary consumption data

*A) Average dietary intake for all groups over the 15-week intervention. Values were calculated from the nutritional information of the food pellets; error bars represent standard error. B) Feed efficiency ratio dot plot, each point represents the average of a cage in the respective dietary group. Bars represent 95 % confidence interval with mean. Significance **** $p < 0.0001$ compared to LF diet. $^{+}$ $p < 0.05$, $^{+++}$ $p < 0.001$, $^{++++}$ $p < 0.0001$ compared to their respective controls (HF with supplements are compared to HF, LF with supplements are compared to LF).*

3.5.4 (−)-Epicatechin but not 34DHPVL supplementation of high-fat diet fed mice caused an improvement in insulin sensitivity compared to high-fat controls

Glucose tolerance tests (GTT) were performed in week-13 of the intervention by supplying a 2 g/kg body weight bolus glucose dose to the mice and measuring their blood glucose and insulin levels over time; if they re-established baseline blood glucose levels within 2-hours, then this was indicative of a good response to insulin. The test provided a measure for insulin resistance, where the HOMA-IR and QUICKI was calculated. This test allowed for the identification of whether EC or 34DHPVL protected against HF diet induced insulin resistance.

Initial results demonstrated that mice on all LF dietary interventions responded quicker in returning their glucose levels than all mice on HF dietary interventions, Figure 3.5 A. Despite all mice having received the same dose of glucose at 2 g/kg body weight, the mice on all LF dietary interventions achieved a lower glucose C_{max} (maximum concentration) than all mice on the HF dietary interventions, (Table 3.5). This indicated that all LF diet fed mice were receptive to the low concentration of insulin released (Figure 3.6 A) to prevent rises in blood glucose. Blood glucose levels in all LF dietary intervention treatment groups rapidly declined between 30-60 mins post-injection, and so they responded quickly in returning glucose homeostasis.

The supplementation of 20 mg/kg body weight EC into LF diet fed mice caused a significant reduction in the glucose area under the curve (A.U.C) when compared to the non-supplemented group (1824 ± 24 mmol/L versus to 2221 ± 394 mmol/L, $p = 0.028$, respectively) (Figure 3.5 B); but, they did not release more insulin to cause this effect, and were thus insulin sensitive.

In contrast, all HF diet fed mice exhibited significantly higher baseline glucose levels (67 ± 3 % more) when compared to the LF mice ($p \leq 0.006$). Therefore, because they also exhibited significantly higher levels of blood insulin ($p \leq 0.002$) (Figure 3.6 A), they were unable to respond to insulin in lowering blood glucose, which is a clear sign of insulin resistance. Immediately following the glucose injection in all HF intervention treatment groups, was a sharp rise in blood glucose where they had 6.32-9.24 mmol/L higher glucose concentrations at the C_{max} compared to LF diet fed mice. Blood glucose levels only started to decline in all HF treatment groups at 60 mins post-injection, which was significantly delayed compared to LF diet fed mice. At 120 mins following the glucose dose, HF diet fed mice reduced their blood glucose levels by only 14 ± 7 % (a drop in 4.92 mmol/L) from their C_{max}, which was much less than the 58 ± 8 % (a drop in 15.72 mmol/L) decrease observed for LF

dietary fed mice. Thus, HF diet fed mice struggled to restore baseline blood glucose levels, and as a consequence of this there was a 73 % higher glucose A.U.C compared to LF diet fed mice.

The addition of EC or 34DHPVL into the HF diet was associated with an improvement in the lowering of blood glucose compared to non-supplemented mice. All HF diet fed mice expressed similar baseline glucose levels, but, only EC supplemented into HF diet fed mice had significantly lower glucose levels from their C_{max} (a reduction by 12.13 mmol/L) by the end of the test, when compared to HF diet fed mice. Additionally, this group also exhibited lower levels of blood insulin, which confirms that EC supplied in combination with the HF diet increased insulin sensitivity and ameliorated HF diet induced insulin resistance. Surprisingly, 34DHPVL supplied in combination with the HF diet caused mice to exhibit lower glucose concentrations throughout the GTT (borderline significance at 120 mins, $p = 0.0609$) in comparison to HF diet fed mice. This could be due to their significantly higher blood insulin levels observed throughout the test, i.e. even though high plasma insulin suggests they are insulin resistant, the fact that insulin levels are so high might mean that there is still an insulin response. Despite these results, there were no differences between the glucose A.U.C concentrations over time between HF fed mice with or without compound supplementation.

Furthermore, LF dietary fed mice supplemented with 34DHPVL also displayed lower glucose levels during the test than LF fed mice, and they expressed significantly higher baseline insulin levels. Therefore, the addition of 34DHPVL into low-fat or high-fat diets seemed to initiate similar effects.

To identify whether blood glucose levels correlated with mice body weight, a regression analysis was performed using individual mouse blood glucose A.U.C values and their respective body weights at week-13 of the intervention (Figure 3.5 B). The results showed a strong positive correlation between the two variables, $p = 0.0191$, $R^2 = 0.67$, i.e. an increase in body weight was strongly associated with an increase in blood glucose concentrations, such that heavier mice struggled to reduce blood glucose compared to lighter mice.

Table 3.5: Glucose and insulin values following GTT

*GTT was performed at week-13 of the dietary intervention study and insulin and glucose concentrations were recorded throughout the 120-minute experiment. Please refer to Figure 3. 5, Figure 3. 6 and Figure 3. 7 for the graphical illustrations. All values illustrated are means with standard deviation. C_{max}: maximum concentration; T_{max}: time to reach maximum concentration; A.U.C: area under curve values from the figures. Significance **** $p < 0.0001$ compared to LF diet. $^{+}$ $p < 0.05$, $^{++}$ $p < 0.01$ compared to their respective controls (HF with supplements are compared to HF, LF with supplements are compared to LF).*

	LF	LF+EC	LF+34DHPVL	HF	HF+EC	HF+34DHPVL
Glucose A.U.C (mmol/L)	2221 ± 394	1824 ± 249^{+}	2029 ± 273	3681 ± 419 ****	3635 ± 621 ****	3513 ± 599 ****
Glucose C_{max} (mmol/L)	26.9	21.3	23.0	36.1	35.2	33.2
Glucose T_{max} (mins)	30	30	30	60	60	60
Insulin A.U.C (ng/ml)	24.4 ± 16.9	20.7 ± 5.07	32.2 ± 11.1	85.2 ± 31.8**	77.4 ± 36.9*	157 ± 98.2 ****$^{++}$
Insulin C_{max} (ng/ml)	0.26	0.21	0.30	1.07	0.82	1.60
Insulin T_{max} (mins)	30	15	15	120	120	120
HOMA-IR	0.58 ± 0.21	0.90 ± 0.20	2.30 ± 0.49	12.2 ± 1.90 ****	6.74 ± 1.76**	21.8 ± 3.61 ****
QUICKI	0.40 ± 0.07	0.44 ± 0.04	0.35 ± 0.01	0.28 ± 0.01***	0.32 ± 0.02*	0.27 ± 0.01 ****

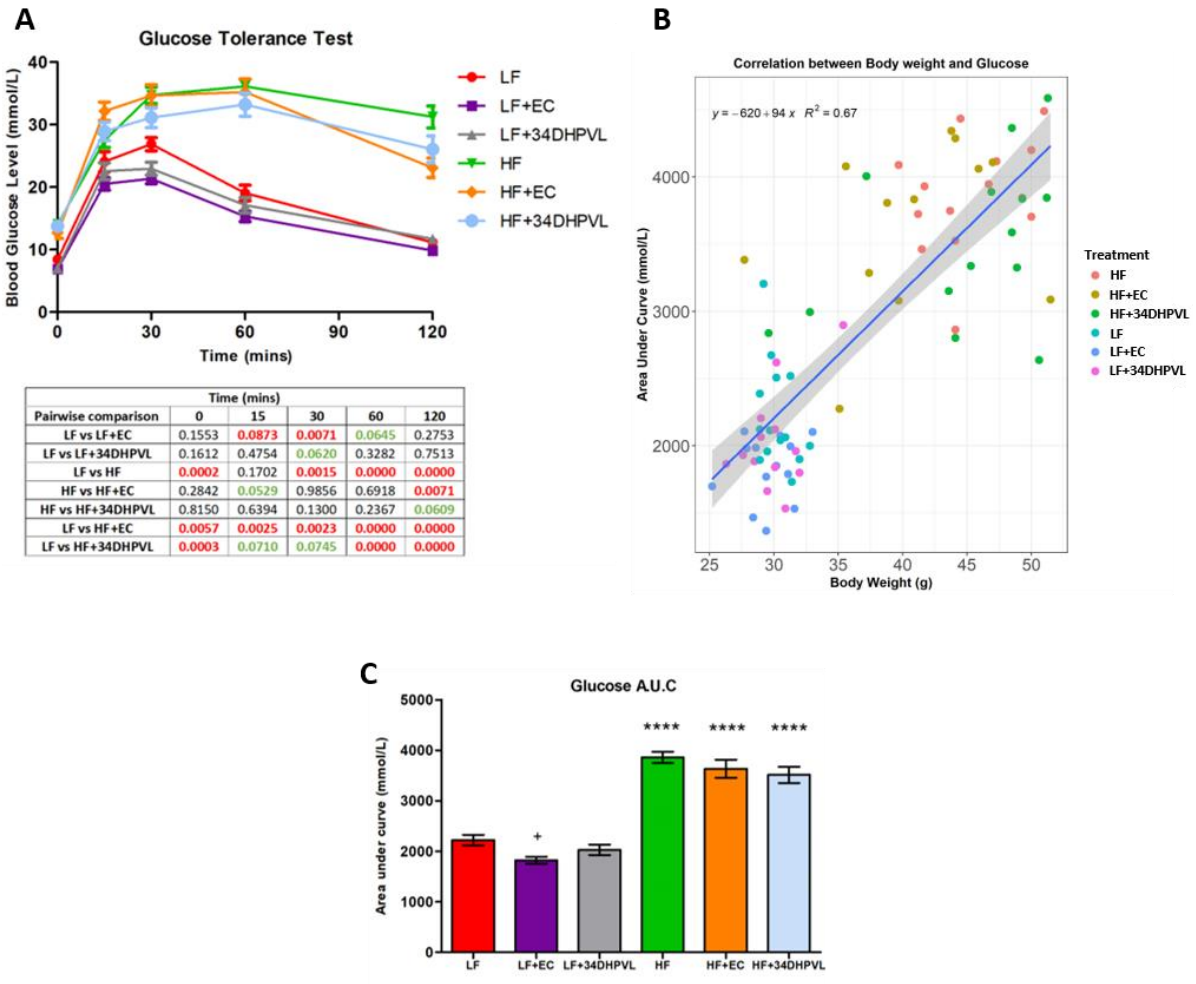

Pairwise comparison	Time (mins) 0	15	30	60	120
LF vs LF+EC	0.1553	0.0873	0.0071	0.0645	0.2753
LF vs LF+34DHPVL	0.1612	0.4754	0.0620	0.3282	0.7513
LF vs HF	0.0002	0.1702	0.0015	0.0000	0.0000
HF vs HF+EC	0.2842	0.0529	0.9856	0.6918	0.0071
HF vs HF+34DHPVL	0.8150	0.6394	0.1300	0.2367	0.0609
LF vs HF+EC	0.0057	0.0025	0.0023	0.0000	0.0000
LF vs HF+34DHPVL	0.0003	0.0710	0.0745	0.0000	0.0000

Figure 3.5: Glucose data from the GTT

*GTT was performed in week-13 of the dietary intervention A) Glucose concentrations in plasma recorded for 120 mins after the glucose injection. Statistical p-values for each comparison at specific time-points are displayed in the table beneath the graph: red values are statistically significant, green values are borderline significant, black values are of no significance; B) Regression line for glucose area under curve values against body weight, each point represents an individual mouse and the grey shading is the 95 % pointwise confidence interval; C) Area under curve (A.U.C) values from graph A for each dietary group. All graphical error bars represent standard error. Significance **** $p < 0.0001$ compared to LF diet. $^{+}$ $p < 0.05$, compared to their respective controls (HF with supplements are compared to HF, LF with supplements are compared to LF).*

3.5.5 Mice on diets supplemented with 3',4'-dihydroxyphenyl-γ-valerolactone exhibited significantly higher baseline insulin levels

Insulin concentrations during the GTT were determined using an insulin ELISA kit and from the plasma samples harvested from the mice at recorded times.

Before the test, baseline blood levels for mice on diets of EC in combination with LF, and LF, were at expected physiological levels, and slowly increased by 15-30 mins post-injection and declined

almost immediately back to baseline by 120 mins (Figure 3.6 A). This small change in insulin response reflects the high level of sensitivity of their insulin receptors to stimulate glucose uptake and induce glycogenesis.

The baseline insulin levels for 34DHPVL supplemented LF diet fed mice were significantly higher by 400 ± 500 % ($p = 0.002$) than LF diet fed mice, and in addition, they expressed modest changes in their insulin levels after injection. It is possible that the mice fed the 34DHPVL supplemented LF diet exhibited more insulin to compensate for the high blood glucose levels that arose after food consumption, although this is unlikely because it was a fasted test. In contrast, EC supplemented LF diet fed mice did not exhibit alterations in insulin levels throughout the test, when compared to LF only fed mice, but they did respond better in restoring their glucose levels by the end of the GTT.

All HF diet fed mice consistently exhibited much higher insulin levels at baseline and throughout the GTT. There was also a clear time lag of 60 mins for the mice to respond to the glucose and raise their insulin levels, consequently, the rise in insulin was not sufficient to restore baseline glucose levels by the end of the 2-hours. Overall, HF intervention fed mice expressed a total rise in insulin of 0.5 ± 0.16 ng/ml compared to the 0.2 ± 0.3 ng/ml rise from LF intervention fed mice. These results show that all the HF diet fed mice are insulin resistant, presumably because the pancreatic β-cells are overworked to produce insulin in order to restore glucose levels, or because 34DHPVL inhibits a regulator of insulin, but because the insulin receptors were desensitised, there was a reduced efficiency to restore blood glucose.

The supplementation of EC in the HF diet of mice lowered baseline insulin levels ($p = 0.18$) and they responded more efficiently in lowering blood glucose levels by the end of the test compared to HF controls. Baseline insulin levels in 34DHPVL supplemented HF diet fed mice were significantly higher than the HF control (1.17 ± 0.68 ng/ml compared to 0.65 ± 0.31 ng/ml, $p = 0.008$, respectively), and this was despite an almost identical starting glucose concentration. The overall pattern in response to the glucose injection was very similar for 34DHPVL supplemented into HF diet fed mice and HF fed mice, where there was a total increase of 0.45 ng/ml insulin in both groups. However, because the experiment was stopped after 2-hours, it was not possible to determine where the end-point insulin C_{max} levels were.

To identify whether there was a correlation between insulin levels and body weight, a regression analysis was performed using the insulin A.U.C values for each mouse and their respective body weights at 13-weeks into the intervention (Figure 3.6 B). This showed there was a strong positive correlation between the two variables ($p < 0.0001$, $R^2 = 0.65$), i.e. higher body weight was associated

with higher blood insulin concentrations. The positive correlations for both glucose and insulin to body weight is indicative that heavier mice required more insulin to lower their blood glucose levels.

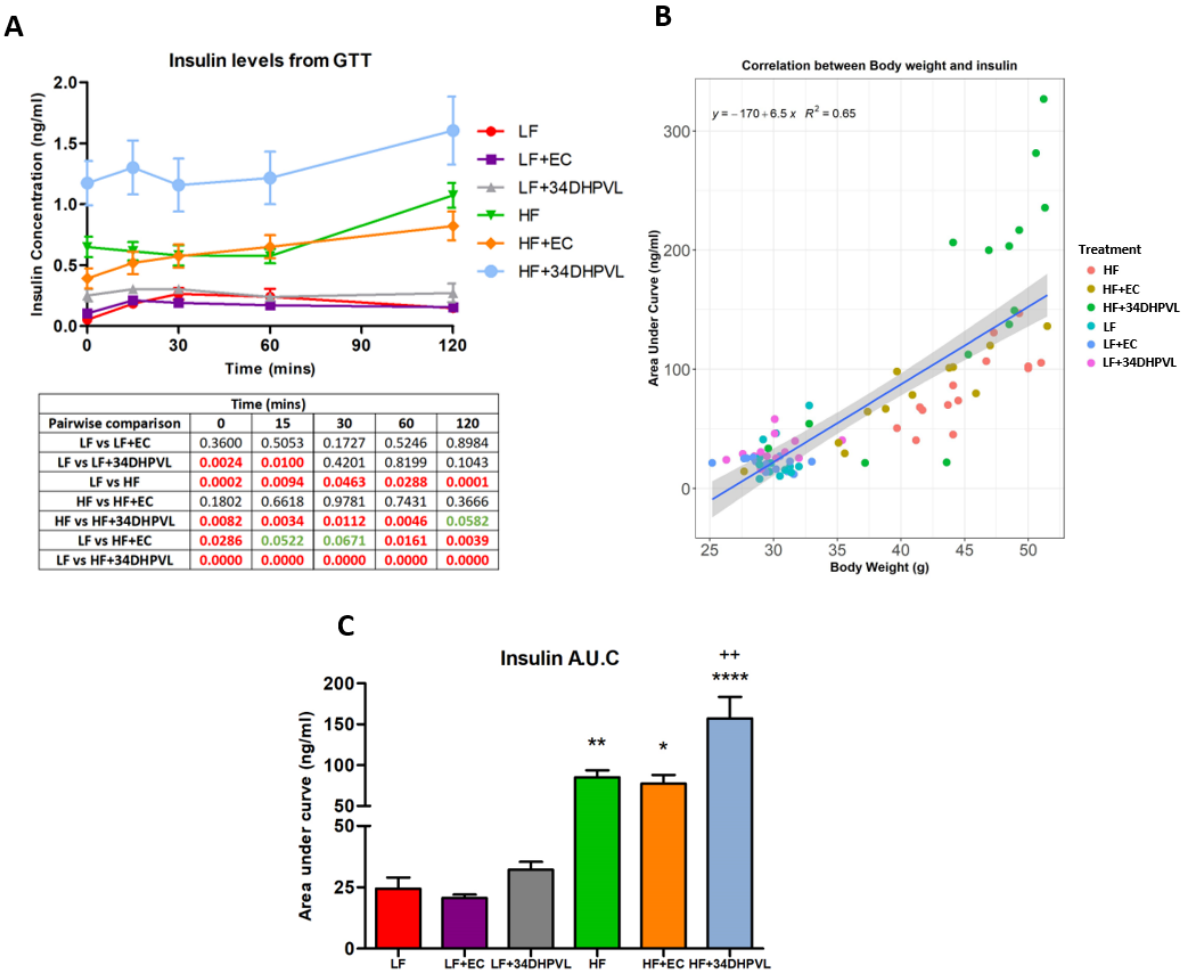

Time (mins)					
Pairwise comparison	0	15	30	60	120
LF vs LF+EC	0.3600	0.5053	0.1727	0.5246	0.8984
LF vs LF+34DHPVL	0.0024	0.0100	0.4201	0.8199	0.1043
LF vs HF	0.0002	0.0094	0.0463	0.0288	0.0001
HF vs HF+EC	0.1802	0.6618	0.9781	0.7431	0.3666
HF vs HF+34DHPVL	0.0082	0.0034	0.0112	0.0046	0.0582
LF vs HF+EC	0.0286	0.0522	0.0671	0.0161	0.0039
LF vs HF+34DHPVL	0.0000	0.0000	0.0000	0.0000	0.0000

Figure 3.6: Insulin data from the GTT

*GTT was performed during week-13 of the dietary intervention and insulin levels were recorded throughout. A) Insulin concentrations in plasma up to 120 mins after the glucose injection. Statistical p-values for each comparison and time point are displayed in the table beneath the graph: red values are statistically significant, green values are borderline significant, black values are of no significance; B) Regression line for insulin area under curve values against body weight, each point represents an individual mouse and the grey shading is the 95 % pointwise confidence interval; C) Area under curve (A.U.C) values from graph A for each dietary group. All graphical error bars represent standard error. Significance * $p < 0.05$, ** $p < 0.01$, **** $p < 0.0001$ compared to LF diet. $^{++}$ $p < 0.01$, compared to their respective controls (with supplements are compared to HF, LF with supplements are compared to LF).*

3.5.6 (−)-Epicatechin supplemented high-fat diets caused an improvement in insulin sensitivity compared to high-fat diet fed mice

The homeostatic model assessment of insulin resistance (HOMA-IR) is a model derived by Matthews *et al* (1985) (343) that has been approved to quantify the levels of insulin resistance; where scores lower than 2.5 are indicative of a 'normal' insulin response to glucose. Conversely, the quantitative insulin sensitivity check index (QUICKI) is a method to quantify insulin sensitivity as opposed to insulin resistance (344); where indexes > 0.382 classify non-obese subjects, ~ 0.331 classifies obese subjects and < 0.304 classifies diabetic subjects (344). Blood insulin and glucose concentrations from the GTT were applied to these checks as per Formulas' 3.3 and 3.4 in the methods section.

Mice fed the EC supplemented LF diet or the non-supplemented LF control diet had HOMA-IR scores < 1.0 and QUICKI scores > 0.38 (Table 3.5, Figure 3.7), which are optimal scores that suggest a normal sensitivity to insulin. In contrast, mice fed the 34DHPVL supplemented LF diet exhibited early signs of insulin resistance, evidenced by a HOMA-IR between 1.9-2.9 (p for difference = 0.062, and QUICKI 0.29-0.43, p = 0.10) when compared to LF diet fed mice; this is mostly due to their higher blood insulin levels.

Moreover, for mice on all HF interventions, they expressed a HOMA-IR > 2.9 and a QUICKI = 0.27, which was significantly higher when compared to LF diet fed mice ($p \leq 0.0002$). Consequently, all HF diet fed mice exhibited insulin resistance. However, EC supplemented into the HF diet and compared to HF diet fed mice caused a reduction in the mean HOMA-IR score (6.74 ± 6.11 compared to 12.23 ± 7.12, p = 0.072, respectively) (Figure 3.7). The large variance seen in the scores in this dietary group shows that the protection against insulin resistance afforded by consuming EC was greater in some mice more than others.

The opposite of this was true for mice fed the 34DHPVL supplemented HF diet, which exhibited a HOMA-IR of 21.76 ± 13.52, and a mean QUICKI score of 0.27 (borderline significant compared to the HF only intervention group, p = 0.078). This would suggest that this group of mice were more insulin resistant.

This study has provided novel data to show that 34DHPVL can promote higher blood insulin levels in both low and high calorie diets. Meanwhile, it has reinforced the existing published evidence surrounding ECs ability to mitigate high-fat diet induced insulin resistance.

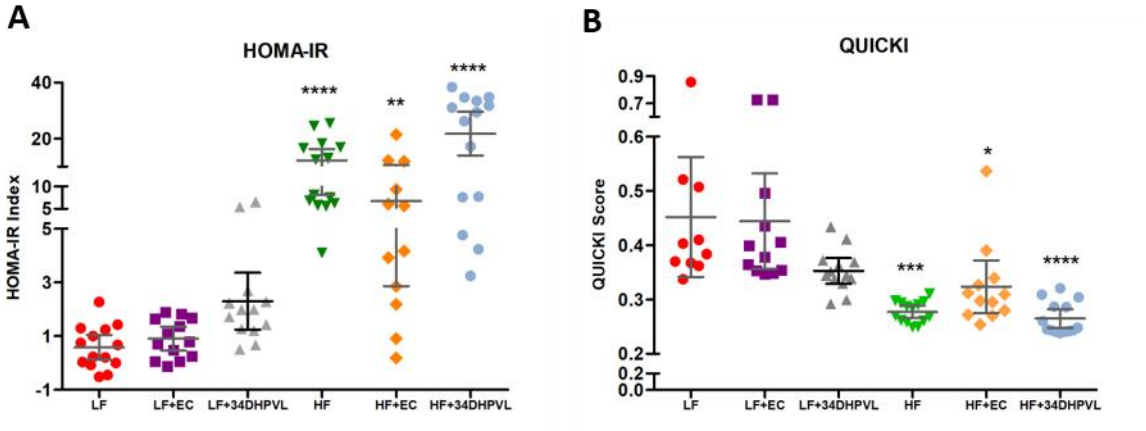

Figure 3.7: Insulin resistance data

*Glucose and insulin concentrations from the GTT for each mouse were used to calculate: A) HOMA-IR (Formula 3.3) and B) QUICKI (Formula 3.4). Each point represents an individual mouse. Bars represent 95 % confidence intervals. Significance * $p < 0.05$, ** $p < 0.01$, *** $p < 0.001$, **** $p < 0.0001$ compared to LF diet.*

3.6 Discussion

This research study was performed to investigate whether 34DHPVL could protect against high fat diet induced insulin resistance, and as such, whether HPVLs were the causative agents for the changes that ultimately manifest as improved sensitivity to insulin by EC consumption in high-fat diets. Subsequently, this work has shown that:

(1) EC slowed the progression of insulin resistance in HF diet fed mice.

(2) 34DHPVL supplementation of both HF and LF diets caused an increase in fasting baseline blood insulin levels when compared to their non-supplemented controls.

(3) 34DHPVL supplementation of both HF and LF diets caused a better response to glucose challenge in lowering blood glucose when compared to their non-supplemented controls.

(4) EC mitigated weight gain when supplemented into HF diet fed mice, whilst 34DHPVL did not.

(5) Mice on LF diets consumed more food but less calories than mice on HF diets.

(6) 34DHPVL affected the daily amount of food consumed in both HF and LF dietary fed mice.

This is the first report describing how HPVLs, when provided directly in the feed of mice, induces the effects observed with relation to insulin resistance. As a result, this discussion will be largely focussing on how EC influences insulin resistance in mice, which can also drive hypothesised mechanisms for how 34DHPVL exerts the effects seen in the mice in this study, and more specifically how it could raise fasting insulin concentrations.

3.6.1 How might 3',4'-dihydroxyphenyl-γ-valerolactone raise baseline insulin concentrations?

EC has been previously reported to protect against insulin resistance in HF diet fed mice/rat models and to mitigate the onset of weight gain (127, 129, 130, 224, 226, 227). However, due to the negligible concentrations of unmetabolized parent EC that enters a human's circulatory system (347, 348) and the understanding that unmetabolized parent EC does not circulate in rodents (1, 5), it is necessary to identify what the active EC metabolite(s) are. Because one third of EC metabolites that reach the systemic circulation are HPVLs in humans (1) and in rodents (5), one of

the main objectives of this research was to investigate whether or not HPVLs are bioactive metabolites of EC.

The prolonged consumption of a HF diet over time can cause obesity and insulin resistance, both hallmarks of metabolic syndrome (MetS) (349-352). MetS increases the incidence of metabolic associated fatty liver disease (MAFLD), itself caused by a series of inflammatory events that lead to dysregulation of liver functions and glucose metabolism (350). The study presented in this chapter reports a potential protective effect of HPVLs against HF diet induced insulin resistance, however, the results are inconclusive. HPVLs supplemented into the LF and HF diets caused lower glucose levels following a glucose challenge compared to their respective controls, however, the results were not statistically significant. These data suggests that HPVLs may be partly responsible for the beneficial effects of EC consumption on HF diet induced insulin resistance, but additional research, for example a more powerful study with greater numbers of mice than the one described here, and testing of more biological markers is necessary to generate further evidence to address this question. The HPVL fed mice also had much higher insulin concentrations than HF diet fed mice, consequently, the insulin sensitivity calculations provided poorer scores (HOMA-IR and QUICKI), which would normally be regarded as a sign of insulin resistance despite exhibiting lower glucose levels than their controls. Normally, a higher fasting insulin concentration implies that the β-cells are continually stimulated to secrete insulin and keep glucose levels down, but the responsiveness of the mice to the insulin in reducing glucose suggests that this might not necessarily be the case here. If the high insulin levels occurred because of impaired hepatic insulin clearance rather than hypersecretion by the pancreas, then this could favour the protection against insulin resistance. But, because this is the first study to provide 34DHPVL into the feed of mice and investigate insulin resistant effects, it has therefore proved to be hypothesis generating.

There are several plasma markers that could have been assessed in this study to provide more information to explain the actions of 34DHPVL on raising fasting insulin concentrations, such as C-peptides (hepatic insulin clearance marker), leptin (a marker that reduces gluconeogenesis and favours glucose uptake), and creatinine (kidney functions for urinary excretions), but aspartate transaminase/alanine transaminase (AST/ALT) levels are reviewed in chapter 4 with histology of the liver. However, because these effects were not anticipated, further plasma marker analysis was not performed. Because of this, a discussion of the current evidence that reports similar effects to those seen in this study will be considered.

Following a randomised control study in humans of different ethnicities, it was reported that non-Hispanic blacks expressed higher fasting insulin concentrations than non-Hispanic White's or

Mexican American's, despite no signs of diabetes and no family history of diabetes (353). But, by assessing plasma insulin and C-peptide concentrations, they could determine that the higher insulin concentrations were most likely due to insufficient insulin clearance via the liver because there was a correlation for high insulin to low C-peptide levels. Meanwhile in White and Mexican individual's they expressed low insulin with high C-peptide levels. C-peptides and insulin are released from pancreatic β-cells at the same time in equimolar amounts (354), but C-peptides are metabolised by the kidneys whereas insulin is metabolised by the liver (355). Because of this, the low level detection of C-peptides and the high level detection of insulin implies that there was an impaired hepatic insulin clearance in non-Hispanic blacks (353). This study's findings were also supported by Rossell *et al* (1983) (355) in obese subjects, where only obese individuals suffered from hyperinsulinemia and low C-peptide levels, and so expressed a low clearance of insulin by the liver. The rationale for this effect was suggested to be because when "the portal insulin concentration increases, the liver is incapable of increasing its capacity to remove insulin" (355). An even earlier study found similar findings for hyperinsulinemia accompanying low C-peptide levels in patients who suffered from liver cirrhosis, where their livers were so badly damaged that they encountered insufficient insulin clearance (354). And, when these patients blood glucose levels were examined, only cirrhotic subjects displayed significantly elevated blood glucose levels, however, the glucose levels and concentration of insulin secreted did not differ between the hyperinsulinemic and normoinsulinemic subjects (354). Furthermore, the effect of weight loss has been shown to increase hepatic insulin clearance and restore insulin sensitivity (356), and so demonstrating that these effects can be reversed. But, because C-peptide levels were not recorded in this current study, it is only a suggestion that 34DHPVL may impair insulin clearance, but it would support the evidence for the lower blood glucose and the higher insulin levels seen in the mice when compared to controls.

If insulin clearance is impaired following 34DHPVL supplementation into the diet, then it could be eliciting actions through several processes. The impairment of insulin clearance can cause hepatic steatosis because chronic hyperinsulinemia can stimulate hepatic *de novo* lipogenesis (357-360), and therefore, the impairment of insulin clearance could be the link between hepatic insulin resistance and steatosis. High circulatory insulin concentrations can also cause the desensitisation and lysosomal degradation of the insulin receptor (361) via inactivating or deleting the glycoprotein 'carcinoembryonic antigen-related cell adhesion molecule 1' (CEACAM1), that has a central role to promote hepatic insulin clearance (362). Chapter 5 discusses in detail the CEACAM1 gene expression changes by the dietary interventions. To summarise, there were marginal reductions in its expression for 34DHPVL supplemented into HF diet fed mice, but there were marginal increases

in its expression for EC supplemented into HF diet fed mice when compared to HF controls. Therefore, this data somewhat supports the notion that 34DHPVL impairs hepatic insulin clearance.

In this current study, 34DHPVL supplemented into high fat diet fed mice expressed lower glucose levels throughout the GTT than their non-supplemented controls. This suggests a pre-diabetic state in this group of mice because they were still responsive to the rise in insulin by lowering their blood glucose, and they did so more rapidly than HF only fed mice. Because of this, it is hypothesised that 34DHPVL supplemented into the diet of mice caused an impairment in insulin clearance through the inactivation or desensitisation of the CEACAM1 receptor, rather than the hypersecretion of insulin. This effect over time would cause insulin resistance and type-2 diabetes, which was seen by the poorer response of the mice to lower blood glucose than LF diet fed mice (363). Finally, because impaired insulin clearance is also inversely correlated with liver lipid accumulation (364), this could help to explain why 34DHPVL supplemented into HF diet fed mice expressed higher liver lipids (as discussed in chapter 4 of this thesis).

3.6.2 Mechanistic insights of how the consumption of (–)-epicatechin can cause improvements in insulin sensitivity

The results presented in this chapter report a protective effect of EC against HF diet induced body weight gain and insulin resistance in mice. EC supplied in combination with the HF diet improved the response to insulin-induced glucose reduction compared to HF diet fed mice which was evidenced by lower insulin levels and an overall improvement in their insulin resistance/sensitivity scores (HOMA-IR and QUICKI). These findings reinforce the literature which report protective effects of EC against HF diet induced insulin resistance and body weight gain, and in the following sections these shall be discussed to establish what is known about how EC induces these positive changes.

In 2019, Cremonini *et al* (128) reviewed ECs role in the mitigation of insulin resistance, specifically focussing on how EC inhibits the production of oxidants through NADPH oxidase and NF-κB, JNK, IKK and protein kinase C (PKC) signalling pathways. As highlighted in chapter 1 of this thesis, the activation of these pathways causes the phosphorylation of serine residues on IRS-1 receptors, and subsequently desensitises these receptors to insulin over time (153-158). Cocoa products which are rich in EC and other flavanols have been shown to decrease the phosphorylation of serine on IRS-1 in Zucker-diabetic fatty rats (199) and in HF diet fed mice that had been supplemented with EC, and this was accompanied by reductions in IR/IRS-1 phosphorylation and downstream signalling

proteins Akt and ERK1/2 in the liver and adipose tissue (127). Similar findings were confirmed following the incubation of EC with HepG2 cells, which restored insulin sensitivity via preventing palmitate induced activation of NADPH oxidase, and by reducing IR phosphorylation in mice (129). Furthermore, EC has been reported to lower the oxidation of lipids or proteins in the liver (129, 229), adipose tissue (229) and intestines (130). These are all putative mechanisms for how EC supplementation could improve insulin sensitivity in mice in this current study.

EC has been well documented to mitigate the inflammatory events caused by HF diet consumption, particularly in the liver and adipose tissue (224, 225), which can subsequently affect glucose metabolism and insulin sensitivity (127). One explanation to describe this effect could be because EC is reported to protect the tight junction barrier integrity of the small intestines in mice (130), and subsequently protected against HF diet induced intestinal inflammation which would otherwise cause a 'leakier' gut and allow for paracellular transport of bacterial and dietary antigens. Consequently, EC ameliorated inflammatory mediated NAFLD and insulin resistance (232, 365-367). It is thought that EC and other polyphenols protect the intestinal barrier by preventing HF diet induced gut microbiome dysbiosis (368). This could be a mechanism of action for the effects seen by EC in this current study, but experimental validation would be required to prove this.

Furthermore, another explanation for the effects seen by EC in combination with the HF diet in this this chapter could be because of enhanced mitochondrial biogenesis. It has been previously reported that EC regulates redox potential and the phosphorylation of IR/IRS-1 whilst preserving mitochondrial biogenesis (227, 230). This is relevant because pancreatic β-cells regulate insulin secretion mostly through their mitochondria, and mitochondrial dysfunction contributes to insulin resistance (369, 370). EC has been shown to increase the protein levels of mitochondrial related biogenesis genes: proliferator-activated receptor gamma coactivator-1-alpha (*PGC1α*), mitochondrial transcription factor A (*TFAM*), sirtuin-1 (*SIRT1*), sirtuin-3 (*SIRT3*), and uncoupling protein 1 (*UCP1*) in adipose tissue and skeletal muscle of mice on HF diets and compared to HF treatments (230). These effects were also confirmed following the isolation and culture of obese participants adipose tissue with EC (230).

In summary, these studies highlight that EC could act to improve insulin sensitivity and mitigate insulin resistance effects by improving mitochondrial function, enhancing mitochondrial biogenesis, deactivation of inflammatory signalling, reductions in ROS production, and by interfering with serine phosphorylation on IR/IRS-1 receptors. Although these markers were not assessed in this current study, these effects could be possibly caused by HPVLs from EC consumption to improve

the response of circulating insulin to lower blood glucose, but because no studies have addressed this question, further studies are required to explore this gap in the literature.

3.6.3 The consumption of high-fat diets caused an increase in body weight gain and a reduction in the mass of food consumed compared to low-fat diet fed mice

Consistent with the literature, this investigation has confirmed that a 60 % kcal from fat in HF diet fed mice can induce a significant increase in body weight, along with the weights of liver and epididymal adipose tissue and the epididymal to body weight ratio throughout the 15-week intervention (371-373). However, the liver to body weight ratio did not alter between the six dietary intervention groups, which has also been confirmed by Sano *et al* (224), and so the increase in liver weight was because of rises in body weight. This chapter also reports a significantly higher epididymal adipose weight to body weight ratio in in all HF intervention fed mice than LF intervention fed mice which implies that the excess calorie consumption was stored as white adipose tissue, as has been previously reported (374).

This chapter also reports a significant decrease in the mass of food consumed by mice on the HF diet when compared to the LF diet. This is due to the greater calorie intake, where HF diet fed mice consumed 5.2 kcal/g compared to 3.8 kcal/g from the LF diet. Mice will only consume the energy that they require, and so to ensure that mice put on weight and become fatter, the diet needs to be modified for where the main source of calories comes from (375). To explain this, the consumption of high calories from fat can suppress the oxidative capacity of the mitochondria in the liver and skeletal muscle (376, 377), and consequently this slows down metabolism and causes greater weight gain. In addition, studies have also shown that mice fed HF diets express high circulatory leptin levels (378); a hormone that regulates appetite and is associated with decreased food consumption (379). Although leptin levels were not recorded in this current study, there is enough evidence in the literature to suggest that the decreased appetite in HF diet fed mice is because of high circulatory leptin levels, which is an active attempt to control excess weight gain in mice (228, 378, 380). Furthermore, this current study shows an increase in the daily average food intake in mice on diets of 34DHPVL supplied in combination with HF and compared to the HF only treatment group. This could be because the mice developed an insensitivity to leptin which is reported to occur by HF diet consumption. For example, Lin *et al* (2000) (378) reported that HF diet fed mice experienced waves of sensitivity to leptin; in the first couple of months they secreted more

leptin to slow down dietary consumption of the excess calories, and after 19-weeks, they developed leptin resistance, and thus caused an increase in dietary consumption and more dramatic weight gain (378). In this current study, the supplementation of 34DHPVL into the HF diet could somehow be exacerbating the effects of leptin resistance. Unfortunately, leptin levels were not recorded throughout this intervention study to understand whether this was an underlying mechanism.

Finally, the amount of polyphenols consumed by mice in this study is representative of a physiological dose consumed in humans, particularly those with high polyphenol diets, and thus the physiological and phenotypical effects seen in mice here could be good predictors for those in humans.

3.6.4 The mechanistic effects of (–)-epicatechin, but not 3',4'-dihydroxyphenyl-γ-valerolactone, in ameliorating high-fat diet induced body weight gain in mice

In this current study, the supplementation of EC at 20 mg/kg body weight significantly mitigated HF diet induced weight gain in mice. This finding has been reinforced by Sano *et al* (224) and Cremonini *et al* (127, 130) where the effects on inhibiting body weight gain were seen at supplied concentrations of EC at 200 mg/kg body weight (224) and at 20 mg/kg body weight (127, 130). And so, the consumption of EC at physiological concentrations are sufficient to induce obesity protective effects.

The metabolic actions underlying how EC prevents body weight gain has been scarcely explored. However, it could act by influencing mitochondrial biogenesis, and by stimulating a brown adipose tissue (BAT) phenotype in white adipose tissue (WAT), as has been shown previously (230). They reported that the BAT phenotype was induced following an increase in mitochondrial density, which subsequently drove the transcription of thermogenic genes and raised fatty acid β-oxidation (230).

The main flavanol researched for its disease protective effects is EGCG, especially with regards to the prevention of weight gain from high calorie consumption/cell culture environments (368, 381-383). Thus, it is assumed that EC has similar effects to EGCG but of lower potency, as it is known that its lack of gallate reduces its bioactivity in comparison to EGC, ECG and EGCG (381, 384, 385). To demonstrate the anti-weight gain effects from these compounds, the *in-vitro* culture of 3T3-L1 mouse pre-adipocyte cell lines with EC, EGC, and EGCG (100-400 μM), showed that all three compounds induced apoptosis in pre-adipocytes and increased the levels of caspase-3 activity, an apoptotic enzyme (384-389). Further findings reported that EGCG binds to the Fas death receptor

to then activate caspase-3 (390, 391). Moreover, EGCG has been shown to phosphorylate (activate) AMPK and its downstream substrates in 3T3-L1 cells through the increase in ROS, resulting in the mitigation of adipocyte differentiation (385) in male Wistar rats (392), male Sprague Dawley rats (393), and female C57BL/6J mice (394). The downstream effects from activated AMPK are to suppress the stimulation of peroxisome proliferator activator receptor-γ (PPARγ) and CCAAT/enhancer binding protein α (C/EBPα), both regulators of adipocyte differentiation (386), and the transcription factor SREBP-1c that enhances lipogenesis and adipogenesis (387). Lu *et al* (2012) (395) has also reported the anti-obesogenic effects of green tea polyphenols, rich in EGCG, via the reversal of 11/12 obesity regulated gene expressions in Virgin Sprague Dawley female rats, in support with other studies (396-398). These actions therefore caused an increased energy expenditure in the rats through the activation of genes such as *Adcyap1r1* and *Adrb1*, and thus increased the rate of lipolysis and a reduction of body fat (398). It is therefore highly plausible that EC in this current study could be inducing these same actions in mice.

By observing the weight gain in mice on all six dietary interventions in this current study, it has allowed for conclusion on whether both EC and 34DHPVL can prevent high fat diet induced weight gain. Taken together, these observations support the notion that EC metabolites (SREMs) and not the respective microbiota derived HPVLs, are the causative agents that cause the reduced weight gain in HF diet fed mice. There is sufficient evidence from published reports to suggest how EC may induce anti-obesogenic effects, and so, both EC and 34DHPVL influenced different pathways and functions in mice once consumed orally.

3.7 Conclusion

The dietary intervention mouse study performed in this chapter has formed the foundations for this thesis and upcoming chapters with a primary aim to determine whether 34DHPVL was responsible for mitigating insulin resistance effects in high fat diet fed mice, using EC as a positive control. The results of this investigation have resulted in the following hypotheses and conclusions in this chapter:

(1) EC reduced weight gain and insulin resistance effects from high fat diet fed mice most likely by mechanisms reported previously in the literature.

(2) 34DHPVL supplementation increased food consumption in high fat diet fed mice possibly by increasing circulatory leptin concentrations and desensitising cells to leptin.

(3) The consumption of both EC and 34DHPVL in mice represent physiological dose consumption in humans, and so the effects seen in mice could be predictive for those in humans.

(4) 34DHPVL supplementation in mice induced hyperinsulinemia through a hypothesised process of decreased insulin clearance by the liver, which in return induced pre-diabetes, seen by impaired glucose metabolism.

Overall, this study provides evidence to suggest that HPVLs could be partly responsible for improving insulin sensitive effects following EC consumption. The study's experimental limitations demonstrate that more research is required to prove the above generated hypotheses. These include recording circulatory leptin and C-peptide levels throughout the entire duration of the intervention, in addition to performing more targeted experiments on insulin sensitive tissues (skeletal muscle, pancreas and liver) to assess the protein concentrations and activity levels of insulin receptors and downstream activation pathways.

Chapter Four

EXPLORING THE BIOLOGICAL CHANGES INDUCED BY (−)-EPICATECHIN AND 3',4'-DIHYDROXYPHENYL-γ-VALEROLACTONE WHEN SUPPLEMENTED INTO HIGH-FAT AND LOW-FAT DIET FED MICE

Chapter 4: Exploring the biological changes induced by (−)-epicatechin and 3',4'-dihydroxyphenyl-γ-valerolactone when supplemented into high-fat and low-fat diet fed mice

4.1 Abstract

Background: Metabolic associated fatty liver disease (MAFLD, formerly known as non-alcoholic fatty liver disease) arises following the continued consumption of high calorie diets which causes its hallmark features for liver steatosis, hepatic insulin resistance and hepatic damage/fibrosis. But there are several studies that report the protection against MAFLD and more specifically hepatic lipid accumulation in high-fat (HF) diet fed rodents that have been supplemented with (−)-epicatechin (EC). The current evidence for this indicates a reduction in hepatic *de novo* lipogenesis (DNL) processes. But there is no evidence to suggest whether hydroxyphenyl-γ-valerolactones (HPVLs), which are the most abundant circulatory metabolites of (−)-epicatechin (EC), mediate these effects from EC consumption. Therefore, the livers from the mouse intervention study (chapter 3) were processed to explore the physiological and phenotypical markers for lipids, fibrosis, and inflammation, in order to assess whether consumption of EC or 34DHPVL caused significant changes in this metabolic organ.

Aim: To quantify the effects of 20 mg/kg body weight consumption of EC and 34DHPVL on liver lipids, and biomarkers of fibrosis and inflammation, and plasma lipids and liver damage markers, when supplemented into low-fat (LF) and HF diets of mice.

Methods: Livers were harvested at the end of the intervention study (chapter 3) and processed as follows: paraffin embedded liver sections were stained for hematoxylin and eosin (H&E), Sirius red, and CD11B to observe the level of steatosis, fibrosis, and inflammation, respectively; cryopreserved liver sections were stained using LipidTox™ to observe liver lipids; and cryopreserved liver lobes were subjected to the Bligh and Dyers method for lipid extraction and quantification. Finally, an alpha amylase enzyme assay was performed using the PAHBAH method to quantify release of maltose from corn starch alone or when incubated in the presence of the α-amylase inhibitor acarbose, or with EGCG or 34DHPVL to determine whether 34DHPVL could inhibit enzyme activity.

Results: Mice on the HF and HF+34DHPVL interventions exhibited a 2-fold increase in hepatic lipids when compared to the LF diet ($p < 0.01$), whilst the mice on the HF+EC diet exhibited a 33 ± 3 % reduction in liver lipids than the HF controls (not significant). Furthermore, all HF intervention fed mice exhibited significantly higher levels of low-density lipoproteins (LDL), cholesterol, high-density

lipoproteins (HDL) and HDL3 levels in plasma when compared to LF diet fed mice ($p < 0.05$). But there were no significant changes observed in plasma lipids following the supplementation of EC or 34DHPVL into HF diets of mice and compared to non-supplemented HF controls. No significant differences were detected in the levels of liver fibrosis between any of the HF and LF intervention fed mice, despite several mice exhibiting severe liver damage on the LF intervention, as determined by Sirius red staining. Finally, the activity of alpha amylase on starch was not inhibited by 34DHPVL, but the well-known inhibitor acarbose almost completely inhibited α-amylase activity.

Conclusion: In line with previous studies, EC was able to mitigate the accumulation of liver lipids in mice fed HF diets. In contrast with the literature, EC supplementation into HF diet fed mice was not successful in lowering serum lipids when compared to non-supplemented mice. This indicates that EC caused a reduction in hepatic DNL but had no effect on circulatory lipid clearance. Moreover, there was no evidence to indicate that 34DHPVL protected against hepatic lipid accumulation in high fat diet fed mice. Furthermore, both the HF and LF (LF was also high in complex carbohydrates) diets induced liver damage, which was most likely to have occurred via the activation of inflammatory signalling pathways, that high-fat and high-carbohydrate diets are known to stimulate. Finally, because 34DHPVL was not successful in inhibiting alpha amylase activity, this was evidence to suggest that it does not affect the digestion of starch and consequently it was not a mechanism for its glucose lowering effects seen in mice. Overall, EC provided a level of protection against hepatic lipid accumulation but not against liver damage or inflammation, whereas, 34DHPVL did not exert protective effects against HF diet induced MAFLD.

4.2 Introduction

The dietary intervention study that was performed in chapter 3 has provided evidence for the protective effects against insulin resistance from EC or 34DHPVL supplemented HF diet fed mice, and these effects also indicate towards the protection against MAFLD. This chapter is purposed to investigate the physiological changes that are induced by MAFLD and whether EC or 34DHPVL influence these. Before this can be discussed, it is essential to understand the relevance and mechanisms of DNL and lipolysis, and so this shall be explained in this introduction.

4.2.1 Regulation of fatty acids

The ingestion of high calorie diets in the form of saturated fats can prove detrimental to health in the long-term, contributing to obesity, cardiovascular disease (CVD), metabolic syndrome, insulin resistance and metabolic associated fatty liver disease (MAFLD) (399). Controlling fat intake, as well as understanding its metabolism and oxidation, can assist in the prevention of disease. Moreover, other dietary components, especially polyphenols, have been shown to modulate lipid metabolism (400-405) such as by slowing down the rate of fat oxidation (129, 130, 229), and so, this highlights the benefits of dietary control.

4.2.1.1 Lipolysis

After food ingestion, the mouth, stomach, and pancreas secrete lipase enzymes to hydrolyse the primary ester bonds of short-chain triglycerides. But, most of the breakdown of triglycerides occurs in the small intestine where around 50-70 % of fatty acids are formed as a result (406). Due to the hydrophilic nature of short and medium chained fatty acids, they can be passively absorbed through the stomach and transported to the liver via the portal vein (407). On the other hand, long chain fatty acids are hydrophobic and form lipid droplets in the form of micelles that are later absorbed through enterocytes into the lymphatic system and eventually transported into the circulation. Moreover, dietary phospholipids continue into the jejunum for continued hydrolysis (407).

In adipose tissue, the enzymes adipose triglyceride lipase (ATGL) and hormone-sensitive lipase (HSL) are responsible for more than 90 % of triglyceride hydrolysis, however, in the liver, ATGL is responsible for less than 50 % of their hydrolysis (408). These enzymes are activated by PPARγ agonists, glucocorticoids and by fasting, whereas insulin decreases their expression levels. The rise in ATGL transcriptomic mRNA levels is initiated by SIRT1-mediated deacetylation of FOXO1, but the levels of ATGL are not always reflective of lipase activity. The further activation of ATGL also occurs

by AMP-activated protein kinase (AMPK) once it has been activated by phosphorylation of a serine residue, cryptically, AMPK has also been shown to inhibit lipolysis (408). An alternative activation approach of ATGL occurs from the β-adrenergic stimulation of perilipin-1 (PLIN-1), subsequently causing the release of comparative gene identification-58 (CGI-58), that binds to and activates ATGL (Figure 4.1) (409). Meanwhile, the actions of HSL are to hydrolyse diacylglycerols, whilst monoacylglycerol lipase (MGL) hydrolyse monoacylglycerols, and both contribute to around 10 % of triglyceride breakdown (410). HSL is activated once it is phosphorylated by PKA and AMPK and fully activated by the binding of phosphorylated PLIN-1.

For non-adipose tissue lipolysis, the mechanism for activation is very similar to that mentioned previously for PLIN-1 activation, but instead for the protein perilipin-5, which recruits both ATGL and CGI-58 for complete ATGL activation (Figure 4.1) (408). The liver also produces autophagy-related protein 7 (Atg7), an autolipophagosome, that consumes cytoplasmic lipid droplets and fuses with lysosomes for their degradation (408). However, chronic fat feeding impairs this process and ultimately causes lipid accumulation in the liver, which is a precursor for the development of MAFLD. In contrast, even under normal fasting conditions, autophagy has been shown to promote lipid accumulation, thus playing pleiotropic roles. Finally, the liver protein PNPLA3 (patatin-like phospholipase domain-containing protein 3), also known as adiponutrin, expresses high homology to ATGL and has been shown to act as a triglyceride hydrolase, however, its exact role remains unclear because it has also been reported to activate genes involved in lipid production (408).

In contrast to lipolysis processes, insulin promotes lipid storage in the liver by "increasing *de novo* lipogenesis (DNL), suppressing fatty acid oxidation, and promoting triglyceride esterification"(411). In normal circumstances, the liver will contribute to around 10-37.5 % of fatty acids produced by DNL processes in the postprandial period (399). Insulin also reduces the rate of lipolysis through transcriptional downregulation of ATGL and HSL and via Akt induced phosphorylation of phosphodiesterase 3B (PDE3B) isoforms that prevents phosphorylation of HSL and PLIN-1 (408). Furthermore, insulin can activate lipoprotein lipase (LPL) on the capillary endothelium of adipocytes, and so, this causes the hydrolysis of triglycerides in chylomicrons and very-low density lipoproteins (vLDL) found in the circulation system (412). Once diacyglycerols are formed they can act as second messengers and activate protein kinase-C (PKC), which in turn can phosphorylate the insulin receptor substrate-1 (IRS-1), and over-time this can cause IR desensitisation in the liver and muscles (408).

4.2.1.2 Lipogenesis

Fatty acid synthesis is an integral process to allow for fat storage, brain myelination and for the survival of cells because they are incorporated into membrane tissue formations (413). Lipogenesis involves the formation of fatty acids as well as triglycerides by the liver and adipose tissue, and is otherwise known more commonly by DNL (414). To stimulate DNL, consuming high carbohydrate diets causes a rise in plasma glucose levels, whereas continuous HF consumption causes the onset of insulin resistance, both of which contribute to DNL activation. High circulatory glucose levels activate lipogenic genes by two mechanisms (1) raising circulatory insulin concentrations, which has been discussed previously to stimulate DNL, and (2) converting glucose to acetyl-CoA, which enters a series of enzymatic reactions to produce triglycerides.

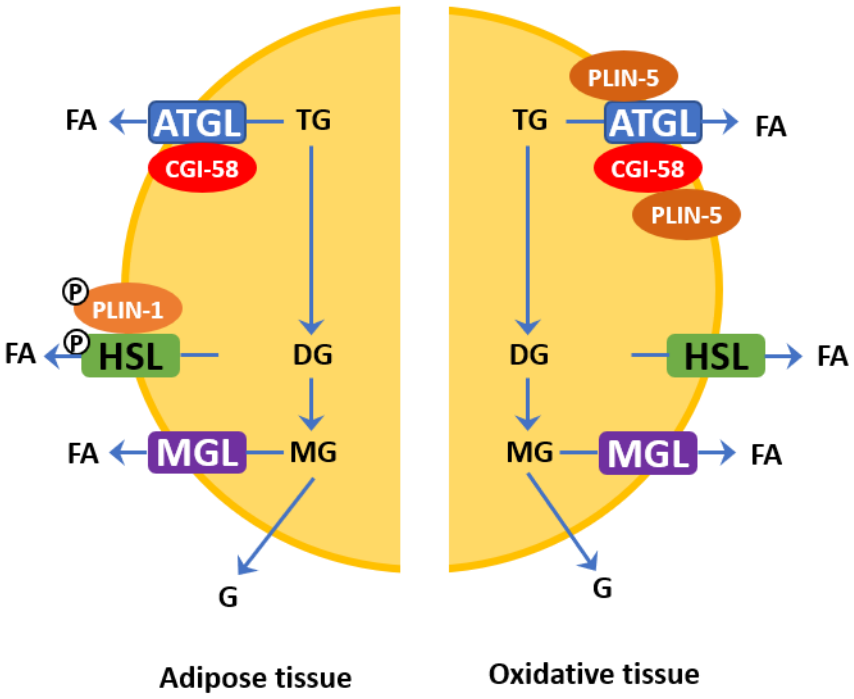

Figure 4.1: Lipolysis during fasting in adipose and oxidative tissues
In adipose tissue, β-adrenergic stimulation of lipolysis activates the three enzymes 'adipose triglyceride lipase' (ATGL), 'hormone-sensitive lipase' (HSL) and 'monoacylglycerol lipase (MGL). ATGL cleaves the first ester bond in triacylglycerols (TG), HSL hydrolyses diacylglycerols (DGs), and MGL hydrolyses MGs. For full activation of ATGL, 'comparative gene identification-58' (CGI-58) binds to it, whereas HSL is phosphorylated by 'protein kinase A' (PKA) or by 'adenosine monophosphate-activated protein kinase' (AMPK) and recruits phosphorylated perilipin (PLIN)-1 for activation. In oxidative tissues, PLIN-5 is present instead of PLIN-1 and interacts with both ATGL and CGI-58. G: glycerols; FA: fatty acids.

To describe the production of triglycerides from acetyl-CoA, firstly it is converted to malonyl-CoA by acetyl-CoA carboxylase (ACC), itself activated by protein phosphatase 2a (PP2a)-mediated

dephosphorylation (415). Fatty acid synthase then acts on malonyl-CoA to elongate the chain by two carbons at a time to a carbon-16 chained molecule, and is finally released as palmitate (416) (Figure 4.2). Moreover, the production of malonyl-CoA from acetyl-CoA can inhibit carnitine palmitoyltransferase (CPT-1) on the mitochondria and thus control the rate of fatty acid entry, as such, high malonyl-CoA levels, as supplied by high carbohydrate diets, can suppress mitochondrial fatty acid oxidation and increase triglyceride formation. The reverse of the above process is mediated by AMPK that can phosphorylate and inhibit ACC and activate malonyl-CoA decarboxylase (MCD) which decarboxylates malonyl-CoA to acetyl-CoA (416).

Enzymes involved in fatty acid biosynthesis are mostly regulated by the transcription factors 'sterol regulatory element binding protein-1c' (SREBP-1c) and carbohydrate response element binding-protein (ChREBP). Fatty acyl-CoA, derived from fatty acids, can enter the mitochondria for β-oxidation via the actions of CPT-1. Alternatively, acyl-CoA is used as a substrate for glycerol phosphate acyltransferase (GPAT1), an enzyme that mostly resides in the outer mitochondrial membrane, and has high activity in the liver and adipose tissues to stimulate the production of phospholipids (417) (Figure 4.2). During the consumption of high carbohydrate diets, hepatic *Gpat1* transcription levels are drastically increased by SREBP-1c. In contrast, the consumption of high fat diets reduces the rate of fatty acid biosynthesis by lowering hepatic *Gpat1* levels (416).

Lipogenesis is also promoted by insulin via the stimulation of SREBP-1c synthesis, subsequently inducing DNL (411). However, in the case of insulin resistance, more triglycerides are secreted into the circulatory system and their metabolism is reduced, causing an impaired clearance of lipids (411).

4.2.2 The effects of flavanols on lipogenesis and lipolysis

As discussed in chapter 3 (section 3.5.1), flavanols have been reported to prevent body weight gain in mammals from high fat diets through several processes, which are summarised here.

In-vitro experiments on HepG2 cells have shown that green tea polyphenols (GTP) comprising of 68 % EGCG, 19 % EC, 7 % EGC, and 1 % ECG, in the presence of glucose and insulin can increase the rate of glycogen synthesis in a dose dependent manner, when compared to the actions of insulin alone (400). Evidence suggests that this occurred by the increase in the phosphorylation levels of glycogen synthase kinase-3β and glycogen synthase. But also, when the cells were incubated with only EGCG, there were raised levels of active (phosphorylated) AMPK and increased inactive

(phosphorylated) ACC. Thus, GTP have been revealed to regulate glycogen synthesis and lipogenesis enzymes.

In a further study, GTP were reported to decrease the adipose tissue expression of SREBP-1c, FASN (fatty acid synthase), SCD-1 (stearoyl-CoA desaturase) and HSL to levels similar to those in lean mice, whereas their levels were significantly overexpressed in obese mice (401). These gene changes were not also observed in the mice livers of the same study despite GTP supplementation causing a reduction in steatosis levels (401), and so the effects of GTP were targeted to decrease only adipose tissue lipogenesis processes. Because of this, it was likely that steatosis was decreased because there was less availability of adipose-derived fatty acids that are otherwise processed by the liver (401). Similarly, Wolfram *et al* (2005) confirmed these results in EGCG supplemented diet fed C57BL/6J mice, for all listed genes (402). Furthermore, they reported a reduction in gene expression for GPAT and LPL but an increase for the fatty acid β-oxidation gene CPT-1. A different study demonstrated that rats supplied with GTP in HF diets caused an increase in AMPK activation and a decrease in active ACC (403). To add to this, it is common that inflammatory marker expressions, such as TNF-α, in the circulation and adipose tissues can stimulate lipogenesis, but GTP supplemented into HF diet fed mice have been shown to reduce these (401, 403).

To focus more specifically on EC, Cheng *et al* (2017) investigated the actions of EC at concentrations of 10, 20, and 40 mg/kg body weight consumption in Sprague-Dawley rats on HF diets (404). In doing so, they found that EC at 20 and 40 mg/kg body weight supplementation was able to reduce the expression of SREBP-1c and *INSIG1*, a gene that regulates lipogenesis in the endoplasmic reticulum. In comparison, for Zucker diabetic fatty rats that were fed a 10 % cocoa diet rich in EC, they expressed lower levels of the proteins SREBP-1c, FASN, and anti-fibrogenic PPARα, in the liver (405). These findings were also reciprocated in the same study for hepatic HepG2 cells that were cultured under a high glucose environment, and their culture with EC (3 mM) also caused higher phosphorylated (active) levels of AMPK (405). Finally, EC cultured onto HepG2 cells has been shown to reduce the protein expressions of FASN, ACC, ACLY (ATP-citrate synthase) and CPT-1, ultimately reducing DNL processes (418).

Overall, there is evidence to imply that EC has an influence on the reduction of DNL processes, however, the addition of the galloyl group intensifies these effects, even at lower concentrations.

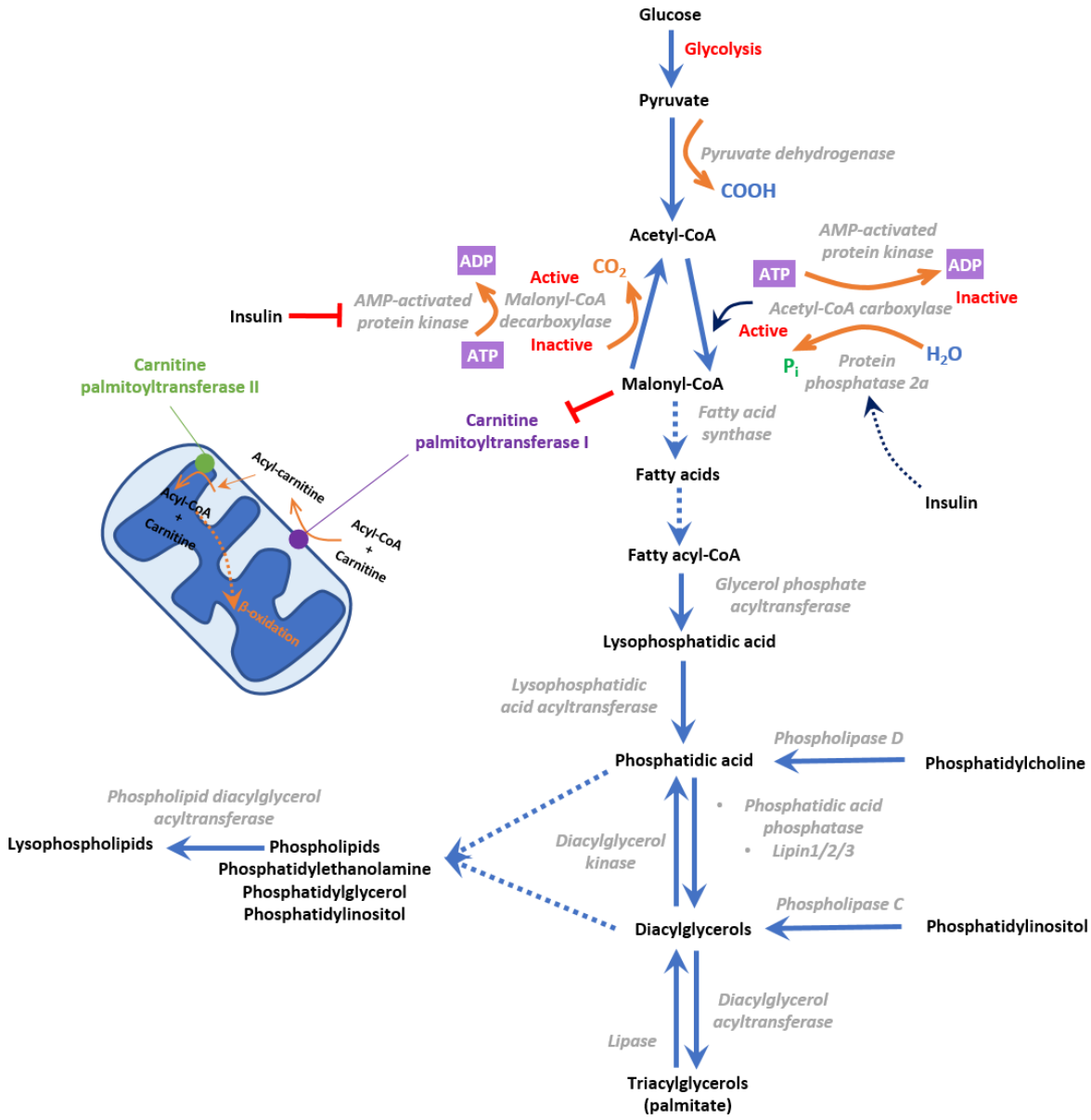

Figure 4.2: Fatty acid and phospholipid biosynthesis

The consumption of glucose or high carbohydrate diets raises blood glucose levels and initiates the biosynthesis of fatty acids and phospholipids in both the liver and adipose tissue. After glycolysis, pyruvate undergoes an enzymatic reaction into acetyl-CoA. Acetyl-CoA is then a substrate for acetyl-CoA carboxylase (ACC) and transformed into malonyl-CoA. Malonyl-CoA can then either be de-carboxylated to acetyl-CoA by malonyl-CoA decarboxylase (MCD) or transformed into fatty acids by fatty acid synthase. Malonyl-CoA also inhibits carnitine palmitoyltransferase-I (CTP-1), a mitochondrial enzyme responsible for producing acyl-carnitines and subsequently β-oxidation. A series of further enzymes are then involved to convert fatty acyl-CoA into triacyglycerols and diacylglycerols. Phosphatidic acid and diacylglycerols can also be re-directed to form phospholipids, glycerophospholipids and lysophospholipids. AMP-activated protein kinase (AMPK) can inhibit the action of ACC through phosphorylation, whilst protein phosphatase 2a (PP2a) activates ACC via dephosphorylation. AMPK can also activate MCD through phosphorylation, thereby lowering malonyl-CoA stores. Insulin can activate pathways that inhibits AMPK activity and increase PP2a activity, thus increasing the biosynthesis of fatty acids and phospholipids and lowering blood glucose levels. Enzymes are represented in grey text.

4.3 Objectives

Following the main dietary intervention study outlined in chapter 3, the purpose of this chapter was to investigate other biological changes induced by the HF diet in mice liver tissue and plasma markers, and to determine whether EC or 34DHPVL can influence these. As such, the aim of this chapter was to provide quantifiable measures for how the HF diet with or without EC or 34DHPVL supplementation alters biological markers. To achieve this, the following were achieved:

(1) Quantify liver lipids following the Bligh and Dyer's extraction protocol.

(2) Quantify plasma lipid concentrations using clinical chemistry.

(3) View the scale of liver inflammation via CD11B immunostaining.

(4) Assess liver damage in mice via hepatic tissue staining and pixel quantification for the fibrosis marker, Sirius red, and from analysing plasma markers for liver damage.

(5) Identify whether 34DHPVL can inhibit the digestion of starch by alpha amylase.

The data produced was used to address the following questions: (1) Can EC and 34DHPVL mitigate the accumulation of liver lipids in HF diet fed mice? (2) Will EC and 34DHPVL reduce the levels of circulatory lipids in HF intervention fed mice? (3) Does EC and 34DHPVL mitigate the onset of liver damage from LF and HF diets? (4) Is 34DHPVL capable of inhibiting alpha amylase activity on starch digestion and therefore lower blood glucose levels in mice? A number of hypotheses were tested, as follows:

(1) EC and 34DHPVL will counteract against HF diet induced liver steatosis.

(2) EC and 34DHPVL will counteract against HF diet induced rises in plasma lipids.

(3) EC and 34DHPVL will mitigate HF or high-complex-carbohydrate (in LF diet) diet induced hepatic damage.

(4) 34DHPVL will inhibit alpha amylase activity on starch digestion and subsequently prevent rises in blood glucose levels.

4.4 Methods

4.4.1 Materials & solutions

Neo-mount® anhydrous mounting medium (1090160100), Sirius red (365548), coverslips (Z692263), paraffin wax (Paraplast®, cat: P3558), A-amylase type I-a PMSF treated from porc (A4268-25MG), starch from corn (S4180-500G), p-hydroxybenzoic acid hydrazide (H9882-25G) (PAHBAH), D-(+)-maltose monohydrate from potato (M5885-100G), hematoxylin harris, eosin, trisodium citrate dehydrate, citric acid pellets, triton-x 100, bovine serum albumin (BSA), goat serum, tris, hydrogen peroxide, tween-20, (−)-epigallocatechin gallate (EGCG) (E4143), acarbose (A8980), hydrochloric acid (HCL) and sodium chloride were purchased from Sigma Aldrich, UK. Fast Green FCF (F7252) was purchased from Merck. Primary CD11B antibody rabbit (ab133357) was purchased from Abcam, UK. OCT (AGR1180) and Histo-Clear II (AGR1353), were purchased from Agar Scientific, UK. HCS LipidTOX™ green neutral lipid stain (H34475), methanol-free formaldehyde ampules (11586711), DAPI (D1306), and superfrost plus microscope slides (12628026), were purchased from ThermoFisher Scientific, UK. Histo-Clear I (HS-200) was purchased from the LabShop, UK. Triglyceride Liquicolor Mono Assay Kit was purchased from Human Gmbh, Germany. Dako antibody diluent buffer (s0809), Dako En Vision secondary anti-rabbit antibody (K4003), and Dako DAB+ Substrate Chromogen System (GV825) were purchased from Agilent technologies, UK. 3’,4’-dihydroxyhydroxyphenyl-γ-valerolactone (34DHPVL) was prepared as previously described in section 3.4.1.

Tris buffer solution (TBS) was made to a 20X stock by dissolving 175.2 g NaCl and 24.28 g Tris in water and adjusted to pH 8.0 with HCL. TBS-Tween (TBS-T) was then made using 949 mL water, 250 mL 20X TBS and 1ml Tween-20. Citrate buffer solution pH 6.0 was made using two pre-made solutions citrate A and citrate B, prepared as follows: citrate A: 10.5 g of citric acid in 500 mL distilled water; citrate B: 14.7 g of trisodium citrate dehydrate in 500 mL distilled water. The final citrate buffer was then made by mixing 18 mL of citrate A with 82 mL of citrate B and brought to a final volume of 1 L with distilled water.

4.4.2 Hematoxylin and eosin (H&E) staining of liver sections

Paraffin embedded liver sections (from the mice dietary intervention study as described in chapter 3) were cut to 5 µm using the Leica Biosystems HistoCore BIOCUT (RM2235, UK) onto superfrost plus slides. Sections were: de-paraffinized in Histo-Clear I for 5 mins, and for 5 mins in Histo-Clear II; hydrated for 2 mins in 100 % ethanol, 2 mins 80 % ethanol, 2 mins 70 % ethanol, and 5 mins

water; incubated for 5 mins in Harris's hematoxylin, and rinsed for 5 mins in running water; incubated for 15 secs in 1 % acid solution (1 % hydrochloric acid in 70 % ethanol) and rinsed with water; immersed in 0.1 % sodium bicarbonate (in water) for 1 min, and rinsed for 5 mins under running water; and counterstained for 30 secs in eosin. Sections were finally dehydrated for 2 mins in 70 % ethanol, 2 mins 80 % ethanol, 2 mins 100 % ethanol, 5 mins Histo-Clear I, and 5 mins Histo-Clear II, and then mounted in Neo-Mount and covered with coverslips.

4.4.3 Sirius red staining of liver sections

Paraffin embedded liver sections were cut to 5 µm using the microtome, onto Superfrost Plus slides. Sections were: de-paraffinized in Histo-Clear I for two changes of 10 mins; hydrated for 2 mins in 100 % ethanol, 2 mins in 80 % ethanol, 2 mins in 70 % ethanol, and 5 mins in water; incubated in 0.01 % Fast Green FCF solution in picric aqueous solution for 15 mins; incubated in 0.04 % Fast green FCF/0.1 % Sirius red in saturated picric aqueous solution for 15 mins. Sections were finally dehydrated in 100 % ethanol for 5 mins and incubated in Histo-Clear I for 10 mins and then mounted in Neo-Mount and covered with coverslips.

4.4.4 LipidTOX™ staining of liver sections

OCT embedded liver sections were cut to 5 µm using the Thermo Scientific Microm HM560 Cryostat (UK) onto Superfrost Plus slides. Sections were then: immersed in 4 % methanol free formaldehyde for 15 mins, removed and evaporated for 20 mins at room temperature; rinsed in 1X PBS twice for 5 mins each; incubated in DAPI (1:1000 in PBS) at room temperature for 1 min; washed in PBS thrice for 8 mins each; and incubated in HCS LipidTOX™ Green Neutral Lipid stain (1:1000 in PBS) at room temperature for 69 mins. Sections were finally mounted in Aqueous Vectamount® for 24-hours at room temperature in the dark. Coverslips were then secured, and the slides were kept at 4 °C.

4.4.5 Staining of liver sections for the inflammatory marker, CD11B

Paraffin mounted liver sections on Superfrost Plus slides were: deparaffinised and rehydrated as per section 4.4.2; blocked with 3 % H_2O_2 in methanol (v/v) at room temperature for 10 mins and rinsed in water; unmasked (antigen retrieval) by boiling for 20 mins in a microwave in Citrate buffer (pH 6.0) and cooled for 20 mins; washed in TBS-T for three sets of 5 mins; blocked in 50 µL of blocking solution (10 % goat serum with 0.1 % triton-x 100 with 1 % BSA in PBS) for one hour at

room temperature; drained and incubated with primary antibody (1:3000 dilution of CD11B anti-rabbit in Dako antibody diluent buffer) overnight at 4 °C; washed in TBS-T for three sets of 5 mins; incubated in Dako En Vision secondary anti-rabbit antibody for 30 mins at room temperature; washed in TBS-T for three sets of 5 mins; developed in Dako DAB+ Substrate Chromogen System until CD11B staining was visible (~30 secs); and the reaction was stopped by placing the slides in water, and counterstained by using the reverse protocol of the H&E staining as described in section 4.4.2, (starting with the hematoxylin step and ending with histoclear). The slides were finally mounted using NeoMount and covered with coverslips.

4.4.6 Imaging the stained liver sections

Hematoxylin and eosin (H&E), Sirius red, and CD11B stained sections were imaged at 4X, 10X an 20X magnification on Olympus BX60 microscope (Olympus) on brightfield mode using a Progress C10 plus camera (2080x1542 HQ, Jenoptik, Germany). LipidTOX stained sections were imaged on the Zeiss Axio Imager 2 microscope (using camera adaptors 60C 1” 1.0x and 60NC 2/3” 0.63x) (Germany) at 358 nm for DAPI and 488 nm for LipidTOX (green). A total of six images were taken for each Sirius red stained section, and two to three images for the LipidTox and CD11B stained sections.

4.4.7 Pixel quantification of imaged liver sections in Fiji

Fiji (419), the image processing package in ImageJ (NIH) was used to quantify pixel intensity for images taken from liver sections stained for Sirius red and LipidTOX. Sirius red pixel intensity was quantified according to documentation on the ImageJ website (420). LipidTOX pixel intensity was quantified according to a method devised by Dr Paul Thomas at the University of East Anglia (Manager of the Henry Wellcome Laboratory for Cell Imaging, UK). Macro plugins were then designed and installed into Fiji software to ensure equal analysis of all the sections.

An average of all the pixel intensities were taken from each section imaged in replicate. An average was then obtained for each dietary intervention group.

4.4.8 Triglyceride extraction from C57BL/6J liver samples

Snap frozen liver samples were processed into a homogenous powder using a pestle and mortar under liquid nitrogen. Livers were then processed according to the Bligh and Dyer method (421) as

follows. Crushed 30 mg liver samples were homogenised in 200 µL chloroform and 400 µL methanol using the Precellys 24 Lysis and Homogeniser at 6000 rpm for 30 secs (Bertin Technologies, France). A further 200 µL of chloroform was added and samples homogenised again. Samples were transferred to new 1.5 mL centrifuge tubes and centrifuged for 10 mins at 4,300 g. The lower layer containing the lipids was transferred into a new 1.5 mL centrifuge tube and the chloroform was evaporated overnight in a fume cupboard. Lipids were then dissolved in 700 µL of 2 % Triton-X-100 in PBS. Samples were then vortexed until lipids were completely dissolved. After this, 2.5 µL of the dissolved liver lipid samples were loaded onto 96 well plates in triplicates and 250 µL of reagent from Triglyceride Liquicolor Mono Assay Kit was added and the plate incubated for 5 mins at 37 °C. A triglyceride standard curve was prepared according to the kit's protocol. The plate was then read on the FLUOstar Optima Microplate Reader (BMG Labtech, Germany) at 500 nm. Mice liver lipids were quantified according to the standard curve and the kit's protocol, values were then converted to obtain mg of lipid mass per mg of liver mass.

4.4.9 Quantification of various plasma biomarkers (RANDOX)

Clinical chemistry analyser kits from RANDOX Daytona plus (UK) for total cholesterol (CH 8310), high-density lipoproteins (CH 8311), high-density lipoprotein-3 (CH 10165), triglycerides (TR 8332), aspartate transaminases (AS 8306), and alanine transaminases (AL 8304) were performed on mouse plasma according to the manufacturer's instructions.

Low-density lipoprotein concentrations were calculated using the Friedewald formula (Formula 4.1).

$$LDL = CHO - \frac{TRIG}{2.18} - HDL$$

Formula 4.1: Friedewald formula to calculate LDL concentration
LDL: low-density lipoproteins; CHO: cholesterol; TRIG: triglycerides; HDL: high-density lipoproteins. All units were in mmol/L (422).

4.4.10 α-amylase enzyme activity

Starch from corn was prepared in PBS buffer to 5 mg/mL and cooked at 90 °C for 20 mins. Aliquots of 5 mLs were then incubated at 37 °C. A 1:1000 dilution of α-amylase was prepared in PBS and 100 µL of this added to 5 mL of 5 mg/ml gelatinised corn starch. At 0, 3, 6, 9 and 12 mins after the addition of the enzyme, 100 µL of the reaction solution was withdrawn and thoroughly mixed with

100 µL of 0.3 M Na_2CO_3 solution to stop the reaction. This mix was then centrifuged at 15,000 g for 5 mins at room temperature. The initial reaction velocity was determined using the PAHBAH method described by Sun *et al* (2016) (423). Briefly, the supernatant was diluted by 4-fold in PBS and 100 µL placed into separate 1.5 mL centrifuge tubes. A 5 % (w/v) final working PAHBAH reagent was prepared in a 1:9 volume of 0.5 M HCl:0.5 M NaOH solution (method with modifications from Lever, 1973 (424)). A 1 mL of PAHBAH reagent was added to duplicate samples (100 µL) and boiled at 99 °C for 5 mins and absorbance measured in a 96-well plate at 380 nm in a FLUOstar Optima Microplate Reader (BMG Labtech). Although 405 nm is the optimum absorbance for the assay, the closest available working filter was 380 nm, accounting for around 80 % of the absorbance value to be captured. Maltose (100 µL) was used as the standard curve at 0.01-1.0 mM in PBS. Absorbance readings acquired were converted to the concentrations of the reduced sugar. Initial reaction velocity and therefore enzyme activity was calculated from the reducing sugar concentration in the reaction solution against time. A-amylase enzyme activity was determined to be 5.2 kU/mL.

4.4.11 Starch digestion kinetics

Once the enzyme activity was determined (section 4.4.10), assessment for the most optimal enzyme concentration was acquired. To achieve this, firstly, α-amylase at 2.5, 5.0, 12.5, and 25 U/mL was prepared from stock solution of 5.2 kU/mL in PBS. Secondly, 50 µL of PBS was incubated for 5 mins at 37 °C with 50 µL of α-amylase pre-prepared stocks, the 100 µL was then added to 5 mL of 5 mg/mL corn starch solution as previously described to make final enzyme reaction concentrations of 0.05, 0.10, 0.25 and 0.30 U/mL. Aliquots of 100 µL reaction solution was withdrawn at 0, 3, 6, 9 and 12 mins. The rest of the protocol described in section 4.4.10 was then performed to calculate the initial rates of the reactions. The reaction that provided a complete linear production of maltose within the 12 mins was selected for future inhibition assays; this was 0.05 U/mL.

4.4.12 Inhibition assays of α-amylase by EGCG and 34DHPVL

As described in section 4.4.10, corn starch was prepared. After that, 50 µL of α-amylase at 5 U/mL was pre-incubated for 5 mins with 50 µL of: PBS, or 15 mM EGCG, or 100 mM 34DHPVL, or 200 µM acarbose, at 37 °C. Once warmed, 100 µL of the enzyme with PBS/compound was added to the 5 mL of 5 mg/mL starch to make 0.05 U/mL α-amylase and 150 µM EGCG and 1mM 34DHPVL. The remaining protocol was then followed.

4.4.13 Statistical Calculations

All statistical analyses were performed as described in section 3.4.7. Datasets with unequal variance were transformed according to Table 4.1 prior to statistical analysis and analysed using the linear model method as listed in the Table 4.1.

Table 4.1: Transformations made on the data for statistical analysis and the linear model R package used

Mouse Measurement	Transformation	R Package used
Sirius red pixels	Log_{10}	nlme
LipidTox pixels	Log_{10}	lmer
Liver lipids per mg liver	$\frac{1}{x^2}$	nlme
Liver lipids in whole liver	$\frac{1}{\sqrt{x}}$	nlme
Liver lipids in whole liver to body weight ratio	$\frac{1}{\sqrt{x}}$	nlme
Plasma aspartate transaminases	Log_{10}	nlme
Plasma alanine transaminases	Log_{10}	nlme
Plasma triglyceride	N/A	lmer
Plasma triglyceride/HDL ratio	N/A	lmer
Plasma LDL	N/A	nlme
Plasma HDL	N/A	lmer
Plasma HDL3	N/A	lmer
Plasma cholesterol	N/A	nlme

4.5 Results

4.5.1 H&E and CD11B staining revealed hepatic liver damage and inflammation by all diets

Liver sections from the mice dietary intervention study (as described in section 3.4.4) were stained using H&E to assess the general physiology of the tissue for steatosis, and fibrosis, which are known precursors for the onset of MAFLD and non-alcoholic steatohepatitis (NASH). The hematoxylin dye stains the nuclei a bluish dark purple colour, whilst eosin counterstains the remaining tissue to become pink, and hence allowing for the recognition of hepatic cellular structures, damage, and nuclei displacement. Non-stained areas that appeared white were lipids, where large fat droplets can be defined as microvesicular or macrovesicular steatosis; the former of the two involves small fat droplets that do not displace the nuclei, whilst the latter displaces the cell nuclei to the cell periphery because of its large size. In a separate immunostaining procedure, liver sections were also assessed for the infiltration of inflammatory leukocytes using a CD11B antibody with hematoxylin as the counterstain.

Healthy functioning livers are defined by the lack of exhibitions for: visible fat deposits, bridging of cellular structures, inflammatory cell accumulation, and lots of mitotic cells (425). It was apparent that a large majority (N = 9) of the mice on all LF dietary interventions (i.e. with or without compound) had 'healthy' liver physiologies (Figure 4.6). Conversely, a total of three mice from the LF diet (Figure 4.3), three mice from the 34DHPVL supplemented LF diet (Figure 4.5) and two mice from the EC supplemented diet LF diet (Figure 4.4) exhibited severe liver inflammation, steatosis, fibrosis and hyperplasic cells. The fibrosis was later confirmed by Sirius red staining (described in section 4.5.2) where these same samples exhibited high collagen levels that appeared in a bridging fashion. CD11B staining confirmed inflammatory cell accumulation in some of the mice on LF intervention livers with or without compound supplementation, and these appeared as dark brown spots on a lighter brown background (Figure 4.8). The liver sections that displayed high inflammatory infiltrates from all LF intervention fed mice were confirmed to be the same mouse livers that exhibited a fibrotic phenotype.

The mice on HF diets presented with extreme hepatic steatosis, and only showed signs of improvement following the addition of EC into the diet (Figure 4.7), this was confirmed visually by H&E and LipidTOX staining, and was quantified by lipid extraction (discussed later in section 4.5.3). There were signs of a reduction in inflammatory infiltrates in the livers of mice on all the HF dietary interventions when compared to those on all LF dietary interventions, as determined visually by H&E and CD11B staining (Figures 4.7 & 4.9). Consequently, this is evidence that the LF diets (which

were also high in carbohydrates and very low in fibre) caused liver damage and inflammation, that could be greater than those exhibited from the HF diets. However, only once the liver damage markers in plasma for AST and ALT were assessed (discussed later in section 4.5.2), there were no significant differences between any of the treatments (Figure 4.13).

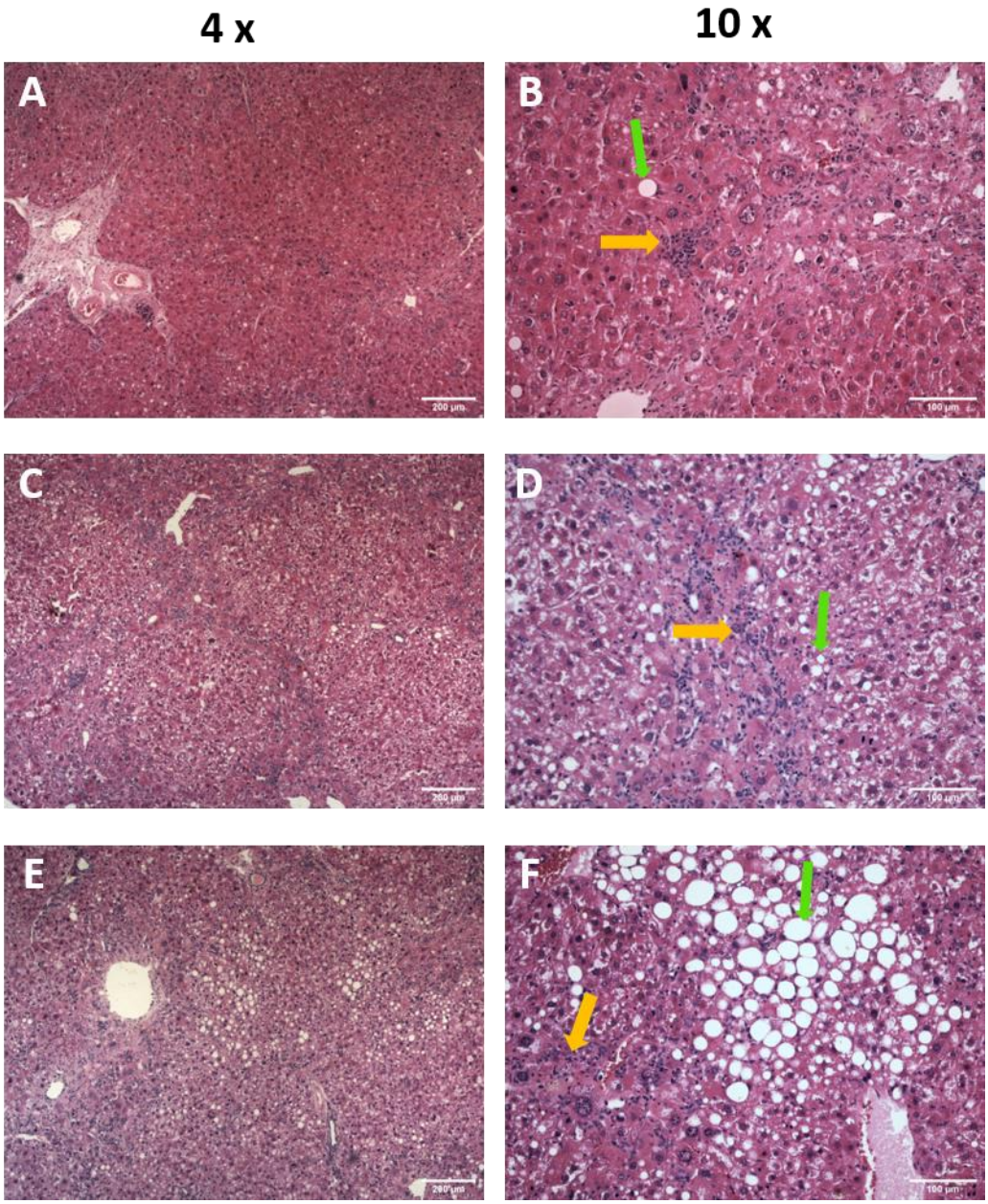

Figure 4.3: Hematoxylin and eosin stains of hepatic sections from LF fed mice that present signs of fibrosis

A/C/E 4x magnification. B/D/F 10x magnification of sections from A/C/E. Yellow arrows point towards an area of inflammation, green arrows point towards a fat droplet. Each row represents a section obtained from a different mouse liver.

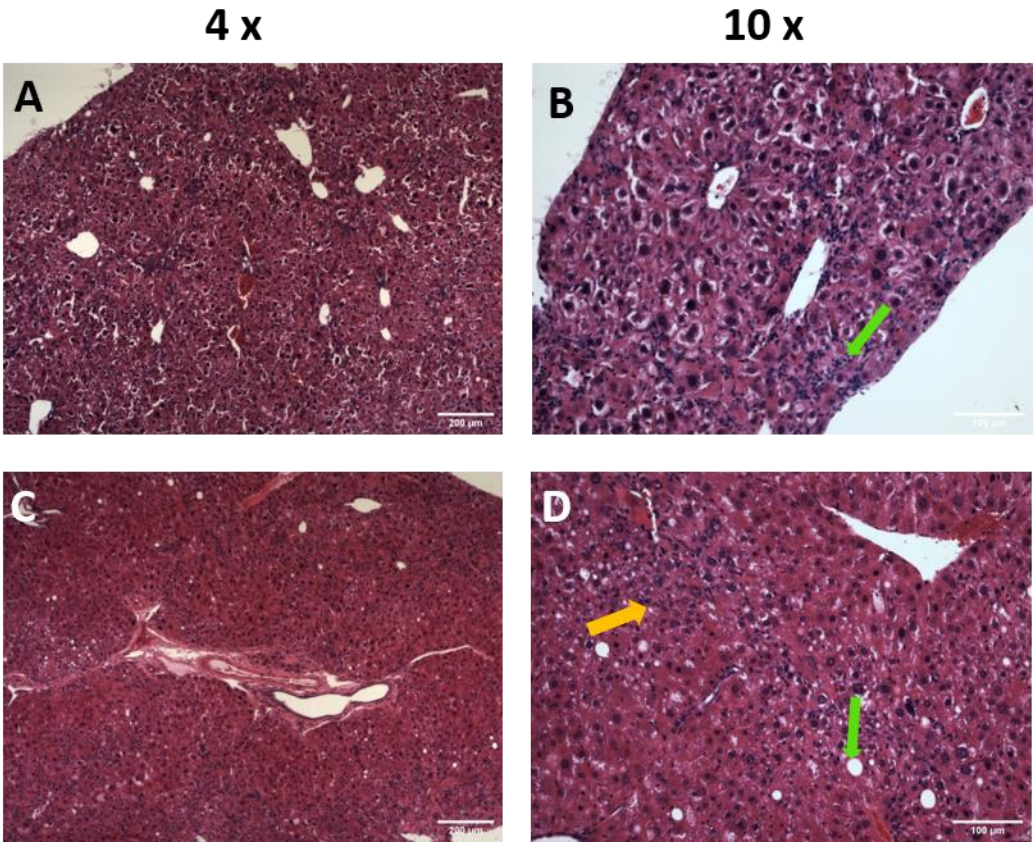

Figure 4.4: Hematoxylin and eosin stains of hepatic sections from LF+EC fed mice that show signs of fibrosis

B/D 10x magnification of sections from A/C. Yellow arrows point towards an area of inflammation, green arrows point towards a fat droplet. Each row represents a section obtained from a different mouse liver.

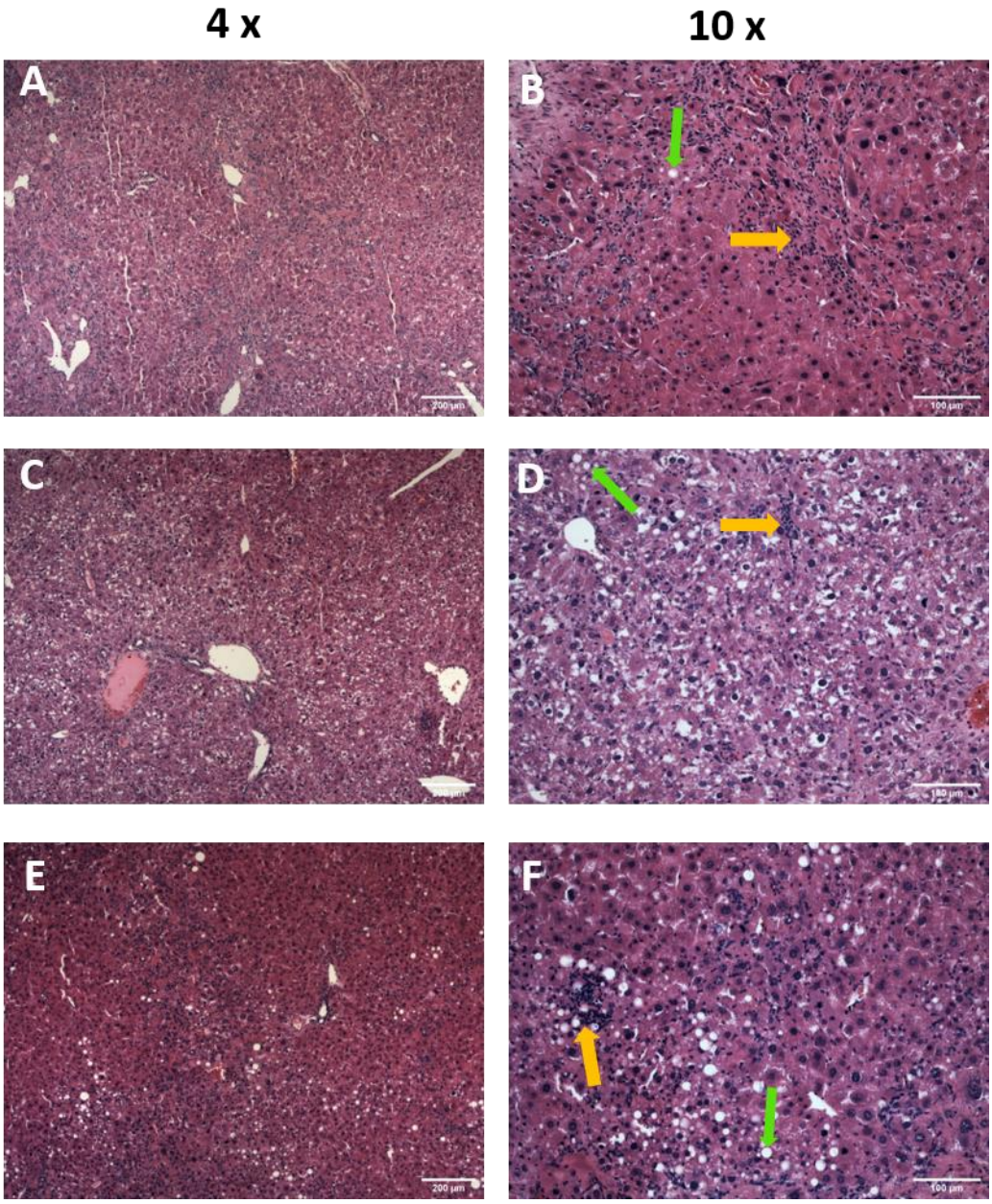

Figure 4.5: Hematoxylin and eosin stains of hepatic sections from LF+34DHPVL fed mice that show signs of fibrosis

A/C/E 4x magnification. B/D/F 10x magnification of sections from A/C/E. Yellow arrows point towards an area of inflammation, green arrows point towards a fat droplet. Each row represents a section obtained from a different mouse liver.

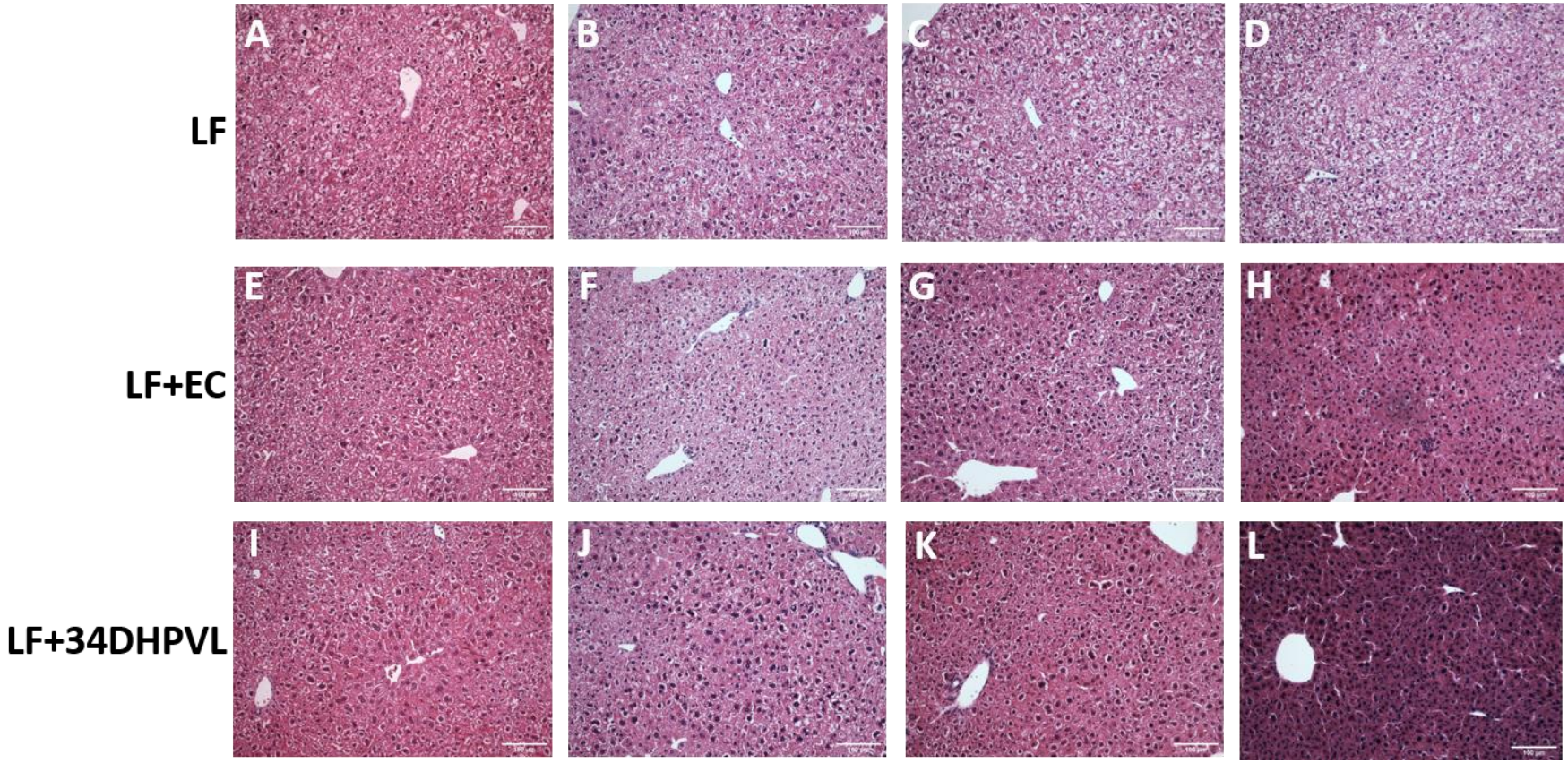

Figure 4.6: Hematoxylin and eosin stains of hepatic sections from LF intervention fed mice that exhibited 'normal' physiology

All sections presented are of 10x magnification. A-D sections were taken from LF fed mice, E-H sections were taken from LF+EC fed mice, I-L sections were taken from LF+34DHPVL fed mice. Each image is obtained from a different mouse liver section.

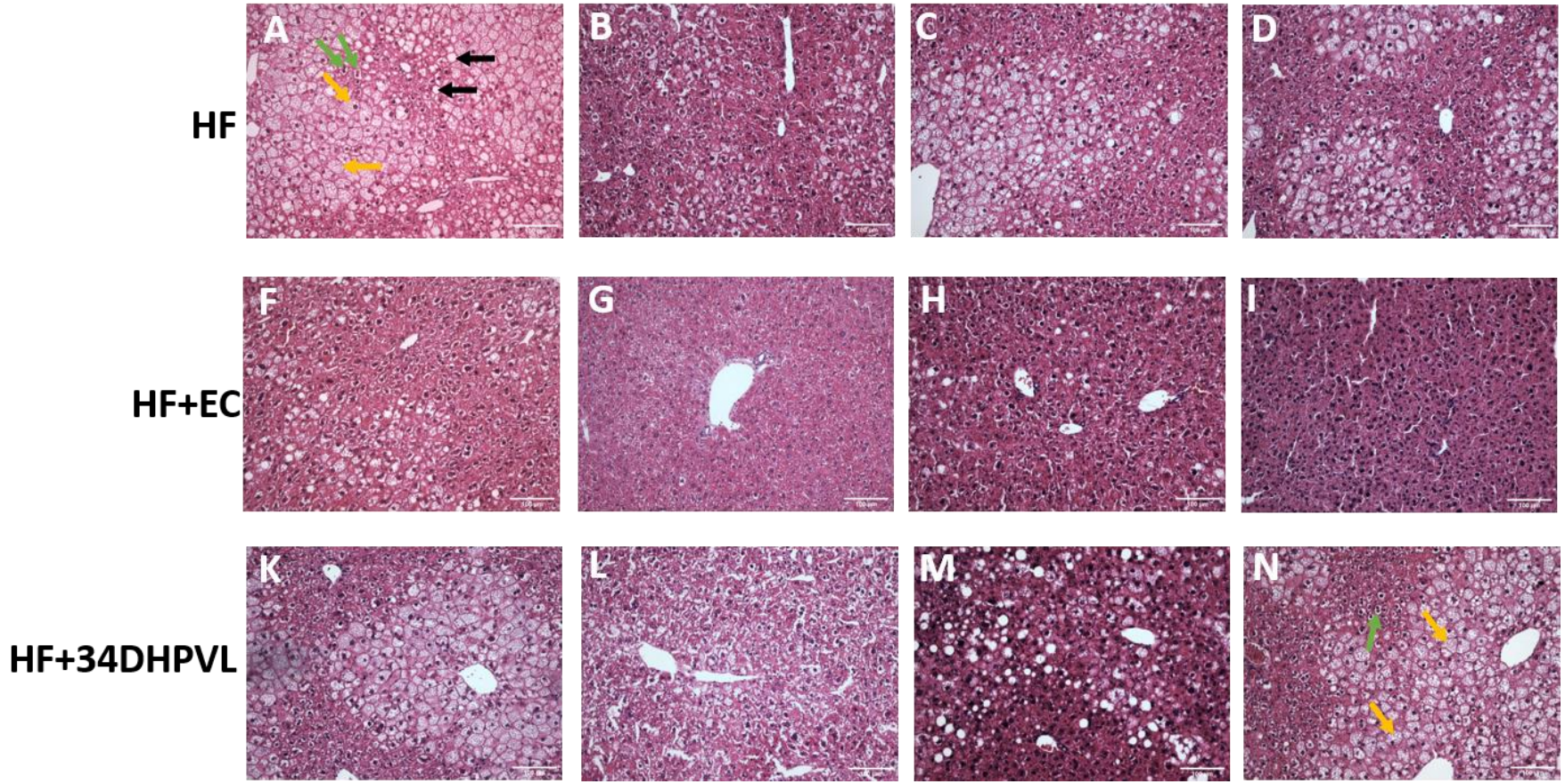

Figure 4.7: Hematoxylin and eosin stains of hepatic sections from HF intervention fed mice

All sections presented are of 10x magnification. A-E sections were taken from HF fed mice, F-I sections were taken from HF+EC fed mice, K-N sections were taken from HF+34DHPVL fed mice. Each image was obtained from a different mouse liver section. Arrows in images A and N: Black arrows point to zones of macrovesicular fat, yellow arrows points towards microvesicular fat and green arrows point to mitotic cells, for examples.

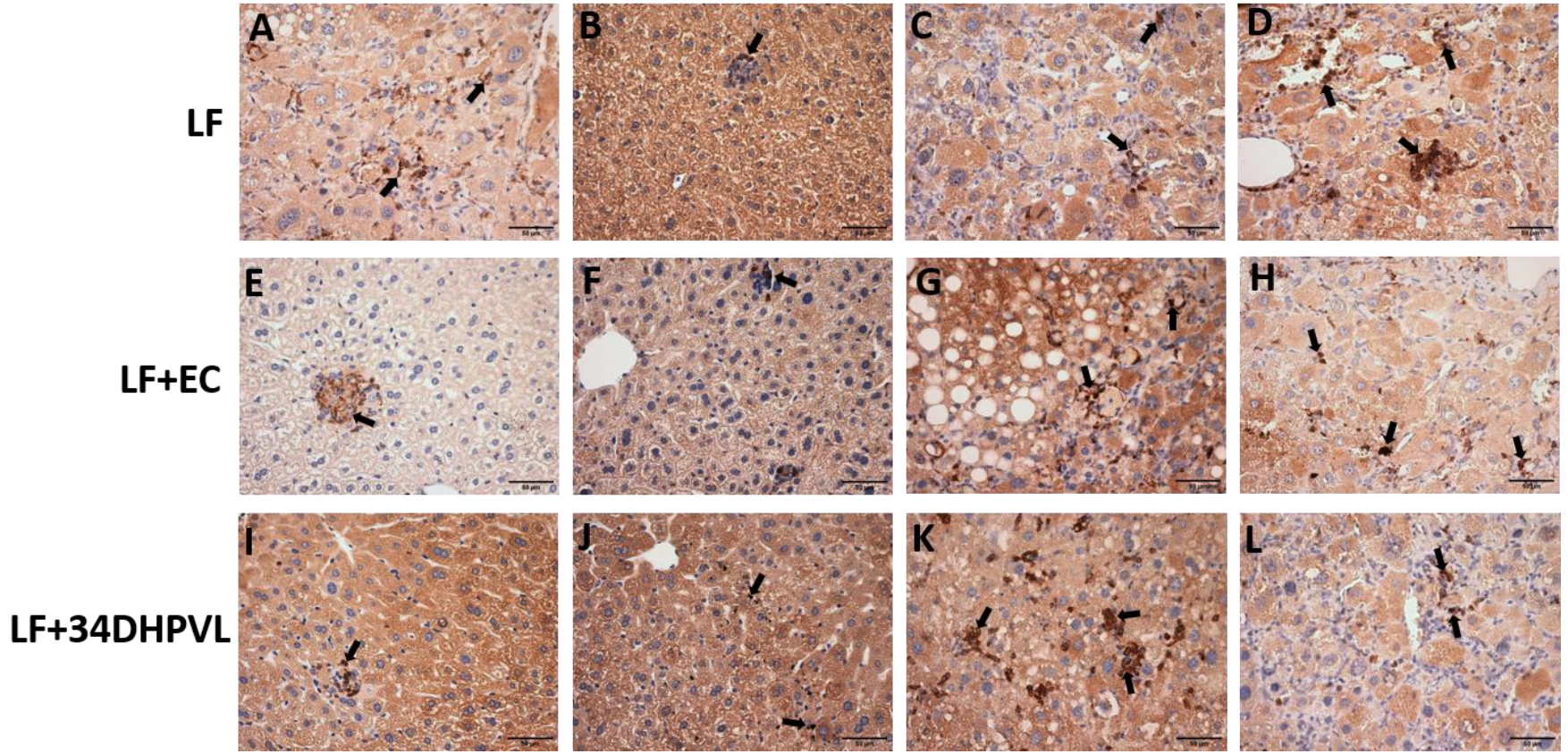

Figure 4.8: CD11B immunostains of hepatic sections from all LF intervention fed mice

All sections presented are of 20x magnification. A-D sections were taken from LF fed mice, E-H sections were taken from LF+EC fed mice, I-L sections were taken from LF+34DHPVL fed mice. Each image was obtained from a different mouse liver section. Positive CD11B cells are represented by dark brown areas that some black arrows point towards. Sections were counterstained with hematoxylin and highlighted the nuclei purple.

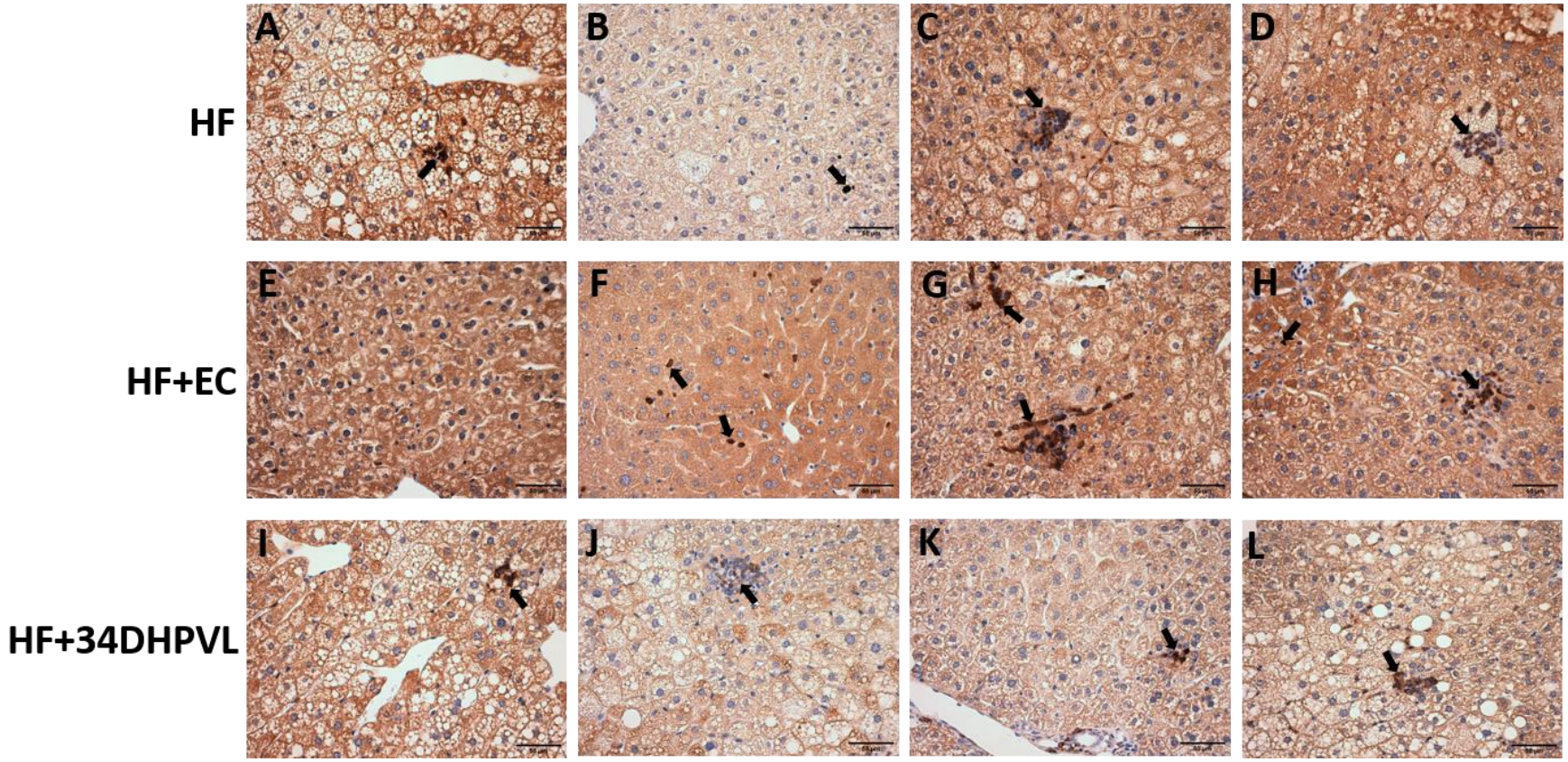

Figure 4.9: CD11B immunostains of hepatic sections from all HF intervention fed mice

All sections presented are of 20x magnification. A-D sections were taken from HF fed mice, E-H sections were taken from HF+EC fed mice, I-L sections were taken from HF+34DHPVL fed mice. Each image was obtained from a different mouse liver section. Positive CD11B cells are represented by dark brown areas that some black arrows point towards. Sections were counterstained with hematoxylin and highlighted the nuclei purple.

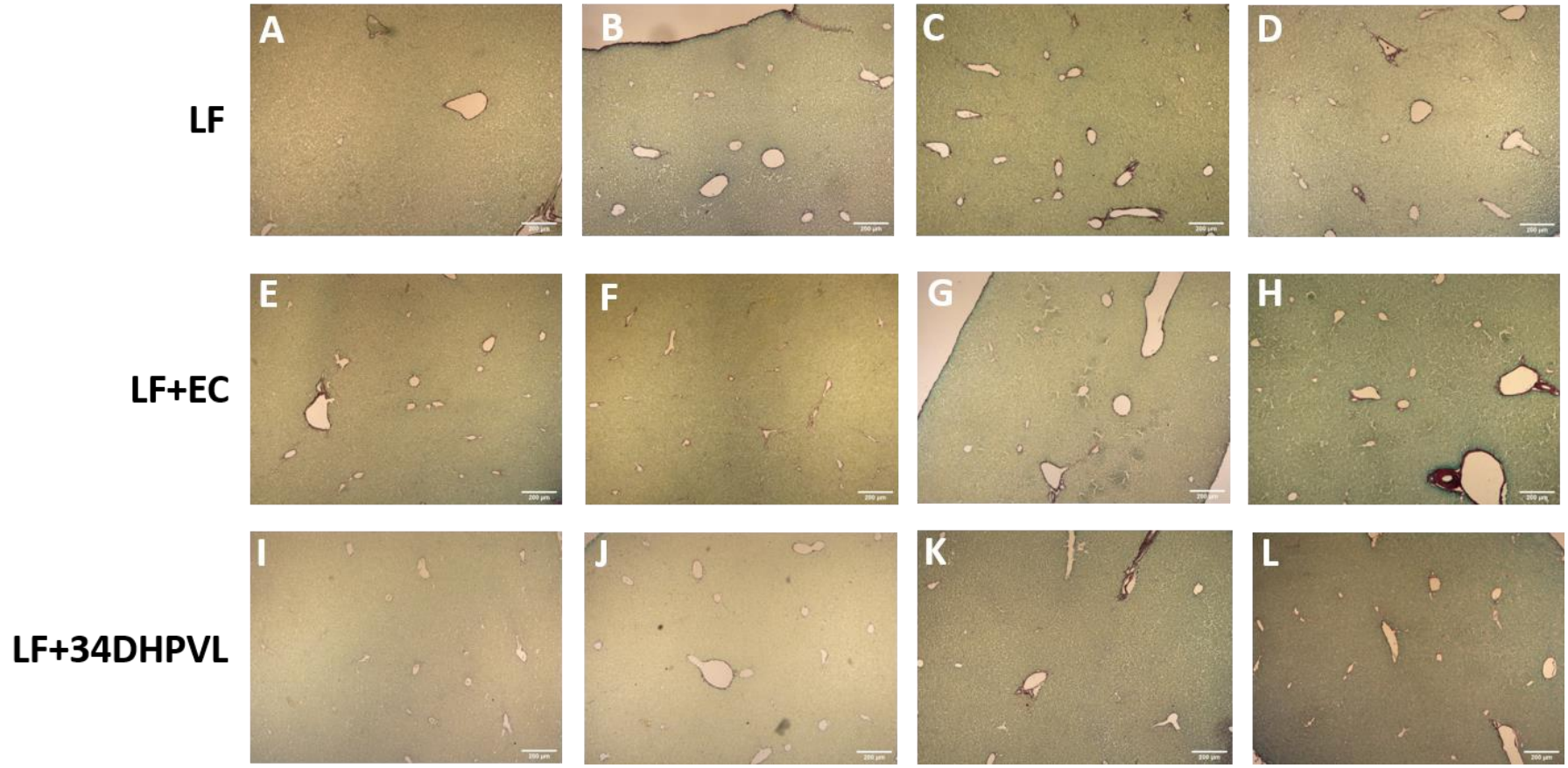

Figure 4.10: Sirius red stains of hepatic sections from all LF intervention fed mice that exhibited no signs of fibrosis

All images presented are of 4x magnification. Sirius red stain binds to tissue collagen and appears red. Sections were counterstained in Fast Green FCF solution and stained the rest of the tissue green. All sections presented do not show signs of fibrosis, but there can be collagen seen around the portal veins, which is normal. A-D sections were taken from LF fed mice, E-H sections were taken from LF+EC fed mice, I-L sections were taken from LF+34DHPVL fed mice. Each image was obtained from a different mouse liver section

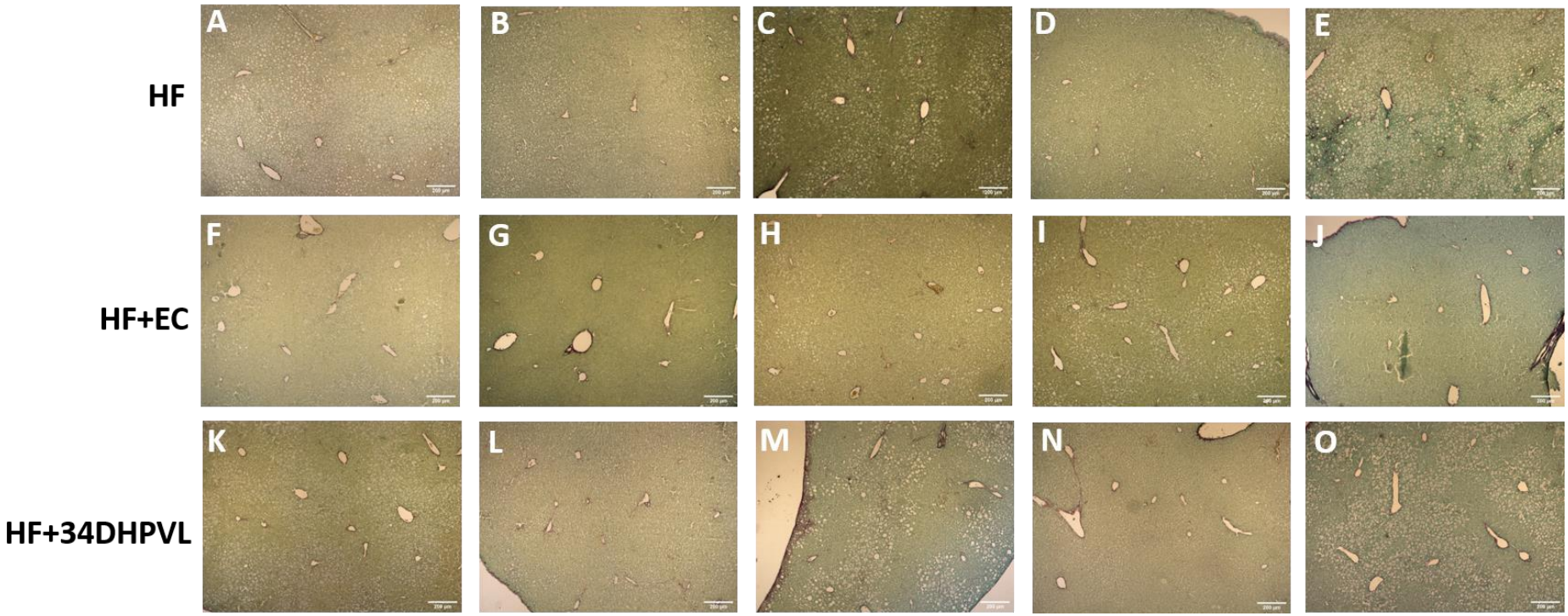

Figure 4.11: Sirius red stains of hepatic sections from all HF intervention fed mice that exhibited no signs of fibrosis

All images presented are of 4x magnification. Sirius red stain binds to tissue collagen and appears red. Sections were counterstained in Fast Green FCF solution and stained the rest of the tissue green. All sections presented do not show signs of fibrosis, but there can be collagen seen around the portal veins, which is normal. A-D sections were taken from HF fed mice, E-H sections were taken from HF+EC fed mice, I-L sections were taken from HF+34DHPVL fed mice. Each image is obtained from a different mouse liver section.

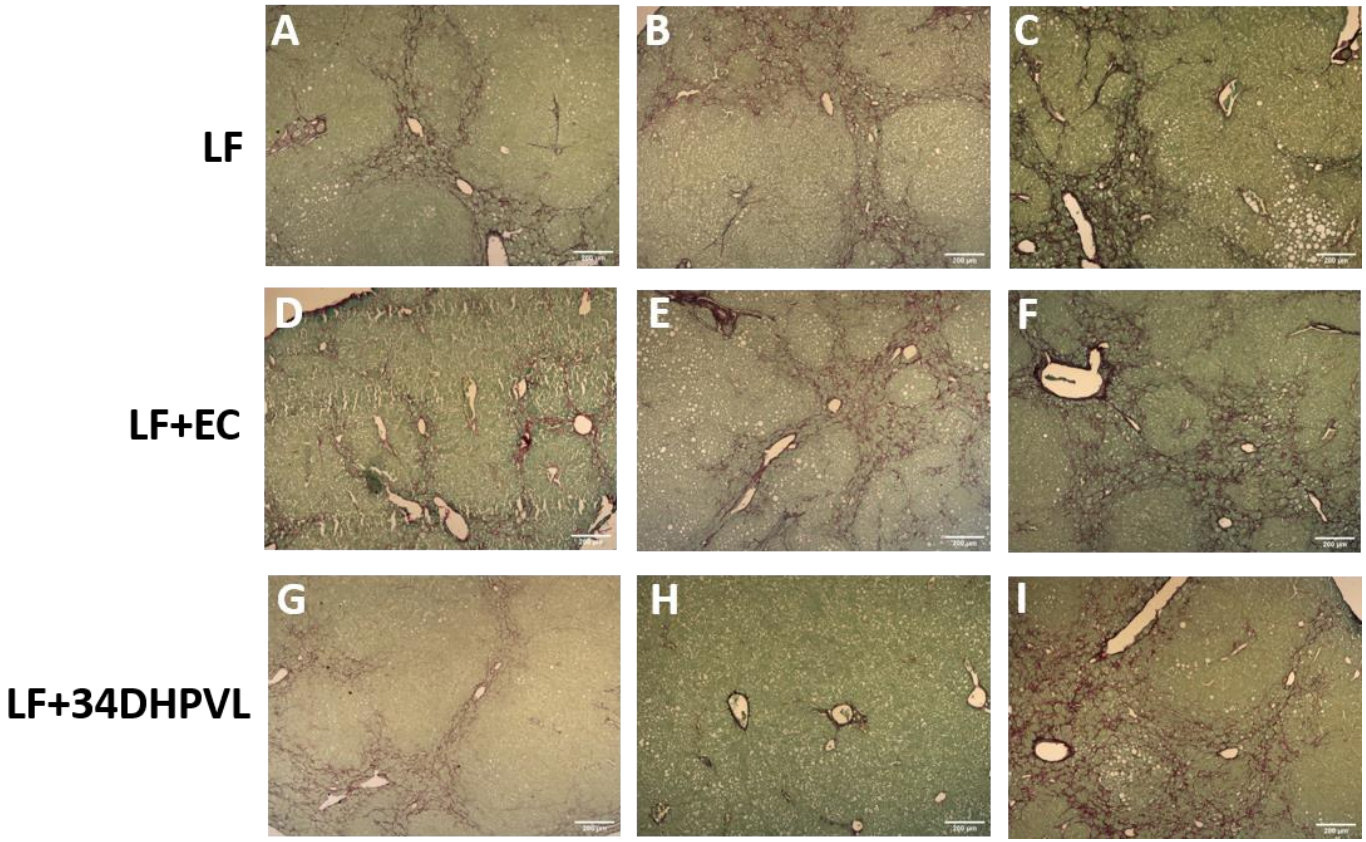

Figure 4.12: Sirius red stains of hepatic sections from all LF intervention fed mice that presented clear signs of fibrosis
All images presented are of 4x magnification. Sirius red stain binds to tissue collagen and appears red. Sections were counterstained in Fast Green FCF solution and stained the rest of the tissue green. All sections presented show clear signs of fibrosis, which represents a build-up of collagen. Collagen also appeared in a bridging fashion across some of the tissues, which is indicative of severe liver damage. A-D sections were taken from HF fed mice, E-H sections were taken from HF+EC fed mice, I-L sections were taken from HF+34DHPVL fed mice. Each image is obtained from a different mouse liver section

4.5.2 The levels of liver fibrosis appeared to be no different across all dietary intervention fed mice

Mice livers from the dietary intervention study were harvested and stained for Sirius red. Sirius red is a dye that binds to collagen, and thus allows for the interpretation for healthy or diseased state livers. A high accumulation of collagen in hepatic tissue can be indicative of fibrosis and a precursor to cancer. Generally, fibrotic livers have approximately four to six times more extracellular matrix than normal (26-28).

Overall, most of the mice did not experience high levels of collagen in their livers (Figure 4.10/11), however, there were noticeably three LF intervention fed mice that exhibited high collagen levels, alongside three EC supplemented LF fed mice and two 34DHPVL supplemented LF fed mice (Figure 4.12), this was illustrated by the ≥ 9-fold, ≥ 5-fold and ≥ 10-fold greater pixel intensities than the remaining mice in their group, respectively. These datasets represent 23 % of the total mice sample size on LF diets with or without supplementation, but were also confirmed outliers from the remaining data for pixel intensity values, however, it does not seem sensible to remove these datasets because they occupy almost a quarter of the LF sample size. Because of the high pixel intensities in these samples and the severe bridging fashion of the collagen, it demonstrates that these particular mice suffered from severe hepatic perisinusoidal and portal/periportal fibrosis, that ultimately could have led to hepatocellular carcinoma. Generally, this implies that the LF high carbohydrate low fibre diet was capable of inducing liver damage, and if the intervention was performed over a longer timeframe, it is very likely that more mice would have exhibited a similar phenotype.

In contrast to the LF diet, HF diet fed mice exhibited uniform Sirius red pixilation in all three dietary groups, except for one mouse on the EC supplemented diet (Figures 4.11, and 4.13 A/B). Yet despite the large differences in the mean values between LF fed and HF fed mice, there were no statistical significances between any of the treatment groups, even following the removal of outliers. This indicates that both the LF and HF diets contributed to hepatic collagen accumulation, and thenceforth a scale of liver damage.

To reinforce the quantified pixilation values from Sirius red staining, mice plasma was assessed for ALT and AST levels, which are markers that directly correlate to the scale of liver damage. There were several mice that exhibited extreme values for AST and ALT (Figure 4.13 C/D), and these mirrored the same mice that exhibited signs of severe fibrosis. Despite this, there was no statistical significance in AST and ALT levels between any of the dietary intervention groups, even once the outliers were removed. Nevertheless, because ~20 % of the mice experienced signs of fibrosis in

conjunction with extreme values for liver damage markers, it is not sensible to exclude these extreme datapoints from the sample size for analysis.

Published studies report reference ranges for AST and ALT to provide a scale on the level of liver damage present, however, these values are very much laboratory dependent (426). As such, a normal AST reference range can lay anywhere within 0-79 U/L, whilst for ALT it can be between 0-65 U/L, and a healthy AST/ALT ratio is around 0.8. In MAFLD, AST can be 2-5 times elevated where the AST/ALT ratio is normally 1.0 or more (427-430). As seen in Table 4.2, all dietary intervention groups exhibited an abnormal AST/ALT ratio that exceeded 1.0, where LF and LF+34DHPVL appeared to be the worst affected. These scores therefore suggest that all dietary groups displayed signs of MAFLD and consequently liver damage. But, because there were no significant changes seen by supplementing EC or 34DHPVL into either HF or LF dietary fed mice for the AST/ALT ratio, this indicates that they did not exert a protective effect against HF or LF high carbohydrate induced liver damage. A regression analysis was also performed for the Log_{10} AST or Log_{10} ALT to body weight ratio, but no correlation was found (data not shown), and so there was no link towards hepatic liver damage and body weight.

Table 4.2: Values for liver damage markers in mice from the dietary intervention study
Sirius red values were obtained from the quantification of red pixels in Fiji software and represent the levels of collagen in the sections. AST: aspartate transaminase. ALT: alanine transaminase. Both AST and ALT were recorded in U/L and are both detected in the plasma of mice and represent the level of liver damage. Values are represented as means of the whole group sample sizes with standard deviation.

	LF	LF+EC	LF+34DHPVL	HF	HF+EC	HF+34DHPVL
Sirius red pixels	$2.50 \times 10^7 \pm 4.02 \times 10^7$	$2.06 \times 10^7 \pm 3.12 \times 10^7$	$1.98 \times 10^7 \pm 3.02 \times 10^7$	$8.96 \times 10^6 \pm 7.24 \times 10^6$	$1.20 \times 10^7 \pm 1.04 \times 10^7$	$1.45 \times 10^7 \pm 1.05 \times 10^7$
Sirius red Log_{10} pixels	7.00 ± 0.56	6.97 ± 0.55	6.91 ± 0.64	6.75 ± 0.47	6.95 ± 0.34	6.99 ± 0.36
AST (IU/L)	372 ± 309	370 ± 330	828 ± 1246	206 ± 65.0	191 ± 88.2	190 ± 68.4
ALT (IU/L)	154 ± 173	179 ± 175	648 ± 1508	87.8 ± 39.6	74.2 ± 44.4	87.9 ± 57.9
AST/ALT Ratio	3.34 ± 1.23	2.49 ± 0.88	4.33 ± 3.14	2.67 ± 1.04	3.02 ± 1.60	2.71 ± 1.19
Log_{10} AST	2.43 ± 0.38	2.42 ± 0.39	2.50 ± 0.63	2.29 ± 0.14	2.23 ± 0.22	2.25 ± 0.15
Log_{10} ALT	1.93 ± 0.51	2.05 ± 0.48	1.97 ± 0.83	1.89 ± 0.21	1.81 ± 0.23	1.86 ± 0.28

Finally, regression analyses were performed to identify whether there was a correlation for AST or ALT levels (Log_{10}) to the levels of red pixels detected from Sirius red staining (Log_{10}) (Figure 4.13 E/F). There was a positive linear relationship between these variables, but because of the high variance, the R^2 values were low and there was not a significant association found (Log_{10} Sirius to Log_{10} ALT, p = 0.974, Log_{10} Sirius to Log_{10} AST, p = 0.139). Correlations for AST/ALT were also performed against body weight, but no correlations were observed (Appendix Figure 7).

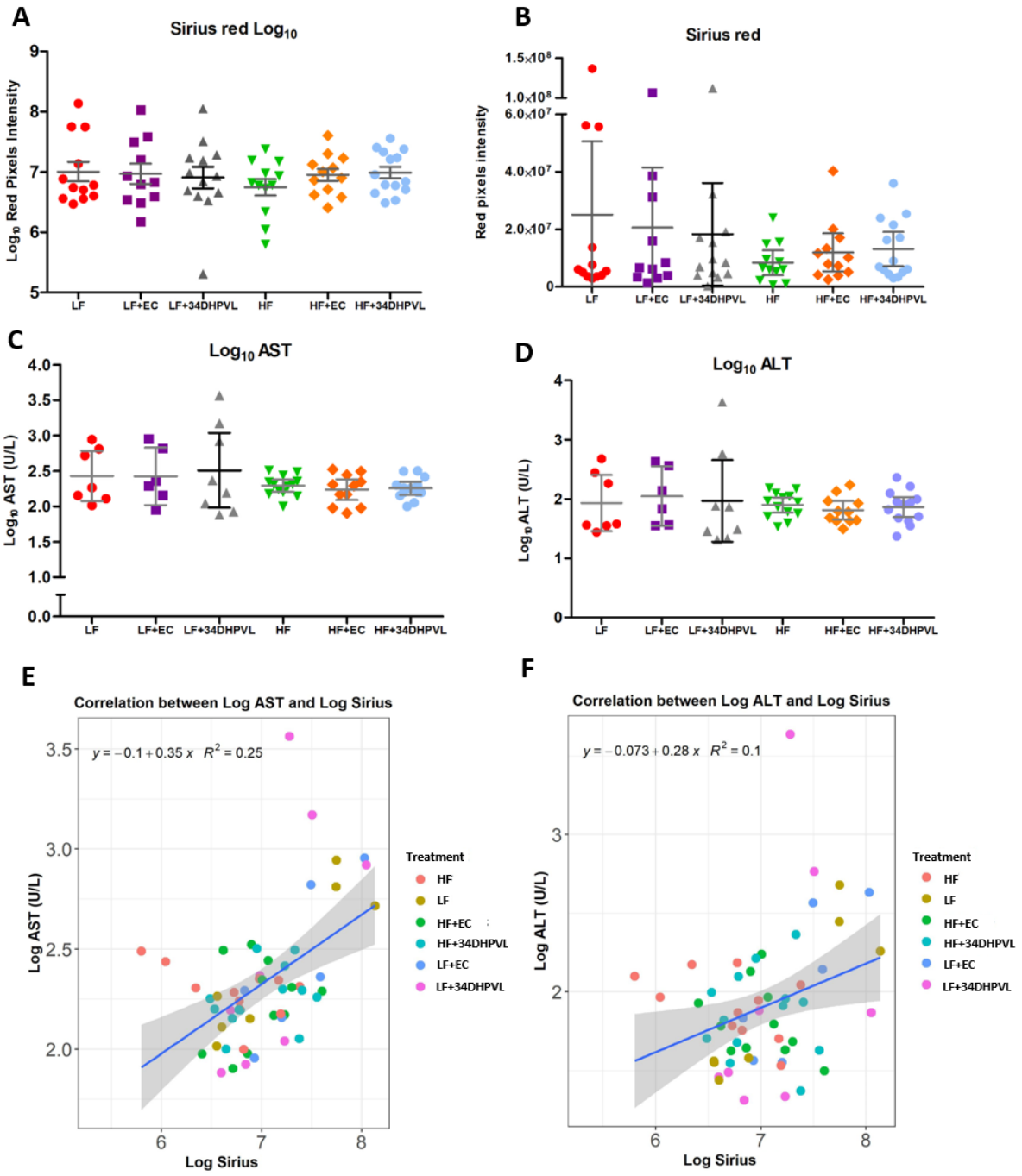

Figure 4.13: Data extracted for hepatic Sirius red and plasma liver damage markers

A) Log_{10} of Sirius red pixels from hepatic sections, dot plot chart; B) Raw Sirius red pixel values from hepatic sections, dot plot chart; C) Log_{10} AST values recorded from the plasma of mice, dot plot; D) Log_{10} ALT values recorded from the plasma of mice, dot plot; E) Regression graph for Log_{10} AST against Log_{10} Sirius red pixels; F) Regression graph for Log_{10} ALT against Log_{10} Sirius red pixels. Each point represents an individual mouse on that respective diet. Bars represent 95 % confidence intervals with mean. Sirius red values are obtained from the quantification of red pixels in Fiji, ImageJ software.

4.5.3 (−)-Epicatechin, but not 3',4'-dihydroxyhydroxyphenyl-γ-valerolactone, reduced hepatic steatosis in high-fat diet fed mice

Mice livers were processed for visual assessment of lipids and processed for lipid quantification. Firstly, snap frozen livers were sectioned and stained for LipidTOX™, a green fluorescent dye that targets lipids, and the pixel intensity was quantified using image processing software Fiji. Secondly, 30 mg portions of snap frozen liver lobes were processed using the Bligh and Dyer (421) method to extract lipids which were later quantified using a Triglyceride Liquicolor Mono assay kit. These allowed for identification of whether EC or 34DHPVL were able to protect against HF diet induced steatosis.

Lipids were quantified from livers and are presented as the mass of lipids (mg) per g of liver tissue. For all LF dietary intervention fed mice there were no significant changes observed following the supplementation of EC or 34DHPVL into the diets of mice (Figure 4.14 C/D and Table 4.3). However, EC supplemented into HF diet fed mice and compared to HF fed mice caused a reduction in liver lipids by ~0.018 mg (p = 0.11) but did not reach statistical significance. However, significant increases in liver lipids were observed for 34DHPVL supplemented into HF diet fed and HF fed mice compared to LF fed mice (p = 0.006 and p = 0.0035, respectively). Moreover, EC supplemented into HF diet fed mice exhibited no significant changes in liver lipid levels to LF diet fed mice, and thus EC protected against lipid accumulation (p = 0.20). The individual mouse liver lipid levels for both the EC and 34DHPVL supplemented into HF diet fed mice were at both high and low levels, and so, this high variation demonstrates a strong or weak response of the mice to the diets with regards to lipid accumulation.

Although the fluorescent staining of lipids cannot be used to quantify mass, it does allow for the visual assessment of lipid coverage in the tissue, and the pixel intensities can be used as a semi-quantitative measure (Appendix Figures 3-6). The effects observed for LipidTOX pixel intensities were comparable to the effects seen for liver lipids and also reinforce the data where statistically significant changes were observed (Figure 4.14 A/B and Table 4.3).

To determine whether there was a correlation between body weight and liver lipid mass, a plot of these two variables was created to identify whether there was a trend in the data (Figure 4.14 E). There was no effect between the two variables up to a body weight of 45 g, however at ≥ 45 g there was a clear positive correlation (R^2 = 0.56, p = 0.0002, Figure 4.14 F). Because of this, it appears the mice were able to metabolise the lipids efficiently from the HF diet up to 45 g in body weight, but beyond this, they were unable to metabolise the excess lipids and subsequently stored them as fat in the liver, most likely because of impaired liver processes.

Finally, because 34DHPVL supplemented into HF diet fed mice exhibited high levels of liver lipids and significantly higher circulatory insulin levels when compared to all other diet fed mice, a regression analysis was performed on all datasets to identify whether there was a correlation between the two (Figure 4.14 G). There was a strong positive correlation between the two variables ($p < 0.0001$, $R^2 = 0.65$) which shows that with rising blood insulin levels there was greater hepatic lipid storage.

Table 4.3: Values for liver lipids in mice from the dietary intervention study
*LipidTox values were obtained from the quantification of green pixels in Fiji software and represent the levels of lipids in the sections. Lipid mass values were obtained from the extraction of lipids from the livers of mice. Values are represented as means of the whole sample sizes with standard deviation. Significance *p < 0.05, **p < 0.01 compared to LF diet.*

	LF	LF+EC	LF+34DHPVL	HF	HF+EC	HF+34DHPVL
LipidTox pixels	$1.64 \times 10^4 \pm 2.55 \times 10^4$	$1.75 \times 10^4 \pm 4.00 \times 10^4$	$3.97 \times 10^3 \pm 7.11 \times 10^3$	$8.11 \times 10^4 \pm 7.19 \times 10^4$ *	$2.00 \times 10^4 \pm 2.93 \times 10^4$	$2.01 \times 10^5 \pm 3.08 \times 10^5$ *
Log_{10} LipidTox pixels	3.64 ± 0.79	3.24 ± 1.15	2.99 ± 0.77	4.51 ± 0.97*	3.78 ± 0.74	4.49 ± 1.17*
Lipid mass (mg per g liver)	25.7 ± 3.23	23.4 ± 5.13	23.2 ± 5.24	55.2 ± 23.7**	36.9 ± 22.0	63.9 ± 34.8**
Lipid mass (mg) in whole liver	32.2 ± 6.54	29.0 ± 5.75	27.7 ± 9.79	106 ± 65.7**	66.6 ± 61.5*	141 ± 120***
Lipid mass in whole liver to body weight ratio	0.001 ± 0.002	0.001 ± 0.000	0.001 ± 0.000	0.002 ± 0.001 *	0.001 ± 0.001	0.003 ± 0.002 **

To conclude, all LF intervention fed mice accumulated minimal liver lipids, however, for HF intervention fed mice, only once they'd exceeded 45 g in body weight did their livers store the excess fat. Finally, only EC supplementation in HF diet fed mice caused changes in liver lipids to protect against hepatic steatosis, and this was almost effective enough to reduce levels down to those alike in LF diet fed mice.

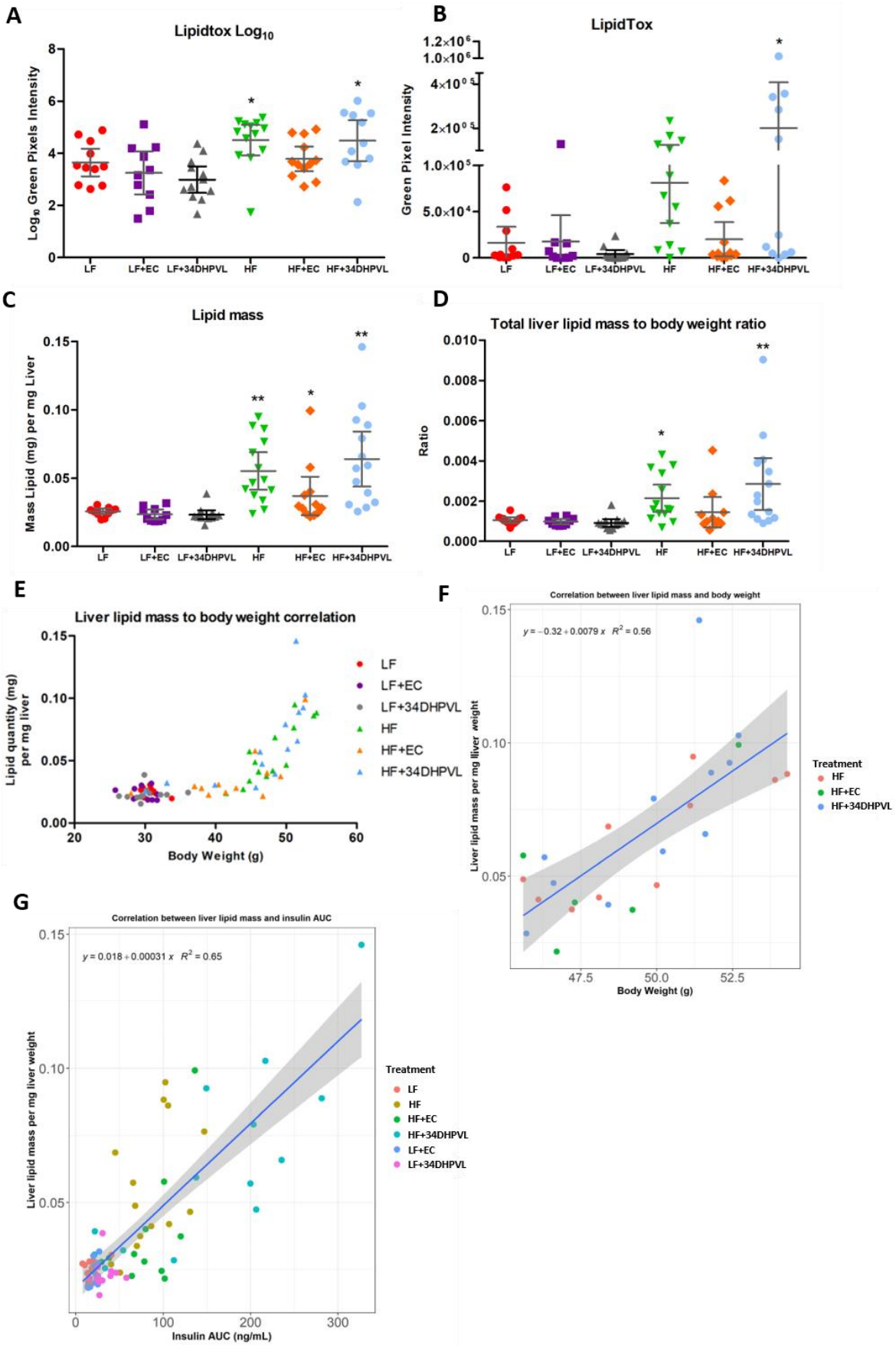

Figure 4.14: Hepatic LipidTox and lipid mass data

Figure 4.14: (continued) *A) Log_{10} of LipidTox green pixels of hepatic sections, dot plot chart; B) Raw LipidTox pixel values from hepatic sections, dot plot chart; C) Mass of lipids present per mg liver tissue, dot plot; D) Mass of lipids in the whole liver tissue of each mouse and then divided by their own body weight, dot plot; E) Correlation graph for lipid mass per mg liver weight against body weight of the mice; there was a stationary phase up to ~45 g body weight followed by a positive correlation after this; F) Regression graph for the mass of lipids per mg liver weight against the body weight of the mice that weighed ≥ 45 g. Each point represents an individual mouse on their respective diet. Bars represent 95 % confidence intervals with mean. LipidTox values are obtained from the quantification of green pixels in Fiji, ImageJ software. Significance *p < 0.05, **p < 0.01 compared to LF diet fed mice.*

4.5.4 Mice on high-fat interventions exhibited significantly more lipids in their circulation than low-fat fed mice

At the point of sacrifice, blood was harvested from the mice and subjected to assays on the RANDOX Daytona$^+$ instrument to measure the levels of cholesterol (CHO), high density lipoprotein (HDL), low density lipoprotein (LDL), high density lipoprotein-3 (HDL3) and triglycerides (TRIG). Thus, this provided quantitative data to identify whether EC or 34DHPVL could mitigate HF-diet induced rises in blood lipids.

Table 4.4: Mice plasma lipid levels
*All plasma lipid values were from week-15 of the dietary intervention study and obtained by following assays according to RANDOX Laboratories. LDL: low-density lipoproteins; HDL: high-density lipoproteins. Values are presented as means of the group sample sizes with standard deviation. Significance *p < 0.05, ***p < 0.001, ****p< 0.0001 compared to LF diet fed mice.*

	LF	LF+EC	LF+34DHPVL	HF	HF+EC	HF+34DHPVL
LDL (mg/dL)	21.4 ± 8.68	23.6 ± 14.5	26.4 ± 12.2	81.5 ± 17.2****	69.8 ± 32.2****	74.9 ± 29.5****
Cholesterol (mg/dL)	86.4 ± 39.7	78.2 ± 31.58	86.5 ± 37.0	189 ± 26.3****	168 ± 32.2****	166 ± 39.0****
Triglyceride (mg/dL)	82.3 ± 50.5	60.5 ± 27.1	75.5 ± 30.8	97.2 ± 31.2	1060 ± 56.6	94.8 ± 49.8
HDL (mg/dL)	55.3 ± 23.20	42.5 ± 19.2	54.6 ± 17.5	88.5 ± 10.3****	76.3 ± 9.23*	88.3 ± 15.9***
HDL3 (mg/dL)	15.8 ± 5.09	13.9 ± 4.96	14.4 ± 5.94	21.0 ± 3.04*	22.1 ± 3.99***	21.8 ± 5.53***
Triglyceride /HDL ratio	0.66 ± 0.25	0.68 ± 0.28	0.62 ± 0.17	0.49 ± 0.16	0.61 ± 0.33	0.49 ± 0.20

It was evident that a 60 % kcal HF diet caused significant rises in circulatory lipids: CHO ($p < 0.0001$), LDL ($p < 0.0001$), HDL ($p \leq 0.01$), and HDL3 ($p \leq 0.01$), when compared to LF diet fed mice (Figure

4.15, Table 4.4). This occurred because the HF diet fed mice had a significantly higher intake of calories and fats compared to LF dietary fed mice (Section 3.5.3, Figure 3.4).

On the other hand, triglyceride blood levels were not significantly affected by any of the diets, as illustrated by the overlapping confidence intervals in Figure 4.15 E/F. This is interesting because HF diet consumption is commonly known to raise blood triglycerides that are associated with an increased cardiometabolic risk (431). The TRIG/HDL ratio was performed (Figure 4.15 F) because it is supposed to provide a better scale to measure cardiometabolic risk (432). High ratios are indicative of smaller and denser LDL particles (very low-density LDL (vLDL)) that directly correlate towards a risk of atherosclerosis (431) and potential insulin resistance (433-435), this is because, the smaller size of vLDLs are considered to be easier to oxidise. In humans, a ratio ≥ 2.5 in women or ≥ 3.5 in men signifies insulin resistance (435), but it is uncertain if these ratios are unanimous in mice. However, despite insulin resistance having been confirmed from HF diet consumption in mice from this study (chapter 3), their TRIG/HDL ratios average < 0.70, and thus this confirms that the human ratios are very different to the mice ratios for concluding insulin resistance. Moreover, for all HF dietary intervention fed mice, their TRIG/HDL averages were lower than all LF diet fed mice (not significant) and so the mice in this study do not support the more generalised associations that have been published.

Plasma lipids were also correlated to body weight (Appendix Figure 7) where LDL (p = 0.01, R^2 = 0.65), HDL3 (p = 0.04, R^2 = 0.17), and cholesterol (p < 0.01, R^2 = 0.68) showed significant positive associations to body weight, whereas HDL (p = 0.19, R^2 = 0.49), and triglycerides (p = 0.08, R^2 = 0.025) were borderline significant. Therefore, heavier mice had higher circulating lipid levels.

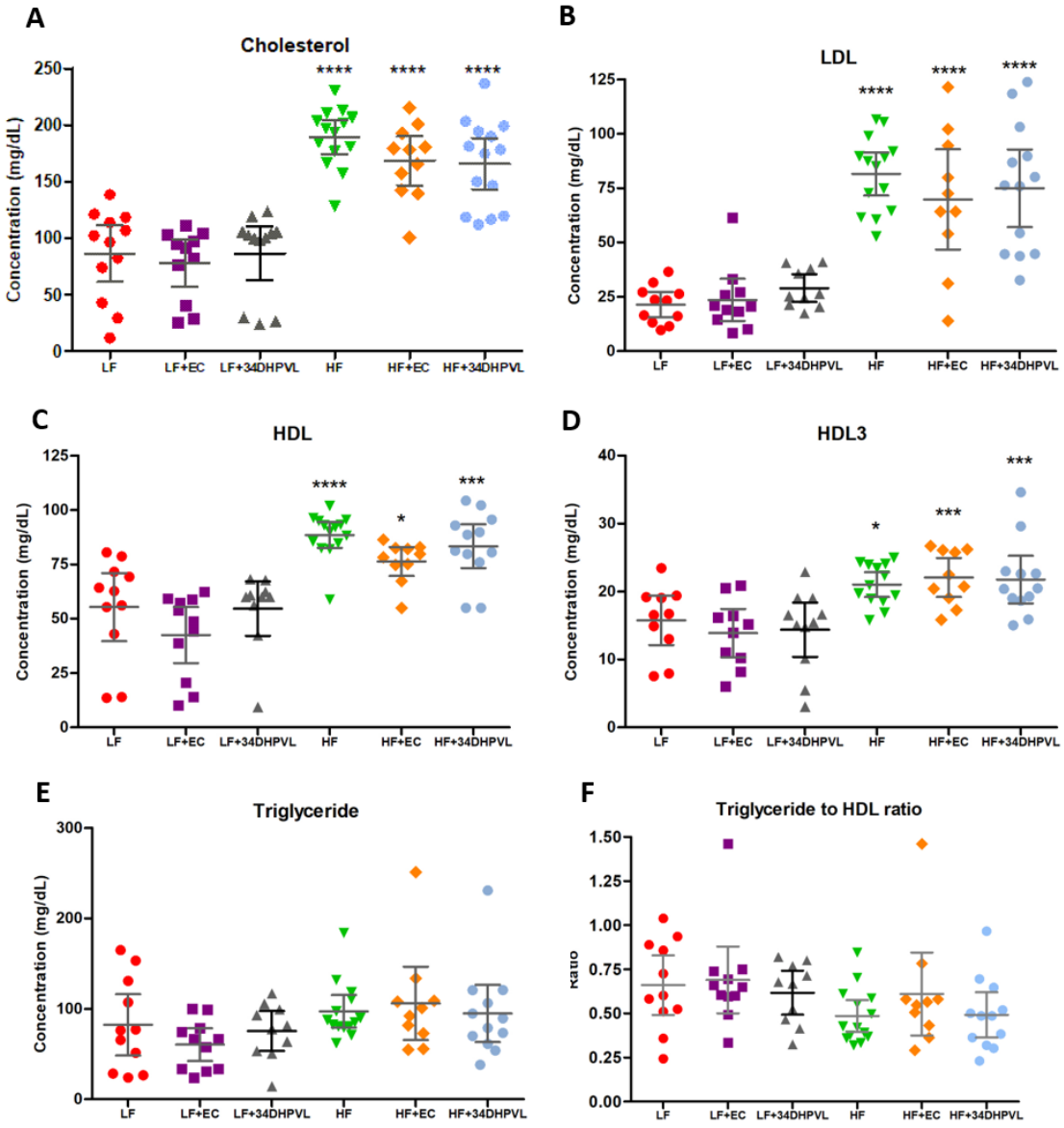

Figure 4.15: Concentrations of plasma lipids in mice from the dietary intervention
*A) Cholesterol concentrations, dot plot chart; B) Low-density lipoprotein concentrations (LDL), dot plot chart; C) High-density lipoprotein concentrations (HDL), dot plot; D) HDL3 concentrations, dot plot; E) Triglyceride concentrations, dot plot chart; F) Triglycerides to HDL ratio, dot plot chart. Each point represents an individual mouse on that respective diet. Bars represent 95 % confidence intervals with mean. Significance *p < 0.05, ***p < 0.001, ****p<0.0001 compared to LF diet fed mice.*

4.5.5 α-amylase activity on starch digestion was not inhibited by 3',4'-dihydroxyphenyl-γ-valerolactone

Polyphenols have been reported to inhibit the enzymatic activity of α-amylase (436), which is an enzyme secreted in saliva and in pancreatic juices following the consumption of food, to digest starch. Because of this, polyphenols could lower the C_{max} of blood glucose after food ingestion and

may perhaps be an underlying action for their effects on hindering the development of insulin resistance. To determine whether 34DHPVL was capable of enzyme inhibition, it was investigated following its incubation with alpha amylase on starch digestion. Positive enzyme inhibitory controls were also performed using EGCG (reported to inhibit α-amylase) and acarbose (a known α-amylase inhibitor).

Firstly, the enzyme activity of α-amylase was determined to be 5.2 kU/mL, (data not shown). For the reaction, starch was used at 5 mg/mL, and the optimal final reaction concentration of α-amylase was confirmed to be 0.05 U/mL, which was the concentration that caused a linear production of maltose over 12-mins (Figure 4.16 A). Although there are published studies that report the inhibition of α-amylase with EGCG at ≥ 100 µM concentrations (243, 437), this could not be reproduced in this study, and the rate of enzyme activity was not lowered by the presence of EGCG (Figure 4.16 B). Because of this, the purity of EGCG was checked using high-performance liquid chromatography mass spectrometry (HPLC-MS), but this confirmed one clear peak for EGCG at a mass of 459 on the LC and diode array (U.V). In contrast, 10 µM acarbose completely inhibited α-amylase activity (Figure 4.16 B).

The concentration selected for 34DHPVL was based on the pellet concentration provided to the mice (200 mg/kg) and from the assumption that density was 1 kg/m^3, subsequently equating to 0.2 g/L of 34DHPVL (0.96 mM). For convenience this was rounded up to 1 mM which was used in the assay. During the assay, the rate of starch degradation in the presence of α-amylase was 161 ± 9.08 µM/min maltose production (Figure 4.16 C), whilst in the presence of 34DHPVL this became 129 ± 0.59 µM/min maltose production, and although this was lower it was not significantly different (p = 0.18, unpaired two sample t-test). Therefore, 1 mM 34DHPVL did not inhibit α-amylase activity when supplied at 0.05 U/mL on 5 mg/mL corn starch. In addition, a separate assay that used 2 µM acarbose was added to the enzyme-starch reaction, and proved to cause incomplete inhibition of α-amylase, and significantly lowered its activity to 46 ± 8.50 µM/min maltose production, which was a 3.5-fold reduction in enzyme activity (p = 0.035, unpaired two sample t-test) (Figure 4.16 C).

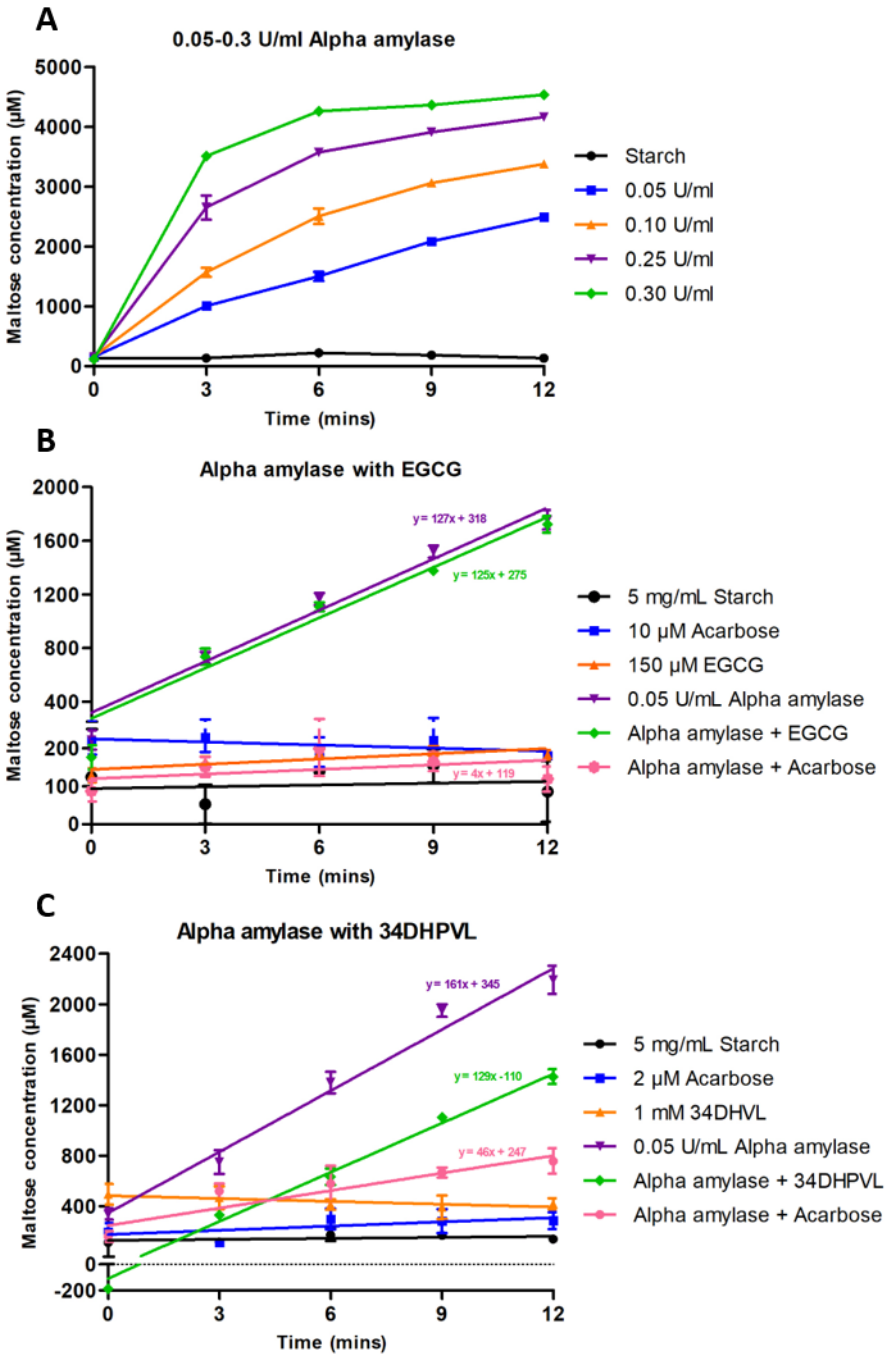

Figure 4.16: Starch digestion assays using alpha amylase
A) Maltose production data from alpha amylase activity at 0.05, 0.10, 0.25 and 0.30 U/mL on 5 mg/mL corn starch over 12 mins. B) Inhibitory assay using either 150 µM EGCG or 10 µM acarbose on the activity of 0.05 U/mL alpha amylase on 5 mg/mL starch over 12 mins. C) Inhibitory assay using either 1 mM 34DHPVL or 2 µM acarbose on the activity of 0.05 U/mL alpha amylase on 5 mg/mL starch over 12 mins.

4.6 Discussion

To investigate whether EC or 34DHPVL protected against HF diet induced steatosis and raised circulatory lipids, several liver histology stains, and plasma assays were performed. A final enzyme assay was performed to investigate whether 34DHPVL could prevent rises in blood glucose levels via the inhibition of alpha amylase activity on starch digestion. The results from these experiments have shown the following:

(1) 34DHPVL supplemented into HF diet fed mice, and HF diet fed mice exhibited significantly greater levels of hepatic steatosis when compared to LF diet fed mice.

(2) EC but not 34DHPVL mitigated HF diet induced liver lipid accumulation.

(3) A HF diet caused a significant rise in plasma LDL, cholesterol, HDL and HDL3 concentrations in mice compared to LF diet fed mice.

(4) The addition of EC or 34DHPVL into the HF diet did not affect plasma lipid levels, when compared to HF diet fed mice.

(5) There were uniform levels of liver damage encountered in all mice dietary treatment groups, but there were approximately 20 % of mice from all LF interventions that exhibited severe damage.

(6) 1 mM of 34DHPVL did not inhibit the activity of 0.05 U/mL of α-amylase on starch digestion.

4.6.1 Hydroxyphenyl-γ-valerolactones do not contribute to the effects seen from EC consumption for mitigating high-fat diet induced hepatic steatosis

It is well reported that HF diets will increase hepatic steatosis from long-term consumption, and this was clearly observed in the mice in this current study (438). It was also observed that EC lowered the levels of hepatic lipids when supplemented into HF diets by approximately 33 %, but this did not reach statistical significance. However, this does suggest that EC protected against HF diet induced liver lipid accumulation, which could occur by EC influencing hepatic *de novo* lipogenesis (DNL). To investigate this, hepatic gene expressions were assessed following RNA-sequencing of the tissue, as described and discussed in chapter 5 section 5.6.2, and there was sufficient gene expression and pathway changes for the lowering of hepatic DNL when compared to HF diet fed mice. This corroborates previous reports for the effects of EC or cocoa polyphenol

extract supplementation into the diets of diabetic rats or as treatments on hepatic cell lines (199, 285, 338, 341, 405, 439, 440). This will be revisited in chapter 5.

In contrast, the addition of 34DHVL into the HF diets of mice was not protective against hepatic lipid accumulation and instead caused ~15 % increase in liver lipids, albeit not significant. Instead of lowering hepatic gene expression for DNL, 34DHPVL increased hepatic gene expression for DNL on the HF diet only (chapter 5, section 5.5.8), which would explain the marginally increased liver lipids in the mice. Therefore, HPVL derived metabolites from EC consumption do contribute to mitigating hepatic steatosis. Additionally, there was a large variance in the hepatic lipid content for the mice fed HF diets supplemented with 34DHPVL, and the variance was greater than those on the HF diet. Accompanying the high liver lipid contents was a positive association for high insulin circulatory levels, which, when assessing Figure 4.14 G, the extreme levels only applied to mice on 34DHPVL supplemented into HF diets. To explain this, studies have found that obese hyperinsulinemic subjects expressed a significantly higher level of DNL in their livers than obese normoinsulinemic subjects, and because of this they were converting carbohydrates to fats even when there was a small dietary contribution of carbohydrates (438). The exact mechanisms that underlie this are not currently well-understood, however, there are the following hypotheses; (1) because insulin resistance causes a reduced glucose uptake by extrahepatic tissues, this could cause more carbohydrates to be directed to the liver for metabolism; (2) hyperinsulinemia can induce hepatic DNL processes in obese subjects, and as a consequence their livers would take up more glucose from carbohydrate stores and convert them into fat in an attempt to control blood glucose (438). And so, because there were two clear groups for the mice on the HF diets supplemented with 34DHPVL for low liver fat/blood insulin and for high liver fat/blood insulin, this could be explained by the hyperinsulinemic effects for raising hepatic DNL processes.

4.6.2 Serum lipids were not affected by the presence of polyphenol supplementation

The addition of EC or 34DHPVL into either the LF or HF diet did not influence the levels of serum lipids levels for LDL, cholesterol, triglycerides, HDL or HDL3. This corroborates a study performed by Hollands *et al* (2018) where healthy men and women consumed either 70 mg of monomeric flavanols with 65 mg of procyanidins or 140 mg of monomeric flavanols with 130 mg of procyanidins for four weeks, however, neither of these doses altered the levels of plasma lipids for HDL, LDL, cholesterol or triglycerides when compared to placebo treatments (441). Similarly, no changes in the same serum lipid profile were observed in obese or overweight participants following 25 mg of

EC consumption for two weeks (442). In contrast to this, EC (5 mg/kg/day) supplied to spontaneously hypertensive rats on HF HC diets for 20-weeks significantly lowered serum LDL and triglyceride levels but not HDL levels compared to the HF HC diet alone (443). In addition, the supply of green tea extracts (delivering 1315 mg catechins) to post-menopausal women for 12-months caused a reduction in serum total cholesterol, and LDL levels, but there were no changes in HDL levels and there was an increase in triglyceride levels compared to the placebo group (444). The effects observed were also greater in those with higher baseline serum total cholesterol levels.

It therefore seems that the model used and the length of dietary intervention with catechin supplementation in either humans or rodents influences whether there are observable changes in plasma lipids.

4.6.3 How high-fat diet fed mice exhibit higher circulatory HDL levels than LF diet fed mice

It has been observed in this current study that HF diet fed mice exhibited significantly higher levels of liver lipids and plasma HDL levels than LF diet fed mice. However, because there were big differences between the carbohydrate and fat content for both the HF and LF diets and there was not an intervention group that received a standard caloric diet for carbohydrate and fat content, this limits the analysis to understand whether the LF mice also exhibited higher circulatory and liver lipid levels than would normally be expected. Nonetheless, there is sufficient evidence in the literature to suggest that the activation of *de novo* lipogenesis (DNL) in the liver is responsible for hepatic fat accumulation and higher levels of circulatory lipids from both HF and HC fed diets.

Plasma LDL levels are positively associated with atherogenic risk (445), whereas HDL levels are inversely associated with atherogenic risk and it is well reported that high-fat diets will increase atherogenic risk, although paradoxically with rises in the levels of HDLs (446), and also with rises in total cholesterol levels. In contrast, LF diets can reduce the total cholesterol levels, with reductions in both the levels of harmful LDL and 'healthy' HDL. In addition, LF HC diets that possess 60 % kcal or more total energy as carbohydrates, can cause an elevation in the levels of plasma triglycerides and a reduction in the levels of HDLs in mammals compared to lower carbohydrate diets (447-454). Although it is well documented that HDL is associated with a decrease in atherogenic risk (455), there are contrasting studies that do not support this (453, 456). For example, some human clinical trial studies have reported positive atherogenic outcomes in patients despite a decrease in their blood HDL levels (456, 457). Because of this, markers for cholesterol efflux capacity and total HDL

are better to measure CVD risk (458, 459). HF diet consumption has also been shown to raise circulatory HDL levels (204, 460-468) largely because of the onset of insulin resistance which has been demonstrated to increase lipoprotein lipase activity in adipose tissue, and subsequently raise circulatory free fatty acids (FFAs). The liver then receives these FFAs and directs them to DNL processes in the liver, causing steatosis and rises in circulatory lipids (464, 469-472). This phenomenon also explains in this current study why liver lipid mass was not positively associated with body weight until > 45g, because this was the point at which insulin resistance effects were mostly recorded, as demonstrated by the positive correlation for liver lipids and circulatory insulin levels.

The lack of a standard diet control group in this study prevented the identification for whether the LF HC diet caused HDL levels to decrease from baseline, or whether the HF diet caused HDL levels to increase from baseline, or whether the two occurred side by side. To have overcame this issue, it would have been necessary to measure the HDL levels in the blood of mice before they commenced the intervention study, and thus this would have provided baseline readings. Regardless, the HF dietary intervention caused higher circulatory HDL levels than the LF diet in mice.

4.6.4 There were no phenotypical changes observed for liver damage in mice supplemented with polyphenols

Liver fibrosis occurs when the liver parenchyma is destroyed and is later replaced by scar tissue (473). Scar tissue is an over-deposition of extracellular matrix (ECM), which impairs the functions of hepatocytes and affects hepatic blood flow. This process is driven by hepatic inflammation, which itself is stimulated from the continued consumption of HF and/or HC diets (474). The main signalling pathways activated during the onset of fibrosis include the JAK-STAT, Smad, ERK and NF-κB pathways, and they cause an increase in the production of inflammatory cytokines, particularly transforming growth factor-β (TGF-β) which is the most potent fibrogenic cytokine, and they activate transcriptional genes involved in extracellular matrix deposition (474, 475).

This dietary intervention study has revealed non-significant effects on liver damage from HF or LF dietary consumption in mice and there were no phenotypical differences observed following the supplementation of EC or 34DHPVL, and there were no changes in plasma transaminase levels, which provide a measurement of liver damage. Although there were no phenotypical differences observed, there were gene expression changes recorded in favour of lowering hepatic fibrosis by EC supplemented into the HF diets of mice (chapter 5, section 5.5.7), so it is plausible that had the

study continued for longer, then phenotypical changes may have been observed for collagen deposition in the livers of mice as well as for changes in serum transaminases. There are several reports that have published the beneficial effects of EC (20-40 mg/kg) (476), EGCG (50 mg/kg) (477) and green tea extracts (1-2 %; 300 mg/kg) (478, 479) on the protection against liver damage in different rodent models (monocrotaline induced hepatic sinusoidal obstruction syndrome in mice; ob/ob mice; choline deficient diet in Wistar rats; high-fat diet fed Sprague-Dawley rats), and following high doses (200 mg) of catechin consumption in humans with MAFLD which significantly lowered serum ALT levels (480).

4.6.5 How high-fat and low-fat high-carbohydrate diets cause inflammatory induced liver fibrosis

Despite a lack of significant changes observed for serum transaminases and collagen deposition in the livers of mice for HF and LF diet fed mice, there were still 23 % of all LF treatment groups that exhibited severe signs of liver damage, which is partly because the diet had 70 % kcal content attributed to complex carbohydrates, and no dietary fibre. Subsequently this can cause an induction of liver damage within these mice, as evidenced by published reports that compare low carbohydrate (LC) and HC diets (481-484). Accompanying the 23 % increase in liver damage markers for LF HC mice in this study were also changes in hepatic gene expressions for an induction of fibrogenic genes when compared to HF treatment groups, as discussed later in chapter 5. To briefly elude to this here, the LF diet caused an induction in the transcriptomic profile for the production of collagen and other ECM proteins and various pro-fibrogenic genes. And so, had the study continued for a longer time-period, there may be more measurable effects seen in the levels of hepatic damage between the mice.

There are several studies that have reported the development of liver fibrosis and inflammation by LF HC and HF diets in mice (460, 472, 481, 483) and in humans (482, 485). But it should be clarified that the effects of the high carbohydrate diets are drastically exacerbated when the diet is lacking in dietary fibre, which the LF diet in this current study was, or is provided as simple rather than complex carbohydrates. A lack of dietary fibre can cause gut microbiota dysbiosis and in turn can increase gut 'leakiness' and stimulate inflammation that can cause liver damage (486-488), and the HC diet can increase hepatic DNL which is closely linked to the development of liver fibrosis (484). Solga *et al* reported that when humans consumed a HC diet (> 54 % kcal energy) versus those who consumed either a LC (32 % kcal energy) or HF diet, they experienced significantly higher odds of developing hepatic inflammation and fibrosis (485). Meanwhile, when mice were fed standard diets

(with fibre, 18 % kcal fat, 58 % kcal carbohydrate – corn starch), HC diets (no fibre, 11 % kcal fat, 73 % kcal carbohydrate – 12 % corn starch, 61 % sucrose) or HF diets (no fibre, 58 % kcal fat, 25 % kcal carbohydrate) for 12 or 18 months, they all experienced very similar levels of hepatic steatosis, fibrosis and inflammation, as well as signs of hepatic tumour growth in all treatment groups (460). However, it was only the standard diet fed mice that exhibited significantly lower levels of fibrosis at both 12 and 18 months, and lower inflammatory accumulation at 18 months, when compared to the HF mice. Furthermore, plasma AST and ALT levels were significantly higher in mice on the LF HC diet after 18 months with clear elevations seen after 12-months, when compared to HF diet fed mice. Similarly, the standard diet fed mice showed higher levels of AST than HF diet fed mice after 18 months. This evidence supports the notion that HC diets in the form of starch or monosaccharides will induce greater liver damage over-time, more so than from HF dietary consumption over the same timeframe. However, had the diets been supplemented with fibre, this could have mitigated fibrosis development and hepatic DNL (489-492). To link this to the results presented in this chapter, because Tessitore *et al* (460) fed the LF intervention mice a lower carbohydrate content than the LF diet fed mice in this current study, it can be assumed that had the study length continued for at least 12-months or more in this current study, the LF diet fed mice would have experienced significantly higher levels of liver damage than the HF diet fed mice.

4.6.6 The actions of α-amylase in raising blood glucose levels from starch ingestion

An enzyme assay was performed to investigate whether 34DHPVL was able to inhibit the actions of α-amylase on starch digestion. Following food ingestion, α-amylase is produced by the salivary glands and is secreted into the upper intestinal tract in pancreatic juices, and acts to digest starch into maltose, and is later digested by further enzymes into monosaccharides (493). The rapid digestion of starch can cause a large glucose load in the circulation over a short-period of time, which, if this happens regularly can raise the risk of developing insulin resistance (494). When the actions of α-amylase are inhibited, it causes a more controlled release of glucose into the blood, and can consequently mitigate against insulin resistance effects (494).

It is well documented that flavanols can inhibit α-amylase's enzyme activity (436, 495-497), and EC does so at high concentrations (243). Because of this, EC could mitigate the development of insulin resistance via this mechanism. In chapter 3 of this thesis, it has been reported that EC lowered the overall glucose A.U.C values when supplemented into LF diet fed mice and compared to LF diet fed mice (rich in starch). In contrast, all the HF diets did not contain starch in their formulation, and as

such, α-amylase inhibition is not a mechanism of action from EC or 34DHPVL in lowering blood glucose levels in HF diet fed mice. In addition, the presence of 34DHPVL into the LF diet caused a reduction in the glucose A.U.C of mice than in its absence, and so 34DHPVL was investigated to identify whether it could inhibit α-amylase activity.

Corn starch was used in the reaction because this was formulated into the LF diet pellets. To this, either EGCG, acarbose or 34DHPVL was incubated in the presence of α-amylase, to record the rate of starch digestion over time. In previous studies, EGCG has been reported to inhibit α-amylase at relatively low concentrations, with reported IC_{50} values of 2 µM, 260 µM, 400 µM and a high 1 mM (126, 243, 437, 498, 499) *in-vitro*. The IC_{50} values were very much dependent on the concentration of starch and enzymes used in addition to the type of reaction performed. EGCG has also been assessed for its enzyme inhibiting ability *in-vivo* in healthy and streptozocin (STZ) injected HF diabetic induced mice (126). It was reported that an oral gavage of 300 mg/kg body weight of EGCG with starch in healthy mice significantly delayed the rise in blood glucose levels compared to the starch group. Similarly, in STZ HF diabetic mice, administration of EGCG (300 mg/kg body weight) for three weeks significantly lowered postprandial blood glucose levels and protected against glucose rises following a glucose tolerance test when compared to diabetic mice (126). Forester *et al* (2012) reported similar effects following corn starch gavage with or without 100 mg/kg body weight of EGCG in CF-1 mice, and reported protective effects of EGCG against rises in postprandial blood glucose levels by the starch (437).

Despite these positive effects observed for EGCG in inhibiting alpha amylase activity *in-vitro* and mitigating glucose rises from starch *in-vivo*, in this current study, EGCG did not inhibit the activity of α-amylase. This could have been due to the type of starch used because most studies perform the reaction using maize or potato starch and show inhibitory effects from EGCG on α-amylase in their assays. In the current study, the incubation of 34DHPVL at the same concentration supplied in the pellets (1 mM), was not effective in inhibiting α-amylase activity. As such, 34DHPVL was not responsible for preventing the breakdown of starch via α-amylase in LF diet fed mice.

EC was not measured in the starch digestion assays because it is reported to inhibit α-amylase at very high concentrations with a small efficacy (243). On the other hand, acarbose was used as a positive control and proved to be an effective inhibitor of α-amylase, as demonstrated by several authors (495).

4.7 Conclusion

This chapter aimed to investigate the biological effects of supplying EC and 34DHPVL into the diets of mice and whether they could improve the hepatic physiology for fibrosis and steatosis. In addition, alpha amylase activity was investigated to highlight whether 34DHPVL could inhibit the digestion of starch. All these examinations were performed to understand how EC could mitigate HF diet induced insulin resistance, and to understand the contribution of 34DHPVL. As such, the following conclusions were drawn:

(1) All HF treatment groups exhibited significantly higher levels of hepatic lipids than the LF treatment groups after 45 g in body weight, which was also the point where greater insulin resistance was recorded and therefore a greater level of hepatic *de novo* lipogenesis.

(2) EC, but not 34DHPVL, protected against HF diet induced hepatic steatosis because of the lower plasma insulin levels and consequently lowered DNL activation.

(3) The LF HC diet induced an equal level of liver damage and hepatic fibrosis when compared to the HF treatment groups, however there were several LF treated mice that exhibited severe signs of fibrosis, which was most likely caused by the high-carbohydrate low-fibre content.

(4) Neither EC nor 34DHPVL mitigated the onset of liver damage/fibrosis when supplemented into LF or HF diet fed mice.

(5) All HF treatment groups with or without polyphenol supplementation exhibited significantly higher levels of plasma cholesterol, LDL and HDL, compared to LF diet fed mice, most likely because of higher lipolysis activity in the adipose tissue.

(6) 34DHPVL was not capable of inhibiting the activity of alpha amylase on starch digestion and was thus not responsible for the reduced glucose A.U.C when supplemented into and compared to LF diet fed mice.

Chapter Five

EFFECTS OF (−)-EPICATECHIN AND 3’,4’-DIHYDROXYPHENYL-γ-VALEROLACTONE ON HEPATIC GENE EXPRESSION IN LOW-FAT AND HIGH-FAT DIET FED MICE

Chapter 5: Effects of (−)-epicatechin and 3',4'-dihydroxyphenyl-γ-valerolactone on hepatic gene expression in low-fat and high-fat diet fed mice

5.1 Abstract

Background: In the previous chapters it was reported that 34DHPVL had a modest, non-significant effect on the glucose response, caused substantial increases in plasma insulin concentrations and increased liver lipid accumulation in liver tissues of high fat (HF) diet fed mice. In order to further assess the effects of 34DHPVL dietary supplementation, a genome wide transcriptomic analysis was undertaken using mouse liver tissue which was exposed to high concentrations of 34DHPVL via the hepatic portal vein, and compared to the non-supplemented HF diet and EC supplemented diet fed mice.

Aim: To identify the hepatic transcriptional pathways that support the actions of 34DHPVL on glucose and insulin changes observed, and to identify whether EC exerts a similar response in the gene changes of mice fed high-fat (HF) or low-fat (LF) diets.

Methods: RNA extracts prepared from mice liver tissue was sent for Illumina NovaSeq RNA-Sequencing and the data were analysed in R studio using the DESeq2 package for comparisons against control treatments (high-fat: HF or low-fat: LF) for polyphenol treatments (EC or 34DHPVL) to obtain differential gene expression (DGE) data. Ranked Log_2 fold-change files were then analysed using gene set enrichment analysis software (Broad Institute) for KEGG and REACTOME pathway analyses.

Results: Large DGE changes were found for the HF versus LF diets (q-value = 0.05, upregulated = 732, downregulated = 713 genes) with a total of 48 significantly enriched KEGG pathways (FDR q-value = 0.25). There were significant changes induced by EC on the HF diet (q-value ≤ 0.05, upregulated = 68, downregulated = 7 genes) with a total of 49 significantly enriched KEGG pathways (FDR q-value ≤ 0.25). In contrast, 34DHPVL did not induce significant gene expression changes (q-value ≤ 0.05, upregulated = 2, downregulated = 4 genes) and only significantly altered 2 KEGG pathways (FDR q-value ≤ 0.25). There were very few differences between EC and 34DHPVL supplemented LF diets and the non-supplemented LF diet, although there were 58-61 significantly enriched KEGG pathway changes (FDR q-value ≤ 0.25).

Conclusion: HF diet caused significant increases in genes involved in pathways for: gluconeogenesis, ribosome, starch and sucrose metabolism, amino acid metabolism and fatty acid metabolic pathways, when compared to the LF treatment, whereas they exhibited a significant reduction in genes involved in *de novo* lipogenesis and fibrosis. The supplementation of EC in the HF diet significantly reversed all these changes, meanwhile the addition of 34DHPVL also reversed these pathway expressions but not significantly. These data suggest that EC protected against MAFLD and insulin resistance by reducing the expression of genes in pathways involved in the mitigation of insulin resistance, and by increasing the transcription of genes involved in the insulin signalling pathway. Further research and a bigger sample size would be required to conclude whether 34DHPVL exerted a protective effect, due to the large variation found.

5.2 Introduction

It is well established that HF diets induce gene expression and metabolic pathway changes associated with the development of metabolic associated fatty liver disease (MAFLD) (formerly known as non-alcoholic fatty liver disease, NAFLD) in rodents. In this introduction, the current state of the art on the effects of HF diets on gene expression profiles and metabolic pathways will be presented, followed by what is known about the effects of EC and 34DHPVL on biomarkers of metabolic syndrome induced by HF diets.

5.2.1 Typical gene expression changes induced by high-fat diets in the livers of mammals

In order to understand how to treat MAFLD and hepatic insulin resistance induced by long-term consumption of HF diets, it is important to understand how such diets can cause changes in gene expression and metabolic disruption in the liver. This not only allows a better understanding of liver disease pathogenesis but also highlights possible targets for preventing or treating disease.

Wang *et al* (2016) assessed gene expression data from the livers of participants who were obese or exhibited MAFLD or NASH (non-alcoholic steatohepatitis) phenotypes, as well as 'normal' control samples (500). In doing so they found some common changes in the expression of genes and pathways that were linked to all three groups where the expression of gene changes were more drastic with progressing disease severity. To summarise their findings compared to control samples, obese livers had 505 differentially expressed genes (DEGs), MAFLD livers had 814 DEGs and NASH livers had 783 DEGs (using p-value < 0.01). Of these, there were 27 significantly enriched pathways that were common to all three groups (using p-value < 0.1), as shown in Table 5.1. The most highly enriched pathways for all three disease phenotypes were for ribosome, ubiquitin mediated proteolysis and focal adhesion and are thus important for the development of MAFLD and NASH.

Similarly, another study investigated hepatic gene expression profiles from the livers of patients that expressed mild MAFLD (very minor fibrosis signs) and those with severe MAFLD (high fibrosis signs) (501). They found a 64 gene expression profile to be consistently associated with MAFLD, these were shown to be involved in cell adhesion and migration (focal adhesion), extracellular matrix (ECM) organisation, fatty acid metabolism, amino acid metabolism, and signal transduction pathways linked to fibrosis (PDGF, IGFBP) (using p-value < 0.05) (501). Furthermore, Huang *et al* (2018) assessed 3 Gene Expression Omnibus (GEO) datasets that contained data for human livers that exhibited positive for MAFLD and used non-diseased subjects as controls (502). As a result,

they reported that the GO ontology pathways and KEGG pathways listed in Table 5.2 were most commonly found in MAFLD when compared to non-diseased controls for all 3 omnibus datasets (using *p*-value < 0.05) (although they did not report the direction of change). Very similar findings were also reported by Ryaboshapkina and Hammar (2018) who also assessed the GEO database, but this time they analysed 7 studies (503), and by Li *et al* (2018) for 2 GEO databases. All these datasets have highlighted how MAFLD affects hepatic transcription and subsequent metabolic processes, showing how severe impairments in 'normal' signalling processes induces the disease.

Table 5.1: The 27 significantly enriched KEGG pathways found by Wang et al (2016) in obese, MAFLD and NASH livers in humans (500).
The pathways presented are those that were commonly enriched in all three groups and compared to non-diseased hepatic controls (using p-value < 0.01).

Significantly enriched KEGG pathways		
Bladder cancer	Ubiquitin mediated proteolysis	RNA degradation
Ribosome	Beta-alanine metabolism	Tryptophan metabolism
N-glycan biosynthesis	*Vibrio cholerae* infection	Nitrogen metabolism
Epithelial cell signalling in *Helicobacter pylori* infection	Valine, leucine and isoleucine degradation	Glycosylphosphatidylinositol (GPI)-anchor biosynthesis
Focal adhesion	Apoptosis	Type-2 diabetes mellitus
Prion disease	P53 signalling pathway	Endocytosis
Steroid hormone biosynthesis	Proteasome	Fc gamma r-mediated phagocytosis
Lysine degradation	Propanoate metabolism	Pathogenic *Escherichia coli* infection
Renal cell carcinoma	Complement and coagulation cascades	PPAR signalling pathway

Another study identified an increase in the 'complement and coagulation cascade' pathway in HF diet fed aged mice, which induced the activation of inflammatory mediators, and ECM deposition for collagen, laminin, hyaluron, elastin, and fibronectin, all of which contribute to the development of fibrosis (504). Similar findings were also reported from a study that used human livers from participants with MAFLD, where pathways for immune system activation, cell cycle progression and extracellular matrix (ECM) reorganisation were upregulated in addition to aforementioned metabolic pathways, but the insulin receptor signalling pathway was downregulated (505).

Table 5.2: The significantly enriched GO or KEGG pathways found by Huang et al in MAFLD patients (502)
The pathway expressions were collated from 3 different Gene Expression Omnibus datasets and were compared against non-diseased hepatic controls (using p-value < 0.05).

Significantly enriched GO ontology pathways		
Cellular lipid metabolic process	Cell adhesion	Transcription from RNA polymerase II promoter
Signal transduction		
Significantly enriched KEGG pathways		
Glycine, serine and threonine metabolism	Cytokine-cytokine receptor interaction	PI3K-Akt signalling pathway
P53 signalling pathway	Glycolysis/gluconeogenesis	MAPK signalling pathway
Apoptosis	Cell cycle	Wnt signalling pathway
Pyruvate metabolism		

For the development of insulin resistance and type-2 diabetes in livers, there are common impairments in fatty acid metabolism, fatty acid oxidation, synthesis and storage, and gluconeogenesis (506). Significant increases in genes *CD36*, *PPARA* (encodes PPARα protein) and *SLC2A2* (GLUT2 transporter) were also reported for diabetic livers. In a study that assessed gene expression differences in genetically obese mice that were either susceptible or resistant to diabetes, they found that *de novo* lipogenesis (DNL) genes were actually reduced in the adipose and hepatic tissue of mice that developed diabetes, when compared to mice that exhibited insulin resistance but did not develop diabetes. These included genes for fatty acid synthase (*FASN*), stearoyl coenzyme A desaturase 1 (*SCD1*), glycerol 3-phosphate acyltransferase (*GPAT*), acetyl CoA carboxylase (*ACC*), sterol regulatory element binding protein-1c (*SREBP1*), and peroxisome proliferator activated receptor gamma (*PPARG*) (507). Meanwhile, there was an increase in inflammatory gene expression in the adipose tissue, which could act to impair DNL processes. Gluconeogenic genes such as phosphoenopyruvate carboxykinase (*PEPCK*) were also suppressed in the livers of pre-diabetic mice but were increased in the presence of diabetes; whilst fatty acid oxidation was decreased in several organs in obese diabetic mice but was low in obese non-diabetic mice. Interestingly, the level of steatosis did not correlate with diabetes onset, where the obese diabetic mice actually expressed reduced hepatic fat than the obese non-diabetic mice (507); this was in support of previous literature (508-511).

Further changes in the expressions of genes for the development of hepatic insulin resistance commonly involve the *IGFBP* (insulin-like growth factor binding proteins) genes and matrix metalloproteinase-7 (*MMP7*) which transcribe proteins for binding to insulin and extracellular matrix degradation, respectively. The name for IGFBP really reflects their role where they bind to

IGF-I (insulin-like growth factor-1) and IGF-II proteins, which causes a decreased binding of IGFs to their receptors and a reduction in insulin signalling; IGFBPs can also prolong the half-life of IGFs (512). IGFBP1 is expressed predominantly in the liver and is mostly regulated by insulin, but their levels fluctuate postprandially and are reduced in the presence of insulin resistance (513), whilst IGFBP-3 regulates the ratio of bound to unbound IGFs and also inhibits cytokine induced insulin resistance, where IGFBP-3 proteolysis positively correlates to obesity induced insulin resistance (514, 515). Furthermore, MMP-7 breaks down IGFBP-3 and promotes IGF-I binding to the insulin receptors to enhance insulin signalling in normoinsulinemic subjects (516). MMP-7 has been shown to be reduced in obese subjects but is restored upon weight loss (517, 518).

5.2.2 Hepatic gene expression changes in diabetic models supplemented with flavanol-3-ol's or flavonoid food extracts

Assessment of the effects of flavan-3-ols on MAFLD have mostly been explored through the use of green tea extracts (GTE) (401, 519-522), cocoa polyphenols (199, 285, 341, 405, 439), epigallocatechin gallate (EGCG) (126, 281, 282, 401, 477, 523-527) and isolated EC (285, 338, 341, 405, 528, 529). In general, these studies have demonstrated that all of these sources of flavan-3-ols mitigate the onset of MAFLD by reducing gluconeogenesis, DNL, TGF-β/SMAD signalling, metabolism of fatty acids, pyruvate, and amino acids and by improving insulin signalling responses for ribosome pathways, cell cycle genes and cell proliferation, and in some cases an upregulation of PI3K/Akt signalling.

In-vitro studies for MAFLD and hepatic insulin resistance have been explored through the use of HepG2 cells in a high glucose environment to mirror an insulin resistant state (530). Most protective effects by polyphenols were observed when the compounds were added to the cells and incubated prior to the addition of glucose. For *in-vivo* modelling of MAFLD there have been a variety of models selected which include SAMP6 mice (senescence-accelerate mouse prone 6), db/db mice (type-2 diabetic and obese), ob/ob mice (obese mice), zucker-diabetic fatty (ZDF) rats, and C57BL/6J mice fed high-fat diets. All these models develop MAFLD and hepatic insulin resistance from high fat/carbohydrate feeding over a length of time (531). Therefore, by supplementing polyphenols into their diet or by means of injection it is possible to identify gene changes taking place in their tissues following sacrifice. A summary of previously reported changes in the expression of genes in HepG2 cells or from mice/rat liver tissue after polyphenol treatments is below.

In the case of EGCG, effects induced at a transcriptomic level in diabetic models and compared to treatments that expressed MAFLD and/or insulin resistance, includes a reduced expression of genes involved with fibrosis, inflammation, gluconeogenesis and DNL, and an increase in gene expression for insulin signalling and related pathways (Table 5.3 summarises this and includes the sources).

Table 5.3: The effects of EGCG on changes in the expression of hepatic genes using in-vivo or in-vitro
The data shows whether EGCG caused genes to be positively or negatively differentially expressed in liver tissues/cells when compared to MAFLD and/or insulin resistant control treatments, and it has been collated from several sources that have been referenced.

Positively regulated	Negatively regulated
Fibrosis markers: TGF-β/SMAD signalling: TGFB1, SMAD1, SMAD2, SMAD4 (477, 519, 523), α-smooth muscle actin (ACTA2) (519, 523), type-I collage (COL1A1) (523, 524), matrix metalloproteinase-9 (MMP9) (523)	PI3K/AKT signalling (477)
Pro-inflammatory markers: inducible nitric oxide synthase (iNOS), Prostaglandin-Endoperoxide Synthase 2 (COX-2), tumour necrosis factor-α (TNFα) (477, 523)	Nuclear factor-κ B (NF-κB) signalling (477)
Gluconeogenesis genes: PEPCK (126, 281, 525, 527), glucose-6-phosphatase (G6PC) (126, 281, 525, 527), FOXO signalling (477)	5' AMP-activated protein kinase (AMPK) signalling (282)
DNL genes: SREBP-1c (126), FASN (126), ACC1 (126), cAMP-response element binding protein (CREB) (126), PGC-1α (PPARGC1A gene) (126), and oxidative stress (477)	Insulin signalling: insulin receptor (IR) (281), insulin receptor substrate-1 (IRS-1) (281)

Table 5.4 shows the changes in the expression of hepatic genes reported for EC dietary supplementation in diabetic rodent models. There are several studies that support the same findings with regards to gene/protein expression changes by EC, but there are also a couple that show opposite effects with regards to NF-κB, JNK and PKC signalling. This is largely due to the experimental design used and the source of diet/media, for example, there was a reduction in the expression of these pathways when EC was supplied in combination with a high fructose diet and not for a HF diet in mice, because it is reported that fructose (carbohydrates) may have a greater impact on transcriptional changes than HF diets (532-534). Interestingly, there were no studies that observed fibrotic markers changed by EC supplementation, and so this is an area that requires further exploration.

Table 5.4: The effects of (−)-epicatechin on changes in the expression of hepatic genes using in-vivo or in-vitro models

The data shows whether (−)-epicatechin caused genes to be positively or negatively differentially expressed in liver tissues/cells when compared to MAFLD and/or insulin resistant control treatments, and it has been collated from several sources that have been referenced.

Positively regulated	Negatively regulated
NF-κB pathway: IκB kinase (IKK) (528), and nuclear factor erythroid 2-related factor 2 (NRF2) (528)	Gluconeogenesis genes: PEPCK (285, 341), and glycogen synthase kinase-3 (GSK-3) (285, 341)
PI3K/AKT signalling (285, 338, 341, 405, 528, 529)	DNL genes: SREBP-1c (405), and FASN (405)
Extracellular signal-regulated kinase (ERK) signalling (338, 528, 529)	JNK signalling: JNK1 (338), JNK2 (338)
c-Jun N-terminal kinases (JNK) signalling: c-JUN (AP-1) (528, 529)	PKC signalling (338)
Protein kinase C (PKC) signalling: PKC (529), and AMPK signalling (341, 405)	Inflammatory mediators: TNFα (338)
Insulin signalling: IR (285, 341), IRS-1 (285, 338, 341), and IRS-2 (285, 341)	
PPAR signalling: PPARα (405)	

Use of GTEs in studies is common. GTEs are rich in polyphenol content, with high concentrations of EGCG, and lower levels of EGC, ECG and EC (535). Because of the polyphenol mixture, it cannot be determined what the active compound(s) are in green tea with regards to hepatic transcriptional changes, but it does provide a valuable insight into this widely consumed drink and its potential health benefits. GTEs have been shown to induce most of the changes in the expression of genes in livers that have been mentioned previously, as listed in Table 5.5.

To briefly put into context some of the changes in the expression of genes induced by the presence of polyphenol extracts, a few studies shall now be described in more detail. Previous evidence has highlighted EGCGs ability to inhibit PKC, a protein that is stimulated by fatty acids to phosphorylate and inhibit the insulin receptor (IR) (525). Consequently, EGCG increased insulin signalling downstream of IR activation. Similar events have also been found following the treatment of HepG2 cells with EC and cocoa polyphenols, where IR, IRS-1, IRS-2 and proteins in the PI3K/Akt pathway were increased, and so counteracted the decreases caused by a high glucose environment (285, 341). Similarly, in a diabetic mouse model (338) and in ZDF rats (199), EC supplemented into their diet induced an increase in the aforementioned insulin signalling markers.

Table 5.5: The effects of green tea extracts on changes in the expression of hepatic genes using in-vivo or in-vitro models

The data shows whether green tea extracts caused genes to be positively or negatively differentially expressed in hepatic tissues/cells when compared to MAFLD and/or insulin resistant control treatments, and it has been collated from several sources that have been referenced.

Positively regulated	Negatively regulated
Insulin signalling: INSR (521), and IRS2 (521)	Fibrosis markers: TGFβ/SMAD signalling: TGFB1 (519, 520, 536), SMAD1 (519), SMAD2 (519), COL1A1 (536), and α-SMA (519, 520)
FOXO signalling (521)	ERK signalling (519)
	JNK signalling: c-JUN (AP-1) (520)
	DNL genes: SREBP1-c (401, 526), FASN (401, 526), SCD-1 (401, 526), and hormone-sensitive lipase (HSL; LIPE gene)
	Gluconeogenesis genes: PEPCK (527), and G6PC (527)

In addition, cocoa polyphenols exhibit high concentrations of EC and catechins, which are second to proanthocyanins, and also possess lower concentrations of anthocyanins (24). The reported hepatic gene expression changes caused by cocoa polyphenols in insulin resistant models are presented in Table 5.6.

Table 5.6: The effects of cocoa polyphenols on changes in the expression of hepatic genes using in-vivo or in-vitro models

The data shows whether cocoa polyphenol extracts caused genes to be positively or negatively differentially expressed in hepatic tissues/cells when compared to MAFLD and/or insulin resistant control treatments, and it has been collated from several sources that have been referenced.

Positively regulated	Negatively regulated
Glucose transporters: GLUT-2 (199, 341)	Gluconeogenesis genes: PEPCK (199, 285, 341), and GSK-3 (199, 285, 341)
Insulin signalling: IR (341) (285), IRS-1 (199, 285, 341), and IRS-2 (285, 341)	DNL genes: SREBP-1c (405), and FASN (405)
PI3K/AKT signalling (285, 341)	PKC signalling (405)
AMPK signalling (341, 405)	

There are therefore many overlapping hepatic gene and pathway changes that have been reported after supplementation of these specific polyphenols and extracts, mostly contributing to protection

against MAFLD and insulin resistance. However, there are also some reports that contradict these findings, consequently, further research and gene expression analyses are required to conclude how specific polyphenols provide protective effects and how translatable these effects are from the foods that are consumed.

There are no reports describing the effects of HPVLs per se on insulin resistance and MAFLD – this remains an important gap in current knowledge.

5.3 Aims and approach

Chapters 3 and 4 have reported evidence for modest protective effects of 34DHPVL on maintaining glucose homeostasis in HF diet fed mice, accompanied with increases in blood insulin and hepatic lipid accumulation. It is thus important to analyse the changes in the expression of genes to understand pathways through which 34DHPVL acts to induce these phenotypical and physiological effects when compared to the EC supplemented and non-supplemented HF diet. Therefore, liver tissue was selected to perform a genome-wide transcriptomic analysis because it is a highly metabolic organ that develops MAFLD and insulin resistance and is exposed to high concentrations of 34DHPVL. The overall aim of the research reported in this chapter was to explore the possible effects of 34DHPVL using a non-targeted (hypothesis-generating) approach and to compare against the effects of EC. This was achieved using two different dietary backgrounds (HF or LF) with or without EC or 34DHPVL supplementation and use of RNA-sequencing to investigate possible effects on gene expression. To investigate this, the below approaches were taken:

(1) Quantify differential gene expression changes in response to different dietary treatments. RNA samples were sent and analysed for transcriptomic profiling by RNA-Sequencing for: HF versus LF, HF+EC versus HF, HF+34DHPVL vs HF, LF+EC vs LF, and LF+34DHPVL vs LF treatments.

(2) Identify significantly enriched pathways in response to the treatments using gene set enrichment analysis.

(3) Assess the genes and pathways where changes had taken place in response to polyphenol treatments and how they impact specifically on MAFLD and insulin sensitive pathways.

(4) Analyse these changes with reference to the biological changes seen in chapter 3 and 4 for the GTT and histology analyses.

The data produced were used to address the following questions: (1) do changes in gene and pathway expressions induced by the HF diet reciprocate those seen in previous studies for the induction of MAFLD and hepatic insulin resistance? (2) Does 34DHPVL alter hepatic gene expression in a HF diet, and if so, are any of these linked to the biological effects observed in the previous chapters? (3) Are the changes in hepatic gene expression caused by 34DHPVL different to those caused by EC supplementation? (4) Do the gene expression changes assist with understanding how 34DHPVL and EC affect MAFLD and insulin resistance? To answer these questions, the following hypotheses were formed:

(1) The HF diet will induce similar pathway changes to those previously published for the induction of MAFLD and hepatic insulin resistance.

(2) 34DHPVL will cause changes in gene expression to protect against HF diet induced metabolic disease.

(3) Based on the findings in the previous chapters, EC will reverse/mitigate the pathway changes induced by the HF diet to protect against MAFLD and insulin resistance.

5.4 Methods

All the methods detailed were performed in-house unless otherwise indicated.

5.4.1 RNA extraction from mice livers

The left lobe of livers from the mice harvested as outlined in chapter 3, Table 3.2 and stored in RNAlater, were homogenised into a fine powder under liquid nitrogen using a pestle and mortar. A mass of 30 mg was transferred to homogenising tubes with glass beads and 1 mL of QIAzol Lysis reagent (Qiagen, UK), and homogenised using the Precellys 24 lysis & homogeniser at 6000 rpm for 4 cycles for 30 secs (Bertin Technologies, France). Total RNA was later extracted using Qiagen's RNeasy Lipid Tissue Mini Kit according to the manufacturer's protocol. Total RNA concentration was assessed using the Nanodrop 1000 (ThermoScientific, UK).

5.4.2 RNA-Sequencing of hepatic mouse tissue

5.4.2.1 Quality control and Illumina NovaSeq

RNA was first checked for quality on the 2100 Bioanalyzer (Agilent, USA) using Agilent RNA 6000 Nano Reagents. Only high-quality RNA was sent for sequencing. To ensure this, the following criteria were used: RNA Integrity value (RIN) had > 7, no visual evidence of cirrhosis, and livers that expressed extreme glucose values (greater than the 95 % confidence intervals) during the GTT were excluded from the analysis. Once this was taken into consideration, seven liver RNA samples from each of the six treatment groups were selected at random and sent to Macrogen (South Korea) for sequencing. Macrogen generated cDNAs and ligated them to Illumina adapters at the 3' and 5' ends using a TruSeq library preparation kit with PolyA pulldown. cDNA libraries were fractionated on agarose gels, and 150 bp fragments were excised and PCR (polymerase chain reaction) amplified. For cluster generation, the library was loaded into a flow cell where fragments were captured onto a lawn of surface-bound oligos complementary to the library adapters. Each fragment was then amplified into distinct clonal clusters by bridge amplification in the Illumina NovaSeq 6000 for a 40 million read depth.

5.4.2.2 Processing, differential gene expression and gene set enrichment analysis

The following was then performed in house by myself, the default parameters were used when not specified. Reads were pre-processed to remove ribosomal RNA (rRNA) reads using SortMeRNA

(version 2.1b), using the parameter *paired_out* (537). Quality control was done with Trim Galore (version 0.5.0_dev) and FASTQ (538) to remove: adaptor sequences, short sequences that were shorter than 60 bp, and low quality reads < 30. The reads were then mapped to the reference genome for Mus Musculus GRCm38.97, where the gene transcripts were extracted from Ensembl database (539), using HISAT2 (version 2.1.0) (540), and further assembled into full length transcripts by the use of StringTie (version 1.3.5) (541). Finally, raw gene counts were estimated using a python script provided by the authors (542). The analysis for differential expression was then performed in R Studio, version 3.6.1, using the DESeq2 package (543) alongside other packages listed in Table 5.7. The analysis started with the raw gene counts.

Very low level expressed genes were removed by only retaining genes with at least 10 counts for 7 samples or more (as each group contained 7 samples). Differential expression analysis was then performed to determine whether the different dietary treatments had an impact on the gene expression profile of the sample, according to the DESeq2 protocol (543, 544). The Wald test was used to estimate differentially expressed genes between the control groups (LF or HF) and the treatments (EC or 34DHPVL). Further testing was performed for differentially expressed genes between the LF and HF control groups by adding these as a dietary group factor in the analysis. The Benjamini-Hochberg (545) adjustment was then performed to calculate adjusted *p*-values by setting the adjusted *p*-value threshold to 0.1. Log_2FC shrinkage was then performed for an adjusted *p*-value < 0.1. Following this, independent filtering was performed to filter genes that had little or no chance of showing significance; this was done by setting the adjusted *p*-value < 0.1. The *p*-values calculated by DESeq2 were used to rank all the expressed genes, which was then used to perform a gene set enrichment analysis. Gene Set Enrichment Analysis (GSEA, Broad Institute, USA) (546) was used for KEGG and REACTOME gene set collections.

5.4.2.3 Data availability

All raw RNA-sequencing data was uploaded to NCBI's Sequence Read Archive (SRA) and is accessible at the following link http://www.ncbi.nlm.nih.gov/bioproject/686430 with BioProject ID PRJNA686430 and BioSample accession numbers SAMN17117538-SAMN17117579 with a release date 31/01/2022 or upon publication.

5.4.2.4 R Studio packages and versions

Table 5.7: R packages and versions used for RNA-sequencing analysis

Package	Version	Package	Version
affy	3.26.7	ggbeeswarm	0.6.0
AnnotationDbi	2.40.5	ggplot2	1.46.1
apeglm	1.32.0	Glimma	1.66.0
genefilter	1.1-2	glmpca	3.8.2
gskb	1.12.0	KEGG.db	0.8.8
org.Mm.eg.db	2.2.2	KEGGREST	1.62.0
pheatmap	1.3.0	magrittr	0.3.3
BiocManager	1.3.1	msigdbr	1.16.0
biomaRt	1.30.10	pathfindR	7.0.1
clusterProfiler	1.24.0	pathview	3.12.0
dendsort	1.5	PoiClaClu	1.24.0
DESeq2	0.1.0	RColorBrewer	1.4.0
devtools	1.0.2.1	ReactomePA	1.4.0
dplyr	0.8.5	readxl	1.28.0
edgeR	3.3.0	reshape	1.24.1
enrichplot	1.0.12	tidyverse	3.2.3
ggbio	1.6.0	UpSetR	1.4.2

5.4.3 cDNA synthesis and Real-time quantitative PCR

For cDNA synthesis, 200 ng of RNA was reverse transcribed using the Precision NanoScript Reverse Transcription kit (Primerdesign, UK) in a final volume of 20 µL according to the manufacturer's instructions. Primers were designed targeting 28 pairs of intron-spanning genes (Table 5.8). This was performed by using the Roche probe library software tool (https://lifescience.roche.com/en_gb/brands/universal-probe-library.html) and the specificity checked against the NCBI BLAST database (https://blast.ncbi.nlm.nih.gov/Blast.cgi). Primers were synthesised by Integrated DNA Technologies (IDT, Belgium).

For qRT-PCR, a 7.5 µL final reaction volume was prepared consisting of 3.33 µL of 2X ImmoMix (Bioline, UK, BIO-25020), 0.40 µL 0.1 % bovine serum albumin (Sigma Aldrich, UK, A2153), 0.07 µL of 37.5 mM $MgCl_2$, 0.04 µL of 100-fold diluted SYBR Green (Sigma Aldrich, UK, S9430), 0.07 µL of 10 nM reverse primer, 0.07 µL of 10 nM forward primer, 0.07 µL of 50X ROX reference dye (ThermoFisher, UK), 1.21 µL of RNAse free water (totalling to 5.27 µL reaction mix) and 1.73 µL of the mouse hepatic cDNA. The reaction mixture was placed into 384-well PCR plates (Applied Biosystems, UK) and the reaction carried out using the VIIA™ 7 PCR System (Life Technologies, UK)

using the following conditions: initial denaturation at 95 °C for 10 mins, followed by amplification and data acquisition for 40 cycles for both 95 °C for 15 sec and annealing/extension at 60 °C for 1 min. This was then followed by a melt curve stage of 95 °C for 15 secs, 60 °C for 1 min and 95 °C for 15 secs. For each gene, the melt curves and standard curves were performed to determine the primer specificity, amplification efficiencies and linearity respectively (Table 5.8). All samples were run in triplicate with a no template control for each gene.

Table 5.8: Primers used for qRT-PCR analysis
The R^2 efficiencies and amplification efficiencies correspond to the primer results from the VIIA7 qRT-PCR machine.

Gene	Full Gene Name	Gene ID	Product Size	Forward Primer	Reverse Primer	R^2 Value	Amplification Efficiency
ACTB	Actin beta	NM_007393.5	74	GCAGGAGTACGATGAGTCCG	ACGCAGCTCAGTAACAGTCC	0.972	108.812
EIF2A	Eukaryotic Translation Initiation Factor 2A	NM_026114.3	78	ACTTTTAGTAAGGATGGGACATTGTT	TCCCTTGTTAGCGACATTGA	0.993	115.372
ACADM	Acyl-CoA Dehydrogenase Medium Chain	NM_007382.5	104	GAGGCAGCAGATCGAGGA	GCTTTCGAGTGTTGTGTTCG	0.968	106.794
ALD3HA2	Aldehyde dehydrogenase 3 family member A2	NM_007437.5	65	TCTAGGCCAGTAGGCGGATA	TATGGATGATGCCACAGCTC	0.976	90.706
ACAA1A	Acetyl-CoA Acyltransferase 1	NM_130864.3	92	GGCAGAAGCAGGATGACTTT	CACAGGCACAATCTCAGCAC	0.997	96.724
ALDH7A1	Aldehyde dehydrogenase 7 family member A1	NM_138600.4	92	TGTCCTTCACTGGGAGCACT	GTTTCCTCCAAGCTCCAACA	0.987	93.698
PDHA1	Pyruvate Dehydrogenase E1 Subunit Alpha 1	NM_008810.3	91	GTAAGGGGCCCATCCTGA	TCTTCTCGAGTGCGGTAGC	0.957	88.148
SUCLG1	Succinate-CoA ligase, GDP-forming, alpha subunit	NM_019879.3	78	CACATTCACAAGAAGGGAAGAAT	GGTTGTTTGGTGAACTGCTTC	0.989	98.834
PPARG	Peroxisome proliferator activated receptor gamma	NM_001308354.1	90	AAGACAACGGACAAATCACCA	GGGGGTGATATGTTTGAACTTG	0.943	119.383

Table 5.8: Primers used for qRT-PCR analysis (continued)

Gene	Full Gene Name	Gene ID	Product Size	Forward Primer	Reverse Primer	R^2 Value	Amplification Efficiency
PPARA	Peroxisome proliferator activated receptor alpha	NM_011144.6	74	CTGAGACCCTCGGGGAAC	AAACGTCAGTTCACAGGGAAG	0.982	81.233
PPARD	Peroxisome proliferator activator receptor delta	NM_011145.3	71	GACGGAGAGTGAGACCTTGC	GGCTGCGGCCTTAGTACAT	0.896	110.945
FABP2	Fatty acid binding protein 2	NM_007980.3	124	ACGGAACGGAGCTCACTG	TGGATTAGTTCATTACCAGAAACCT	0.968	81.239
SLC2A2	Solute carrier family 2 (facilitated glucose transporter), member 2	NM_031197.2	96	GTCAGCTATTCATCCACATTCAGT	AGCCAAGGTTCCGGTGAT	0.914	122.984
AGL	Amylo-1,6-glucosidase, 4-alpha-glucanotransferase	NM_001362367.1	90	GCAGTGCTGTGCCTCCTTA	CGAAGGGCAATGAAAGTGTC	0.97	80.801
GYS2	Glycogen synthase 2	NM_145572.2	70	TTTTGGGTGTTTCGTGCAG	GCGTCTGTCCACGATGTAAA	0.972	95.821
GBE1	Glucan (1,4-alpha-), branching enzyme 1	NM_028803.4	77	CAAGAGCTATACGGACTACCGAGT	CCGCTGCGTCAGAATCTAGT	0.988	98.464
IGFBP1	Insulin-like growth factor binding protein 1	NM_008341.4	78	GATCGCCGACCTCAAGAA	TGGGCTGCAGCTAATCTCTC	0.988	92.446
STEAP4	STEAP family member 4	NM_054098.3	93	TGATTCCTATCCGTTACTATGTTCG	AAGAGGTAATAAATGGGCTGTCTTT	0.942	69.821
ENPP2	Ectonucleotide pyrophosphatase/phosphodiesterase 2	NM_001136077.3	71	TGGCTTACGTGACATTGAGG	AGTGGGTAGGGACAGGAATAGAG	0.974	96.141

Table 5.8: Primers used for qRT-PCR analysis (continued)

Gene	Full Gene Name	Gene ID	Product Size	Forward Primer	Reverse Primer	R^2 Value	Amplification Efficiency
SOCS5	Suppressor of cytokine signalling 5	NM_019654.2	92	AGGACATGGACAGCGTTTCT	TCTCATGGGAAAACACAAACC	0.965	61.702
TNF	Tumour necrosis factor	NM_001278601.1	166	CGGGCAGGTCTACTTTGGAG	ACCCTGAGCCATAATCCCCT	0.899	43.845
BAX	BCL2-associated X protein	NM_007527.3	73	GTGAGCGGCTGCTTGTCT	GTGGGGGTCCCGAAGTAG	0.967	95.818
CASP9	Caspase 9	NM_001355176.1	95	GTACATCGAGACCTTGGATGG	TCGCAGAAACAGCATTGG	0.989	88.584
PTEN	Phosphatase and tensin homolog	NM_008960.2	74	AGGCACAAGAGGCCCTAGAT	CTGACTGGGAATTGTGACTCC	0.999	100.821
CHUK	Conserved helix-loop-helix ubiquitous kinase	NM_007700.2	113	AGGCACAGTAACCCCTCCA	TCATTTGTGCTAACGTCTCTCC	0.923	100.741
AKT1	AKT serine/threonine kinase 1	NM_001331107.1	78	TCGTGTGGCAGGATGTGTAT	ACCTGGTGTCAGTCTCAGAGG	0.975	100.851
ITGAM	Integrin Subunit Alpha M (also known as CD11B)	NM_008401.2	77	TGTCCCTGGCTGTTTCTACTG	ATTCTCCTTGCAGTTTTGGTG	0.886	109.186
CD86	CD86 Molecule	NM_019388.3	65	GAAGCCGAATCAGCCTAGC	CAGCGTTACTATCCCGCTCT	0.825	108.444
CD14	CD14 Molecule	NM_009841.4	89	AAAGAAACTGAAGCCTTTCTCG	AGCAACAAGCCAAGCACAC	0.985	64.223

5.4.4 qRT-PCR housekeeping gene validation and statistical analysis

To validate the most stably expressed housekeeping gene prior to data analysis, 12 sets of primer pairs were selected: *ACTB, EIF2A, YWHAZ, TBP1, GAK, RPL27, HMBS, RPLP0, GAPDH, B2M, RPL4,* and *OAZ1* (listed in Appendix Table 1), and were designed and purchased according to that described in section 5.4.3. Bestkeeper, Normfinder and GeNorm programmes (547-549) were then used to validate the most stably expressed pairs of housekeeping genes, where *EIF2A* was found to be the most stable and *ACTB* was the second most stably expressed gene. Changes in gene expressions were calculated using the delta CT method ($2^{-\Delta CT}$) (550) for the housekeeping genes *EIF2A* and *ACTB*, and then statistical analysis was performed as described previously in chapter 3, section 3.4.7. Please see Table 5.9 for the transformations made on the delta CT values and the linear method applied to the data in R studio. For fold-change analysis, all treatments were compared against their respective controls; for example, for a LF+34DHPVL vs LF comparison the LF+34DHPVL mean group average delta CT was divided against the LF mean group average delta CT.

Table 5.9: Transformations performed on qRT-PCR gene expression data for statistical analysis and the R packages used

Gene	Transformation	R Package used	Gene	Transformation	R Package used
ACTB	Log_2	NA	***GBE1***	Log_2	nlme
EIF2A	Log_2	NA	***IGFBP1***	Log_2	lmer
ACADM	Log_2	nlme	***STEAP4***	Log_2	lmer
ALD3HA2	Log_2	lmer	***ENPP2***	Log_2	nlme
ACAA1A	Log_2	lmer	***SOCS5***	Log_2	nlme
ALDH7A1	Log_2	lmer	***TNF***	Log_2	lmer
PDHA1	Log_2	nlme	***BAX***	Log_2	lmer
SUCLG1	Log_2	lmer	***CASP9***	Log_2	lmer
PPARG	Log_2	lmer	***PTEN***	Log_2	nlme
PPARA	Log_2	lmer	***CHUK***	Log_2	lmer
PPARD	Log_2	lmer	***AKT1***	Log_2	lmer
FABP2	Log_2	lmer	***ITGAM***	Log_2	lmer
SLC2A2	Log_2	lmer	***CD86***	Log_2	lmer
AGL	Log_2	lmer	***CD14***	Log_2	lmer
GYS2	Log_2	nlme			

5.5 Results

5.5.1 RNA-sequencing data analysis and identification of treatment clustering

A total of seven hepatic RNA samples per dietary treatment from the intervention study were sent for RNA-sequencing (RNA-seq). The raw RNA-seq data was processed according to the protocol by Pertea *et al* (2016) (551) to estimate raw gene counts using the Norwich Bioscience Institute's (UK) high-performance computers (HPC). The gene counts were loaded and analysed in R studio. First, removing lowly expressed genes and keeping only those genes with at least 7 out of the 42 samples expressing a count of 10 or more for annotated and non-annotated genes. The data was then analysed using the *DESeq2* package, this was selected over the commonly used *edgeR* package because it accounts for gene specific normalisation factors to reduce technical bias towards high GC content, gene length, and amongst others (552, 553). Although *edgeR* was initially trialled on the dataset, it was soon apparent that this package would not be suitable due to a higher variation in the data spread within groups, as later explained. Using *DESeq2*, each gene was treated separately to calculate gene wise dispersion estimates and later shrunk (LFCshrink) through an empirical Bayes approach to obtain final dispersion values; *DESeq2* performs this by estimating the width of the prior distribution of the data and controlling the level of shrinkage automatically from the observed data properties, thereby reducing the occurrence of false positives. It is these shrunken LFCs (log-fold change) and standard errors that were used to discover differentially expressed genes (section 5.5.2). Significance testing was applied using the Wald test by *DESeq2* and adjusted for multiple testing by Benjamini and Hochberg (545).

Data was then transformed for visualisation using *regularised logarithm* (rlog) (543) and *variance stabilising transformation* (vst) (554-556) and assessed for heteroscedasticity (Figure 5.1). Heatmap of the Euclidean distance of the samples was created using the rlog transformed data, as the rlog transformation uses the same empirical Bayes approach applied by *DESeq2* and creates a matrix with a coefficient for each sample. Whilst vst looks for a trend in the variance and mean of the dataset, applying a transformation to remove the trend, and does not consider the differences in size factors. Figure 5.1 shows that the rlog transformation versus the vst transformation had the same range of variance at different ranges of mean values, this is ideal for exploratory analysis.

Figure 5.2 highlights the unnormalised versus the normalised box plots. Samples 23.2 (LF diet), 3.2, 20.2 (LF+34DHPVL diet), 19.1 and 19.2 (LF+EC diet) (where the first number represents the cage number and the second number represents the mouse ID in the cage, i.e. 23.2 corresponds to cage 23 and the 2nd mouse in the cage) were still not normalised to the mean sample distribution after

transformation in comparison to the rest of the dataset. When Euclidean distance heatmaps (Figure 5.3), and principal components analysis (PCA) plots were inspected (Figures 5.4 and 5.5), it was obvious that samples 23.2, 3.2, 20.2, 19.1 and 19.2 did not fit with the rest of the samples within their dietary groups, as shown mapped to the left of the image (Figure 5.4). This was the major reason that *DESeq2* was selected over *edgeR* as it can cope with these datasets without them interfering with downstream statistical testing. Nonetheless, these samples were investigated further with a bioinformatician (Dr Perla Rey, QIB, UK), and in doing so, it was shown that these particular samples expressed a higher read count coverage to the reference genome, in addition to expressing more zero count values versus the other samples (data not shown). By way of caution, the data was then assessed differently to see if these samples would affect the overall outcome of the data prior to exclusion: (1) the raw RNA-Seq data was processed to obtain raw gene counts for only annotated genes, and later processed for differential expression values; (2) the 'outlier' samples were removed completely from the analysis, and the remaining samples were processed for differential gene expression. In performing both the above two steps, it did not affect the outcome results for differential gene expression. The changes were so negligible that they did not have any substantial effects, and so there was not felt a need to exclude them. Therefore, all the 42 samples sent off for sequencing were processed in the final downstream analysis to provide differential gene expression data and gene set enrichment analysis outcomes.

The generalised version for a PCA plot (Figure 5.4), highlights the groupings for the LF versus the HF diets, showing that these two diets distinctively induced hepatic transcriptional changes. In contrast, there were no distinctive groupings revealed for the inclusion of either EC or 34DHPVL into the LF or HF diets. This suggests that there may be some transcriptional changes induced by EC and 34DHPVL, but these were not enough to alter hepatic transcriptional activity in a way that was individually definable.

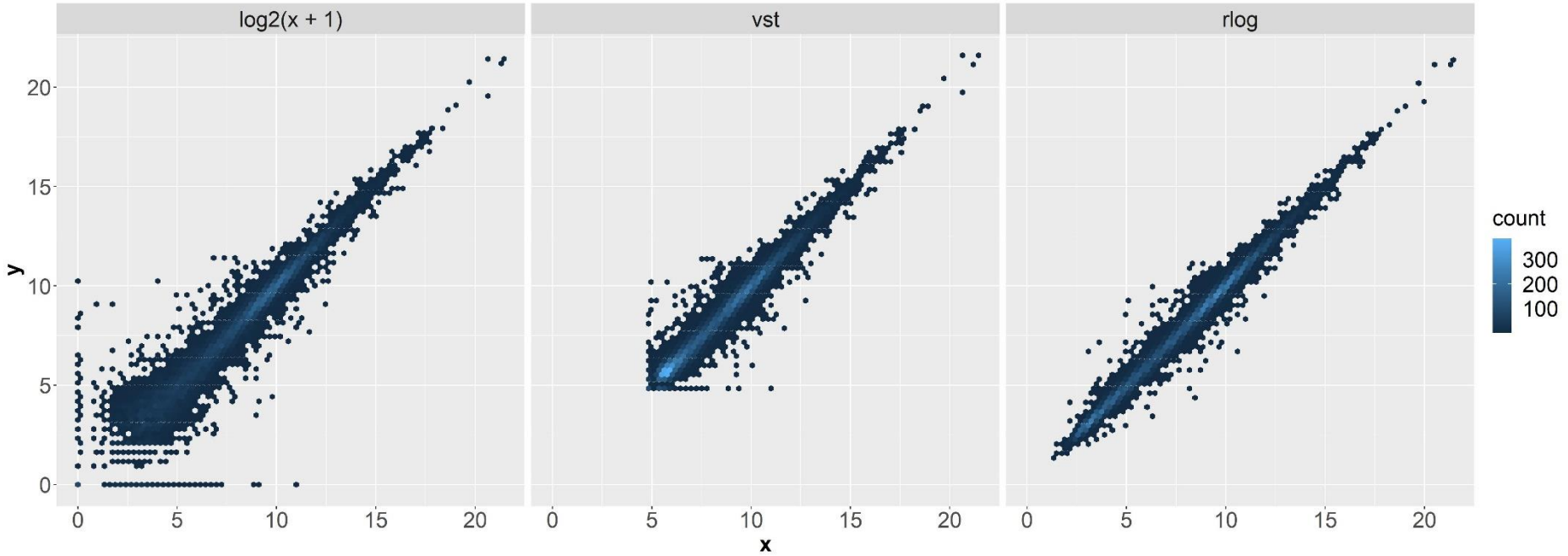

Figure 5.1: Gene expression profiles for different transformations of RNA-sequenced data by Log_2, vst or rlog
These data are from RNA-sequenced mouse livers from the dietary intervention study and plotted in R Studio.

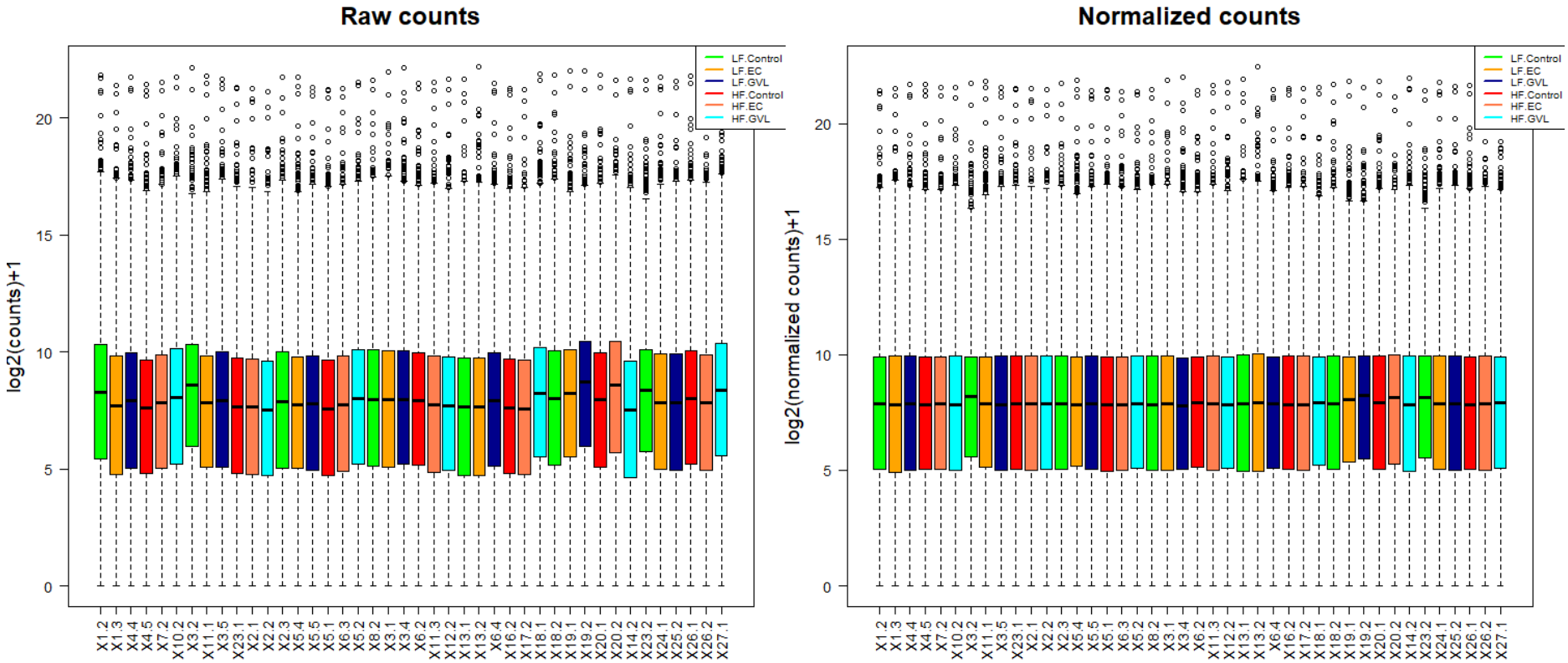

Figure 5.2: Boxplots for the Log₂ datasets of RNA-Sequenced raw gene counts and normalised gene counts

These data are from RNA-sequenced mouse livers from the dietary intervention study and plotted in R Studio. Each number represents an individual mouse ID, where the first number represents the cage number and the second number represents the mouse ID in the cage, i.e. 23.2 corresponds to cage 23 and the 2nd mouse in the cage. LF: low fat; LF.EC: low fat supplemented with (−)-epicatechin; LF.GVL: low fat supplemented with 3',4'-dihydroxyphenyl-γ-valerolactone; HF: high fat; HF.EC: high fat supplemented with (−)-epicatechin; HF.GVL: high fat supplemented with 3',4'-dihydroxyphenyl-γ-valerolactone dietary fed mice.

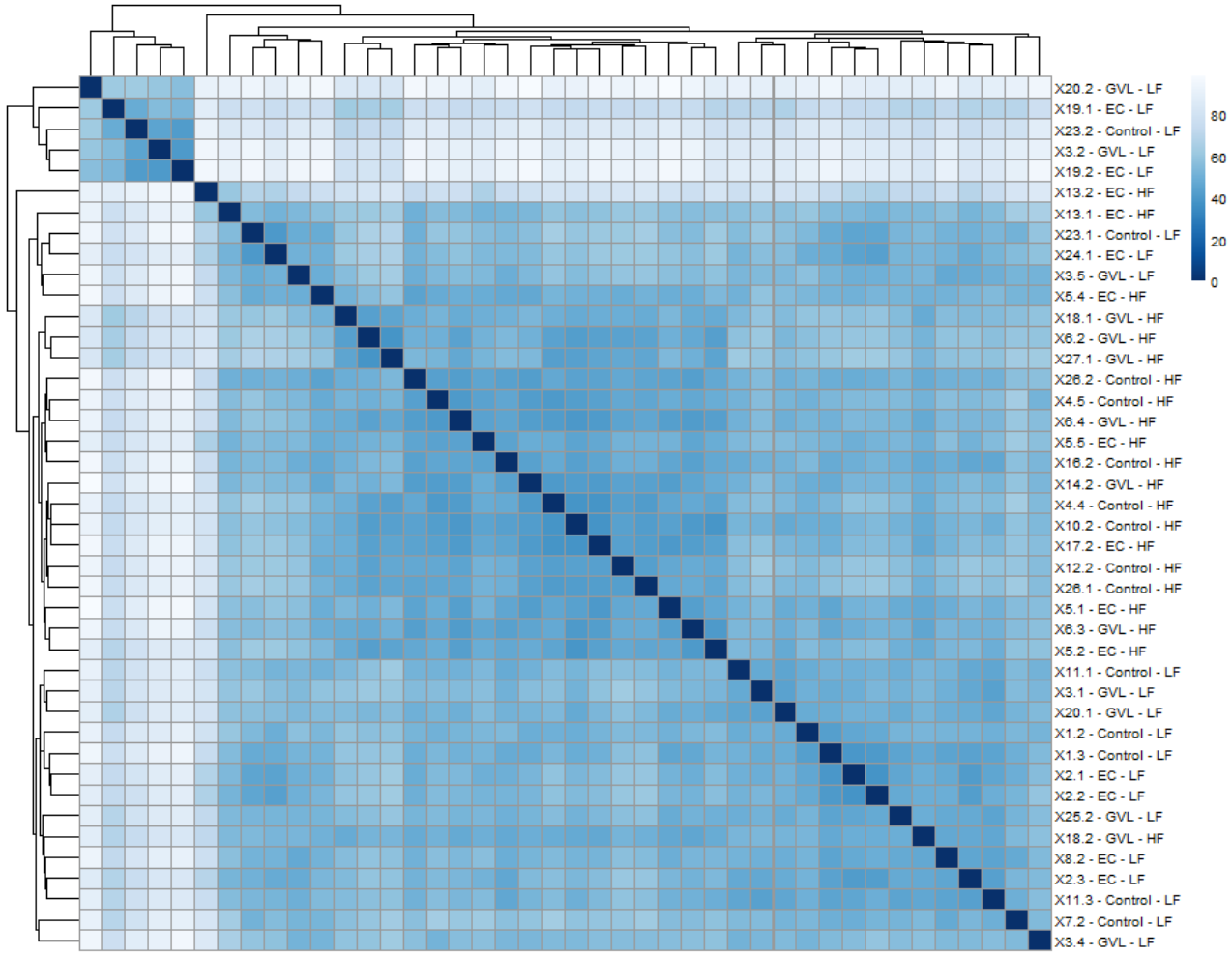

Figure 5.3: Euclidean distance heatmap for each sample/treatment transformed by rlog

These data are from RNA-sequenced mouse livers from the dietary intervention study and this plot was performed using R package pheatmap. Each number represents an individual mouse ID, where the first number represents the cage number and the second number represents the mouse ID in the cage, i.e. 23.2 corresponds to cage 23 and the 2nd mouse in the cage. Control - LF: low fat; EC - LF: low fat supplemented with (−)-epicatechin; GVL - LF: low fat supplemented with 3',4'-dihydroxyphenyl-γ-valerolactone; Control - HF: high fat; EC - HF: high fat supplemented with (−)-epicatechin; GVL - HF: high fat supplemented with 3',4'-dihydroxyphenyl-γ-valerolactone dietary fed mice.

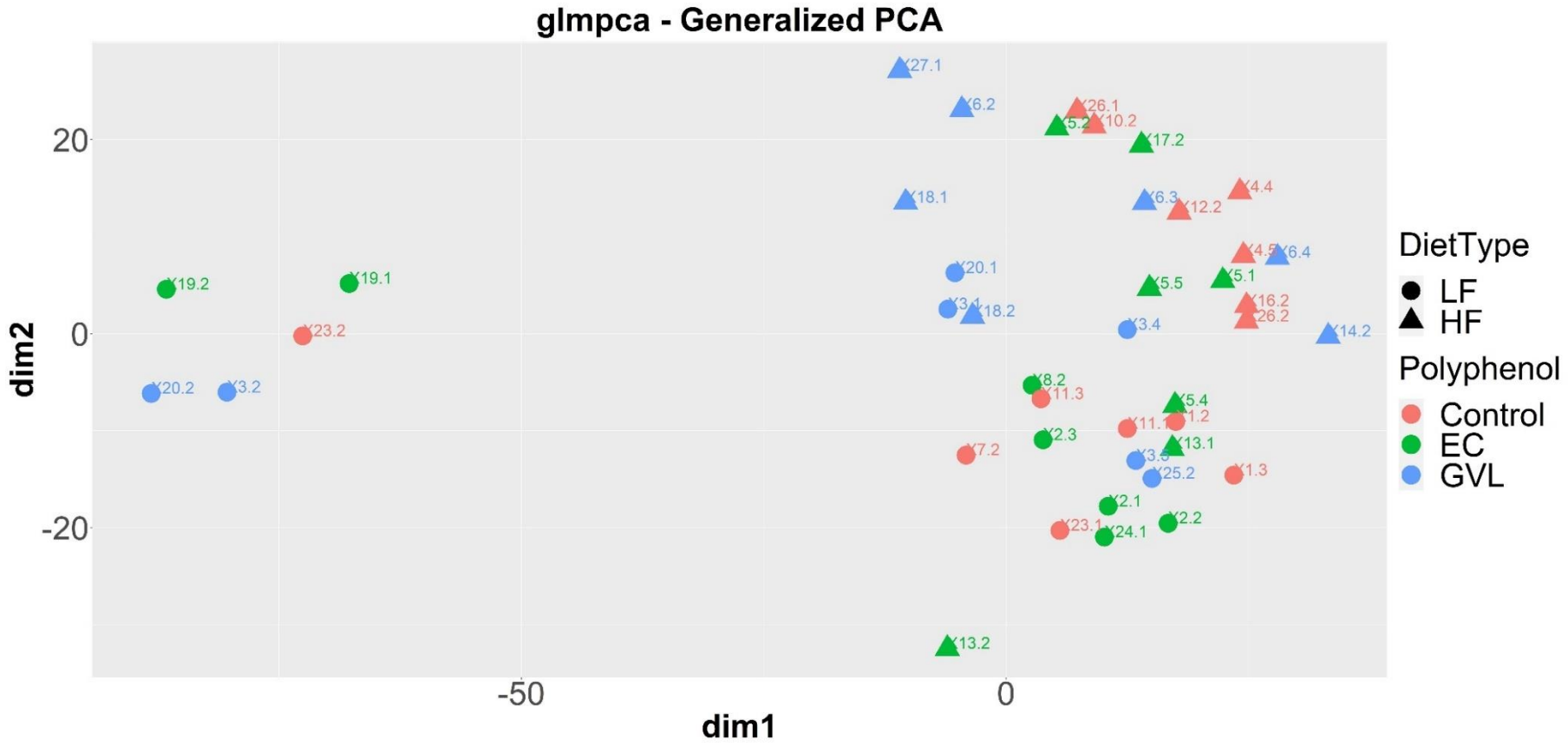

Figure 5.4: Generalised principal component analysis (PCA) plot on raw count data for first and second dimensions

These data are from RNA-sequenced mouse livers from the dietary intervention study and plotted in R Studio. Each number represents an individual mouse ID, where the first number represents the cage number and the second number represents the mouse ID in the cage, i.e. 23.2 corresponds to cage 23 and the 2nd mouse in the cage. LF: low fat; HF: high fat; Control: either LF or HF; EC: supplemented with (−)-epicatechin; GVL: supplemented with 3',4'-dihydroxyphenyl-γ-valerolactone dietary fed mice.

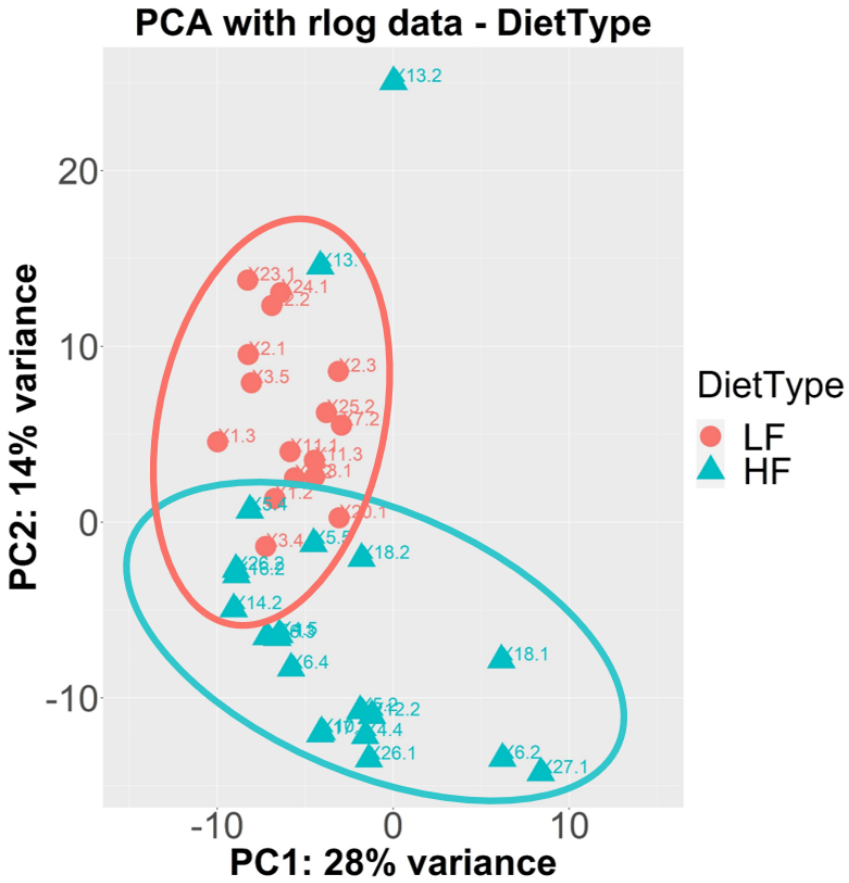

Figure 5.5: Principal component analysis (PCA) plot on rlog transformed data separated for DietType (HF or LF treatments)
These data are from RNA-sequenced mouse livers from the dietary intervention study and plotted in R Studio. Each number represents an individual mouse ID, where the first number represents the cage number and the second number represents the mouse ID in the cage, i.e. 23.2 corresponds to cage 23 and the 2nd mouse in the cage. LF: low fat; HF: high fat; dietary fed mice.

5.5.2 Differential expression analysis highlights significant changes conferred by EC but not by 34DHPVL supplementation of HF and LF diets

As detailed above (section 5.5.1), differential expression analysis was performed on the gene counts via *DESeq2*'s LFCshrink and adjusted for multiple testing by Benjamini and Hochberg. The aim was to investigate (1) whether 34DHPVL causes changes in gene expression, (2) if so, are the changes observed different to those caused by EC, and (3) do the gene expression changes assist with understanding how EC and 34DHPVL affect MAFLD and insulin resistance.

A total of seven pairwise-comparisons were performed to identify differentially expressed genes as follows: (where LF or HF fed mice acted as controls respectively)

1. HF fed mice versus LF control fed mice
2. HF+EC fed mice versus HF control fed mice
3. HF+34DHPVL fed mice versus HF control fed mice
4. LF+EC fed mice versus LF control mice
5. LF+34DHPVL fed mice versus LF control mice
6. HF+EC fed mice versus LF control fed mice
7. HF+34DHPVL fed mice versus LF control fed mice

Table 5.10 highlights the number of genes differentially expressed per comparison at different significance levels (*q*-value). At a significance level of 0.05 there were a total of 1445 differentially expressed genes for the HF vs LF comparison, indicating that the HF diet caused many changes at a transcription level. On the other hand, EC caused 77 gene changes at 0.05 significance in the HF diet, increasing to 112 at 0.1 significance. Therefore, EC induced changes transcriptionally for a small proportion of genes. In contrast, 34DHPVL only altered 6 genes at 0.05 significance in the HF diet, and only increased to 7 genes at 0.3 significance.

Additionally, in the LF diet group, EC supplementation was only able to induce 5 transcriptional changes at 0.05 significance, with only 1 more gene expression change when 0.3 significance level was applied. Therefore, EC caused modest changes in gene expression when supplemented into the LF diet, but it was stronger at causing changes in gene expression when supplemented into the HF diet. Conversely, 34DHPVL caused more changes in gene expression when supplemented into the LF diet, more strongly than its supplementation into the HF diet (using a 0.3 significance level).

Above all, there were many transcriptional changes for the HF+EC and HF+34DHPVL vs LF comparisons at a 0.05 significance threshold. Nonetheless, the changes were fewer than the HF vs LF comparison, where there were 1445 transcriptional changes, whilst the HF+EC vs LF diets

induced 560 transcriptional changes and the HF+34DHPVL vs LF diets induced 940 transcriptional changes.

Table 5.10: Differential gene expression changes for pairwise comparisons
Performed using the DESeq2 package for q-values 0.05-0.3. Up corresponds to the number of genes found to be upregulated for the comparison, and down corresponds to downregulated genes.

***q*-value**	**≤ 0.05**		**≤ 0.1**		**≤ 0.2**		**≤ 0.25**		**≤ 0.3**	
Altered expression	**Up**	**Down**	**Up**	**Down**	**Up**	**Down**	**Up**	**Down**	**Up**	**Down**
HF.Control vs LF.Control	732	713	1024	1163	1514	1990	1791	2466	2086	2873
HF.EC vs HF.Control	68	7	102	10	169	29	206	51	253	73
HF.34DHPVL vs HF.Control	2	4	2	4	2	5	2	5	2	5
LF.EC vs LF.Control	2	3	2	4	2	4	2	4	2	4
LF.34DHPVL vs LF.Control	2	1	8	6	14	10	41	26	76	46
HF.EC vs LF.Control	326	234	512	416	878	883	1069	1144	1261	1419
HF.34DHPVL vs LF.Control	533	407	775	673	1141	1246	1334	1557	1521	1832

5.5.3 Gene set enrichment analysis identifies significantly altered pathways for each pairwise-comparison

Following processing of the RNA-Seq dataset, only annotated genes were considered and the pairwise comparisons were ranked according to their *p.*value multiplied by the sign of the $\log_2$-fold change. The ranked list was then input to Broad Institute's gene set enrichment analysis (GSEA) software (546) for REACTOME and KEGG pathway analysis. This was performed by collapsing the mouse gene symbols to be remapped to human symbols via use of the Chip platform 'Mouse_ENSEMBL_Gene_ID_to_Human_Orthologs_MSigDB.v7.1.chip' for 1000 permutations. This computed the pathways that were significantly altered in the liver for a positive or negative direction by the dietary comparisons. In total, 16,413 genes were input into GSEA and 12,682 had genes mapped to gene symbols for analysis. Table 5.11 illustrates the number of gene sets found to be enriched per pairwise comparison at different FDR (false discovery rate) *q*-values (0.05, 0.1 and 0.25) for KEGG pathway analysis, and Table 5.12 for REACTOME pathway analysis.

Table 5.11: Summary of numbers of significantly enriched KEGG pathways
Data were obtained from GSEA, Broad Institute, for 0.05, 0.10 and 0.25 FDR q-values. Up corresponds to the number of pathways found to be upregulated for the comparison, and down corresponds to downregulated pathways.

***q*-value**	**≤ 0.05**		**≤ 0.10**		**≤ 0.25**	
Altered expression	**Up**	**Down**	**Up**	**Down**	**Up**	**Down**
HF.Control vs LF.Control	24	1	33	2	44	4
HF.EC vs HF.Control	6	10	7	23	15	34
HF.34DHPVL vs HF.Control	0	0	0	0	2	0
LF.EC vs LF.Control	33	0	42	0	56	2
LF.34DHPVL vs LF.Control	37	0	39	1	59	2
HF.EC vs LF.Control	16	4	23	4	42	14
HF.34DHPVL vs LF.Control	28	2	32	2	49	2

Table 5.12: Summary of numbers of significantly enriched REACTOME pathways
Data were obtained from GSEA, Broad Institute, for 0.05, 0.10 and 0.25 FDR q-values. Up corresponds to the number of pathways found to beupregulated for the comparison, and down corresponds to downregulated pathways.

***q*-value**	**≤ 0.05**		**≤ 0.10**		**≤ 0.25**	
Altered expression	**Up**	**Down**	**Up**	**Down**	**Up**	**Down**
HF.Control vs LF.Control	39	24	56	36	104	86
HF.EC vs HF.Control	40	16	60	20	88	52
HF.34DHPVL vs HF.Control	0	0	0	0	19	0
LF.EC vs LF.Control	56	5	98	7	220	9
LF.34DHPVL vs LF.Control	128	16	177	22	325	62
HF.EC vs LF.Control	59	21	79	33	170	126
HF.34DHPVL vs LF.Control	40	43	51	55	121	80

For GSEA analysis, the FDR *q*-values were selected over the nominal *p*-values, because the FDR *q*-values are an estimated probability that the normalised enrichment score will represent as a false positive finding. For example, using the recommended 0.25 *q*-value indicates that the result will be valid 3 out of 4 times as it is adjusted for gene set size and multiple hypothesis testing. Conversely, the nominal *p*-value estimates statistical significance of the enrichment score for a single gene set, not correcting for gene set size and multiple hypothesis testing and is therefore not suitable. To

briefly summarise the results for ≤ 0.25 *q*-value: there were 48 KEGG and 190 REACTOME pathways significantly enriched for the HF versus LF diet comparison; 49 KEGG and 140 REACTOME pathways significantly enriched for the HF+EC versus HF diet comparison; 2 KEGG and 19 REACTOME pathways significantly enriched for the HF+34DHPVL versus HF diet comparison; 58 KEGG and 229 REACTOME pathways significantly enriched for the LF+EC versus LF diet comparison; 61 KEGG and 387 REACTOME pathways significantly enriched for the LF+34DHPVL versus LF diet comparison; 56 KEGG and 296 REACTOME pathways significantly enriched for the HF+EC versus LF diet comparison; and 51 KEGG and 201 REACTOME pathways significantly enriched for the HF34DHPVL versus LF diet comparison. Ultimately, EC supplied in combination with the HF diet of mice significantly affected many hepatic pathways, as it did when supplied to the LF diet. On the other hand, 34DHPVL had almost no significant effects on pathways under HF diet fed conditions but had a large effect under LF diet fed conditions.

The top 10 upregulated and top 10 downregulated KEGG and REACTOME pathways affected by the diets are displayed in Appendix Tables 2-15. The sign in front of the normalised enrichment score (NES) indicates whether the specific pathway was up or downregulated. The top hepatic pathways upregulated for the HF versus LF diets include: amino acid metabolism, fatty acid metabolism, drug metabolism and the PPAR signalling pathway, all of which are strongly linked to the pathogenesis of MAFLD, whilst the top downregulated pathways include a reduction in gene transcriptions associated with cell adhesion molecules, tight junctions and cell cycle progression (Appendix Tables 2 & 9). In contrast, the HF+EC diet compared to the HF diet reversed some of these changes by downregulating amino acid, fatty acid, starch and sucrose metabolic pathways as well as PPAR signalling and transcriptome which are involved in the citrate cycle. This therefore suggests the protective effects that EC confer on hepatic tissues to reduce MAFLD, including lipid storage, and glucose production, which in return have favourable outcomes of mitigating insulin resistance (Appendix Tables 3 & 10). Interestingly, supplementation of EC into the HF diet also upregulated genes involved in immune response and inflammatory pathway activation such as toll like receptor signalling (TLR), Jak-Stat signalling, NOD like receptor signalling, cytokine-cytokine signalling, amongst others, whilst also increasing the expression of the 'ribosome' pathway, which has been shown to have antifibrotic effects as well as supporting cell cycle progression, apoptosis and DNA damage responses (557).

No enriched pathways were detected for the HF+34DHPVL versus HF diet comparison as can be seen by the large FDR *q*-values (Appendix Table 4). The only two KEGG pathways that had an FDR *q*-value < 0.25 are involved in the increased regulation of mismatch repair and base excision repair pathways, which indicates that the addition of 34DHPVL may act to improve and repair damaged

DNA, most likely caused by the HF diet and MAFLD. All other pathways listed were not significantly enriched. This result was also confirmed in the REACTOME pathway analysis of the pairwise comparison (Appendix Table 11).

Like the effects of EC supplemented into the HF diet, EC supplemented into the LF diet and compared to the LF control caused an increase in pathways involved with immune response and inflammation. For pathway downregulation, oxidative phosphorylation was a significantly enriched KEGG pathway (Appendix Table 7). REACTOME pathway analysis also confirms these results, in addition, there was also a significant downregulation in 'CHREBP metabolic gene expression' (Appendix Table 14) which is involved in DNL processes.

Although 34DHPVL did not cause pathway changes under HF diet fed conditions, it was able to significantly increase the expression of many pathways, particularly with regards to inflammation and immune responses, and decreased pathway expression for amino acid metabolism, oxidative phosphorylation, and CHREBP under LF diet fed conditions (Appendix Tables 8 & 15). Therefore, 34DHPVL caused gene expression changes comparable to those caused by EC under LF diet fed conditions.

The pathways enriched for the comparisons of HF+EC versus LF (Tables 7 & 14), and HF+34DHPVL versus LF (Tables 8 & 15), illustrates the general changes for the effects of HF diets on hepatic transcription for: raising amino acid, fatty acid, pyruvate, and lipid metabolism as well as the citric acid cycle, but reduces the expressions for cell cycle and ribosomal genes. Nonetheless, these effects were weaker in HF+EC conditions when compared to HF or HF+34DHPVL conditions, and their expression was downregulated when compared to the HF diet.

5.5.4 qRT-PCR confirms differential expression changes identified via RNA-sequencing

To validate the changes seen from differential gene expression following RNA-seq, qRT-PCR was run on a selection of 28 genes for validation of different pathways for genes: *SOCS5, TNF, ITGAM* (encoding CD11B), *CD86, CD14, BAX, CASP9, PTEN, CHUK, SLC2A2, ENPP2, ALDH7A1, ACADM, ALD3HA2, ACAA1, AGL1, GYS2, GBE1, PDHA1, SUCLG1, PPARG, PPARA, PPARD, FABP2, IGFBP1, STEAP4, AKT1*, and housekeeping genes *EIF2A* and *ACTB*. These represent pathways involved in cytokine signalling, inflammation, P53 signalling, glucose transporters, lipid metabolism, fatty acid metabolism, starch and sucrose metabolism, citric acid cycle, PPAR signalling, insulin resistance,

and MAPK signalling; all reported to be involved in the development of MAFLD and type-2 diabetes. As qRT-PCR is a more sensitive method for determining gene expression values, it was of interest to determine how close the RNA-seq gene expression fold changes were to qRT-PCR fold changes for sequenced only samples in addition to all of the mice samples used in the intervention, in order to determine if the samples selected were reflective of the overall sample size.

Changes in gene expressions were calculated using the delta CT method for the housekeeping gene *EIF2A*, this was validated to be the most stably expressed gene for hepatic tissues from this dietary intervention study (Appendix Table 1). Although *ACTB* was also validated as the 2nd most stably expressed gene, the results were almost identical following delta CT calculations, so only the results optimised relative to *EIF2A* have been shown here. These data were then transformed (natural logarithm) to produce the graphs in Figure 5.6, and statistical analyses were performed by linear regression models in R studio. To summarise statistical significance, upregulated changes were found for HF versus LF pairwise comparison for the following genes: P53 signalling - *PTEN* (p = 0.0007), *CHUK* (p = 0.0024); lipid metabolism - *ENPP2* (p < 0.0001); fatty acid metabolism - *ALDH7A1* (p = 0.0003), *ACADM* (p = 0.0001), *ACAA1* (p = 0.0006); starch and sucrose metabolism - *AGL1* (p = 0.0316), *GYS2* (p = 0.0019), *GBE1* (p = 0.0136); citric acid cycle - *PDHA1* (p = 0.0006), *SUCLG1* (p = 0.0024), and PPAR signalling - *PPARG* (p < 0.0001), and *FABP2* (p = 0.0195).

For HF+EC versus HF comparison, the following genes were significantly downregulated: cytokine signalling - *SOCS5* (p = 0.0459); P53 signalling - *PTEN* (p = 0.0807), *CHUK* (p = 0.030); lipid metabolism - *ENPP2* (p = 0.0207); and citric acid cycle - *PDHA1* (p = 0.0386). None of the genes investigated by qRT-PCR were significantly altered for the HF+34DHPVL versus HF comparison.

For the LF+EC and LF+34DHPVL versus LF comparison, only one gene was significantly downregulated according to the qRT-PCR data, this was for the inflammatory marker *CD86* (p < 0.05).

Graphs were then plotted to visualise the Log_2 fold change for pairwise comparisons from: RNA-Seq differential expression values, qRT-PCR data on only the samples used for RNA-Seq, and finally following qRT-PCR from all the mice liver samples obtained from the intervention. As can be seen in Figure 5.7 and Table 5.13, the general change in regulation for most of the genes was consistent for each of the data points, indicating that the samples used for RNA-Seq were representative of the whole population of mice from the intervention. The few cases where this did not apply are highlighted in red in Table 5.13. For example, with regards to the HF vs LF comparison for *SOCS5*, differential expression from RNA-Seq highlights an increased regulation, whilst qRT-PCR highlighted no altered expression for the samples that were sent off for RNA-Seq or for all the samples from

the intervention. Although there are some highlighted expressions that have opposing regulations, some of the differences are minimal and were not considered different.

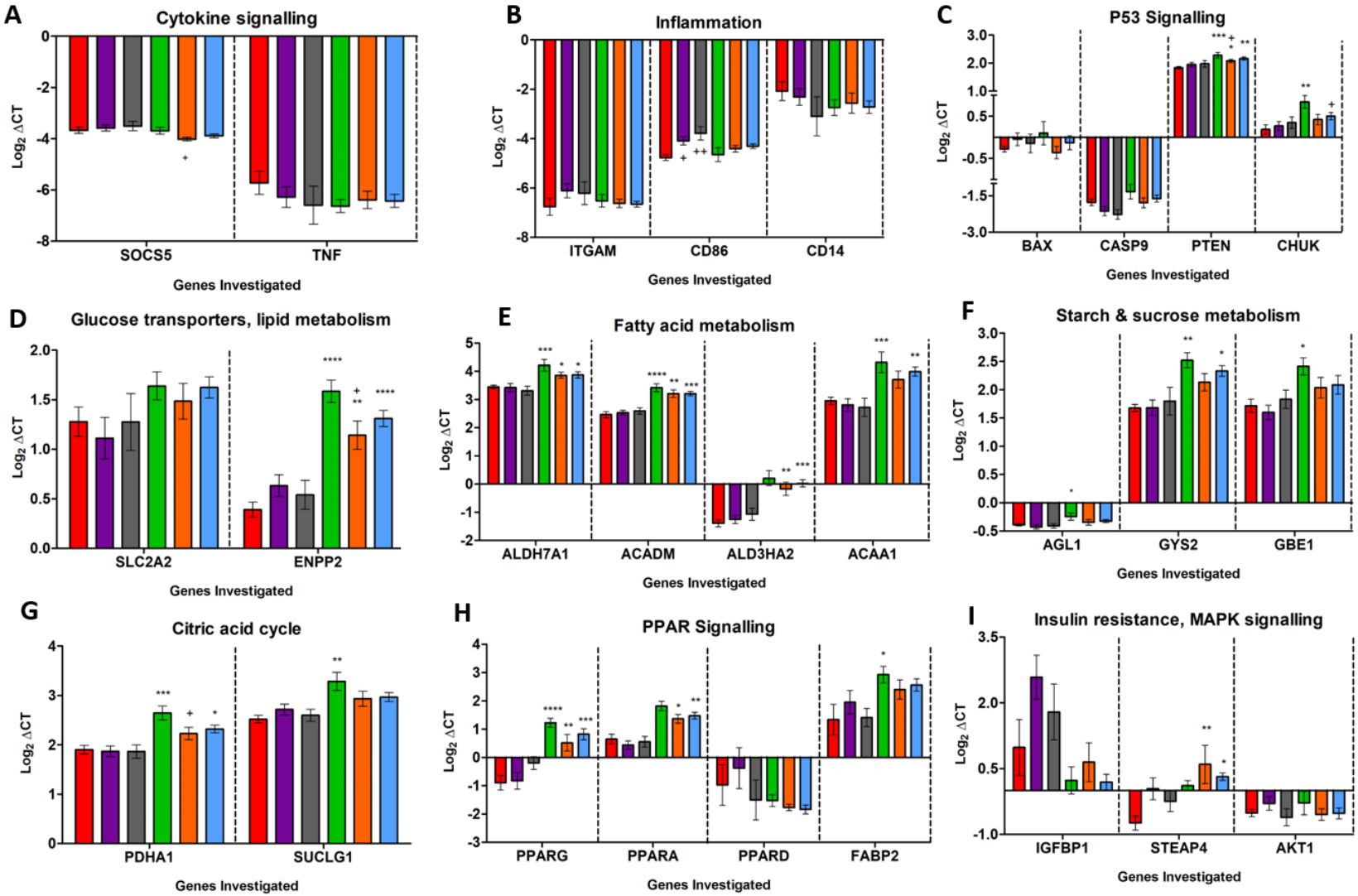
A
Cytokine signalling
Log2 ΔCT
SOCS5
TNF
Genes Investigated
B
Inflammation
ITGAM
CD86
CD14
C
P53 Signalling
BAX
CASP9
PTEN
CHUK
D
Glucose transporters, lipid metabolism
SLC2A2
ENPP2
E
Fatty acid metabolism
ALDH7A1
ACADM
ALD3HA2
ACAA1
F
Starch & sucrose metabolism
AGL1
GYS2
GBE1
G
Citric acid cycle
PDHA1
SUCLG1
H
PPAR Signalling
PPARG
PPARA
PPARD
FABP2
I
Insulin resistance, MAPK signalling
IGFBP1
STEAP4
AKT1
LF
LF+EC
LF+34DHPVL
HF
HF+EC
HF+34DHPVL

Figure 5.6: qRT-PCR delta CT expressions of genes

*Bar graphs for genes amplified via qRT-PCR from the hepatic tissues of the mice from the dietary intervention study. All data is presented as Log_2 transformations for the expressions of genes relative to the housekeeping gene EIF-2α. Error bars represent standard error. A) Genes involved in cytokine signalling; B) Genes involved in inflammation; C) Genes involved in P53 signalling; D) Genes involved with glucose transporters and lipid metabolism; E) Genes involved in fatty acid metabolism; F) Genes involved in starch and sucrose metabolism; G) Genes involved in the citric acid cycle; H) Genes involved in PPAR signalling; I) Genes involved in insulin resistance and MAPK signalling. Significance * $p < 0.05$, ** $p < 0.01$, *** $p < 0.001$, **** $p < 0.0001$ compared to LF diet. $_{+}p < 0.05$, $_{++}p < 0.01$, compared to their respective controls (HF with supplements are compared to HF, LF with supplements are compared to LF).*

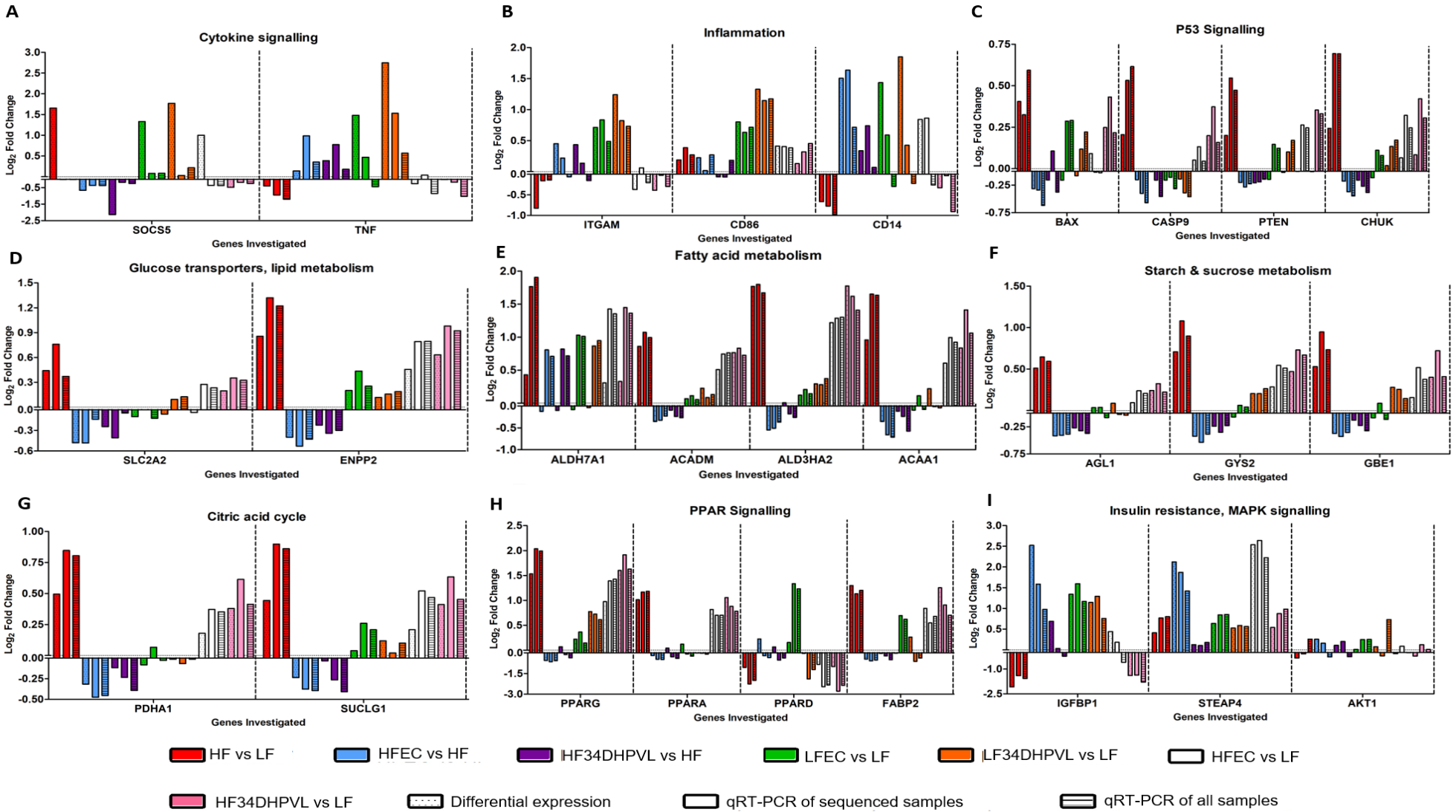
A
Cytokine signalling
Log2 Fold Change
SOCS5
TNF
Genes Investigated
B
Inflammation
ITGAM
CD86
CD14
C
P53 Signalling
BAX
CASP9
PTEN
CHUK
D
Glucose transporters, lipid metabolism
SLC2A2
ENPP2
E
Fatty acid metabolism
ALDH7A1
ACADM
ALD3HA2
ACAA1
F
Starch & sucrose metabolism
AGL1
GYS2
GBE1
G
Citric acid cycle
PDHA1
SUCLG1
H
PPAR Signalling
PPARG
PPARA
PPARD
FABP2
I
Insulin resistance, MAPK signalling
IGFBP1
STEAP4
AKT1
HF vs LF
HFEC vs HF
HF34DHPVL vs HF
LFEC vs LF
LF34DHPVL vs LF
HFEC vs LF
HF34DHPVL vs LF
Differential expression
qRT-PCR of sequenced samples
qRT-PCR of all samples

Figure 5.7: qRT-PCR Log_2 fold changes and differential expressions of genes per treatment comparison

Bar graphs for genes from the hepatic tissues of the mice from the dietary intervention study: from RNA-Seq differential gene expressions (DGE) (bars with dots); amplified via qRT-PCR for the 42 samples sent off for sequencing (bars with no pattern); amplified by qRT-PCR for the mice livers harvested (bars with horizontal lines). All data is presented as Log_2 fold-changes for gene expressions (DGE data), relative to the housekeeping gene EIF-2α (qRT-PCR data), per pairwise comparison. A) Genes involved in cytokine signalling; B) Genes involved in inflammation; C) Genes involved in P53 signalling; D) Genes involved with glucose transporters and lipid metabolism; E) Genes involved in fatty acid metabolism; F) Genes involved in starch and sucrose metabolism; G) Genes involved in the citric acid cycle; H) Genes involved in PPAR signalling; I) Genes involved in insulin resistance and MAPK signalling.

5.5.5 Hepatic genes and pathway expressions increased in response to HF diet fed mice for MAFLD

Following differential gene expression and GSEA results, this section will focus on the genes and pathways that have been induced and downregulated in response to a HF fed diet when compared to the LF fed conditions. It will then explore how EC mitigated these changes whilst 34DHPVL caused no significant impact.

Some of the most significantly enriched KEGG pathways (FDR *q*-value ≤ 0.25) upregulated in this current study and shown to be linked to MAFLD are: ABC transporters, amino acid metabolism (butanoate, glycine, serine, threonine, valine, tryptophan, leucine and isoleucine), citrate cycle, ether/glycerolipid/pyruvate/starch and sucrose metabolism, fatty acid metabolism, glycolysis/gluconeogenesis, metabolism of xenobiotics by cytochrome P450, oxidative phosphorylation, peroxisome, PPAR signalling, and steroid biosynthesis. The top downregulated pathways includes ribosome and spliceosome, with subtle decreases for cell-cycle, cytokine receptors, MAPK signalling, NOD like receptor signalling, phosphatidylinositol signalling and T-cell receptor signalling. Therefore, the development of MAFLD is strongly associated with increased metabolism including oxidative phosphorylation, and PPAR signalling, and decreased ribosomal activity. A comparison of these effects to a published study is provided later (section 5.6.1).

In contrast, the addition of EC into the HF diet and compared to the HF treatment group reversed expression in all of the aforementioned pathways except for PPAR signalling, cell cycle, and steroid biosynthesis. This suggests that EC had protective effects against insulin resistance and MAFLD by modifying these pathways/functions. Moreover, although in the majority of cases the effects were not significant, the addition of 34DHPVL into the HF diet and compared to the HF treatment group also reversed nearly all of the aforementioned pathways except for spliceosome, cell cycle, ABC transporters, pyruvate metabolism, and metabolism of xenobiotics by cytochrome P450. However, the effects were not as strong as those induced by EC which was seen by the higher FDR *q*-values, but it does provide evidence that 34DHPVL provides a level of protection against MAFLD.

5.5.6 (–)-Epicatechin and 3',4'-dihydroxyphenyl-γ-valerolactone supplementation caused improvements in insulin sensitivity in both the high-fat and low-fat diets

The overarching aim of the investigation was to determine whether 34DHPVL could mitigate against insulin resistance effects, as a metabolite of EC, and to determine which genes and pathways

showed altered expression. In chapter 3, a GTT experiment in mice revealed whether they were insulin resistant or insulin sensitive, and the HF+EC fed mice exhibited slightly lower blood insulin levels than the HF fed mice but responded more quickly in lowering their glucose levels. Contrary to expectations, HF+34DHPVL fed mice exhibited substantially increased insulin levels but lower glucose concentrations throughout the GTT. Gene expression analysis has provided insights to help explain these results.

From investigating genes involved in insulin signalling, there was a clear reduction in gene expression in the HF versus LF comparison, and included *PRKAA1, PRKAB1, PRKAB2, PRKAG1, LEPR, CREB1, MMP7, H19, IRS2, PIK3CB, PIK3CD, PIK3CG, HMGA1, SHC1, SHC2, AKT1* and *IGFBP1*. Meanwhile, genes that are involved in causing a reduction in insulin signalling included *FAS, FOXO1, FOXO3, FOXO4, PD1, PDK2, PDK3, PDK4, MAPK9* (JNK2), and *SOCS5*, (Table 5.15). The insulin signalling KEGG pathway was also negatively enriched (NES = -0.78, FDR *q*-value = 1.00).

In contrast, EC in the HF diet altered the expression levels for most of these genes to promote insulin sensitivity, by increasing the expression of genes linked to insulin signalling for *PRKAB1, PRKAG1, LEPR, CREB1, STEAP4, MMP7, IRS2, PIK3CB, PIK3CD, PIK3CG, INSR, SHC1, SHC2, GRB2, IGFBP1* and *AKT1*. Whilst there was a decrease in gene expression linked to promote insulin resistance for *PDK1, PDK2, PDK3, PDK4, MAPK8* (JNK1), *MAPK9* (JNK2) and *SOCS5*. The insulin signalling KEGG pathway was also positively enriched (NES = 1.08, FDR *q*-value = 0.66).

The addition of 34DHPVL into the HF diet induced an increase in a few insulin signalling genes, but with weaker fold-change effects in comparison to EC (not significant) for *PRKAB1, PRKAB2, LEPR, STEAP4, H19, PIK3CD, PIK3CG, HMGA1, SHC1, SHC2, GRB2,* and *AKT1*. In addition, there was a reduction in the expression for genes that promote insulin resistance for *PDK1, PDK3, MAPK8* (JNK1)*, MAPK9* (JNK2) and *SOCS5*. Despite this, the combination of gene changes in favour of insulin resistance was associated with the insulin signalling KEGG pathway being negatively regulated (NES = -0.90, FDR *q*-value = 1.00), although this was not significant. To further explain the lower circulatory glucose concentrations throughout the GTT, there was a large fold change for the increase in gene SLC2A1 that encodes protein GLUT-1 and is primarily involved in the uptake of glucose into hepatocytes (558). Furthermore, there was a large decrease in fold change for *SLC2A2*, coding for protein GLUT-2 and has been reported to primarily regulate glucose efflux from hepatocytes (558).

To investigate whether the dietary interventions impacted against insulin degradation for decreased insulin clearance from the blood, the gene *CEACAM1* was examined. Although the gene expression of *CEACAM1* was not considered significant for any of the dietary comparisons, there

was a decreased fold change in *CEACAM1* for these comparisons: HF vs LF (Log_2FC = -0.01), HF+34DHPVL vs HF (Log_2FC = -0.04), LF+EC vs LF (Log_2FC = -0.09) , LF+34DHPVL vs LF(Log_2FC = -0.23), and HF+34DHPVL vs LF (Log_2FC = -0.05). The reduction in expression for these comparisons is consistent with the decreased hepatic insulin clearance in MAFLD and insulin resistance, it also highlights a possible reason why 34DHPVL decreased insulin clearance in both LF and HF diets where the effects were seen to be greater than the HF vs LF comparison, but the changes were stronger when 34DHPVL was supplemented into the LF diet.

When having assessed gene changes linked to insulin signalling for the LF+EC and LF+34DHPVL versus LF treatments, genes for insulin signalling expressed an increase in Log_2FC for *PRKAA1, PRKAA2, CREB1, FOXO3, STEAP4, MMP7, H19, IRS2, PIK3CA, PIK3CD, PIK3CG, HMGA1, SHC2, GRB2, IGFBP1,* and *AKT1*, and in addition to a decreased expression for genes linked to insulin resistance (*PDK1, PDK2, PDK3, PDK4*, and *MAPK9* (JNK2)). The fold changes were always larger in EC fed mice compared to 34DHPVL fed mice.

Further gene changes and pathways were also assessed that are directly or indirectly linked to the onset/prevention of insulin resistance. These included genes and pathways involved with oxidative phosphorylation, gluconeogenesis (mentioned in section 5.5.8), amino acid metabolism, P53 signalling and the starch and sucrose metabolic pathway. Oxidative phosphorylation was increased for the HF versus LF treatment (NES = 1.58, FDR *q*-value = 0.058) and was linked to an increase in the citric acid cycle (NES = 1.79, FDR *q*-value = 0.09) which are consistent with the onset of insulin resistance. In contrast, EC in the HF diet (oxidative phosphorylation: NES = -1.15, FDR *q*-value = 0.442; citric acid cycle: NES = -1.80, FDR *q*-value = 0.023) and in the LF diet (oxidative phosphorylation: NES = -1.71, FDR *q*-value = 0.150; citric acid cycle: NES = -0.91, FDR *q*-value = 0.851) reversed pathway expressions for oxidative phosphorylation and the citric acid cycle which contributes to improving insulin sensitivity. Similarly, 34DHPVL also lowered the expression of these pathways, but not significantly (oxidative phosphorylation: NES = -0.69, FDR *q*-value = 1.00; citric acid cycle: NES = -0.82, FDR *q*-value =1.00).

The 'starch and sucrose metabolism' KEGG pathway is closely linked to gluconeogenesis because it metabolises carbohydrates for glucose production and it was shown to be increased by the HF diet when compared to the LF diet, as represented by gene expression increases in *AGL, AMY1, GYS2, PGM1*, and *GBE1*, (Table 5.15). All of these HF diet-induced gene and pathway changes were reversed when EC was supplemented into the HF diet (NES = -1.86, FDR *q*-value = 0.014) and LF diet (NES = -0.95, FDR *q*-value = 0.875), whilst 34DHPVL only reversed these in the HF diet (NES = -1.11, FDR *q*-value = 0.792).

In addition to alterations in the citric acid cycle and oxidative phosphorylation, amino acid metabolism is also impaired in the presence of MAFLD and strongly correlates to insulin resistance (559). This has been demonstrated in this study for the HF versus LF treatment comparison where the following increases in enrichments for the following pathways were observed: 'valine, leucine and isoleucine degradation' (NES = 2.56, FDR *q*-value = 0.000), 'lysine degradation' (NES = 1.77, FDR *q*-value = 0.012), 'arginine and proline metabolism' (NES = 1.55, FDR *q*-value = 0.068), 'proteasome' (NES = 1.88, FDR *q*-value = 0.004), 'selenoamino acid metabolism' (NES = 0.78, FDR *q*-value = 0.961), 'phenylalanine metabolism' (NES = 1.15, FDR *q*-value = 0.397), 'tryptophan metabolism' (NES = 2.09, FDR *q*-value = 0.000), 'tyrosine metabolism' (NES = 0.91, FDR *q*-value = 0.785), 'alanine, aspartate and glutamate metabolism' (NES = 1.43, FDR *q*-value = 0.127), all of which are substrates for the citric acid cycle for energy production and linked to increases in oxidative phosphorylation.

To support EC's role in mitigating insulin resistance effects and the development of MAFLD, amino acid KEGG pathways were reversed for: 'valine, leucine and isoleucine degradation' (NES = -2.53, FDR *q*-value = 0.000), 'lysine degradation' (NES = -1.36, FDR *q*-value = 0.201), 'arginine and proline metabolism' (NES = -0.75, FDR *q*-value = 1.000), 'phenylalanine metabolism' (NES = -0.90, FDR *q*-value = 0.857), 'tryptophan metabolism' (NES = -1.79, FDR *q*-value = 0.022), and 'tyrosine metabolism' (NES = -0.97, FDR *q*-value = 0.738), in HF diet fed conditions. Additional evidence to support an effect of 34DHPVL in protecting against insulin resistance in HF fed conditions, was downregulation of the following KEGG pathways: 'valine, leucine and isoleucine degradation' (NES = -1.69, FDR *q*-value = 0.422), 'lysine degradation' (NES = -0.94, FDR *q*-value = 0.965), 'arginine and proline metabolism' (NES = -0.73, FDR *q*-value = 1.000), 'tryptophan metabolism' (NES = -0.74, FDR *q*-value = 1.000), 'proteasome; (NES = -1.10, FDR *q*-value = 0.791), and 'alanine, aspartate and glutamate metabolism' (NES = -1.04, FDR *q*-value = 0.869). Both EC and 34DHPVL in LF conditions caused a reduction in a couple of the amino acid KEGG pathways listed, whilst the others had no change. So, although there were not any significantly enriched pathways found for the HF+34DHPVL versus HF treatment, the collective observations of gene and pathways changes could possibly increase the sensitivity of hepatocytes to insulin.

The P53 signalling pathway has been shown to negatively regulate the influx of glucose into tissues via GLUT transporters (560). Here it was shown for the HF versus LF comparison that there was an increase in P53 signalling (NES = 0.83, FDR *q*-value = 0.944), but this was decreased by the presence of EC in combination with the HF treatment (NES = -1.05, FDR *q*-value = 0.59) and compared to the HF treatment. Despite this, in the LF interventions, the addition of EC (NES = 1.00, FDR *q*-value = 0.669) or 34DHPVL (NES = 1.19, FDR *q*-value = 0.378) caused an increase in the pathway expression

for P53 signalling. These changes also suggest a lower uptake of glucose into hepatic tissue from the circulation.

5.5.7 Hepatic genes and pathway expressions enriched with regards to fibrosis

Chapter 4 reported evidence that there were signs of fibrosis in several mice on LF fed diets, and thus gene expression changes were analysed in relation to fibrosis and the following was discovered.

Genes involved in the development of hepatic fibrosis were overall more highly expressed in LF diet fed mice compared to HF diet fed mice, and these were particularly linked to the TGF-β and PDGF pathways that ultimately lead to an increase in the rate of hepatic fibrosis (Table 5.15). As an overview of the results, for the HF versus LF comparison there was a negative Log_2FC for differential gene expression for the vast majority of genes related to fibrosis (*EGFR, VEGFA, TGFB1, TGFB2, BMP2, BMP4, BMP5, BMP6, SMAD1, SMAD4, ACTA2, COL1A1, HGF, NFKB1, NFKB2, PDGFA, PDGFB, PDGFC, PDGFD, PDGFRA, PDGFRB, MMP2, SEL1L3,* and *LOXL1)*, where there was a decrease in the KEGG 'TGF-β signalling pathway' (NES = -1.37, FDR *q*-value = 0.66). Meanwhile, the genes that exert anti-fibrotic effects and were upregulated included: *PPARA, SMAD6, CEBPA, HORMAD2*, and *APOF*. The adjusted *p*-values have been provided in Table 5.15 to highlight the level of significance of these gene changes. These data largely support the notion that the LF (also high in carbohydrate) diet induces hepatic fibrosis more strongly than the HF diet.

The inclusion of EC into the HF diet and compared to the HF control caused changes in expression for a reduction in genes involved in the development of hepatic fibrosis (albeit insignificantly), including *PRKCA, CDC42, TGFB1, TGFB2, SMAD2, SMAD5, PDGFD*, and *COL1A1*, and there was an increase in anti-fibrotic genes (*C1QTNF2, IFNGR2, HORMAD2*, and *APOF*). However, there was also an increase in pro-fibrotic genes (*EGFR, VEGFA, BMP4, SMAD1, HGF, NFKB1, NFKB2, PDGFC, PDGFRA, PDGFRB,* and *SEL1L3*), and a decrease in anti-fibrotic genes (*PPARA* and *SMAD6*). Nonetheless, the TGF-β signalling pathway was downregulated when compared to the HF control (NES = -0.88, FDR *q*-value = 0.889), but this was not significant. Therefore, the overall effects of EC on hepatic fibrosis within the HF diet background suggests that it could be protective against the development of hepatic fibrosis.

In contrast, although there were not significant changes in fibrosis related genes for the HF+34DHPVL versus HF comparison, there was a large increase in their Log_2FC for *EGFR, BMP4,*

ACTA2, COL1A1, HGF, NFKB2, PDGFA, PDGFB, PDGFC, PDGFRA, PDGFRB, MMP2, SEL1L3, and *LOXL1*. However, the TGF-β signalling pathway was downregulated (NES = -1.43, FDR *q*-value = 0.451). Despite this, the increase in the above changes in the expression of genes would explain the marginally increased mean values for Sirius red staining presented in chapter 4, which stains for fibrotic tissues.

The addition of EC into the LF diet and compared to the LF control did not induce any significant gene changes. But, there were several Log_2FC changes similar to those seen for EC supplemented into the HF diet in mice and caused an overall reduction in the expression of the TGF-β signalling pathway (NES = -1.23, FDR *q*-value = 0.72). Moreover, the addition of 34DHPVL into the LF diet and compared to the LF control induced a reduction in Log_2FC for *EGFR, VEGFA, BMP5, SMAD1, ACTA2, COL1A1* and *LOX1*, implying that it could provide a protective effect from the HC diet on fibrosis, despite the fact there were increases in PDGF and TGF signalling genes (TGF-β signalling pathway, NES = 1.03, FDR *q*-value = 0.59).

5.5.8 High-fat diet fed mice experienced more gluconeogenesis and reduced de novo lipogenesis compared to low-fat high carbohydrate fed mice

Gene expression and pathway analysis was assessed for changes in DNL and gluconeogenesis. This is because there is an existing body of evidence supporting the notion that LF (high carbohydrate (HC)) diets can induce DNL more strongly than HF diets, while HF diets will induce gluconeogenesis genes more strongly. Thus, genes were assessed from the mouse livers to determine if such findings have been reciprocated in this study.

The extent to which LF HC diets can extensively affect DNL is discussed later in this chapter. Here, the gene changes confirming the effects of HC on DNL are listed in Table 5.15. For the HF versus LF diets, there was a downregulation in the following genes: *SREBF* (SREBP-1c), *MLXIPL* (ChREBP), *G6PC, INSIG1, ACACA, AACS, AGPAT1, GPAM* (GPAT1), *SCAP, PRKAA1, PRKAB1, PRKAB2*, and *PRKAG1*. The combination of these gene changes suggests a reduction in DNL processes which is linked to the pathway change seen for an increase in the enrichment for 'fatty acid metabolism' KEGG pathway (NES = 2.50, FDR *q*-value = 0.000), and its associated genes (*ACOX1, ACADM, ACAA1, ECI2, ALDH3A2,* and *ALDH7A1*; significantly upregulated, $p < 0.001$) (to list but a few of the genes). A consequence of increased fatty acid metabolism is an increase in glucose production via gluconeogenesis, as will be outlined later.

EC supplemented into the HF diet reduced the expression of genes involved in DNL more than the HF diet alone (although they were not significantly altered), and there was a reduction in the expression of *SREBF, G6PC, LIPE, INSIG1, AACS, GPAM, PRKAA1, PRKAA2, PRKAB2*, and *PRKAG2*. Additionally, there were reductions in the expression of genes for fatty acid metabolism (*ACOX1, ACADM, ACCA1, ECI2, ALDH3A2*, and *ALDH7A1*) where the KEGG pathway was also significantly downregulated (NES = -2.27, FDR *q*-value = 0.000). In turn, this highlights that EC induced a protective effect on hepatocytes by reducing the production of lipids, and ultimately mitigating against the severity of hepatic steatosis effects induced by HF diets.

HF+34DHPVL fed mice compared to HF fed mice exhibited an overall increase (but not statistically significant) in the expression of DNL genes including *MLXIPL, INSIG1, ACACA, AACS, AGPAT1, GPAM, PRKAB1, PRKAB2*, and *PRKAG1*. Interestingly, there was a decrease in the expression of fatty acid metabolism genes (*ACOX1, ACADM, ACAA1, ECI2*, and *ALDH7A1*), and although the KEGG pathway was not significantly enriched (NES = -1.33, FDR *q*-value = 0.523), it was still one of the top 20 downregulated pathways.

With regards to gluconeogenesis there were several genes that were shown to be changing in the pairwise comparisons (Table 5.15). In the HF versus LF comparison, the KEGG 'gluconeogenesis-glycolysis' pathway was significantly enriched (NES = 1.55, FDR *q*-value = 0.070), and the gluconeogenesis genes that were upregulated included (but were not limited to) *PCK1* (PEPCK), *FOXO1, FOXO3, FOXO4, ALDH3A2, ALDH7A1, PDHA1*, and *CEBPA*. Meanwhile *PPARGC1A*, coding for protein PGC-1α (peroxisome proliferator-activated receptor γ coactivator 1α) was downregulated.

In contrast, EC in the HF diet reversed the gluconeogenesis process, showing a significant reduction in its KEGG pathway (NES = -1.49, FDR *q*-value = 0.118), and also caused a reversal in gene expressions for: *PPARGC1A, CREB1, FOXO1, FOXO3, FOXO4, ALDH3A2, ALDH7A1, PDHA1* and *CEBPA*.

Interestingly, HF+34DHPVL fed mice in comparison to HF fed mice showed a downregulation in gluconeogenic genes (*PCK1, PPARGC1A, G6PC, CREB1, FOXO1, FOXO3, FOXO4, ALDH7A1, PDHA1*, and *CEBPA*), whereas the KEGG pathway was upregulated for glycolysis linked genes (NES = 1.47, FDR *q*-value = 0.361), but not for gluconeogenic genes, although none of these changes reached statistical significance.

In contrast to the HF diet, EC supplemented into the LF diet and compared to the LF control induced a slight increase in the expression of gluconeogenic genes except for *PPARGC1A, FOXO4, ALDH7A1, PDHA1*, and *CEBPA*, although all listed gene changes did not reach significance (p.adjust = 1.00) and

the gluconeogenesis-glycolysis KEGG pathway was not significantly enriched (NES = 0.84, FDR *q*-value = 0.854). Similar observations applied to mice provided diets of 34DHPVL in combination with the LF diet, where genes except for *PPARGC1A, G6PC, FOXO1, ALDH7A1, PDHA1* and *CEPBA* were increased (not significant) and the gluconeogenesis-glycolysis KEGG pathway was not significantly enriched (NES = 0.91, FDR *q*-value = 0.723).

Table 5.13: Log_2FC values for changes in gene expression following qRT-PCR or RNA-sequencing analysis

For each pairwise comparison shown are gene expressions from the liver tissues of the mice from the dietary intervention study: from RNA-Seq differential gene expressions (DGE); amplified via qRT-PCR for the 42 samples sent off for sequencing; amplified by qRT-PCR for all the mice livers harvested. Only genes targeted by qRT-PCR have been presented here alongside the main biological pathways they are involved with. Red text highlights genes that have non-consistent regulation as detected by qRT-PCR or RNA-Seq; for example; the ITGAM gene for comparison HF+34DHPVL vs HF shows positive regulation by RNA-Seq and qRT-PCR of only the samples sent for sequencing, whilst there was a negative regulation when performing qRT-PCR on all of the mice livers harvested.

Pairwise comparison		HF vs LF			HF+EC vs HF			HF+34DHPVL vs HF			LF+EC vs LF			LF+34DHPVL vs LF			HF+EC vs LF			HF+34DHPVL vs LF		
Pathway involved	Genes	RNA-Seq	qRT-PCR RNA-Seq	qRT-PCR all samples	RNA-Seq	qRT-PCR RNA-Seq	qRT-PCR all samples	RNA-Seq	qRT-PCR RNA-Seq	qRT-PCR all samples	RNA-Seq	qRT-PCR RNA-Seq	qRT-PCR all samples	RNA-Seq	qRT-PCR RNA-Seq	qRT-PCR all samples	RNA-Seq	qRT-PCR RNA-Seq	qRT-PCR all samples	RNA-Seq	qRT-PCR RNA-Seq	qRT-PCR all samples
Cytokine signalling	***SOCS5***	1.66	0.00	0.00	-0.66	-0.36	-0.37	-2.13	-0.17	-0.24	1.33	0.08	0.08	1.77	0.03	0.22	1.00	-0.37	-0.37	-0.47	-0.18	-0.24
	TNF	-0.40	-0.95	-1.21	0.14	0.99	0.35	0.39	0.77	0.18	1.48	0.47	-0.44	2.75	1.53	0.57	-0.25	0.04	-0.85	-0.01	-0.17	-1.03
Inflammation	***ITGAM***	-0.82	-0.16	-0.14	0.45	0.22	-0.06	0.43	0.14	-0.16	0.71	0.83	0.49	1.24	0.82	0.73	-0.37	0.06	-0.20	-0.39	-0.02	-0.30
	CD86	0.19	0.39	0.27	0.22	0.02	0.27	-0.06	-0.07	0.18	0.80	0.63	0.71	1.33	1.14	1.17	0.41	0.40	0.38	0.13	0.32	0.45
	CD14	-0.66	-0.77	-0.98	1.50	1.64	0.72	0.34	0.74	0.07	1.43	0.59	-0.30	1.85	0.42	-0.22	0.84	0.86	-0.26	-0.33	-0.03	-0.91
P53 signalling	***BAX***	0.41	0.33	0.59	-0.31	-0.34	-0.62	-0.16	0.11	-0.38	-0.16	0.29	0.29	-0.08	0.12	0.22	0.09	-0.01	-0.02	0.25	0.43	0.22
	CASP9	0.20	0.53	0.62	-0.15	-0.40	-0.57	-0.01	-0.16	-0.46	-0.16	-0.11	-0.32	-0.14	-0.39	-0.46	0.05	0.13	0.05	0.20	0.37	0.16
	PTEN	0.20	0.55	0.47	-0.20	-0.28	-0.23	-0.21	-0.19	-0.14	-0.15	0.15	0.12	-0.02	0.10	0.17	0.00	0.26	0.25	-0.01	0.35	0.33
	CHUK	0.24	0.69	0.69	-0.18	-0.37	-0.45	-0.16	-0.27	-0.39	-0.12	0.11	0.08	0.02	0.13	0.17	0.07	0.32	0.25	0.08	0.42	0.31
Glucose transporter	***SLC2A2***	0.44	0.76	0.37	-0.48	-0.48	-0.14	-0.25	-0.41	-0.05	-0.10	0.00	-0.12	-0.06	0.09	0.13	-0.04	0.28	0.23	0.20	0.35	0.32
Lipid metabolism	***ENPP2***	0.86	1.32	1.22	-0.40	-0.53	-0.43	-0.22	-0.34	-0.30	0.20	0.43	0.25	0.12	0.16	0.19	0.46	0.79	0.79	0.63	0.98	0.92
Fatty acid metabolism	***ALDH7A1***	0.43	1.77	1.91	-0.12	0.81	0.71	-0.10	0.82	0.72	-0.08	1.03	1.01	-0.04	0.87	0.95	0.31	1.43	1.35	0.33	1.45	1.36
	ACADM	0.86	1.07	0.99	-0.35	-0.33	-0.23	-0.10	-0.24	-0.27	0.07	0.11	0.06	0.23	0.09	0.13	0.51	0.75	0.76	0.77	0.83	0.73
	ALDH3A2	1.77	1.80	1.67	-0.55	-0.51	-0.37	0.01	-0.18	-0.26	0.12	0.21	0.14	0.29	0.28	0.37	1.22	1.29	1.30	1.78	1.62	1.41
	ACAA1	0.96	1.65	1.64	-0.35	-0.66	-0.71	-0.12	-0.24	-0.57	-0.10	0.11	-0.08	0.22	-0.02	-0.04	0.61	0.99	0.92	0.84	1.41	1.06

Table 5.13: Gene expression Log_2FC values for differential gene expression or qRT-PCR (continued)

Pairwise comparison		HF vs LF			HF+EC vs HF			HF+34DHPVL vs HF			LF+EC vs LF			LF+34DHPVL vs LF			HF+EC vs LF			HF+34DHPVL vs LF		
Pathway involved	Genes	RNA-Seq	qRT-PCR RNA-Seq	qRT-PCR all samples	RNA-Seq	qRT-PCR RNA-Seq	qRT-PCR all samples	RNA-Seq	qRT-PCR RNA-Seq	qRT-PCR all samples	RNA-Seq	qRT-PCR RNA-Seq	qRT-PCR all samples	RNA-Seq	qRT-PCR RNA-Seq	qRT-PCR all samples	RNA-Seq	qRT-PCR RNA-Seq	qRT-PCR all samples	RNA-Seq	qRT-PCR RNA-Seq	qRT-PCR all samples
Starch & sucrose metabolism	***AGL1***	0.51	0.65	0.59	-0.42	-0.41	-0.39	-0.27	-0.32	-0.37	0.04	0.04	-0.08	0.09	-0.02	-0.04	0.09	0.24	0.21	0.24	0.32	0.22
	GYS2	0.71	1.08	0.90	-0.42	-0.54	-0.39	-0.24	-0.35	-0.23	-0.07	0.06	0.04	0.21	0.20	0.26	0.29	0.54	0.51	0.47	0.73	0.67
	GBE1	0.53	0.95	0.73	-0.37	-0.43	-0.36	-0.13	-0.23	-0.32	-0.09	0.09	-0.11	0.28	0.26	0.14	0.16	0.52	0.38	0.40	0.72	0.41
Citric acid cycle	***PDHA1***	0.49	0.85	0.80	-0.32	-0.48	-0.45	-0.12	-0.23	-0.39	-0.08	0.07	-0.03	-0.01	-0.07	-0.01	0.18	0.37	0.35	0.38	0.61	0.41
	SUCLG1	0.44	0.90	0.86	-0.24	-0.38	-0.39	-0.03	-0.26	-0.41	0.04	0.26	0.21	0.12	0.02	0.10	0.21	0.52	0.47	0.41	0.63	0.45
PPAR signalling	***PPARG***	1.53	2.04	1.99	-0.56	-0.65	-0.57	0.07	-0.12	-0.36	0.22	0.36	0.15	0.78	0.73	0.62	0.97	1.39	1.43	1.60	1.92	1.63
	PPARA	1.01	1.17	1.18	-0.20	-0.47	-0.48	0.04	-0.29	-0.40	0.12	-0.08	-0.24	-0.02	-0.03	-0.09	0.82	0.70	0.70	1.05	0.88	0.78
	PPARD	-1.06	-2.26	-2.00	0.23	-0.20	-0.34	0.07	-0.53	-0.37	0.16	1.34	1.23	-0.04	-1.89	-1.21	-0.83	-2.46	-2.34	-0.99	-2.78	-2.36
	FABP2	1.30	1.13	1.20	-0.46	-0.58	-0.52	-0.04	-0.23	-0.50	-0.03	0.69	0.62	0.26	-0.62	-0.37	0.84	0.55	0.68	1.25	0.91	0.70
Insulin resistance	***IGFBP1***	-2.08	-1.40	-1.57	2.52	1.59	0.98	0.69	0.03	-0.22	1.34	1.60	1.17	1.14	1.29	0.76	0.44	0.18	-0.59	-1.39	-1.37	-1.79
	STEAP4	0.41	0.77	0.80	2.12	1.87	1.42	0.13	0.11	0.18	0.64	0.84	0.85	0.53	0.59	0.57	2.54	2.64	2.22	0.54	0.88	0.98
MAPK signalling	***AKT1***	-0.32	-0.08	0.26	0.26	0.16	-0.26	0.11	0.20	-0.25	0.01	0.25	0.25	0.08	-0.20	0.73	-0.07	0.09	0.00	-0.21	0.13	0.01

Table 5.14: Gene set enrichment analysis KEGG pathway changes for data obtained by me (Helleur) and compared to Teufel et al (561)

The KEGG pathways listed are those seen to be enriched in both the current study and in Teufel's study. Whilst the current study shows the GSEA results for the livers of high-fat diet (HFD) versus low-fat diet (LFD) fed mice treatments, Teufel's study is for GSEA results from the livers of: healthy obese humans, human livers exhibiting MAFLD, human livers exhibiting NASH, mice livers fed HFD for 12-weeks/18-weeks/30 weeks, and all compared to 'normal' control subjects. This table highlights the strong similarities seen from the current study and a published study with regards to pathway changes on HF diets. KEGG pathways highlighted in: red – reflects pathways that are not expressed in the same direction for my data in the current study versus any of Teufel's data; green – reflects pathways that are expressed in the same direction for data in the current study and for at least one sample of Teufel's human data and one sample of their mice data; blue – pathways that are expressed in the same direction for data in the current study and at least one of Teufel's mice data. FDR q-values higlighted in red corresponds to those pathways that are seen to be significantly enriched, where q < 0.25 was set as the threshold

GSEA Treatments	Helleur's data		Teufel *et al's* data											
	HFD vs LFD mice		Healthy obese humans		MAFLD humans		NASH humans		12-week HFD mice		18-week HFD mice		30-week HFD mice	
KEGG Pathway	Altered expression	FDR *q*-value neg	Altered expression	FDR *q*-value	Altered expression	FDR *q*-value	Altered expression	FDR *q*-value	Altered expression	FDR *q*-value	Altered expression	FDR *q*-value	Altered expression	FDR *q*-value
ABC TRANSPORTERS	up	0.058	up	0.606	up	0.034	up	0.355	up	0.863	up	0.012	down	0.854
ALLOGRAFT REJECTION	down	0.993	up	0.891	up	0.211	up	0.022	down	0.774	up	0.460	up	0.547
ANTIGEN PROCESSING AND PRESENTATION	down	1.000	up	1.000	up	0.060	up	0.025	down	0.133	up	0.368	up	0.087
ARGININE AND PROLINE METABOLISM	up	0.068	down	0.659	down	0.260	down	0.040	down	0.098	down	0.843	down	0.965
ARRHYTHMOGENIC RIGHT VENTRICULAR CARDIOMYOPATHY (ARVC)	down	0.647	up	0.211	up	0.061	up	0.024	down	0.961	down	0.960	down	0.933
ASTHMA	down	0.979	down	0.839	up	0.121	up	0.046	down	0.416	up	0.101	up	0.178
AUTOIMMUNE THYROID DISEASE	down	1.000	up	0.326	up	0.050	up	0.008	down	0.821	up	0.354	up	0.501
AXON GUIDANCE	down	0.808	up	0.118	up	0.047	up	0.053	up	0.818	down	0.960	down	0.951
B CELL RECEPTOR SIGNALING PATHWAY	up	1.000	up	0.057	up	0.004	up	0.002	up	0.940	up	0.992	down	0.974
BLADDER CANCER	down	0.429	down	0.688	up	0.171	up	0.001	up	0.831	down	0.908	down	0.879
BUTANOATE METABOLISM	up	0.000	down	0.885	up	0.914	down	1.000	down	0.126	up	0.003	up	0.109
CELL ADHESION MOLECULES (CAMS)	down	0.287	up	0.205	up	0.017	up	0.001	down	0.316	up	0.587	up	0.238

Table 5.14: Gene set enrichment analysis KEGG pathway changes for data obtained by me (Helleur) and compared to Teufel et al (561) (continued)

GSEA Treatments	Helleur's data		Teufel *et al's* data											
	HFD vs LFD mice		Healthy obese humans		MAFLD humans		NASH humans		12-week HFD mice		18-week HFD mice		30-week HFD mice	
KEGG Pathway	Altered expression neg	FDR *q*-value	Altered expression	FDR *q*-value	Altered expression	FDR *q*-value	Altered expression	FDR *q*-value	Altered expression	FDR *q*-value	Altered expression	FDR *q*-value	Altered expression	FDR *q*-value
CELL CYCLE	down	0.590	down	0.122	up	0.191	up	0.000	down	0.914	down	0.680	up	0.914
CHEMOKINE SIGNALING PATHWAY	down	0.971	up	0.569	up	0.115	up	0.004	up	0.829	up	0.604	down	0.857
CHRONIC MYELOID LEUKEMIA	down	0.848	up	0.827	up	0.345	up	0.028	up	0.732	down	0.965	down	0.905
CITRATE CYCLE (TCA CYCLE)	up	0.009	down	0.905	down	1.000	down	1.000	down	0.000	up	0.583	up	0.124
COLORECTAL CANCER	down	0.768	up	0.608	up	0.116	up	0.017	up	0.891	down	0.971	up	0.792
COMPLEMENT AND COAGULATION Cascades	up	0.606	up	0.172	up	0.018	up	0.175	down	0.010	down	0.004	up	0.281
CYTOKINE-CYTOKINE RECEPTOR INTERACTION	down	0.792	down	0.387	up	0.099	up	0.004	down	0.819	up	0.612	up	0.753
DNA REPLICATION	up	0.957	down	0.989	up	0.013	up	0.000	up	0.924	down	0.680	up	0.417
ECM-RECEPTOR INTERACTION	down	0.137	up	0.170	up	0.000	up	0.000	up	0.917	up	0.359	up	0.135
EPITHELIAL CELL SIGNALING IN HELICOBACTER PYLORI INFECTION	down	1.000	up	0.781	up	0.410	up	0.044	down	0.829	up	0.497	up	0.265
ERBB SIGNALING PATHWAY	down	0.777	up	0.419	up	0.490	up	0.023	up	0.844	up	0.976	up	0.736
ETHER LIPID METABOLISM	up	0.091	up	0.350	up	0.181	up	0.323	up	0.931	up	0.326	up	0.007
FATTY ACID METABOLISM	up	0.000	up	0.496	up	0.749	up	0.666	down	0.068	up	0.014	up	0.012
FC EPSILON RI SIGNALING PATHWAY	down	1.000	up	0.055	up	0.000	up	0.001	down	0.972	up	0.775	up	0.943
FC GAMMA R-MEDIATED PHAGOCYTOSIS	down	0.635	up	0.113	up	0.003	up	0.000	down	0.919	up	0.583	up	0.817
FOCAL ADHESION	down	0.335	up	0.082	up	0.000	up	0.000	up	0.906	up	0.504	up	0.286
GLIOMA	down	0.879	up	0.545	up	0.195	up	0.021	up	1.000	up	0.669	up	0.877
GLUTATHIONE METABOLISM	up	0.440	down	0.060	down	0.041	down	1.000	down	0.024	up	0.085	up	0.003
GLYCEROLIPID METABOLISM	up	0.086	up	0.657	up	0.037	up	0.051	up	1.000	up	0.075	up	0.506

Table 5.14: Gene set enrichment analysis KEGG pathway changes for data obtained by me (Helleur) and compared to Teufel et al (561) (continued)

GSEA Treatments	Helleur's data		Teufel *et al's* data											
	HFD vs LFD mice		Healthy obese humans		MAFLD humans		NASH humans		12-week HFD mice		18-week HFD mice		30-week HFD mice	
KEGG Pathway	Altered expression	FDR *q*-value neg	Altered expression	FDR *q*-value	Altered expression	FDR *q*-value	Altered expression	FDR *q*-value	Altered expression	FDR *q*-value	Altered expression	FDR *q*-value	Altered expression	FDR *q*-value
GLYCINE, SERINE AND THREONINE metabolism	up	0.318	up	0.541	down	1.000	down	0.498	down	0.027	up	0.517	down	0.791
GLYCOLYSIS_GLUCONEOGENESIS	up	0.070	up	0.417	up	0.019	up	0.107	down	0.020	down	0.553	up	0.440
GNRH SIGNALING PATHWAY	down	0.839	up	0.173	up	0.068	up	0.025	up	0.907	down	0.843	up	0.851
GRAFT-VERSUS-HOST DISEASE	down	1.000	up	0.887	up	0.179	up	0.010	down	0.122	down	0.839	up	0.751
HEMATOPOIETIC CELL LINEAGE	down	0.773	up	0.494	up	0.013	up	0.000	down	0.273	down	0.661	down	1.000
HOMOLOGOUS RECOMBINATION	down	1.000	up	0.651	up	0.104	up	0.002	down	0.785	down	0.993	down	0.995
HUNTINGTON'S DISEASE	up	0.818	down	0.401	down	0.027	down	0.035	down	0.009	down	0.695	up	0.003
INTESTINAL IMMUNE NETWORK FOR IGA PRODUCTION	up	1.000	up	0.766	up	0.067	up	0.018	down	0.613	up	0.338	up	0.695
LEISHMANIA Infection	down	0.801	up	0.170	up	0.000	up	0.000	down	0.455	down	0.683	down	0.968
LEUKOCYTE TRANSENDOTHELIAL MIGRATION	down	0.690	up	0.128	up	0.002	up	0.000	up	0.930	up	0.349	up	0.517
LINOLEIC ACID METABOLISM	up	0.167	up	0.542	up	0.775	down	0.986	down	0.789	up	0.265	up	0.041
MAPK SIGNALING PATHWAY	down	0.817	up	0.169	up	0.093	up	0.014	up	0.839	down	0.686	down	0.862
MELANOMA	up	0.660	up	0.770	up	0.402	up	0.084	up	0.751	up	0.924	up	0.738
METABOLISM OF XENOBIOTICS BY CYTOCHROME P450	up	0.106	down	0.591	down	0.039	down	0.038	down	0.025	up	0.008	up	0.002
NATURAL KILLER CELL MEDIATED CYTOTOXICITY	down	1.000	up	0.341	up	0.019	up	0.004	up	0.779	up	0.601	down	0.868
NEUROTROPHIN SIGNALING PATHWAY	down	0.798	up	0.389	up	0.209	up	0.023	down	0.629	down	0.667	down	0.884
NOD-LIKE RECEPTOR SIGNALING PATHWAY	down	1.000	down	1.000	up	0.170	up	0.004	down	0.190	down	0.605	down	0.936
NON-SMALL CELL LUNG CANCER	down	1.000	up	0.209	up	0.078	up	0.012	up	1.000	up	0.918	up	0.932
OLFACTORY TRANSDUCTION	down	0.787	down	0.439	up	0.000	down	0.006	up	1.000	up	0.963	down	0.893
OXIDATIVE PHOSPHORYLATION	up	0.058	down	0.428	down	0.039	down	0.036	down	0.000	down	0.924	up	0.003

Table 5.14: Gene set enrichment analysis KEGG pathway changes for data obtained by me (Helleur) and compared to Teufel et al (561) (continued)

GSEA Treatments	Helleur's data		Teufel *et al's* data											
	HFD vs LFD mice		Healthy obese humans		MAFLD humans		NASH humans		12-week HFD mice		18-week HFD mice		30-week HFD mice	
KEGG Pathway	Altered expression	FDR *q*-value neg	Altered expression	FDR *q*-value	Altered expression	FDR *q*-value	Altered expression	FDR *q*-value	Altered expression	FDR *q*-value	Altered expression	FDR *q*-value	Altered expression	FDR *q*-value
P53 SIGNALING PATHWAY	up	0.944	down	0.165	down	0.919	up	0.045	up	0.798	down	0.838	down	0.982
PANCREATIC CANCER	down	0.760	up	0.501	up	0.033	up	0.000	up	0.780	up	0.610	down	0.908
PARKINSON'S DISEASE	up	0.089	down	0.662	down	0.033	down	0.018	down	0.000	down	0.780	up	0.001
PATHOGENIC ESCHERICHIA COLI infection	down	0.873	down	0.430	down	0.839	up	0.768	down	0.001	down	0.548	up	0.041
PATHWAYS IN CANCER	down	0.831	up	0.376	up	0.094	up	0.002	up	0.765	up	0.502	up	0.694
PENTOSE PHOSPHATE PATHWAY	down	0.827	down	0.997	up	0.955	up	1.000	down	0.050	down	0.677	down	0.932
PEROXISOME	up	0.000	up	1.000	up	0.485	up	1.000	down	0.017	up	0.000	up	0.111
PHOSPHATIDYLINOSITOL SIGNALING SYSTEM	down	0.763	up	0.061	up	0.018	up	0.011	up	0.826	down	0.872	down	0.839
PPAR SIGNALING PATHWAY	up	0.001	up	0.383	up	0.000	up	0.000	up	0.814	up	0.015	up	0.462
PRIMARY BILE ACID BIOSYNTHESIS	up	0.008	up	0.123	up	0.099	up	0.093	up	0.692	up	0.026	up	0.064
PRIMARY IMMUNODEFICIENCY	down	0.817	down	0.821	up	0.351	up	0.026	up	0.907	up	0.985	down	0.902
PRION DISEASES	down	1.000	up	0.011	up	0.013	up	0.083	down	0.188	down	0.349	up	0.374
PROPANOATE METABOLISM	up	0.000	down	0.901	down	0.947	down	0.617	down	0.043	up	0.004	up	0.096
PROSTATE CANCER	down	0.755	down	0.895	up	0.282	up	0.045	up	0.686	up	0.641	up	0.910
PROTEASOME	up	0.004	down	0.408	down	0.230	down	0.976	down	0.097	down	0.915	up	0.003
PROTEIN EXPORT	down	0.785	up	1.000	down	1.000	down	1.000	down	0.000	down	0.000	up	0.321
PROXIMAL TUBULE BICARBONATE reclamation	down	1.000	up	0.997	down	1.000	up	0.972	down	0.025	down	0.337	down	0.861
PYRIMIDINE METABOLISM	up	0.374	down	0.752	up	0.926	up	0.699	down	0.436	down	0.917	up	0.379
PYRUVATE METABOLISM	up	0.021	up	1.000	up	0.101	up	0.095	down	0.025	up	0.375	up	0.786
REGULATION OF ACTIN CYTOSKELETON	down	0.694	up	0.205	up	0.082	up	0.008	up	0.887	up	0.619	up	0.732
RENIN-ANGIOTENSIN SYSTEM	up	0.093	up	0.201	up	0.048	up	0.044	up	0.686	up	0.611	up	0.794

Table 5.14: Gene set enrichment analysis KEGG pathway changes for data obtained by me (Helleur) and compared to Teufel et al (561) (continued)

GSEA Treatments	Helleur's data		Teufel *et al's* data											
	HFD vs LFD mice		Healthy obese humans		MAFLD humans		NASH humans		12-week HFD mice		18-week HFD mice		30-week HFD mice	
KEGG Pathway	Altered expression	FDR *q*-value neg	Altered expression	FDR *q*-value	Altered expression	FDR *q*-value	Altered expression	FDR *q*-value	Altered expression	FDR *q*-value	Altered expression	FDR *q*-value	Altered expression	FDR *q*-value
RIBOSOME	down	0.000	down	0.179	down	0.001	down	0.003	down	0.000	down	0.000	up	0.084
RNA POLYMERASE	down	0.991	down	0.405	down	0.075	down	0.208	down	0.631	down	0.098	down	0.985
SMALL CELL LUNG CANCER	down	0.757	up	0.349	up	0.000	up	0.000	up	0.752	up	0.491	up	0.548
SNARE INTERACTIONS IN VESICULAR transport	up	0.669	up	0.956	up	0.790	up	0.096	down	0.055	down	0.347	up	0.298
SPHINGOLIPID METABOLISM	up	0.414	down	0.897	up	0.349	up	0.391	up	0.944	down	0.783	up	0.020
SPLICEOSOME	down	0.085	down	0.996	down	0.151	down	0.891	down	0.328	down	0.009	down	0.876
STARCH AND SUCROSE METABOLISM	up	0.187	up	0.368	up	0.085	up	0.032	down	0.088	down	0.225	up	0.773
STEROID BIOSYNTHESIS	up	0.349	up	0.105	up	0.192	up	0.111	down	0.026	up	0.000	down	0.156
STEROID HORMONE BIOSYNTHESIS	up	0.368	up	0.377	up	0.107	up	0.470	down	0.626	up	0.214	up	0.378
SYSTEMIC LUPUS ERYTHEMATOSUS	down	1.000	down	0.679	up	0.482	up	0.405	down	0.026	down	0.120	up	0.173
T CELL RECEPTOR SIGNALING PATHWAY	down	1.000	up	0.381	up	0.066	up	0.002	down	0.799	down	0.957	down	0.871
TOLL-LIKE RECEPTOR SIGNALING PATHWAY	down	1.000	down	0.824	up	0.194	up	0.002	down	0.508	up	0.509	up	0.548
TRYPTOPHAN METABOLISM	up	0.000	up	0.758	down	0.743	down	0.739	down	0.016	up	0.210	up	0.160
TYROSINE METABOLISM	up	0.785	up	0.220	down	1.000	down	1.000	down	0.038	down	0.407	down	0.997
VALINE, LEUCINE AND ISOLEUCINE degradation	up	0.000	up	0.997	down	1.000	down	1.000	down	0.027	up	0.007	up	0.028
VASCULAR SMOOTH MUSCLE CONTRACTION	down	0.996	up	0.081	up	0.100	up	0.026	down	0.797	down	0.921	down	0.920
VEGF SIGNALING PATHWAY	down	0.916	up	0.079	up	0.010	up	0.041	up	0.779	up	0.668	up	0.661
VIRAL MYOCARDITIS	down	1.000	up	0.353	up	0.047	up	0.019	down	0.820	up	0.647	up	0.437

Table 5.15: Differential gene expression results for some important genes highlighted to be of importance for MAFLD and hepatic insulin resistance

All data is obtained following DESeq2 analysis of RNA-Sequencing data from the livers of mice from the dietary intervention study. Genes selected were chosen based on their involvement in pathways/metabolic functions altered in metabolic syndrome. p.adj = adjusted p-value. A negative Log_2FC corresponds to a downregulation of the gene for the pairwise comparison, and vice versa.

Pairwise comparison			HF vs LF		HF+EC vs HF		HF+34DHPVL vs HF		LF+EC vs LF		LF+34DHPVL vs LF		HF+EC vs LF		HF+34DHPVL vs LF	
Pathway/Disease/Biological function the gene is involved in	**Gene Name**	**Gene**	**p.adj**	**Log_2FC**	**p.adj**	**Log_2FC**	**p.adj**	**Log_2FC**	**p.adj**	**Log_2FC**	**p.adj**	**Log_2FC**	**p.adj**	**Log_2FC**	**p.adj**	**Log_2FC**
De novo lipogenesis	Sterol regulatory element binding protein-1c	***SREBF (SREBP-1C)***	0.869	-0.132	1.000	-0.005	0.997	-0.028	1.000	-0.412	0.958	-0.173	0.905	-0.138	0.872	-0.160
De novo lipogenesis	Carbohydrate response element binding protein	***MLXIPL (CHREBP)***	0.419	-0.382	0.954	0.181	0.998	0.048	1.000	-0.250	0.821	-0.359	0.784	-0.201	0.566	-0.334
De novo lipogenesis/glycogenolysis/gluconeogenesis	Glucose 6-phosphatase	***G6PC***	0.759	-0.241	0.983	-0.124	0.998	-0.346	1.000	0.046	0.958	-0.171	0.695	-0.365	0.426	-0.587
De novo lipogenesis/ anti-lipolysis	Hormone sensitive lipase (HSL)	***LIPE***	0.040	0.507	0.971	-0.089	0.998	-0.065	1.000	-0.181	0.845	-0.200	0.167	0.418	0.114	0.442
De novo lipogenesis	Insulin induced gene 1	***INSIG1***	0.733	-0.203	0.993	-0.054	0.998	0.088	1.000	0.300	0.817	-0.384	0.728	-0.258	0.895	-0.116
De novo lipogenesis/Apoptosis	Acetyl-coa carboxylase 1	***ACACA***	0.012	-0.853	0.995	0.030	0.998	0.095	1.000	-0.399	0.674	-0.452	0.032	-0.822	0.045	-0.758
De novo lipogenesis	Acetoacetyl-coa Synthetase	***AACS***	0.301	-0.802	0.995	-0.059	0.998	0.092	1.000	-0.178	0.158	-1.752	0.343	-0.861	0.448	-0.711
De novo lipogenesis	1-Acylglycerol-3-Phosphate O-Acyltransferase 1 (lysophosphatidic acid acyltransferase)	***AGPAT1***	0.240	-0.305	0.843	0.202	0.998	0.219	1.000	-0.103	0.507	-0.395	0.819	-0.103	0.849	-0.086
De novo lipogenesis	Glycerol-3-phosphate acyltransferase 1, mitochondrial	***GPAM (GPAT1)***	0.718	-0.223	0.906	-0.290	0.998	0.110	1.000	-0.310	0.547	-0.697	0.400	-0.513	0.904	-0.113
De novo lipogenesis	SREBF Chaperone	***SCAP***	0.594	-0.176	0.981	0.064	0.999	-0.004	1.000	-0.085	0.717	-0.296	0.819	-0.112	0.651	-0.180

Table 5.15: Differential gene expression results for some important genes highlighted to be of importance for MAFLD and hepatic insulin resistance (continued)

Pairwise comparison			HF vs LF		HF+EC vs HF		HF+34DHPVL vs HF		LF+EC vs LF		LF+34DHPVL vs LF		HF+EC vs LF		HF+34DHPVL vs LF	
Pathway/Disease/Biological function the gene is involved in	**Gene Name**	**Gene**	**p.adj**	**Log_2FC**	**p.adj**	**Log_2FC**	**p.adj**	**Log_2FC**	**p.adj**	**Log_2FC**	**p.adj**	**Log_2FC**	**p.adj**	**Log_2FC**	**p.adj**	**Log_2FC**
De novo lipogenesis /inhibits glycogen synthesis, increases glucose uptake, increases fatty acid uptake but reduces their synthesis/positive for insulin signalling	Protein Kinase AMP-Activated Catalytic Subunit Alpha 1 (AMPK1)	***PRKAA1***	0.521	-0.118	0.976	-0.048	0.998	-0.113	1.000	0.085	0.735	0.166	0.424	-0.166	0.180	-0.232
De novo lipogenesis/inhibits glycogen synthesis, increases glucose uptake, increases fatty acid uptake but reduces their synthesis/positive for insulin signalling	Protein Kinase AMP-Activated Catalytic Subunit Alpha 2 (AMPK2)	***PRKAA2***	0.880	0.064	0.972	-0.093	0.998	-0.153	1.000	0.070	0.864	0.197	0.967	-0.029	0.867	-0.089
De novo lipogenesis/inhibits glycogen synthesis, increases glucose uptake, increases fatty acid uptake but reduces their synthesis/positive for insulin signalling	Protein Kinase AMP-Activated Catalytic Subunit beta 1 (AMPK)	***PRKAB1***	0.493	-0.115	0.717	0.163	0.998	0.116	1.000	-0.008	0.930	0.067	0.866	0.048	0.999	0.000
De novo lipogenesis/inhibits glycogen synthesis, increases glucose uptake, increases fatty acid uptake but reduces their synthesis/positive for insulin signalling	Protein Kinase AMP-Activated Catalytic Subunit beta 2 (AMPK)	***PRKAB2***	0.285	-0.636	0.998	-0.031	0.998	0.085	1.000	0.196	1.000	-0.006	0.342	-0.667	0.446	-0.552
De novo lipogenesis/inhibits glycogen synthesis, increases glucose uptake, increases fatty acid uptake but reduces their synthesis/positive for insulin signalling	Protein Kinase AMP-Activated Catalytic Subunit gamma 1 (AMPK)	***PRKAG1***	0.330	-0.162	0.822	0.134	0.998	0.053	1.000	0.142	0.890	-0.095	0.934	-0.028	0.621	-0.109
De novo lipogenesis/inhibits glycogen synthesis, increases glucose uptake, increases fatty acid uptake but reduces	Protein Kinase AMP-Activated Catalytic Subunit gamma 2 (AMPK)	***PRKAG2***	0.233	0.254	0.929	-0.114	0.998	-0.247	1.000	-0.094	0.930	-0.096	0.665	0.140	0.990	0.007

Table 5.15: Differential gene expression results for some important genes highlighted to be of importance for MAFLD and hepatic insulin resistance (continued)

Pairwise comparison			HF vs LF		HF+EC vs HF		HF+34DHPVL vs HF		LF+EC vs LF		LF+34DHPVL vs LF		HF+EC vs LF		HF+34DHPVL vs LF	
Pathway/Disease/Biological function the gene is involved in	**Gene Name**	**Gene**	**p.adj**	**Log_2FC**	**p.adj**	**Log_2FC**	**p.adj**	**Log_2FC**	**p.adj**	**Log_2FC**	**p.adj**	**Log_2FC**	**p.adj**	**Log_2FC**	**p.adj**	**Log_2FC**
their synthesis/positive for insulin signalling																
Fatty acid metabolism/PPAR signalling/Fatty acid beta oxidation	Acyl-coa Oxidase 2	***ACOX1***	0.000	0.979	0.731	-0.251	0.998	-0.114	1.000	0.036	0.998	0.007	0.000	0.728	0.000	0.865
Fatty acid metabolism/PPAR signalling	Acyl-coa Dehydrogenase Medium Chain	***ACADM***	0.000	0.862	0.291	-0.354	0.998	-0.095	1.000	0.068	0.692	0.226	0.005	0.508	0.000	0.767
Fatty acid metabolism/PPAR signalling	Acetyl-coa Acyltransferase 1	***ACAA1***	0.000	0.959	0.518	-0.352	0.998	-0.121	1.000	-0.096	0.920	0.219	0.008	0.606	0.000	0.838
Fatty acid metabolism	Enoyl-coa Delta Isomerase 2	***ECI2***	0.020	0.670	0.933	-0.171	0.998	-0.195	1.000	0.042	0.871	0.216	0.170	0.499	0.177	0.475
Lipolysis/lipid transport	Retinoic Acid Receptor Alpha	***RARA***	0.681	0.137	0.930	-0.142	0.998	0.176	1.000	-0.219	0.987	-0.023	0.993	-0.005	0.317	0.313
Lipolysis (INHIBITS SREBP/ChREBP)	Nuclear Receptor Subfamily 1 Group I Member 2 (pregnane x receptor)	***NR1I2 (PXR)***	0.943	-0.030	0.887	0.170	1.000	0.003	1.000	0.231	0.944	-0.103	0.738	0.141	0.965	-0.026
Lipolysis (INHIBITS SREBP)/Liver fibrosis	Nuclear Receptor Subfamily 1 Group H Member 4 (farnesoid x receptor)	***NR1H4 (FXR)***	0.405	0.349	0.956	-0.157	0.998	-0.082	1.000	-0.259	0.915	0.206	0.767	0.192	0.624	0.266
Lipolysis	Lipoprotein lipase	***LPL***	0.002	-1.814	0.997	0.046	0.998	0.331	1.000	0.486	0.892	0.421	0.006	-1.768	0.027	-1.483
Lipolysis/Ether lipid metabolism	Phospholipid Phosphatase 2	***PLPP2***	0.139	-0.522	0.942	0.173	0.998	0.498	1.000	0.447	0.328	0.685	0.466	-0.350	0.978	-0.025
Lipolysis/Ether lipid metabolism	Phospholipase A2, group VI	***PLA2G6***	0.082	0.320	0.351	-0.326	0.998	0.185	1.000	0.027	0.950	0.067	0.990	-0.006	0.003	0.505
Lipolysis/Ether lipid metabolism	Ectonucleotide pyrophosphatase/phosphodiesterase 2	***ENPP2***	0.000	0.855	0.344	-0.399	0.998	-0.223	1.000	0.200	0.925	0.118	0.060	0.456	0.002	0.632
Fatty acid uptake	CD36 molecule	***CD36***	0.042	1.516	0.714	-0.904	0.998	0.075	1.000	0.550	0.880	0.513	0.613	0.612	0.043	1.591

Table 5.15: Differential gene expression results for some important genes highlighted to be of importance for MAFLD and hepatic insulin resistance (continued)

Pairwise comparison			HF vs LF		HF+EC vs HF		HF+34DHPVL vs HF		LF+EC vs LF		LF+34DHPVL vs LF		HF+EC vs LF		HF+34DHPVL vs LF	
Pathway/Disease/Biological function the gene is involved in	**Gene Name**	**Gene**	**p.adj**	**Log_2FC**	**p.adj**	**Log_2FC**	**p.adj**	**Log_2FC**	**p.adj**	**Log_2FC**	**p.adj**	**Log_2FC**	**p.adj**	**Log_2FC**	**p.adj**	**Log_2FC**
Fatty acid beta oxidation	Carnitine palmitoyltransferase 1	***CPT1A***	0.001	0.702	0.942	-0.123	0.998	-0.100	1.000	0.049	0.972	-0.054	0.020	0.579	0.010	0.602
Fatty acid beta oxidation	Carnitine palmitoyltransferase 2	***CPT2***	0.006	0.406	0.976	0.052	0.998	0.016	1.000	0.058	0.967	0.040	0.003	0.459	0.006	0.423
Fatty acid Biosynthesis	Monoacylglycerol O-acyltransferase 1	***MOGAT1***	0.000	3.825	0.664	-1.053	0.998	0.313	1.000	-0.251	0.947	0.341	0.000	2.771	0.000	4.138
Fatty acid Biosynthesis	Cell death-inducing DNA fragmentation factor	***CIDEA***	0.000	7.114	0.822	-1.645	0.998	1.198	1.000	2.120	0.526	3.175	0.004	5.469	0.000	8.312
Fatty acid Biosynthesis	Microfibril Associated Protein 2	***MFAP2***	0.239	-2.110	0.995	-0.154	0.998	0.879	1.000	0.204	0.987	0.155	0.277	-2.264	0.612	-1.231
Fatty acid biosynthesis	Stearoyl-coa desaturase	***SCD1***	0.003	-1.676	0.978	-0.179	0.998	0.671	1.000	-0.879	0.856	-0.487	0.002	-1.854	0.168	-1.005
Reduces fatty acid oxidation/Programmed cell death/Type I diabetes mellitus/Insulin resistance/ P53 Signalling pathway/Apoptosis	Fatty cell surface death receptor	***FAS***	0.065	0.498	0.991	0.044	0.998	0.071	1.000	0.285	0.656	0.345	0.070	0.542	0.040	0.568
Apoptosis (in damaged cells)/ Cell survival & proliferation (in healthy proliferative cells)	Jun Proto-Oncogene, AP-1 Transcription Factor Subunit	***JUN (AP-1)***	0.130	-0.760	0.34	0.873	1.000	0.218	1.000	0.504	0.950	0.183	0.920	0.115	0.400	-0.540
Fatty acid Biosynthesis	Fatt acid synthase	***FASN***	0.062	-1.283	0.998	0.036	0.998	0.158	1.000	-0.582	0.319	-1.416	0.113	-1.247	0.150	-1.125
Liver regeneration	Hepatocyte growth factor receptor	***MET***	0.540	0.370	0.999	-0.003	0.998	-0.078	1.000	-0.365	0.938	-0.225	0.641	0.367	0.713	0.292
Liver fibrosis	Protein kinase C α	***PRKCA***	0.671	0.147	0.727	-0.299	0.998	0.067	1.000	0.069	0.988	0.023	0.738	-0.152	0.569	0.214
Liver fibrosis	Cell division cycle 42	***CDC42***	0.958	0.013	0.784	-0.141	0.999	0.002	1.000	0.053	0.817	0.127	0.549	-0.127	0.965	0.015
Liver fibrosis	Vascular endothelial growth factor A	***VEGFA***	0.074	-0.397	0.790	0.217	0.998	-0.011	1.000	-0.112	0.441	-0.396	0.603	-0.181	0.085	-0.409
Liver fibrosis/TGF pathway	Transforming growth factor B 1	***TGFB1***	0.733	-0.181	0.977	-0.107	0.998	0.087	1.000	0.226	0.621	0.519	0.638	-0.288	0.998	0.087

Table 5.15: Differential gene expression results for some important genes highlighted to be of importance for MAFLD and hepatic insulin resistance (continued)

Pairwise comparison			HF vs LF		HF+EC vs HF		HF+34DHPVL vs HF		LF+EC vs LF		LF+34DHPVL vs LF		HF+EC vs LF		HF+34DHPVL vs LF	
Pathway/Disease/Biological function the gene is involved in	**Gene Name**	**Gene**	**p.adj**	**Log_2FC**	**p.adj**	**Log_2FC**	**p.adj**	**Log_2FC**	**p.adj**	**Log_2FC**	**p.adj**	**Log_2FC**	**p.adj**	**Log_2FC**	**p.adj**	**Log_2FC**
Liver fibrosis/TGF pathway	Transforming growth factor B 2	***TGFB2***	0.319	-1.032	0.884	-0.680	0.998	-0.372	1.000	0.266	0.996	0.049	0.105	-1.712	0.189	-1.404
Liver fibrosis/TGF pathway	E2F Transcription Factor 4	***E2F4***	0.012	-0.393	0.708	0.202	0.998	0.078	1.000	-0.035	0.864	-0.124	0.409	-0.191	0.080	-0.316
Liver fibrosis/TGF pathway/lipogenesis	Bone morphogenic protein 2	***BMP2***	0.359	-0.260	0.998	0.005	0.998	-0.256	1.000	-0.039	0.891	0.157	0.467	-0.255	0.043	-0.516
Liver fibrosis/TGF pathway/lipogenesis	Bone morphogenic protein 4	***BMP4***	0.178	-0.465	0.775	0.333	0.998	0.202	1.000	-0.113	0.966	-0.084	0.833	-0.132	0.572	-0.264
Liver fibrosis/TGF pathway/lipogenesis	Bone morphogenic protein 5	***BMP5***	0.171	-0.432	0.998	0.017	0.998	0.086	1.000	-0.022	0.737	-0.319	0.268	-0.415	0.373	-0.346
Liver fibrosis/TGF pathway/lipogenesis	Bone morphogenic protein 6	***BMP6***	0.044	-0.550	0.965	-0.107	0.998	0.030	1.000	-0.181	0.972	0.059	0.022	-0.656	0.081	-0.519
Liver fibrosis/TGF pathway/lipogenesis	SMAD Family Member 1	***SMAD1***	0.000	-0.456	0.731	0.173	0.999	-0.003	1.000	-0.065	0.859	-0.113	0.099	-0.283	0.001	-0.459
Liver fibrosis/TGF pathway/lipogenesis	SMAD Family Member 2	***SMAD2***	0.779	0.124	0.932	-0.170	0.998	-0.343	1.000	-0.103	0.972	-0.065	0.949	-0.047	0.633	-0.219
Anti-fibrogenic/TGF pathway	SMAD Family Member 3	***SMAD3***	0.631	-0.179	0.976	-0.088	0.998	0.046	1.000	-0.148	0.794	0.276	0.530	-0.267	0.790	-0.134
Liver fibrosis/TGF pathway/lipogenesis	SMAD Family Member 4	***SMAD4***	0.804	-0.053	0.964	-0.057	0.998	-0.154	1.000	0.104	0.946	0.059	0.636	-0.109	0.224	-0.207
Liver fibrosis/TGF pathway/lipogenesis	SMAD Family Member 5	***SMAD5***	0.646	0.234	0.933	-0.218	0.998	-0.217	1.000	-0.063	0.947	0.150	0.987	0.016	0.986	0.017
Liver fibrosis	A-smooth muscle actin	***ACTA2***	0.245	-0.656	0.995	0.045	0.998	0.488	1.000	-0.005	0.735	-0.573	0.378	-0.611	0.869	-0.168
Liver fibrosis	Type I collagen	***COL1A1***	0.180	-1.453	0.970	-0.360	0.998	0.735	1.000	0.101	0.964	-0.274	0.119	-1.813	0.645	-0.719
Liver fibrosis	Hepatocyte growth factor	***HGF***	0.436	-0.530	0.859	0.458	0.998	0.414	1.000	0.359	0.984	0.075	0.960	-0.072	0.925	-0.115
Liver fibrosis/inflammation	Nuclear factor kappa B 1	***NFKB1***	0.690	-0.188	0.666	0.442	0.998	0.021	1.000	0.258	0.909	0.205	0.658	0.254	0.783	-0.167
Liver fibrosis/inflammation	Nuclear factor kappa B 2	***NFKB2***	0.646	-0.417	0.400	1.176	0.998	0.281	1.000	0.740	0.869	0.492	0.426	0.759	0.928	-0.136
Liver fibrosis	Platelet derived growth factor alpha	***PDGFA***	0.215	-0.516	0.995	0.035	0.998	0.269	0.872	-0.042	0.975	-0.077	0.340	-0.481	0.684	-0.247
Liver fibrosis	Platelet derived growth factor beta	***PDGFB***	0.683	-0.376	0.998	0.006	0.998	0.200	0.145	0.668	0.795	0.651	0.763	-0.370	0.902	-0.176
Liver fibrosis	Platelet derived growth factor c	***PDGFC***	0.459	-0.386	0.848	0.362	0.998	0.246	0.256	0.332	0.647	0.566	0.983	-0.024	0.872	-0.140

Table 5.15: Differential gene expression results for some important genes highlighted to be of importance for MAFLD and hepatic insulin resistance (continued)

Pairwise comparison			HF vs LF		HF+EC vs HF		HF+34DHPVL vs HF		LF+EC vs LF		LF+34DHPVL vs LF		HF+EC vs LF		HF+34DHPVL vs LF	
Pathway/Disease/Biological function the gene is involved in	**Gene Name**	**Gene**	**p.adj**	**Log_2FC**	**p.adj**	**Log_2FC**	**p.adj**	**Log_2FC**	**p.adj**	**Log_2FC**	**p.adj**	**Log_2FC**	**p.adj**	**Log_2FC**	**p.adj**	**Log_2FC**
Liver fibrosis	Platelet derived growth factor d	***PDGFD***	0.468	-0.440	0.785	-0.513	0.998	-0.248	0.860	0.059	0.999	0.008	0.101	-0.952	0.266	-0.688
Liver fibrosis	Platelet derived growth factor receptor alpha	***PDGFRA***	0.240	-0.906	0.965	0.274	0.998	0.205	0.214	0.588	0.959	0.209	0.552	-0.632	0.467	-0.701
Liver fibrosis	Platelet derived growth factor receptor beta	***PDGFRB***	0.205	-0.774	0.976	0.180	0.998	0.354	0.699	0.147	0.993	-0.039	0.456	-0.594	0.623	-0.420
Liver fibrosis	Matrix metalloproteinase 2	***MMP2***	0.047	-1.589	0.994	0.085	0.998	0.420	1.000	0.312	0.976	0.152	0.105	-1.504	0.229	-1.169
Liver fibrosis	SEL1L Family Member 3	***SEL1L3***	0.006	-0.556	0.475	0.358	0.998	0.253	1.000	0.182	0.967	-0.055	0.561	-0.198	0.269	-0.303
Liver fibrosis	Lysyl Oxidase Like 1	***LOXL1***	0.120	-1.340	0.998	0.040	0.998	0.487	1.000	0.167	0.967	-0.206	0.197	-1.300	0.450	-0.853
Anti-fibrogenic	C1Q and TNF related 2	***C1QTNF2***	0.112	-0.759	0.912	0.297	0.998	0.280	1.000	-0.123	0.972	-0.097	0.485	-0.461	0.439	-0.479
Anti-fibrogenic/anti-inflammatory	Peroxisome proliferator activated receptor alpha	***PPARA***	0.046	1.014	0.965	-0.197	0.998	0.040	1.000	0.120	0.997	-0.018	0.189	0.818	0.050	1.055
Anti-fibrogenic	SMAD Family Member 7	***SMAD7***	0.004	-0.654	0.994	-0.029	0.998	-0.171	1.000	-0.433	0.737	-0.270	0.005	-0.683	0.000	-0.825
Anti-fibrogenic	SMAD Family Member 6	***SMAD6***	0.943	0.037	0.965	-0.118	0.998	-0.082	1.000	-0.066	0.985	-0.037	0.906	-0.080	0.948	-0.044
Anti-fibrogenic	Interferon gamma receptor 2	***IFNGR1***	0.730	-0.229	0.989	-0.081	0.998	-0.080	1.000	0.036	0.987	-0.046	0.700	-0.310	0.679	-0.309
Anti-fibrogenic	Interferon gamma receptor 2 (non ligand binging of beta chain)	***IFNGR2***	0.940	-0.058	0.936	0.239	0.998	0.104	1.000	0.278	0.824	0.386	0.833	0.181	0.967	0.047
Anti-fibrogenic	HORMA Domain Containing 2	***HORMAD2***	NA	0.586	0.995	0.122	0.998	0.450	1.000	0.791	0.935	0.675	NA	0.708	0.633	1.037
Anti-fibrogenic	Apolipoprotein F	***APOF***	0.908	0.031	0.722	0.189	0.998	0.090	1.000	0.057	0.879	-0.110	0.286	0.220	0.623	0.121
Anti-fibrogenic/increased adipogenesis/increased gluconeogenesis	CCAAT/enhancer binding protein alpha	***CEBPA***	0.607	0.212	0.998	0.003	0.999	0.006	1.000	-0.316	0.791	-0.311	0.690	0.216	0.661	0.219
Anti-oxidative defence/(reduced in DNL) anti-fibrotic/protective	Nuclear factor erythroid 2 like 2	***NFE2L2 (NRF2)***	0.423	0.242	0.725	-0.296	0.999	0.004	1.000	-0.020	0.960	0.074	0.927	-0.054	0.486	0.246
Anti-oxidative defence	Cytochrome p450 2E1	***CYP2E1***	0.033	0.384	0.957	-0.246	0.998	-0.421	1.000	-0.169	0.958	0.178	0.173	0.928	0.288	0.753

Table 5.15: Differential gene expression results for some important genes highlighted to be of importance for MAFLD and hepatic insulin resistance (continued)

Pairwise comparison			HF vs LF		HF+EC vs HF		HF+34DHPVL vs HF		LF+EC vs LF		LF+34DHPVL vs LF		HF+EC vs LF		HF+34DHPVL vs LF	
Pathway/Disease/Biological function the gene is involved in	**Gene Name**	**Gene**	**p.adj**	**Log_2FC**	**p.adj**	**Log_2FC**	**p.adj**	**Log_2FC**	**p.adj**	**Log_2FC**	**p.adj**	**Log_2FC**	**p.adj**	**Log_2FC**	**p.adj**	**Log_2FC**
Gluconeogenesis	Phosphoenolpyruvate carboxykinase (PEPCK)	***PCK1***	0.534	0.390	0.831	0.450	0.998	-0.095	1.000	0.619	0.904	0.306	0.161	0.839	0.724	0.295
Gluconeogenesis (when fasting)/ fatty acid beta oxidation/reduced in MAFLD and insulin resistance	Peroxisome proliferator-activated receptor γ coactivator 1α (PGC-1a)	***PPARGC1A***	0.271	-0.512	0.959	0.176	0.998	-0.143	1.000	-0.039	0.870	-0.298	0.613	-0.337	0.176	-0.655
Gluconeogenesis/Insulin secretion	Camp response element binding protein	***CREB1***	0.970	-0.044	0.954	0.300	0.998	-0.156	1.000	0.612	0.873	0.469	0.848	0.256	0.884	-0.200
Gluconeogenesis/Raised insulin resistance/De novo lipogenesis	Forkhead box class Os 1	***FOXO1***	0.191	0.276	0.998	0.006	0.998	-0.256	1.000	0.074	0.967	-0.050	0.248	0.282	0.967	0.020
Gluconeogenesis/Raised insulin resistance/De novo lipogenesis	Forkhead box class Os 3	***FOXO3***	0.001	0.671	0.741	-0.254	0.998	-0.256	1.000	0.328	0.972	0.050	0.111	0.417	0.097	0.414
Gluconeogenesis/Raised insulin resistance/De novo lipogenesis	Forkhead box class Os 4	***FOXO4***	0.284	0.215	0.844	-0.152	0.998	-0.139	1.000	-0.131	1.000	0.002	0.864	0.064	0.819	0.076
Glycogenolysis/gluconeogenesis	Glycogen Synthase Kinase 3 Alpha	***GSK3A***	0.630	-0.060	0.860	0.077	1.000	0.095	1.000	-0.040	0.800	-0.090	0.940	0.016	0.850	0.034
Glycogenolysis/gluconeogenesis	Glycogen Synthase Kinase 3 Beta	***GSK3B***	0.400	0.353	0.950	-0.170	1.000	-0.110	1.000	0.252	0.950	0.131	0.780	0.182	0.660	0.246
Fatty acid metabolism/ Gluconeogenesis	Aldehyde dehydrogenase 3 family member A2	***ALDH3A2***	0.000	1.768	0.537	-0.549	0.999	0.008	1.000	0.121	0.845	0.292	0.000	1.220	0.000	1.776
Fatty acid metabolism/Pyruvate metabolism/Gluconeogenesis	Aldehyde dehydrogenase 7 family member A1	***ALDH7A1***	0.004	0.431	0.883	-0.122	0.998	-0.103	1.000	-0.084	0.971	-0.038	0.105	0.309	0.063	0.328
Gluconeogenesis/Pyruvate metabolism/Citric acid cycle	Pyruvate Dehydrogenase E1 Subunit Alpha 1	***PDHA1***	0.000	0.494	0.243	-0.316	0.998	-0.115	1.000	-0.083	0.990	-0.013	0.414	0.179	0.015	0.379
Citric acid cycle	Succinate-coa ligase, GDP-forming, alpha subunit	***SUCLG1***	0.000	0.443	0.310	-0.236	0.998	-0.033	1.000	0.039	0.804	0.118	0.168	0.208	0.000	0.410

Table 5.15: Differential gene expression results for some important genes highlighted to be of importance for MAFLD and hepatic insulin resistance (continued)

Pairwise comparison			HF vs LF		HF+EC vs HF		HF+34DHPVL vs HF		LF+EC vs LF		LF+34DHPVL vs LF		HF+EC vs LF		HF+34DHPVL vs LF	
Pathway/Disease/Biological function the gene is involved in	**Gene Name**	**Gene**	**p.adj**	**Log_2FC**	**p.adj**	**Log_2FC**	**p.adj**	**Log_2FC**	**p.adj**	**Log_2FC**	**p.adj**	**Log_2FC**	**p.adj**	**Log_2FC**	**p.adj**	**Log_2FC**
Citric acid cycle/Oxidative phosphorylation	Succinate Dehydrogenase Complex Flavoprotein Subunit A	***SDHA***	0.032	0.377	0.783	-0.182	0.998	-0.177	1.000	0.077	0.982	-0.028	0.446	0.195	0.412	0.200
PPAR signalling pathway/Fatty acid oxidation	Peroxisome proliferator activated receptor gamma	***PPARG***	0.007	1.532	0.826	-0.557	0.998	0.069	1.000	0.222	0.668	0.775	0.193	0.975	0.006	1.601
PPAR signalling pathway/Fatty acid oxidation	Peroxisome proliferator activated receptor alpha	***PPARA***	0.046	1.014	0.965	-0.197	0.998	0.040	1.000	0.120	0.997	-0.018	0.189	0.818	0.050	1.055
PPAR signalling pathway	Peroxisome proliferator activator receptor delta	***PPARD***	0.046	-1.061	0.959	0.226	0.998	0.067	1.000	0.156	0.993	-0.038	0.201	-0.835	0.088	-0.994
PPAR signalling pathway	Fatty acid binding protein 2	***FABP2***	0.000	1.298	0.600	-0.459	0.998	-0.044	1.000	-0.029	0.847	0.261	0.012	0.839	0.000	1.253
PPAR signalling pathway/Fatty acid Biosynthesis	Fatty acid binding protein 5	***FABP5***	0.000	-4.180	0.313	1.377	0.998	0.319	1.000	-0.152	0.448	-1.310	0.000	-2.804	0.000	-3.861
Starch and sucrose metabolism	Amylo-1,6-glucosidase, 4-alpha-glucanotransferase	***AGL***	0.012	0.511	0.288	-0.416	0.998	-0.270	1.000	0.035	0.947	0.088	0.820	0.095	0.408	0.242
Starch and sucrose metabolism	Amylase 1, salivary	***AMY1***	0.005	0.607	0.567	-0.344	0.998	-0.154	1.000	-0.117	0.999	0.005	0.434	0.262	0.079	0.453
Starch and sucrose metabolism	Glycogen synthase 2	***GYS2***	0.028	0.709	0.676	-0.423	0.998	-0.238	1.000	-0.071	0.903	0.206	0.584	0.286	0.246	0.471
Starch and sucrose metabolism	Phosphoglucomutase 1	***PGM1***	0.001	0.488	0.802	-0.164	0.998	-0.080	1.000	-0.062	0.883	0.113	0.094	0.323	0.015	0.408
Starch and sucrose metabolism	Glucan (1,4-alpha-), branching enzyme 1	***GBE1***	0.095	0.531	0.710	-0.374	0.998	-0.129	1.000	-0.085	0.819	0.280	0.782	0.157	0.306	0.402
Insulin signalling/Cell growth	Insulin-like growth factor binding protein 1	***IGFBP1***	0.024	-2.079	0.035	2.522	0.998	0.691	1.000	1.342	0.700	1.145	0.805	0.443	0.228	-1.388
Insulin signalling/Cell growth	Insulin-like growth factor binding protein 3	***IGFBP3***	0.620	-0.210	0.930	-0.180	1.000	0.352	1.000	-0.150	1.000	-0.150	0.380	-0.400	0.820	0.140
Insulin signalling	STEAP family member 4	***STEAP4***	0.642	0.414	0.003	2.122	0.998	0.128	1.000	0.641	0.850	0.530	0.000	2.536	0.590	0.541
Insulin signalling	Matrix metalloproteinase 7	***MMP7***	0.122	-3.586	0.998	0.071	0.998	-0.394	1.000	1.474	0.982	0.327	0.194	-3.515	0.107	-3.980

Table 5.15: Differential gene expression results for some important genes highlighted to be of importance for MAFLD and hepatic insulin resistance (continued)

Pairwise comparison			HF vs LF		HF+EC vs HF		HF+34DHPVL vs HF		LF+EC vs LF		LF+34DHPVL vs LF		HF+EC vs LF		HF+34DHPVL vs LF	
Pathway/Disease/Biological function the gene is involved in	**Gene Name**	**Gene**	**p.adj**	**Log_2FC**	**p.adj**	**Log_2FC**	**p.adj**	**Log_2FC**	**p.adj**	**Log_2FC**	**p.adj**	**Log_2FC**	**p.adj**	**Log_2FC**	**p.adj**	**Log_2FC**
Insulin signalling	H19 Imprinted Maternally Expressed Transcript	***H19***	0.020	-3.902	0.979	-0.497	0.998	0.764	1.000	0.380	0.987	0.198	0.015	-4.399	0.106	-3.138
Insulin signalling	Insulin receptor substrate 1	***IRS1***	0.584	0.185	0.775	-0.268	0.998	-0.388	1.000	-0.225	0.939	-0.121	0.885	-0.083	0.609	-0.203
Insulin signalling	Insulin receptor substrate 2 (more significant)	***IRS2***	0.551	-0.475	0.541	0.933	0.998	-0.056	1.000	0.632	0.913	0.369	0.664	0.458	0.564	-0.532
Insulin signalling	Phosphatidylinositol-4,5-Bisphosphate 3-Kinase Catalytic Subunit ALPHA (PI3K)	***PIK3CA***	0.971	0.014	0.844	-0.198	0.998	-0.081	1.000	0.112	0.947	0.092	0.624	-0.183	0.890	-0.066
Insulin signalling	Phosphatidylinositol-4,5-Bisphosphate 3-Kinase Catalytic Subunit BETA	***PIK3CB***	0.955	-0.038	0.993	0.051	0.998	-0.041	1.000	-0.100	0.982	-0.055	0.989	0.013	0.921	-0.079
Insulin signalling	Phosphatidylinositol-4,5-Bisphosphate 3-Kinase Catalytic Subunit delta	***PIK3CD***	0.631	-0.316	0.844	0.424	0.998	0.426	1.000	0.371	0.611	0.705	0.927	0.107	0.919	0.109
Insulin signalling	Phosphatidylinositol-4,5-Bisphosphate 3-Kinase Catalytic Subunit Gamma	***PIK3CG***	0.121	-1.019	0.853	0.526	0.998	0.445	1.000	0.527	0.778	0.608	0.623	-0.493	0.510	-0.574
Insulin signalling	Insulin receptor	***INSR***	0.922	0.100	0.984	0.121	0.998	-0.153	1.000	-0.078	0.967	-0.156	0.858	0.221	0.973	-0.053
Insulin signalling	High mobility group AT-Hook 1	***HMGA1***	0.52	-0.29	0.98	-0.1	1.00	0.23	1.00	0.137	0.770	0.373	0.450	-0.400	0.940	-0.060
Insulin signalling/cell growth	SHC adaptor protein 1	***SHC1***	0.531	-0.117	0.817	0.138	0.998	0.115	1.000	0.166	0.916	-0.086	0.954	0.021	0.998	-0.001
Insulin signalling/cell growth	SHC adaptor protein 2	***SHC2***	0.012	-3.594	0.998	0.072	0.998	1.980	1.000	1.031	0.966	0.394	0.028	-3.521	0.428	-1.614
Insulin signalling/cell growth	Growth factor receptor-bound protein 2	***GRB2***	0.019	0.147	0.770	0.069	0.998	0.027	1.000	0.025	0.451	0.115	0.000	0.216	0.005	0.174
Insulin signalling/Appetite	Leptin Receptor	***LEPR***	0.000	-2.484	0.994	0.055	0.998	0.029	1.000	-0.250	0.988	0.049	0.000	-2.430	0.000	-2.455

Table 5.15: Differential gene expression results for some important genes highlighted to be of importance for MAFLD and hepatic insulin resistance (continued)

Pairwise comparison			HF vs LF		HF+EC vs HF		HF+34DHPVL vs HF		LF+EC vs LF		LF+34DHPVL vs LF		HF+EC vs LF		HF+34DHPVL vs LF	
Pathway/Disease/Biological function the gene is involved in	**Gene Name**	**Gene**	**p.adj**	**Log_2FC**	**p.adj**	**Log_2FC**	**p.adj**	**Log_2FC**	**p.adj**	**Log_2FC**	**p.adj**	**Log_2FC**	**p.adj**	**Log_2FC**	**p.adj**	**Log_2FC**
Insulin clearance	CEA Cell Adhesion Molecule 1	***CEACAM1***	0.980	-0.010	0.980	0.054	1.000	-0.040	1.000	-0.090	0.770	-0.230	0.930	0.044	0.920	-0.050
Decreased insulin signalling/decreased fatty acid synthesis (higher levels in MAFLD)	Pyruvate dehydrogenase kinase 2 (main PDK in liver)	***PDK2***	0.048	0.429	0.940	-0.115	0.998	0.011	1.000	-0.201	0.737	-0.237	0.255	0.314	0.057	0.440
Decreased insulin signalling/decreased fatty acid synthesis (lower levels in MAFLD)	Pyruvate dehydrogenase kinase 4	***PDK4***	0.534	-0.561	0.993	-0.098	0.998	0.315	1.000	0.817	0.880	0.492	0.547	-0.659	0.864	-0.246
Decreased insulin signalling/JNK pathway	Mitogen-activated protein kinase 8	***MAPK8 (JNK1)***	0.980	-0.010	0.740	-0.130	1.000	-0.110	1.000	-0.030	0.870	0.079	0.400	-0.130	0.470	-0.110
Decreased insulin signalling/JNK pathway	Mitogen-activated protein kinase 9	***MAPK9 (JNK2)***	0.100	0.587	0.860	-0.280	1.000	-0.290	1.000	0.174	0.820	0.308	0.580	0.302	0.560	0.296
P53 Signalling pathway/Apoptosis	BCL2-associated X protein	***BAX***	0.068	0.405	0.577	-0.314	0.998	-0.157	1.000	-0.160	0.951	-0.080	0.833	0.091	0.401	0.248
P53 Signalling pathway/Apoptosis	Caspase 9	***CASP9***	0.379	0.205	0.870	-0.153	0.999	-0.006	1.000	-0.160	0.876	-0.138	0.910	0.052	0.470	0.199
P53 Signalling pathway/Apoptosis	Phosphatase and tensin homolog	***PTEN***	0.285	0.200	0.706	-0.203	0.998	-0.207	1.000	-0.146	0.986	-0.020	0.995	-0.002	0.989	-0.006
P53 Signalling pathway/Apoptosis	Conserved helix-loop-helix ubiquitous kinase	***CHUK***	0.166	0.243	0.760	-0.178	0.998	-0.160	1.000	-0.117	0.987	0.019	0.841	0.066	0.768	0.084
P53 Signalling pathway/Apoptosis	Caspase 7	***CASP7***	0.170	0.252	0.982	0.042	0.998	-0.115	1.000	-0.110	0.967	-0.043	0.147	0.294	0.590	0.138
Oxidative phosphorylation/Insulin resistance	Inorganic Pyrophosphatase 2	***PPA2***	0.028	0.359	0.753	-0.184	0.998	-0.117	1.000	-0.097	0.906	0.103	0.472	0.175	0.236	0.242
Oxidative phosphorylation/Insulin resistance	NADH:Ubiquinone Oxidoreductase Subunit A10	***NDUFA10***	0.000	0.426	0.364	-0.245	0.998	-0.106	1.000	-0.012	0.977	0.026	0.315	0.181	0.021	0.320
Oxidative phosphorylation/Insulin resistance	Atpase H+ Transporting V1 Subunit D	***ATP6V1D***	0.054	0.551	0.983	0.061	0.998	-0.171	1.000	0.245	0.668	0.363	0.050	0.612	0.289	0.380
MAPK signalling/Chemokine signalling/insulin signalling	AKT serine/threonine kinase 1	***AKT1***	0.020	-0.322	0.374	0.257	0.998	0.112	1.000	0.012	0.925	0.077	0.813	-0.065	0.230	-0.210

Table 5.15: Differential gene expression results for some important genes highlighted to be of importance for MAFLD and hepatic insulin resistance (continued)

Pairwise comparison			HF vs LF		HF+EC vs HF		HF+34DHPVL vs HF		LF+EC vs LF		LF+34DHPVL vs LF		HF+EC vs LF		HF+34DHPVL vs LF	
Pathway/Disease/Biological function the gene is involved in	**Gene Name**	**Gene**	**p.adj**	**Log_2FC**	**p.adj**	**Log_2FC**	**p.adj**	**Log_2FC**	**p.adj**	**Log_2FC**	**p.adj**	**Log_2FC**	**p.adj**	**Log_2FC**	**p.adj**	**Log_2FC**
MAPK signalling/Chemokine signalling/insulin signalling/Liver fibrosis	Epidermal growth factor receptor	***EGFR***	0.054	-1.277	0.512	1.024	0.998	0.179	1.000	0.083	0.862	-0.497	0.849	-0.253	0.147	-1.098
MAPK signalling/Chemokine signalling/insulin signalling	Mitogen-Activated Protein Kinase 7	***MAPK7***	0.010	-0.947	0.917	0.249	0.998	0.494	1.000	0.078	0.988	0.036	0.132	-0.698	0.388	-0.452
MAPK signalling/TGF-Beta signalling	Transforming Growth Factor Beta 3	***TGFB3***	0.100	-1.319	0.998	0.030	0.998	0.419	1.000	0.077	0.921	-0.426	0.168	-1.289	0.381	-0.900
Inflammatory genes	Integrin Subunit Alpha M (also known as CD11B)	***ITGAM***	0.477	-0.823	0.952	0.451	0.998	0.434	1.000	0.714	0.647	1.241	0.844	-0.372	0.826	-0.389
Inflammatory genes	CD86 antigen	***CD86***	0.823	0.189	0.963	0.223	0.998	-0.061	1.000	0.802	0.220	1.328	0.650	0.412	0.915	0.128
Cytokine mediated signalling pathway /inhibits IRS-1 in insulin signalling	Suppressor of cytokine signaling 5	***SOCS5***	0.012	1.657	0.817	-0.657	0.032	-2.131	1.000	1.330	0.186	1.770	0.268	1.000	0.676	-0.474
Cytokine mediated signalling pathway	Tumour necrosis factor	***TNF***	0.863	-0.396	0.994	0.142	0.998	0.387	1.000	1.481	0.355	2.748	0.940	-0.254	0.998	-0.009
Glucose transporters (glucose influx)	solute carrier family 2 (facilitated glucose transporter), member 1	***SLC2A1 (Glut-1)***	0.863	-0.113	0.957	0.177	0.998	0.324	1.000	0.074	0.608	0.581	0.949	0.064	0.765	0.210
Glucose transporters (glucose efflux, increased in type-2 diabetes))	solute carrier family 2 (facilitated glucose transporter), member 2	***SLC2A2 (Glut-2)***	0.327	0.441	0.704	-0.481	0.998	-0.245	1.000	-0.101	0.981	-0.062	0.969	-0.039	0.774	0.196
Glucose transporters	solute carrier family 2 (facilitated glucose transporter), member 3	***SLC2A3 (Glut-3)***	0.501	-0.573	0.919	0.431	0.998	0.447	1.000	0.440	0.944	0.292	0.929	-0.142	0.932	-0.126
Glucose transporters	solute carrier family 2 (facilitated glucose transporter), member 4	***SLC2A4 (Glut-4)***	0.058	-1.755	0.994	0.096	0.998	-0.289	1.000	-1.702	0.674	-1.153	0.124	-1.659	0.031	-2.044
Glucose transporters	solute carrier family 2 (facilitated glucose transporter), member 8	***SLC2A8 (Glut-8)***	0.483	-0.211	0.885	0.179	0.998	0.081	1.000	-0.014	0.948	-0.094	0.960	-0.032	0.759	-0.131

Table 5.15: Differential gene expression results for some important genes highlighted to be of importance for MAFLD and hepatic insulin resistance (continued)

Pairwise comparison			HF vs LF		HF+EC vs HF		HF+34DHPVL vs HF		LF+EC vs LF		LF+34DHPVL vs LF		HF+EC vs LF		HF+34DHPVL vs LF	
Pathway/Disease/Biological function the gene is involved in	**Gene Name**	**Gene**	**p.adj**	**Log_2FC**	**p.adj**	**Log_2FC**	**p.adj**	**Log_2FC**	**p.adj**	**Log_2FC**	**p.adj**	**Log_2FC**	**p.adj**	**Log_2FC**	**p.adj**	**Log_2FC**
Glucose transporters (increased in type-2 diabetes)	solute carrier family 2 (facilitated glucose transporter), member 9	***SLC2A9 (Glut-9)***	0.168	0.397	0.740	-0.302	0.998	-0.152	1.000	-0.296	0.949	-0.102	0.865	0.095	0.520	0.245

5.6 Discussion

Here, RNA-seq and qRT-PCR was employed followed by differential expression analyses and GSEA to understand how EC and 34DHPVL could protect against HF diet induced insulin resistance and MAFLD. Several metabolic and signalling pathways have been shown to be affected by these polyphenol treatments and how these may act in synergy to induce the overall changes. The main observations from this study include the following:

(1) MAFLD and insulin resistant mice, from the HF diet, expressed a significant increase in genes involved in gluconeogenesis and a decrease in DNL compared to mice on LF HC diets, contributing to increased circulatory glucose concentrations.

(2) EC but not 34DHPVL reversed the expression of a large number of differentially expressed genes and pathways enriched in HF fed conditions.

(3) 34DHPVL caused an increase in gene expression in favour of promoting insulin sensitivity and leptin sensitivity, although the changes were not significant, the combination of gene changes across different pathways could act in synergy to enhance the response to insulin, or independently of insulin, in lowering blood glucose.

(4) EC significantly increased gene expression in favour of insulin signalling and decreased gene expression in favour of inducing insulin resistance.

(5) LF HC diets induced significant gene changes involved in hepatic fibrosis development over the 15-week intervention, more so than the LC HF diets.

5.6.1 The effects of high-fat and high-carbohydrate diets on de novo lipogenesis and gluconeogenesis

Subjects with MAFLD and insulin resistance are known to exhibit increased hepatic gluconeogenesis and DNL. In this study, the HF fed mice without polyphenols displayed a significant increase in gluconeogenesis than LF fed mice, but also exhibited a reduction in DNL gene expression. The reduction in DNL gene expression was most likely caused by the HC content of the LF diet which can be more powerful than HF diets in the induction of DNL (438, 484, 562, 563). Here, a discussion of the gene changes that occurred to support DNL and gluconeogenesis will be detailed for HF and LF HC dietary treatment groups, and later it will discuss a paper that directly complements the findings here for HF diet induced MAFLD pathway changes.

Please refer to chapter 4, Figure 4.2, for the pathway of DNL and chapter 1, Figure 1.8 for the gluconeogenesis pathway. DNL is activated primarily by SREBP-1c (*SREBF* gene) and ChREBP (*MLXIPL* gene) to stimulate enzyme activation for lipogenesis, which include: ACC, FASN, SCD-1, PKLR, GPAT1 (*GPAM* gene), AGPAT1, and others (564). CHREBP is a transcription factor increased in response to HC diets for DNL activation (564). In this current study, it was shown that the LF HC diet caused a much higher expression of several genes involved in DNL processes than the HF treatment group, including *MLXIPL* and *SREBF*. Previous studies support this finding where it has been shown that mice fed a HC diet from a fasted state expressed a 20-fold increase in hepatic *GPAT1* mRNA, namely because of SREBP-1c activation (565). The effects of reduced DNL processes in the HF diet fed mice compared to the LF diet fed mice in this current study, caused an increase in fatty acid metabolism that can increase blood glucose levels via stimulating gluconeogenesis (566).

In contrast, HF diets cause hepatic lipid accumulation through the actions of insulin. Insulin will activate SREBP-1c and subsequent lipogenic enzymes whilst repressing the activity of glucose-6-phosphatase (G6Pase), which is also a mechanism of 'selective insulin resistance' in type-2 diabetics (567). When there are high nuclear levels of SREBP-1c, this stimulates the synthesis of fatty acids, and consequently causes lipid storage in the liver, and an increase in the secretion of vLDLs into the plasma, which can directly influence insulin resistance in muscles and adipose tissues (567).

The effects of the HF diet compared to the LF diet in this study were to significantly raise genes and pathway expressions involved in gluconeogenesis, which is well reported in cases such as MAFLD because the circulating insulin levels are ineffective at inhibiting gluconeogenesis due to the presence of insulin resistance (568). Just a few of the gene changes seen to be increased in the HF versus LF comparison included *FOXO, PCK1* (PEPCK) and *CEBPA*. The roles that the proteins transcribed by these genes perform in gluconeogenesis are now described and explain why they are more highly expressed under HF conditions. FOXO is phosphorylated and rendered inactive by insulin, as a consequence it binds directly with G6Pase and PEPCK proteins and inhibits their role in gluconeogenesis and promotes glycogenesis (569), therefore, active FOXO is known to stimulate gluconeogenesis. However, PEPCK converts oxaloacetate to phosphoenolpyruvate, whilst G6Pase acts to convert glucose-6-phosphate to glucose (outlined in chapter 3, section 3.2.1), both of which are inhibited by insulin in the fed state and stimulated by glucagon during fasting (570). Insulin inhibits the actions of FOXO via the activation of PI3K, PDK-1 and Akt (571), but this does not happen in insulin resistant cells (569) and therefore explains why FOXO is more highly expressed under HF conditions. Furthermore, FOXO can directly interact with C/EBPa (*CEBPA* gene) to drive gene transcription of G6Pase (*G6PC* gene), PEPCK (*PCK1* gene) and ACC and again stimulate

gluconeogenesis (572). Moreover, C/EBPa can induce PPARγ expression, known to be the master regulator of adipogenesis (572), but C/EBP levels are increased in insulin resistant mice (572, 573). Moreover, *PPARGC1A*, coding for protein PGC-1α (peroxisome proliferator-activated receptor γ coactivator 1α) was downregulated for HF versus LF treatment groups, which is known to occur in the presence of MAFLD and insulin resistance and is also shown to regulate the ratio of IRS1 and IRS2 (66-69).

To add to these findings, in this current study, the HF diet fed mice expressed a reduced expression in *CREB*, and *PXR* (pregnane x receptor; *NR1I2* gene: nuclear receptor subfamily 1 group I member 2) in conjunction with *PPARGC1A* (encoding PGC-1α) and a rise in *PCK1* (encoding PEPCK) levels, but not for *G6PC*, when compared to the LF treatment. This data is supported by Li *et al* (2018) (126) in diabetic mice where they expressed raised levels of protein and mRNA levels for PEPCK and G6Pase and a decrease in protein and mRNA levels of CREB and PGC-1α expression. These gene changes can be driven by PXR binding to CREB (cAMP responsive element binding protein) and PGC-1α to suppress gluconeogenic gene activation (*PEPCK* and *G6PC*) (126). Therefore, for the HF diet fed mice in this current study, the lower levels of *PXR*, *PPARGC1A* and *CREB* prevented gene suppression for gluconeogenesis processes such as *PCK1*.

Pyruvate dehydrogenase kinase (PDK) enzymes are also highly important in the gluconeogenesis process, and it has been shown in this study that *PDK2* was more highly expressed and *PDK4* was more lowly expressed in the livers of the HF treatment group when compared to the LF treatment. In the liver PDK inhibits the enzyme 'pyruvate dehydrogenase', that acts to convert pyruvate to acetyl-CoA, and so, insulin acts to inhibit PDK, and when this protein is directly targeted it can partially improve insulin sensitivity in diabetics (574). From all four PDK proteins that are present, the liver expresses highest levels of PDK2 than other variants and its levels have been shown to be higher in the livers of HF diet fed mice in conjunction with a reduction in PDK4 levels (575), which has also been shown in this current study. As a result of the raised PDK2 levels there are spared gluconeogenic substrates for glucose production which can progress to insulin resistant hepatocytes (575).

With regards to MAFLD, it was clear that the HF diet increased the expression levels for several pathways involved in its pathogenesis in this current study, which have been commonly reported by several authors (501-505, 561, 576, 577). Across these studies, there was not a complementary change for specific genes in MAFLD development, but there were similar pathways that were regulated, which was vastly due to the experimental design and model used, where humans have been found to express a different subset of enriched pathways leading to steatosis than mice (561).

The length of dietary intervention is also important, where Teufel *et al* (2016) showed that the length of HF diet feeding in C57BL6/J mice can determine which pathways become upregulated or downregulated over time; where an enrichment of a hepatic pathway could be upregulated after 12-weeks of feeding but then downregulated after 18-weeks of feeding, and vice versa (561). Additionally, Teufel *et al* compared the differences in the hepatic GSEA profile in the livers of humans who either were obese, had MAFLD or had NASH, and in livers from HF diet mice fed for 12-weeks, 18-weeks and 30-weeks (561). As such, Table 5.14 shows a composite table for the pathways that have been found to be enriched in humans and mice from Teufel *et al*'s study in conjunction with being enriched in the hepatic tissue in this current mouse intervention study. A total of 89 KEGG pathways were enriched in both this study for HF vs LF fed mice and in the human and mice livers from the study by Teufel *et al*. A total of 76 out of the 90 KEGG pathways were complementary (upregulated or downregulated) to the human and mice study by Teufel *et al* (561). Pathways highlighted in blue show complementarity to the mouse samples (47 confirmed pathways), whilst pathways highlighted in green show complementarity to both human and mouse samples (30 confirmed pathways), and pathways in red correspond to no pathway crossover between all treatments (13 confirmed pathways) (complementarity refers to the pathways expressed in this current study by HF versus LF fed mice and to those specified by Teufel *et al*). Both this study (60 % kcal fat and 20 % kcal carbohydrates) and the study by Teufel *et al* supplied mice with similar diets, with the exception that Teufel *et* al supplied their carbohydrate source into drinking water rather than the pellets (59 % kcal fat and 26 % kcal carbohydrates); this is therefore a positive indication for the large similarity of enriched pathways between the studies. Although other studies have highlighted several pathways enriched following their treatments, Teufel *et al's* study is the closest study that matches the current study with regards to dietary composition, intervention length and mouse breed and age. Please refer to the results section 5.5.5 for the description of hepatic pathways regulated by HF diets, but overall, they are involved mostly in metabolic processes.

5.6.2 The mechanisms underlying the effects of EC in lowering hepatic DNL and lipogenesis processes to protect against steatosis

In this study, it was evident that EC protected against HF diet induced hepatic steatosis by lowering the expression of genes involved in DNL and gluconeogenesis pathways, and there was also evidence to suggest that 34DHPVL complemented the reduction in gluconeogenesis, but with a much lower effect, and instead increased the expression of DNL genes. These effects will be

discussed in relation to previous evidence for the actions of polyphenols on the aforementioned processes.

Although it was shown that the HF diet lowered the expression of genes involved in DNL when compared to the LF diet, the effects were far greater when EC was supplied into the HF diet. To summarise just a few of the genes changes that arose following EC supplementation into the HF diet, these included the reduction in the expressions of *SREBF*, *G6PC* and *AMPK* and several genes involved in the fatty acid metabolic pathway. As mentioned previously, a reduction in fatty acid metabolism causes a reduction in gluconeogenesis and therefore lowers blood glucose levels and protects against insulin resistant effects. Meanwhile, phosphorylated AMPK (active) is known to be a negative regulator of DNL by inhibiting the expression of ACC, and FASN and reducing the expression of SREBP-1c, in return promoting fatty acid uptake, β-oxidation and downregulating gluconeogenesis (578). However, the presence of MAFLD is shown to reduce hepatic phosphorylated AMPK levels, whilst polyphenols have been reported to upregulate them and thus mitigate liver lipid accumulation (579), as has been shown in this current study and supports the previous findings in chapter 4 for the reduced liver lipid mass for HF+EC mice compared to HF mice. Evidence for when this has been reported to occur by polyphenols and the mechanisms that underlie them, has been previously demonstrated using EGCG, where it was reported to activate AMPK at concentrations of ≤ 1 μM in isolated hepatocytes through the upstream stimulation of Ca^{2+}/calmodulin-dependent protein kinase kinase (CaMKK), which is one of two known mediators of AMPK, and initiated by ROS production (282). In further studies, cocoa polyphenols or EC have been provided as treatments in diabetic cells or animal models to assess DNL and gluconeogenesis (199, 285, 338, 341, 405, 439, 440). As such, it was reported that the treatment of insulin resistant HepG2 cells with either cocoa polyphenols or EC re-activated (phosphorylated) the AMPK and PI3K pathways (341, 405), and in the hepatic tissue of Zucker diabetic fatty (ZDF) rats fed with 10 % cocoa polyphenols (405).

Moreover, both EC and 34DHPVL in this study were shown to reduce the expression of DNL genes *FASN* and *SREBF* in all LF intervention fed mice but not in all HF intervention fed mice. This was most likely because the LF HC interventions caused a much higher expression of DNL genes than the HF diet, and thus the compounds were more effective at counteracting this increase in the LF diet. For *AMPK* expression, only some of their subunits were more highly expressed by both EC and 34DHPVL when supplied into the LF diet, and so it would be more conclusive to assess AMPK at a protein level to determine whether their abundance and activity was affected. Previous reports for the reduction in the expression of genes *FASN* and *SREBF* were shown by EC (20-40 mg/kg body weight)

or 10 % cocoa polyphenols supplemented into ZDF rats and insulin resistant HepG2 cells (10 µM EC) (405).

This current study also revealed a reduction in the expression of gene *SCD-1* by EC in the LF and HF dietary interventions but only in the LF intervention by 34DHPVL. SCD-1 is a rate limiting enzyme for the synthesis of fatty acids (522), and the gene expression changes by EC in this current study are supported by several studies, such as when EGCG was supplemented into the diets of HF fed mice (522), and in EGCG supplemented high fructose fed rats (526) and diabetic mice (126) for a dose dependent reduction in hepatic gene expressions: *SCD-1,* SREBP-1c *(SREBF gene), FASN*, and *PPARG*. The PPARγ protein (encoded by the *PPARG* gene) can drive lipogenic gene transcription including *SREBF*, both of which were decreased in this current study when EC was supplied in combination with the HF diet. In contrast, a further study investigated the effects of green tea extracts (GTE) in genetically obese mice, and found no reductions in hepatic *SREBF, FASN* and *SCD-1* expression, however these same genes were significantly reduced in the adipose tissue of these same mice, however the GTE concentration used was lower than those used in other studies (401).

The addition of either EC or 34DHPVL into the HF diet induced a decreased expression of *FOXO* genes, which was discussed previously to cause a reduction in circulatory glucose concentrations (section 5.6.2). For the *CEBPA* gene, EC and 34DHPVL were only successful in lowering its expression levels when supplemented into the LF diet and not for the HF diet. Therefore, in this current study, EC and 34DHPVL targeted specific genes in the gluconeogenic pathway to reduce glucose production. To continue, the expression of genes *PIK3CD*, *PIK3CG* (isoforms of PI3K) and *AKT1* was reduced in the HF versus LF treatment, and were more highly expressed in all EC and 34DHPVL supplemented diets, but the polyphenols had greater effects on changes in gene expression in the HF diets. This is evidence to support the stimulation of the PI3K/Akt pathway by EC and 34DHPVL, where Akt can directly phosphorylate and inactivate FOXO to reduce the transcription of gluconeogenic genes (569).

The addition of EC into the HF diet also caused an increase in the expression of *PPARGC1A* and in both the HF and LF diets for *CREB* and *PXR*. The regulations of these genes and their impact were briefly mentioned in section 5.6.2, but their increase is reported to slow down gluconeogenesis processes. To add to the aforementioned effects in the changes in expression of these three genes, CREB1 has been previously shown to positively regulate gluconeogenesis by activating PGC-1α (569), in addition to regulating insulin secretion in pancreatic β-cells (580, 581), however, in the liver it is commonly linked to insulin resistance. As CREB also drives the transcription of PEPCK (*PCK1*) and PGC1-α (*PPARGC1A*) (582), which were both seen to be increased in mice who

consumed EC supplemented into HF diets, this could also explain why this group exhibited a rise in blood glucose equal to that of the HF diet fed mice within 15 mins of the GTT, because EC caused an increase in a few gluconeogenic genes. However, the increase in genes for insulin signalling (detailed in section 5.5.6) counteracted the increased glucose production later in the GTT. In contrast, Koyama *et al* (2004) who fed mice a 0.15 % EGCG diet for 7-days discovered that their hepatic mRNA levels for *PEPCK* were significantly reduced, but in keeping with the observations from this current study, their *G6PC* levels were also reduced in the presence of EGCG (527). These results were further reiterated in rat hepatoma cells treated with EGCG via the activation of the PI3K pathway (281), and in a diabetic mouse model through an increase in PXR (pregnane x receptor; *NR1I2* gene: nuclear receptor subfamily 1 group I member 2) protein and mRNA expression levels following EGCG supplementation (126).

This current study reports an increase in the expression of several gluconeogenesis genes when EC and 34DHPVL were supplemented into LF HC diets of mice, which is a result that cannot be explained by this study because polyphenols have been mostly reported to decrease HC diet induced gluconeogenesis (241) and requires further investigation.

Further changes in the expression of gluconeogenic genes in this study following EC supplementation included an increase in *PCK1* levels in both the LF and HF diets and a reduction in *G6PC* (encoding G6Pase) by both EC and 34DHPVL supplementation in the HF treatment groups. These dual action effects suggest that EC may have upstream effects on different signalling pathways. Additionally, this study has shown that the gene *GSK3B*, a subunit of GSK-3 (glycogen synthase kinase 3), had raised expression levels in the HF versus LF treatment, but reduced expression levels following the addition of EC or 34DHPVL into the HF diet; subsequently, this would promote glycogen formation from glucose in the polyphenol supplemented treatment groups. This finding is supported by studies that assessed the hepatic protein levels following EC and cocoa polyphenol treatments in HepG2 cells, where a reduction in PEPCK was observed, accompanied with an increase in GSK-3 phosphorylation levels, thus causing an inhibition of its actions on inhibiting glycogen synthase, i.e. GSK-3 inhibition promotes the synthesis of glycogen (285, 341). In addition, the phosphorylated levels of Akt and AMPK rose with polyphenol addition, which also stimulated the phosphorylation of GSK-3 and the suppression of PEPCK and G6Pase (285). Similarly, when cocoa was supplemented into the diets of ZDF rats, it prevented the inactivation of hepatic glycogen synthase and reduced PEPCK levels and increased glucokinase levels (alike hexokinase but only expressed in the liver for the conversion of glucose to glucose-6-phosphate) (199).

Because HF diet fed mice in this study expressed much higher levels of *PDK2* than LF diet fed mice (discussed in section 5.6.1), it was exciting to discover that when EC was supplemented into the HF and LF diet it caused a reduction in the expression of *PDK2*, whilst 34DHPVL was successful at lowering its levels only in the LF intervention. Ultimately, this change caused by EC would promote the synthesis of fatty acids from glucose precursors and to reduce blood glucose levels (574), which to our knowledge is the first time a catechin has been reported to induce this effect.

In addition, it was highlighted that the starch and sucrose metabolic pathway was upregulated in HF versus LF diet fed mice and decreased following the addition of EC in both the LF and HF diets, and by 34DHPVL in the HF diet. The rise in starch and sucrose metabolism in the HF vs LF diet could be because of the limited carbohydrate content of the diet, and therefore almost all of the carbohydrates that were consumed were directed into the citric acid cycle for acetyl-CoA synthesis, which was another pathway more highly expressed in the HF vs LF treatment. These effects would increase the production of glucose from carbohydrates because it is linked to gluconeogenesis processes.

The effects reported following the supplementation of 34DHPVL in the diets of mice in this study have been briefly covered in this section. However, to summarise its effects, 34DHPVL caused an increase in several DNL genes (section 5.5.8) when combined with the HF diet in mice, and as such this supports the effect for an increase in hepatic lipid build-up, which was reported in chapter 4 (section 4.5.3) following the quantification of liver lipids. Furthermore, although the decrease in the expression of genes for fatty acid metabolism and gluconeogenesis by 34DHPVL in HF diet fed mice did not reach statistical significance, the gene changes supports the physiological evidence found in chapter 3 for the reduction in blood glucose levels when compared to those in HF diet fed mice. For example, the gene *ACOX1* (acyl-CoA oxidase-1) encodes an enzyme that is the rate limiting step for fatty acid β-oxidation (583), and so a reduction in its expression levels would have effects on the production of acetyl-CoA and later on for glucose. In addition, there were modest increases in the expression of genes *PRKAB1*, *PRKAB2*, and *PRKAG2*, which encode the AMPK protein and can stimulate glucose uptake to drive glycolysis and inhibit gluconeogenesis via inhibition of gluconeogenic enzymes, such as ACC (584). Furthermore, there is evidence to suggest increased leptin sensitivity by 34DHPVL in the HF diet of mice which promotes the reduction of gluconeogenesis and stimulation of glycogenesis, as discussed in section 5.6.4.

In summary, this study has shown that EC, and in some cases 34DHPVL, can mitigate gluconeogenic gene transcription events in HF insulin resistant mice and DNL gene transcription events in LF HC fed mice. The data obtained in mice supplemented with EC in their diets supports the existing

literature for how EGCG, cocoa polyphenols, GTE or EC cause changes in the liver transcriptome for gluconeogenesis and DNL, whilst also providing new evidence for gene changes that are more specifically assigned to EC and 34DHPVL. In addition, the gene changes caused by EC when supplemented in HF diet fed mice has supported the findings reported in chapter 3 of this thesis for the reduction in blood glucose levels and hepatic lipid accumulation.

5.6.3 Gene transcription targets for (–)-epicatechin and 3',4'-dihydroxyphenyl-γ-valerolactone in mitigating insulin resistance effects

Previous sections have demonstrated the specific pathways that may impact insulin sensitivity and downstream insulin signalling. These changes will now be discussed, with a particular focus on how the addition of EC or 34DHPVL into HF and LF diets may have caused the physiological changes observed in chapter 3, and how the current literature supports these changes.

Several gene changes were shown to be altered following the addition of EC or 34DHPVL into the HF diet for P53 signalling processes, where the HF compared to LF diet raised the expression of genes involved in this pathway, whereas the addition of EC reversed these effects. P53 signalling is very important in the development of insulin resistance and MAFLD, as shall now be explained. The severity of hepatic steatosis is closely associated to the expression of P53 signalling proteins/genes (585) mostly because of DNA damage and apoptotic stimulation. Reviews by Kung *et al* (2016) (586) and Strycharz *et al* (2017) (587) have summarised the involvement of P53 in metabolic syndrome, which includes the stimulation of gluconeogenic genes (588), and the negative regulation of the IGF-I/Akt pathway (589). This was demonstrated to occur in diabetic mice which exhibited higher expression of the P53 pathway when compared to non-diabetic mice, and subsequently this induced gluconeogenesis that caused a rise in their blood glucose levels and triggered insulin receptor desensitisation to glucose (590). These events are very likely to have occurred here in this current study because the HF versus LF mice had a higher expression of P53 signalling and these mice also presented with high blood glucose levels and high expressions of gluconeogenesis genes, whereas the addition of EC reversed all these effects and 34DHPVL partially reversed them. Moreover, P53 has been reported previously to negatively repress glucose influx through lowering the expression of glucose transporters GLUT1 and GLUT4 (560) and indirectly repressing GLUT3 through a reduction in NF-κB signalling caused by the reduction in glycolysis (591). These changes were also confirmed in this current study where the HF versus LF diet caused a decrease in the expression of genes *NFKB1, NFKB2, SLC2A1* (encodes proteins GLUT1), *SLC2A3* (encodes proteins GLUT3), and *SLC2A4* (encodes proteins GLUT4), but the addition of EC reversed these, and the

addition of 34DHPVL reversed all except for *SLC2A4*. Therefore, both EC and 34DHPVL promoted an increase in the uptake/binding of glucose to the receptors for influx into hepatocytes and reduced its efflux, which would explain the lower glucose levels during the glucose tolerance test in chapter 3. The combination of these changes alongside the reduced expression for some gluconeogenic genes could be sufficient to lower circulatory glucose levels and somewhat counteract the negative effects of insulin resistance. Of course, this is just one theory of mechanism behind this and more functional experimental validation and protein expression data would be required to prove this.

However, when EC and 34DHPVL were combined with the LF diet in mice in this current study, there was an increase in P53 pathway expression. This could be explained by the greater hepatic damage that was seen in mice on the LF diets than the HF diets in chapter 4, where it is understood that stimulation of the P53 pathway is in aid to stimulate repair of damaged tissue via apoptosis to remove damaged cells. These changes have also been reported in previous studies following the treatment of EGCG with damaged hepatocellular carcinoma cell lines (592), as well as in colon cancer (593) and lung cancer cells (594) for an increase in P53 signalling. The evidence reported in this current study supports the notion that EC and 34DHPVL could have protected against the development of hepatocellular carcinoma by raising P53 signalling.

The HF insulin resistant mice in this current study exhibited an increase in the expression of pathways: oxidative phosphorylation, citric acid cycle and fatty acid β-oxidation, when compared to LF diet fed mice. Whereas, the addition of EC into the HF diet reversed all these pathway expressions which are known to be interconnected. The higher expression of the citric acid cycle would re-direct more acetyl-CoA to the mitochondria for oxidative phosphorylation of fatty acids, which in return would raise ROS levels that are associated with the pathogenesis of MAFLD and insulin resistance (595). These aforementioned pathways have also been reported to be more highly expressed in subjects with type-2 diabetes (595-597). Moreover, an increase in fatty acid β-oxidation is commonly linked to an increase in genes encoding PPARα and PPARβ (*PPARA* and *PPARB* respectively), which were also shown to be significantly increased in this current study for the HF vs LF treatment, but were significantly reduced by the addition of EC but not 34DHPVL into the HF diet. A consequence of the high ROS levels produced by these pathway activations in the HF diet provides a negative feedback mechanism to enhance insulin resistance effects, most likely through triggering P53 signalling, known to also feedback and activate β-oxidation, oxidative phosphorylation and gluconeogenesis (587). Thus, all these pathways are strongly linked to the onset of MAFLD and insulin resistance (586) and could be another mechanism explaining how EC protects against their pathogenesis in this current study (please refer to chapter 3 and chapter 4 for the physiological effects seen by EC in mice).

In this current study, the HF diet caused a reduction in the expression of gene *CREB1* compared to the LF diet, and significantly increased the expression of *PPARG*, *NR1H4* (encoding protein FXR) and *CD36*, whereas the addition of EC, but not 34DHPVL, reversed these changes, which is indicative of an improved insulin sensitivity in these mice, as shall now be explained. The expression of CREB has been shown to play pleiotropic roles, where its reduction (598) and increase (599) has been reported to be associated with improved insulin sensitivity, however, this current study supports its increase for improved insulin sensitivity by EC. Phosphorylated CREB is also reported to inhibit PPARγ in the liver (600), and so all of these aforementioned proteins/genes directly or indirectly regulate another, as now described. The mRNA and protein expressions of CD36 levels are associated with hepatic fatty acid uptake which could contribute to hepatic steatosis, as has been shown in this study and also by Liu *et al* (2017) (599) in mice fed the exact same HF diets over an almost identical study length. And the mRNA and protein expressions for CD36 were seen to be much greater in HF diet fed mice than in mice on LF HC diets in both this study and Liu *et al* (599). CD36 mediated hepatic fatty acid uptake is transcriptionally regulated by PXR, LXR, PPARγ (601) and FXR (602); but Liu *et al* found that PPARγ was responsible for the increase in CD36 (599). They also showed that the addition of the natural polyphenol curcumin into the diets caused a decrease in CD36 expression at both a protein and mRNA level, as well as a decrease in PPARγ and an increase in CREB protein and mRNA levels (599). This process could be translated to the findings in this current study where EC most likely influenced lipid metabolism to limit hepatic fat build-up via eliciting an increase in total and phosphorylated CREB levels, which would cause the inhibition of PPARγ and lower the synthesis of CD36, ultimately causing a reduction in triglyceride synthesis (599). However, because this current study also reports higher expression levels of *NR1H4* (encoding protein *FXR*) in the HF compared to LF diet fed mice, it is not possible to establish whether *CD36* levels were only affected by *PPARG*, or whether it was a combination effect from both *NR1H4* and *PPARG*. Nonetheless, the increase in *CREB1* gene expression levels were associated with improved insulin sensitivity rather than a decreased sensitivity by EC in the HF diet, as indicated by the lower blood glucose levels in chapter 3.

The findings for reduced expression levels of *IGFBP1* and *IGFBP3* have been shown in this study for insulin resistant HF diet versus LF diet fed mice, whereas the addition of EC into the diet caused a significant increase in the expression of *IGFBP1* but a further decrease for *IGFBP3*; this is a normal response when insulin signalling is being restored because IGFBP-1 is mostly regulated by insulin, but is reduced in the presence of insulin resistance (513), and IGFBP-3 can inhibit cytokine induced insulin resistance (514, 515) (please see section 5.2.1 for the roles of IGFBPs). Furthermore, MMP-7 is reported to degrade IGFBP-3 to promote IGF-I binding to the insulin receptors and enhance

insulin signalling (516), and *MMP7* levels were largely reduced in this current study for HF diet fed mice when compared to LF diet fed mice, but their levels were only modestly increased when EC was supplemented into the HF diet but more highly expressed when supplemented into LF diet fed mice. It is not possible to identify why this occurred without having assessed protein expression levels for MMPs and TIMPs (tissue inhibitor of metalloproteinase), but it could be linked to extracellular matrix (ECM) remodelling in the liver or further downstream effects such as IGFBP degradation. The only case where MMP-7 levels were reported to increase following EGCG addition, was in colorectal cancer cells through the activation of JNK1/2 and c-JUN (AP-1) (603). Because the expression levels of *JUN* were also shown to be increased in this current study by EC when supplemented in HF diets of mice, this could explain why *MMP7* levels were raised.

For gene changes that are directly involved in the insulin signalling pathway and seen in this current study, included an increase in the expression of genes *IRS2, PI3K, AKT*, and *MAPK*, and a decrease in *PRKCA* (PKC-α protein) only following the supplementation of EC and occasionally 34DHPVL into the HF diet and compared to HF diet fed mice. These results imply a greater insulin sensitivity in the livers of mice following supplementation of the HF diet with EC and 34DHPVL, and it would explain why both groups exhibited lower glucose levels during the glucose tolerance test (as described in chapter 3). For a comparison of these changes to the literature, it has been reported that EGCG can inhibit PKC, an inhibitory protein of the insulin receptor (IR) (525), and that EC and cocoa polyphenols stimulated IR, IRS-1, IRS-2 and proteins in the PI3K/Akt pathway when treated in insulin resistant HepG2 cells (285, 341) (described in more detail in section 5.2.2).

Finally, chapter 3 of this thesis reported significantly higher blood insulin levels in 34DHPVL supplemented HF diet fed mice and it discussed this against a plausible scenario of impaired hepatic clearance of insulin rather than hypersecretion. To identify whether there was any evidence from the RNA-seq data for this, the gene *CEACAM1* (CEA cell adhesion molecule 1) was assessed and it was shown to exhibit a lower expression in HF+34DHPVL and HF treatment groups when compared to HF and LF treatment groups, respectively; but the effects were stronger when 34DHPVL was present. Although the changes were not significant, it could possibly explain the significantly higher levels of blood insulin in the 34DHPVL combined with HF diet fed mice (chapter 3). Because the liver is the main site for insulin degradation (604, 605) and CEACAM1 mediates insulin degradation by binding to and internalising the insulin bound insulin receptor for enzymatic degradation (357, 358), it can provide an indirect measure for hepatic insulin clearance. It is understood that obesity and type-2 diabetes are associated with a reduced hepatic clearance of insulin (358), and that there is an association between hepatic fat concentration and impaired insulin clearance (358, 364) (discussed in chapter 4), and so the reduction in *CEACAM1* expression in this study supports the

phenotypical observations in the mice. However, this study also showed a higher expression of *CEACAM1* in HF+EC versus HF mice, which suggests that this group would be more responsive to insulin bound receptors for internalisation and degradation. To confirm if insulin degradation was really affected by the different dietary interventions in this study, more tests would be required as outlined in chapter 4, but the differential expression data has provided a valuable start to generate hypotheses for future experiments

Overall, this study has shown that EC mitigates HF diet induced insulin resistance and MAFLD, which was shown by increases in the expressions of genes directly linked to insulin signalling and the PI3K/Akt pathway as well as for other metabolic genes and pathways. This therefore highlights the protective effects of EC on transcriptomic changes caused by HF diets and is currently the first study to have assessed gene expression changes by EC at an RNA-seq level. Moreover, this current study provides evidence for modest protective effects of 34DHPVL against HF diet induced insulin resistance by causing changes in the expression of genes involved in insulin signalling and indirectly via gluconeogenesis, leptin metabolism (discussed in section 5.6.4) and the citrate cycle. Although the changes in the expressions of genes caused by 34DHPVL were not as strong as those caused by EC, it does support the physiological reductions in blood glucose levels following glucose challenge in HF+34DHPVL fed mice in comparison to HF fed mice. Therefore, 34DHPVL could be partly responsible for mitigating the insulin resistant effects as a metabolite of EC, but it is not responsible for the mitigation of MAFLD in the mice livers. Again, this is the first study of its kind to investigate the effects of 34DHPVL in an *in-vivo* model of insulin resistance, as such, the gene expression data is invaluable for hypothesis generating and designing future experiments with this compound.

5.6.4 Does 3',4'-dihydroxypenyl-y-valerolactone improve leptin sensitivity to aid the lowering of blood glucose levels in high fat diet fed mice?

Leptin is an important regulator of food intake, energy homeostasis and glucose metabolism and its effects depend on its binding to the leptin receptor (LEPR). In the liver, leptin enhances glycogen storage and inhibits gluconeogenesis, but it also has critical regulatory effects in the hypothalamus (606). In chapter 3, it was demonstrated that 34DHPVL drastically increased the levels of insulin in HF diet fed mice and caused the lowering of glucose levels compared to HF fed controls. The rise in insulin could be because of hypersecretion or impaired clearance, but 34DHPVL may affect pathways independent of insulin for the glucose lowering effects. Although leptin levels were not measured in this current study, there was evidence for a significant reduction in the expression of *LEPR* in the HF versus LF diet fed mice. Lower levels of LEPR and increased circulatory leptin levels

are regularly reported in obesity (607, 608). The increased leptin levels act to decrease appetite and increase satiety (607), the effects of which cause leptin resistance. A reduced response to leptin stimulates hepatic DNL and an increase in gluconeogenesis (609). This current study shows that EC and 34DHPVL supplementation into the HF diet and compared to HF controls caused a modest increase in the expression of the *LEPR* gene. It cannot be established whether this was also associated with changes in leptin levels without having investigated this, but it could imply greater sensitivity to leptin.

Leptin is reported to increase insulin sensitivity in subjects with type-2 diabetes and lower gluconeogenesis to favour a reduction in blood glucose independently of blood insulin levels (610-612). Leptin regulates insulin levels in a dual hormonal feedback loop mechanism (adipoinsular axis), i.e. high leptin lowers insulin secretion, and insulin stimulates leptin production in adipocytes. Leptin signals through the JAK/STAT (primarily JAK2/STAT3) pathway to stimulate Akt/PI3K to promote insulin signalling, and STAT3 also suppresses the expression of gluconeogenic genes (613). Alongside the marginal increases in *LEPR* expression in this current study for EC and 34DHPVL supplemented HF diet fed mice, was the increase in *STAT3* expression, and the decrease in the leptin signalling inhibitor, *SOCS3* (613, 614) for 34DHPVL but not EC supplemented HF diet fed mice. In fact, there were rises in *SOCS3* expression levels in the presence of EC, when compared to HF control fed mice. The lowering of *SOCS3* expression in 34DHPVL supplemented HF diet fed mice could explain why there was an increase in several cytokine genes by 34DHPVL in the HF diet (namely *TNFA* and interleukin genes variants: *CXCL*) because it suppresses their expression under inflammatory conditions (615). These changes would favour an increase in leptin signalling in 34DHPVL supplemented HF diet fed mice, more so than in the EC supplemented diets, which consequently could contribute to explaining the lower glucose levels in the mice during the fasted glucose challenge.

Although the high insulin levels in mice on 34DHPVL supplemented HF diets cannot be clarified from the data in this study, if it occurred via hypersecretion by the pancreas, then this could possibly be explained by higher leptin levels, because leptin promotes insulin secretion, and because the mice appeared to have a better sensitivity to leptin (from the gene expression changes) which would increase the uptake of glucose into the liver for glycogenesis. Furthermore, higher leptin levels can also increase adipose lipolysis which consequently could increase hepatic steatosis through the higher uptake of FFAs (616, 617). This could also be another mechanism to explain how 34DHPVL increased the hepatic lipid content in HF mice when compared to HF controls.

5.6.5 The effects of low-fat high-carbohydrate diets on hepatic fibrosis

It has been discussed previously in chapter 4, section 4.6.3, the effects of high carbohydrate diets and the induction of liver fibrosis and DNL. Therefore, this section will discuss in more detail the possible pathways and gene changes affected by the LF HC diets and how it may explain the phenotypical changes observed and discussed in chapters 3 and 4.

In this current study, it was clear that the LF HC diet induced DNL more strongly than the HF diet in mice (as discussed in section 5.6.1), and the effects of this are understood to induce hepatic fibrosis more strongly, which was shown by visual observation of the LF HC fed mice hepatic tissues (chapter 4) and also confirmed here for gene expression changes. Gene expressions that are reported to be linked to the development of fibrosis involve those in the TGFβ-BMP-SMAD pathway (618), and it was identified that the transcriptional events for a large selection of genes in this pathway were more highly expressed by the mice on the LF HC diet than the HF diet in this study (section 5.5.7). Some of these gene changes will now be explained with explanation to their contribution to fibrosis, specifically with regards to the TBFβ-BMP-SMAD pathway. In the presence of liver damage, hepatic stellate cells (HSCs) are activated to initiate repair processes and it does so via the synthesis of TGF-β (618). It was clear that TGF-β transcription levels were higher in the LF mice than the HF mice in this study because there was higher expression levels of genes *TGFB1*, *TGFB2* and *TGFB3*. The TGF-β protein then binds to initiate the phosphorylation of SMAD2 and SMAD3 proteins that now bind to SMAD4 and translocate to the nucleus to activate gene transcription for the production of extracellular matrix proteins, like α-smooth muscle actin (αSMA, *ACTA2* gene) and type-I collagen (*COL1A1*) (618), both of which were expressed at much higher levels in the LF mice in this study compared to HF diet fed mice. Furthermore, the LF fed mice in this study showed lower expression levels of *SMAD2* and higher levels of *SMAD3* and *SMAD4* compared to HF diet fed mice. These changes can be explained because SMAD3 phosphorylation is crucial for activating gene transcription and is pro-fibrogenic (619), where its inhibition inhibits type-I collagen production, whereas SMAD2 has been shown to be anti-fibrogenic where its upregulation promotes HSC apoptosis and its decrease further promotes collagen production (620). An additional role of TGF-β1 in supporting fibrosis development is to suppress MMP activity and thereby inhibit ECM degradation (621). Alternatively, the BMP pathway can be activated to stimulate ECM gene transcription, and in this study the genes for *BMP2-6* were more highly expressed in the LF diet compared to the HF diet, further supporting fibrosis development. However, BMP proteins signal through the downstream activation of SMAD1, SMAD5 and SMAD8 proteins (622), but only *SMAD1* was more highly expressed in this current study.

Further genes that are involved in the development of fibrosis and were shown to be more highly expressed in the LF versus HF diet includes *EGFR* and *VEGFA*. This is because EGFs are known to bind to its receptor EGFR and stimulate the proliferation and migration of hepatic stellate cells (HSC), and subsequently the deposition of ECM (623). Whereas, VEGF is known for its role in being pro-angiogenic, where angiogenesis has been shown to be a pre-requisite for MAFLD and fibrosis (624, 625), in addition, VEGF supports the proliferation of HSC's.

In addition, the genes *SEL1L3*, and *LOXL1* were more highly expressed in the LF versus HF diet fed mice in this study, and *APOF* and *HORMAD2* were more lowly expressed. The expression of genes *HORMAD2* and *APOF* have also been reported by Ryaboshapkina and Hammer (2017) to be decreased in cases of increasing hepatic fibrosis severity, in addition to increased expression levels of *LOXL1* (503), previously shown to stimulate TGF-βI induced ECM deposition (626), and its inhibition retarded liver fibrosis (627). Additionally, the expression of *SEL1L3* has been reported to increase with fibrosis severity and is associated with hepatic ballooning (503). This is further evidence supporting the ideology that the LF HC diet induced hepatic fibrosis more strongly than the HF diet in mice in this study.

5.6.6 How (–)-epicatechin protected against high-fat but not high-carbohydrate diet induced TGF-β activation for fibrosis

HF fed diets and insulin resistance have been shown to induce an increase in TGF-β signalling through upregulation of TGF-β1 (628). Despite the LF HC diet having induced fibrotic genes more strongly than the HF diet, the protective effects were seen by EC when supplemented into the HF diet for the reversal of fibrotic genes, which is suggestive that EC can protect against HF diet induced hepatic fibrosis, as shall now be discussed.

In this study, it was observed that EC supplemented HF diet and compared to HF diet fed mice caused a reduction in the differential expression for genes *TGFB1* (TGF-βI), *TGFB2* (TGF-βII), *SMAD2-5*, *COL1A1* (type-I collagen) and increased the expression for *NFKB1* (NF-κB), *NFKB2* (NF-κB), *AKT1*, *PIK3CB* (PI3K), *PIK3CD* (PI3K), *PIK3CG* (PI3K), and *JUN* (AP-1) but not for *NRF2*. This supports the evidence reported by previous authors with regards to the effects of EC stimulating the PI3K/Akt and NF-κB pathways, but this is new evidence to indicate that EC can reduce TGF-β/SMAD and type-I collagen transcriptional events. Furthermore, this study showed that these gene changes caused by EC in the HF diet marginally reversed the expression of the KEGG TGF-β signalling pathway. These observations are consistent with previous findings *in-vitro* where EC (10 μM) caused an increase in

pathway expressions for NF-κB (528), PI3K/Akt (528, 529), ERK (529), AP-1 and NRF2 (528) in HepG2 cells. These specific gene changes caused by EC were shown to arise by (1) rises in IKK (IκB kinase) and phosphorylated IκBα stimulated NF-κB, where the absence of IKK caused extensive liver damage due to apoptosis (528); (2) EC counteracted the rise in ROS levels and stimulated cell survival/proliferation through the PI3K/Akt pathway (528, 529), along with the sustained enhancement of the AP-1 transcription factor (c-JUN gene) (528), which is known to trigger apoptosis in damaged cells, and their survival/proliferation in capable cells, and low ROS stimulated NRF2 for cell survival functions (528). Overall, these pathways have been shown to retard fibrosis development.

There are several other studies that support the changes in the expression of fibrotic genes by EC when supplemented into HF diets in mice in this current study, and also provides evidence for changes in protein levels; although protein levels were not assessed in this study, the transcript levels can suggest a level of protein expression. Xiao *et al* (2012) investigated the effects of EGCG (50 mg/kg body weight) on hepatic fibrosis in HF diet fed rats for 8-weeks and found that EGCG counteracted the HF diet induced rise in active protein expression in the TGFβ-SMAD pathway for SMAD2, SMAD4, FOXO1, and NF-κB active levels and counteracted the decrease in PI3K and Akt active levels, which subsequently caused a reduction in α-SMA deposits (477). In addition, EGCG has been reported to lower the expression of genes encoding proteins TNF-α, IL-1β, TGF-βI, MMP-9, α-SMA and COL1A1, and suppressed the phosphorylation of SMAD2 and SMAD3 in a fibrotic rat model and in HSCs (523). Moreover, EGCG and ECG have also been shown to dose dependently inhibit the production of type-I collagen as well as collagenase activity (MMP-1) in HSCs at a protein level whilst also transcriptionally increasing type-I collagen (*COL1A1*) and *TIMP1* and reducing *MMP1* (524) and *EGFR* (579). Similar changes were also shown by GTE in rats (519, 536). These studies therefore highlight the similar effects that both EC and EGCG had on hepatic pathway activation, specifically for PI3K/Akt and NF-κB stimulation and for the repression of TGFβ-SMAD signalling.

In this study, the inclusion of EC and 34DHPVL into the HF and LF diet was able to increase differential gene expression for *HORMAD2*, which was mentioned in section 5.6.5 to be associated with the severity of hepatic fibrosis (503). However, the role HORMAD2 plays in the liver has not been investigated previously and there are no known effects of green tea polyphenols or catechins on altering the expression levels of this gene or of *APOF*, *LOXL1* and *SEL1L3*. Thus, this would be interesting to investigate further, particularly as their expressions are altered in MAFLD and with fibrosis severity.

Furthermore, in this study, EC significantly upregulated the ribosome KEGG pathway in the HF diet, which has also been shown to occur by EGCG in a previous study (557), because the ribosome pathway is involved in protecting the liver through cell cycle progression and responding to DNA damage, whereas MAFLD commonly causes a depression in the ribosome pathway to induce apoptosis and cell death (500, 557).

In summary, the LF HC diet induced differential gene expression changes in favour of the development of liver fibrosis, more strongly than the HF diet, by significantly increasing the expression of genes involved in the TGF-β/SMAD pathway and subsequent ECM genes for type-I collagen and α-SMA, as well as other fibrosis linked gene changes. In this study, we have shown that EC supplementation in the LF and HF diet can cause changes in the expression of genes that favour the mitigation of fibrosis via a reduction in TGF-β/SMAD pathway and an increase in PI3K/Akt and NF-κB pathway related genes, which causes a reduction in apoptosis and promotes cell survival/proliferation and ROS scavenging (although these effects did not always reach statistical significance). This study also reports similar effects following dietary supplementation of 34DHPVL, however, the effects were seen to be stronger in the LF diet than the HF diet.

5.6.7 Summary – bringing everything together

This discussion has explained the evidence for the changes in the expression of hepatic genes following each dietary treatment with reference to the literature for how flavanols and their food extracts have caused changes in the expression of hepatic genes. This will now be summarised with the aid of Figures 5.8 and 5.9 to understand how the major pathways are interlinked.

In the fed-state, the liver should respond metabolically as depicted in Figure 5.8, with a clear influx of glucose that then enters glycolysis for pyruvate production or glycogenesis to produce glycogen. Pyruvate then forms acetyl-CoA that enters the citric acid cycle or is directed to fatty acid biosynthesis and triglyceride formation (lipogenesis). In the presence of a LF HC diet there was a much higher expression of fatty acid biosynthesis and DNL than the HF diet because of the high concentration of carbohydrates that reached the liver, which can also induce hepatic damage and high circulatory lipid concentrations. When EC or 34DHPVL was combined with the LF diet there was an increase in gluconeogenesis, fatty acid metabolism, and a reduction in oxidative phosphorylation, DNL and citric acid cycle pathways; these favour an increase in glucose production and a decrease in lipid production.

However, during insulin resistance, the liver is unresponsive to insulin in lowering glucose levels following food consumption, and instead can stimulate gluconeogenesis to continue the production of glucose. This was mainly how the HF diet compared to the LF diet acted in mice in this study, as demonstrated by Figure 5.9. For this there was an increase in fatty acid metabolism, citric acid cycle, oxidative phosphorylation, amino acid metabolism and gluconeogenesis pathways, which all favour glucose production. Moreover, there was an increase in P53 signalling which can drive gluconeogenic genes (588) and suppress insulin signalling (589), and a decrease in PPAR signalling which can regulate fatty acid uptake and β-oxidation (629), and there was a decrease in the ribosome pathway which is inversely linked to the P53 signalling for a reduction in glycolysis (630), and there was a reduction in insulin signalling. However, the supplementation of EC and 34DHPVL to the HF diet reversed nearly all these processes, and favours the reduction of blood glucose levels seen in the mice in chapter 3, because they were more insulin sensitive and exhibited a reduction in the expression of pathways that drive gluconeogenesis. EC was more effective than 34DHPVL in counteracting the HF diet induced pathway changes. All these events are summarised in Figures 5.8 and 5.9 and illustrates how the pathways are interlinked, Figure 5.9 also shows in detail the citric acid cycle and where the amino acids enter for their metabolism.

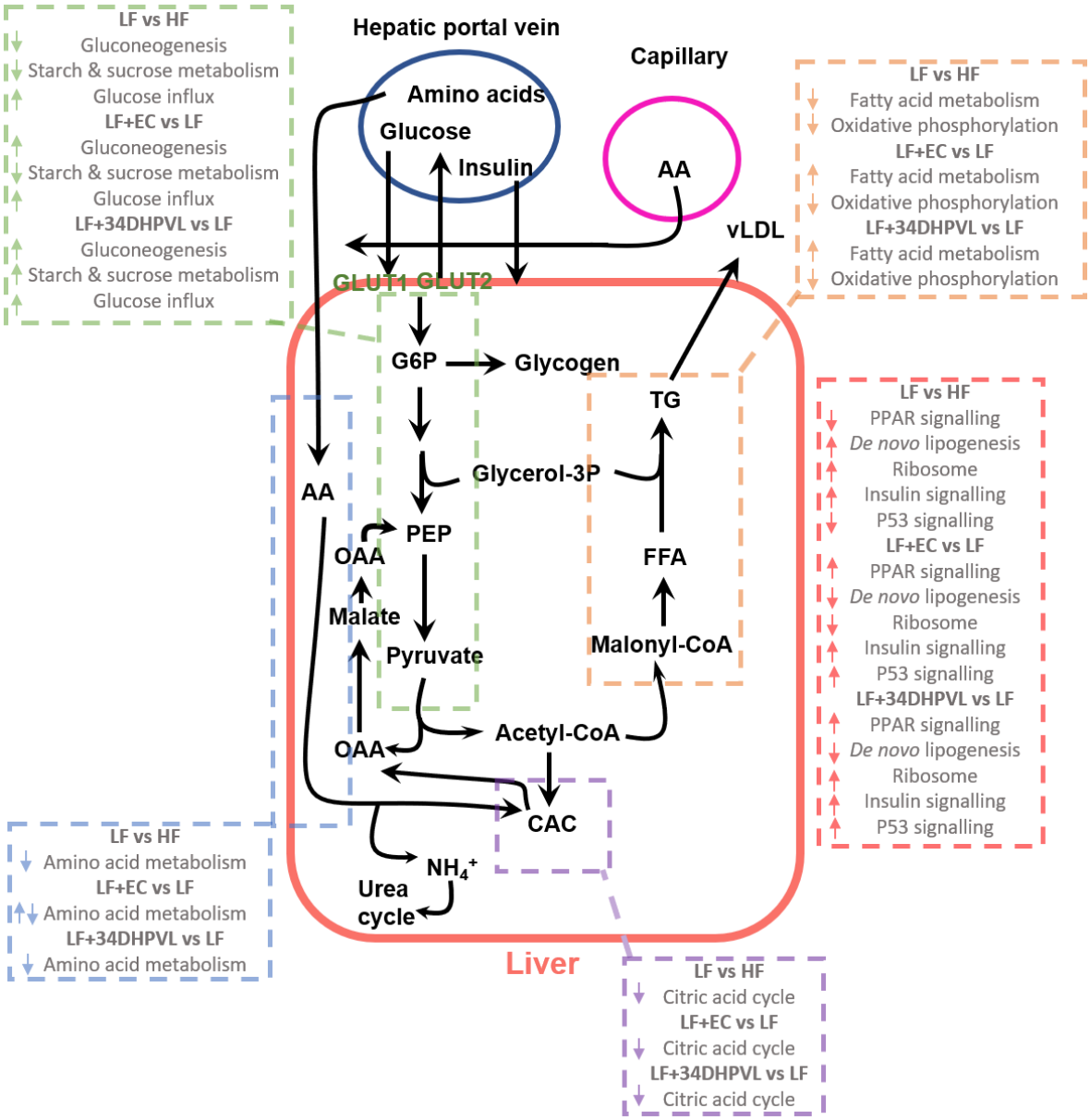

Figure 5.8: Liver metabolism in the well-fed state

Hormones and fuels in the hepatic portal vein are directly delivered to the liver to stimulate processes for glycolysis, glycogenesis, fatty acid biosynthesis and lipogenesis. The hepatic pathway changes that all link to this process are highlighted for the LF versus HF, LF+EC versus LF, and LF+34DHPVL versus LF dietary fed mice, where the dashed boxes indicate where those respective pathways are. AA: amino acids; G6P: glucose-6-phosphate; PEP: phosphoenolpyruvate; OAA: oxaloacetate; CAC, citric acid cycle; FFA: free-fatty acids; TG: triglycerides; vLDL: very-low-density lipoprotein.

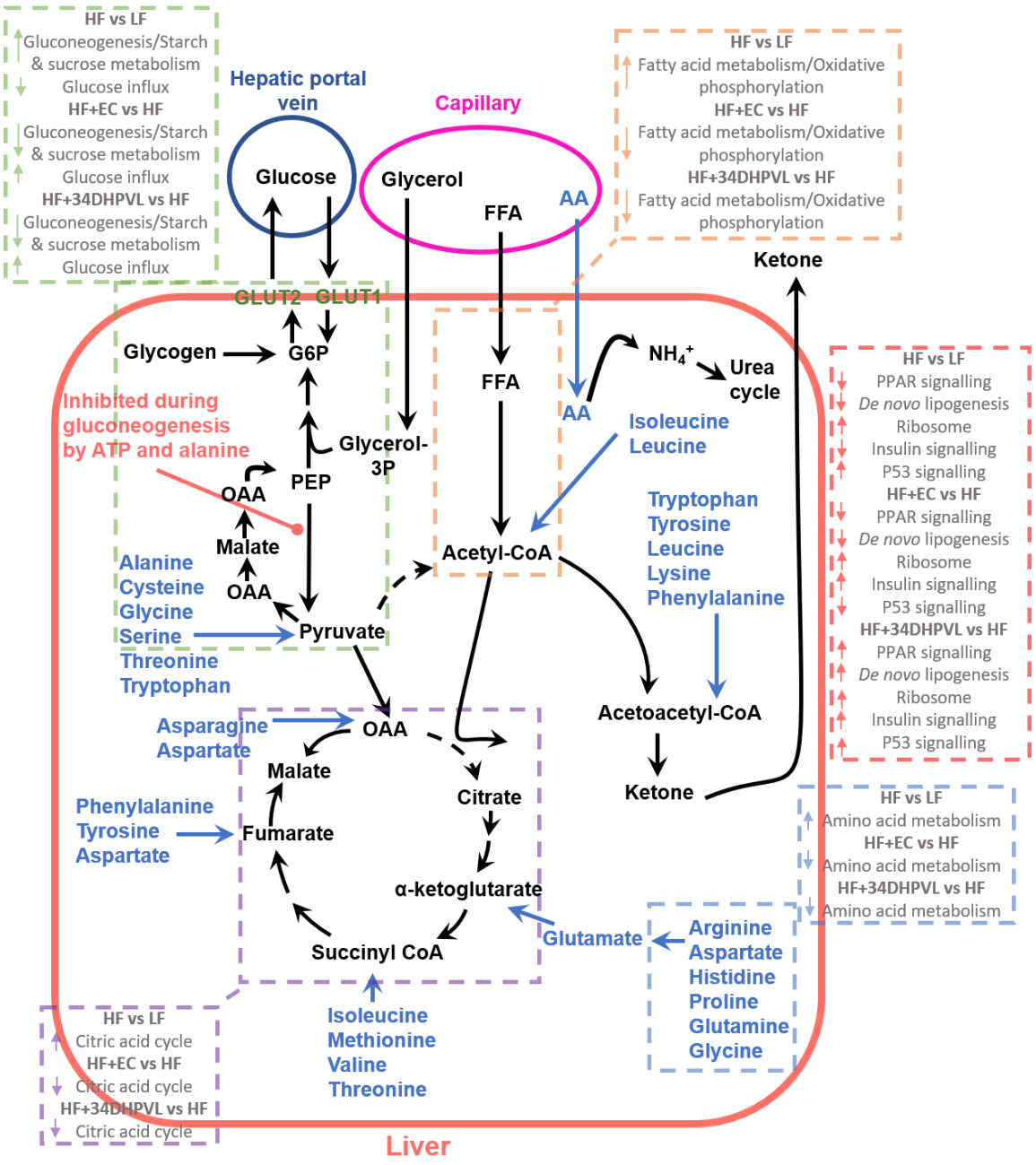

Figure 5.9: Liver metabolism when insulin resistant

Hormones and fuels in the hepatic portal vein are directly delivered to the liver, or from the general circulation (capillaries). Due to insulin resistance, there is a delayed response to insulin in lowering glucose levels, and therefore pathways for fatty acid, pyruvate, amino acid, and starch and sucrose metabolism are increased which stimulate gluconeogenesis for further glucose production. This is highly demonstrated in the HF versus LF treated mice. The hepatic pathway changes that all link to this process are highlighted for the HF versus LF, HF+EC versus HF, and HF+34DHPVL versus HF dietary fed mice, where the dashed boxes indicate where those respective pathways are. Blue text and blue arrows indicate amino acids. AA: amino acids; G6P: glucose-6-phosphate; PEP: phosphoenolpyruvate; OAA: oxaloacetate; CAC, citric acid cycle; FFA: free-fatty acids.

5.7 Conclusion

Data presented in chapters 3 and 4 have aimed to investigate the phenotypical changes of HF diets in mice and their tissues to understand whether there were physiological effects of supplying EC and 34DHPVL into their diets. From this, it was then important to understand how these changes may arise from gene expression changes in the liver, where the liver was selected because: (1) it is a highly metabolic organ, (2) it comes into contact with high concentrations of the polyphenols and their metabolites following pellet consumption, (3) it is affected by HF diets to develop insulin resistance, and (4) it develops MAFLD in mice on the HF diet. The following conclusions can be made in this chapter:

(1) HF diet fed mice that expressed MAFLD and insulin resistance demonstrated a significant increase in the expression of genes in gluconeogenesis and other metabolic pathways for starch and sucrose metabolism, amino acid metabolism, citrate cycle, and oxidative phosphorylation.

(2) EC and sometimes 34DHPVL supplementation into HF diet fed mice was able to reverse these pathway changes and assist the lowering of blood glucose levels and regulate the expression of genes to promote insulin signalling, and thus improve insulin sensitivity.

(3) The LF HC diet induced gene changes for DNL and fibrosis more strongly than the HF diet largely through increasing the expression of genes involved in the TGFβ-BMP-SMAD pathway; and could thus be a stronger driver for the development of hepatocellular carcinoma.

(4) EC was shown to mitigate gene expression changes for fibrosis development and DNL on the LF and HF diets, whilst 34DHPVL exerted similar protective changes for fibrosis development but raised the expression of genes for DNL, explaining why HF+34DHPVL fed mice exhibited a higher average concentration of liver lipids.

Overall, there is sufficient evidence from this dietary intervention study to conclude that EC protects the liver from damage induced by HC and HF diets and protects the liver from the development of MAFLD and insulin resistance through a reduction in hepatic lipogenesis and an increase in insulin signalling processes, respectively. The evidence obtained for 34DHPVL is more modest, where its inclusion in the HF diet was associated with an increase in hepatic lipogenesis but a decrease in circulating glucose through reduced gluconeogenesis, whilst there is some evidence to suggest improved insulin signalling responses in the livers of the mice. More experimental research would be required to understand the exact mechanisms of action for

34DHPVL in order to collate enough evidence to understand whether it protects against HF diet induced insulin resistance.

Chapter Six

GENERAL DISCUSSION AND FURTHER RESEARCH RECOMMENDATIONS

Chapter 6: General Discussion and further research recommendations

6.1 Summary of main findings

The purpose of the four methods and results chapters in this thesis were to investigate the following main aims (1) assess the pharmacokinetics of hydroxyphenyl-γ-valerolactones (HPVL) in plasma and urine over 24-hours when provided as an oral dose in mice, (2) investigate the physiological and phenotypical effects of (−)-epicatechin (EC) and 3',4'-dihydroxyphenyl-γ-valerolactone (34DHPVL) when supplied in combination with a high-fat (HF) diet in a mouse model of high-fat diet induced insulin resistance and metabolic associated fatty liver disease (MAFLD), and (3) explore the hepatic gene expression changes induced by EC and 34DHPVL in HF diet fed mice to understand the mechanisms that underly their protective effects against HF diet induced hepatic insulin resistance and MAFLD. The main findings from these investigations include the following points:

1. When HPVLs were provided as an oral dose in mice, they were rapidly absorbed and substantially conjugated to phase-II metabolites and were still detectable at 24-hours (the end of the study).
2. EC supplemented into HF diets in mice mitigated HF diet induced insulin resistance, MAFLD, body weight gain and steatosis. EC was also successful in reversing the expression of several genes involved in the progression of liver fibrosis in both the HF and LF diets when compared to their respective controls. Finally, EC raised the expressions of hepatic genes involved in insulin signalling and reduced the expressions of genes involved in gluconeogenesis, consequently causing a more efficient reduction in blood glucose levels than HF diet fed mice.
3. The main effects observed for 34DHPVL supplemented into HF diets in mice were to improve fasting glucose concentrations, raise blood insulin levels, increase liver lipids in line with rises in blood insulin, increase hepatic *de novo* lipogenesis (DNL), and increase the expressions of hepatic genes involved in insulin signalling and for leptin signalling and reduced the expressions of genes involved in fibrosis and gluconeogenesis, which all support the observations for lower blood glucose levels. However, 34DHPVL did not mitigate against HF diet induced body weight gain and did not alter the profile of plasma lipids. Evidence from the intervention suggests an impaired hepatic insulin clearance rather than hypersecretion to explain the high blood insulin levels.

4. Mice fed a 60 % kcal diet from fat exhibited observational changes that were consistent with the literature compared to mice fed a 10 % kcal diet from fat, for the following: significant gain in body weight, development of insulin resistance, significantly higher plasma cholesterol and low-density lipoproteins (LDL), and hepatic gluconeogenesis. However, they also exhibited higher levels of plasma high-density lipoproteins (HDL) than LF fed mice.
5. The overall level of hepatic damage was higher in mice on the LF compared to the HF diet, which corresponded with an increase in hepatic DNL and pathways involved in extracellular matrix production.

The following sections in this chapter are to discuss the novelty and wider importance of the research presented in this thesis and to make some recommendations for future work.

6.2 Developing evidence that hydroxyphenyl-γ-valerolactones are bioactive

It is clear in this thesis and from previous publications (127, 128, 130) that EC supplemented into the diets of HF diet fed mice mitigated HF diet induced body weight gain and insulin resistance, and the data presented here supports that reported in previous publications. But this thesis has helped to answer whether the structurally related EC metabolites (SREMs) or whether the colonic ring fission metabolites (RFMs) are responsible for inducing the protective effects seen by EC consumption. The ingestion of EC gives rise to both SREMs and RFMs, whilst the ingestion of HPVLs, and in this case 34DHPVL will only give rise to RFMs and its conjugates, and so, this thesis has isolated a fraction of EC metabolites and investigated these in mice.

To identify whether HPVLs possess bioactive properties, this thesis looked to compare the effects of 34DHPVL against those reported for EC following their consumption in mice for the following: (1) establish whether 34DHPVL caused the previously reported reductions by EC for weight gain and insulin resistance in mice fed HF diets, (2) assess the effects of 34DHPVL dietary supplementation on liver histology and liver biomarkers related to MAFLD for steatosis and fibrosis, and (3) assess the effects of 34DHPVL dietary supplementation on global hepatic gene expression via genome-wide transcriptomics.

6.2.1 Do hydroxyphenyl-γ-valerolactones have biological activities and are they potentially beneficial?

Although, there is an existing body of evidence to support the notion that HPVLs possess bioactive properties (covered in section 1.5 of chapter 1), they have not been investigated for their effects on insulin sensitivity, and so the findings in this thesis are completely novel with regards to the effects induced by HPVLs, in addition to the effects of both EC and HPVLs on hepatic transcriptomic effects at a high-throughput RNA-Sequencing level.

The question for whether HPVLs ameliorate HF-diet induced insulin resistance has been partly answered by the research in this thesis. It has been reported here that the supplementation of 34DHPVL into both HF and LF diets caused an overall reduction in blood glucose levels when compared to their respective controls during a glucose challenge in mice, but this did not reach statistical significance. This was later found to be accompanied by gene and pathway changes that favour a reduction in glucose production and an improvement in insulin signalling responses. This is evidence to support the notion that HPVLs contribute to ameliorating insulin resistance effects, however, the gene and pathway changes were not significantly different to the control treatments possibly due to the high variance in the group, and thus makes it difficult to conclude whether HPVLs exert protective effects. However, there were slight changes in the expressions of genes encoding proteins for rate limiting steps in pathways such as fatty acid metabolism and gluconeogenesis, and this evidence supports the notion that 34DHPVL has a beneficial effect on insulin resistance. Accompanying these changes for 34DHPVL fed mice were higher fasting blood insulin concentrations both prior to and during the glucose challenge, when compared to their controls. Although it was hypothesised that the high insulin concentrations occurred because of impaired hepatic insulin clearance, there was not enough evidence in this thesis to conclude this, and it could be because of high insulin secretion which would not favour the mitigation of insulin resistance. Consequently, there is not enough evidence from the research in these chapters to conclude whether HPVLs contribute to ameliorating HF diet induced insulin resistance, but there is some evidence that they have a modest protective effect.

The power of the dietary intervention study in mice was based on the data reported by Cremonini *et al* (127) and this suggested a power of 60 %, which provided a minimum mouse sample size of 12 per group. However, the changes observed when 34DHPVL was supplemented into the HF diet did not reach statistical significance. If the power of the study were designed at 80 % or more then there could have been greater effects observed by 34DHPVL to cause significant changes from the HF diet in mice.

The research presented in this thesis suggests that structurally related EC metabolites (SREMs) are most likely the metabolic derivates that ameliorate insulin resistance effects following EC consumption, but does not exclude the possibility that ring fission metabolites (RFMs) also contribute, albeit less effectively; see section 6.4 where this is discussed in more detail.

6.3 Evidence to support the biological effects induced by gut-microbiota dependent metabolites derived from flavonoids

This thesis reports some evidence to show that 34DHPVL and its metabolites have biological activities. The evidence from the fasted glucose tolerance test and biomarkers of insulin sensitivity, and from liver tissue histology highlight modest changes by supplementation of HF diet fed mice with 34DHPVL, but the effects were not statistically significant. However, transcriptomic analysis of the liver tissue of mice demonstrated that there were changes in gene expressions by 34DHPVL in HF diet fed mice for metabolic pathways that favour a reduction in insulin resistance and gluconeogenesis, but although these effects were not significant they support the changes observed in the mice throughout the GTT. Overall, these findings suggest that HPVLs may have modest effects on these processes, however, the beneficial effects on insulin-resistance and body weight gain on the HF diet following EC consumption were mostly driven by SREMs. But, is this also the case for other dietary flavonoids, or is there evidence to show that the gut microbiota metabolites of flavonoids are responsible for the beneficial effects associated with their consumption?

Only about a third of humans in Western countries can metabolise the isoflavone daidzein into equol by the gut microbiota, whereas the prevalence is 40-60 % in Asian countries, and so, humans are termed as equol or non-equol producers (631). Although both equol and non-equol producers exhibit microbiota involved in the production of equol, the differences reported for whether or not equol is produced is in the abundance of equol producing gut microbiota (631, 632), and although the exact reasons defining this are not known, it is thought that the regularity and types of soy products consumed (631), as well as genetics, and overall dietary factors contributes to interindividual differences in the conversion of daidzein to equol (633). This is important because there is a strong relationship for positive health benefits for those that can produce equol at high concentrations for positive outcomes in vasomotor symptoms (634), protection against the loss of mineral bone density (635), a reduction in body weight (636), a reduced prostate cancer risk and improvements in biomarkers for cardiovascular health (634). Equol has also been reported to

possess anti-depressant properties (636). Therefore, this is evidence to suggest that metabolites derived from the metabolism of flavonoids by the gut microbiota have stronger bioactive properties than the parent compounds to initiate positive health effects.

Furthermore, daidzein can also be metabolised to *O*-desmethylangolensin (DMA) by the gut microbiota, but DMA is less active than equol (637). Both equol and DMA are otherwise known as non-steroidal oestrogens for their high binding affinity to the oestrogen receptor (638-640) and consequently have been used to alleviate the symptoms of menopause (641). *In-vitro* studies with these metabolites have revealed strong anti-cancer effects such as the inhibition of cancer cell proliferation and migration and the promotion of cancer cell apoptosis (640, 642-644), in addition to exhibiting strong anti-inflammatory activities including the inhibition of iNOS and activation of eNOS (645-647). Very similar effects have been reported to be elicited by urolithins, which are catabolites of ellagitannins, and enterolactones and enterodiols, which are catabolites of lignans, and all exhibit similar bioactive properties to those of equol and DMA for oestrogen receptor binding, anti-inflammatory activity and inhibition of cancer cell development (648-655). However, the concentrations of catabolites produced and the strength of these beneficial effects is very much dependent on the age of the individual and their gut microbiotic signature (656, 657), for example, humans are split into three different urolithin producing metabotypes: non-producers, urolithin B producers, and urolithin A producers, and the health benefits differ considerably between these groups following ellagitannin consumption (658).

Complex polyphenols such as anthocyanins and procyanidins are metabolised by the gut microbiota to form metabolites such as protocatechuic acid (PCA). The biological effects of PCA are stronger than the effects of its parent compounds *in-vitro*, such as cyanidin glycoside, and is more physiologically relevant because substantial levels of PCA are produced *in-vivo* (659). PCA has been reported to possess anti-inflammatory, antioxidant, anticancer and neuroprotective activities as well as protecting against hyperglycaemia and atherosclerosis, as reviewed by Masella *et al* (2012) (660). PCAs anti-atherogenic effects are thought to occur via its anti-inflammatory actions (661), and its anticancer effects due to its antiproliferative and pro-apoptotic actions (660). PCA also possesses anti-apoptotic effects and protects against mitochondrial dysfunction, which is important for protecting against neurodegenerative diseases (660). Moreover, PCAs antihyperglycemic activity has been demonstrated *in-vivo* where its administration (50-200 mg/kg body weight) orally to streptozotocin diabetic rats for 45-days prevented glucose and insulin rises and inhibited gluconeogenic enzyme activation (662).

Carregosa *et al* (2001) reviewed the literature for the biological effects of flavonoid colonic metabolites on neuronal inflammation, and to briefly summarise, benzoic acids, cinnamic acids, phenylacetic acids and phenylpropionic acids inhibited lipopolysaccharide induced inflammatory activation for cytokine production such as interleukins, tumour necrosis factor-α, and signalling molecules involved in inflammatory pathway activation, such as p38, MAPK, NF-κB, and others (663). These metabolites could therefore exert similar protective effects in other tissues of the body.

There are some metabolic derivatives of flavonoids that exert pleiotropic effects, such as 3,4-dihydroxyphenylacetic acid which is a metabolite of quercetin and rutin, where it has been reported to possess anticancer (664, 665), anti-inflammatory (666), cardioprotective (664) and neuroprotective properties (667), however, it can also inhibit mitochondrial respiration and lead to mitochondrial dysfunction in the presence of NO radicals, which could contribute to the onset of Parkinson's disease (668, 669).

Overall, bacterial derived flavonoid metabolites possess bioactive properties that can protect against disease progression and onset, but the level of protection is very much concentration dependent and treatments on *in-vitro* models should look to use physiological concentrations to reflect those produced via the gut following food consumption.

6.4 Structurally related (−)-epicatechin metabolites are responsible for ameliorating high-fat diet induced weight gain

This thesis has reported evidence that when EC is supplemented into HF diets it mitigates HF diet induced body weight gain and liver weight gain, where the body weight was seen to be reduced by the reduction in epididymal fat mass, and liver weight was reduced because body weight was lowered. Following the consumption of EC, its metabolism and catabolism gives rise to SREMs and RFMs, where the effects on body weight could be attributed to each or both groups of metabolites. And so, by feeding mice 34DHPVL directly, this removed the production of SREMs in the mice, and allowed for the complete production of RFMs and its conjugates to identify whether they contributed to the protection against weight gain. The results of this showed that the supplementation of 34DHPVL into the HF diets of mice had no effect on preventing HF diet induced weight gain, and consequently this suggests that EC SREMs mediated protection and not RFMs. In fact, it was observed that 34DHPVL caused an increase in liver steatosis as determined by the isolation and quantification of liver lipids which was in direct correlation with the concentration

under the pharmacokinetic curve of blood insulin levels. This finding was discussed in chapter 4 of this thesis with relevance to the literature for explanation, but it supports the gene changes for an induction of DNL processes in 34DHPVL supplemented into HF diet fed mice and compared to HF controls.

Section 6.5 discusses how mouse models could be designed to identify whether SREMs are responsible for mitigating HF diet induced insulin resistance, but it should be recognised that there are very limited *in-vivo* and *in-vitro* models that use EC conjugates (SREMs) because they are extremely difficult and expensive to synthesise and are not available commercially (348, 670).

6.5 Performing studies to identify whether structurally related (−)-epicatechin metabolites are bioprotective against insulin resistance

The findings in this thesis provide modest evidence to support an effect of HPVLs for protection against HF diet-induced insulin resistance, but no evidence that they protect against HF diet induced body weight gain, and therefore EC SREMs most likely contribute to the physiological changes seen following EC consumption. This also makes it interesting to query whether the physiological changes induced by EC following its consumption would be greater in ameliorating insulin resistance if the production of RFMs and HPVLs were limited (and in doing so the absorption of EC would be maximised). But to fully investigate this, different animal models would be required as detailed below.

Because ECs give rise to SREMS and RFMs, a study would need to be performed that completely prevented the production of RFMs from EC, which is somewhat difficult to perform. To do this, there could be two approaches used, first a germ-free mouse model, and second an antibiotic treated mouse model. For the former, mice are kept and maintained in a completely sterile environment to avoid exposure to microorganisms and can be used to model mice with the complete absence of microorganisms or for the generation of gnotobiotic mice with specific strains only (671). To generate gnotobiotic mice, it would first need to be identified which colonic microorganisms are involved in the metabolism of EC and its conjugates to produce RFMs. Only then could a mouse model be designed for the absence of those microorganisms. A gnotobiotic mouse model containing no gut microbiota involved in RFM production from EC would only allow for the production of SREMs and for their circulation and excretion, and would not affect other processes performed in the gut by other microbiota species. Subjecting these mice to a dietary

intervention with EC in combination with a HF diet would then allow for the identification of whether SREMs were responsible for ameliorating HF diet induced insulin resistance. However, at present, very few bacterial species are reportedly involved in the production of RFMs and HPVLs specifically (57) but there could be many others. And so, until the full microbiota profile involved in EC catabolism has been identified, this model is not a realistic one, unless the mice were germ-free. However, to maintain germ-free and gnotobiotic mice it is very expensive, labour intensive and it requires the right skills, which can make this model inaccessible to many researchers (671).

Alternatively, an antibiotic treated mouse model could be used which overhauls most of the difficulties associated with maintaining gnotobiotic and germ-free mice. However, one disadvantage includes that antibiotics almost completely deplete the gut microbiota and does not allow for strain specific species to colonise (671). In addition, it is hard to completely eradicate the gut microbiota, so there could still be species present that are involved in EC catabolism. More importantly, antibiotics have been shown to affect glucose tolerance in diabetic mouse models by improving glycaemic control (672), and because this is a primary marker recorded to identify insulin resistance it would be hard to establish if positive changes occurred as a result of EC or the antibiotics in HF diet fed mice. Despite these drawbacks, antibiotics could be used to deplete different members of the gut microbiota with specific functions, for example, vancomycin depletes gram-positive bacteria (671).

Both germ-free and antibiotic mouse models require routine validation for the depletion of bacterial species, of which there are several methods to choose from (671). Nonetheless, the best model that could be used to identify whether SREMs mediate the mitigation of HF diet induced insulin resistance from EC consumption would be the germ-free model, because all bacteria have not currently been identified for their involvement in EC catabolism to be targeted with antibiotics. This would then allow for the identification of whether SREMs provided a greater effect for physiological changes in EC fed mice once the production of RFMs were removed.

Another approach would be to investigate the effects of SREMs in cell culture models of insulin resistance. This would prove to be more beneficial than incubating EC directly with the cells because EC is not absorbed into the circulation of humans unmetabolized, and thus SREM treatments would be physiological and best reflect the *in-vivo* situation. However, as mentioned previously, SREMs are not commercially available and are hard to synthesise which explains why there are very few studies reported ((673) this is one study that incubates SREMs in different cell models to determine their uptake into cells).

6.6 Recommendations for future work

A number of recommendations for future work to clarify whether HPVLs are protective against HF diet induced insulin resistance or have other health-protective biological activities are summarised here.

Firstly, the results reported in this thesis and from previous published reports suggests that the LF high carbohydrate low fibre diet induced hepatic gene expression increases in mice for DNL, which was accompanied by stronger phenotypical and physiological evidence for hepatic fibrosis and lower plasma HDL levels when compared to HF diet fed mice. All of these effects from the LF HC low fibre diet support the notion that this model is not ideal to use as a 'normal' control treatment group (488), because it proves difficult to compare how the HF diet induces changes against the 'normal' physiological and phenotypical displays in mice. Instead, it is recommended that a control 'standard' diet should be used which is not high or low in either carbohydrates or fats, such as the standard SDS diet (RM3, UK) the mice were on prior to their placing on a LF intervention for 2-weeks. This would then provide a better comparison for how the HF diet induces changes from the typical baseline values seen in mice.

Secondly, the glucose tolerance test showed mice that consumed 34DHPVL in combination with the HF diet exhibited significantly higher fasting baseline insulin concentrations than the HF treatment groups. However, it would be of interest to determine whether this occurred because of impaired hepatic insulin clearance or because of insulin hypersecretion by the pancreas which would help identify whether 34DHPVL provided a greater protection against insulin resistance, i.e. mice on diets of 34DHPVL in combination with HF displayed lower blood glucose levels and high insulin because of impaired hepatic insulin clearance would suggest that 34DHPVL protects against HF diet induced insulin resistance, whereas if it was because of hypersecretion of insulin then it could favour a progression of insulin resistance. To determine this, plasma C-peptide levels should be recorded in mice who consume 34DHPVL in combination with the HF diet. Since C-peptides and insulin are released in equimolar amounts by the pancreas, and insulin is only cleared by the liver, it will provide a direct measure to identify whether hepatic insulin clearance or insulin hypersecretion by the pancreas is the cause of the high blood insulin levels (354).

Furthermore, 34DHPVL induced hepatic gene expression changes that favour an increase in leptin sensitivity when supplemented into HF diets of mice. This could provide evidence for the lowering of blood glucose levels in this group independently of insulin. However, blood and tissue leptin levels would also need to have been recorded to confirm whether this was plausible. Moreover, because 34DHPVL also altered the dietary consumption in mice when compared to control

treatments, measuring leptin levels would provide another physiological parameter to confirm whether this occurred because of changes in this satiety hormone.

In future mouse polyphenol interventions that model diabetes and/or insulin resistance, it is recommended to harvest the pancreas and assess protein and gene expression levels of β-receptors and other markers involved in the production and secretion of insulin. This thesis has reported in detail the hepatic gene expression changes from EC and 34DHPVL supplementation in HF diets of mice, which are also publicly available for other scientists to examine further genes of interest, but this study is lacking the assessment of hepatic protein changes and the assessment of the pancreatic tissue for markers involved in insulin resistance/sensitivity. Performing these extra analyses will provide a more detailed account for how EC protects against insulin resistance and whether HPVLs can influence pancreatic protein/gene expressions from a HF diet.

In addition, it may be beneficial to measure bile acid production in future *in-vivo* models with HPVL supplementation, as it is reported that the composition and concentration of bile acids produced can influence hyperglycaemia (674). Bile acids are produced by hepatocytes, and chapter 5 of this thesis has highlighted the effects of 34DHPVL supplementation on gene and pathway expression changes in mice livers, and although we have not investigated the effects of bile acid production, the overall changes in gene expressions could influence the levels and types of bile acids produced by the liver and ultimately influence the regulation of glucose homeostasis (674).

Finally, the models outlined in section 6.5 for either germ-free or gnotobiotic mouse models will allow identification for whether SREMs mediate the bioprotective effects seen from EC consumption because it will remove the production of HPVLs via the gut microbiota.

Overall, the investigation of HPVLs is a new emerging research area with regards to the health benefits that polyphenols and their metabolites can induce. There is evidence to suggest that HPVLs possess bioactive properties, and this thesis has highlighted that they may confer protective effects against the onset of high-fat diet induced insulin resistance. However, further research is required into this interesting group of metabolites to elucidate their biological effects and to identify whether they do or do not contribute to the array of health benefits observed from the consumption of their parent compounds.

References

1. Ottaviani JI, Borges G, Momma TY, Spencer JP, Keen CL, Crozier A*, et al.* The metabolome of [2-14C](−)-epicatechin in humans: implications for the assessment of efficacy, safety, and mechanisms of action of polyphenolic bioactives. Scientific reports. 2016;6.

2. Hollands WJ, Philo M, Perez-Moral N, Needs PW, Savva GM, Kroon PA. Monomeric Flavanols are More Efficient Substrates for gut Microbiota Conversion to Hydroxyphenyl-γ-Valerolactone Metabolites than Oligomeric Procyanidins: A Randomized, Placebo-Controlled Human Intervention Trial. Molecular Nutrition & Food Research. 2020;64(10):1901135.

3. Takagaki A, Nanjo F. Metabolism of (−)-Epigallocatechin Gallate by Rat Intestinal Flora. Journal of Agricultural and Food Chemistry. 2010;58(2):1313-21.

4. Manach C, Scalbert A, Morand C, Rémésy C, Jiménez L. Polyphenols: food sources and bioavailability. The American journal of clinical nutrition. 2004;79(5):727-47.

5. Borges G, van der Hooft JJ, Crozier A. A comprehensive evaluation of the [2-14C](-)-epicatechin metabolome in rats. Free Radic Biol Med. 2016;99:128-38.

6. Tsao R. Chemistry and biochemistry of dietary polyphenols. Nutrients. 2010;2(12):1231-46.

7. Abbas M, Saeed F, Anjum FM, Afzaal M, Tufail T, Bashir MS*, et al.* Natural polyphenols: An overview. International Journal of Food Properties. 2017;20(8):1689-99.

8. Singla RK, Dubey AK, Garg A, Sharma RK, Fiorino M, Ameen SM*, et al.* Natural polyphenols: Chemical classification, definition of classes, subcategories, and structures. Journal of AOAC International. 2019;102(5):1397-400.

9. Manach C, Williamson G, Morand C, Scalbert A, Rémésy C. Bioavailability and bioefficacy of polyphenols in humans. I. Review of 97 bioavailability studies. The American journal of clinical nutrition. 2005;81(1):230S-42S.

10. Cutrim CS, Cortez MAS. A review on polyphenols: Classification, beneficial effects and their application in dairy products. International Journal of Dairy Technology. 2018;71(3):564-78.

11. Rasmussen SE, Frederiksen H, Struntze Krogholm K, Poulsen L. Dietary proanthocyanidins: occurrence, dietary intake, bioavailability, and protection against cardiovascular disease. Mol Nutr Food Res. 2005;49(2):159-74.

12. Scalbert A, Williamson G. Dietary Intake and Bioavailability of Polyphenols. The Journal of Nutrition. 2000;130(8):2073S-85S.

13. Hackman RM, Polagruto JA, Zhu QY, Sun B, Fujii H, Keen CL. Flavanols: digestion, absorption and bioactivity. Phytochemistry Reviews. 2007;7(1):195.

14. Neveu V, Perez-Jiménez J, Vos F, Crespy V, du Chaffaut L, Mennen L*, et al.* Phenol-Explorer: an online comprehensive database on polyphenol contents in foods. Database. 2010;2010.

15. Rothwell JA, Urpi-Sarda M, Boto-Ordoñez M, Knox C, Llorach R, Eisner R*, et al.* Phenol-Explorer 2.0: a major update of the Phenol-Explorer database integrating data on polyphenol metabolism and pharmacokinetics in humans and experimental animals. Database. 2012;2012.

16. Rothwell JA, Perez-Jimenez J, Neveu V, Medina-Remón A, M'Hiri N, García-Lobato P*, et al.* Phenol-Explorer 3.0: a major update of the Phenol-Explorer database to incorporate data on the effects of food processing on polyphenol content. Database. 2013;2013.

17. Kiely M, Black LJ, Plumb J, Kroon PA, Hollman PC, Larsen JC*, et al.* EuroFIR eBASIS: application for health claims submissions and evaluations. European Journal of Clinical Nutrition. 2010;64:S101-S7.

18. Haytowitz DB, Wu X, Bhagwat S. USDA Database for the Flavonoid Content of Selected Foods, Release 3.3 US Department of Agriculture, Agricultural Research Service. Nutrient Data Labrotatory.2018 [Available from: https://www.ars.usda.gov/nutrientdata/flav.

19. Fernández-Millán E, Cordero-Herrera I, Ramos S, Escrivá F, Alvarez C, Goya L*, et al.* Cocoa-rich diet attenuates beta cell mass loss and function in young Zucker diabetic fatty rats by preventing oxidative stress and beta cell apoptosis. Molecular nutrition & food research. 2015;59(4):820-4.

20. Khan N, Khymenets O, Urpi-Sarda M, Tulipani S, Garcia-Aloy M, Monagas M*, et al.* Cocoa polyphenols and inflammatory markers of cardiovascular disease. Nutrients. 2014;6(2):844-80.

21. Lee KW, Kim YJ, Lee HJ, Lee CY. Cocoa has more phenolic phytochemicals and a higher antioxidant capacity than teas and red wine. Journal of agricultural and food chemistry. 2003;51(25):7292-5.

22. Khan N, Khymenets O, Urpí-Sardà M, Tulipani S, Garcia-Aloy M, Monagas M*, et al.* Cocoa Polyphenols and Inflammatory Markers of Cardiovascular Disease. Nutrients. 2014;6(2):844-80.

23. Ostertag LM, O'Kennedy N, Kroon PA, Duthie GG, de Roos B. Impact of dietary polyphenols on human platelet function–a critical review of controlled dietary intervention studies. Mol Nutr Food Res. 2010;54(1):60-81.

24. Urbańska B, Kowalska J. Comparison of the total polyphenol content and antioxidant activity of chocolate obtained from roasted and unroasted cocoa beans from different regions of the World. Antioxidants. 2019;8(8):283.

25. Wollgast J, Anklam E. Polyphenols in chocolate: is there a contribution to human health? Food Research International. 2000;33(6):449-59.

26. Andújar I, Recio MC, Giner RM, Ríos JL. Cocoa Polyphenols and Their Potential Benefits for Human Health. Oxidative Medicine and Cellular Longevity. 2012;2012:906252.

27. Lakenbrink C, Lapczynski S, Maiwald B, Engelhardt UH. Flavonoids and other polyphenols in consumer brews of tea and other caffeinated beverages. Journal of agricultural and food chemistry. 2000;48(7):2848-52.

28. Arts IC, van de Putte B, Hollman PC. Catechin contents of foods commonly consumed in The Netherlands. 1. Fruits, vegetables, staple foods, and processed foods. Journal of agricultural and food chemistry. 2000;48(5):1746-51.

29. Balentine DA, Wiseman SA, Bouwens LC. The chemistry of tea flavonoids. Critical Reviews in Food Science & Nutrition. 1997;37(8):693-704.

30. Yang CS, Wang Z-Y. Tea and cancer. JNCI: Journal of the National Cancer Institute. 1993;85(13):1038-49.

31. Higdon JV, Frei B. Tea catechins and polyphenols: health effects, metabolism, and antioxidant functions. 2003.

32. Scalbert A, Johnson IT, Saltmarsh M. Polyphenols: antioxidants and beyond. The American journal of clinical nutrition. 2005;81(1):215S-7S.

33. Arts IC, Hollman PC. Polyphenols and disease risk in epidemiologic studies. The American journal of clinical nutrition. 2005;81(1):317S-25S.

34. Cardona F, Andres-Lacueva C, Tulipani S, Tinahones FJ, Queipo-Ortuno MI. Benefits of polyphenols on gut microbiota and implications in human health. J Nutr Biochem. 2013;24(8):1415-22.

35. Scalbert A, Morand C, Manach C, Rémésy C. Absorption and metabolism of polyphenols in the gut and impact on health. Biomedicine & Pharmacotherapy. 2002;56(6):276-82.

36. Hollman PC, de Vries JH, van Leeuwen SD, Mengelers MJ, Katan MB. Absorption of dietary quercetin glycosides and quercetin in healthy ileostomy volunteers. The American journal of clinical nutrition. 1995;62(6):1276-82.

37. Wu X, Cao G, Prior RL. Absorption and metabolism of anthocyanins in elderly women after consumption of elderberry or blueberry. J Nutr. 2002;132(7):1865-71.

38. Passamonti S, Vrhovsek U, Mattivi F. The interaction of anthocyanins with bilitranslocase. Biochem Biophys Res Commun. 2002;296(3):631-6.

39. Németh K, Plumb GW, Berrin JG, Juge N, Jacob R, Naim HY*, et al.* Deglycosylation by small intestinal epithelial cell beta-glucosidases is a critical step in the absorption and metabolism of dietary flavonoid glycosides in humans. Eur J Nutr. 2003;42(1):29-42.

40. Day AJ, Cañada FJ, Díaz JC, Kroon PA, Mclauchlan R, Faulds CB*, et al.* Dietary flavonoid and isoflavone glycosides are hydrolysed by the lactase site of lactase phlorizin hydrolase. FEBS letters. 2000;468(2-3):166-70.

41. Day AJ, DuPont MS, Ridley S, Rhodes M, Rhodes MJ, Morgan MR*, et al.* Deglycosylation of flavonoid and isoflavonoid glycosides by human small intestine and liver β-glucosidase activity. FEBS letters. 1998;436(1):71-5.

42. Marin L, Miguelez EM, Villar CJ, Lombo F. Bioavailability of dietary polyphenols and gut microbiota metabolism: antimicrobial properties. Biomed Res Int. 2015;2015:905215.

43. Kalt W. Anthocyanins and their C6-C3-C6 metabolites in humans and animals. Molecules. 2019;24(22):4024.

44. Marín L, Miguélez EM, Villar CJ, Lombó F. Bioavailability of dietary polyphenols and gut microbiota metabolism: antimicrobial properties. BioMed research international. 2015;2015.

45. Stevens JF, Maier CS. The Chemistry of Gut Microbial Metabolism of Polyphenols. Phytochem Rev. 2016;15(3):425-44.

46. Conlon MA, Bird AR. The impact of diet and lifestyle on gut microbiota and human health. Nutrients. 2014;7(1):17-44.

47. Hills RD, Jr., Pontefract BA, Mishcon HR, Black CA, Sutton SC, Theberge CR. Gut Microbiome: Profound Implications for Diet and Disease. Nutrients. 2019;11(7):1613.

48. Holt RR, Lazarus SA, Sullards MC, Zhu QY, Schramm DD, Hammerstone JF*, et al.* Procyanidin dimer B2 [epicatechin-(4β-8)-epicatechin] in human plasma after the consumption of a flavanol-rich cocoa. The American journal of clinical nutrition. 2002;76(4):798-804.

49. Appeldoorn MM, Vincken J-P, Aura A-M, Hollman PC, Gruppen H. Procyanidin dimers are metabolized by human microbiota with 2-(3, 4-dihydroxyphenyl) acetic acid and 5-(3, 4-dihydroxyphenyl)-γ-valerolactone as the major metabolites. Journal of agricultural and food chemistry. 2009;57(3):1084-92.

50. Aura A-M, Martin-Lopez P, O'Leary KA, Williamson G, Oksman-Caldentey K-M, Poutanen K*, et al.* In vitro metabolism of anthocyanins by human gut microflora. European journal of nutrition. 2005;44(3):133-42.

51. Kay CD, Mazza G, Holub BJ, Wang J. Anthocyanin metabolites in human urine and serum. British Journal of Nutrition. 2004;91(6):933-42.

52. Ichiyanagi T, Shida Y, Rahman MM, Sekiya M, Hatano Y, Matsumoto H*, et al.* Effect on both aglycone and sugar moiety towards Phase II metabolism of anthocyanins. Food chemistry. 2008;110(2):493-500.

53. Czank C, Cassidy A, Zhang Q, Morrison DJ, Preston T, Kroon PA*, et al.* Human metabolism and elimination of the anthocyanin, cyanidin-3-glucoside: a 13C-tracer study. The American of Clinical Nutrition. 2013;97(5):995-1003.

54. Serra A, Macià A, Romero M-P, Reguant J, Ortega N, Motilva M-J. Metabolic pathways of the colonic metabolism of flavonoids (flavonols, flavones and flavanones) and phenolic acids. Food chemistry. 2012;130(2):383-93.

55. Chadwick RW, Elizabeth George S, Claxton LD. Role of the gastrointestinal mucosa and microflora in the bioactivation of dietary and environmental mutagens or carcinogens. Drug Metabolism Reviews. 1992;24(4):425-92.

56. Takagaki A, Nanjo F. Catabolism of (+)-Catechin and (−)-Epicatechin by Rat Intestinal Microbiota. Journal of Agricultural and Food Chemistry. 2013;61(20):4927-35.

57. Kutschera M, Engst W, Blaut M, Braune A. Isolation of catechin-converting human intestinal bacteria. J Appl Microbiol. 2011;111(1):165-75.

58. Stoupi S, Williamson G, Drynan JW, Barron D, Clifford MN. A comparison of the in vitro biotransformation of (–)-epicatechin and procyanidin B2 by human faecal microbiota. Molecular nutrition & food research. 2010;54(6):747-59.

59. Roowi S, Stalmach A, Mullen W, Lean ME, Edwards CA, Crozier A. Green tea flavan-3-ols: colonic degradation and urinary excretion of catabolites by humans. Journal of agricultural and food chemistry. 2009;58(2):1296-304.

60. Williamson G, Kay CD, Crozier A. The Bioavailability, Transport, and Bioactivity of Dietary Flavonoids: A Review from a Historical Perspective. Comprehensive Reviews in Food Science and Food Safety. 2018;17(5):1054-112.

61. Nielsen ILF, Chee WS, Poulsen L, Offord-Cavin E, Rasmussen SE, Frederiksen H*, et al.* Bioavailability is improved by enzymatic modification of the citrus flavonoid hesperidin in humans: a randomized, double-blind, crossover trial. The Journal of nutrition. 2006;136(2):404-8.

62. Hollman PC, Van Trijp JM, Buysman MN, vd Gaag MS, Mengelers MJ, De Vries JH*, et al.* Relative bioavailability of the antioxidant flavonoid quercetin from various foods in man. FEBS letters. 1997;418(1-2):152-6.

63. Hollman PC, Bijsman MN, Van Gameren Y, Cnossen EP, De Vries JH, Katan MB. The sugar moiety is a major determinant of the absorption of dietary flavonoid glycosides in man. Free radical research. 1999;31(6):569-73.

64. Williamson G, Clifford MN. Role of the small intestine, colon and microbiota in determining the metabolic fate of polyphenols. Biochemical Pharmacology. 2017;139:24-39.

65. Erlund I, Meririnne E, Alfthan G, Aro A. Plasma kinetics and urinary excretion of the flavanones naringenin and hesperetin in humans after ingestion of orange juice and grapefruit juice. The Journal of nutrition. 2001;131(2):235-41.

66. Fuhr U, Kummert AL. The fate of naringin in humans: A key to grapefruit juice-drug interactions? Clinical Pharmacology & Therapeutics. 1995;58(4):365-73.

67. Lee YS, Reidenberg MM. A method for measuring naringenin in biological fluids and its disposition from grapefruit juice by man. Pharmacology. 1998;56(6):314-7.

68. Manach C, Morand C, Gil-Izquierdo A, Bouteloup-Demange C, Rémésy C. Bioavailability in humans of the flavanones hesperidin and narirutin after the ingestion of two doses of orange juice. European Journal of Clinical Nutrition. 2003;57(2):235-42.

69. de Ferrars RM, Czank C, Zhang Q, Botting NP, Kroon PA, Cassidy A*, et al.* The pharmacokinetics of anthocyanins and their metabolites in humans. Br J Pharmacol. 2014;171(13):3268-82.

70. Watanabe S, Yamaguchi M, Sobue T, Takahashi T, Miura T, Arai Y*, et al.* Pharmacokinetics of Soybean Isoflavones in Plasma, Urine and Feces of Men after Ingestion of 60 g Baked Soybean Powder (Kinako). The Journal of Nutrition. 1998;128(10):1710-5.

71. Xu X, Wang H-J, Murphy PA, Cook L, Hendrich S. Daidzein is a more bioavailable soymilk isoflavone than is genistein in adult women. The Journal of nutrition. 1994;124(6):825-32.

72. King RA, Bursill DB. Plasma and urinary kinetics of the isoflavones daidzein and genistein after a single soy meal in humans. The American journal of clinical nutrition. 1998;67(5):867-72.

73. Gradolatto A, Basly J-P, Berges R, Teyssier C, Chagnon M-C, Siess M-H*, et al.* Pharmacokinetics and metabolism of apigenin in female and male rats after a single oral administration. Drug Metabolism and Disposition. 2005;33(1):49-54.

74. Liang M, Xu W, Zhang W, Zhang C, Liu R, Shen Y*, et al.* Quantitative LC/MS/MS method and in vivo pharmacokinetic studies of vitexin rhamnoside, a bioactive constituent on cardiovascular system from hawthorn. Biomed Chromatogr. 2007;21(4):422-9.

75. Dai W, Ruan C, Zhang Y, Wang J, Han J, Shao Z*, et al.* Bioavailability enhancement of EGCG by structural modification and nano-delivery: A review. Journal of Functional Foods. 2020;65:103732.

76. Kohri T, Matsumoto N, Yamakawa M, Suzuki M, Nanjo F, Hara Y*, et al.* Metabolic Fate of (−)-[4-3H]Epigallocatechin Gallate in Rats after Oral Administration. Journal of Agricultural and Food Chemistry. 2001;49(8):4102-12.

77. Takagaki A, Nanjo F. Metabolism of (-)-epigallocatechin gallate by rat intestinal flora. J Agric Food Chem. 2010;58(2):1313-21.

78. Suganuma M, Okabe S, Oniyama M, Tada Y, Ito H, Fujiki H. Wide distribution of [3H](−)-epigallocatechin gallate, a cancer preventive tea polyphenol, in mouse tissue. Carcinogenesis. 1998;19(10):1771-6.

79. Cai Z-Y, Li X-M, Liang J-P, Xiang L-P, Wang K-R, Shi Y-L*, et al.* Bioavailability of tea catechins and its improvement. Molecules. 2018;23(9):2346.

80. Lambert JD, Lee M-J, Lu H, Meng X, Hong JJJ, Seril DN*, et al.* Epigallocatechin-3-Gallate Is Absorbed but Extensively Glucuronidated Following Oral Administration to Mice. The Journal of Nutrition. 2003;133(12):4172-7.

81. Lee M-J, Maliakal P, Chen L, Meng X, Bondoc FY, Prabhu S*, et al.* Pharmacokinetics of tea catechins after ingestion of green tea and (−)-epigallocatechin-3-gallate by humans. Cancer Epidemiology and Prevention Biomarkers. 2002;11(10):1025-32.

82. Chow H-HS, Cai Y, Alberts DS, Hakim I, Dorr R, Shahi F*, et al.* Phase I Pharmacokinetic Study of Tea Polyphenols following Single-dose Administration of Epigallocatechin Gallate and Polyphenon E. Cancer Epidemiology Biomarkers & Prevention. 2001;10(1):53-8.

83. Mereles D, Hunstein W. Epigallocatechin-3-gallate (EGCG) for clinical trials: more pitfalls than promises? International journal of molecular sciences. 2011;12(9):5592-603.

84. Henning SM, Niu Y, Liu Y, Lee NH, Hara Y, Thames GD*, et al.* Bioavailability and antioxidant effect of epigallocatechin gallate administered in purified form versus as green tea extract in healthy individuals. The Journal of Nutritional Biochemistry. 2005;16(10):610-6.

85. Wei B-B, Liu M-Y, Zhong X, Yao W-F, Wei M-J. Increased BBB permeability contributes to EGCG-caused cognitive function improvement in natural aging rats: pharmacokinetic and distribution analyses. Acta Pharmacologica Sinica. 2019;40(11):1490-500.

86. Stalmach A, Troufflard S, Serafini M, Crozier A. Absorption, metabolism and excretion of Choladi green tea flavan-3-ols by humans. Molecular Nutrition & Food Research. 2009;53(S1):S44-S53.

87. Kida K, Suzuki M, Matsumoto N, Nanjo F, Hara Y. Identification of Biliary Metabolites of (−)-Epigallocatechin Gallate in Rats. Journal of Agricultural and Food Chemistry. 2000;48(9):4151-5.

88. Mena P, Bresciani L, Brindani N, Ludwig IA, Pereira-Caro G, Angelino D*, et al.* Phenyl-γ-valerolactones and phenylvaleric acids, the main colonic metabolites of flavan-3-ols: synthesis, analysis, bioavailability, and bioactivity. Natural product reports. 2019.

89. Mullen W, Borges G, Donovan JL, Edwards CA, Serafini M, Lean ME*, et al.* Milk decreases urinary excretion but not plasma pharmacokinetics of cocoa flavan-3-ol metabolites in humans. The American journal of clinical nutrition. 2009;89(6):1784-91.

90. Rodriguez-Mateos A, Cifuentes-Gomez T, Gonzalez-Salvador I, Ottaviani JI, Schroeter H, Kelm M*, et al.* Influence of age on the absorption, metabolism, and excretion of cocoa flavanols in healthy subjects. Molecular nutrition & food research. 2015;59(8):1504-12.

91. Ottaviani JI, Kwik-Uribe C, Keen CL, Schroeter H. Intake of dietary procyanidins does not contribute to the pool of circulating flavanols in humans. The American journal of clinical nutrition. 2012;95(4):851-8.

92. Vitaglione P, Lumaga RB, Ferracane R, Sellitto S, Morelló JR, Miranda JR*, et al.* Human bioavailability of flavanols and phenolic acids from cocoa-nut creams enriched with free or microencapsulated cocoa polyphenols. British Journal of Nutrition. 2013;109(10):1832-43.

93. Urpi-Sarda M, Garrido I, Monagas MA, GóMez-CordovéS C, Medina-RemóN A, Andres-Lacueva C*, et al.* Profile of Plasma and Urine Metabolites after the Intake of Almond [Prunus dulcis (Mill.) D.A. Webb] Polyphenols in Humans. Journal of Agricultural and Food Chemistry. 2009;57(21):10134-42.

94. Borges G, Mullen W, Mullan A, Lean MEJ, Roberts SA, Crozier A. Bioavailability of multiple components following acute ingestion of a polyphenol-rich juice drink. Molecular Nutrition & Food Research. 2010;54(S2):S268-S77.

95. Wiese S, Esatbeyoglu T, Winterhalter P, Kruse H-P, Winkler S, Bub A*, et al.* Comparative biokinetics and metabolism of pure monomeric, dimeric, and polymeric flavan-3-ols: A randomized cross-over study in humans. Molecular Nutrition & Food Research. 2015;59(4):610-21.

96. Borges G, Ottaviani JI, van der Hooft JJJ, Schroeter H, Crozier A. Absorption, metabolism, distribution and excretion of (−)-epicatechin: A review of recent findings. Molecular Aspects of Medicine. 2018;61:18-30.

97. Chen W, Zhu X, Lu Q, Zhang L, Wang X, Liu R. C-ring cleavage metabolites of catechin and epicatechin enhanced antioxidant activities through intestinal microbiota. Food Research International. 2020;135:109271.

98. Kohri T, Suzuki M, Nanjo F. Identification of metabolites of (−)-epicatechin gallate and their metabolic fate in the rat. Journal of agricultural and food chemistry. 2003;51(18):5561-6.

99. Meng X, Sang S, Zhu N, Lu H, Sheng S, Lee M-J*, et al.* Identification and characterization of methylated and ring-fission metabolites of tea catechins formed in humans, mice, and rats. Chemical research in toxicology. 2002;15(8):1042-50.

100. Li C, Lee M-J, Sheng S, Meng X, Prabhu S, Winnik B*, et al.* Structural identification of two metabolites of catechins and their kinetics in human urine and blood after tea ingestion. Chemical research in toxicology. 2000;13(3):177-84.

101. Li C, Meng X, Winnik B, Lee M-J, Lu H, Sheng S*, et al.* Analysis of Urinary Metabolites of Tea Catechins by Liquid Chromatography/Electrospray Ionization Mass Spectrometry. Chemical Research in Toxicology. 2001;14(6):702-7.

102. Borges G, van der Hooft JJ, Crozier A. A comprehensive evaluation of the [2-14 C](–)-epicatechin metabolome in rats. Free Radical Biol Med. 2016;99:128-38.

103. Lambert JD, Rice JE, Hong J, Hou Z, Yang CS. Synthesis and biological activity of the tea catechin metabolites, M4 and M6 and their methoxy-derivatives. Bioorg Med Chem Lett. 2005;15(4):873-6.

104. Uhlenhut K, Hogger P. Facilitated cellular uptake and suppression of inducible nitric oxide synthase by a metabolite of maritime pine bark extract (Pycnogenol). Free Radic Biol Med. 2012;53(2):305-13.

105. Sun YN, Li W, Song SB, Yan XT, Zhao Y, Jo AR*, et al.* A new phenolic derivative with soluble epoxide hydrolase and nuclear factor-kappaB inhibitory activity from the aqueous extract of Acacia catechu. Natural Product Research. 2016;30(18):2085-92.

106. Aktan F. iNOS-mediated nitric oxide production and its regulation. Life Sciences. 2004;75(6):639-53.

107. Grimm T, Schafer A, Hogger P. Antioxidant activity and inhibition of matrix metalloproteinases by metabolites of maritime pine bark extract (pycnogenol). Free Radic Biol Med. 2004;36(6):811-22.

108. Vacek TP, Rehman S, Neamtu D, Yu S, Givimani S, Tyagi SC. Matrix metalloproteinases in atherosclerosis: role of nitric oxide, hydrogen sulfide, homocysteine, and polymorphisms. Vasc Health Risk Manag. 2015;11:173-83.

109. Lee CC, Kim JH, Kim JS, Oh YS, Han SM, Park JHY*, et al.* 5-(3',4'-Dihydroxyphenyl-γ-valerolactone), a Major Microbial Metabolite of Proanthocyanidin, Attenuates THP-1 Monocyte-Endothelial Adhesion. International journal of molecular sciences. 2017;18(7):1363.

110. Cybulsky M, Gimbrone M. Endothelial expression of a mononuclear leukocyte adhesion molecule during atherogenesis. Science. 1991;251(4995):788-91.

111. Takagaki A, Nanjo F. Effects of Metabolites Produced from (−)-Epigallocatechin Gallate by Rat Intestinal Bacteria on Angiotensin I-Converting Enzyme Activity and Blood Pressure in Spontaneously Hypertensive Rats. Journal of Agricultural and Food Chemistry. 2015;63(37):8262-6.

112. Van Rymenant E, Grootaert C, Beerens K, Needs PW, Kroon PA, Kerimi A*, et al.* Vasorelaxant activity of twenty-one physiologically relevant (poly)phenolic metabolites on isolated mouse arteries. Food & Function. 2017;8(12):4331-5.

113. Mele L, Carobbio S, Brindani N, Curti C, Rodriguez-Cuenca S, Bidault G*, et al.* Phenyl-γ-valerolactones, flavan-3-ol colonic metabolites, protect brown adipocytes from oxidative stress without affecting their differentiation or function. Molecular Nutrition & Food Research. 2017:1700074-n/a.

114. Mena P, González de Llano D, Brindani N, Esteban-Fernández A, Curti C, Moreno-Arribas MV*, et al.* 5-(3',4'-Dihydroxyphenyl)-γ-valerolactone and its sulphate conjugates, representative circulating metabolites of flavan-3-ols, exhibit anti-adhesive activity against uropathogenic Escherichia coli in bladder epithelial cells. Journal of Functional Foods. 2017;29:275-80.

115. Hara-Terawaki A, Takagaki A, Kobayashi H, Nanjo F. Inhibitory Activity of Catechin Metabolites Produced by Intestinal Microbiota on Proliferation of HeLa Cells. Biological and Pharmaceutical Bulletin. 2017;40(8):1331-5.

116. Pittayapruek P, Meephansan J, Prapapan O, Komine M, Ohtsuki M. Role of Matrix Metalloproteinases in Photoaging and Photocarcinogenesis. International journal of molecular sciences. 2016;17(6):868.

117. Unno K, Pervin M, Nakagawa A, Iguchi K, Hara A, Takagaki A*, et al.* Blood–Brain Barrier Permeability of Green Tea Catechin Metabolites and their Neuritogenic Activity in Human Neuroblastoma SH-SY5Y Cells. Molecular Nutrition & Food Research. 2017;61(12):1700294.

118. Angelino D, Carregosa D, Domenech-Coca C, Savi M, Figueira I, Brindani N*, et al.* 5-(Hydroxyphenyl)-γ-valerolactone-sulfate, a key microbial metabolite of flavan-3-ols, is able to reach the brain: Evidence from different in silico, in vitro and in vivo experimental models. Nutrients. 2019;11(11):2678.

119. Ruotolo R, Minato I, La Vitola P, Artioli L, Curti C, Franceschi V*, et al.* Flavonoid-Derived Human Phenyl-γ-Valerolactone Metabolites Selectively Detoxify Amyloid-β Oligomers and Prevent Memory Impairment in a Mouse Model of Alzheimer's Disease. Molecular Nutrition & Food Research. 2020;64(5):1900890.

120. Forloni G, Balducci C. Alzheimer's Disease, Oligomers, and Inflammation. Journal of Alzheimer's Disease. 2018;62:1261-76.

121. Aucott L, Poobalan A, Smith W, Avenell A, Jung R, Broom J*, et al.* Weight loss in obese diabetic and non-diabetic individuals and long-term diabetes outcomes–a systematic review. Diabetes, Obesity and Metabolism. 2004;6(2):85-94.

122. Avenell A, Broom J, Brown TJ, Poobalan A, Aucott L, Stearns S*, et al.* Systematic review of the long-term effects and economic consequences of treatments for obesity and implications for health improvement. Health technology assessment. 2004;8(21).

123. Bramante CT, Lee CJ, Gudzune KA. Treatment of Obesity in Patients With Diabetes. Diabetes Spectrum. 2017;30(4):237-43.

124. Tang L, Li L, Yang J, Zeng C. Potential benefit of (-)-epigallocatechin-3-gallate for macrovascular complications in diabetes. Brazilian Journal of Medical and Biological Research. 2017;50(10).

125. Meng J-M, Cao S-Y, Wei X-L, Gan R-Y, Wang Y-F, Cai S-X*, et al.* Effects and Mechanisms of Tea for the Prevention and Management of Diabetes Mellitus and Diabetic Complications: An Updated Review. Antioxidants (Basel). 2019;8(6):170.

126. Li X, Li S, Chen M, Wang J, Xie B, Sun Z. (−)-Epigallocatechin-3-gallate (EGCG) inhibits starch digestion and improves glucose homeostasis through direct or indirect activation of PXR/CAR-mediated phase II metabolism in diabetic mice. Food & function. 2018;9(9):4651-63.

127. Cremonini E, Bettaieb A, Haj FG, Fraga CG, Oteiza PI. (-)-Epicatechin improves insulin sensitivity in high fat diet-fed mice. Archives of biochemistry and biophysics. 2016;599:13-21.

128. Cremonini E, Fraga CG, Oteiza PI. (–)-Epicatechin in the control of glucose homeostasis: Involvement of redox-regulated mechanisms. Free Radical Biology and Medicine. 2019;130:478-88.

129. Cremonini E, Oteiza PI. (-)-Epicatechin and its metabolites prevent palmitate-induced NADPH oxidase upregulation, oxidative stress and insulin resistance in HepG2 cells. Archives of biochemistry and biophysics. 2018;646:55-63.

130. Cremonini E, Wang Z, Bettaieb A, Adamo AM, Daveri E, Mills DA*, et al.* (-)-Epicatechin protects the intestinal barrier from high fat diet-induced permeabilization: Implications for steatosis and insulin resistance. Redox biology. 2018;14:588-99.

131. Hruby VJ. Chapter 16 Glucagon: Molecular biology and structure-activity. Principles of Medical Biology C edn. 10. Elsevier Inc.1997.

132. Cersosimo E, Triplitt C, Solis-Herrera C, Mandarino LJ, DeFronzo RA. Pathogenesis of Type 2 Diabetes Mellitus. In: Feingold KR, Anawalt B, Boyce A, Chrousos G, Dungan K, Grossman A*, et al.*, editors. Endotext. South Dartmouth (MA).2000.

133. Feher J. 2.9 - ATP Production I: Glycolysis. In: Feher J, editor. Quantitative Human Physiology (Second Edition). Boston: Academic Press; 2017. p. 218-26.

134. Paredes-Flores MA, Mohiuddin SS. Biochemistry, Glycogenolysis. StatPearls [Internet]: StatPearls Publishing; 2020.

135. Bhagavan NV, Ha C-E. Chapter 14 - Carbohydrate Metabolism II: Gluconeogenesis, Glycogen Synthesis and Breakdown, and Alternative Pathways. In: Bhagavan NV, Ha C-E, editors. Essentials of Medical Biochemistry (Second Edition). San Diego: Academic Press; 2015. p. 205-25.

136. Röder PV, Wu B, Liu Y, Han W. Pancreatic regulation of glucose homeostasis. Experimental & molecular medicine. 2016;48(3):e219-e.

137. Feher J. 9.4 - The Endocrine Pancreas and Control of Blood Glucose. In: Feher J, editor. Quantitative Human Physiology (Second Edition). Boston: Academic Press; 2012. p. 895-905.

138. Evans M. Chapter 36 - Diabetes mellitus, insulin, oral antidiabetes agents, obesity. In: Bennett PN, Brown MJ, Sharma P, editors. Clinical Pharmacology (Eleventh Edition). Oxford: Churchill Livingstone; 2012. p. 572-86.

139. Kaplan SA. The insulin receptor. The Journal of Pediatrics. 1984;104(3):327-36.

140. Lee J, Pilch PF. The insulin receptor: structure, function, and signaling. American Journal of Physiology-Cell Physiology. 1994;266(2):C319-C34.

141. Guo S. Insulin signaling, resistance, and the metabolic syndrome: insights from mouse models to disease mechanisms. Journal of Endocrinology. 2013:JOE-13-0327.

142. Saltiel AR, Kahn CR. Insulin signalling and the regulation of glucose and lipid metabolism. Nature. 2001;414(6865):799.

143. McManus EJ, Sakamoto K, Armit LJ, Ronaldson L, Shpiro N, Marquez R*, et al.* Role that phosphorylation of GSK3 plays in insulin and Wnt signalling defined by knockin analysis. The EMBO journal. 2005;24(8):1571-83.

144. Baumann CA, Ribon V, Kanzaki M, Thurmond DC, Mora S, Shigematsu S*, et al.* CAP defines a second signalling pathway required for insulin-stimulated glucose transport. Nature. 2000;407(6801):202.

145. Foretz M, Pacot C, Dugail I, Lemarchand P, Guichard C, le Lièpvre X*, et al.* ADD1/SREBP-1c is required in the activation of hepatic lipogenic gene expression by glucose. Molecular and cellular biology. 1999;19(5):3760-8.

146. Ronald Kahn C. Insulin resistance, insulin insensitivity, and insulin unresponsiveness: A necessary distinction. Metabolism - Clinical and Experimental. 1978;27(12):1893-902.

147. Tilg H, Effenberger M. From NAFLD to MAFLD: when pathophysiology succeeds. Nature Reviews Gastroenterology & Hepatology. 2020;17(7):387-8.

148. Tolman KG, Fonseca V, Dalpiaz A, Tan MH. Spectrum of liver disease in type 2 diabetes and management of patients with diabetes and liver disease. Diabetes care. 2007;30(3):734-43.

149. Flier JS. Insulin receptors and insulin resistance. Annual review of medicine. 1983;34(1):145-60.

150. Shulman GI, Rothman DL, Jue T, Stein P, DeFronzo RA, Shulman RG. Quantitation of muscle glycogen synthesis in normal subjects and subjects with non-insulin-dependent diabetes by 13C nuclear magnetic resonance spectroscopy. New England Journal of Medicine. 1990;322(4):223-8.

151. Samuel VT, Petersen KF, Shulman GI. Lipid-induced insulin resistance: unravelling the mechanism. The Lancet. 2010;375(9733):2267-77.

152. Savage DB, Petersen KF, Shulman GI. Disordered lipid metabolism and the pathogenesis of insulin resistance. Physiological reviews. 2007;87(2):507-20.

153. Perry RJ, Samuel VT, Petersen KF, Shulman GI. The role of hepatic lipids in hepatic insulin resistance and type 2 diabetes. Nature. 2014;510(7503):84-91.

154. Samuel VT, Liu Z-X, Qu X, Elder BD, Bilz S, Befroy D*, et al.* Mechanism of hepatic insulin resistance in non-alcoholic fatty liver disease. Journal of Biological Chemistry. 2004;279(31):32345-53.

155. Kumashiro N, Erion DM, Zhang D, Kahn M, Beddow SA, Chu X*, et al.* Cellular mechanism of insulin resistance in nonalcoholic fatty liver disease. Proceedings of the National Academy of Sciences. 2011;108(39):16381-5.

156. Yuan M, Konstantopoulos N, Lee J, Hansen L, Li Z-W, Karin M*, et al.* Reversal of obesity-and diet-induced insulin resistance with salicylates or targeted disruption of Ikkβ. Science. 2001;293(5535):1673-7.

157. Samuel VT, Liu Z-X, Wang A, Beddow SA, Geisler JG, Kahn M*, et al.* Inhibition of protein kinase Cε prevents hepatic insulin resistance in nonalcoholic fatty liver disease. The Journal of clinical investigation. 2007;117(3):739-45.

158. Rains JL, Jain SK. Oxidative stress, insulin signaling, and diabetes. Free Radical Biology and Medicine. 2011;50(5):567-75.

159. Dasgupta S, Bhattacharya S, Maitra S, Pal D, Majumdar SS, Datta A*, et al.* Mechanism of lipid induced insulin resistance: activated PKCε is a key regulator. Biochimica et Biophysica Acta (BBA)-Molecular Basis of Disease. 2011;1812(4):495-506.

160. Bazotte RB, Silva LG, Schiavon FP. Insulin resistance in the liver: deficiency or excess of insulin? Cell Cycle. 2014;13(16):2494-500.

161. Pagadala M, Kasumov T, McCullough AJ, Zein NN, Kirwan JP. Role of ceramides in nonalcoholic fatty liver disease. Trends in Endocrinology & Metabolism. 2012;23(8):365-71.

162. Magkos F, Su X, Bradley D, Fabbrini E, Conte C, Eagon JC*, et al.* Intrahepatic diacylglycerol content is associated with hepatic insulin resistance in obese subjects. Gastroenterology. 2012;142(7):1444-6. e2.

163. Ottaviani JI, Britten A, Lucarelli D, Luben R, Mulligan AA, Lentjes MA*, et al.* Biomarker-estimated flavan-3-ol intake is associated with lower blood pressure in cross-sectional analysis in EPIC Norfolk. Scientific Reports. 2020;10(1):17964.

164. Zamora-Ros R, Forouhi NG, Sharp SJ, González CA, Buijsse B, Guevara M*, et al.* Dietary Intakes of Individual Flavanols and Flavonols Are Inversely Associated with Incident Type 2 Diabetes in European Populations. The Journal of Nutrition. 2013;144(3):335-43.

165. Del Bo C, Bernardi S, Marino M, Porrini M, Tucci M, Guglielmetti S*, et al.* Systematic review on polyphenol intake and health outcomes: is there sufficient evidence to define a health-promoting polyphenol-rich dietary pattern? Nutrients. 2019;11(6):1355.

166. Wedick NM, Pan A, Cassidy A, Rimm EB, Sampson L, Rosner B*, et al.* Dietary flavonoid intakes and risk of type 2 diabetes in US men and women. The American journal of clinical nutrition. 2012;95(4):925-33.

167. Zamora-Ros R, Forouhi NG, Sharp SJ, González CA, Buijsse B, Guevara M*, et al.* The Association Between Dietary Flavonoid and Lignan Intakes and Incident Type 2 Diabetes in European Populations. The EPIC-InterAct study. 2013;36(12):3961-70.

168. Grosso G, Stepaniak U, Micek A, Kozela M, Stefler D, Bobak M*, et al.* Dietary polyphenol intake and risk of type 2 diabetes in the Polish arm of the Health, Alcohol and Psychosocial factors in Eastern Europe (HAPIEE) study. British Journal of Nutrition. 2017;118(1):60-8.

169. Jacques PF, Cassidy A, Rogers G, Peterson JJ, Meigs JB, Dwyer JT. Higher dietary flavonol intake is associated with lower incidence of type 2 diabetes. The Journal of nutrition. 2013;143(9):1474-80.

170. Oh JS, Kim H, Vijayakumar A, Kwon O, Kim Y, Chang N. Association of dietary flavonoid intake with prevalence of type 2 diabetes mellitus and cardiovascular disease risk factors in Korean women aged≥ 30 years. Journal of nutritional science and vitaminology. 2017;63(1):51-8.

171. Jennings A, Welch AA, Spector T, Macgregor A, Cassidy A. Intakes of anthocyanins and flavones are associated with biomarkers of insulin resistance and inflammation in women. The Journal of nutrition. 2014;144(2):202-8.

172. Kim K, Vance TM, Chun OK. Greater flavonoid intake is associated with improved CVD risk factors in US adults. British Journal of Nutrition. 2016;115(8):1481-8.

173. Akiyama S, Katsumata S-i, Suzuki K, Nakaya Y, Ishimi Y, Uehara M. Hypoglycemic and hypolipidemic effects of hesperidin and cyclodextrin-clathrated hesperetin in Goto-Kakizaki rats with type 2 diabetes. Bioscience, biotechnology, and biochemistry. 2009;73(12):2779-82.

174. Agrawal YO, Sharma PK, Shrivastava B, Ojha S, Upadhya HM, Arya DS*, et al.* Hesperidin produces cardioprotective activity via PPAR-γ pathway in ischemic heart disease model in diabetic rats. PLoS One. 2014;9(11):e111212.

175. Jung UJ, Lee M-K, Jeong K-S, Choi M-S. The hypoglycemic effects of hesperidin and naringin are partly mediated by hepatic glucose-regulating enzymes in C57BL/KsJ-db/db mice. The Journal of nutrition. 2004;134(10):2499-503.

176. Jung UJ, Lee M-K, Park YB, Kang MA, Choi M-S. Effect of citrus flavonoids on lipid metabolism and glucose-regulating enzyme mRNA levels in type-2 diabetic mice. The international journal of biochemistry & cell biology. 2006;38(7):1134-45.

177. Akiyama S, Katsumata S-i, Suzuki K, Ishimi Y, Wu J, Uehara M. Dietary hesperidin exerts hypoglycemic and hypolipidemic effects in streptozotocin-induced marginal type 1 diabetic rats. Journal of clinical biochemistry and nutrition. 2009;46(1):87-92.

178. Rizza S, Muniyappa R, Iantorno M, Kim J-a, Chen H, Pullikotil P*, et al.* Citrus polyphenol hesperidin stimulates production of nitric oxide in endothelial cells while improving endothelial function and reducing inflammatory markers in patients with metabolic syndrome. The Journal of Clinical Endocrinology & Metabolism. 2011;96(5):E782-E92.

179. Koch CE, Ganjam GK, Steger J, Legler K, Stöhr S, Schumacher D*, et al.* The dietary flavonoids naringenin and quercetin acutely impair glucose metabolism in rodents possibly via inhibition of hypothalamic insulin signalling. British journal of nutrition. 2013;109(6):1040-51.

180. Ong KC, Khoo H-E. Effects of myricetin on glycemia and glycogen metabolism in diabetic rats. Life Sciences. 2000;67(14):1695-705.

181. Liu I-M, Liou S-S, Lan T-W, Hsu F-L, Cheng J-T. Myricetin as the active principle of Abelmoschus moschatus to lower plasma glucose in streptozotocin-induced diabetic rats. Planta medica. 2005;71(07):617-21.

182. Liu IM, Tzeng T-F, Liou S-S, Lan T-W. Myricetin, a naturally occurring flavonol, ameliorates insulin resistance induced by a high-fructose diet in rats. Life Sciences. 2007;81(21):1479-88.

183. Valsa AK, Sudheesh S, Vijayalakshmi NR. Effect of catechin on carbohydrate metabolism. Indian J Biochem Biophys. 1997;34(4):406-8.

184. Vessal M, Hemmati M, Vasei M. Antidiabetic effects of quercetin in streptozocin-induced diabetic rats. Comparative Biochemistry and Physiology Part C: Toxicology & Pharmacology. 2003;135(3):357-64.

185. Potenza MA, Marasciulo FL, Tarquinio M, Tiravanti E, Colantuono G, Federici A*, et al.* EGCG, a green tea polyphenol, improves endothelial function and insulin sensitivity, reduces blood pressure, and protects against myocardial I/R injury in SHR. American Journal of Physiology-Endocrinology and Metabolism. 2007;292(5):E1378-E87.

186. Wolfram S, Raederstorff D, Preller M, Wang Y, Teixeira SR, Riegger C*, et al.* Epigallocatechin Gallate Supplementation Alleviates Diabetes in Rodents. The Journal of Nutrition. 2006;136(10):2512-8.

187. Brown AL, Lane J, Coverly J, Stocks J, Jackson S, Stephen A*, et al.* Effects of dietary supplementation with the green tea polyphenol epigallocatechin-3-gallate on insulin resistance and associated metabolic risk factors: randomized controlled trial. British journal of nutrition. 2008;101(6):886-94.

188. Sabu M, Smitha K, Kuttan R. Anti-diabetic activity of green tea polyphenols and their role in reducing oxidative stress in experimental diabetes. Journal of ethnopharmacology. 2002;83(1-2):109-16.

189. Tsuneki H, Ishizuka M, Terasawa M, Wu J-B, Sasaoka T, Kimura I. Effect of green tea on blood glucose levels and serum proteomic patterns in diabetic (db/db) mice and on glucose metabolism in healthy humans. BMC pharmacology. 2004;4(1):18.

190. Suliburska J, Bogdanski P, Szulinska M, Stepien M, Pupek-Musialik D, Jablecka A. Effects of green tea supplementation on elements, total antioxidants, lipids, and glucose values in the serum of obese patients. Biological trace element research. 2012;149(3):315-22.

191. Bogdanski P, Suliburska J, Szulinska M, Stepien M, Pupek-Musialik D, Jablecka A. Green tea extract reduces blood pressure, inflammatory biomarkers, and oxidative stress and improves parameters associated with insulin resistance in obese, hypertensive patients. Nutrition research. 2012;32(6):421-7.

192. Fukino Y, Ikeda A, Maruyama K, Aoki N, Okubo T, Iso H. Randomized controlled trial for an effect of green tea-extract powder supplementation on glucose abnormalities. European journal of clinical nutrition. 2008;62(8):953-60.

193. Liu CY, Huang CJ, Huang LH, Chen IJ, Chiu JP, Hsu CH. Effects of green tea extract on insulin resistance and glucagon-like peptide 1 in patients with type 2 diabetes and lipid abnormalities: a randomized, double-blinded, and placebo-controlled trial. PLoS One. 2014;9(3):e91163.

194. Almoosawi S, Fyfe L, Ho C, Al-Dujaili E. The effect of polyphenol-rich dark chocolate on fasting capillary whole blood glucose, total cholesterol, blood pressure and glucocorticoids in healthy overweight and obese subjects. British journal of nutrition. 2010;103(6):842-50.

195. Curtis PJ, Sampson M, Potter J, Dhatariya K, Kroon PA, Cassidy A. Chronic ingestion of flavan-3-ols and isoflavones improves insulin sensitivity and lipoprotein status and attenuates estimated 10-year CVD risk in medicated postmenopausal women with type 2 diabetes: a 1-year, double-blind, randomized, controlled trial. Diabetes care. 2012:DC_111443.

196. Davison K, Coates A, Buckley J, Howe P. Effect of cocoa flavanols and exercise on cardiometabolic risk factors in overweight and obese subjects. International journal of obesity. 2008;32(8):1289-96.

197. Grassi D, Lippi C, Necozione S, Desideri G, Ferri C. Short-term administration of dark chocolate is followed by a significant increase in insulin sensitivity and a decrease in blood pressure in healthy persons–. The American journal of clinical nutrition. 2005;81(3):611-4.

198. Mastroiacovo D, Kwik-Uribe C, Grassi D, Necozione S, Raffaele A, Pistacchio L*, et al.* Cocoa flavanol consumption improves cognitive function, blood pressure control, and metabolic profile in elderly subjects: the Cocoa, Cognition, and Aging (CoCoA) Study—a randomized controlled trial. The American journal of clinical nutrition. 2015;101(3):538-48.

199. Cordero-Herrera I, Martín MÁ, Escrivá F, Álvarez C, Goya L, Ramos S. Cocoa-rich diet ameliorates hepatic insulin resistance by modulating insulin signaling and glucose homeostasis in Zucker diabetic fatty rats. The Journal of nutritional biochemistry. 2015;26(7):704-12.

200. Dorenkott MR, Griffin LE, Goodrich KM, Thompson-Witrick KA, Fundaro G, Ye L*, et al.* Oligomeric cocoa procyanidins possess enhanced bioactivity compared to monomeric and polymeric cocoa procyanidins for preventing the development of obesity, insulin resistance, and impaired glucose tolerance during high-fat feeding. Journal of agricultural and food chemistry. 2014;62(10):2216-27.

201. Gu Y, Yu S, Lambert JD. Dietary cocoa ameliorates obesity-related inflammation in high fat-fed mice. Eur J Nutr. 2014;53(1):149-58.

202. Jalil AMM, Ismail A, Pei CP, Hamid M, Kamaruddin SHS. Effects of cocoa extract on glucometabolism, oxidative stress, and antioxidant enzymes in obese-diabetic (Ob-db) rats. Journal of agricultural and food chemistry. 2008;56(17):7877-84.

203. Jalil AMM, Ismail A, Chong PP, Hamid M, Syed Kamaruddin SH. Effects of cocoa extract containing polyphenols and methylxanthines on biochemical parameters of obese-diabetic rats. Journal of the Science of Food and Agriculture. 2009;89(1):130-7.

204. Ruzaidi A, Amin I, Nawalyah A, Hamid M, Faizul H. The effect of Malaysian cocoa extract on glucose levels and lipid profiles in diabetic rats. Journal of ethnopharmacology. 2005;98(1-2):55-60.

205. Ruzaidi AMM, Abbe MMJ, Amin I, Nawalyah AG, Muhajir H. Protective effect of polyphenol-rich extract prepared from Malaysian cocoa (Theobroma cacao) on glucose levels and lipid profiles in streptozotocin-induced diabetic rats. Journal of the Science of Food and Agriculture. 2008;88(8):1442-7.

206. Tomaru M, Takano H, Osakabe N, Yasuda A, Inoue K-i, Yanagisawa R*, et al.* Dietary supplementation with cacao liquor proanthocyanidins prevents elevation of blood glucose levels in diabetic obese mice. Nutrition. 2007;23(4):351-5.

207. Grassi D, Necozione S, Lippi C, Croce G, Valeri L, Pasqualetti P*, et al.* Cocoa reduces blood pressure and insulin resistance and improves endothelium-dependent vasodilation in hypertensives. Hypertension. 2005;46(2):398-405.

208. Grassi D, Desideri G, Necozione S, Lippi C, Casale R, Properzi G*, et al.* Blood pressure is reduced and insulin sensitivity increased in glucose-intolerant, hypertensive subjects after 15 days of consuming high-polyphenol dark chocolate. The Journal of nutrition. 2008;138(9):1671-6.

209. Sánchez D, Moulay L, Muguerza B, Quinones M, Miguel M, Aleixandre A. Effect of a soluble cocoa fiber-enriched diet in Zucker fatty rats. Journal of medicinal food. 2010;13(3):621-8.

210. Hooper L, Kay C, Abdelhamid A, Kroon PA, Cohn JS, Rimm EB*, et al.* Effects of chocolate, cocoa, and flavan-3-ols on cardiovascular health: a systematic review and meta-analysis of randomized trials–. The American journal of clinical nutrition. 2012;95(3):740-51.

211. Shrime MG, Bauer SR, McDonald AC, Chowdhury NH, Coltart CE, Ding EL. Flavonoid-Rich Cocoa Consumption Affects Multiple Cardiovascular Risk Factors in a Meta-Analysis of Short-Term Studies1. The Journal of nutrition. 2011;141(11):1982-8.

212. Chondronikola M, Volpi E, Børsheim E, Porter C, Annamalai P, Enerbäck S*, et al.* Brown adipose tissue improves whole body glucose homeostasis and insulin sensitivity in humans. Diabetes. 2014:DB_140746.

213. Curtis PJ, Potter J, Kroon PA, Wilson P, Dhatariya K, Sampson M*, et al.* Vascular function and atherosclerosis progression after 1 y of flavonoid intake in statin-treated postmenopausal women with type 2 diabetes: a double-blind randomized controlled trial–. The American of Clinical Nutrition. 2013;97(5):936-42.

214. Mellor DD, Madden LA, Smith KA, Kilpatrick ES, Atkin SL. High-polyphenol chocolate reduces endothelial dysfunction and oxidative stress during acute transient hyperglycaemia in Type 2 diabetes: a pilot randomized controlled trial. Diabetic Medicine. 2013;30(4):478-83.

215. Basu A, Betts NM, Leyva MJ, Fu D, Aston CE, Lyons TJ. Acute Cocoa Supplementation Increases Postprandial HDL Cholesterol and Insulin in Obese Adults with Type 2 Diabetes after Consumption of a High-Fat Breakfast. The Journal of nutrition. 2015;145(10):2325-32.

216. Choi MS, Jung UJ, Yeo J, Kim MJ, Lee MK. Genistein and daidzein prevent diabetes onset by elevating insulin level and altering hepatic gluconeogenic and lipogenic enzyme activities in non-obese diabetic (NOD) mice. Diabetes/Metabolism Research and Reviews. 2008;24(1):74-81.

217. Park SA, Choi M-S, Cho S-Y, Seo J-S, Jung UJ, Kim M-J*, et al.* Genistein and daidzein modulate hepatic glucose and lipid regulating enzyme activities in C57BL/KsJ-db/db mice. Life sciences. 2006;79(12):1207-13.

218. Huang P-L, Chi C-W, Liu T-Y. Areca nut procyanidins ameliorate streptozocin-induced hyperglycemia by regulating gluconeogenesis. Food and Chemical Toxicology. 2013;55:137-43.

219. Guo H, Xia M, Zou T, Ling W, Zhong R, Zhang W. Cyanidin 3-glucoside attenuates obesity-associated insulin resistance and hepatic steatosis in high-fat diet-fed and db/db mice via the transcription factor FoxO1. The Journal of Nutritional Biochemistry. 2012;23(4):349-60.

220. Pinent M, Blay M, Bladé MC, Salvadó MJ, Arola L, Ardévol A. Grape Seed-Derived Procyanidins Have an Antihyperglycemic Effect in Streptozotocin-Induced Diabetic Rats and Insulinomimetic Activity in Insulin-Sensitive Cell Lines. Endocrinology. 2004;145(11):4985-90.

221. Prince PSM, Kamalakkannan N. Rutin improves glucose homeostasis in streptozotocin diabetic tissues by altering glycolytic and gluconeogenic enzymes. Journal of Biochemical and Molecular Toxicology. 2006;20(2):96-102.

222. Kobori M, Masumoto S, Akimoto Y, Takahashi Y. Dietary quercetin alleviates diabetic symptoms and reduces streptozotocin-induced disturbance of hepatic gene expression in mice. Molecular nutrition & food research. 2009;53(7):859-68.

223. Coskun O, Kanter M, Korkmaz A, Oter S. Quercetin, a flavonoid antioxidant, prevents and protects streptozotocin-induced oxidative stress and β-cell damage in rat pancreas. Pharmacological research. 2005;51(2):117-23.

224. Sano T, Nagayasu S, Suzuki S, Iwashita M, Yamashita A, Shinjo T*, et al.* Epicatechin downregulates adipose tissue CCL19 expression and thereby ameliorates diet-induced obesity and insulin resistance. Nutrition, Metabolism and Cardiovascular Diseases. 2017;27(3):249-59.

225. Vazquez-Prieto MA, Bettaieb A, Haj FG, Fraga CG, Oteiza PI. (−)-Epicatechin prevents TNFα-induced activation of signaling cascades involved in inflammation and insulin sensitivity in 3T3-L1 adipocytes. Archives of biochemistry and biophysics. 2012;527(2):113-8.

226. Gutiérrez-Salmeán G, Ortiz-Vilchis P, Vacaseydel CM, Garduño-Siciliano L, Chamorro-Cevallos G, Meaney E*, et al.* Effects of (−)-epicatechin on a diet-induced rat model of cardiometabolic risk factors. European journal of pharmacology. 2014;728:24-30.

227. Ramírez-Sánchez I, Rodríguez A, Moreno-Ulloa A, Ceballos G, Villarreal F. (-)-Epicatechin-induced recovery of mitochondria from simulated diabetes: Potential role of endothelial nitric oxide synthase. Diabetes and Vascular Disease Research. 2016;13(3):201-10.

228. Hoek-van den Hil EF, Schothorst EM, Stelt I, Swarts HJ, Vliet M, Amolo T*, et al.* Direct comparison of metabolic health effects of the flavonoids quercetin, hesperetin, epicatechin, apigenin and anthocyanins in high-fat-diet-fed mice. Genes & nutrition. 2015;10(4):23.

229. Bettaieb A, Cremonini E, Kang H, Kang J, Haj FG, Oteiza PI. Anti-inflammatory actions of (−)-epicatechin in the adipose tissue of obese mice. The international journal of biochemistry & cell biology. 2016;81:383-92.

230. Varela CE, Rodriguez A, Romero-Valdovinos M, Mendoza-Lorenzo P, Mansour C, Ceballos G*, et al.* Browning effects of (-)-epicatechin on adipocytes and white adipose tissue. European journal of pharmacology. 2017;811:48-59.

231. Bischoff SC, Barbara G, Buurman W, Ockhuizen T, Schulzke J-D, Serino M*, et al.* Intestinal permeability–a new target for disease prevention and therapy. BMC gastroenterology. 2014;14(1):189.

232. Cani PD, Amar J, Iglesias MA, Poggi M, Knauf C, Bastelica D*, et al.* Metabolic endotoxemia initiates obesity and insulin resistance. Diabetes. 2007;56(7):1761-72.

233. Dower JI, Geleijnse JM, Gijsbers L, Zock PL, Kromhout D, Hollman PC. Effects of the pure flavonoids epicatechin and quercetin on vascular function and cardiometabolic health: a randomized, double-blind, placebo-controlled, crossover trial. Am J Clin Nutr. 2015;101(5):914-21.

234. Gutierrez-Salmean G, Ortiz-Vilchis P, Vacaseydel CM, Rubio-Gayosso I, Meaney E, Villarreal F*, et al.* Acute effects of an oral supplement of (-)-epicatechin on postprandial fat and carbohydrate metabolism in normal and overweight subjects. Food Funct. 2014;5(3):521-7.

235. Moreno-Ulloa A, Nájera-García N, Hernández M, Ramírez-Sánchez I, Taub PR, Su Y*, et al.* A pilot study on clinical pharmacokinetics and preclinical pharmacodynamics of (+)-epicatechin on cardiometabolic endpoints. Food & function. 2018;9(1):307-19.

236. Henry R. Early Phase Pre-Clinical and Initial Clinical Research on Epicatechin (Epicatechin): clinicaltrials.gov; 2015 [Available from: https://clinicaltrials.gov/ct2/show/NCT02330276?term=epicatechin&cond=Diabetes&draw=2&rank=2.

237. Henry R. Early Phase Pre-Clinical and Initial Clinical Research on Epicatechin (Part 2) (Epicatechin): clinicaltrials.gov; 2016 [Available from: https://clinicaltrials.gov/ct2/show/NCT02656212?term=epicatechin&cond=Diabetes&draw=2&rank=1.

238. Atkin SL. A Comparison Chocolate With and Without High Cocoa Solids in Patients With Type 2 Diabetes in a Randomised Clinical Trial: clinicaltrials.gov; 2012 [Available from:

https://clinicaltrials.gov/ct2/show/NCT01617603?term=epicatechin&cond=Diabetes&draw=2&rank=4.

239. Decroix L, van Schuerbeek P, Tonoli C, van Cutsem J, Soares DD, Heyman E*, et al.* The effect of acute cocoa flavanol intake on the BOLD response and cognitive function in type 1 diabetes: a randomized, placebo-controlled, double-blinded cross-over pilot study. Psychopharmacology (Berl). 2019;236(12):3421-8.

240. Meeusen R. The Effect of Cocoa Flavanol on the BOLD Response and Cognitive Function in Type 1 Diabetes: clinicaltrials.gov; 2018 [Available from: https://clinicaltrials.gov/ct2/show/NCT03452605?term=epicatechin&cond=Diabetes&draw=2&rank=5.

241. Hanhineva K, Törrönen R, Bondia-Pons I, Pekkinen J, Kolehmainen M, Mykkänen H*, et al.* Impact of dietary polyphenols on carbohydrate metabolism. International journal of molecular sciences. 2010;11(4):1365-402.

242. Iwai K, Kim M-Y, Onodera A, Matsue H. α-Glucosidase Inhibitory and Antihyperglycemic Effects of Polyphenols in the Fruit of Viburnum dilatatum Thunb. Journal of agricultural and food chemistry. 2006;54(13):4588-92.

243. Tadera K, Minami Y, Takamatsu K, Matsuoka T. Inhibition of α-glucosidase and α-amylase by flavonoids. Journal of nutritional science and vitaminology. 2006;52(2):149-53.

244. Lo Piparo E, Scheib H, Frei N, Williamson G, Grigorov M, Chou CJ. Flavonoids for controlling starch digestion: structural requirements for inhibiting human α-amylase. Journal of medicinal chemistry. 2008;51(12):3555-61.

245. Kim J-S, Kwon C-S, Son KH. Inhibition of alpha-glucosidase and amylase by luteolin, a flavonoid. Bioscience, biotechnology, and biochemistry. 2000;64(11):2458-61.

246. Funke I, Melzig M. Effect of different phenolic compounds on α-amylase activity: screening by microplate-reader based kinetic assay. Die Pharmazie-An International Journal of Pharmaceutical Sciences. 2005;60(10):796-7.

247. Adisakwattana S, Charoenlertkul P, Yibchok-anun S. α-Glucosidase inhibitory activity of cyanidin-3-galactoside and synergistic effect with acarbose. Journal of Enzyme Inhibition and Medicinal Chemistry. 2009;24(1):65-9.

248. Adisakwattana S, Ngamrojanavanich N, Kalampakorn K, Tiravanit W, Roengsumran S, Yibchok-Anun S. Inhibitory Activity of Cyanidin-3-rutinoside on α-Glucosidase. Journal of Enzyme Inhibition and Medicinal Chemistry. 2004;19(4):313-6.

249. Matsui T, Ueda T, Oki T, Sugita K, Terahara N, Matsumoto K. α-Glucosidase Inhibitory Action of Natural Acylated Anthocyanins. 1. Survey of Natural Pigments with Potent Inhibitory Activity. Journal of Agricultural and Food Chemistry. 2001;49(4):1948-51.

250. Ishikawa A, Yamashita H, Hiemori M, Inagaki E, Kimoto M, Okamoto M*, et al.* Characterization of inhibitors of postprandial hyperglycemia from the leaves of Nerium indicum. Journal of nutritional science and vitaminology. 2007;53(2):166-73.

251. Welsch CA, Lachance PA, Wasserman BP. Effects of Native and Oxidized Phenolic Compounds on Sucrase Activity in Rat Brush Border Membrane Vesicles. The Journal of Nutrition. 1989;119(11):1737-40.

252. Welsch CA, Lachance PA, Wasserman BP. Dietary phenolic compounds: inhibition of Na+-dependent D-glucose uptake in rat intestinal brush border membrane vesicles. The Journal of nutrition. 1989;119(11):1698-704.

253. Levin RJ. Digestion and absorption of carbohydrates—from molecules and membranes to humans. The American journal of clinical nutrition. 1994;59(3):690S-8S.

254. Hanamura T, Hagiwara T, Kawagishi H. Structural and Functional Characterization of Polyphenols Isolated from Acerola (Malpighia emarginata DC.) Fruit. Bioscience, Biotechnology, and Biochemistry. 2005;69(2):280-6.

255. Lee D-S, Lee S-H. Genistein, a soy isoflavone, is a potent α-glucosidase inhibitor. FEBS letters. 2001;501(1):84-6.

256. Johnston K, Sharp P, Clifford M, Morgan L. Dietary polyphenols decrease glucose uptake by human intestinal Caco-2 cells. FEBS Letters. 2005;579(7):1653-7.

257. Manzano S, Williamson G. Polyphenols and phenolic acids from strawberry and apple decrease glucose uptake and transport by human intestinal Caco-2 cells. Molecular Nutrition & Food Research. 2010;54(12):1773-80.

258. Zhang ZF, Li Q, Liang J, Dai XQ, Ding Y, Wang JB*, et al.* Epigallocatechin-3-O-gallate (EGCG) protects the insulin sensitivity in rat L6 muscle cells exposed to dexamethasone condition. Phytomedicine. 2010;17(1):14-8.

259. Fang X-K, Gao J, Zhu D-N. Kaempferol and quercetin isolated from Euonymus alatus improve glucose uptake of 3T3-L1 cells without adipogenesis activity. Life sciences. 2008;82(11-12):615-22.

260. Bazuine M, van den Broek PJ, Maassen JA. Genistein directly inhibits GLUT4-mediated glucose uptake in 3T3-L1 adipocytes. Biochemical and biophysical research communications. 2005;326(2):511-4.

261. Montagut G, Onnockx S, Vaqué M, Bladé C, Blay M, Fernández-Larrea J*, et al.* Oligomers of grape-seed procyanidin extract activate the insulin receptor and key targets of the insulin signaling pathway differently from insulin. The Journal of Nutritional Biochemistry. 2010;21(6):476-81.

262. Ueda-Wakagi M, Mukai R, Fuse N, Mizushina Y, Ashida H. 3-O-Acyl-epicatechins Increase Glucose Uptake Activity and GLUT4 Translocation through Activation of PI3K Signaling in Skeletal Muscle Cells. International journal of molecular sciences. 2015;16(7):16288-99.

263. Vuong T, Martineau LC, Ramassamy C, Matar C, Haddad PS. Fermented Canadian lowbush blueberry juice stimulates glucose uptake and AMP-activated protein kinase in insulin-sensitive cultured muscle cells and adipocytes. Can J Physiol Pharmacol. 2007;85(9):956-65.

264. Kurimoto Y, Shibayama Y, Inoue S, Soga M, Takikawa M, Ito C*, et al.* Black soybean seed coat extract ameliorates hyperglycemia and insulin sensitivity via the activation of AMP-activated protein kinase in diabetic mice. J Agric Food Chem. 2013;61(23):5558-64.

265. Röder PV, Geillinger KE, Zietek TS, Thorens B, Koepsell H, Daniel H. The role of SGLT1 and GLUT2 in intestinal glucose transport and sensing. PloS one. 2014;9(2):e89977-e.

266. Cermak R, Landgraf S, Wolffram S. Quercetin glucosides inhibit glucose uptake into brush-border-membrane vesicles of porcine jejunum. British Journal of Nutrition. 2004;91(6):849-55.

267. Kobayashi Y, Suzuki M, Satsu H, Arai S, Hara Y, Suzuki K*, et al.* Green tea polyphenols inhibit the sodium-dependent glucose transporter of intestinal epithelial cells by a competitive mechanism. Journal of Agricultural and Food Chemistry. 2000;48(11):5618-23.

268. Shimizu M, Kobayashi Y, Suzuki M, Satsu H, Miyamoto Y. Regulation of intestinal glucose transport by tea catechins. Biofactors. 2000;13(1-4):61-5.

269. Li JM, Che CT, Lau CB, Leung PS, Cheng CH. Inhibition of intestinal and renal Na+-glucose cotransporter by naringenin. The international journal of biochemistry & cell biology. 2006;38(5-6):985-95.

270. Ong KC, Khoo H-E. Insulinomimetic effects of myricetin on lipogenesis and glucose transport in rat adipocytes but not glucose transporter translocation. Biochemical Pharmacology. 1996;51(4):423-9.

271. Harmon AW, Patel YM. Naringenin inhibits phosphoinositide 3-kinase activity and glucose uptake in 3T3-L1 adipocytes. Biochemical and Biophysical Research Communications. 2003;305(2):229-34.

272. Smith RM, Tiesinga JJ, Shah N, Smith JA, Jarett L. Genistein Inhibits Insulin-Stimulated Glucose Transport and Decreases Immunocytochemical Labeling of GLUT4 Carboxyl-Terminus without Affecting Translocation of GLUT4 in Isolated Rat Adipocytes: Additional Evidence of GLUT4 Activation by Insulin. Archives of Biochemistry and Biophysics. 1993;300(1):238-46.

273. Strobel P, Allard C, Perez-Acle T, Calderon R, Aldunate R, Leighton F. Myricetin, quercetin and catechin-gallate inhibit glucose uptake in isolated rat adipocytes. Biochemical Journal. 2005;386(3):471-8.

274. Jakobs S, Fridrich D, Hofem S, Pahlke G, Eisenbrand G. Natural flavonoids are potent inhibitors of glycogen phosphorylase. Molecular nutrition & food research. 2006;50(1):52-7.

275. Estrada O, Hasegawa M, Gonzalez-Mujíca F, Motta N, Perdomo E, Solorzano A*, et al.* Evaluation of flavonoids from Bauhinia megalandra leaves as inhibitors of glucose-6-phosphatase system. Phytotherapy Research. 2005;19(10):859-63.

276. Gonzalez-Mujica F, Motta N, Estrada O, Perdomo E, Méndez J, Hasegawa M. Inhibition of hepatic neoglucogenesis and glucose-6-phosphatase by quercetin 3-O-α (2 ″-galloyl) rhamnoside isolated from Bauhinia megalandra leaves. Phytotherapy Research: An International Journal Devoted to Pharmacological and Toxicological Evaluation of Natural Product Derivatives. 2005;19(7):624-7.

277. Cai EP, Lin J-K. Epigallocatechin Gallate (EGCG) and Rutin Suppress the Glucotoxicity through Activating IRS2 and AMPK Signaling in Rat Pancreatic β Cells. Journal of Agricultural and Food Chemistry. 2009;57(20):9817-27.

278. Hii CS, Howell SL. Effects of flavonoids on insulin secretion and 45Ca2+ handling in rat islets of Langerhans. J Endocrinol. 1985;107(1):1-8.

279. Fu Z, Liu D. Long-term exposure to genistein improves insulin secretory function of pancreatic β-cells. European journal of pharmacology. 2009;616(1-3):321-7.

280. Jayaprakasam B, Vareed SK, Olson LK, Nair MG. Insulin secretion by bioactive anthocyanins and anthocyanidins present in fruits. Journal of Agricultural and Food Chemistry. 2005;53(1):28-31.

281. Waltner-Law ME, Wang XL, Law BK, Hall RK, Nawano M, Granner DK. Epigallocatechin gallate, a constituent of green tea, represses hepatic glucose production. Journal of Biological Chemistry. 2002;277(38):34933-40.

282. Collins QF, Liu H-Y, Pi J, Liu Z, Quon MJ, Cao W. Epigallocatechin-3-gallate (EGCG), a green tea polyphenol, suppresses hepatic gluconeogenesis through 5'-AMP-activated protein kinase. The Journal of biological chemistry. 2007;282(41):30143-9.

283. Sears B, Perry M. The role of fatty acids in insulin resistance. Lipids in health and disease. 2015;14:121-.

284. Giacco F, Brownlee M. Oxidative stress and diabetic complications. Circulation research. 2010;107(9):1058-70.

285. Cordero-Herrera I, Martín MÁ, Goya L, Ramos S. Cocoa flavonoids attenuate high glucose-induced insulin signalling blockade and modulate glucose uptake and production in human HepG2 cells. Food and chemical toxicology. 2014;64:10-9.

286. Wang J, Obici S, Morgan K, Barzilai N, Feng Z, Rossetti L. Overfeeding rapidly induces leptin and insulin resistance. Diabetes. 2001;50(12):2786-91.

287. Cordero-Herrera I, Martín MA, Goya L, Ramos S. Cocoa flavonoids protect hepatic cells against high-glucose-induced oxidative stress: Relevance of MAPKs. Molecular nutrition & food research. 2015;59(4):597-609.

288. Álvarez-Cilleros D, Martín MÁ, Goya L, Ramos S. (−)-Epicatechin and the colonic metabolite 3, 4-dihydroxyphenylacetic acid protect renal proximal tubular cell against high glucose-induced oxidative stress by modulating NOX-4/SIRT-1 signalling. Journal of Functional Foods. 2018;46:19-28.

289. Liang F, Kume S, Koya D. SIRT1 and insulin resistance. Nature Reviews Endocrinology. 2009;5(7):367.

290. Wu X, Koh EK, Williams KJ, editors. The NOX4 pathway as a source of selective insulin resistance and responsiveness in endothelium. Diabetes; 2012; 1701 N Beauregard St, Alexandria, VA 22311-1717 USA

Amer Diabetes Assoc

291. Martín MÁ, Fernández-Millán E, Ramos S, Bravo L, Goya L. Cocoa flavonoid epicatechin protects pancreatic beta cell viability and function against oxidative stress. Molecular nutrition & food research. 2014;58(3):447-56.

292. Fernández-Millán E, Ramos S, Alvarez C, Bravo L, Goya L, Martín MÁ. Microbial phenolic metabolites improve glucose-stimulated insulin secretion and protect pancreatic beta cells against tert-butyl hydroperoxide-induced toxicity via ERKs and PKC pathways. Food and Chemical Toxicology. 2014;66:245-53.

293. Yang K, Chan CB. Epicatechin potentiation of glucose-stimulated insulin secretion in INS-1 cells is not dependent on its antioxidant activity. Acta Pharmacologica Sinica. 2018;39(5):893-902.

294. Kim M-J, Ryu GR, Chung J-S, Sim SS, Rhie D-J, Yoon SH*, et al.* Protective effects of epicatechin against the toxic effects of streptozotocin on rat pancreatic islets: in vivo and in vitro. Pancreas. 2003;26(3):292-9.

295. Hii CS, Howell SL. Effects of epicatechin on rat islets of Langerhans. Diabetes. 1984;33(3):291-6.

296. Rodriguez-Mateos A, Vauzour D, Krueger CG, Shanmuganayagam D, Reed J, Calani L*, et al.* Bioavailability, bioactivity and impact on health of dietary flavonoids and related compounds: an update. Arch Toxicol. 2014;88(10):1803-53.

297. Panche AN, Diwan AD, Chandra SR. Flavonoids: an overview. J Nutr Sci. 2016;5:e47-e.

298. Kozłowska A, Szostak-Wegierek D. Flavonoids--food sources and health benefits. Rocz Panstw Zakl Hig. 2014;65(2):79-85.

299. Ottaviani JI, Fong R, Kimball J, Ensunsa JL, Gray N, Vogiatzoglou A*, et al.* Evaluation of (−)-epicatechin metabolites as recovery biomarker of dietary flavan-3-ol intake. Scientific Reports. 2019;9(1):13108.

300. Chang XW, Peng WM, Yao YF, Koek J. Concise Synthesis of Ring-Fission Metabolites of Epicatechin: 5-(3,4-Dihydroxybenzyl)dihydrofuran-2(3H)-one M6. Synthetic Commun. 2010;40(22):3346-52.

301. Miranda AM, Steluti J, Fisberg RM, Marchioni DM. Dietary intake and food contributors of polyphenols in adults and elderly adults of Sao Paulo: a population-based study. British Journal of Nutrition. 2016;115(6):1061-70.

302. Knaze V, Zamora-Ros R, Luján-Barroso L, Romieu I, Scalbert A, Slimani N*, et al.* Intake estimation of total and individual flavan-3-ols, proanthocyanidins and theaflavins, their food sources and determinants in the European Prospective Investigation into Cancer and Nutrition (EPIC) study. British Journal of Nutrition. 2012;108(6):1095-108.

303. Pérez-Jiménez J, Fezeu L, Touvier M, Arnault N, Manach C, Hercberg S*, et al.* Dietary intake of 337 polyphenols in French adults. The American Journal of Clinical Nutrition. 2011;93(6):1220-8.

304. Cassidy A, O'Reilly ÉJ, Kay C, Sampson L, Franz M, Forman J*, et al.* Habitual intake of flavonoid subclasses and incident hypertension in adults. The American Journal of Clinical Nutrition. 2010;93(2):338-47.

305. Escobar-Cévoli R, Castro-Espín C, Béraud V, Buckland G, Zamora-Ros R, Béraud G. An overview of global flavonoid intake and its food sources. Flavonoids-From Biosynthesis to Human Health. 2017.

306. Vogiatzoglou A, Mulligan AA, Lentjes MAH, Luben RN, Spencer JPE, Schroeter H*, et al.* Flavonoid Intake in European Adults (18 to 64 Years). PLOS ONE. 2015;10(5):e0128132.

307. Nair AB, Jacob S. A simple practice guide for dose conversion between animals and human. Journal of basic and clinical pharmacy. 2016;7(2):27.

308. Flórez-Vargas O, Brass A, Karystianis G, Bramhall M, Stevens R, Cruickshank S*, et al.* Bias in the reporting of sex and age in biomedical research on mouse models. Elife. 2016;5:e13615.

309. Mülek M, Seefried L, Genest F, Högger P. Distribution of constituents and metabolites of maritime pine bark extract (Pycnogenol®) into serum, blood cells, and synovial fluid of patients with severe osteoarthritis: a randomized controlled trial. Nutrients. 2017;9(5):443.

310. Kurlbaum M, Mülek M, Högger P. Facilitated uptake of a bioactive metabolite of maritime pine bark extract (pycnogenol) into human erythrocytes. PloS one. 2013;8(4):e63197-e.

311. Mülek M, Högger P. Highly sensitive analysis of polyphenols and their metabolites in human blood cells using dispersive SPE extraction and LC-MS/MS. Analytical and Bioanalytical Chemistry. 2015;407(7):1885-99.

312. Mülek M. Distribution and metabolism of constituents and metabolites of a standardized maritime pine bark extract (Pycnogenol®) in human serum, blood cells and synovial fluid of patients with severe osteoarthritis. Germany: University of Würzburg; 2015.

313. Mülek M, Fekete A, Wiest J, Holzgrabe U, Mueller MJ, Högger P. Profiling a gut microbiota-generated catechin metabolite's fate in human blood cells using a metabolomic approach. Journal of Pharmaceutical and Biomedical Analysis. 2015;114:71-81.

314. Yan L, Yin P, Ma C, Liu Y. Method development and validation for pharmacokinetic and tissue distributions of ellagic acid using ultrahigh performance liquid chromatography-tandem mass spectrometry (UPLC-MS/MS). Molecules. 2014;19(11):18923-35.

315. Gallant VA. Liquid chromatography tandem mass spectrometry identification of apple polyphenol metabolites in human urine and plasma: University of Nottingham; 2010.

316. Feliciano RP, Mecha E, Bronze MR, Rodriguez-Mateos A. Development and validation of a high-throughput micro solid-phase extraction method coupled with ultra-high-performance liquid chromatography-quadrupole time-of-flight mass spectrometry for rapid identification and quantification of phenolic metabolites in human plasma and urine. Journal of Chromatography A. 2016;1464:21-31.

317. Castello F, Costabile G, Bresciani L, Tassotti M, Naviglio D, Luongo D*, et al.* Bioavailability and pharmacokinetic profile of grape pomace phenolic compounds in humans. Archives of biochemistry and biophysics. 2018;646:1-9.

318. Yuste S, Macià A, Ludwig IA, Romero MP, Fernández-Castillejo S, Catalán Ú*, et al.* Validation of Dried Blood Spot Cards to Determine Apple Phenolic Metabolites in Human Blood and Plasma After an Acute Intake of Red-Fleshed Apple Snack. Molecular nutrition & food research. 2018;62(23):1800623.

319. de Ferrars RM, Czank C, Saha S, Needs PW, Zhang Q, Raheem KS*, et al.* Methods for isolating, identifying, and quantifying anthocyanin metabolites in clinical samples. Anal Chem. 2014;86(20):10052-8.

320. Byers JP, Sarver JG. Chapter 10 - Pharmacokinetic Modeling. In: Hacker M, Messer W, Bachmann K, editors. Pharmacology. San Diego: Academic Press; 2009. p. 201-77.

321. Research NCftRRRoAi. Decision Tree: How much blood does a mouse have? London: NC3R's; [Available from: https://www.nc3rs.org.uk/mouse-decision-tree-blood-sampling.

322. Noh J-Y, Han D-H, Yoon J-A, Kim M-H, Kim S-E, Ko I-G*, et al.* Circadian rhythms in urinary functions: possible roles of circadian clocks? International neurourology journal. 2011;15(2):64.

323. Demetrius L. Of mice and men. When it comes to studying ageing and the means to slow it down, mice are not just small humans. EMBO Rep. 2005;6 Spec No(Suppl 1):S39-S44.

324. Perlman RL. Mouse models of human disease: An evolutionary perspective. Evol Med Public Health. 2016;2016(1):170-6.

325. Yue F, Cheng Y, Breschi A, Vierstra J, Wu W, Ryba T*, et al.* A comparative encyclopedia of DNA elements in the mouse genome. Nature. 2014;515(7527):355-64.

326. Trends in adult body-mass index in 200 countries from 1975 to 2014: a pooled analysis of 1698 population-based measurement studies with 19·2 million participants. The Lancet. 2016;387(10026):1377-96.

327. Keaver L, Xu B, Jaccard A, Webber L. Morbid obesity in the UK: A modelling projection study to 2035. Scand J Public Health. 2018;48(4):422-7.

328. Heart N, Lung, Institute B, Diabetes NIo, Digestive, Diseases K. Clinical guidelines on the identification, evaluation, and treatment of overweight and obesity in adults: the evidence report: National Heart, Lung, and Blood Institute; 1998.

329. Bhaskaran K, Douglas I, Forbes H, dos-Santos-Silva I, Leon DA, Smeeth L. Body-mass index and risk of 22 specific cancers: a population-based cohort study of 5·24 million UK adults. The Lancet. 2014;384(9945):755-65.

330. Kasen S, Cohen P, Chen H, Must A. Obesity and psychopathology in women: a three decade prospective study. International Journal of Obesity. 2008;32(3):558-66.

331. Luppino FS, de Wit LM, Bouvy PF, Stijnen T, Cuijpers P, Penninx BWJH*, et al.* Overweight, Obesity, and Depression: A Systematic Review and Meta-analysis of Longitudinal Studies. Archives of General Psychiatry. 2010;67(3):220-9.

332. Roberts RE, Deleger S, Strawbridge WJ, Kaplan GA. Prospective association between obesity and depression: evidence from the Alameda County Study. International Journal of Obesity. 2003;27(4):514-21.

333. Members EP, Jensen MD, Ryan DH, Donato KA, Apovian CM, Ard JD*, et al.* Executive summary: Guidelines (2013) for the management of overweight and obesity in adults. Obesity. 2014;22(S2):S5-S39.

334. Guasch-Ferré M, Merino J, Sun Q, Fitó M, Salas-Salvadó J. Dietary Polyphenols, Mediterranean Diet, Prediabetes, and Type 2 Diabetes: A Narrative Review of the Evidence. Oxidative Medicine and Cellular Longevity. 2017;2017:6723931.

335. Kang GG, Francis N, Hill R, Waters D, Blanchard C, Santhakumar AB. Dietary Polyphenols and Gene Expression in Molecular Pathways Associated with Type 2 Diabetes Mellitus: A Review. International Journal of Molecular Sciences. 2020;21(1):140.

336. Mihaylova D, Popova A, Alexieva I, Krastanov A, Lante A. Polyphenols as Suitable Control for Obesity and Diabetes. The Open Biotechnology Journal. 2018;12(1).

337. Aryaeian N, Sedehi SK, Arablou T. Polyphenols and their effects on diabetes management: A review. Med J Islam Repub Iran. 2017;31:134-.

338. Bettaieb A, Vazquez Prieto MA, Rodriguez Lanzi C, Miatello RM, Haj FG, Fraga CG*, et al.* (−)-Epicatechin mitigates high-fructose-associated insulin resistance by modulating redox signaling and endoplasmic reticulum stress. Free Radical Biology and Medicine. 2014;72:247-56.

339. Aguirre V, Uchida T, Yenush L, Davis R, White MF. The c-Jun NH2-terminal kinase promotes insulin resistance during association with insulin receptor substrate-1 and phosphorylation of Ser307. Journal of Biological Chemistry. 2000;275(12):9047-54.

340. Cai D, Yuan M, Frantz DF, Melendez PA, Hansen L, Lee J*, et al.* Local and systemic insulin resistance resulting from hepatic activation of IKK-β and NF-κB. Nature medicine. 2005;11(2):183-90.

341. Cordero-Herrera I, Martín MA, Bravo L, Goya L, Ramos S. Cocoa flavonoids improve insulin signalling and modulate glucose production via AKT and AMPK in H ep G 2 cells. Molecular nutrition & food research. 2013;57(6):974-85.

342. Knopp JL, Holder-Pearson L, Chase JG. Insulin Units and Conversion Factors: A Story of Truth, Boots, and Faster Half-Truths. Journal of diabetes science and technology. 2019;13(3):597-600.

343. Matthews DR, Hosker JP, Rudenski AS, Naylor BA, Treacher DF, Turner RC. Homeostasis model assessment: insulin resistance and ?-cell function from fasting plasma glucose and insulin concentrations in man. Diabetologia. 1985;28(7):412-9.

344. Katz A, Nambi SS, Mather K, Baron AD, Follmann DA, Sullivan G*, et al.* Quantitative insulin sensitivity check index: a simple, accurate method for assessing insulin sensitivity in humans. The Journal of Clinical Endocrinology & Metabolism. 2000;85(7):2402-10.

345. Bates D, Mächler M, Bolker B, Walker S. Fitting linear mixed-effects models using lme4. arXiv preprint arXiv:14065823. 2014.

346. Pinheiro J, Bates D, DebRoy S, Sarkar D. R Core Team. 2019. nlme: linear and nonlinear mixed effects models. R package version 3.1-141. Available at http://CRANR-ProjectOrg/Package=Nlme. 2019.

347. Actis-Goretta L, Lévèques A, Giuffrida F, Romanov-Michailidis F, Viton F, Barron D*, et al.* Elucidation of (−)-epicatechin metabolites after ingestion of chocolate by healthy humans. Free Radical Biology and Medicine. 2012;53(4):787-95.

348. Ottaviani JI, Momma TY, Kuhnle GK, Keen CL, Schroeter H. Structurally related (−)-epicatechin metabolites in humans: assessment using de novo chemically synthesized authentic standards. Free Radical Biology and Medicine. 2012;52(8):1403-12.

349. Waqar AB, Koike T, Yu Y, Inoue T, Aoki T, Liu E*, et al.* High-fat diet without excess calories induces metabolic disorders and enhances atherosclerosis in rabbits. Atherosclerosis. 2010;213(1):148-55.

350. Moreno-Fernández S, Garcés-Rimón M, Vera G, Astier J, Landrier JF, Miguel M. High Fat/High Glucose Diet Induces Metabolic Syndrome in an Experimental Rat Model. Nutrients. 2018;10(10):1502.

351. Lasker S, Rahman MM, Parvez F, Zamila M, Miah P, Nahar K*, et al.* High-fat diet-induced metabolic syndrome and oxidative stress in obese rats are ameliorated by yogurt supplementation. Scientific Reports. 2019;9(1):20026.

352. Panchal SK, Poudyal H, Iyer A, Nazer R, Alam A, Diwan V*, et al.* High-carbohydrate, high-fat diet–induced metabolic syndrome and cardiovascular remodeling in rats. Journal of cardiovascular pharmacology. 2011;57(5):611-24.

353. Harris MI, Cowie CC, Gu K, Francis ME, Flegal K, Eberhardt MS. Higher fasting insulin but lower fasting C-peptide levels in African Americans in the US population. Diabetes/Metabolism Research and Reviews. 2002;18(2):149-55.

354. Johnston DG, Alberti KGMM, Wright R, Smith-Laing G, Stewart AM, Sherlock S*, et al.* C-peptide and Insulin in Liver Disease. Diabetes. 1978;27(Supplement 1):201.

355. Rossell R, Gomis R, Casamitjana R, Segura R, Vilardell E, Rivera F. Reduced Hepatic Insulin Extraction in Obesity: Relationship with Plasma Insulin Levels. The Journal of Clinical Endocrinology & Metabolism. 1983;56(3):608-11.

356. Jones CNO, Abbasi F, Carantoni M, Polonsky KS, Reaven GM. Roles of insulin resistance and obesity in regulation of plasma insulin concentrations. American Journal of Physiology-Endocrinology and Metabolism. 2000;278(3):E501-E8.

357. Najjar SM, Perdomo G. Hepatic Insulin Clearance: Mechanism and Physiology. Physiology. 2019;34(3):198-215.

358. Bojsen-Møller KN, Lundsgaard A-M, Madsbad S, Kiens B, Holst JJ. Hepatic Insulin Clearance in Regulation of Systemic Insulin Concentrations—Role of Carbohydrate and Energy Availability. Diabetes. 2018;67(11):2129.

359. Corkey BE. Banting lecture 2011: hyperinsulinemia: cause or consequence? Diabetes. 2012;61(1):4-13.

360. Pories WJ, Dohm GL. Diabetes: have we got it all wrong?: hyperinsulinism as the culprit: Surgery provides the evidence. Diabetes care. 2012;35(12):2438-42.

361. Knutson V, Ronnett G, Lane MD. Rapid, reversible internalization of cell surface insulin receptors. Correlation with insulin-induced down-regulation. Journal of Biological Chemistry. 1983;258(20):12139-42.

362. Poy MN, Yang Y, Rezaei K, Fernstrom MA, Lee AD, Kido Y*, et al.* CEACAM1 regulates insulin clearance in liver. Nat Genet. 2002;30(3):270-6.

363. Bergman RN, Piccinini F, Kabir M, Kolka CM, Ader M. Hypothesis: Role of Reduced Hepatic Insulin Clearance in the Pathogenesis of Type 2 Diabetes. Diabetes. 2019;68(9):1709.

364. Kotronen A, Juurinen L, Tiikkainen M, Vehkavaara S, Yki–Järvinen H. Increased liver fat, impaired insulin clearance, and hepatic and adipose tissue insulin resistance in type 2 diabetes. Gastroenterology. 2008;135(1):122-30.

365. Ménard S, Cerf-Bensussan N, Heyman M. Multiple facets of intestinal permeability and epithelial handling of dietary antigens. Mucosal Immunology. 2010;3(3):247-59.

366. Vancamelbeke M, Vermeire S. The intestinal barrier: a fundamental role in health and disease. Expert Rev Gastroenterol Hepatol. 2017;11(9):821-34.

367. Hollander D, Kaunitz JD. The “Leaky Gut”: Tight Junctions but Loose Associations? Digestive Diseases and Sciences. 2020;65(5):1277-87.

368. Li Y, Rahman SU, Huang Y, Zhang Y, Ming P, Zhu L*, et al.* Green tea polyphenols decrease weight gain, ameliorate alteration of gut microbiota, and mitigate intestinal inflammation in canines with high-fat-diet-induced obesity. The Journal of Nutritional Biochemistry. 2020;78:108324.

369. Lowell BB, Shulman GI. Mitochondrial dysfunction and type 2 diabetes. Science. 2005;307(5708):384-7.

370. Koliaki C, Roden M. Alterations of mitochondrial function and insulin sensitivity in human obesity and diabetes mellitus. Annual review of nutrition. 2016;36:337-67.

371. Schreyer SA, Wilson DL, Leboeuf RC. C57BL/6 mice fed high fat diets as models for diabetes-accelerated atherosclerosis. Atherosclerosis. 1998;136(1):17-24.

372. Schreyer SA, Vick C, Lystig TC, Mystkowski P, LeBoeuf RC. LDL receptor but not apolipoprotein E deficiency increases diet-induced obesity and diabetes in mice. Am J Physiol Endocrinol Metab. 2002;282(1):E207-14.

373. Fraulob JC, Ogg-Diamantino R, Fernandes-Santos C, Aguila MB, Mandarim-De-Lacerda CA. A Mouse Model of Metabolic Syndrome: Insulin Resistance, Fatty Liver and Non-Alcoholic Fatty Pancreas Disease (NAFPD) in C57BL/6 Mice Fed a High Fat Diet. Journal of Clinical Biochemistry and Nutrition. 2010;46(3):212-23.

374. Altintas MM, Rossetti MA, Nayer B, Puig A, Zagallo P, Ortega LM*, et al.* Apoptosis, mastocytosis, and diminished adipocytokine gene expression accompany reduced epididymal fat mass in long-standing diet-induced obese mice. Lipids in Health and Disease. 2011;10(1):198.

375. Austad SN, Kristan DM. Are mice calorically restricted in nature? Aging Cell. 2003;2(4):201-7.

376. Iossa S, Lionetti L, Mollica MP, Crescenzo R, Botta M, Barletta A*, et al.* Effect of high-fat feeding on metabolic efficiency and mitochondrial oxidative capacity in adult rats. British Journal of Nutrition. 2003;90(05):953.

377. Gao M, Ma Y, Liu D. High-Fat Diet-Induced Adiposity, Adipose Inflammation, Hepatic Steatosis and Hyperinsulinemia in Outbred CD-1 Mice. PLOS ONE. 2015;10(3):e0119784.

378. Lin S, Thomas TC, Storlien LH, Huang XF. Development of high fat diet-induced obesity and leptin resistance in C57Bl/6J mice. International Journal of Obesity. 2000;24(5):639-46.

379. Gruzdeva O, Borodkina D, Uchasova E, Dyleva Y, Barbarash O. Leptin resistance: underlying mechanisms and diagnosis. Diabetes Metab Syndr Obes. 2019;12:191-8.

380. Van Heek M, Compton DS, France CF, Tedesco RP, Fawzi AB, Graziano MP*, et al.* Diet-induced obese mice develop peripheral, but not central, resistance to leptin. The Journal of Clinical Investigation. 1997;99(3):385-90.

381. Hung P-F, Wu B-T, Chen H-C, Chen Y-H, Chen C-L, Wu M-H*, et al.* Antimitogenic effect of green tea (−)-epigallocatechin gallate on 3T3-L1 preadipocytes depends on the ERK and Cdk2 pathways. American Journal of Physiology-Cell Physiology. 2005;288(5):C1094-C108.

382. Wang S, Moustaid-Moussa N, Chen L, Mo H, Shastri A, Su R*, et al.* Novel insights of dietary polyphenols and obesity. The Journal of nutritional biochemistry. 2014;25(1):1-18.

383. Meydani M, Hasan ST. Dietary polyphenols and obesity. Nutrients. 2010;2(7):737-51.

384. Wu B-T, Hung P-F, Chen H-C, Huang R-N, Chang H-H, Kao Y-H. The apoptotic effect of green tea (−)-epigallocatechin gallate on 3T3-L1 preadipocytes depends on the Cdk2 pathway. Journal of agricultural and food chemistry. 2005;53(14):5695-701.

385. Moon HS, Chung CS, Lee HG, Kim TG, Choi YJ, Cho CS. Inhibitory effect of (−)-Epigallocatechin-3-gallate on lipid accumulation of 3T3-L1 cells. Obesity. 2007;15(11):2571-82.

386. Chan CY, Wei L, Castro-Muñozledo F, Koo WL. (−)-Epigallocatechin-3-gallate blocks 3T3-L1 adipose conversion by inhibition of cell proliferation and suppression of adipose phenotype expression. Life sciences. 2011;89(21-22):779-85.

387. Kim H, Hiraishi A, Tsuchiya K, Sakamoto K. (−) Epigallocatechin gallate suppresses the differentiation of 3T3-L1 preadipocytes through transcription factors FoxO1 and SREBP1c. Cytotechnology. 2010;62(3):245-55.

388. Lee M-S, Kim Y. (−)-Epigallocatechin-3-gallate enhances uncoupling protein 2 gene expression in 3T3-L1 adipocytes. Bioscience, biotechnology, and biochemistry. 2009;73(2):434-6.

389. Lin J, Della-Fera MA, Baile CA. Green tea polyphenol epigallocatechin gallate inhibits adipogenesis and induces apoptosis in 3T3-L1 adipocytes. Obesity research. 2005;13(6):982-90.

390. Saeki K, Hayakawa S, Isemura M, Miyase T. Importance of a pyrogallol-type structure in catechin compounds for apoptosis-inducing activity. Phytochemistry. 2000;53(3):391-4.

391. Hayakawa S, Saeki K, Sazuka M, Suzuki Y, Shoji Y, Ohta T*, et al.* Apoptosis Induction by Epigallocatechin Gallate Involves Its Binding to Fas. Biochemical and Biophysical Research Communications. 2001;285(5):1102-6.

392. Ashida H, Furuyashiki T, Nagayasu H, Bessho H, Sakakibara H, Hashimoto T*, et al.* Anti-obesity actions of green tea: Possible involvements in modulation of the glucose uptake system and suppression of the adipogenesis-related transcription factors. Biofactors. 2004;22(1-4):135-40.

393. Chen N, Bezzina R, Hinch E, Lewandowski PA, Cameron-Smith D, Mathai ML*, et al.* Green tea, black tea, and epigallocatechin modify body composition, improve glucose tolerance, and differentially alter metabolic gene expression in rats fed a high-fat diet. Nutrition research. 2009;29(11):784-93.

394. Axling U, Olsson C, Xu J, Fernandez C, Larsson S, Strom K*, et al.* Green tea powder and Lactobacillus plantarum affect gut microbiota, lipid metabolism and inflammation in high-fat fed C57BL/6J mice. Nutr Metab (Lond). 2012;9(1):105.

395. Lu C, Zhu W, Shen C-L, Gao W. Green Tea Polyphenols Reduce Body Weight in Rats by Modulating Obesity-Related Genes. PLOS ONE. 2012;7(6):e38332.

396. Rumpler W, Seale J, Clevidence B, Judd J, Wiley E, Yamamoto S*, et al.* Oolong tea increases metabolic rate and fat oxidation in men. J Nutr. 2001;131(11):2848-52.

397. Dulloo AG, Duret C, Rohrer D, Girardier L, Mensi N, Fathi M*, et al.* Efficacy of a green tea extract rich in catechin polyphenols and caffeine in increasing 24-h energy expenditure and fat oxidation in humans. The American journal of clinical nutrition. 1999;70(6):1040-5.

398. Chantre P, Lairon D. Recent findings of green tea extract AR25 (Exolise) and its activity for the treatment of obesity. Phytomedicine. 2002;9(1):3-8.

399. Wallace M, Metallo CM. Tracing insights into de novo lipogenesis in liver and adipose tissues. Seminars in Cell & Developmental Biology. 2020.

400. Kim JJY, Tan Y, Xiao L, Sun Y-L, Qu X. Green Tea Polyphenol Epigallocatechin-3-Gallate Enhance Glycogen Synthesis and Inhibit Lipogenesis in Hepatocytes. BioMed Research International. 2013;2013:920128.

401. Park HJ, DiNatale DA, Chung M-Y, Park Y-K, Lee J-Y, Koo SI*, et al.* Green tea extract attenuates hepatic steatosis by decreasing adipose lipogenesis and enhancing hepatic antioxidant defenses in ob/ob mice. The Journal of Nutritional Biochemistry. 2011;22(4):393-400.

402. Wolfram S, Raederstorff D, Wang Y, Teixeira SR, Elste V, Weber P. TEAVIGO (epigallocatechin gallate) supplementation prevents obesity in rodents by reducing adipose tissue mass. Ann Nutr Metab. 2005;49(1):54-63.

403. Tan Y, Kim J, Cheng J, Ong M, Lao W-G, Jin X-L*, et al.* Green tea polyphenols ameliorate non-alcoholic fatty liver disease through upregulating AMPK activation in high fat fed Zucker fatty rats. World journal of gastroenterology. 2017;23(21):3805-14.

404. Cheng H, Xu N, Zhao W, Su J, Liang M, Xie Z*, et al.* (-)-Epicatechin regulates blood lipids and attenuates hepatic steatosis in rats fed high-fat diet. Molecular nutrition & food research. 2017;61(11):1700303.

405. Cordero-Herrera I, Martín MÁ, Fernández-Millán E, Álvarez C, Goya L, Ramos S. Cocoa and cocoa flavanol epicatechin improve hepatic lipid metabolism in in vivo and in vitro models. Role of PKCζ. Journal of Functional Foods. 2015;17:761-73.

406. Bauer E, Jakob S, Mosenthin R. Principles of Physiology of Lipid Digestion. Asian-Australas J Anim Sci. 2005;18(2):282-95.

407. Carey MC, Small DM, Bliss CM. Lipid Digestion and Absorption. Annual Review of Physiology. 1983;45(1):651-77.

408. Zechner R, Zimmermann R, Eichmann Thomas O, Kohlwein Sepp D, Haemmerle G, Lass A*, et al.* FAT SIGNALS - Lipases and Lipolysis in Lipid Metabolism and Signaling. Cell Metabolism. 2012;15(3):279-91.

409. Morigny P, Houssier M, Mouisel E, Langin D. Adipocyte lipolysis and insulin resistance. Biochimie. 2016;125:259-66.

410. Wang S, Soni KG, Semache M, Casavant S, Fortier M, Pan L*, et al.* Lipolysis and the integrated physiology of lipid energy metabolism. Molecular Genetics and Metabolism. 2008;95(3):117-26.

411. Titchenell PM, Lazar MA, Birnbaum MJ. Unraveling the Regulation of Hepatic Metabolism by Insulin. Trends in Endocrinology & Metabolism. 2017;28(7):497-505.

412. Engelking LR. Chapter 70 - Lipolysis. In: Engelking LR, editor. Textbook of Veterinary Physiological Chemistry (Third Edition). Boston: Academic Press; 2015. p. 444-9.

413. de Mendoza D, Schujman G. Lipid Biosynthesis. Physiology. 2014:219-28.

414. Kersten S. Mechanisms of nutritional and hormonal regulation of lipogenesis. EMBO Rep. 2001;2(4):282-6.

415. Berg J, Tymoczko J, Stryer L. Acetyl Coenzyme A Carboxylase Plays a Key Role in Controlling Fatty Acid Metabolism. Biochemistry. 5th Edition ed. New York2002.

416. Clarke SD, Nakamura MT. Fatty Acid Structure and Synthesis. In: Lennarz WJ, Lane MD, editors. Encyclopedia of Biological Chemistry (Second Edition). Waltham: Academic Press; 2013. p. 285-9.

417. Wendel AA, Lewin TM, Coleman RA. Glycerol-3-phosphate acyltransferases: rate limiting enzymes of triacylglycerol biosynthesis. Biochimica et biophysica acta. 2009;1791(6):501-6.

418. Khiewkamrop P, Phunsomboon P, Richert L, Pekthong D, Srisawang P. Epistructured catechins, EGCG and EC facilitate apoptosis induction through targeting de novo lipogenesis pathway in HepG2 cells. Cancer Cell International. 2018;18(1):46.

419. Schindelin J, Arganda-Carreras I, Frise E, Kaynig V, Longair M, Pietzsch T*, et al.* Fiji: an open-source platform for biological-image analysis. Nature methods. 2012;9(7):676-82.

420. DebRoy A. Quantifying Stained Liver Tissue University of Iowa [Available from: https://imagej.nih.gov/ij/docs/examples/stained-sections/index.html.

421. Bligh EG, Dyer WJ. A rapid method of total lipid extraction and purification. Canadian Journal of Biochemistry and Physiology. 1959;37(8):911-7.

422. Friedewald WT, Levy RI, Fredrickson DS. Estimation of the concentration of low-density lipoprotein cholesterol in plasma, without use of the preparative ultracentrifuge. Clin Chem. 1972;18(6):499-502.

423. Sun L, Warren FJ, Netzel G, Gidley MJ. 3 or 3'-Galloyl substitution plays an important role in association of catechins and theaflavins with porcine pancreatic α-amylase: The kinetics of inhibition of α-amylase by tea polyphenols. Journal of Functional Foods. 2016;26:144-56.

424. Lever M. Colorimetric and fluorometric carbohydrate determination with p-hydroxybenzoic acid hydrazide. Biochemical medicine. 1973;7(2):274-81.

425. Kalra A, Tuma F. Physiology, Liver. StatPearls [Internet]: StatPearls Publishing; 2018.

426. Neuschwander-Tetri BA, Unalp A, Creer MH, Nonalcoholic Steatohepatitis Clinical Research N. Influence of local reference populations on upper limits of normal for serum alanine aminotransferase levels. Archives of internal medicine. 2004;168(6):663-6.

427. Wieckowska A, Feldstein AE. 74 - Nonalcoholic Fatty Liver Disease. In: Wyllie R, Hyams JS, editors. Pediatric Gastrointestinal and Liver Disease (Fourth Edition). Saint Louis: W.B. Saunders; 2011. p. 804-10.e2.

428. Neuschwander-Tetri BA. Chapter 7 - Fatty liver and nonalcoholic steatohepatitis. In: Friedman LS, Keeffe EB, editors. Handbook of Liver Disease (Third Edition). Philadelpia: W.B. Saunders; 2012. p. 106-14.

429. de Alwis NMW. Chapter 9 - Obesity and Nonalcoholic Fatty Liver Disease. In: Weaver JU, editor. Practical Guide to Obesity Medicine: Elsevier; 2018. p. 89-97.

430. Dasgupta A. Chapter 5 - Liver Enzymes as Alcohol Biomarkers. In: Dasgupta A, editor. Alcohol and its Biomarkers. San Diego: Elsevier; 2015. p. 121-37.

431. Koba S, Hirano T, Ito Y, Tsunoda F, Yokota Y, Ban Y*, et al.* Significance of small dense low-density lipoprotein-cholesterol concentrations in relation to the severity of coronary heart diseases. Atherosclerosis. 2006;189(1):206-14.

432. Pacifico L, Bonci E, Andreoli G, Romaggioli S, Di Miscio R, Lombardo CV*, et al.* Association of serum triglyceride-to-HDL cholesterol ratio with carotid artery intima-media thickness, insulin resistance and nonalcoholic fatty liver disease in children and adolescents. Nutrition, Metabolism and Cardiovascular Diseases. 2014;24(7):737-43.

433. Giannini C, Santoro N, Caprio S, Kim G, Lartaud D, Shaw M*, et al.* The Triglyceride-to-HDL Cholesterol Ratio. Association with insulin resistance in obese youths of different ethnic backgrounds. 2011;34(8):1869-74.

434. McLaughlin T, Reaven G, Abbasi F, Lamendola C, Saad M, Waters D*, et al.* Is There a Simple Way to Identify Insulin-Resistant Individuals at Increased Risk of Cardiovascular Disease? The American Journal of Cardiology. 2005;96(3):399-404.

435. Murguía-Romero M, Jiménez-Flores JR, Sigrist-Flores SC, Espinoza-Camacho MA, Jiménez-Morales M, Piña E*, et al.* Plasma triglyceride/HDL-cholesterol ratio, insulin resistance, and cardiometabolic risk in young adults. Journal of Lipid Research. 2013;54(10):2795-9.

436. Xiao J, Ni X, Kai G, Chen X. A review on structure–activity relationship of dietary polyphenols inhibiting α-amylase. Critical reviews in food science and nutrition. 2013;53(5):497-506.

437. Forester SC, Gu Y, Lambert JD. Inhibition of starch digestion by the green tea polyphenol, (−)-epigallocatechin-3-gallate. Molecular Nutrition & Food Research. 2012;56(11):1647-54.

438. Schwarz J-M, Linfoot P, Dare D, Aghajanian K. Hepatic de novo lipogenesis in normoinsulinemic and hyperinsulinemic subjects consuming high-fat, low-carbohydrate and low-fat, high-carbohydrate isoenergetic diets. The American Journal of Clinical Nutrition. 2003;77(1):43-50.

439. Cordero-Herrera I, Martín MÁ, Goya L, Ramos S. Cocoa intake ameliorates hepatic oxidative stress in young Zucker diabetic fatty rats. Food Research International. 2015;69:194-201.

440. Ramos S, Martín MA, Goya L. Effects of Cocoa Antioxidants in Type 2 Diabetes Mellitus. Antioxidants (Basel). 2017;6(4):84.

441. Hollands WJ, Tapp H, Defernez M, Perez Moral N, Winterbone MS, Philo M*, et al.* Lack of acute or chronic effects of epicatechin-rich and procyanidin-rich apple extracts on blood pressure and cardiometabolic biomarkers in adults with moderately elevated blood pressure: a randomized, placebo-controlled crossover trial. The American Journal of Clinical Nutrition. 2018;108(5):1006-14.

442. Kirch N, Berk L, Liegl Y, Adelsbach M, Zimmermann BF, Stehle P*, et al.* A nutritive dose of pure (–)-epicatechin does not beneficially affect increased cardiometabolic risk factors in overweight-to-obese adults—a randomized, placebo-controlled, double-blind crossover study. The American Journal of Clinical Nutrition. 2018;107(6):948-56.

443. Connolly K, Jackson D, Batacan R, Fenning A. Epicatechin improves lipid profile and oxidative stress status, but does not reduce abdominal fat or blood pressure in an obese SHR model of metabolic syndrome. Heart, Lung and Circulation. 2015;24:S187.

444. Samavat H, Newman AR, Wang R, Yuan J-M, Wu AH, Kurzer MS. Effects of green tea catechin extract on serum lipids in postmenopausal women: a randomized, placebo-controlled clinical trial. The American journal of clinical nutrition. 2016;104(6):1671-82.

445. Ference BA, Ginsberg HN, Graham I, Ray KK, Packard CJ, Bruckert E*, et al.* Low-density lipoproteins cause atherosclerotic cardiovascular disease. 1. Evidence from genetic, epidemiologic, and clinical studies. A consensus statement from the European Atherosclerosis Society Consensus Panel. European heart journal. 2017;38(32):2459-72.

446. Wolf G. High-fat, high-cholesterol diet raises plasma HDL cholesterol: studies on the mechanism of this effect. Nutr Rev. 1996;54(1):34-5.

447. Krauss RM, Eckel RH, Howard B, Appel LJ, Daniels SR, Deckelbaum RJ*, et al.* AHA Dietary Guidelines. Circulation. 2000;102(18):2284-99.

448. Starc TJ, Shea S, Cohn LC, Mosca L, Gersony WM, Deckelbaum RJ. Greater dietary intake of simple carbohydrate is associated with lower concentrations of high-density-lipoprotein cholesterol in hypercholesterolemic children. The American Journal of Clinical Nutrition. 1998;67(6):1147-54.

449. Dreon DM, Fernstrom HA, Miller B, Krauss RM. Low-density lipoprotein subclass patterns and lipoprotein response to a reduced-fat diet in men. The FASEB Journal. 1994;8(1):121-6.

450. Mensink RP, Katan MB. Effect of a diet enriched with monounsaturated or polyunsaturated fatty acids on levels of low-density and high-density lipoprotein cholesterol in healthy women and men. New England Journal of Medicine. 1989;321(7):436-41.

451. Hudgins LC, Hellerstein MK, Seidman CE, Neese RA, Tremaroli JD, Hirsch J. Relationship between carbohydrate-induced hypertriglyceridemia and fatty acid synthesis in lean and obese subjects. Journal of Lipid Research. 2000;41(4):595-604.

452. Garg A, Grundy SM, Unger RH. Comparison of Effects of High and Low Carbohydrate Diets on Plasma Lipoproteins and Insulin Sensitivity in Patients With Mild NIDDM. Diabetes. 1992;41(10):1278-85.

453. Oster P, Schlierf G, Heuck CC, Hahn S, Szymanski H, Schellenberg B. Diet and high density lipoproteins. Lipids. 1981;16(2):93-7.

454. Turley M, Skeaff C, Mann J, Cox B. The effect of a low-fat, high-carbohydrate diet on serum high density lipoprotein cholesterol and triglyceride. European journal of clinical nutrition. 1998;52(10):728-32.

455. Castelli WP. Epidemiology of coronary heart disease: the Framingham study. Am J Med. 1984;76(2a):4-12.

456. Linton MF, Yancey PG, Davies SS, Jerome WG, Linton EF, Song WL*, et al.* The role of lipids and lipoproteins in atherosclerosis. Endotext [Internet]. South Dartmouth: MDText. com, Inc.; 2019.

457. Tall AR, Rader DJ. Trials and Tribulations of CETP Inhibitors. Circ Res. 2018;122(1):106-12.

458. Rohatgi A, Khera A, Berry JD, Givens EG, Ayers CR, Wedin KE*, et al.* HDL cholesterol efflux capacity and incident cardiovascular events. N Engl J Med. 2014;371(25):2383-93.

459. Saleheen D, Scott R, Javad S, Zhao W, Rodrigues A, Picataggi A*, et al.* Association of HDL cholesterol efflux capacity with incident coronary heart disease events: a prospective case-control study. Lancet Diabetes Endocrinol. 2015;3(7):507-13.

460. Tessitore A, Mastroiaco V, Vetuschi A, Sferra R, Pompili S, Cicciarelli G*, et al.* Development of hepatocellular cancer induced by long term low fat-high carbohydrate diet in a NAFLD/NASH mouse model. Oncotarget. 2017;8(32):53482.

461. Chen Q, Xiong C, Jia K, Jin J, Li Z, Huang Y*, et al.* Hepatic transcriptome analysis from HFD-fed mice defines a long noncoding RNA regulating cellular cholesterol levels. Journal of lipid research. 2019;60(2):341-52.

462. Chen Y, Wu Y, Yang Y, Xu Z, Tong J, Li Z*, et al.* Transcriptomic and proteomic analysis of potential therapeutic target genes in the liver of metformin-treated Sprague-Dawley rats with type 2 diabetes mellitus. International journal of molecular medicine. 2018;41(6):3327-41.

463. Toye AA, Dumas ME, Blancher C, Rothwell AR, Fearnside JF, Wilder SP*, et al.* Subtle metabolic and liver gene transcriptional changes underlie diet-induced fatty liver susceptibility in insulin-resistant mice. Diabetologia. 2007;50(9):1867-79.

464. Wu X, Xu H, Zhang Z, Chang Q, Liao S, Zhang L*, et al.* Transcriptome Profiles Using Next-Generation Sequencing Reveal Liver Changes in the Early Stage of Diabetes in Tree Shrew (Tupaia belangeri chinensis). Journal of Diabetes Research. 2016;2016:6238526.

465. Hayek T, Ito Y, Azrolan N, Verdery RB, Aalto-Setälä K, Walsh A*, et al.* Dietary fat increases high density lipoprotein (HDL) levels both by increasing the transport rates and decreasing the fractional catabolic rates of HDL cholesterol ester and apolipoprotein (Apo) A-I. Presentation of a new animal model and mechanistic studies in human Apo A-I transgenic and control mice. The Journal of clinical investigation. 1993;91(4):1665-71.

466. Brinton EA, Eisenberg S, Breslow JL. A low-fat diet decreases high density lipoprotein (HDL) cholesterol levels by decreasing HDL apolipoprotein transport rates. The Journal of clinical investigation. 1990;85(1):144-51.

467. Ruanpang J, Pleumsamran A, Pleumsamran J, Mingmalairak S. Effect of a high-fat diet and cholesterol levels on depression-like behavior in mice. Chiang Mai University Journal of Natural Sciences. 2018.

468. Schwingshackl L, Hoffmann G. Comparison of Effects of Long-Term Low-Fat vs High-Fat Diets on Blood Lipid Levels in Overweight or Obese Patients: A Systematic Review and Meta-Analysis. Journal of the Academy of Nutrition and Dietetics. 2013;113(12):1640-61.

469. Lomas-Soria C, Reyes-Castro LA, Rodríguez-González GL, Ibáñez CA, Bautista CJ, Cox LA*, et al.* Maternal obesity has sex-dependent effects on insulin, glucose and lipid metabolism and the liver transcriptome in young adult rat offspring. The Journal of physiology. 2018;596(19):4611-28.

470. Day CP, James OF. Steatohepatitis: a tale of two “hits”? : Elsevier; 1998.

471. Fabbrini E, Sullivan S, Klein S. Obesity and nonalcoholic fatty liver disease: biochemical, metabolic, and clinical implications. Hepatology. 2010;51(2):679-89.

472. Sanders FWB, Griffin JL. De novo lipogenesis in the liver in health and disease: more than just a shunting yard for glucose. Biol Rev Camb Philos Soc. 2016;91(2):452-68.

473. Gressner OA, Weiskirchen R, Gressner AM. Biomarkers of liver fibrosis: Clinical translation of molecular pathogenesis or based on liver-dependent malfunction tests. Clinica Chimica Acta. 2007;381(2):107-13.

474. Brenner DA. Molecular pathogenesis of liver fibrosis. Trans Am Clin Climatol Assoc. 2009;120:361-8.

475. Hernandez-Gea V, Friedman SL. Pathogenesis of Liver Fibrosis. Annual Review of Pathology: Mechanisms of Disease. 2011;6(1):425-56.

476. Huang Z, Jing X, Sheng Y, Zhang J, Hao Z, Wang Z*, et al.* (-)-Epicatechin attenuates hepatic sinusoidal obstruction syndrome by inhibiting liver oxidative and inflammatory injury. Redox biology. 2019;22:101117-.

477. Xiao J, Ho CT, Liong EC, Nanji AA, Leung TM, Lau TYH*, et al.* Epigallocatechin gallate attenuates fibrosis, oxidative stress, and inflammation in non-alcoholic fatty liver disease rat model through TGF/SMAD, PI3 K/Akt/FoxO1, and NF-kappa B pathways. European journal of nutrition. 2014;53(1):187-99.

478. Bruno RS, Dugan CE, Smyth JA, DiNatale DA, Koo SI. Green Tea Extract Protects Leptin-Deficient, Spontaneously Obese Mice from Hepatic Steatosis and Injury. The Journal of Nutrition. 2008;138(2):323-31.

479. Nakamoto K, Takayama F, Mankura M, Hidaka Y, Egashira T, Ogino T*, et al.* Beneficial effects of fermented green tea extract in a rat model of non-alcoholic steatohepatitis. Journal of clinical biochemistry and nutrition. 2009;44(3):239-46.

480. Sakata R, Nakamura T, Torimura T, Ueno T, Sata M. Green tea with high-density catechins improves liver function and fat infiltration in non-alcoholic fatty liver disease (NAFLD) patients: A double-blind placebo-controlled study. Int J Mol Med. 2013;32(5):989-94.

481. Basaranoglu M, Basaranoglu G, Bugianesi E. Carbohydrate intake and nonalcoholic fatty liver disease: fructose as a weapon of mass destruction. Hepatobiliary Surg Nutr. 2015;4(2):109-16.

482. Abdelmalek MF, Suzuki A, Guy C, Unalp-Arida A, Colvin R, Johnson RJ*, et al.* Increased fructose consumption is associated with fibrosis severity in patients with nonalcoholic fatty liver disease. Hepatology. 2010;51(6):1961-71.

483. Sumiyoshi M, Sakanaka M, Kimura Y. Chronic intake of a high-cholesterol diet resulted in hepatic steatosis, focal nodular hyperplasia and fibrosis in non-obese mice. British Journal of Nutrition. 2010;103(3):378-85.

484. Menezes AL, Pereira MP, Buzelle SL, dos Santos MP, de França SA, Baviera AM*, et al.* A low-protein, high-carbohydrate diet increases de novo fatty acid synthesis from glycerol and glycerokinase content in the liver of growing rats. Nutrition Research. 2013;33(6):494-502.

485. Solga S, Alkhuraishe AR, Clark JM, Torbenson M, Greenwald A, Diehl AM*, et al.* Dietary composition and nonalcoholic fatty liver disease. Digestive diseases and sciences. 2004;49(10):1578-83.

486. Kieffer DA, Martin RJ, Adams SH. Impact of dietary fibers on nutrient management and detoxification organs: gut, liver, and kidneys. Advances in Nutrition. 2016;7(6):1111-21.

487. Sonnenburg ED, Smits SA, Tikhonov M, Higginbottom SK, Wingreen NS, Sonnenburg JL. Diet-induced extinctions in the gut microbiota compound over generations. Nature. 2016;529(7585):212-5.

488. Pellizzon MA, Ricci MR. Choice of Laboratory Rodent Diet May Confound Data Interpretation and Reproducibility. Current Developments in Nutrition. 2020;4(4).

489. Zolfaghari H, Askari G, Siassi F, Feizi A, Sotoudeh G. Intake of Nutrients, Fiber, and Sugar in Patients with Nonalcoholic Fatty Liver Disease in Comparison to Healthy Individuals. Int J Prev Med. 2016;7:98-.

490. Xia Y, Zhang S, Zhang Q, Liu L, Meng G, Wu H*, et al.* Insoluble dietary fibre intake is associated with lower prevalence of newly-diagnosed non-alcoholic fatty liver disease in Chinese men: a large population-based cross-sectional study. Nutrition & Metabolism. 2020;17(1):4.

491. Brockman DA, Chen X, Gallaher DD. High-viscosity dietary fibers reduce adiposity and decrease hepatic steatosis in rats fed a high-fat diet. J Nutr. 2014;144(9):1415-22.

492. Cantero I, Abete I, Monreal JI, Martinez JA, Zulet MA. Fruit Fiber Consumption Specifically Improves Liver Health Status in Obese Subjects under Energy Restriction. Nutrients. 2017;9(7):667.

493. Butterworth PJ, Warren FJ, Ellis PR. Human α-amylase and starch digestion: An interesting marriage. Starch-Stärke. 2011;63(7):395-405.

494. Dhital S, Warren FJ, Butterworth PJ, Ellis PR, Gidley MJ. Mechanisms of starch digestion by α-amylase—Structural basis for kinetic properties. Critical reviews in food science and nutrition. 2017;57(5):875-92.

495. Nyambe-Silavwe H, Villa-Rodriguez JA, Ifie I, Holmes M, Aydin E, Jensen JM*, et al.* Inhibition of human α-amylase by dietary polyphenols. Journal of Functional Foods. 2015;19:723-32.

496. Martinez-Gonzalez AI, Díaz-Sánchez Á, de La Rosa L, Bustos-Jaimes I, Alvarez-Parrilla E. Inhibition of α-amylase by flavonoids: Structure activity relationship (SAR). Spectrochimica Acta Part A: Molecular and Biomolecular Spectroscopy. 2019;206:437-47.

497. Proença C. FM, Ribeiro D., Tomé S.M., Oliveira E.F.T., Viegas M.F., Araújo A.N., Ramos M.J., Silva. A.M.S., Fernandes P.A. & Fernandes E. Evaluation of a flavonoids library for inhibition of pancreatic α-amylase towards a structure–activity relationship. Journal of Enzyme Inhibition and Medicinal Chemistry. 2019;34:577-88.

498. Hara Y, Honda M. The inhibition of α-amylase by tea polyphenols. Agricultural and Biological Chemistry. 1990;54(8):1939-45.

499. Koh LW, Wong LL, Loo YY, Kasapis S, Huang D. Evaluation of different teas against starch digestibility by mammalian glycosidases. Journal of agricultural and food chemistry. 2010;58(1):148-54.

500. Wang R, Wang X, Zhuang L. Gene expression profiling reveals key genes and pathways related to the development of non-alcoholic fatty liver disease. Annals of hepatology. 2016;15(2):190-9.

501. Moylan CA, Pang H, Dellinger A, Suzuki A, Garrett ME, Guy CD*, et al.* Hepatic gene expression profiles differentiate presymptomatic patients with mild versus severe nonalcoholic fatty liver disease. Hepatology. 2014;59(2):471-82.

502. Huang S, Sun C, Hou Y, Tang Y, Zhu Z, Zhang Z*, et al.* A comprehensive bioinformatics analysis on multiple Gene Expression Omnibus datasets of nonalcoholic fatty liver disease and nonalcoholic steatohepatitis. Scientific reports. 2018;8(1):7630-.

503. Ryaboshapkina M, Hammar M. Human hepatic gene expression signature of non-alcoholic fatty liver disease progression, a meta-analysis. Scientific Reports. 2017;7(1):12361.

504. Almanza D, Gharaee-Kermani M, Zhilin-Roth A, Rodriguez-Nieves JA, Colaneri C, Riley T*, et al.* Nonalcoholic Fatty Liver Disease Demonstrates a Pre-fibrotic and Premalignant Molecular Signature. Digestive Diseases and Sciences. 2019;64(5):1257-69.

505. Hoang SA, Oseini A, Feaver RE, Cole BK, Asgharpour A, Vincent R*, et al.* Gene Expression Predicts Histological Severity and Reveals Distinct Molecular Profiles of Nonalcoholic Fatty Liver Disease. Scientific Reports. 2019;9(1):12541.

506. Zhang F, Xu X, Zhang Y, Zhou B, He Z, Zhai Q. Gene expression profile analysis of type 2 diabetic mouse liver. PloS one. 2013;8(3):e57766-e.

507. Lan H, Rabaglia ME, Stoehr JP, Nadler ST, Schueler KL, Zou F*, et al.* Gene expression profiles of nondiabetic and diabetic obese mice suggest a role of hepatic lipogenic capacity in diabetes susceptibility. Diabetes. 2003;52(3):688-700.

508. Way JM, Harrington WW, Brown KK, Gottschalk WK, Sundseth SS, Mansfield TA*, et al.* Comprehensive messenger ribonucleic acid profiling reveals that peroxisome proliferator-activated receptor γ activation has coordinate effects on gene expression in multiple insulin-sensitive tissues. Endocrinology. 2001;142(3):1269-77.

509. Suzuki A, Yasuno T, Kojo H, Hirosumi J, Mutoh S, Notsu Y. Alteration in expression profiles of a series of diabetes-related genes in db/db mice following treatment with thiazolidinediones. The Japanese Journal of Pharmacology. 2000;84(2):113-23.

510. Chao L, Marcus-Samuels B, Mason MM, Moitra J, Vinson C, Arioglu E*, et al.* Adipose tissue is required for the antidiabetic, but not for the hypolipidemic, effect of thiazolidinediones. The Journal of clinical investigation. 2000;106(10):1221-8.

511. Yahagi N, Shimano H, Hasty AH, Matsuzaka T, Ide T, Yoshikawa T*, et al.* Absence of sterol regulatory element-binding protein-1 (srebp-1) ameliorates fatty livers but not obesity or insulin resistance inlep ob/lep ob mice. Journal of Biological Chemistry. 2002;277(22):19353-7.

512. Rajaram S, Baylink DJ, Mohan S. Insulin-like growth factor-binding proteins in serum and other biological fluids: regulation and functions. Endocr Rev. 1997;18(6):801-31.

513. Rajwani A, Ezzat V, Smith J, Yuldasheva NY, Duncan ER, Gage M*, et al.* Increasing circulating IGFBP1 levels improves insulin sensitivity, promotes nitric oxide production, lowers blood pressure, and protects against atherosclerosis. Diabetes. 2012;61(4):915-24.

514. Cai Q, Oh Y. The Impact of IGFBP-3/IGFBP-3R System on Obesity-associated Insulin Resistance. 2019.

515. Heald A, Anderson S, Cruickshank J, Gibson J, editors. Circulating IGFBP-3 concentration is independently associated with insulin resistance and BMI. 22nd Joint Meeting of the British Endocrine Societies; 2003: BioScientifica.

516. Ohashi S, Natsuizaka M, Nakagawa H. MMP7 and activation of IGF-1R: a new insight into anti-EGFR therapeutic resistance in metastatic colorectal cancer. Cancer biology & therapy. 2011;11(2):184-7.

517. Claudia R, Alexander T, Christian C, Markus WL, Julia WE, Wolfgang S*, et al.* Influence of significant weight loss on serum matrix metalloproteinase (MMP)-7 levels. European Cytokine Network. 2010;21(1):65-70.

518. Maquoi E, Munaut C, Colige A, Collen D, Lijnen HR. Modulation of Adipose Tissue Expression of Murine Matrix Metalloproteinases and Their Tissue Inhibitors With Obesity. Diabetes. 2002;51(4):1093-101.

519. Wang L, Yang G, Yuan L, Yang Y, Zhao H, Ho C-T*, et al.* Green tea catechins effectively altered hepatic fibrogenesis in rats by inhibiting ERK and Smad1/2 phosphorylation. Journal of agricultural and food chemistry. 2018;67(19):5437-45.

520. Kobayashi H, Tanaka Y, Asagiri K, Asakawa T, Tanikawa K, Kage M*, et al.* The antioxidant effect of green tea catechin ameliorates experimental liver injury. Phytomedicine. 2010;17(3):197-202.

521. Ferreira LT, de Sousa Filho CPB, Marinovic MP, Rodrigues AC, Otton R. Green tea polyphenols positively impact hepatic metabolism of adiponectin-knockout lean mice. Journal of Functional Foods. 2020;64:103679.

522. Wolfram S, Wang Y, Thielecke F. Anti-obesity effects of green tea: From bedside to bench. Molecular Nutrition & Food Research. 2006;50(2):176-87.

523. Yu DK, Zhang CX, Zhao SS, Zhang SH, Zhang H, Cai SY*, et al.* The anti-fibrotic effects of epigallocatechin-3-gallate in bile duct-ligated cholestatic rats and human hepatic stellate LX-2 cells are mediated by the PI3K/Akt/Smad pathway. Acta Pharmacol Sin. 2015;36(4):473-82.

524. Nakamuta M, Higashi N, Kohjima M, Fukushima M, Ohta S, Kotoh K*, et al.* Epigallocatechin-3-gallate, a polyphenol component of green tea, suppresses both collagen production and collagenase activity in hepatic stellate cells. Int J Mol Med. 2005;16(4):677-81.

525. Bose M, Lambert JD, Ju J, Reuhl KR, Shapses SA, Yang CS. The Major Green Tea Polyphenol, (-)-Epigallocatechin-3-Gallate, Inhibits Obesity, Metabolic Syndrome, and Fatty Liver Disease in High-Fat–Fed Mice. The Journal of Nutrition. 2008;138(9):1677-83.

526. Shrestha S, Ehlers SJ, Lee J-Y, Fernandez M-L, Koo SI. Dietary green tea extract lowers plasma and hepatic triglycerides and decreases the expression of sterol regulatory element-binding protein-1c mRNA and its responsive genes in fructose-fed, ovariectomized rats. The Journal of nutrition. 2009;139(4):640-5.

527. Koyama Y, Abe K, Sano Y, Ishizaki Y, Njelekela M, Shoji Y*, et al.* Effects of Green Tea on Gene Expression of Hepatic Gluconeogenic Enzymes in vivo. Planta Med. 2004;70(11):1100-2.

528. Granado-Serrano AB, Martín MA, Haegeman G, Goya L, Bravo L, Ramos S. Epicatechin induces NF-κB, activator protein-1 (AP-1) and nuclear transcription factor erythroid 2p45-related factor-2 (Nrf2) via phosphatidylinositol-3-kinase/protein kinase B (PI3K/AKT) and extracellular regulated kinase (ERK) signalling in HepG2 cells. British Journal of Nutrition. 2010;103(2):168-79.

529. Granado-Serrano AB, Martín MA, Goya L, Bravo L, Ramos S. Time-course regulation of survival pathways by epicatechin on HepG2 cells. The Journal of nutritional biochemistry. 2009;20(2):115-24.

530. Mohamadpour Z, Sharifi L, Norouzzadeh M, Kalikias Y, Mahmoudi M. Hyperglycemia induction in HepG2 cell line. International Journal of Health Studies. 2016;2(1):28-9.

531. Fang J-Y, Lin C-H, Huang T-H, Chuang S-Y. In Vivo Rodent Models of Type 2 Diabetes and Their Usefulness for Evaluating Flavonoid Bioactivity. Nutrients. 2019;11(3):530.

532. Ferramosca A, Conte A, Damiano F, Siculella L, Zara V. Differential effects of high-carbohydrate and high-fat diets on hepatic lipogenesis in rats. European Journal of Nutrition. 2014;53(4):1103-14.

533. Parry SA, Hodson L. Influence of dietary macronutrients on liver fat accumulation and metabolism. Journal of Investigative Medicine. 2017;65(8):1102-15.

534. Axen KV, Harper MA, Kuo YF, Axen K. Very low-carbohydrate, high-fat, weight reduction diet decreases hepatic gene response to glucose in obese rats. Nutrition & Metabolism. 2018;15(1):54.

535. Smith TJ. Green Tea Polyphenols in drug discovery - a success or failure? Expert Opin Drug Discov. 2011;6(6):589-95.

536. Abe K, Suzuki T, Ijiri M, Koyama Y, Isemura M, Kinae N. The anti-fibrotic effect of green tea with a high catechin content in the galactosamine-injured rat liver. Biomedical Research. 2007;28(1):43-8.

537. Kopylova E, Noé L, Touzet H. SortMeRNA: fast and accurate filtering of ribosomal RNAs in metatranscriptomic data. Bioinformatics. 2012;28(24):3211-7.

538. Andrews S. FastQC: a quality control tool for high throughput sequence data: Babraham Bioinformatics, Babraham Institute, Cambridge, United Kingdom; 2010 [Available from: http://www.bioinformatics.babraham.ac.uk/projects/fastqc/.

539. Yates AD, Achuthan P, Akanni W, Allen J, Allen J, Alvarez-Jarreta J*, et al.* Ensembl 2020. Nucleic Acids Research. 2020;48(D1):D682-D8.

540. Kim D, Langmead B, Salzberg SL. HISAT: a fast spliced aligner with low memory requirements. Nature Methods. 2015;12(4):357-60.

541. Pertea M, Pertea GM, Antonescu CM, Chang T-C, Mendell JT, Salzberg SL. StringTie enables improved reconstruction of a transcriptome from RNA-seq reads. Nat Biotechnol. 2015;33(3):290-5.

542. M P, D K, GM P, JT L, SL S. RNA-Sequencing raw gene count script John Hopkins University, USA: The Center for Computational Biology; 2020 [Available from: https://ccb.jhu.edu/software/stringtie/dl/prepDE.py.

543. Love MI, Huber W, Anders S. Moderated estimation of fold change and dispersion for RNA-seq data with DESeq2. Genome biology. 2014;15(12):550.

544. Love MI, Anders S, Kim V, Huber W. RNA-seq workflow: gene-level exploratory analysis and differential expression Rowell Park, New York: Bioconductor; 2019 [cited 2020.

545. Benjamini Y, Hochberg Y. Controlling the false discovery rate: a practical and powerful approach to multiple testing. Journal of the Royal statistical society: series B (Methodological). 1995;57(1):289-300.

546. Subramanian A, Tamayo P, Mootha VK, Mukherjee S, Ebert BL, Gillette MA*, et al.* Gene set enrichment analysis: a knowledge-based approach for interpreting genome-wide expression profiles. Proceedings of the National Academy of Sciences. 2005;102(43):15545-50.

547. Vandesompele J, De Preter K, Pattyn F, Poppe B, Van Roy N, De Paepe A*, et al.* Accurate normalization of real-time quantitative RT-PCR data by geometric averaging of multiple internal control genes. Genome biology. 2002;3(7):research0034. 1.

548. Andersen CL, Jensen JL, Ørntoft TF. Normalization of real-time quantitative reverse transcription-PCR data: a model-based variance estimation approach to identify genes suited for normalization, applied to bladder and colon cancer data sets. Cancer research. 2004;64(15):5245-50.

549. Pfaffl MW, Tichopad A, Prgomet C, Neuvians TP. Determination of stable housekeeping genes, differentially regulated target genes and sample integrity: BestKeeper–Excel-based tool using pair-wise correlations. Biotechnology letters. 2004;26(6):509-15.

550. Rao X, Huang X, Zhou Z, Lin X. An improvement of the 2ˆ(-delta delta CT) method for quantitative real-time polymerase chain reaction data analysis. Biostat Bioinforma Biomath. 2013;3(3):71-85.

551. Pertea M, Kim D, Pertea GM, Leek JT, Salzberg SL. Transcript-level expression analysis of RNA-seq experiments with HISAT, StringTie and Ballgown. Nature Protocols. 2016;11(9):1650-67.

552. Seyednasrollah F, Laiho A, Elo LL. Comparison of software packages for detecting differential expression in RNA-seq studies. Brief Bioinform. 2015;16(1):59-70.

553. Costa-Silva J, Domingues D, Lopes FM. RNA-Seq differential expression analysis: An extended review and a software tool. PloS one. 2017;12(12):e0190152-e.

554. Tibshirani R. Estimating transformations for regression via additivity and variance stabilization. Journal of the American Statistical Association. 1988;83(402):394-405.

555. Huber W, von Heydebreck A, Sültmann H, Poustka A, Vingron M. Parameter estimation for the calibration and variance stabilization of microarray data. Statistical applications in genetics and molecular biology. 2003;2(1).

556. Anders S, Huber W. Differential expression analysis for sequence count data. Genome Biology. 2010;11(10):R106.

557. Li Y, Zhu M, Huo Y, Zhang X, Liao M. Anti-fibrosis activity of combination therapy with epigallocatechin gallate, taurine and genistein by regulating glycolysis, gluconeogenesis, and ribosomal and lysosomal signaling pathways in HSC-T6 cells. Exp Ther Med. 2018;16(6):4329-38.

558. Karim S, Adams DH, Lalor PF. Hepatic expression and cellular distribution of the glucose transporter family. World journal of gastroenterology. 2012;18(46):6771-81.

559. Gaggini M, Carli F, Rosso C, Buzzigoli E, Marietti M, Della Latta V*, et al.* Altered amino acid concentrations in NAFLD: Impact of obesity and insulin resistance. Hepatology. 2018;67(1):145-58.

560. Schwartzenberg-Bar-Yoseph F, Armoni M, Karnieli E. The tumor suppressor p53 down-regulates glucose transporters GLUT1 and GLUT4 gene expression. Cancer Res. 2004;64(7):2627-33.

561. Teufel A, Itzel T, Erhart W, Brosch M, Wang XY, Kim YO*, et al.* Comparison of gene expression patterns between mouse models of nonalcoholic fatty liver disease and liver tissues from patients. Gastroenterology. 2016;151(3):513-25. e0.

562. Parks EJ, Krauss RM, Christiansen MP, Neese RA, Hellerstein MK. Effects of a low-fat, high-carbohydrate diet on VLDL-triglyceride assembly, production, and clearance. The Journal of clinical investigation. 1999;104(8):1087-96.

563. Paglialunga S, Dehn CA. Clinical assessment of hepatic de novo lipogenesis in non-alcoholic fatty liver disease. Lipids in health and disease. 2016;15(1):1-10.

564. Agius L. High-carbohydrate diets induce hepatic insulin resistance to protect the liver from substrate overload. Biochemical Pharmacology. 2013;85(3):306-12.

565. Shin DH, Paulauskis JD, Moustaïd N, Sul HS. Transcriptional regulation of p90 with sequence homology to Escherichia coli glycerol-3-phosphate acyltransferase. Journal of Biological Chemistry. 1991;266(35):23834-9.

566. Pelley JW. 13 - Integration of Carbohydrate, Fat, and Amino Acid Metabolism. In: Pelley JW, editor. Elsevier's Integrated Review Biochemistry (Second Edition). Philadelphia: W.B. Saunders; 2012. p. 109-17.

567. Brown MS, Goldstein JL. Selective versus total insulin resistance: a pathogenic paradox. Cell Metab. 2008;7(2):95-6.

568. Edgerton DS, Cardin S, Emshwiller M, Neal D, Chandramouli V, Schumann WC*, et al.* Small increases in insulin inhibit hepatic glucose production solely caused by an effect on glycogen metabolism. Diabetes. 2001;50(8):1872-82.

569. Oh K-J, Han H-S, Kim M-J, Koo S-H. CREB and FoxO1: two transcription factors for the regulation of hepatic gluconeogenesis. BMB reports. 2013;46(12):567-74.

570. Lee S, Dong HH. FoxO integration of insulin signaling with glucose and lipid metabolism. The Journal of endocrinology. 2017;233(2):R67-R79.

571. Sutherland C, O'Brien RM, Granner DK. Insulin Action Gene Regulation. Mechanisms of Insulin Action: Springer; 2007. p. 110-32.

572. Gross D, Van den Heuvel A, Birnbaum M. The role of FoxO in the regulation of metabolism. Oncogene. 2008;27(16):2320-36.

573. Arizmendi C, Liu S, Croniger C, Poli V, Friedman JE. The transcription factor CCAAT/enhancer-binding protein β regulates gluconeogenesis and phosphoenolpyruvate

carboxykinase (GTP) gene transcription during diabetes. Journal of Biological Chemistry. 1999;274(19):13033-40.

574. Lee I-K. The role of pyruvate dehydrogenase kinase in diabetes and obesity. Diabetes Metab J. 2014;38(3):181-6.

575. Jeoung NH. Pyruvate Dehydrogenase Kinases: Therapeutic Targets for Diabetes and Cancers. Diabetes Metab J. 2015;39(3):188-97.

576. Li L, Liu H, Hu X, Huang Y, Wang Y, He Y*, et al.* Identification of key genes in non-alcoholic fatty liver disease progression based on bioinformatics analysis. Mol Med Rep. 2018;17(6):7708-20.

577. Almanza D. RNA Seq Analysis of Non-Alcoholic Fatty Liver Disease (NAFLD) Induced by Metabolic Syndrome in a Mouse Model [Honors College Theses]. Boston: University of Massachusetts-Boston; 2016.

578. Zeng L, Tang WJ, Yin JJ, Zhou BJ. Signal transductions and nonalcoholic fatty liver: a mini-review. International journal of clinical and experimental medicine. 2014;7(7):1624.

579. Li S, Tan HY, Wang N, Cheung F, Hong M, Feng Y. The Potential and Action Mechanism of Polyphenols in the Treatment of Liver Diseases. Oxidative Medicine and Cellular Longevity. 2018;2018:8394818.

580. Blanchet E, Van de Velde S, Matsumura S, Hao E, LeLay J, Kaestner K*, et al.* Feedback inhibition of CREB signaling promotes beta cell dysfunction in insulin resistance. Cell Rep. 2015;10(7):1149-57.

581. Jansson D, Ng AC-H, Fu A, Depatie C, Al Azzabi M, Screaton RA. Glucose controls CREB activity in islet cells via regulated phosphorylation of TORC2. Proceedings of the National Academy of Sciences. 2008;105(29):10161-6.

582. Yang H, Yang L. Targeting cAMP/PKA pathway for glycemic control and type 2 diabetes therapy. J Mol Endocrinol. 2016;57(2):R93-R108.

583. Moreno-Fernandez ME, Giles DA, Stankiewicz TE, Sheridan R, Karns R, Cappelletti M*, et al.* Peroxisomal β-oxidation regulates whole body metabolism, inflammatory vigor, and pathogenesis of nonalcoholic fatty liver disease. JCI Insight. 2018;3(6):e93626.

584. Srivastava RAK, Pinkosky SL, Filippov S, Hanselman JC, Cramer CT, Newton RS. AMP-activated protein kinase: an emerging drug target to regulate imbalances in lipid and carbohydrate metabolism to treat cardio-metabolic diseases. Journal of lipid research. 2012;53(12):2490-514.

585. Panasiuk A, Dzieciol J, Panasiuk B, Prokopowicz D. Expression of p53, Bax and Bcl-2 proteins in hepatocytes in non-alcoholic fatty liver disease. World journal of gastroenterology: WJG. 2006;12(38):6198.

586. Kung C-P, Murphy ME. The role of the p53 tumor suppressor in metabolism and diabetes. The Journal of endocrinology. 2016;231(2):R61.

587. Strycharz J, Drzewoski J, Szemraj J, Sliwinska A. Is p53 Involved in Tissue-Specific Insulin Resistance Formation? Oxidative medicine and cellular longevity. 2017;2017:9270549-.

588. Goldstein I, Yizhak K, Madar S, Goldfinger N, Ruppin E, Rotter V. p53 promotes the expression of gluconeogenesis-related genes and enhances hepatic glucose production. Cancer & Metabolism. 2013;1(1):9.

589. Feng Z, Hu W, de Stanchina E, Teresky AK, Jin S, Lowe S*, et al.* The Regulation of AMPK β1, TSC2, and PTEN Expression by p53: Stress, Cell and Tissue Specificity, and the Role of These Gene Products in Modulating the IGF-1-AKT-mTOR Pathways. Cancer Research. 2007;67(7):3043-53.

590. Ghosh S, Bhattacharyya S, Rashid K, Sil PC. Curcumin protects rat liver from streptozotocin-induced diabetic pathophysiology by counteracting reactive oxygen species and inhibiting the activation of p53 and MAPKs mediated stress response pathways. Toxicology Reports. 2015;2:365-76.

591. Kawauchi K, Araki K, Tobiume K, Tanaka N. p53 regulates glucose metabolism through an IKK-NF-kappaB pathway and inhibits cell transformation. Nat Cell Biol. 2008;10(5):611-8.

592. Bimonte S, Albino V, Piccirillo M, Nasto A, Molino C, Palaia R*, et al.* Epigallocatechin-3-gallate in the prevention and treatment of hepatocellular carcinoma: experimental findings and translational perspectives. Drug Des Devel Ther. 2019;13:611-21.

593. Cordero-Herrera I, Martín MA, Bravo L, Goya L, Ramos S. Epicatechin Gallate Induces Cell Death via p53 Activation and Stimulation of p38 and JNK in Human Colon Cancer SW480 Cells. Nutrition and Cancer. 2013;65(5):718-28.

594. Jin L, Li C, Xu Y, Wang L, Liu J, Wang D*, et al.* Epigallocatechin gallate promotes p53 accumulation and activity via the inhibition of MDM2-mediated p53 ubiquitination in human lung cancer cells. Oncol Rep. 2013;29(5):1983-90.

595. Takamura T, Misu H, Matsuzawa-Nagata N, Sakurai M, Ota T, Shimizu A*, et al.* Obesity upregulates genes involved in oxidative phosphorylation in livers of diabetic patients. Obesity (Silver Spring). 2008;16(12):2601-9.

596. Misu H, Takamura T, Matsuzawa N, Shimizu A, Ota T, Sakurai M*, et al.* Genes involved in oxidative phosphorylation are coordinately upregulated with fasting hyperglycaemia in livers of patients with type 2 diabetes. Diabetologia. 2007;50(2):268-77.

597. Ciapaite J, Bakker SJL, Van Eikenhorst G, Wagner MJ, Teerlink T, Schalkwijk CG*, et al.* Functioning of oxidative phosphorylation in liver mitochondria of high-fat diet fed rats. Biochimica et Biophysica Acta (BBA) - Molecular Basis of Disease. 2007;1772(3):307-16.

598. Erion DM, Ignatova ID, Yonemitsu S, Nagai Y, Chatterjee P, Weismann D*, et al.* Prevention of hepatic steatosis and hepatic insulin resistance by knockdown of cAMP response element-binding protein. Cell metabolism. 2009;10(6):499-506.

599. Liu Y, Cheng F, Luo Y, Zhan Z, Hu P, Ren H*, et al.* PEGylated curcumin derivative attenuates hepatic steatosis via CREB/PPAR-γ/CD36 pathway. BioMed research international. 2017;2017.

600. Herzig S, Hedrick S, Morantte I, Koo S-H, Galimi F, Montminy M. CREB controls hepatic lipid metabolism through nuclear hormone receptor PPAR-γ. Nature. 2003;426(6963):190-3.

601. Zhou J, Febbraio M, Wada T, Zhai Y, Kuruba R, He J*, et al.* Hepatic fatty acid transporter Cd36 is a common target of LXR, PXR, and PPARγ in promoting steatosis. Gastroenterology. 2008;134(2):556-67. e1.

602. Ma Y, Huang Y, Yan L, Gao M, Liu D. Synthetic FXR agonist GW4064 prevents diet-induced hepatic steatosis and insulin resistance. Pharmaceutical research. 2013;30(5):1447-57.

603. Kim M, Murakami A, Kawabata K, Ohigashi H. (−)-Epigallocatechin-3-gallate promotes pro-matrix metalloproteinase-7 production via activation of the JNK1/2 pathway in HT-29 human colorectal cancer cells. Carcinogenesis. 2005;26(9):1553-62.

604. Bansal DD, Bajaj JS, McMaster D, Vallance-Owen J. Hepatic degradation of insulin and the release of its component A and B chains. Irish Journal of Medical Science. 1975;144(1):375-8.

605. Duckworth WC, Bennett RG, Hamel FG. Insulin Degradation: Progress and Potential*. Endocrine Reviews. 1998;19(5):608-24.

606. Morton GJ. Hypothalamic leptin regulation of energy homeostasis and glucose metabolism. The Journal of physiology. 2007;583(Pt 2):437-43.

607. Liu ZJ, Bian J, Liu J, Endoh A. Obesity reduced the gene expressions of leptin receptors in hypothalamus and liver. Horm Metab Res. 2007;39(7):489-94.

608. Nason SR, Kim T, Antipenko JP, Finan B, DiMarchi R, Hunter CS*, et al.* Glucagon-Receptor Signaling Reverses Hepatic Steatosis Independent of Leptin Receptor Expression. Endocrinology. 2019;161(1).

609. Perfield JW, 2nd, Ortinau LC, Pickering RT, Ruebel ML, Meers GM, Rector RS. Altered hepatic lipid metabolism contributes to nonalcoholic fatty liver disease in leptin-deficient Ob/Ob mice. J Obes. 2013;2013:296537.

610. Cohen B, Novick D, Rubinstein M. Modulation of insulin activities by leptin. Science. 1996;274(5290):1185-8.

611. Sivitz WI, Walsh SA, Morgan DA, Thomas MJ, Haynes WG. Effects of Leptin on Insulin Sensitivity in Normal Rats*. Endocrinology. 1997;138(8):3395-401.

612. Kamohara S, Burcelin R, Halaas JL, Friedman JM, Charron MJ. Acute stimulation of glucose metabolism in mice by leptin treatment. Nature. 1997;389(6649):374-7.

613. Amitani M, Asakawa A, Amitani H, Inui A. The role of leptin in the control of insulin-glucose axis. Frontiers in Neuroscience. 2013;7(51).

614. Lubis AR, Widia F, Soegondo S, Setiawati A. The role of SOCS-3 protein in leptin resistance and obesity. Acta Med Indones. 2008;40(2):89-95.

615. Carow B, Rottenberg ME. SOCS3, a Major Regulator of Infection and Inflammation. Front Immunol. 2014;5:58-.

616. Müller G, Ertl J, Gerl M, Preibisch G. Leptin impairs metabolic actions of insulin in isolated rat adipocytes. J Biol Chem. 1997;272(16):10585-93.

617. Kaplan LM. Leptin, obesity, and liver disease. Gastroenterology. 1998;115(4):997-1001.

618. Dewidar B, Meyer C, Dooley S, Meindl B, Nadja. TGF-β in Hepatic Stellate Cell Activation and Liver Fibrogenesis-Updated 2019. Cells. 2019;8(11):1419.

619. Xu F, Liu C, Zhou D, Zhang L. TGF-β/SMAD pathway and its regulation in hepatic fibrosis. Journal of Histochemistry & Cytochemistry. 2016;64(3):157-67.

620. Xu F, Zhou D, Meng X, Wang X, Liu C, Huang C*, et al.* Smad2 increases the apoptosis of activated human hepatic stellate cells induced by TRAIL. International Immunopharmacology. 2016;32:76-86.

621. Dudás J, Kovalszky I, Gallai M, Nagy JO, Schaff Z, Knittel T*, et al.* Expression of decorin, transforming growth factor-beta1, tissue inhibitor metalloproteinase 1 and 2, and type IV collagenases in chronic hepatitis. American journal of clinical pathology. 2001;115(5):725-35.

622. Wang RN, Green J, Wang Z, Deng Y, Qiao M, Peabody M*, et al.* Bone Morphogenetic Protein (BMP) signaling in development and human diseases. Genes & Diseases. 2014;1(1):87-105.

623. Yang C, Zeisberg M, Mosterman B, Sudhakar A, Yerramalla U, Holthaus K*, et al.* Liver fibrosis: insights into migration of hepatic stellate cells in response to extracellular matrix and growth factors. Gastroenterology. 2003;124(1):147-59.

624. Kitade M, Yoshiji H, Kojima H, Ikenaka Y, Noguchi R, Kaji K*, et al.* Leptin-mediated neovascularization is a prerequisite for progression of nonalcoholic steatohepatitis in rats. Hepatology. 2006;44(4):983-91.

625. Yoshiji H, Kuriyama S, Yoshii J, Ikenaka Y, Noguchi R, Hicklin D*, et al.* Vascular endothelial growth factor and receptor interaction is a prerequisite for murine hepatic fibrogenesis. Gut. 2003;52(9):1347-54.

626. Ma L, Zeng Y, Wei J, Yang D, Ding G, Liu J*, et al.* Knockdown of LOXL1 inhibits TGF-β1-induced proliferation and fibrogenesis of hepatic stellate cells by inhibition of Smad2/3 phosphorylation. Biomedicine & Pharmacotherapy. 2018;107:1728-35.

627. Zhao W, Yang A, Chen W, Wang P, Liu T, Cong M*, et al.* Inhibition of lysyl oxidase-like 1 (LOXL1) expression arrests liver fibrosis progression in cirrhosis by reducing elastin crosslinking. Biochimica et Biophysica Acta (BBA) - Molecular Basis of Disease. 2018;1864(4, Part A):1129-37.

628. Yadav H, Quijano C, Kamaraju Anil K, Gavrilova O, Malek R, Chen W*, et al.* Protection from Obesity and Diabetes by Blockade of TGF-β/Smad3 Signaling. Cell Metabolism. 2011;14(1):67-79.

629. Lamichane S, Dahal Lamichane B, Kwon S-M. Pivotal roles of peroxisome proliferator-activated receptors (PPARs) and their signal cascade for cellular and whole-body energy homeostasis. International journal of molecular sciences. 2018;19(4):949.

630. Calamita P, Gatti G, Miluzio A, Scagliola A, Biffo S. Translating the Game: Ribosomes as Active Players. Front Genet. 2018;9:533-.

631. Iino C, Shimoyama T, Iino K, Yokoyama Y, Chinda D, Sakuraba H*, et al.* Daidzein Intake Is Associated with Equol Producing Status through an Increase in the Intestinal Bacteria Responsible for Equol Production. Nutrients. 2019;11(2):433.

632. Zheng W, Ma Y, Zhao A, He T, Lyu N, Pan Z*, et al.* Compositional and functional differences in human gut microbiome with respect to equol production and its association with blood lipid level: a cross-sectional study. Gut Pathogens. 2019;11(1):20.

633. Lampe JW. Is equol the key to the efficacy of soy foods? The American Journal of Clinical Nutrition. 2009;89(5):1664S-7S.

634. Jackson RL, Greiwe JS, Schwen RJ. Emerging evidence of the health benefits of S-equol, an estrogen receptor β agonist. Nutr Rev. 2011;69(8):432-48.

635. Mathey J, Mardon J, Fokialakis N, Puel C, Kati-Coulibaly S, Mitakou S*, et al.* Modulation of soy isoflavones bioavailability and subsequent effects on bone health in ovariectomized rats: the case for equol. Osteoporosis international. 2007;18(5):671-9.

636. Blake C, Fabick KM, Setchell KD, Lund TD, Lephart ED. Neuromodulation by soy diets or equol: anti-depressive & anti-obesity-like influences, age-& hormone-dependent effects. BMC neuroscience. 2011;12(1):28.

637. Frankenfeld CL. O-Desmethylangolensin: The Importance of Equol's Lesser Known Cousin to Human Health. Advances in Nutrition. 2011;2(4):317-24.

638. Duda-Chodak A, Tarko T, Satora P, Sroka P. Interaction of dietary compounds, especially polyphenols, with the intestinal microbiota: a review. European journal of nutrition. 2015;54(3):325-41.

639. Högger P. Nutrition-derived bioactive metabolites produced by gut microbiota and their potential impact on human health. Science. 2013;10:177.

640. Hwang CS, Kwak HS, Lim HJ, Lee SH, Kang YS, Choe TB*, et al.* Isoflavone metabolites and their in vitro dual functions: they can act as an estrogenic agonist or antagonist depending on the estrogen concentration. The Journal of steroid biochemistry and molecular biology. 2006;101(4-5):246-53.

641. Low Y-L, Dunning AM, Dowsett M, Folkerd E, Doody D, Taylor J*, et al.* Phytoestrogen exposure is associated with circulating sex hormone levels in postmenopausal women and interact with ESR1 and NR1I2 gene variants. Cancer Epidemiology and Prevention Biomarkers. 2007;16(5):1009-16.

642. Kang NJ, Lee KW, Rogozin EA, Cho YY, Heo YS, Bode AM*, et al.* Equol, a metabolite of the soybean isoflavone daidzein, inhibits neoplastic cell transformation by targeting the MEK/ERK/p90RSK/activator protein-1 pathway. J Biol Chem. 2007;282(45):32856-66.

643. Zheng W, Zhang Y, Ma D, Shi Y, Liu C, Wang P. (±)Equol inhibits invasion in prostate cancer DU145 cells possibly via down-regulation of matrix metalloproteinase-9, matrix metalloproteinase-2 and urokinase-type plasminogen activator by antioxidant activity. J Clin Biochem Nutr. 2012;51(1):61-7.

644. Raschke M, Wähälä K, Pool-Zobel BL. Reduced isoflavone metabolites formed by the human gut microflora suppress growth but do not affect DNA integrity of human prostate cancer cells. British journal of nutrition. 2006;96(3):426-34.

645. Kang JS, Yoon YD, Han MH, Han SB, Lee K, Park SK*, et al.* Equol inhibits nitric oxide production and inducible nitric oxide synthase gene expression through down-regulating the activation of Akt. Int Immunopharmacol. 2007;7(4):491-9.

646. Gredel S, Grad C, Rechkemmer G, Watzl B. Phytoestrogens and phytoestrogen metabolites differentially modulate immune parameters in human leukocytes. Food and Chemical toxicology. 2008;46(12):3691-6.

647. Joy S, Siow RC, Rowlands DJ, Becker M, Wyatt AW, Aaronson PI*, et al.* The Isoflavone Equol Mediates Rapid Vascular Relaxation Ca2+-independent activation of endothelial nitric-oxide synthase/hsp90 involving erk1/2 and akt phosphorylation in human endothelial cell. Journal of Biological Chemistry. 2006;281(37):27335-45.

648. Danbara N, Yuri T, Tsujita-Kyutoku M, Tsukamoto R, Uehara N, Tsubura A. Enterolactone induces apoptosis and inhibits growth of Colo 201 human colon cancer cells both in vitro and in vivo. Anticancer research. 2005;25(3B):2269-76.

649. Lindahl G, Saarinen N, Abrahamsson A, Dabrosin C. Tamoxifen, flaxseed, and the lignan enterolactone increase stroma-and cancer cell–derived IL-1Ra and decrease tumor angiogenesis in estrogen-dependent breast cancer. Cancer research. 2011;71(1):51-60.

650. Mueller SO, Simon S, Chae K, Metzler M, Korach KS. Phytoestrogens and their human metabolites show distinct agonistic and antagonistic properties on estrogen receptor α (ERα) and ERβ in human cells. Toxicological Sciences. 2004;80(1):14-25.

651. Corsini E, Dell'Agli M, Facchi A, De Fabiani E, Lucchi L, Boraso MS*, et al.* Enterodiol and enterolactone modulate the immune response by acting on nuclear factor-κB (NF-κB) signaling. Journal of agricultural and food chemistry. 2010;58(11):6678-84.

652. Ishimoto H, Shibata M, Myojin Y, Ito H, Sugimoto Y, Tai A*, et al.* In vivo anti-inflammatory and antioxidant properties of ellagitannin metabolite urolithin A. Bioorganic & medicinal chemistry letters. 2011;21(19):5901-4.

653. Larrosa M, González-Sarrías A, García-Conesa MT, Tomás-Barberán FA, Espín JC. Urolithins, ellagic acid-derived metabolites produced by human colonic microflora, exhibit estrogenic and antiestrogenic activities. Journal of agricultural and food chemistry. 2006;54(5):1611-20.

654. Seeram NP, Aronson WJ, Zhang Y, Henning SM, Moro A, Lee R-p*, et al.* Pomegranate ellagitannin-derived metabolites inhibit prostate cancer growth and localize to the mouse prostate gland. J of Agricultural and Food Chemistry. 2007;55(19):7732-7.

655. Adams LS, Zhang Y, Seeram NP, Heber D, Chen S. Pomegranate ellagitannin–derived compounds exhibit antiproliferative and antiaromatase activity in breast cancer cells in vitro. Cancer Prevention Research. 2010;3(1):108-13.

656. Sidhu H, Enatska L, Ogden S, Williams WN, Allison MJ, Peck AB. Evaluating children in the Ukraine for colonization with the intestinal bacterium Oxalobacter formigenes, using a polymerase chain reaction-based detection system. Molecular Diagnosis. 1997;2(2):89-97.

657. Zoetendal EG, Akkermans AD, Akkermans-van Vliet WM, de Visser JAG, de Vos WM. The host genotype affects the bacterial community in the human gastronintestinal tract. Microbial ecology in health and disease. 2001;13(3):129-34.

658. Selma MV, Beltrán D, Luna MC, Romo-Vaquero M, García-Villalba R, Mira A*, et al.* Isolation of Human Intestinal Bacteria Capable of Producing the Bioactive Metabolite Isourolithin A from Ellagic Acid. Frontiers in Microbiology. 2017;8(1521).

659. Vitaglione P, Donnarumma G, Napolitano A, Galvano F, Gallo A, Scalfi L*, et al.* Protocatechuic acid is the major human metabolite of cyanidin-glucosides. The Journal of nutrition. 2007;137(9):2043-8.

660. Masella R, Santangelo C, D'archivio M, LiVolti G, Giovannini C, Galvano F. Protocatechuic acid and human disease prevention: biological activities and molecular mechanisms. Current medicinal chemistry. 2012;19(18):2901-17.

661. Wang D, Wei X, Yan X, Jin T, Ling W. Protocatechuic Acid, a Metabolite of Anthocyanins, Inhibits Monocyte Adhesion and Reduces Atherosclerosis in Apolipoprotein E-Deficient Mice. Journal of Agricultural and Food Chemistry. 2010;58(24):12722-8.

662. Harini R, Pugalendi KV. Antihyperglycemic effect of protocatechuic acid on streptozotocin-diabetic rats. Journal of basic and clinical physiology and pharmacology. 2010;21(1):79-92.

663. Carregosa D, Carecho R, Figueira I, N Santos Cu. Low-Molecular weight metabolites from polyphenols as effectors for attenuating neuroinflammation. Journal of Agricultural and Food Chemistry. 2019;68(7):1790-807.

664. Kim D-H, Jung E-A, Sohng I-S, Han J-A, Kim T-H, Han MJ. Intestinal bacterial metabolism of flavonoids and its relation to some biological activities. Archives of pharmacal research. 1998;21(1):17-23.

665. Gao K, Xu A, Krul C, Venema K, Liu Y, Niu Y*, et al.* Of the major phenolic acids formed during human microbial fermentation of tea, citrus, and soy flavonoid supplements, only 3, 4-dihydroxyphenylacetic acid has antiproliferative activity. The Journal of nutrition. 2006;136(1):52-7.

666. Monagas M, Khan N, Andrés-Lacueva C, Urpí-Sardá M, Vázquez-Agell M, Lamuela-Raventós RM*, et al.* Dihydroxylated phenolic acids derived from microbial metabolism reduce lipopolysaccharide-stimulated cytokine secretion by human peripheral blood mononuclear cells. British journal of nutrition. 2009;102(2):201-6.

667. Pavlica S, Gebhardt R. Protective effects of flavonoids and two metabolites against oxidative stress in neuronal PC12 cells. Life Sciences. 2010;86(3-4):79-86.

668. Nunes C, Almeida L, Laranjinha J. Synergistic inhibition of respiration in brain mitochondria by nitric oxide and dihydroxyphenylacetic acid (DOPAC). Implications for Parkinson's disease. Neurochem Int. 2005;47(3):173-82.

669. Nunes C, Barbosa RM, Almeida L, Laranjinha J. Nitric oxide and DOPAC-induced cell death: from GSH depletion to mitochondrial energy crisis. Mol Cell Neurosci. 2011;48(1):94-103.

670. Zhang M, Jagdmann GE, Van Zandt M, Sheeler R, Beckett P, Schroeter H. Chemical Synthesis and Characterization of Epicatechin Glucuronides and Sulfates: Bioanalytical Standards for Epicatechin Metabolite Identification. Journal of Natural Products. 2013;76(2):157-69.

671. Kennedy EA, King KY, Baldridge MT. Mouse Microbiota Models: Comparing Germ-Free Mice and Antibiotics Treatment as Tools for Modifying Gut Bacteria. Front Physiol. 2018;9:1534-.

672. Membrez M, Blancher F, Jaquet M, Bibiloni R, Cani PD, Burcelin RG*, et al.* Gut microbiota modulation with norfloxacin and ampicillin enhances glucose tolerance in mice. The FASEB Journal. 2008;22(7):2416-26.

673. Rodriguez-Mateos A, Toro-Funes N, Cifuentes-Gomez T, Cortese-Krott M, Heiss C, Spencer JPE. Uptake and metabolism of (−)-epicatechin in endothelial cells. Archives of Biochemistry and Biophysics. 2014;559:17-23.

674. Ahmad TR, Haeusler RA. Bile acids in glucose metabolism and insulin signalling—Mechanisms and research needs. Nature Reviews Endocrinology. 2019:1-12.

Appendix

Appendix

This figure is with reference to the data in chapter 2.

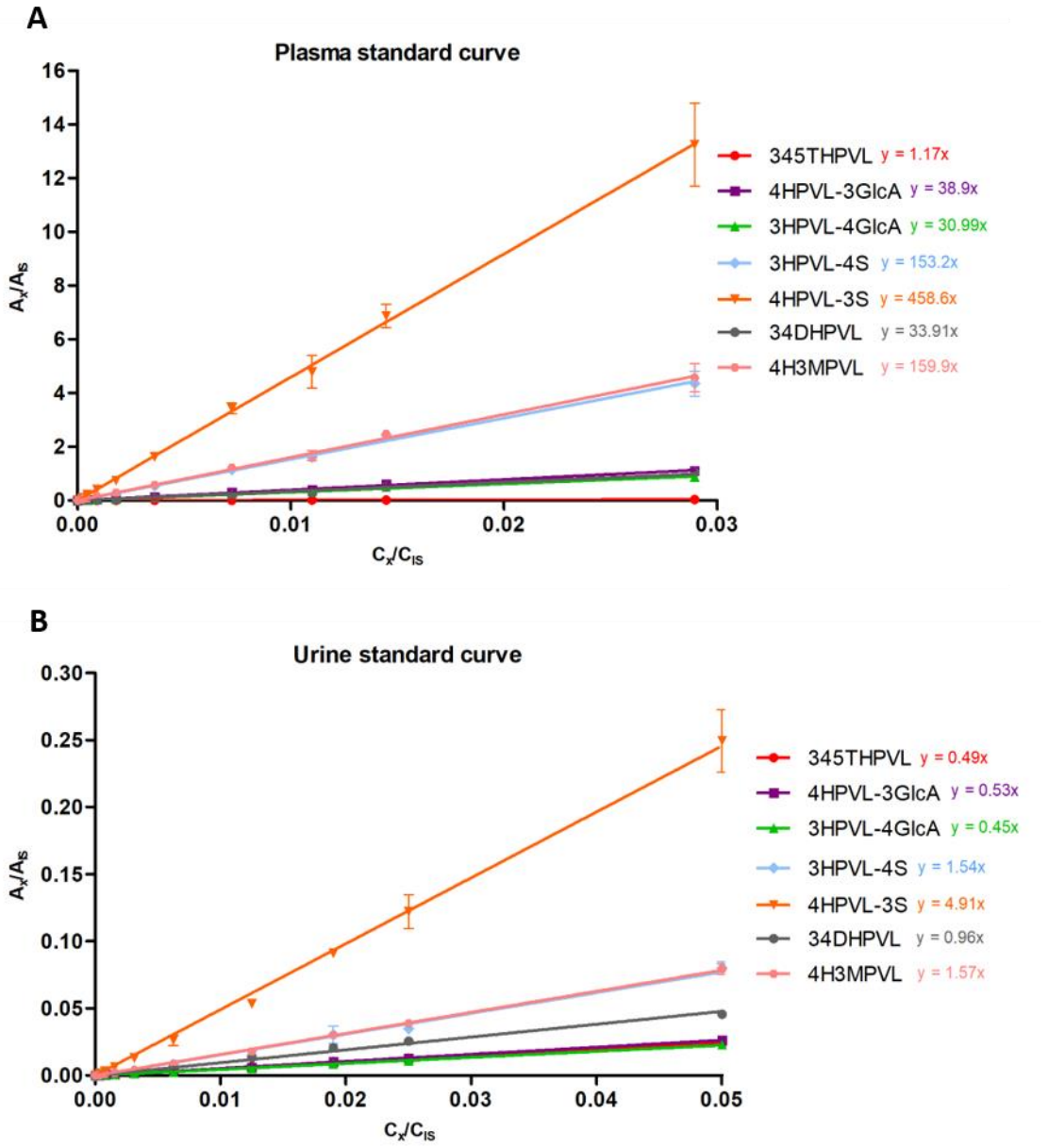

Appendix Figure 1: Hydroxyphenyl-γ-valerolactone standard curves for plasma and urine UPLC-MS² analysis

A) Standard curves for hydroxyphenyl-γ-valerolactones that were spiked into plasma after processing using the protein precipitation method in section 2.4.7.3. The internal standard used was protocatechuic acid. B) Standard curves for hydroxyphenyl-γ-valerolactones that were spiked into urine after processing using the method outlined in section x. The internal standard used was taxifolin. Cx: Concentration of analyte spiked; CIS: concentration of internal standard spiked; Ax: area under the peak curve for the analyte following the UPLC-MS² run; AIS: area under the peak curve for the analyte following the UPLC-MS² run. Error bars represent standard deviation of the standard replicates Line equations are stated next to the line legend.

This figure is with reference to the data in chapter 2.

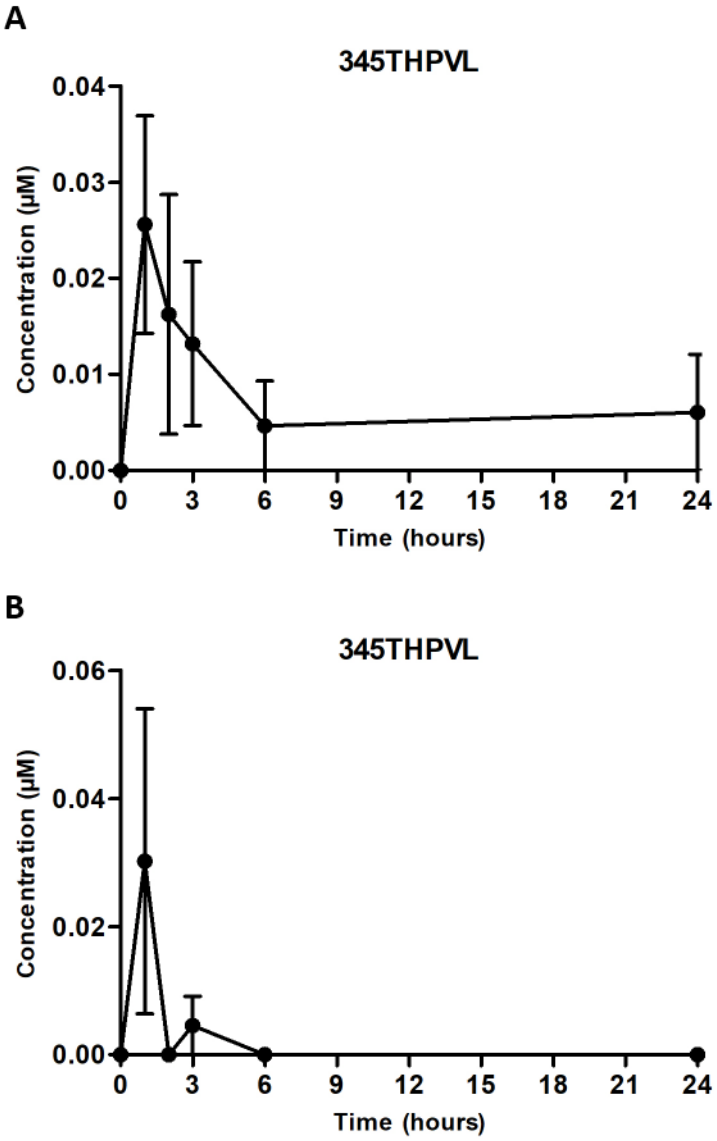

Appendix Figure 2: Plasma and urine pharmacokinetics of 3',4',5'-trihydroxyphenyl-γ-valerolactone (345THPVL) in mice

Mice were oral gavaged with 2 mg of 3',4'-dihydroxyphenyl-γ-valerolactone and the pharmacokinetic profile of 345THPVL was analysed over 24-hours in A) plasma , and B) urine. Error bars represent standard error of the mean (SEM).

This figure is with reference to the data in chapter 4.

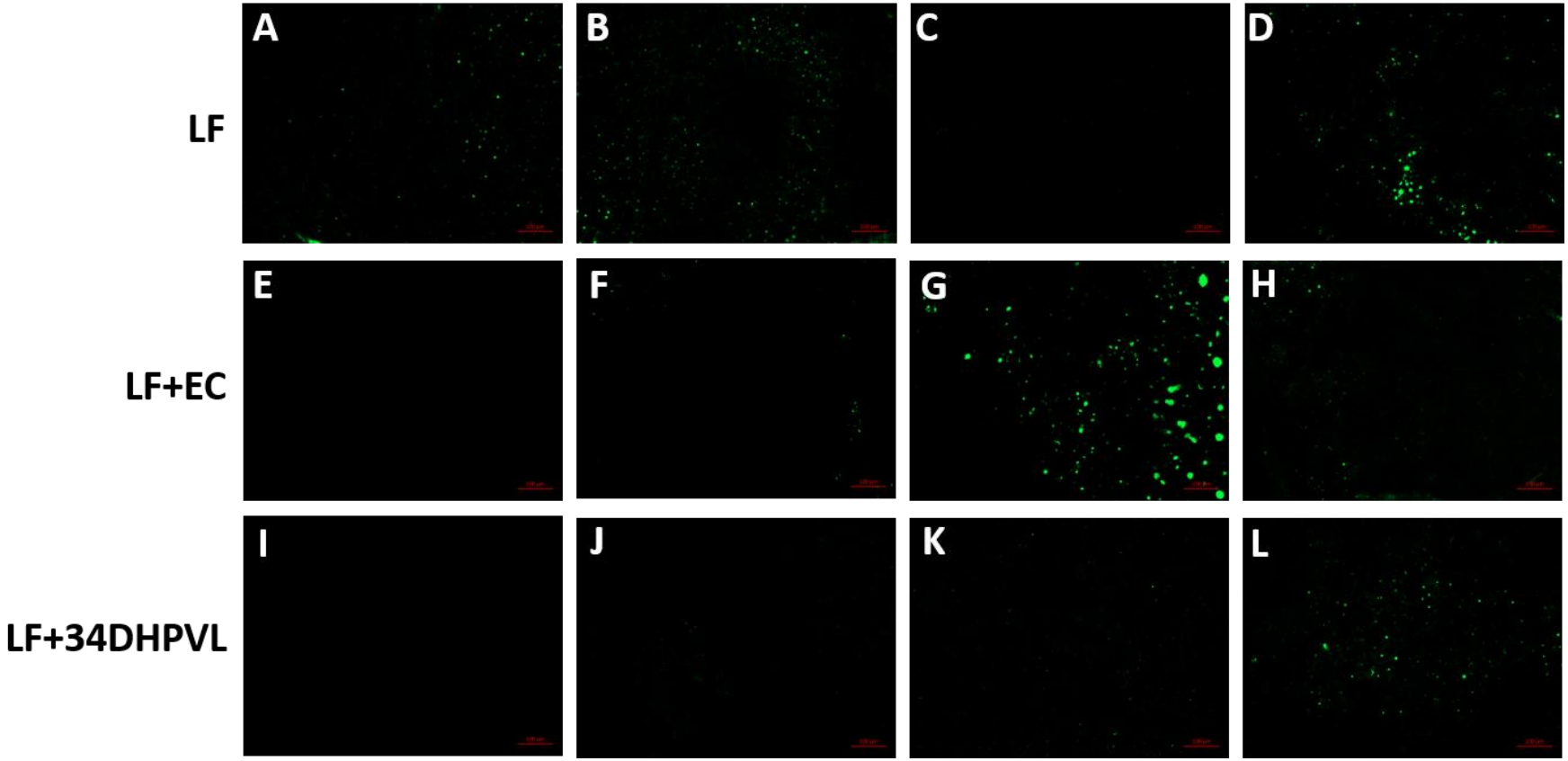

Appendix Figure 3: Lipid fluorescence in the livers of LF intervention mice

Livers from low-fat (LF) fed mice supplemented with or without (−)-epicatechin (EC) or 3',4'-dihydroxyphenyl-γ-valerolactone (34DHPVL), were processed and stained for lipids using LipidTox™ (ThermoFisher) and imaged under a Zeiss Axiocam fluorescence microscope. Images were taken at 10x magnification and the scale bar is 100 µm. Each image is taken from a section of a different mouse liver in the respective groups A-D: LF, E-F: LF+EC, I-L: LF+34DHPVL.

This figure is with reference to the data in chapter 4.

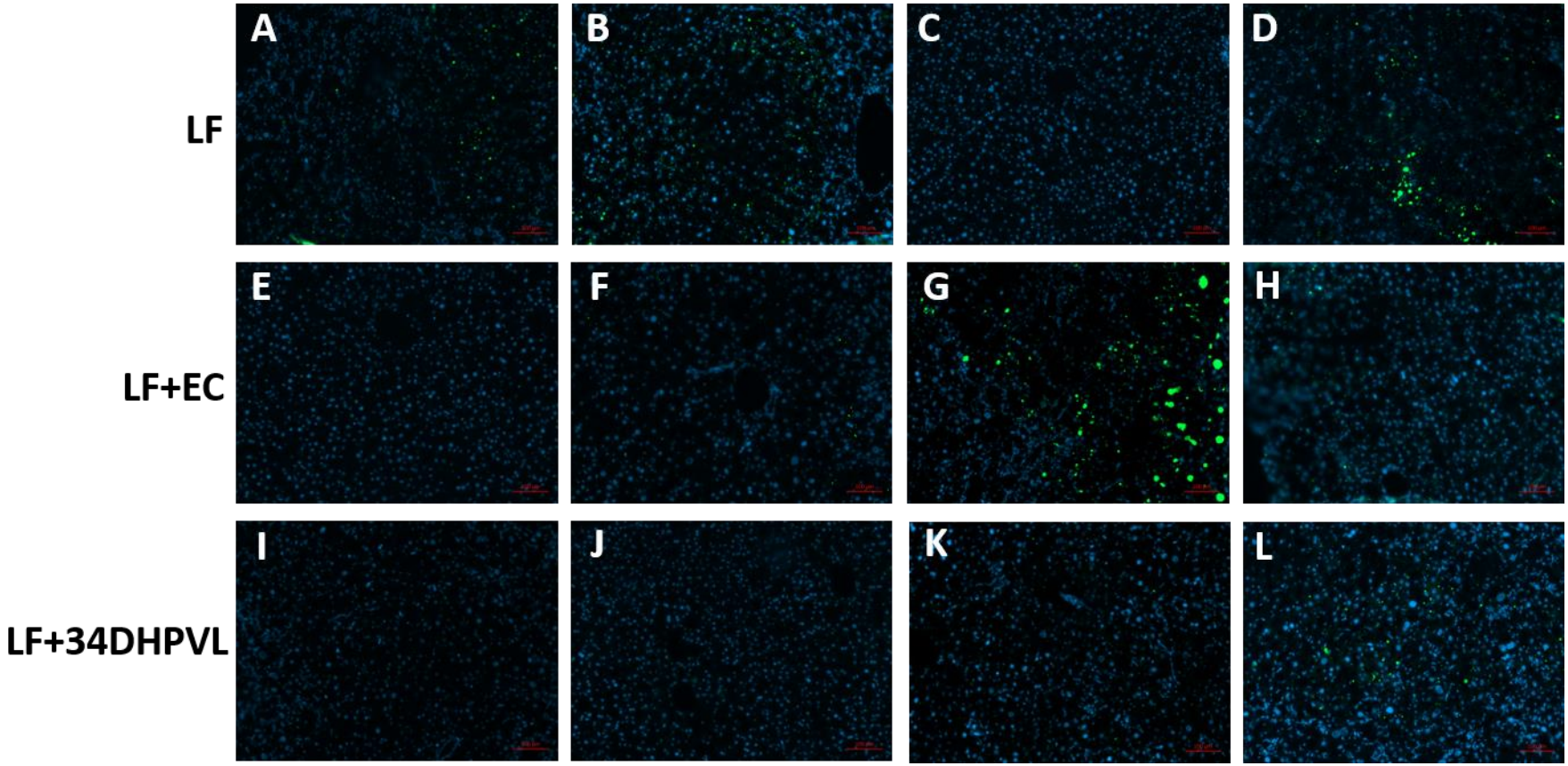

Appendix Figure 4: Lipid and nuclei fluorescence in the livers of LF intervention mice

Livers from low-fat (LF) fed mice supplemented with or without (−)-epicatechin (EC) or 3',4'-dihydroxyphenyl-γ-valerolactone (34DHPVL), were processed and stained for lipids using LipidTox™ green(ThermoFisher) and the nuclei with DAPI and imaged under a Zeiss Axiocam fluorescence microscope. Images were taken at 10x magnification and the scale bar is 100 µm. Each image is taken from a section of a different mouse liver in the respective groups A-D: LF, E-F: LF+EC, I-L: LF+34DHPVL.

This figure is with reference to the data in chapter 4.

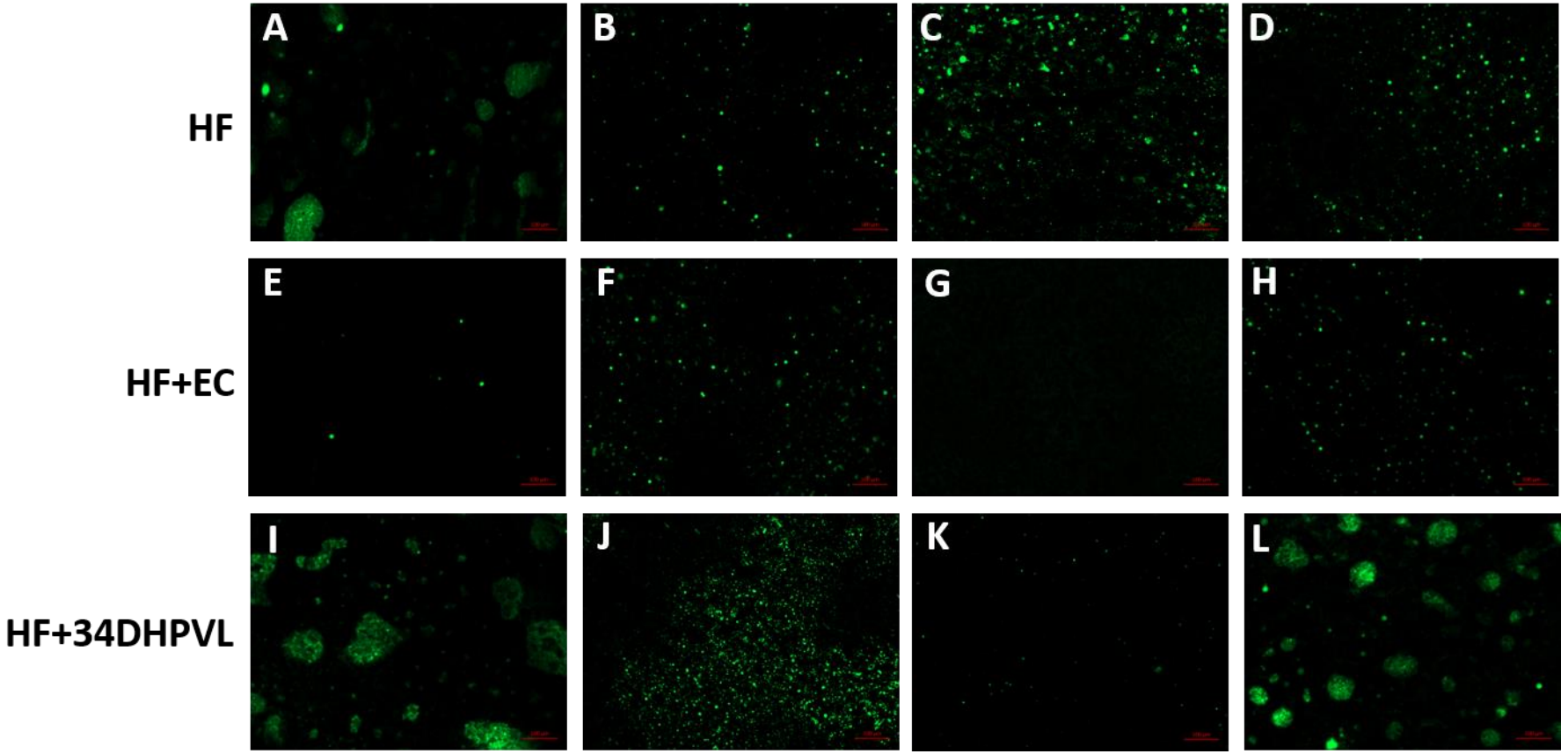

Appendix Figure 5: Lipid fluorescence in the livers of HF intervention mice

Livers from high-fat (HF) fed mice supplemented with or without (−)-epicatechin (EC) or 3',4'-dihydroxyphenyl-γ-valerolactone (34DHPVL), were processed and stained for lipids using LipidTox™ (ThermoFisher) and imaged under a Zeiss Axiocam fluorescence microscope. Images were taken at 10x magnification and the scale bar is 100 µm. Each image is taken from a section of a different mouse liver in the respective groups A-D: HF, E-F: HF+EC, I-L: HF+34DHPVL.

This figure is with reference to the data in chapter 4.

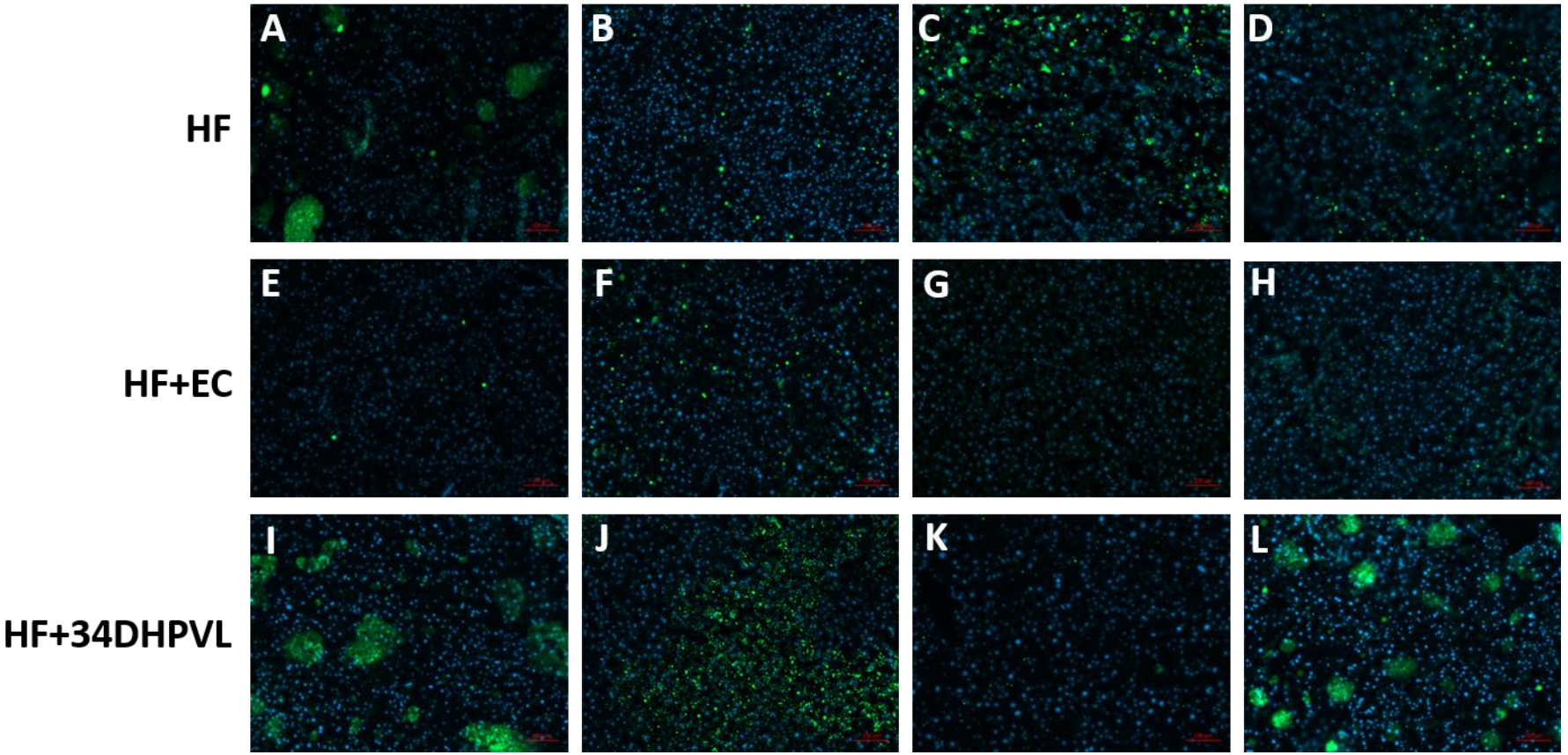

Appendix Figure 6: Lipid and nuclei fluorescence in the livers of HF intervention mice

Livers from high-fat (HF) fed mice supplemented with or without (−)-epicatechin (EC) or 3',4'-dihydroxyphenyl-γ-valerolactone (34DHPVL), were processed and stained for lipids using LipidTox™ (ThermoFisher) and the nuclei with DAPI imaged under a Zeiss Axiocam fluorescence microscope. Images were taken at 10x magnification and the scale bar is 100 µm. Each image is taken from a section of a different mouse liver in the respective groups A-D: HF, E-F: HF+EC, I-L: HF+34DHPVL.

This figure is with reference to the data in chapter 4.

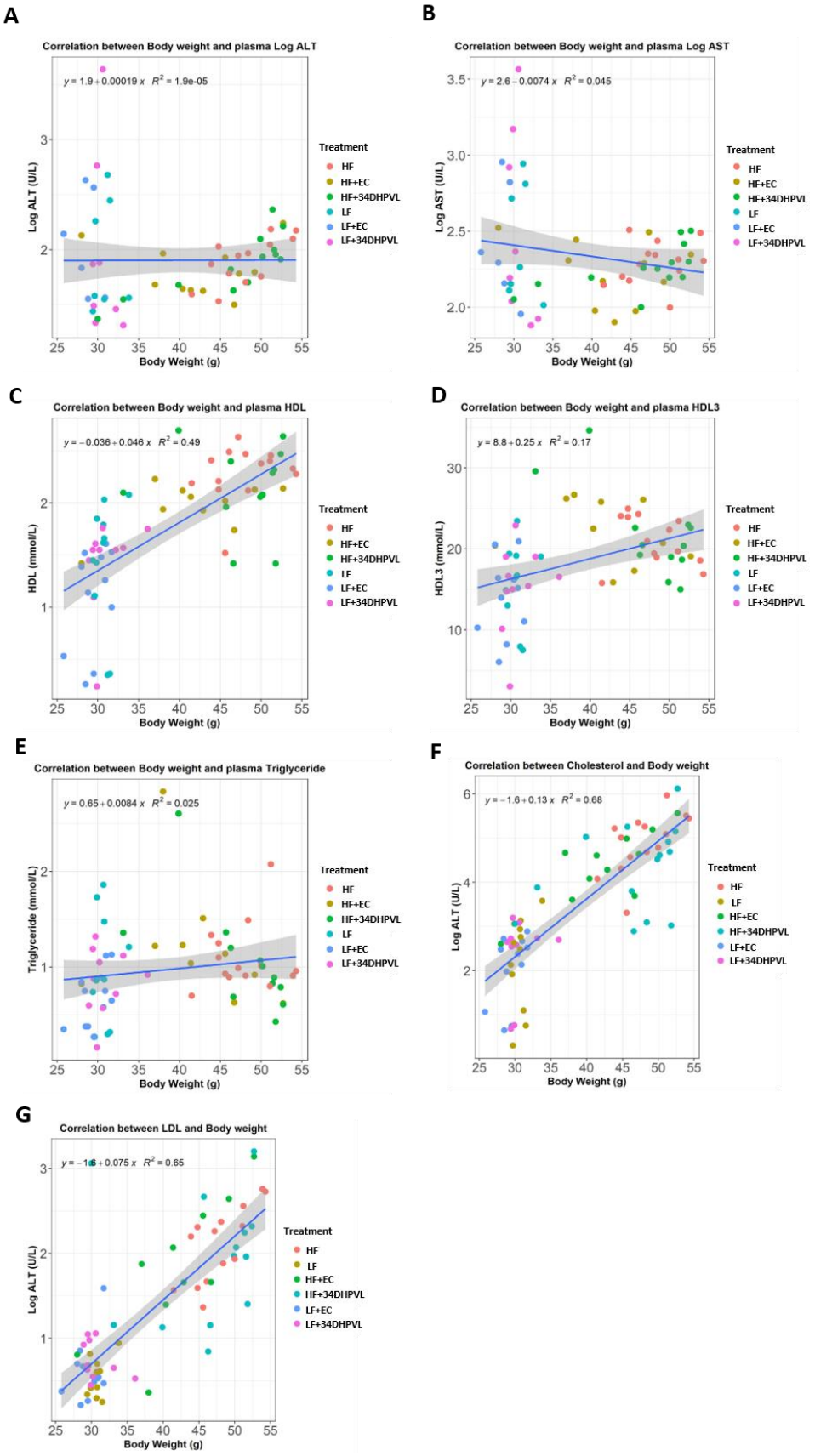

Appendix Figure 7: Correlation analyses for plasma biomarkers against body weight

Appendix Figure 7: Correlation analyses for plasma biomarkers against body weight (continued)
Mouse plasma was assayed using clinical chemistry and regression analyses against body weight were plotted for A) Log ALT (alanine transaminases), B) Log AST (aspartate transaminases), C) HDL (high-density lipoproteins), D) HDL3, E) Triglyceride, F) Cholesterol, G) LDL (low-density lipoproteins).

The following tables are with reference to the data in chapter 5.

Appendix Table 1: Primers used to optimise housekeeping gene selection for the livers of mice from the dietary intervention study

Liver cDNA of the mice from the dietary intervention study outlined in chapter 3 were analysed by qRT-PCR for the following list of primers to optimise housekeeping gene selection. All primers accept YWHAZ provided a single melt curve with R^2 values and amplification efficiencies as outlined below. EIF2A and ACTB were the top ranked most stable housekeeping genes and were used to normalise cDNA expression for further genes of interest.

Gene	Full Gene Name	Gene ID	Product Size	Forward Primer	Reverse Primer	R^2 Value	Amplification Efficiency
ACTB	Actin beta	NM_007393.5	74	GCAGGAGTACGATGAGTCCG	ACGCAGCTCAGTAACAGTCC	0.972	108.812
EIF2A	Eukaryotic Translation Initiation Factor 2A	NM_026114.3	78	ACTTTTAGTAAGGATGGGACATTGTT	TCCCTTGTTAGCGACATTGA	0.994	90.034
YWHAZ	Tyrosine 3-monooxygenase/ tryptophan 5-monooxygenase activation protein, zeta polypeptide	NM_011740.3	78	CCAGACTGAGGAAGATTAAGCAAT	CCAGACTGAGGAAGATTAAGCAAT	0.991	120.535
TBP1	TATA box binding protein	NM_013684	187	ATCAACATCTCAGCAACCCA	TTGAAGCTGCGGTACAATTC	0.99	106.153
GAK	Cyclin G associated kinase	NM_153569.1	111	GGTCATCCAGTCTGTGGCTAAC	TTGATTGCAGACTCCACACC	0.998	91.132
RPL27	Ribosomal protein L27	NM_000988.4	80	TGAAAGGTTAGCGGAAGTGC	TTTCATGAACTTGCCCATCTC	0.994	92.018
HMBS	Hydroxymethylbilane	NM_013551.2	250	GAATTCAGTGCCATCGTCCT	CTTCTGGGTGCAAAATCTGG	0.993	98.225
RPLP0	60 S acidic ribosomal protein P0	NM_007475.5	124	ACTGGTCTAGGACCCGAGAAG	CTCCCACCTTGTCTCCAGTC	0.983	121.137
GAPDH	Glyceraldehyde-3-phosphate dehydrogenase	NM_001289726.1	266	ACAGTCCATGCCATCACTGCC	GCCTGCTTCACCACCTTCTTG	0.998	107.409
B2M	β−2-microglobulin	NM_009735.3	241	CTGCTACGTAACACAGTTCCACCC	CATGATGCTTGATCACATGTCTCG	0.993	107.992
RPL4	Ribosomal protein L4	NM_024212.4	95	AGCAGCCGGGTAGAGAGG	ATGACTCTCCCTTTTCGGAGT	0.997	73.248
OAZ1	Ornithine Decarboxylase Antizyme 1	NM_001301034.1	121	CTCTGCCTGAGGGCAGTAAG	AGTAGGGCGGCTCTGTCC	N/A	N/A

Appendix Table 2: Top 20 KEGG enriched pathways for the HF versus LF treatment

The number of genes involved corresponds to the number of genes found to be significant out of the total number of genes involved in that pathway. Where the normalised enrichment score is a positive number then the pathway was upregulated for the comparison, and vice versa. The FDR q-value highlights how significantly enriched the pathway was.

Top 20 KEGG Pathways	Number of genes involved	Normalised Enrichment Score	FDR *q*-value
Valine Leucine and isoleucine degradation	32/37	2.56	0.000
Peroxisome	46/73	2.53	0.000
Fatty acid metabolism	20/35	2.50	0.000
Butanoate metabolism	17/26	2.30	0.000
Propanoate metabolism	18/28	2.20	0.000
Beta alanine metabolism	12/20	2.10	0.000
Tryptophan metabolism	14/30	2.09	0.000
Drug metabolism other enzymes	16/28	2.02	0.001
PPAR signalling pathway	20/56	1.97	0.001
Limonene and pinene degradation	6/9	1.88	0.004
Ribosome	32/77	-2.33	0.000
Spliceosome	43/116	-1.75	0.085
ECM receptor interaction	34/69	-1.68	0.137
Notch signalling pathway	16/40	-1.68	0.106
Focal adhesion	58/169	-1.55	0.335
Cell adhesion molecules	23/96	-1.54	0.287
Bladder cancer	24/37	-1.48	0.429
Progesterone mediated oocyte maturation	31/73	-1.48	0.377
Cell cycle	42/117	-1.41	0.590
Tight junction	40/101	-1.370	0.694

Appendix Table 3: Top 20 KEGG enriched pathways for the HF+EC versus HF treatment

The number of genes involved corresponds to the number of genes found to be significant out of the total number of genes involved in that pathway. Where the normalised enrichment score is a positive number then the pathway was upregulated for the comparison, and vice versa. The FDR q-value highlights how significantly enriched the pathway was.

Top 20 KEGG Pathways	Number of genes involved	Normalised Enrichment Score	FDR *q*-value
Ribosome	43/77	2.15	0.000
Toll like receptor signalling pathway	21/80	1.94	0.004
Leishmania infection	11/53	1.84	0.015
Jak-Stat signalling pathway	31/95	1.77	0.032
Cytokine-cytokine receptor interaction	42/158	1.77	0.028
Cytosolic DNA sensing pathway	15/38	1.73	0.038
NOD like receptor signalling pathway	10/51	1.66	0.081
Acute myeloid leukaemia	18/56	1.63	0.104
Apoptosis	19/80	1.59	0.137
Spliceosome	35/116	1.53	0.218
Valine Leucine and isoleucine degradation	23/37	-2.53	0.000
Fatty acid metabolism	17/35	-2.27	0.000
Butanoate metabolism	14/26	-2.22	0.000
Propanoate metabolism	15/28	-2.19	0.000
Peroxisome	33/73	-1.97	0.004
Starch and sucrose metabolism	13/29	-1.86	0.014
PPAR signalling pathway	16/56	-1.83	0.018
Citrate cycle (TCA cycle)	15/28	-1.80	0.023
Tryptophan metabolism	14/30	-1.79	0.022
Beta alanine metabolism	13/20	-1.77	0.026

Appendix Table 4: Top 20 KEGG enriched pathways for the HF+34DHPVL and HF treatment

The number of genes involved corresponds to the number of genes found to be significant out of the total number of genes involved in that pathway. Where the normalised enrichment score is a positive number then the pathway was upregulated for the comparison, and vice versa. The FDR q-value highlights how significantly enriched the pathway was.

Top 20 KEGG Pathways	Number of genes involved	Normalised Enrichment Score	FDR *q*-value
Notch signalling pathway	15/40	1.67	0.730
DNA replication	7/33	1.67	0.370
Other glycan degradation	6/15	1.65	0.312
Hematopoietic cell lineage	17/64	1.63	0.262
ECM receptor interaction	29/69	1.59	0.320
Ribosome	22/77	1.57	0.309
Amino sugar and nucleotide sugar metabolism	19/41	1.57	0.267
Mismatch repair	4/21	1.56	0.247
Base excision repair	15/30	1.56	0.227
Histidine metabolism	9/25	1.53	0.261
Valine Leucine and isoleucine degradation	19/37	-1.69	0.422
Primary bile acid biosynthesis	10/13	-1.53	0.780
Regulation of autophagy	10/18	-1.50	0.655
Drug metabolism other enzymes	16/28	-1.49	0.516
Riboflavin metabolism	10/12	-1.47	0.478
Terpenoid backbone biosynthesis	7/12	-1.43	0.526
TGF beta signalling	19/72	-1.43	0.451
Ubiquitin mediated proteolysis	33/126	-1.39	0.515
Butanoate metabolism	13/26	-1.36	0.536
Glycosphingolipid biosynthesis lacto and neolacto series	5/15	-1.34	0.546

Appendix Table 5: Top 20 KEGG pathways for the LF+EC versus LF treatment

The number of genes involved corresponds to the number of genes found to be significant out of the total number of genes involved in that pathway. Where the normalised enrichment score is a positive number then the pathway was upregulated for the comparison, and vice versa. The FDR q-value highlights how significantly enriched the pathway was.

Top 20 KEGG Pathways	Number of genes involved	Normalised Enrichment Score	FDR *q*-value
Leishmania infection	34/53	2.28	0.000
Natural killer cell mediated cytotoxicity	40/86	2.25	0.000
Chemokine signalling pathway	61/147	2.19	0.001
Epithelial cell signalling in helicobacter pylori infection	28/59	2.14	0.001
Antigen processing and presentation	30/47	2.13	0.001
NOD like receptor signalling pathway	22/51	2.01	0.004
Cell adhesion molecules	41/96	2.00	0.004
Graft versus host disease	15/21	1.95	0.014
T-cell receptor signalling pathway	34/92	1.94	0.015
Cytokine-cytokine receptor interaction	61/158	1.92	0.023
Parkinsons disease	50/94	-1.78	0.138
Oxidative phosphorylation	53/99	-1.71	0.150
Regulation of autophagy	6/18	-1.56	0.347
RNA polymerase	9/26	-1.52	0.337
Maturity onset diabetes of the young	7/12	-1.50	0.313
Folate biosynthesis	4/8	-1.48	0.306
Spliceosome	32/116	-1.43	0.342
Glycosaminoglycan biosynthesis keratin sulfate	5/10	-1.40	0.365
Riboflavin metabolism	6/12	-1.38	0.376
Pyruvate metabolism	12/33	-1.28	0.573

Appendix Table 6: Top 20 KEGG enriched pathways for the LF+34DHPVL versus LF treatment

The number of genes involved corresponds to the number of genes found to be significant out of the total number of genes involved in that pathway. Where the normalised enrichment score is a positive number then the pathway was upregulated for the comparison, and vice versa. The FDR q-value highlights how significantly enriched the pathway was.

Top 20 KEGG Pathways	Number of genes involved	Normalised Enrichment Score	FDR *q*-value
Leishmania infection	32/53	2.31	0.000
FC Epsilon RI signalling pathway	23/59	2.25	0.000
Natural killer cell mediated cytotoxicity	36/86	2.25	0.000
Cytokine-cytokine receptor interaction	78/158	2.20	0.000
B cell receptor signalling pathway	33/74	2.17	0.000
Cell adhesion molecules	42/96	2.14	0.000
Leukocyte transendothelial migration	47/93	2.11	0.000
Hematopoietic cell lineage	31/64	2.11	0.000
Graft versus host disease	18/21	2.10	0.000
NOD like receptor signalling	29/51	2.08	0.000
Maturity onset diabetes of the young	56/147	2.08	0.000
Glycosaminoglycan biosynthesis heparan sulfate	6/12	-1.93	0.021
Basal cell carcinoma	10/19	-1.60	0.390
Terpenoid backbone biosynthesis	10/41	-1.57	0.313
Selenoamino acid metabolism	7/12	-1.54	0.304
Glycine serine and threonine metabolism	17/27	-1.54	0.243
Oxidative phosphorylation	47/99	-1.51	0.257
Melanogenesis	11/75	-1.48	0.271
Sulfur metabolism	5/9	-1.44	0.305
Tyrosine metabolism	14/28	-1.43	0.282

Appendix Table 7: Top 20 KEGG pathways for the HF+EC versus LF treatments

The number of genes involved corresponds to the number of genes found to be significant out of the total number of genes involved in that pathway. Where the normalised enrichment score is a positive number then the pathway was upregulated for the comparison, and vice versa. The FDR q-value highlights how significantly enriched the pathway was.

Top 20 KEGG Pathways	Number of genes involved	Normalised Enrichment Score	FDR *q*-value
Peroxisome	40/73	2.41	0.000
Valine leucine and isoleucine degradation	24/37	2.39	0.000
Fatty acid metabolism	19/35	2.28	0.000
Proteasome	23/41	2.02	0.002
Tryptophan metabolism	16/30	1.95	0.003
Butanoate metabolism	15/26	1.90	0.006
Beta alanine metabolism	14/20	1.80	0.024
Pantothenate and COA biosynthesis	9/13	1.78	0.029
Drug metabolism other enzymes	13/28	1.74	0.041
Propanoate metabolism	15/28	1.72	0.046
Ribosome	37/77	-2.01	0.003
Cell cycle	51/117	-1.81	0.044
ECM receptor interaction	34/69	-1.79	0.039
TGF beta signalling pathway	25/72	-1.77	0.039
Focal adhesion	70/169	-1.63	0.141
Arrhythmogenic right ventricular cardiomyopathy	18/52	-1.63	0.125
Cell adhesion molecules	16/96	-1.61	0.125
Progesterone mediated oocyte maturation	31/73	-1.59	0.133
Oocyte meiosis	28/93	-1.59	0.121
Hypertrophic cardiomyopathy HCM	29/57	-1.55	0.155

Appendix Table 8: Top 20 KEGG enriched pathways for the HF+34DHPVL versus LF treatments

The number of genes involved corresponds to the number of genes found to be significant out of the total number of genes involved in that pathway. Where the normalised enrichment score is a positive number then the pathway was upregulated for the comparison, and vice versa. The FDR q-value highlights how significantly enriched the pathway was.

Top 20 KEGG Pathways	Number of genes involved	Normalised Enrichment Score	FDR *q*-value
Valine leucine and isoleucine degradation	29/37	2.47	0.000
Fatty acid metabolism	21/35	2.45	0.000
Peroxisome	35/73	2.43	0.000
Butanoate Metabolism	17/26	2.29	0.000
Tryptophan metabolism	12/30	2.21	0.000
Propanoate metabolism	21/28	2.16	0.000
Drug metabolism cytochrome P450	14/35	2.01	0.000
Beta alanine metabolism	12/20	1.97	0.000
PPAR signalling pathway	28/56	1.94	0.001
Ascorbate and aldarate metabolism	4/8	1.84	0.001
Ribosome	51/77	-2.23	0.000
Spliceosome	52/116	-2.07	0.000
TGF beta signalling pathway	23/72	-1.60	0.330
Basal transcription factors	13/29	-1.58	0.281
Arrhythmogenic right ventricular cardiomyopathy	19/52	-1.57	0.262
RNA degradation	23/55	-1.54	0.274
Notch signalling pathway	18/40	-1.52	0.282
Bladder cancer	15/37	-1.47	0.370
Hypertrophic cardiomyopathy HCM	26/57	-1.43	0.426
mTOR signalling pathway	11/48	-1.42	0.423

Appendix Table 9: Top 20 REACTOME enriched pathways for the HF versus LF treatments

The number of genes involved corresponds to the number of genes found to be significant out of the total number of genes involved in that pathway. Where the normalised enrichment score is a positive number then the pathway was upregulated for the comparison, and vice versa. The FDR q-value highlights how significantly enriched the pathway was.

Top 20 REACTOME Pathways	Number of genes involved	Normalised Enrichment Score	FDR *q*-value
Protein localisation	67/153	2.54	0.000
Peroxisomal protein import	36/58	2.46	0.000
Mitochondrial fatty acid beta oxidation	21/30	2.45	0.000
Fatty acid metabolism	53/145	2.39	0.000
Peroxisomal lipid metabolism	15/26	2.27	0.000
The citric acid cycle and respiratory electron transport	75/145	2.26	0.000
Respiratory electron transport ATP synthesis by chemiosmotic coupling and heat production by uncoupling proteins	54/101	2.23	0.000
Respiratory electron transport	47/82	2.23	0.000
Glyoxylate metabolism and glycine degradation	14/26	2.21	0.000
Branched chain amino acid catabolism	14/18	2.21	0.000
Eukaryotic translation elongation	35/81	-2.31	0.000
Response of EIF2AK4 GCN2 to amino acid deficiency	48/91	-2.31	0.000
SRP dependent co-translational protein targeting to membrane	59/101	-2.26	0.000
Nonsense mediated decay	56/104	-2.24	0.000
Influenza infection	57/135	-2.21	0.000
Eukaryotic translation initiation	60/108	-2.19	0.000
Extracellular matrix organisation	114/232	-2.14	0.000
RRNA processing	87/188	-2.14	0.000
Selenoamino acid metabolism	49/106	-2.11	0.000
Integrin cell surface interactions	50/73	-2.02	0.001

Appendix Table 10: Top 20 REACTOME enriched pathways for the HF+EC versus HF treatments

The number of genes involved corresponds to the number of genes found to be significant out of the total number of genes involved in that pathway. Where the normalised enrichment score is a positive number then the pathway was upregulated for the comparison, and vice versa. The FDR q-value highlights how significantly enriched the pathway was.

Top 20 REACTOME Pathways	Number of genes involved	Normalised Enrichment Score	FDR *q*-value
SRP dependent co-translational protein targeting to membrane	57/101	2.22	0.000
Eukaryotic translation elongation	45/81	2.15	0.000
Response of EIF2AK4 GCN2 to amino acid deficiency	47/91	2.15	0.000
Interferon alpha beta signalling	22/44	2.13	0.000
Antimicrobial peptides	9/20	2.08	0.000
Selenoamino acid metabolism	65/106	2.07	0.000
Regulation of TLR by endogenous ligand	8/18	2.07	0.000
Toll like receptor cascades	36/144	2.03	0.001
RRNA Processing	82/188	2.02	0.001
Interleukin 10 signalling	14/31	2.01	0.001
Mitochondrial fatty acid beta oxidation	16/30	-2.30	0.000
Peroxisomal lipid metabolism	15/26	-2.02	0.022
Fatty acid metabolism	44/145	-1.97	0.038
Mitochondrial fatty acid beta oxidation of saturated fatty acids	6/9	-1.95	0.034
Class I peroxisomal membrane protein import	10/19	-1.92	0.043
Beta oxidation of decanoyl COA to octanoyl COA	4/6	-1.91	0.044
The citric acid cycle and respiratory electron transport	52/145	-1.89	0.048
Branched chain amino acid catabolism	11/18	-1.89	0.043
Mitochondrial fatty acid beta oxidation of unsaturated fatty acids	6/6	-1.89	0.040
Glyoxylate metabolism and glycine degradation	11/26	-1.89	0.037

Appendix Table 11: Top 20 REACTOME enriched pathways for the HF+34DHPVL versus HF treatments
The number of genes involved corresponds to the number of genes found to be significant out of the total number of genes involved in that pathway. Where the normalised enrichment score is a positive number then the pathway was upregulated for the comparison, and vice versa. The FDR q-value highlights how significantly enriched the pathway was.

Top 20 REACTOME Pathways	Number of genes involved	Normalised Enrichment Score	FDR *q*-value
Polymerase switching	5/13	1.96	0.151
Lagging strand synthesis	5/19	1.93	0.128
Polymerase switching on the C strand of the telomere	5/15	1.88	0.153
O glycosylation of TSR domain containing proteins	16/31	1.88	0.126
DNA strand elongation	14/31	1.87	0.116
Assembly of collagen fibrils and other multimeric structures	29/52	1.81	0.187
PCNA dependent long patch base excision repair	4/19	1.79	0.230
Extracellular matrix organisation	114/232	1.77	0.242
ECM proteoglycans	34/59	1.77	0.217
Carboxyterminal post translational modifications of tubulin	13/24	1.75	0.244
FOXO mediated transcription of cell cycle genes	7/15	-1.89	0.488
Neurotransmitter release cycle	7/33	-1.87	0.292
FOXO mediated transcription of oxidative stress metabolic and neuronal genes	13/25	-1.83	0.365
Signalling by BMP	12/25	-1.78	0.512
Regulation of FOXO transcriptional activity by acetylation	4/10	-1.74	0.651
Dopamine neurotransmitter release cycle	4/17	-1.72	0.624
Signalling by Hippo	6/18	-1.72	0.564
Deadenylation of mRNA	11/24	-1.70	0.592
UB specific processing proteases	50/163	-1.69	0.603
Establishment of sister chromatid cohesion	5/11	-1.68	0.583

Appendix Table 12: Top 20 REACTOME enriched pathways for the LF+EC versus LF treatments

The number of genes involved corresponds to the number of genes found to be significant out of the total number of genes involved in that pathway. Where the normalised enrichment score is a positive number then the pathway was upregulated for the comparison, and vice versa. The FDR q-value highlights how significantly enriched the pathway was.

Top 20 REACTOME Pathways	Number of genes involved	Normalised Enrichment Score	FDR *q*-value
Immunoregulatory interactions between a lymphoid and a non-lymphoid cell	51/78	2.45	0.000
Interferon alpha beta signalling	20/44	2.14	0.001
RHO GTPases activate NADPH oxidases	12/21	2.11	0.001
Interleukin 10 signalling	21/31	2.10	0.001
ROS and RNS production in phagocytes	15/28	2.08	0.002
Interleukin 4 and interleukin 13 signalling	55/85	2.06	0.002
FCGR3A mediated IL-10 synthesis	17/34	2.05	0.002
Semaphorin interactions	25/59	2.02	0.003
Antimicrobial peptides	13/20	2.01	0.004
Signalling by interleukins	156/364	2.00	0.004
Respiratory electron transport	52/82	-2.43	0.000
Respiratory electron transport ATP synthesis by chemiosmotic coupling and heat production by uncoupling proteins	54/101	-2.323	0.000
Complex I biogenesis	31/44	-2.25	0.000
Mitochondrial translation	41/94	-2.14	0.001
Class I peroxisomal membrane protein import	10/19	-1.96	0.040
The citric acid cycle and respiratory electron transport	72/145	-1.92	0.056
CHREBP activates metabolic gene expression	8/8	-1.87	0.085
RNF mutants show enhcanced Wnt signalling and proliferation	4/7	-1.80	0.169
HIV transcription elongation	21/40	-1.76	0.247
Degradation of cysteine and homocysteine	10/12	-1.74	0.270

Appendix Table 13: Top 20 REACTOME enriched pathways for the LF+34DHPVL versus LF treatments
The number of genes involved corresponds to the number of genes found to be significant out of the total number of genes involved in that pathway. Where the normalised enrichment score is a positive number then the pathway was upregulated for the comparison, and vice versa. The FDR q-value highlights how significantly enriched the pathway was.

Top 20 REACTOME Pathways	Number of genes involved	Normalised Enrichment Score	FDR *q*-value
Immunoregulatory interactions between a lymphoid and a non-lymphoid cell	48/78	2.52	0.000
Interferon gamma signalling	35/65	2.34	0.000
DAP12 interactions	14/31	2.30	0.000
RHO GTPases activate NADPH oxidases	12/21	2.22	0.000
Interleukin 4 and interleukin 13 signalling	37/85	2.21	0.000
Interleukin 10 signalling	28/31	2.20	0.000
Signalling by interleukins	168/364	2.20	0.000
GPVI mediated activation cascade	17/33	2.20	0.000
Signalling by the B cell receptor BCR	64/108	2.19	0.000
Neutrophil degranulation	167/396	2.18	0.000
Formation of the beta catenin TCF transactivating complex	24/54	-2.21	0.000
Respiratory electron transport	51/82	-2.21	0.000
Activation of gene expression by SREBF SREBP	17/41	-2.20	0.000
Respiratory electron transport ATP synthesis by chemiosmotic coupling and heat production by uncoupling proteins	54/101	-2.19	0.000
Regulation of cholesterol biosynthesis by SREBP SREBF	20/54	-2.18	0.001
HDACS deacetylate histones	21/50	-2.10	0.003
Complex I biogenesis	29/44	-2.06	0.005
CHREBP activates metabolic gene expression	8/8	-2.02	0.007
HATS acetylate histones	39/97	-1.98	0.011
Mitochondrial translation	42/94	-1.96	0.014

Appendix Table 14: Top 20 REACTOME enriched pathways for the HF+EC versus LF treatments

The number of genes involved corresponds to the number of genes found to be significant out of the total number of genes involved in that pathway. Where the normalised enrichment score is a positive number then the pathway was upregulated for the comparison, and vice versa. The FDR q-value highlights how significantly enriched the pathway was.

Top 20 REACTOME Pathways	Number of genes involved	Normalised Enrichment Score	FDR *q*-value
Peroxisomal protein import	30/58	2.37	0.000
Mitochondrial fatty acid beta oxidation	19/30	2.34	0.000
Protein localisation	75/153	2.34	0.000
Metabolism of polyamines	31/57	2.12	0.001
Interleukin 15 signalling	5/13	2.08	0.002
Interleukin 1 signalling	45/95	2.04	0.005
Peroxisomal lipid metabolism	11/26	2.04	0.004
Interleukin 20 family signalling	5/14	2.04	0.004
Branched chain amino acid catabolism	12/18	2.03	0.004
Fatty acid metabolism	48/145	2.03	0.004
ECM proteoglycans	33/59	-2.04	0.011
Eukaryotic translation elongation	46/81	-2.00	0.012
Collagen chain trimerization	28/32	-1.99	0.010
Eukaryotic translation initiation	37/108	-1.98	0.010
RHO GTPases activate formins	50/123	-1.97	0.008
Extracellular matrix organisation	97/232	-1.96	0.007
Nonsense mediated decay	38/104	-1.95	0.008
Resolution of sister chromatid cohesion	45/109	-1.94	0.009
Influenza infection	65/135	-1.93	0.011
SRP dependent co-translational protein targeting to membrane	49/101	-1.92	0.012

Appendix Table 15: Top 20 REACTOME enriched pathways for the HF+34DHPVL versus LF treatments
The number of genes involved corresponds to the number of genes found to be significant out of the total number of genes involved in that pathway. Where the normalised enrichment score is a positive number then the pathway was upregulated for the comparison, and vice versa. The FDR q-value highlights how significantly enriched the pathway was.

Top 20 REACTOME Pathways	Number of genes involved	Normalised Enrichment Score	FDR *q*-value
Protein localisation	67/153	2.37	0.000
Fatty acid metabolism	56/145	2.35	0.000
Peroxisomal protein import	28/58	2.32	0.000
Mitochondrial fatty acid beta oxidation	21/30	2.28	0.000
The citric acid and respiratory electron transport	53/145	2.21	0.000
Peroxisomal lipid metabolism	15/26	2.16	0.000
Pyruvate metabolism and citric acid cycle	22/48	2.13	0.000
Branched chain amino acid catabolism	12/18	2.08	0.001
Respiratory electron transport ATP synthesis by chemiosmotic coupling and heat production by uncoupling proteins	54/101	2.07	0.001
Glutathione conjugation	10/27	2.00	0.004
Nonsense mediated decay	64/104	-2.32	0.000
RRNA processing	107/188	-2.32	0.000
Eukaryotic translation initiation	70/108	-2.31	0.000
Eukaryotic translation elongation	55/81	-2.30	0.000
Influenza infection	70/135	-2.29	0.000
SRP dependent co-translational protein targeting to membrane	60/101	-2.27	0.000
Response of EIF2AK4 GCN2 to amino acid deficiency	56/91	-2.26	0.000
Processing of capped intron containing pre-mRNA	103/222	-2.19	0.000
RRNA modification in the nucleus and cytosol	32/58	-2.18	0.000
Selenoamino acid metabolism	58/106	-2.15	0.000